Petrogenesis of the Acasta Gneiss Complex, Northwest Territories, Canada

by

Jesse Ray Reimink

A thesis submitted in partial fulfillment of the requirements for the degree of

Doctor of Philosophy

Department of Earth and Atmospheric Sciences
University of Alberta

Abstract

This contribution presents the results of a new mapping and geochemical investigation of well-preserved rock units in the Acasta Gneiss Complex (AGC), Canada, and provides additional support for a broadly mafic Hadean Earth, in which the first evolved crust formation took place in a geodynamic environment unlike modern subduction zones. Rocks in the AGC, with crystallization ages spanning a billion years, document a transition in crust-forming processes starting in a shallow petrogenetic setting with the involvement of plagioclase that eventually evolves to a deep-seated regime dominated by partial melting in the presence of residual garnet. As part of this mapping campaign, we identified and mapped a well-preserved rock unit with an igneous crystallization age of 4.02 Ga, a unit informally termed the Idiwhaa tonalitic gneiss (Idiwhaa meaning "ancient" in the local aboriginal language).

The unique geochemical signatures of the Idiwhaa unit are distinct from typical Archean (4.0–2.5 billion year old) evolved crust. Specifically, the strong iron-enrichments and flat rare-earth-element patterns contained in this unit imply a distinct environment of formation; these signatures suggest a petrogenesis involving high degrees of crystal fractionation from a relatively water-poor basaltic magma at shallow levels. Additionally, well-preserved zircons in this unit allow a further investigation of the geochemical evolution as zircon can retain geochemical information through high-temperature metamorphism. In particular, changes in oxygen isotope ratios between two phases of zircon growth, both with ~4.02 Ga crystallization ages, indicate assimilation by the Idiwhaa magma of pre-existing rocks that had been altered by high temperature surface waters. Combined with the whole-rock signatures discussed above, these data imply petrologic processes strikingly similar to those operating on modern Iceland, a setting that has long been proposed as a suitable analog for crust formation on the early Earth.

Because of the presence of very well preserved zircons in the Idiwhaa unit, we are also able to evaluate the composition and age of pre-existing crust into which the Idiwhaa magma intruded, as well as the differentiation state of the mantle from which the magma was derived. To this end, Hf isotope data were obtained from two igneous phases of 4.02 Ga zircon material, as well as the highest precision dating yet undertaken on AGC rocks. These isotopic data, combined with the whole-rock data described above, suggest that there was little or no interaction with typical Archean continental crust during the formation of the Idiwhaa unit. This result, along with evolved Hf isotope signatures contained in zircon with mantle-like oxygen isotope ratios, suggests interaction with very ancient mafic crust or an ear-

ly-enriched mafic reservoir. The combination of early enriched reservoirs and no evidence for interaction with evolved, continental crust suggests that the Hadean Earth may have been dominated by mafic rocks.

Whole-rock major- and trace-element data combined with zircon uranium-lead and oxygen isotope data obtained from younger rocks from the AGC, including rocks formed at ~3.95, 3.75, 3.5–3.6 and 3.4–2.9 Ga, document a transition in crust-forming and likely tectonic processes over that time interval. Specifically, the earliest components of the AGC (~4.02 Ga) formed in an oceanic plateau-like environment and produced primarily mafic- to intermediate-composition rocks with flat REE patterns. Episodic melting of this thickened and partially hydrated pile at ~3.95 and 3.75 Ga at moderate depths produced tonalitic magmas with somewhat more fractionated REE patterns. The volumetrically dominant 3.5–3.6 Ga rocks of the AGC have steep REE patterns similar to those found in Archean granitoids worldwide. These patterns require deep-seated melting in the presence of abundant residual garnet in the source rock and possibly occurred in a subduction-like setting. Thus, the AGC as a whole records a gradual transition from an oceanic plateau setting to a subduction-like setting over an ~400 million year time interval. Similar models have been proposed for other ancient gneiss terranes, but this process occurred a few hundred million years earlier in the AGC.

Preface

Some of the research conducted during this thesis forms part of international and national research collaboration. Though I conducted most of the field mapping, many people provided assistance over the years. These include Drs. Tom Chacko, Larry Heaman, Richard Stern, John Ketchum, Joshua Davies, as well as Eric Thiessen and Ronald Reimink. Fieldwork was only possible with the assistance of staff from the Northwest Territories Geological Survey, namely Dr. John Ketchum, Scott Cairns, Luke Ootes, and Valerie Jackson. In particular, Dr. Ketchum's personal interest and involvement in this project has provided a vast amount of expertise and field assistance throughout the entire process.

Chapter 2 has been published in Nature Geoscience as Reimink, J. R., Chacko, T., Stern, R. A. & Heaman, L. M. Earth's earliest evolved crust generated in an Iceland-like setting. Nature Geoscience 7 (2014) 529–533. Mapping and sample collection was conducted by J.R.R. and T.C. Sample crushing, processing, and zircon separations were carried out by J.R.R. R.A.S. and J.R.R. carried out collection of zircon oxygen and U-Th-Pb isotopic data by SIMS. Chemical abrasion of zircon was carried out by J.R.R. and L.M.H. All authors contributed to discussion of results and their implications, as well as preparation of the manuscript. J.R.R. wrote the initial manuscript and oversaw every stage of revision and editing.

Chapter 3 is in review with Nature Geoscience as Reimink, J.R., Davies, J.H.F.L., Chacko, T., Stern, R.A., Heaman, L.M., Pearson, D.G., Sarkar, C., Schaltegger, U., Creaser, R.A. No evidence for Hadean continents within Earth's oldest evolved rock unit. Mapping and sample collection was conducted by J.R.R. and T.C. Sample crushing, processing, and zircon separations were carried out by J.R.R. J.D. and J.R.R. carried out collection of bulk zircon Hf and U-Th-Pb isotopic data. C.S. and J.R.R. collected zircon laser ablation Hf and U-Pb data. R.A.C. collected whole-rock Nd isotope data. Modeling was conducted by J.R.R. and T.C. All authors contributed to project design, discussion of results and their implications, as well as preparation of the manuscript. J.R.R. wrote the initial manuscript and will oversee every stage of revision and editing.

Chapter 4 will be submitted to Precambrian Research as Reimink, J. R., Chacko, T., Stern, R. A. & Heaman, L. M. The birth of a cratonic nucleus: Lithogeochemical evolution of the 4.02–2.94 Ga Acasta Gneiss Complex. J.R.R. and T.C. performed the mapping and sample collection. R.A.S. and J.R.R. collected SIMS oxygen isotope and U-Th-Pb analysis of zircon material. J.R.R. collected

LA-ICPMS U-Pb data. All authors contributed to project design, discussion of results and their implications, as well as preparation of the manuscript. J.R.R. wrote the initial manuscript and will oversee every stage of revision and editing.

The ideas presented here are my own, although they have been developed and refined by many discussions with co-authors. All the writing and figures presented here are my own, as are any errors or omissions.

Acknowledgements:

Far too many people deserve space here. First and foremost, Tom Chacko has never ceased to advise me on all aspects of life and science. His open door policy, in conjunction with deep interest in high-quality science led to innumerable discussions from which I inevitably walked away having learned a great deal. He has never faltered from his role as supervisor and role model, even during many long drives across this country and others. He taught me to produce a more careful brand of science and forced me to write clearly. Any coherence and logic that is found in this thesis undoubtedly commenced with Tom. I will forever strive to be as good of a supervisor and friend, and I am forever in his debt. A finer supervisor I could not ask for.

My scientific education and this thesis greatly benefited from fruitful and enlightening conversations with too many people to mention here. Dr. Richard Stern is thanked for the maintanance and set-up of a high quality SIMS facility allowing for the collection of excellent data presented here, as well as many though-provoking discussions. Dr. Larry Heaman is thanked for training and access to his lab and zircon separation facilities as well as many fruitful and informative discussions including a great deal of encouragement, both on and off the golf course. Dr. Graham Pearson is thanked for unlimited access to both the lab facilities under his direction and his wealth of knowledge, as well as allowing me to tag along to many of his research group's activities. Dr. John Ketchum is thanked for providing a great deal of advice and encouragement throughout this thesis, both in the field and out.

Any personal development that has taken place during this experience can be attributed to a variety of friends and colleagues. Josh Davies provided many free-spirited adventures and discussions without any semblance of constraint. Eric Thiessen, Laura Barker, and Natasha Oviatt incited many episodes of procrastination and enjoyment in the mountains. Rasmus Haugaard and Joseph Magnall provided innumerable discussions on the finer points of life. Xavier Rojas added a touch of culture to any proceeding. Alberto Reyes, Sarah Gleeson, and Duane Petts were reliable coffee procrastination companions and advised me on many important subjects including science, life, career, and film. Janina Czas helped me understand that diamonds are maybe interesting. Michelle Speta, Dave Dockman, Naomi Miles, and Shawna White are great friends and never stopped attempting to keep me in line.

I would be remiss to not mention my parents, Ron and Linda, and sister Kelsey, who put up with my many rock collections and helped develop an interest in the outdoors, eventually leading me to

geology. Chris Bolhuis has always been an enthusiastic and influencial teacher and mentor, while the combined forces of Dr. Edward Hansen and Dr. Jon Peterson fostered my burgeoning interest in geology during undergrad.

Table of Contents

List of Tables:

Chapter 2:

Chapter 3:

Chapter 4:

List of Figures

Chapter 2:

Chapter 3:

Chapter 4:

Chapter 1: Introduction

Our understanding of the earliest history of Earth is restricted by a paucity of materials preserved from early in its history. Surprisingly, thanks to various sample return missions, we have a much more substantial knowledge of the earliest history of the Moon than we do of our own planet. Undoubtedly, this is in part due to Earth's long history of plate tectonics, which serves to rework and recycle existing crust thereby masking or eliminating pre-existing rocks and their geochemical signatures. One fundamental aspect that remains unresolved despite decades of work is our understanding of how and when the early continental crust formed. Today, continental crust is formed in a multi-stage process typically occurring along subduction zones. However, further back in time it becomes increasingly less clear how evolved rock types comparable to our modern continents formed.

Some locations on Earth do contain intact relics from early in our planet's history. Detailed studies within the few localities that contain these very ancient terrestrial materials have provided a broad spectrum of theories regarding the timing and processes involved in early terrestrial crust formation. These hypotheses may be broadly categorized into two end members. The first presents a largely uniformitarian view that the early Earth was not drastically different from the modern world; it was influenced by low-temperature surface waters and contained large quantities of evolved continental crust that formed in settings broadly analogous to modern subduction zones. The opposing view somewhat reinforces the long-held belief that the early Earth was drastically different from what we observe today. This view contends that the early Earth was hotter, contained little evolved (i.e. continental) crust, and operated under a different geodynamic regime. The volume of early-formed continental crust and its mechanism of formation carry important implications for the ancient atmosphere, the development of life, the chemical evolution of the crust-mantle system, and the impact of the proposed late heavy bombardment of Earth by bolides.

The first, broadly uniformitarian, view of the early Earth is supported in part by geochemical signatures in 4.0–4.4 Ga detrital zircon grains from Western Australia (Froude et al., 1983; Valley et al., 2014), broadly referred to as the Jack Hills zircon suite. These zircons were eroded from their original magmatic source rocks and are now found entrained in much younger (~3.0 Ga) quartzites and conglomerates. These sub-millimeter grains represent the oldest known terrestrial materials and, despite their ultimate source rock remaining yet undiscovered, a vast quantity of geochemical data has been acquired

from these mineral grains, with varied interpretations. Specifically, the presence of higher-than-mantle oxygen isotope ratios (Mojzsis et al., 2001; Wilde et al., 2001), diverse Hf isotope signatures (Blichert-Toft et al., 1997; Amelin et al., 1999; 2000; Harrison, 2005; Harrison et al., 2008), and mineral inclusion suites typical of granitic compositions (Hopkins et al., 2008; 2010; Bell et al., 2014) may point towards an early Earth that had a hydrosphere, a chemically differentiated mantle, and evolved granitic-composition crust formed by melting of subducted sediments (Mojzsis et al., 2001; Harrison, 2009; Hopkins et al., 2010). The broadly uniformitarian view of the early Earth has also been used to explain isotope tracer data from the Acasta Gneiss Complex, Northwest Territories, Canada (Bowring et al., 1989a; Bowring and Housh, 1995; Amelin et al., 1999; Iizuka et al., 2006; 2009) as well as a variety of structural and geochemical information from the Isua Supracrustal Belt of SW Greenland, widely regarded as the world's oldest known supracrustal sequence (>3.8 Ga), and its surrounding gneisses (e.g., Nutman et al., 2007; 2002; Friend and Nutman, 2005).

The opposing view contends that processes and rock types on the early Earth were distinctly different from those we see today. This viewpoint envisions an early Earth that was dominated by mafic rocks, broadly comparable to today's oceanic crust, as well as long-lived geochemical domains preserved for many hundreds of millions of years (Caro et al., 2003; Kamber et al., 2003; 2005; O'Neil et al., 2008; 2013; Kamber, 2010; 2015; Kemp et al., 2010; 2015; Rizo et al., 2012; Debaille et al., 2013; Roth et al., 2014). This view is mainly evidenced by re-evaluation of the Jack Hills data sets mentioned above (e.g., Nemchin et al., 2006; Kemp et al., 2010; Rasmussen et al., 2011; Nebel et al., 2013), as well as very unradiogenic nature of Pb-isotope ratios in ancient cratons requiring ancient mafic crust (Kamber, 2003; Kamber et al., 2007). Additional evidence may be found in northern Quebec, Canada, where a package of mafic rocks is purported to have erupted at ~4.4 Ga (O'Neil et al., 2008; 2012; 2013). It should be noted that the ages of these Quebec rocks are still in question (David et al., 2009; Roth et al., 2013) and some geochemical features suggest that this belt might have formed by subduction-like processes (Adam et al., 2012). Recent geodynamic modeling reinforces the stable, mafic early Earth viewpoint, in that strictly modern-style plate tectonics seem untenable over long periods of time in a hotter early Earth with higher radiogenic heat production (e.g., O'Neill et al., 2007; O'Neill and Debaille, 2014). Rather, a stagnant-lid regime, where large, thick plates remain in place, may in fact be more likely (e.g., Debaille et al., 2013).

Of the localities worldwide containing very ancient materials, certainly one of the most famous is the Acasta Gneiss Complex (AGC) of the Northwest Territories, Canada. The AGC represents a large (>1300 km^2) exposure of basement gneisses located on the western margin of the Slave Craton. Certain samples within the AGC have long been known to contain zircon that is approximately four billion years old (Bowring et al., 1989b; Stern and Bleeker, 1998; Bowring and Williams, 1999).

Despite the scientific value of the area and many research groups previously and currently working on AGC samples, fundamental knowledge gaps remain. Due in part to the complexities involved in dealing with multiply deformed and metamorphosed four-billion-year-old rocks, basic geologic mapping within the AGC has thus far defined areas of high and low strain mapped using broad chemical divisions of rock units (Bowring and Williams, 1999; Iizuka et al., 2007; 2010), as opposed to dividing units based on age. Indeed, rock units with zircon U-Pb ages ranging from 4.02 Ga to 3.4 Ga exist (e.g., Bleeker and Stern, 2000; Iizuka et al., 2007) within the relatively small portion (~30 km^2) of the broader AGC where essentially all previous research has been conducted, and compositional variability within this wide age range so far remains unknown. Additionally, although a significant amount of complex isotopic data have been published on rock samples from the AGC (Bowring and Housh, 1995; Moorbath et al., 1997; Amelin et al., 1999; 2000; Iizuka and Hirata, 2005; Iizuka et al., 2010; 2009; Guitreau et al., 2014; Mojzsis et al., 2014; Roth et al., 2014), very little basic petrologic information has been reported (Bowring et al., 1990; Iizuka et al., 2010; Mojzsis et al., 2014). This has served to mask potentially important changes in the geochemical character of rock units with age, which I attempt to resolve here.

Most of the limited petrologic data that has been published from the AGC comes from highly strained samples (Bowring et al., 1990; Iizuka et al., 2010; Mojzsis et al., 2014) with cm-scale banding, mingling multiple unrelated rock types together, often resulting in a wide range of crystallization ages (e.g., Mojzsis et al., 2014). Due in part to this complexity, the prevailing viewpoint regarding the chemical nature of even the oldest units within the AGC is that they are composed of broadly felsic gneisses with compositions comparable to the Archean tonalite-trondhjemite-granodiorite (TTG) suite of granitoids. Archean TTGs are felsic rocks that comprise a large portion of cratonic basement gneisses worldwide. Originally called “a sea of granite” (Glikson, 1979), Archean TTGs carry a distinct chemical character defined by high Na_2O and fractionated rare-earth-element patterns (i.e., high light rare-earth-element concentrations and low heavy rare-earth element concentrations; Barker and Arth,

1976; Martin, 1986; Moyen, 2011; Moyen and Martin, 2012). These important rock types are thought to represent the dominant mode of continental growth through the Archean and are formed by partial melting of hydrated mafic rocks at depths great enough to stabilize significant quantities of residual garnet (e.g. Martin, 1986; Moyen and Stevens, 2006; Nair and Chacko, 2008; Moyen and Martin, 2012).

Despite a general consensus regarding the petrological requirements for TTG formation, the tectonic setting of TTG production remains controversial and can again be broadly categorized into two endmembers. The first is again analogous to modern subduction settings, whereby the hotter Archean Earth allowed for direct partial melting of subducting oceanic crust, producing significant Archean continental crust in subduction-like environments (Martin, 1986). The opposing view suggests that continental crust formation was initiated by delamination and partial melting at the base of oceanic plateaus (Zegers and van Keken, 2001; Bedard, 2006; Smithies et al., 2009), a setting distinctly different from modern subduction zones. As the above discussion has hopefully portrayed, the geochemical nature of the oldest known evolved rocks on Earth, present within the Acasta Gneiss Complex, has significant implications for the state of the Hadean Earth (>4.0 Ga) and the mechanism for crust formation early in Earth's history.

In this thesis I aim to address two main questions. The first is to investigate the character of Hadean rocks preserved in the Acasta Gneiss Complex (AGC) to gain insight into the petrogenesis of Hadean crust on Earth. The second objective is to evaluate the compositions of rock units formed in the AGC and how crust-forming processes evolved throughout the magmatic history of the area. The present work used basic field mapping to produce a new geological map of key areas within the AGC that separates rock units based on age as well as composition. This mapping has allowed the separation of a suite of well-preserved samples with which to evaluate crust formation processes. The methods that are used include whole-rock major- and trace-element geochemistry and Nd isotope analysis, zircon U-Pb, O, and Hf isotope analysis as well as zircon trace-element analysis.

Throughout this thesis I hope to convince the reader that evidence within the AGC points towards an early Earth that lacked significant quantities of continental crust, and that the first crust formation within the AGC took place in thickening mafic crust, analogous to oceanic plateaus. After the formation of this evolved nucleus subduction-like processes, initiated by the evolved nucleus, then produced voluminous Archean TTG-like magmatism.

References:

Adam, J., Rushmer, T., O'Neil, J., Francis, D., 2012. Hadean greenstones from the Nuvvuagittuq fold belt and the origin of the Earth's early continental crust. Geology 40, 363–366.

Amelin, Y., Lee, D.C., Halliday, A.N., 2000. Early-middle Archaean crustal evolution deduced from Lu-Hf and U-Pb isotopic studies of single zircon grains. Geochimica et Cosmochimica Acta.

Amelin, Y., Lee, D.C., Halliday, A.N., Pidgeon, R.T., 1999. Nature of the Earth's earliest crust from hafnium isotopes in single detrital zircons. Nature.

Barker, F., Arth, J.G., 1976. Generation of trondhjemitic-tonalitic liquids and Archean bimodal trondhjemite-basalt suites. Geology 4, 596–600.

Bedard, J. H., 2006. A catalytic delamination-driven model for coupled genesis of Archaean crust and sub-continental lithospheric mantle. Geochimica et Cosmochimica Acta 70, 1188–1214.

Bell, E.A., Harrison, T.M., Kohl, I.E., Young, E.D., 2014. Eoarchean crustal evolution of the Jack Hills zircon source and loss of Hadean crust. Geochimica et Cosmochimica Acta 146, 27–42.

Bleeker, W., Stern, R., 2000. Why the Slave Province, Northwest Territories, got a little bigger, Geological Survey of Canada Current Research.

Blichert-Toft, J., Gleason, J.D., Telouk, P., Albarède, F., 1997. The Lu–Hf isotope geochemistry of shergottites and the evolution of the Martian mantle–crust system. Earth and Planetary Science Letters 173, 25–39.

Bowring, S.A., Housh, T., 1995. The Earth's early evolution. Science 269, 1535–1540.

Bowring, S.A., Williams, I.S., 1999. Priscoan (4.00–4.03 Ga) orthogneisses from northwestern Canada. Contributions to Mineralogy and Petrology 134, 3–16.

Bowring, S.A., Housh, T.B., Isachsen, C.E., 1990. The Acasta Gneisses: Remnant of Earth's Early Crust. In: Origin of the Earth 1–25.

Bowring, S.A., King, J.E., Housh, T.B., C.E., Isachsen, C.E., Podosek, F.A., 1989a. Neodymium and lead isotope evidence for enriched early Archaean crust in North America. Nature 340, 222–225.

Bowring, S.A., Williams, I.S., Compston, W., 1989b. 3.96 Ga gneisses from the Slave province, Northwest Territories, Canada. Geology 17, 971–975.

Caro, G., Bourdon, B., Birck, J.-L., Moorbath, S., 2003. 146Sm-142Nd evidence from Isua metamorphosed sediments for early differentiation of the Earth's mantle. Nature 423, 428–432.

David, J., Godin, L., Stevenson, R.K., O'Neil, J., Francis, D., 2009. U-Pb ages (3.8–2.7 Ga) and Nd isotope data from the newly identified Eoarchean Nuvvuagittuq supracrustal belt, Superior Craton, Canada. Geological Society of America Bulletin 121, 150–163.

Debaille, V., O'Neill, C., Brandon, A.D., Haenecour, P., 2013. Stagnant-lid tectonics in early Earth revealed by 142Nd variations in late Archean rocks. Earth and Planetary Science Letters 373, 83–92.

Friend, C.R.L., Nutman, A.P., 2005. Complex 3670–3500 Ma Orogenic Episodes Superimposed on Juvenile Crust Accreted between 3850 and 3690 Ma, Itsaq Gneiss Complex, Southern West Greenland. The Journal of Geology 113, 375–397.

Froude, D.O., Ireland, T.R., Kinny, P.D., Williams, I.S., Compston, W., Williams, I.R., Myers, J.S., 1983. Ion microprobe identification of 4,100–4,200 Myr-old terrestrial zircons. Nature 304, 616–618.

Glikson, A.Y., 1979. Early Precambrian Tonalite-Trondhjemite Sialic Nuclei. Earth Science Reviews 1–73.

Guitreau, M., Guitreau, M., Guitreau, M., Blichert-Toft, J., Blichert-Toft, J., Blichert-Toft, J., Mojzsis, S.J., Mojzsis, S.J., Mojzsis, S.J., Roth, A., Roth, A.S.G., Roth, A.S.G., Bourdon, B., Bourdon, B., Cates, N.L., Cates, N.L., Bleeker, W., Bleeker, W., 2014. Lu–Hf isotope systematics of the Hadean–Eoarchean Acasta Gneiss Complex (Northwest Territories, Canada). Geochimica et Cosmochimica Acta 135, 251–269.

Harrison, T.M., 2005. Heterogeneous Hadean Hafnium: Evidence of Continental Crust at 4.4 to 4.5 Ga.

Science 310, 1947–1950.
Harrison, T.M., 2009. The hadean crust: Evidence from >4 ga zircons. Annual Review of Earth and Planetary Sciences 37, 479–505.
Harrison, T.M., Schmitt, A.K., McCulloch, M.T., Lovera, O.M., 2008. Early (≥ 4.5 Ga) formation of terrestrial crust: Lu-Hf, $\delta^{18}O$, and Ti thermometry results for Hadean zircons. Earth and Planetary Science Letters 268, 476–486.
Hopkins, M., Harrison, T.M., Manning, C.E., 2008. Low heat flow inferred from >4 Gyr zircons suggests Hadean plate boundary interactions. Nature 456, 493–496.
Hopkins, M.D., Harrison, T.M., Manning, C.E., 2010. Constraints on Hadean geodynamics from mineral inclusions in >4Ga zircons. Earth and Planetary Science Letters 298, 367–376.
Iizuka, T., Hirata, T., 2005. Improvements of precision and accuracy in in situ Hf isotope microanalysis of zircon using the laser ablation-MC-ICPMS technique. Chemical Geology.
Iizuka, T., Horie, K., Komiya, T., Maruyama, S., Hirata, T., Hidaka, H., Windley, B.F., 2006. 4.2 Ga zircon xenocryst in an Acasta gneiss from northwestern Canada: Evidence for early continental crust. Geology 34, 245–248.
Iizuka, T., Komiya, T., Johnson, S.P., Kon, Y., Maruyama, S., Hirata, T., 2009. Reworking of Hadean crust in the Acasta gneisses, northwestern Canada: Evidence from in-situ Lu–Hf isotope analysis of zircon. Chemical Geology 259, 230–239.
Iizuka, T., Komiya, T., Ueno, Y., Katayama, I., Uehara, Y., Maruyama, S., Hirata, T., Johnson, S.P., Dunkley, D.J., 2007. Geology and zircon geochronology of the Acasta Gneiss Complex, northwestern Canada: New constraints on its tectonothermal history. Precambrian Res 153, 179–208.
Iizuka, T., Nakai, S., Sahoo, Y.V., Takamasa, A., Hirata, T., Maruyama, S., 2010. The tungsten isotopic composition of Eoarchean rocks: Implications for early silicate differentiation and core–mantle interaction on Earth. Earth and Planetary Science Letters 291, 189–200.
Kamber, B.S., 2007. Chapter 2.4 The Enigma of the Terrestrial Protocrust: Evidence for Its Former Existence and the Importance of Its Complete Disappearance, in: Developments in Precambrian Geology, Developments in Precambrian Geology. Elsevier, pp. 75–89.
Kamber, B.S., 2010. Archean mafic–ultramafic volcanic landmasses and their effect on ocean–atmosphere chemistry. Chemical Geology 274, 19–28.
Kamber, B.S., 2015. The evolving nature of terrestrial crust from the Hadean, through the Archaean, into the Proterozoic. Precambrian Res 258, 48–82.
Kamber, B.S., Collerson, K.D., Moorbath, S., Whitehouse, M.J., 2003. Inheritance of early Archaean Pb-isotope variability from long-lived Hadean protocrust. Contributions to Mineralogy and Petrology 145, 25–46.
Kamber, B.S., Greig, A., Collerson, K.D., 2005. A new estimate for the composition of weathered young upper continental crust from alluvial sediments, Queensland, Australia. Geochimica et Cosmochimica Acta 69, 1041–1058.
Kemp, A.I.S., Hickman, A.H., Kirkland, C.L., Vervoort, J.D., 2015. Hf isotopes in detrital and inherited zircons of the Pilbara Craton provide no evidence for Hadean continents. Precambrian Res 261, 112–126.
Kemp, A.I.S., Wilde, S.A., Hawkesworth, C.J., Coath, C.D., Nemchin, A., Pidgeon, R.T., Vervoort, J.D., DuFrane, S.A., 2010. Hadean crustal evolution revisited: New constraints from Pb–Hf isotope systematics of the Jack Hills zircons. Earth and Planetary Science Letters 296, 45–56.
Martin, H., 1986. Effect of steeper Archean geothermal gradient on geochemistry of subduction-zone magmas. Geology 14, 753–756.
Mojzsis, S.J., Cates, N.L., Caro, G., Trail, D., Abramov, O., Guitreau, M., Blichert-Toft, J., Hopkins, M.D., Bleeker, W., 2014. Component geochronology in the polyphase ca. 3920Ma Acasta Gneiss.

Geochimica et Cosmochimica Acta 133, 68–96.
Mojzsis, S.J., Harrison, T.M., Pidgeon, R.T., 2001. Oxygen-isotope evidence from ancient zircons for liquid water at the Earth's surface 4,300 Myr ago. Nature 409, 178–181.
Moorbath, S., Whitehouse, M.J., Kamber, B.S., 1997. Extreme Nd-isotope heterogeneity in the early Archaean - Fact or fiction? Case histories from northern Canada and West Greenland. Chemical Geology 135, 213–231.
Moyen, J.-F., 2011. The composite Archaean grey gneisses: Petrological significance, and evidence for a non-unique tectonic setting for Archaean crustal growth. Lithos 123, 21–36.
Moyen, J.-F., Martin, H., 2012. Forty years of TTG research. Lithos 148, 312–336.
Moyen, J.-F., Stevens, G., 2006. Experimental constraints on TTG petrogenesis: Implications for Archean geodynamics, Geophysical Monograph Series.
Nair, R., Chacko, T., 2008. Role of oceanic plateaus in the initiation of subduction and origin of continental crust. Geology 36, 583–586.
Nebel, O., Rapp, R.P., Yaxley, G.M., 2013. The role of detrital zircons in Hadean crustal research. Lithos 190-191, 313–327.
Nemchin, A.A., Pidgeon, R.T., Whitehouse, M.J., 2006. Re-evaluation of the origin and evolution of >4.2 Ga zircons from the Jack Hills metasedimentary rocks. Earth and Planetary Science Letters 244, 218–233.
Nutman, A.P., Friend, C.R.L., Horie, K., Hidaka, H., 2007. Chapter 3.3 The Itsaq Gneiss Complex of Southern West Greenland and the Construction of Eoarchaean Crust at Convergent Plate Boundaries, Developments in Precambrian Geology, Developments in Precambrian Geology. Elsevier.
Nutman, A.P., McGregor, V.R., Shiraishi, K., Friend, C.R.L., Bennett, V.C., Kinny, P.D., 2002. ⩾3850 Ma BIF and mafic inclusions in the early Archaean Itsaq Gneiss Complex around Akilia, southern West Greenland? The difficulties of precise dating of zircon-free protoliths in migmatites. Precambrian Res 117, 185–224.
O'Neil, J., Carlson, R.W., Francis, D., Stevenson, R.K., 2008. Neodymium-142 evidence for Hadean mafic crust. Science 321, 1828–1831.
O'Neill, C., Debaille, V., 2014. The evolution of Hadean–Eoarchaean geodynamics. Earth and Planetary Science Letters 406, 49–58.
O'Neil, J., Boyet, M., Carlson, R.W., Paquette, J.-L., 2013. Half a billion years of reworking of Hadean mafic crust to produce the Nuvvuagittuq Eoarchean felsic crust. Earth and Planetary Science Letters 379, 13–25.
O'Neil, J., Carlson, R.W., Paquette, J.-L., Francis, D., 2012. Formation age and metamorphic history of the Nuvvuagittuq Greenstone Belt. Precambrian Res 220-221, 23–44.
O'Neill, C., Lenardic, A., Moresi, L., Torsvik, T.H., 2007. Episodic Precambrian subduction. Earth and Planetary Science Letters.
Rasmussen, B., Fletcher, I.R., Muhling, J.R., Gregory, C.J., Wilde, S.A., 2011. Metamorphic replacement of mineral inclusions in detrital zircon from Jack Hills, Australia: Implications for the Hadean Earth. Geology 39, 1143–1146.
Rizo, H., Boyet, M., Blichert-Toft, J., O'Neil, J., Rosing, M.T., Paquette, J.-L., 2012. The elusive Hadean enriched reservoir revealed by 142Nd deficits in Isua Archaean rocks. Nature 491, 96–99.
Roth, A.S.G., Bourdon, B., Mojzsis, S.J., Rudge, J.F., Guitreau, M., Blichert-Toft, J., 2014. Combined 147,146Sm- 143,142Nd constraints on the longevity and residence time of early terrestrial crust. Geochem. Geophys. Geosyst. 15, 2329–2345.
Roth, A.S.G., Bourdon, B., Mojzsis, S.J., Touboul, M., Sprung, P., Guitreau, M., Blichert-Toft, J., 2013. Inherited 142Nd anomalies in Eoarchean protoliths. Earth and Planetary Science Letters 361, 50–57.
Smithies, R.H., Champion, D.C., Van Kranendonk, M.J., 2009. Formation of Paleoarchean continental

crust through infracrustal melting of enriched basalt. Earth and Planetary Science Letters 281, 298–306.
Stern, R., Bleeker, W., 1998. Age of the world's oldest rocks refined using Canada's SHRIMP: The Acasta Gneiss Complex, Northwest Territories, Canada. Geosci Can 25, 27–31.
Valley, J.W., Cavosie, A.J., Ushikubo, T., Reinhard, D.A., Lawrence, D.F., Larson, D.J., Clifton, P.H., Kelly, T.F., Wilde, S.A., Moser, D.E., Spicuzza, M.J., 2014. Hadean age for a post-magma-ocean zircon confirmed by atom-probe tomography. Nature Geoscience.
Wilde, S.A., Valley, J.W., Peck, W.H., Graham, C.M., 2001. Evidence from detrital zircons for the existence of continental crust and oceans on the Earth 4.4 Gyr ago. Nature 409, 175–178.
Zegers, T.E., van Keken, P.E., 2001. Middle Archean continent formation by crustal delamination. Geology 29, 1083–1086.

Chapter 2: Earth's earliest evolved crust generated in an Iceland-like setting

Introduction

Our understanding of early Earth processes is limited by the paucity of rock and mineral samples older than 3.6 billion-years-old (Ga). The available data come from 4.0–4.4 Ga detrital zircon grains from Western Australia (Harrison et al., 2008) and small, scattered blocks of ancient crust, most being younger than 3.9 Ga and nearly all of which have experienced multiple later magmatic or metamorphic events (Condie, 2007). Like their younger Archean counterparts, these ancient terranes are typically dominated by tonalite-trondhjemite-granodiorite (TTG) suite rocks, which are the main plutonic rock package of the Archean and represent significant growth of continental crust. General geochemical characteristics of these Archean TTGs include high Na, high Sr/Y, strong depletions in the heavy rare earth elements (HREEs), and minor or absent Eu anomalies (Barker and Arth, 1976; Martin, 1986; Moyen, 2011; Moyen and Martin, 2012). These characteristics are best explained by partial melting of hydrated basaltic rocks at depths great enough to stabilize significant quantities of residual garnet, a high pressure phase with an affinity for HREEs (Martin, 1986; Rapp et al., 1991; Nair and Chacko, 2008). The lack of a significant Eu anomaly in TTGs indicates that plagioclase, a lower pressure mineral that incorporates Eu^{2+}, had little involvement in their petrogenesis. Two main tectonic models have been proposed for the formation of Archean TTGs and in turn early continental crust: i) subduction and subsequent partial melting of the down-going oceanic slab (Martin, 1986); and ii) partial melting at the base of plume-generated oceanic plateaus (Zegers and van Keken, 2001; Smithies et al., 2009). Though these models differ substantially with regard to tectonic setting, both invoke the deep-seated magmatic processes necessary to generate the geochemical features observed in TTGs. Though many detailed studies have investigated the formation of Archean TTG suites (Barker and Arth, 1976; Martin, 1986; Rapp et al., 1991; Zegers and van Keken, 2001; Nair and Chacko, 2008; Smithies et al., 2009; Moyen, 2011; Moyen and H. Martin, 2012), little is known regarding the nature and petrogenesis of Earth's earliest (>3.9 Ga) sialic crust and its relationship to continental crust formed later in Earth history (e.g. Archean TTGs).

Regional Geology

The Acasta Gneiss Complex (AGC), in northwestern Canada, contains the oldest known terrestrial rocks directly dated by zircon U-Pb isotope methods. The AGC comprises poly-deformed granitic to tonalitic and amphibolitic gneisses with igneous crystallization ages ranging from 4.03 to 3.40 Ga (Bowring et al., 1989; Stern and Bleeker, 1998; Bowring and Williams, 1999). Some units contain still older xenocrystic zircon cores up to 4.2 Ga (Bowring and Williams, 1999; Iizuka et al., 2006). The various components of the AGC, like those of most ancient gneiss terranes, are typically interlayered at the decimeter to centimeter scale, making sampling of individual components difficult. Due in part to their inherent complexity, very little whole-rock, major- and trace-element data has previously been reported for rocks of the AGC and therefore basic petrogenetic information is missing. Additionally, rocks with crystallization ages >4.0 Ga are rare and many of the exposed rock units have significantly younger crystallization ages (~3.8–3.6 Ga; Iizuka et al., 2007). However, as part of a detailed mapping campaign we have identified, from a low strain zone of the AGC, a relatively homogeneous and mappable tonalitic gneiss unit yielding abundant well-preserved igneous zircons with a U-Pb crystallization age of 4.02 Ga (See Supplementary Discussion for details regarding the zircon U-Pb systematics). We refer to this unit as the Idiwhaa ('ancient times' in the local aboriginal language) Tonalitic Gneiss (ITG). This unit affords a rare opportunity to investigate directly the processes responsible for forming pre-4.0 Ga sialic crust. To elucidate the petrogenetic history of this earliest known sample of evolved crust, we conducted whole-rock major- and trace-element analyses of the unit as well as detailed zircon oxygen-isotopes, U-Pb geochronology, and trace-element analyses of zircons by secondary ion mass spectrometry (SIMS).

Whole-rock geochemistry

The ITG is relatively a homogenous mafic tonalite, with small, cross-cutting leucocratic veins (Fig. 2.6). The ITG consists primarily of plagioclase, quartz, hornblende, biotite, and minor garnet. Whole-rock major-element compositions (Table 2.1) are characterized by intermediate levels of SiO_2 (57.9–66.9 wt.%), relatively low Al_2O_3 (13.8–14.1 wt.%), high total iron (8.6–15.3 wt.% FeO) and

correspondingly low Mg-numbers (100 × (MgO/(MgO + FeO) = 13–18). The latter two characteristics are distinct from average Archean TTGs (Moyen, 2011; Moyen and Martin, 2012; 2.7 wt.% and 43, respectively) and indicate magma evolution along an iron enrichment trend (Fig. 2.1A). These geochemical characteristics can be produced by shallow-level fractional crystallization of a relatively reduced, low-H_2O basaltic magma in which the low-pressure mineral plagioclase is a major constituent of the fractionating assemblage (along with clinopyroxene and olivine) and Fe-Ti oxide crystallization is suppressed until late in the differentiation process (Grove and Kinzler, 1986; Bindeman et al., 2012).

The whole-rock trace-element systematics of the ITG are also markedly different from average Archean TTGs (Fig. 2.1B and Fig. 2.7). Unlike TTGs, the REE patterns of the ITG show little fractionation of light from heavy REEs and pronounced negative Eu anomalies. These features indicate, respectively, that garnet was not involved in magma genesis or evolution, but that plagioclase fractionation played a significant role. The high-field-strength elements Zr and Hf are also elevated in the ITG relative to Archean TTGs (Moyen, 2011; Fig. 2.7).

Zircon geochemistry

Given the protracted post-magmatic history of rocks of the AGC (Stern and Bleeker, 1998; Iizuka et al., 2007), it is important to evaluate whether the whole-rock trace-element composition of this unit faithfully reflects that of its igneous precursor. The refractory mineral zircon is useful in this regard because it is strongly resistant to compositional overprinting during post-magmatic processes (Page et al., 2007). Zircons extracted from one sample of the ITG, sample TC-3, are particularly well preserved and consist mainly of magmatic zircon with metamorphic overgrowths. There are two phases of magmatic zircon in the ITG that have identical U-Pb dates; unzoned cores (Phase I) and oscillatory-zoned mantles (Phase II). There are also two later phases involving either recrystallization of pre-existing zircon or new growth during metamorphism (Phases III and IV; Fig. 2.2A-B)

Phase I and II magmatic zircon, both of which record U-Pb ages of ~4.02 Ga, have typical igneous zircon REE profiles that follow those predicted by equilibrium lattice strain models (Fig. 2.13). Importantly, whole-rock REE profiles derived from the zircon REE data using published zircon-melt or zircon-whole-rock partition coefficients share all key features of the measured ITG whole-rock profiles

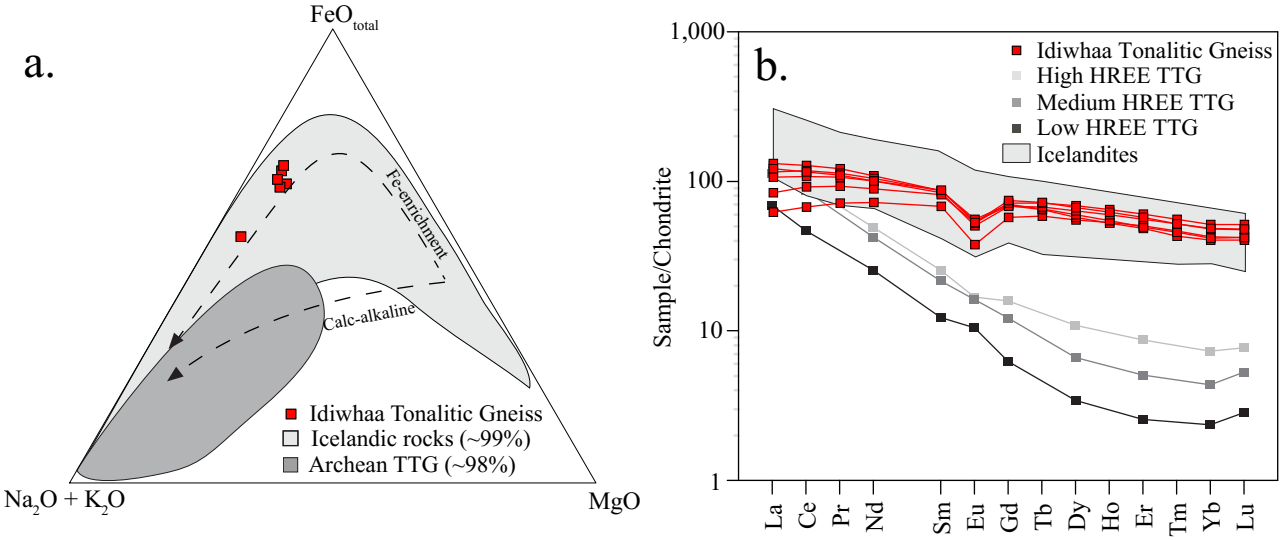

Figure 2.1: Comparison of the whole-rock chemical compositions of the Idiwhaa Tonalitic Gneiss with Icelandic igneous rocks and Archean TTGs. (TTG data are from Moyen, 2011); Icelandic data from the GEOROC database (http://georoc.mpch-mainz.gwdg.de/georoc/). (A) Major-element compositions plotted on a standard alkali-iron-magnesium diagram. The fields shown for Icelandic rocks and Archean TTG's include 99 and 98% of the total 3763 and 1673 total analyses, respectively. (B) Chondrite-normalized REE plot comparing Idiwhaa tonalite data to Archean TTGs and icelandites. The field for icelandites was extracted from the larger Icelandic database (3763 analyses) using: SiO_2 (55–65 wt.%), Al_2O_3 (<15 wt.%), and total FeO (>8 wt.%). This left a total of 90 'icelandite' analyses, 37 containing rare earth element data plotted in B.

described above (Fig. 2.14). This analysis confirms: (i) that igneous zircons present in the ITG were in magmatic equilibrium with a melt equivalent to the whole rock, and therefore provide a good estimate of the igneous crystallization age of the rock; and (ii) the validity of petrogenetic inferences drawn from the whole-rock trace-element data, namely shallow- rather than deep-level processes controlled the magmatic evolution of this unit.

Oxygen isotope data also provide important insights on the petrogenesis of the ITG, in particular the role of exogenic processes in magma evolution. Here again zircon has the capacity to provide the most robust indication of the primary oxygen isotope composition of the magma (Valley et al., 1998; Page et al., 2007). Phase I and II zircon growth zones are indistinguishable in terms of their U-Pb age but show a 0.8‰ difference in $\delta^{18}O_{VSMOW}$ values: Phase I zircon (CL-unzoned cores) have a weighted average = +5.6 ± 0.7‰ (2 s.d.; n = 62), while Phase II (zoned mantles) = +4.7 ± 0.6‰ (2 s.d.; n = 66) (Fig. 2.2C). The average $\delta^{18}O$ values of Phase I zircon are within the +5.3 ± 0.6‰ range of zircon crystallized directly from a primary mantle melt (Valley et al., 1998). In contrast, Phase II zircon

has $\delta^{18}O$ values below +5‰, which requires that the parental magma either directly assimilated, or mixed with, partial melts of low $\delta^{18}O$ rocks that had previously undergone relatively high-temperature hydrothermal alteration by surface waters (Taylor and Sheppard, 1986; Nicholson et al., 1991; Bindeman and Valley, 2001). Later metamorphic zircon overgrowths in the ITG (Phases III–IV) have $\delta^{18}O$ values above +6‰, indicating equilibration with metamorphic fluids enriched in ^{18}O (Fig. 2.2C). Although it appears some Phase I zircons have $\delta^{18}O$ values above the mantle zircon field (Fig. 2.2C), we attribute this to preferential alteration and partial resetting of the oxygen isotope systematics of a small subset of Phase I zircon by a later metamorphic fluid. The full oxygen isotope dataset for Phase I zircon has only a small portion of analyses outside of uncertainty of the mantle zircon field (Fig. 2.15).

Discussion

A petrogenetic model involving assimilation of low $\delta^{18}O$ crust is consistent with the REE systematics of Phase I and II zircon growth zones in that the low $\delta^{18}O$ Phase II igneous mantles have larger positive Ce anomalies than the unzoned cores (Figs. 2.11 and 2.12), indicating the mantles crystallized under more oxidizing conditions than the cores (Trail et al., 2011). Such a result would be expected if the assimilant comprised rocks that had interacted with surface waters.

The Jack Hills detrital zircons from Australia with U-Pb ages up to ~4.4 Ga have $\delta^{18}O$ values higher than those of pristine mantle zircon (Harrison, 2009), implying low-temperature interaction with surface waters in the Hadean. Although the ITG zircons indicate high-, as opposed to low-, temperature water-rock interactions, both indicate the existence of a pre-4.0 Ga hydrosphere on Earth. Ce-anomalies in the Australian detrital zircons (Trail et al., 2011) and ITG zircons also indicate similar magmatic oxidation states.

Though distinct from later-formed Archean TTGs as well as igneous rocks from many modern-day tectonic settings, the geochemical features of the ITG are nearly identical to those of some intermediate rocks from Iceland (Fig. 2.1). In particular, a suite of rocks commonly referred to as icelandites are characterized by ~60 wt.% SiO_2, low Al_2O_3, high FeO, and low Mg-numbers (Muehlenbachs et al., 1974; Bindeman et al., 2012). These rocks also share many of the trace-element features of the ITG including negative Eu anomalies, little fractionation of LREE from HREE (Fig.

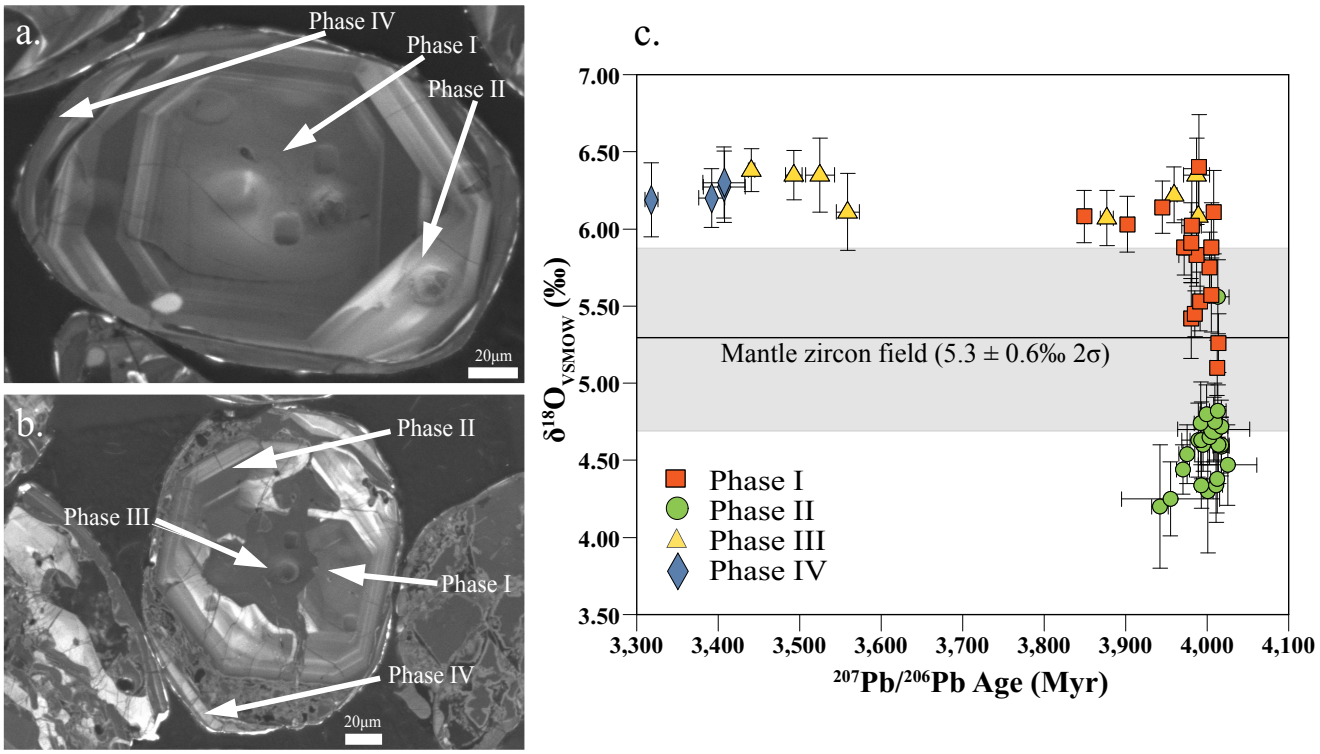

Figure 2.2: Zircon phase relations and correlated zircon U-Pb and oxygen isotopic data from Idiwhaa sample. (A–B) Cathodoluminescence images of representative zircons in Idiwhaa tonalite sample TC-3, which show the zoning characteristics used to distinguish different phases of zircon growth. Phase I growth zones represent unzoned igneous cores. Phase II comprises fine-scale oscillatory-zoned igneous zircon, which commonly conformably overgrows Phase I zircon. Phase III growth dominantly occurs as dark metamorphic incursions grown into all earlier phases. Phase IV growth consists of metamorphic rims overgrowing all phases. (C) Plot of $\delta^{18}O$ values versus $^{207}Pb/^{206}Pb$ for various zircon growth phases. The field for mantle zircon is from Valley et al (1998). Uncertainties on all data points are shown at the 95% confidence level.

2.1B), and elevated concentrations of high-field-strength elements (Fig. 2.7).

Icelandites are thought to result from some combination of low-pressure fractional crystallization of basaltic magma, hybridization of mafic and silicic magma, and assimilation of hydrothermally altered, low-^{18}O crust (Muehlenbachs et al., 1974; Nicholson et al., 1991; Bindeman et al., 2012). The latter process lowers the primary $\delta^{18}O$ values of some icelandite magmas to below pristine mantle values (+5.3 ± 0.3‰; Valley et al., 1998). In this regard, low-^{18}O magmatic rocks are relatively rare worldwide and have most commonly been documented in rift- or plume-related settings (e.g., Iceland, Yellowstone, Hawaii, Skye) in which the shallow-level intrusion of hot, dry magmas have produced high geothermal gradients and in turn driven hydrothermal circulation cells above the magma chambers (Taylor and Sheppard, 1986; Nicholson et al., 1991; Balsley and Gregory, 1998; Bindeman and Valley, 2001).

A number of plausible tectonic scenarios have been suggested for forming sialic crust on the Early Earth. We have documented the need for shallow-level fractionation of basaltic magma and assimilation of hydrothermally altered crust to generate the observed geochemical characteristics of the ~4.02 Ga ITG. On the modern Earth, zones of mantle upwelling such as plumes, rifts or ocean ridges create the necessary conditions for generation of evolved rocks similar to the ITG. Rift- and ridge-related settings, however, produce only a very small proportion of such rocks. In contrast, the combined thermal effects of the mid-Atlantic Ridge and a mantle plume, as well as a high degree of hydrothermal activity, has produced in Iceland a crustal thickness approaching that of typical continental crust (Allen, 2002), as well as a larger proportion of intermediate and felsic composition rocks (~25%) (Jakobsson et al., 2008) than in ocean ridges and other oceanic plateau. The greater thickness and buoyancy of

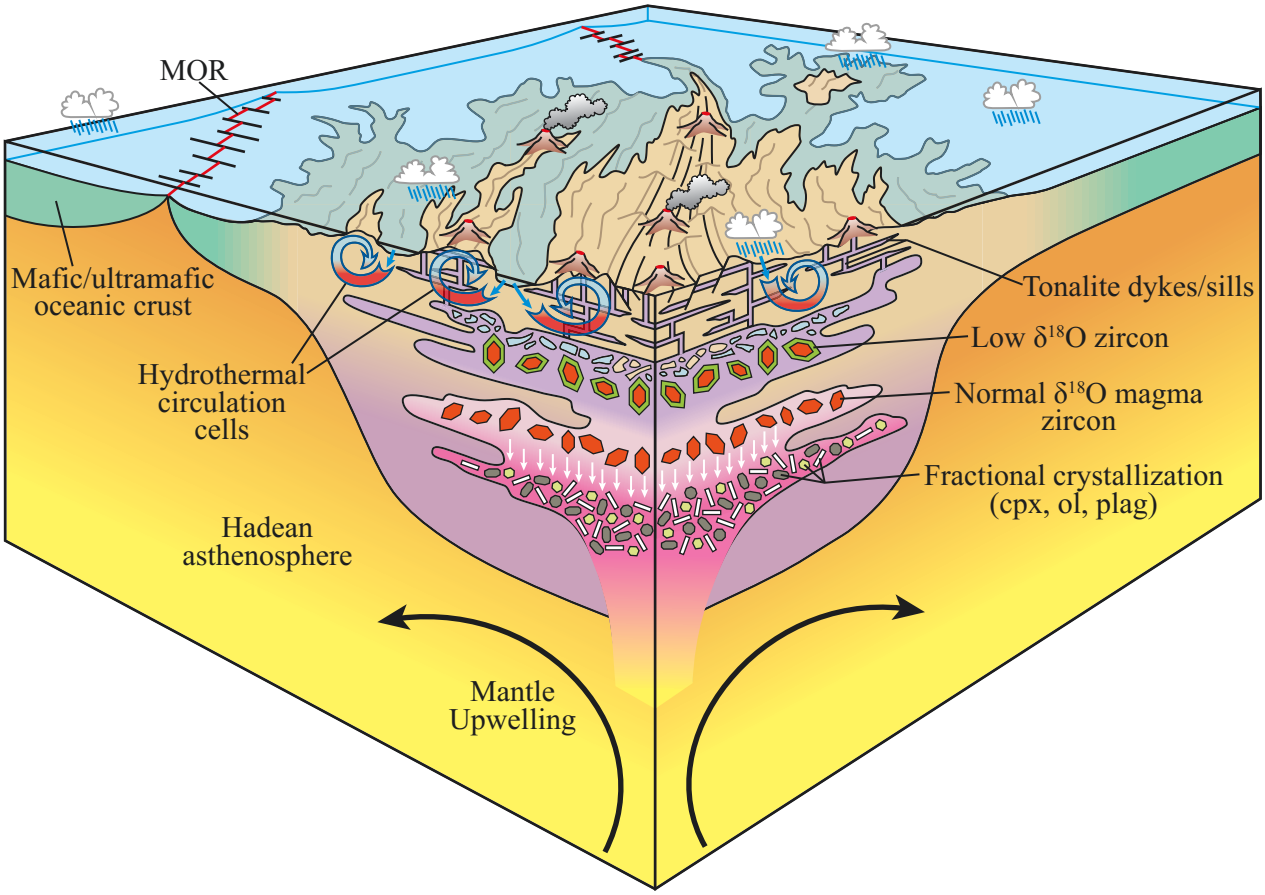

Figure 2.3: Schematic diagram illustrating the major process responsible for formation of the Idiwhaa Tonalitic Gneiss. Basaltic melts are fractionated at shallow crustal levels to produce Fe-enriched intermediate magmas. These magmas initially crystallize zircon with mantle-like $\delta^{18}O$ values. Assimilation of overlying rocks that have been hydrothermally altered by surface waters lowers the $\delta^{18}O$ values of later-stage magmas and in turn produces magmatic zircon rims that have lower than mantle (+5‰) $\delta^{18}O$ values. All of aforementioned processes have been documented in modern-day Iceland, suggesting that Earth's earliest known sialic crust may have formed in an Iceland-like tectonic setting

Icelandic-type crust makes it less likely that it would be recycled back in to the mantle in subduction zones or some other form of mantle down-welling. Therefore, we suggest that a setting similar to modern Iceland, where mantle upwelling creates a thickened plateau with a relatively high proportion of evolved rocks, would be most likely to form and preserve the ITG unit (Fig. 2.3).

Although the formation of Earth's earliest continental crust in an Iceland-like setting has been suggested on theoretical grounds (Kroner, 1985), no direct geological evidence supporting this hypothesis has previously been available (Martin et al., 2008). The data presented here indicate that the oldest known sialic rock unit bears the geochemical fingerprints of shallow-level magmatic and hydrothermal processes involved in the formation of evolved Icelandic rocks. Thus, we propose that such a setting on the early Earth may have generated an analogous proto-continental crust that was sufficiently thick and buoyant to avoid later recycling into the mantle. Notably, owing to Earth's higher heat production at 4 Ga, the confluence of a mantle plume and an ocean ridge, such as is present in modern Iceland, may not have been necessary to generate Iceland-like crust. Rather, any long-lived mantle upwelling in a planet with an operating hydrosphere may have been capable of producing the requisite conditions for formation of this type of crust. Once formed, these small continental nuclei may have served as the substrate for later, deeper-seated TTG magmatism.

Methods

SIMS Analytical Methods

Three epoxy grain mounts (M1070, M1093, M1180) containing zircon from sample TC3 (CCIM sample number S1425) and various reference materials (RM) were prepared for SIMS analysis. Zircon RM for U-Pb calibration were TEM2 (S0022; 416.8 Ma (Black et al., 2004)), 6266 (S0023; $^{206}Pb/^{238}U$ = 559.0 Ma (Stern and Amelin, 2003)), and OG1 (S0030; $^{207}Pb/^{206}Pb$ age = 3465.4 Ma; $^{206}Pb/^{238}U$ = 3441 ± 3 Ma (Stern et al., 2009)) and for oxygen isotopes were TEM2 ($\delta^{18}O_{V\text{-}SMOW}$ = +8.2‰ (Black et al., 2004); $^{18}O/^{16}O_{V\text{-}SMOW}$ = 0.0020052) and our lab zircon UAMT1 (S0081 = $\delta^{18}O_{V\text{-}SMOW}$ = +4.87‰; R. Stern, unpublished data). Weighted mean and age calculations were carried out using Isoplot v. 3.76 (Ludwig, 2001). Uranium decay constants are those of (Jaffey et al., 1971).

M1070 and M1093 contained natural TC3 zircon, whereas M1180 contained TC3 zircon having been subjected to varying levels of annealing and chemical abrasion. The mounts were ground and polished with diamond compounds to expose zircon grain interiors, cleaned with alkaline soap, deionized water, and, in the case of U-Pb analyses, weak HCl. Surfaces were coated with 5 nm of Au for scanning electron microscopy (SEM), followed by an additional 20 nm prior to SIMS analysis. A Zeiss EVO MA15 SEM fitted with a broadband CL detector (ETP Semra, Pty. Ltd., Sydney, Australia) and semiconductor backscattered electron detector was employed for characterizing internal grain zonation. Typical beam conditions were 15 or 20 kV, and 3–5 nA.

Oxygen isotope (^{18}O, ^{16}O) compositions, which were measured prior to U-Pb isotopes, were determined from 156 spots on zircon TC3 in M1070 and M1093 in between March 2011 and March 2012 using the CCIM IMS 1280 ion microprobe. The $^{133}Cs^+$ primary beam conditions included an impact energy of 20 keV, ~15 µm diameter, and 3 nA current. A single analysis lasted 4.5 minutes and entailed rastering the probe for 30–45 s over a 20 × 20 µm area to clean and implant Cs, automated secondary ion tuning, and finally 100 s of isotopic measurements. The normal incidence electron gun was utilized for charge compensation. Negative secondary ions were extracted from the sample mount (–10 kV potential) into the secondary (transfer) column. Transfer conditions included a 120 µm entrance slit, a 5 mm wide rectangular field aperture, and 100× sample image magnification at the field aperture plane. The energy window utilized through 2011 was 50 eV, truncating high-energy ions, but subsequently no energy filtering was applied. The mass-separated oxygen isotopes were detected

simultaneously in dual Faraday cups at the L'2 ($^{16}O^-$) and either H1 or H'2 ($^{18}O^-$) positions in the multi-detector array. Mass resolution (Δm/M at 10% peak height) was typically 1900 and 2250, respectively. Secondary ion count rates for $^{16}O^-$ were ~3 × 10^9 c/s. Faraday cup baselines were measured at the start of the day, and were sufficiently stable and low that no further measurements were necessary. Instrumental mass fractionation was monitored by analysis of TEM2 zircon once after every four unknowns, and data for the RM processed collectively for the analytical session lasting usually several hours. There was either no significant drift in the IMF during a session, or it was smoothly varying, in which case the data for unknowns were time-corrected back to the start of the session. Individual spot uncertainties at 95% confidence are typically ± 0.25‰ (range: 0.14–0.37‰), and include errors relating to within-spot counting statistics, between-spot (geometric) effects, and instrumental mass fractionation. Matrix effects relating to variations in zircon composition and structure (e.g., metamictization) are assumed to be negligible. The analytical results for the zircon RM S0081 run concurrently give an error-weighted mean for $\delta^{18}O$ = +4.87 ± 0.033 (n = 51; MSWD = 1.4; P = 0.039), and with two outliers rejected = +4.87 ± 0.031 (MSWD = 1.12; P = 0.27), identical to the reference value. $\delta^{18}O_{VSMOW}$ was calculated as follows:

$$\delta^{18}O_{VSMOW} = (({}^{18}O / {}^{16}O_{SAMPLE}) / ({}^{18}O / {}^{16}O_{VSMOW}) - 1)$$

where $^{18}O / {}^{16}O_{VSMOW}$ = 0.0020052, and reported in ‰.

SIMS analyses of U-Pb isotopes in TC3 zircon were carried out in six sessions, initially in December 2011, with most analyses occurring in January–February 2013. The methods varied slightly between sessions in experimenting with optimal analytical conditions. The primary beam characteristics included either $^{16}O^-$ (beam current = 4–11 nA) or $^{16}O_2^-$ (0.5–4 nA), impact energy = 23 keV, projected (Kohler) image mode, with probe (longest axis) diameter 10–25 μm. The primary beam was rastered around the analysis site for 2–3 minutes prior to data collection with a stationary primary beam. IMS1280 secondary ion extraction conditions included a sample image magnification of 200× at the field aperture, entrance slit width = 65–75 μm, and field aperture width = 4–6 mm. The energy slit was maintained fully open, except for one session (IP13010) where it was 75 eV and transmitting low energy ions. Positive secondary ions were collected sequentially with the axial electron multiplier and an exit

slit width = 175 μm, giving a mass resolution (1% peak height definition) = 4500–4900.

Ten secondary ion mass positions (typical count times in seconds) were collected over five or six cycles: $^{196}Zr_2O^+$ (2), $^{204}Pb^+$(20), $^{204.05}background^+$(20), $^{206}Pb^+$(10), $^{207}Pb^+$(20), $^{208}Pb^+$(3), $^{238}U^+$(3), $^{248}ThO^+$(3), $^{254}UO^+$(3), and $^{270}UO_2^+$(5). Data were processed using SQUID2 software (Ludwig, 2009), in a custom version designed for processing data output from the IMS 1280. The $^{206}Pb/^{238}U$ ages were calibrated against TEM2 zircon, using a calibration constant ('a') determined from the relationship $^{206}Pb^+/^{270}UO_2^+ = a \times (^{270}UO_2^+/^{254}UO^+)^m$, where the *m* ranged from 0.2 to 0.8 (average 0.5) for TEM2 data. Spot-to-spot excess uncertainties in the $^{206}Pb/^{238}U$ values (not accounted for by within-spot counting uncertainties) determined from analyses of TEM2 ranged from ± 0% to 1.1% (68% confidence), and a minimum of ± 0.5% was propagated to the unknowns (see Stern and Amelin, 2003). Uranium abundances were calibrated against 6266 zircon with U = 903 ppm, utilizing $^{270}UO_2^+/^{196}Zr_2O^+$. The Th/U ratios and Th abundances were determined from $^{248}ThO^+/^{254}UO^+$ using measured $^{232}Th/^{238}U$ discrimination factors for the session (~1.0).

The radiogenic Pb-isotopes were corrected for common Pb using ^{204}Pb, assuming a model crustal composition (Stacey and Kramers, 1975) at the $^{206}Pb/^{238}U$ age of the sample. All count rates were corrected for deadtime = 44 ns. The mean $^{206}Pb/^{238}U$ age determined for 6266 zircon (n = 28) analyzed concurrently is 564 ± 2.9 (MSWD = 5.2), a value that is marginally but statistically higher than the reference age of 559 Ma. The mean $^{206}Pb/^{238}U$ age determined for OG1 zircon (n = 50, minus 3 outliers) is 3436 ± 5 Ma (MSWD =1.05), which is within uncertainty of the reference value of 3441 Ma. The data for the secondary RM's suggest that inaccuracies in the $^{206}Pb/^{238}U$ ages for the unknowns will be < ± 1.0%. The mean $^{207}Pb/^{206}Pb$ age calculated for secondary RM OG1 zircon (n = 50) is 3463.6 ± 1.3 (MSWD = 1.5), and allowing for six rejects (high and low), is 3463.8 ± 1.0 (MSWD = 0.72). These mean values are slightly but statistically lower than the reference value of 3465.4 Ma, suggesting that the $^{207}Pb/^{206}Pb$ ratios for the unknowns are also likely to be biased slightly low. In this study, the $^{207}Pb/^{206}Pb$ ratios were not corrected for this bias, which is probably due to instrumental mass fractionation, with a mean IMF for $^{207}Pb/^{206}Pb$ of –0.97‰ (Stern et al., 2009), equivalent to -1.5 Ma at 4000 Ma.

Zircon trace-element analyses were obtained using the Cameca IMS 4f Ion Microprobe at the Edinburgh Ion Microprobe Facility, University of Edinburgh following the procedures of (Hinton and

Upton, 1991). Uncertainties in the trace-element analyses are dependent on the concentration of the elements measured. Typical uncertainties for elements with concentrations >100 ppm are ≤1% while for elements with concentration between 1–10 ppm uncertainties are ≤10%. La concentrations, which are typically less than 0.1 ppm, may have uncertainties ≥50%.

Whole-Rock Analytical Methods:

Samples were collected during 2010 and 2011 field seasons in the Acasta river area, Northwest Territories, Canada. In order to conduct whole-rock geochemical analyses and zircon mineral separation, between 0.5–2 kg of rock from each sample was pulverized using a shatterbox. Whole-rock major-, minor-, and trace-element geochemistry by XRF (Johnson et al., 1999) and ICP-MS (Knaack et al., 1994) was conducted at the Washington State University's GeoAnalytical Laboratory.

Map:

Figure 2.4 locates the Acasta Gneiss Complex (AGC) on the western margin of the Slave Craton,

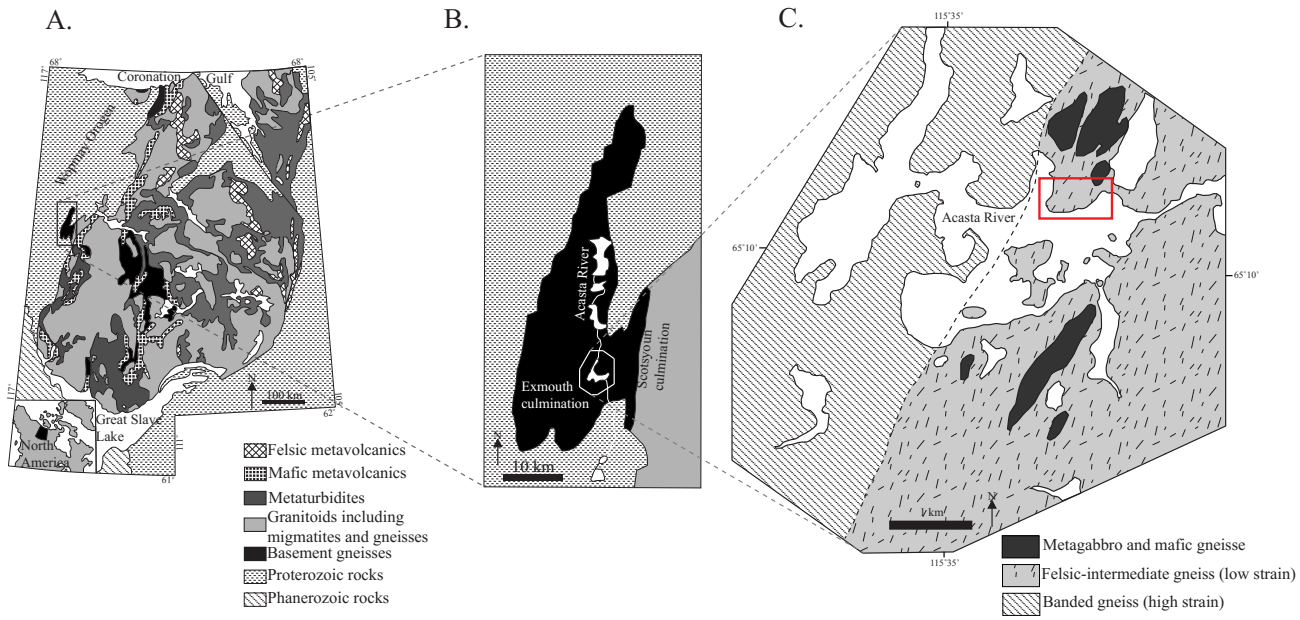

Figure 2.4: Simplified geologic map: (A) The simplified geology of the Slave craton showing location of the Acasta Gneiss Complex on its western margin (B) modified after St. Onge et al. (1988) and Bleeker and Davis (1999) . (C): Simplified lithologic map of the area immediately surrounding the mapped study area, modified after Iizuka et al. (2007). Extent of detailed mapping of the peninsula containing the 4.02 Gyr Idiwhaa Tonalitic Gneiss is shown in red.

Northwest Territories, Canada. Figure 2.5 provides a simplified geologic map of the area surrounding the Idiwhaa Tonalitic Gneiss. The rocks in the mapped area are generally less strained than those in many other parts of the AGC, particularly the highly strained western portion (Bowring and Williams, 1999; Iizuka et al., 2007). We have identified 5 major rock units in this simplified map. The five rocks units (see Fig. 2.6 for field photos) are as follows; 1) the Idiwhaa Tonalitic Gneiss 2) banded biotite

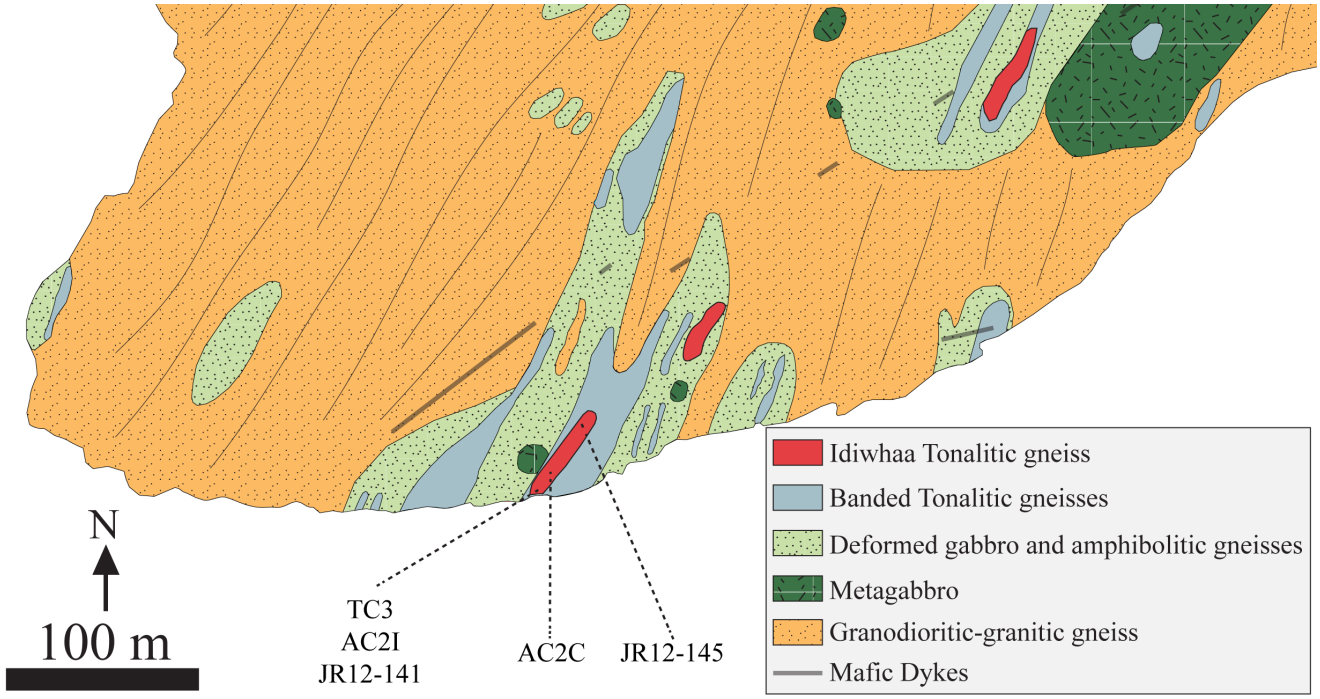

Figure 2.5: Detailed geologic map of the region where the Idiwhaa Tonalitic Gneiss is exposed. Units in the legend are described in the text. Most contacts are inferred. Locations of samples discussed in the study are shown on the map.

tonalitic gneiss interlayered at a decimeter scale, but differentiated from the Idiwhaa Tonalitic Gneiss by lack of combined garnet and amphibole and overall more felsic compositions; 3) a coarse-grained metagabbro dominated by plagioclase and amphibole (after pyroxene) and lacking significant fabric; 4) amphibolite gneisses commonly associated with the banded tonalitic gneisses and cross-cut by leucocratic veinlets; 5) foliated biotite granodiorite and granite that intrude units 1-4. A single mafic dike, likely of Paleoproterozoic age, cross-cuts all the units and is discontinuously traceable across the map area.

The Idiwhaa Tonalitic Gneiss extends for at least 5 x 40 meters (see Table 1.5 for GPS coordinates), trending ~210°, parallel to the local foliation. At the outcrop scale, the unit is variably

intruded by cm-scale white leucocratic veinlets with foliation defined by biotite and amphibole trending roughly parallel to the unit strike. Bounded on both sides by banded biotite tonalitic gneiss, the ITG is a garnet-biotite-hornblende tonalitic gneiss. Modal abundance determinations on one sample (TC3) yielded the following mineral proportions: plagioclase (32%), quartz (23%), hornblende (20%), biotite (19%), Fe-Ti oxides (4%), and garnet (1.4%), along with accessory K-feldspar, apatite, titanite, and zircon.

Supplementary Discussion:

Zircon U-Pb Systematics

Zircons were extracted from one pulverized sample of Idiwhaa Tonalitic Gneiss (sample TC3, CCIM internal sample S1425) by standard magnetic and heavy liquid mineral separation techniques. A subset of these zircons was selected based on clarity and lack of inclusions and subsequently mounted in epoxy resin for later CL imaging and analysis by SIMS.

Zircons from sample TC3 can collectively be subdivided into four distinct morphological or textural phases (see zircon phases I–IV in Fig. 2.2A). These zircon phases are strikingly similar to those described by previous workers from other ca. 4.0 Ga AGC rocks (Bowring and Williams, 1999). Phase I zircon comprises less CL-responsive grain centers of various sizes with generally well-formed crystal boundaries. These are overgrown by Phase II zircon, a chemically distinct CL responsive growth zone characterized by fine-scale oscillatory zoning. Phases I and II are both interpreted to be of magmatic origin (Fig. 2.2A). Phase III zircon consists of dark-CL areas, generally occurring as cross-cutting embayments and irregular incursions into Phase I and II zones (Fig. 2.2B). Phases I–III are overgrown by Phase IV zircon, which consists of thin (5–30 μm wide) overgrowths (Fig. 2.2B) exhibiting no zoning, which we interpret to be of metamorphic origin.

We obtained a total of 160 U-Pb isotope analyses from 68 zircon grains extracted from sample TC3 (Fig. 2.8). The ages of Phase I and II zircon are indistinguishable within analytical uncertainty; both record $^{207}Pb/^{206}Pb$ ages ranging from 4030 to 3840 Ma (Table 1.2; Fig. 2.9) with variable degrees of discordance. Phase I zircon records $^{207}Pb/^{206}Pb$ dates between 3849 and 4041 Ma and discordance between -1.5 and 3%. Phase II zones record a similar span in $^{207}Pb/^{206}Pb$ ages (3844–4033 Ma) but with

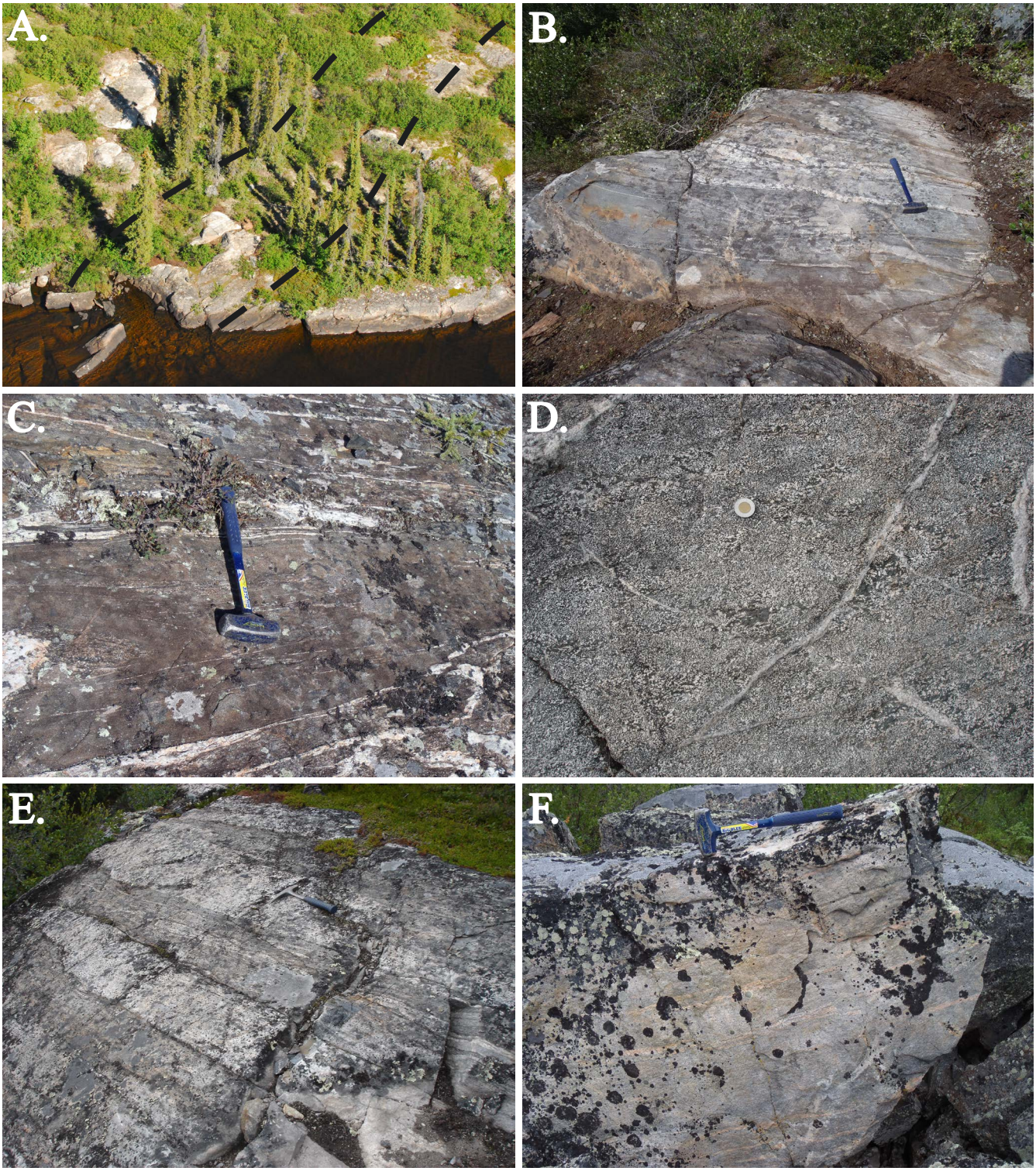

Figure 2.6: Outcrop photos of rock units mapped within the low-strain study area. A: Aerial photo of the portion of the mapped peninsula containing the TC3 sample locality. The boundaries for the Idiwhaa Tonalitic Gneiss are roughly outlined. B: Outcrop photo of the TC3 sample locality. C: Photo of the deformed amphibolitic gneiss. D: Outcrop of coarse-grained metagabbro. E: Example of the banded biotite tonalitic gneiss interlayered at a decimeter scale. F: Outcrop of foliated granitic gneiss

more variable discordance (-1.3% to 6.7%; Fig. 2.8). Approximately half of the Phase II analyses with discordance >1% record $^{207}Pb/^{206}Pb$ ages >4000 Ma, suggesting that recent Pb-loss has occurred within these grains. Both igneous phases of zircon growth show signs of recent and ancient Pb-loss (Fig. 2.10).

It is important to note that nearly all of the analyses (n = 121) of Phase I and II magmatic zircon plot near the upper end of a broad discordia array with an upper intercept exceeding 4.0 Ga (Fig. 2.8). This observation strongly suggests that Phase I and II comprise a single population of magmatic zircon that records the crystallization age of the magmatic protolith of Idiwhaa Tonalitic Gneiss. Analyses from Phase III areas are discordant and generally fall toward the lower end of a discordia array with an upper intercept of >4.0 Ga and lower intercept of ~3.2 Ga. Phase IV overgrowths yielded a wider range of $^{207}Pb/^{206}Pb$ ages between 3.75 and 3.17 Ga and typically have low Th/U (<0.3 in Table 1.2). The most concordant of these data cluster at ~3.2 Ga, which we interpret to represent the approximate time of metamorphic zircon growth. Phase IV analyses with older $^{207}Pb/^{206}Pb$ ages may

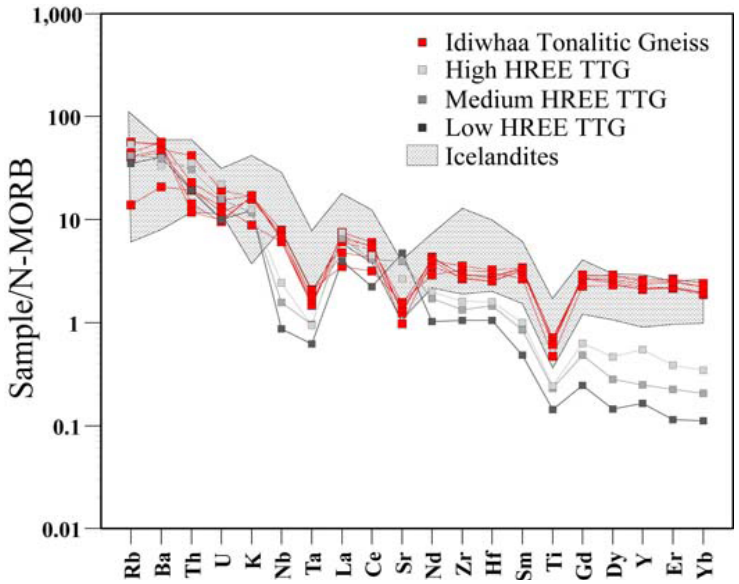

Figure 2.7: Trace-element composition of the Idiwhaa Tonalitic Gneiss. Comparison of trace-element composition of Idiwhaa Tonalitic Gneiss with Icelandite and average Archean TTGs. Data sources same as Fig. 1.1. Note the relative enrichment of the Idiwhaa unit in high-field-strength elements (Hf, Zr, Nb, and Ta) relative to Archean TTG. Samples normalized to 'normal mid-ocean ridge basalt' (Niu, 2003)

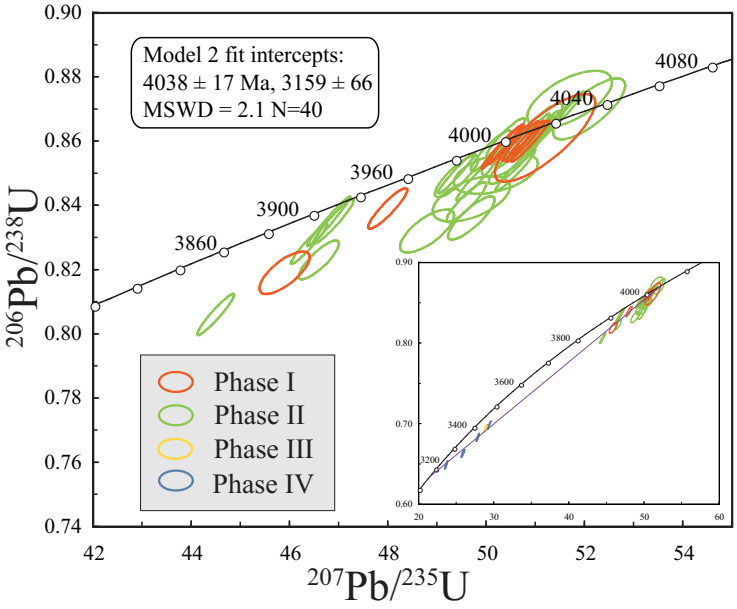

Figure 2.8: Concordia plot of older SIMS U-Pb data obtained from Idiwhaa Tonalitic Gneiss sample TC3. The inset plot shows the full dataset including all zircon growth phases. For clarity, uncertainty ellipses are shown at the 1σ level.

reflect incorporation of some proportion of older zircon phases (I–III) in the analyses due to the small size of the Phase IV overgrowths. Younger, discordant ages from Phase IV areas likely reflect ~3.2 Ga metamorphic zircon that has undergone more recent Pb-loss.

The reason for the spread in $^{207}Pb/^{206}Pb$ ages of Phase I and II zircon between ~4030 and ~3940 Ma is unclear. This age dispersion along concordia has also been documented in previous studies of ancient AGC samples (Bowring et al., 1989; Stern and Bleeker, 1998; Iizuka et al., 2006; 2007) and may reflect Pb-loss during a younger (ca. ~3200 Ma) metamorphic event, or an even earlier (ca. ~3900–3950 Ma) disturbance.

In order to better understand the nature of this shallow 'smearing' of ages along concordia, we performed chemical abrasion (Mattinson, 2005) on aliquots of TC3 zircon, before subsequent analysis by SIMS. Grains were annealed at 1000 °C for up to 48 hours followed by etching with solution of HF and H_2O (50:50) for up to 28 hours. The probability of obtaining >4.0 Ga $^{207}Pb/^{206}Pb$ ages is higher in TC3 zircons that have undergone chemical abrasion. Although some of this increase may be due to removal of domains where Pb-loss was significant, we suggest that the main effect of chemical abrasion was to highlight radiation damaged regions within the zircons so that they could be avoided in SIMS analysis.

Ninety-two analyses of Phase I and II zircon yield $^{207}Pb/^{206}Pb$ dates $\geq$ 3980 Ma. The results of a three-component unmixing treatment (Sambridge and Compston, 1994) of these data indicate a dominant age peak (51% of the analyses) of 4013.3 ± 1.0 Ma. A similar weighted mean $^{207}Pb/^{206}Pb$ date of 4014.6 ± 1.1 Ma (MSWD = 0.96) is obtained based on the 40 oldest zircon analyses. Due to the slight bias in the SIMS $^{207}Pb/^{206}Pb$ ages (see above), these results should be corrected by +1.5 Ma, i.e. 4014.8 ± 1.1 Ma and 4016.1 ± 1.1 Ma, respectively. We interpret these calculations to give a minimum estimate for the crystallization age of the igneous protolith of the ITG.

A regression of 34 Phase I and II zircon analyses of zircon that had been treated by chemical abrasion yields an upper intercept age of 4026 ± 18 Ma (MSWD = 2.2), which is in agreement with the age estimate noted above. Based on the similarity of ages for the oldest zircon analyses calculated in various ways and the large number of concordant or near concordant (≤2% discordant) analyses with $^{207}Pb/^{206}Pb$ ages between 4032 and 4015 Ma (n = 18) within this population, our preferred estimate for the time of igneous zircon crystallization (both Phase I and Phase II growth zones) is 4.02 Ga. We conclude that the

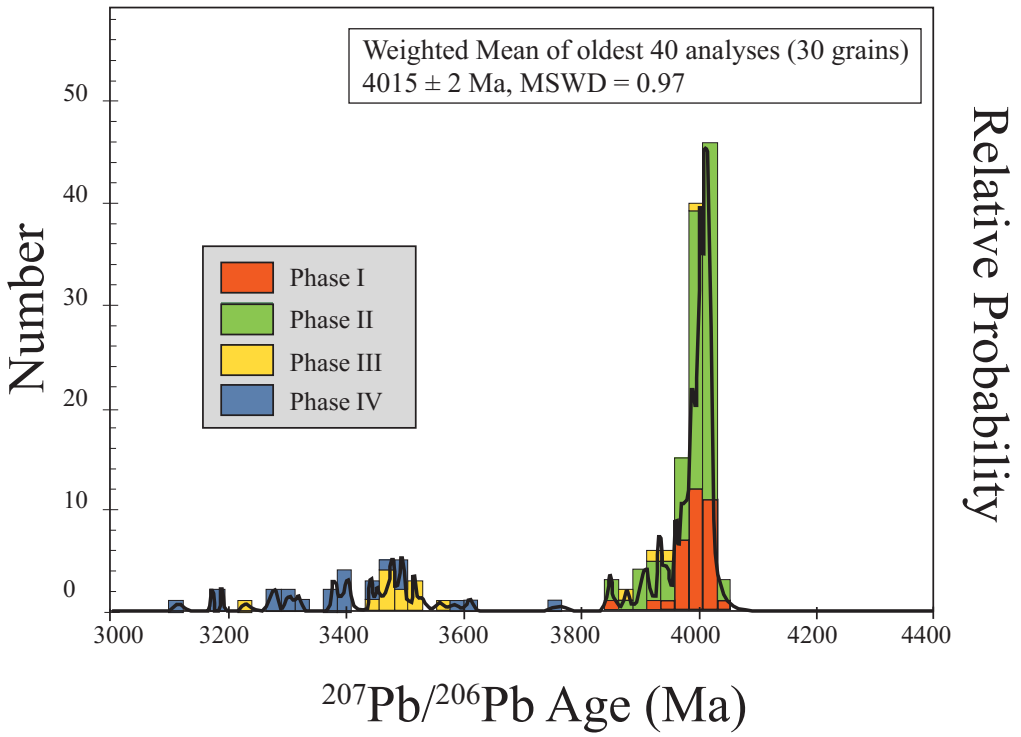

Figure 2.9: Probability density plot of $^{207}Pb/^{206}Pb$ ages from all TC3 zircon SIMS data. Also shown is a histogram of $^{207}Pb/^{206}Pb$ ages, colored according to zircon growth phase. The main peak in relative probability occurs at 4013 Myr and is dominated by Phase I and Phase II zircon, whereas the younger analyses (< 3800 Myr) are exclusively from the two metamorphic domains (Phase III and Phase IV zircon).

Idiwhaa unit represents a single-phase tonalite with a coherent zircon U-Pb dataset. These igneous growth phases were subsequently overprinted by one or more metamorphic recrystallization events, the most recent occurred at ~3.2 Ga.

Zircon Trace-Element Systematics

A suite of trace-elements were analyzed for at the Edinburgh Ion Microprobe Facility (Hinton and Upton, 1991) from each of the four different phases of zircon identified in sample TC3 of the ITG. These data are presented in Table 1.4 along with other data (U-Th-Pb and O-isotope) that correlates to the same spot or growth zone from which the trace-element data were obtained.

REE abundances and patterns vary significantly with zircon growth phase. Phase I and II magmatic zircon domains have broadly similar REE patterns typical of igneous zircons, including highly enriched HREE (relative to LREE) and significant positive Ce and negative Eu anomalies (Fig. 2.11A). Phase III and IV metamorphic zircon display REE patterns much more enriched in the LREE, typical of metamorphic and hydrothermal zircons (Hoskin, 2003).

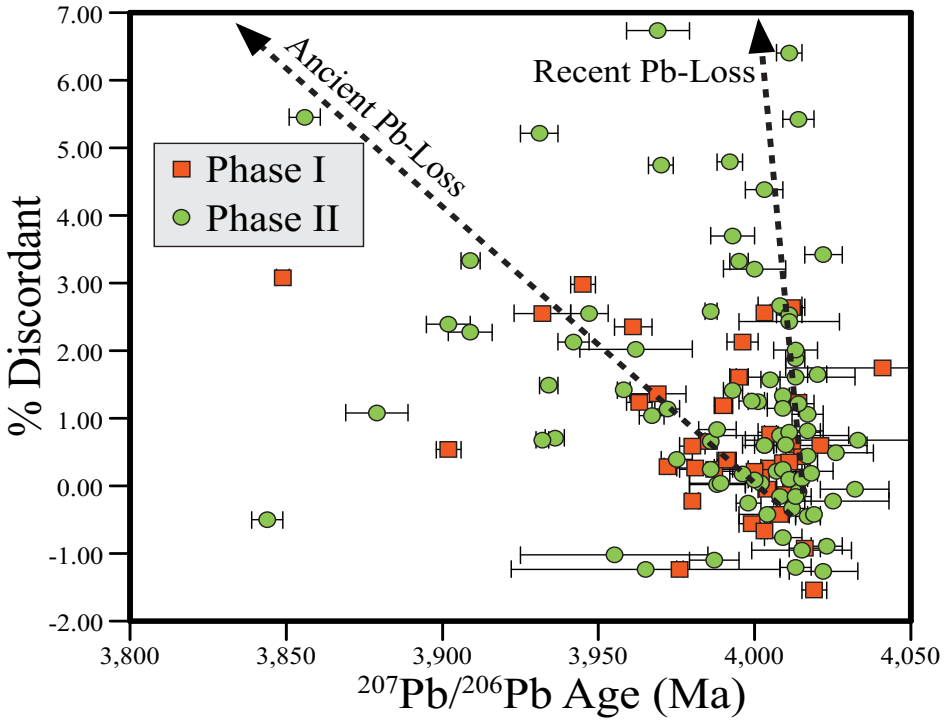

Figure 2.10: $^{207}Pb/^{206}Pb$ age versus discordancy for Phase I and II zircon (sample TC3). Both zircon domains define two contrasting trends: i) decreasing age with increasing discordance, a sign of ancient Pb-loss; and ii) little change in $^{207}Pb/^{206}Pb$ age with increasing discordance, a sign of recent Pb-loss. The majority of all Phase I and II zircon analyses that are ≤ ± 1% discordant record $^{207}Pb/^{206}Pb$ ages > 4000 Myr.

We focus specifically on the REE patterns recorded in Phase I and II igneous zircon. Notably, the REE content of the radiation-damaged parts of igneous zircon can be affected by fluid alteration. Calcium is commonly used as an indicator of the degree of fluid alteration as it tends to be enriched in metamict zones (Geisler et al., 2002). We have therefore filtered out Phase I and II analyses with >4 ppm Ca, as analyses with higher Ca contents have variably enriched LREE contents (Fig. 2.11B). After filtering, the Phase I and II analyses produce a coherent data set for both growth phases of TC3 zircon inferred to be of igneous origin (Fig. 2.11A)

Though the two igneous phases of TC3 zircon have similar shaped REE patterns, they differ in their overall abundance of REEs, except the Ce content. This similarity in Ce content may be viewed as an increase in degree of Ce anomaly. Specifically, Phase II zircon has a larger positive Ce anomaly than Phase I, which, given the greater affinity of zircon for Ce^{4+} relative to Ce^{3+}, requires that Phase II zircon has a higher Ce^{4+}/ Ce^{3+}.

Figure 2.12 shows the relationships between the magnitude of the Ce anomaly (Ce/Ce*), zircon crystallization temperature, and oxygen fugacity as calibrated by (Trail et al., 2011). The temperature of

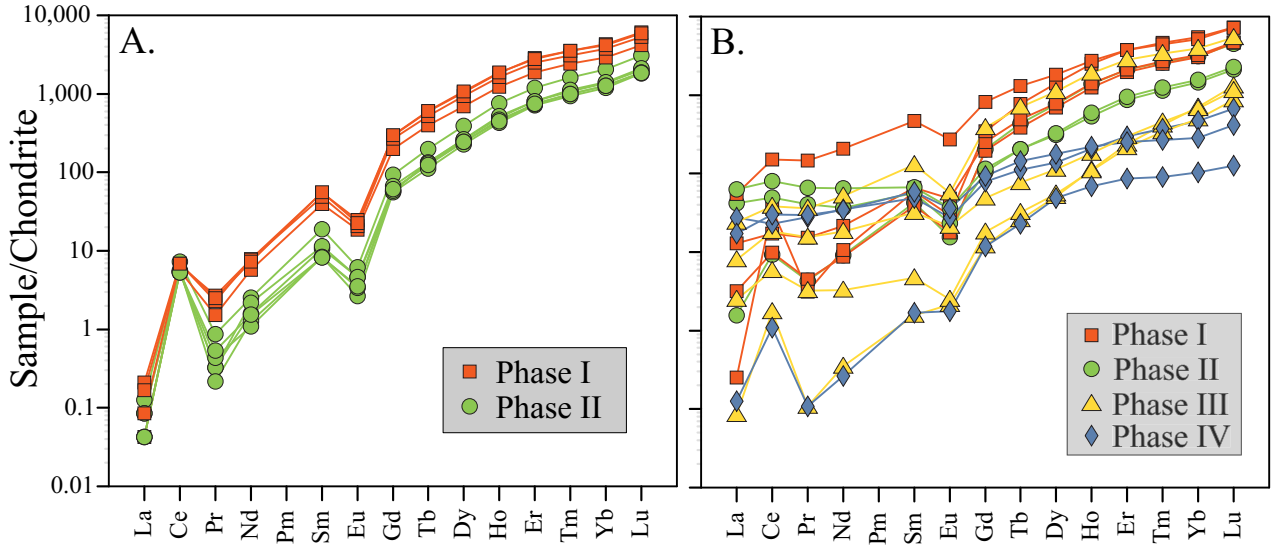

Figure 2.11: REE patterns of TC3 zircon. (A) Chondrite normalized[63] plot showing the REE profiles of igneous zircon phases (Phases I and II) with > 4 ppm Ca analyses removed. We attribute the decrease in total REE from Phase I to II zircon to a decrease in the overall REE content of the magma, potentially due to the crystallization of another REE-bearing accessory phase (e.g., titanite). (B) Chondrite normalized (McDonough and Sun, 1995) REE profiles of analyses with > 4 ppm Ca, which includes analyses of altered Phase I and II zircon and metamorphic growth phases III and IV. Note the flatter REE profiles of altered igneous and metamorphic growth phases compared to those of unaltered igneous growth phases.

zircon crystallization is inferred from Ti-in-zircon geothermometry (Ferry and Watson, 2007) and the oxygen fugacity is referenced to several common oxygen fugacity buffer equilibria. Overall, this plot shows that, at comparable Ti-in-zircon temperatures, Phase II zircon crystallized from a more oxidized magma (i.e., has a larger Ce anomaly) than Phase I zircon. We suggest that this oxidation of the magma occurred due to assimilation of rocks previously altered by surface waters. Even under the reducing atmospheric conditions of the early Earth (i.e., O_2 at ~10^{-13} present atmospheric levels; Kasting, 1993; Catling and Claire, 2005), surface-water alteration would have caused rocks to become more oxidized than their unaltered, mantle-derived precursors.

Validity of Whole-Rock REE Patterns

Although REEs are considered to be relatively immobile during metamorphism, the ability of whole-rocks to preserve primary igneous REE signatures in ancient, poly-metamorphic terranes such as the AGC must be evaluated. An initial check on the robustness of the Idiwhaa whole-rock REE data may be done by comparing the pattern of measured zircon/whole-rock REE ratios with those predicted by

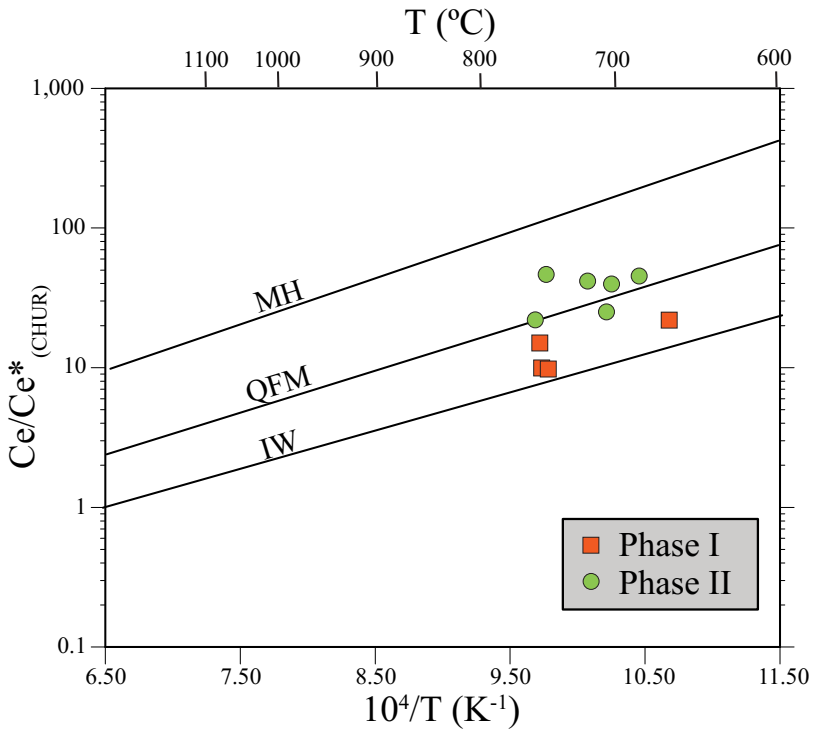

Figure 2.12: Magnitude of Ce anomaly versus 10^4/T (K^{-1}) for Phase I and II zircon (sample TC3). Shown is a plot of Ce anomaly (Ce/Ce*) versus inverse temperature for Phase I and II zircon. The Ce anomaly is calculated as $(Ce/Ce^*)_{CHUR} = (Ce_N)/[(La_N \times Pr_N)^{0.5}]$ where Ce_N, La_N, and Pr_N are the Ce, La, and Pr concentrations normalized to chondrite. Temperatures were calculated by Ti-in-zircon thermometry (Ferry and Watson, 2007), assuming an activity of TiO_2 in the melt of 0.6. As determined by Trail et al. (2011), the plot also shows the magnitudes of Ce anomalies in zircon associated with several common oxygen fugacity buffers (MH = magnetite-hematite; QFM = quartz-fayalite-magnetite; IW = iron-wüstite). Note that at similar Ti-in-zircon temperatures, Phase II zircon is consistently more oxidized (higher Ce/Ce*) than Phase I.

lattice strain theory (Onuma et al., 1968; Blundy and Wood, 1994). In particular, if the REE systematics of the whole-rock have not been disturbed by metamorphism, and if the zircon in question was part of the crystallizing magmatic assemblage, then REE data plotted on a so-called Onuma diagram should be well fit by an equation of the form:

$$D_i = D_o \times \exp\left\{\frac{-4\pi E N_A\left[\frac{r_o}{2}\left(r_i - r_o\right)^2 + \frac{1}{3}\left(r_i - r_o\right)^3\right]}{RT}\right\}$$

where E is the Young's Modulus of the REE-bearing site (in GPa), and D_i is the partition coefficient for an ion of radius r_i (in Å) within a specific structural site. D_0 is then the theoretical partition coefficient for an ion with ideal radius r_0. Finally, N_A is Avagadro's number, R is the gas constant, and T is the temperature in K (Blundy and Wood, 1994). As shown in Figure 2.13, the data for both

Phase I and II zircon show a good parabolic fit to the lattice strain equation as is typical for zircon hosted in the magmatic rock in which it crystallized (Hanchar and van Westrenen, 2007). In contrast, average metamorphic zircon is not well fit by the lattice strain equation (Fig. 2.13). It should be noted that three elements were excluded from the fitting procedure for both the Phase I and II data: Ce and Eu were not included because of their divergence from theoretical partitioning due to variable valence states; La was excluded from all fits because its very low concentration in zircon leads to large relative uncertainties in the measured values in zircon. General conclusions that may be drawn from this analysis are the whole-rock REE systematics of the Idiwhaa unit and Phase I and II zircon REE patterns are broadly in equilibrium, indicating that ITG whole-rock REE compositions have not been greatly modified by post-magmatic processes.

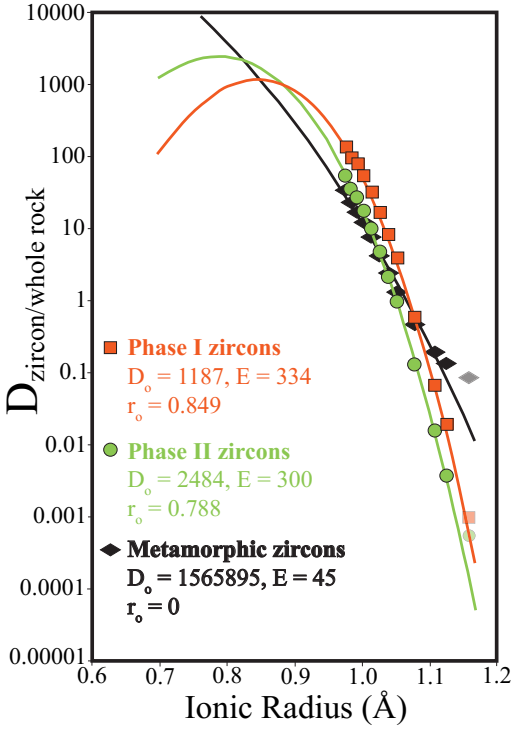

Figure 2.13: Onuma plot of REE partition coefficients. Partition coefficients defined by zircon/whole-rock REE values of the Idiwhaa Tonalitic Gneiss (sample TC3), plotted against ionic radii. Each curve represents a fit to the corresponding data using the lattice strain equation of Onuma et al. (1968). Eu and Ce (not shown) as well as La (lightly shaded symbols) were excluded from each fit. For each curve, the parameters of the equation used are presented, including the ideal cationic radius (r_0), the theoretical partition coefficient for an ideal cation (D_0), and the Young's Modulus (E). The Phase I and II zircon data both yield plausible solutions to the fit function, whereas average Phase III and IV zircon of metamorphic origin yields a geologically unreasonable solution.

A second test of the robustness of the REE systematics within the ITG is to compare the measured whole-rock REE pattern for tonalite sample TC3 with a theoretical REE pattern calculated to be in equilibrium with Phase I and II zircon. We undertook two different sets calculations: first, we employed the widely used zircon/ground-mass partition coefficients of (Sano et al., 2002) derived from a felsic volcanic rock (~73 wt.% SiO_2); and secondly, we used zircon/whole-rock partition coefficients deduced from diorite (BP39) and mafic granodiorite (BP7) samples from the well characterized Boggy Plain pluton of Australia (Hoskin et al., 2000a;b), which contain ~52 and 61 wt.% SiO_2, respectively. Melt composition can have a significant

affect on mineral/melt or whole-rock partition coefficients and thus the partition coefficients deduced from the Boggy Plain samples may be more appropriate than the partition (Sano et al., 2002) coefficients for Idiwhaa tonalite sample TC3 investigated in the present study, which contains ~58 wt.% SiO_2.

Though the whole-rock REE abundances deduced from Phase II zircon are distinctly lower than measured whole-rock abundances, both sets of calculated REE patterns provide a reasonably good match to the overall shape of the measured pattern (Fig. 2.14). Specifically, both calculated and measured patterns show a negative Eu anomaly and relatively little LREE to HREE fractionation when the patterns are calculated using the Boggy Plain partition coefficients. Importantly, none of the calculated patterns resemble the steep REE patterns of later Archean TTGs (Martin, 1986; Moyen, 2011; Moyen and Martin, 2012).

The difference in whole-rock REE contents calculated from Phase I and II zircon requires some evaluation (Fig. 2.14). One possible explanation for this difference is that the crystallization of another REE-rich accessory mineral occurred after the crystallization of Phase I zircon but before the crystallization of Phase II. In particular, the crystallization of titanite, which has an overall affinity for

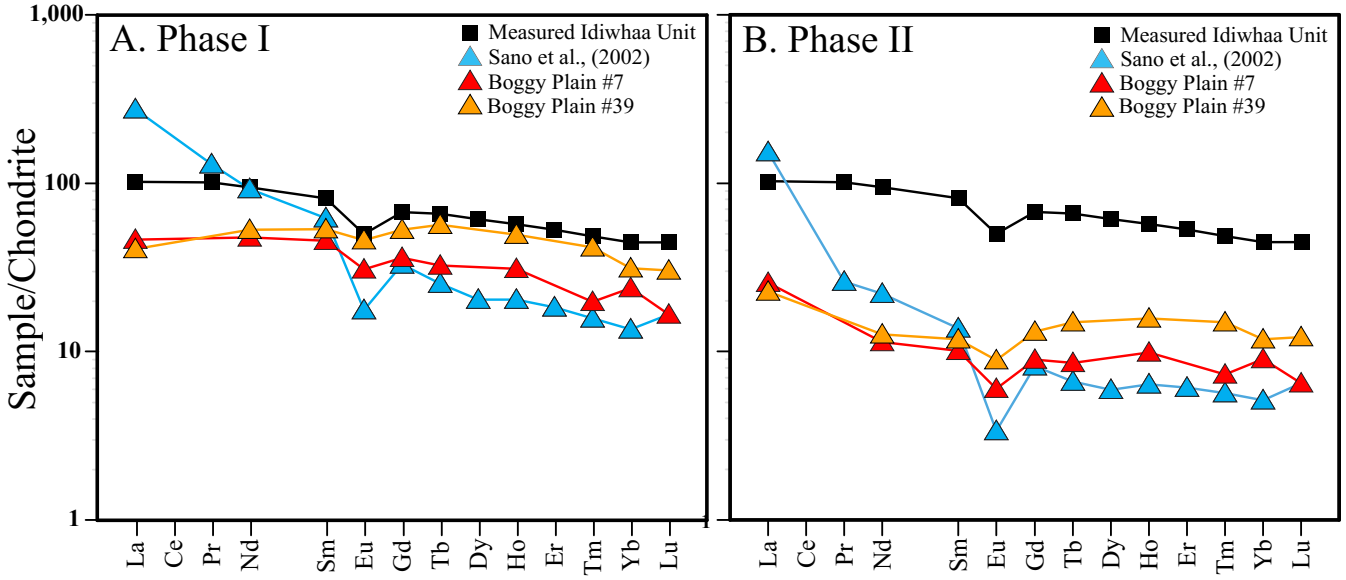

Figure 2.14: REE diagrams showing 'measured' versus 'calculated' whole-rock compositions of the Idiwhaa Tonalitic Gneiss unit (sample TC3). Calculation of REE patterns was carried out assuming the whole-rock was in equilibrium with average Phase I (A) and II (B) zircon. Zircon-whole-rock partition coefficient data used in the calculations are from Sano et al. (2002) for a dacite composition and Hoskin et al. (2000a;b) for a diorite (BP39) and a granodiorite (BP7) composition. Note that the calculated whole-rock REE patterns for Phase I zircon share many of the features of the measured whole-rock pattern for sample TC3 including relatively low La/Yb, a negative Eu anomaly, and a lack of strong HREE depletion. This suggests that the measured whole-rock patterns of the Idiwhaa Tonalitic Gneiss generally reflect those of its igneous precursor.

REE but does not strongly fractionate LREE from HREE (Prowatke and Klemme, 2005), could cause an overall decrease in melt REE content without greatly affecting the overall shape of the melt REE pattern. It then follows that late-crystallizing Phase II zircon would inherit these lower REE contents, yet still exhibit the same basic REE profile as Phase I zircon. Our proposed model of magma evolution through combined assimilation-fractional crystallization (AFC) processes is consistent with such a scenario.

On the basis of these zircon trace-element analyses, we conclude that the measured whole-rock REE composition of this ancient Acasta gneiss sample provides a good approximation of the REE composition of the igneous protolith of the sample. Thus, petrogenetic inferences drawn from these whole-rock REE data should provide robust constraints on the origin and formation of the earliest known continental crust on Earth.

Zircon Oxygen-Isotope Systematics

Because of the slow diffusion rates of oxygen in zircon, this mineral has the capacity to retain a record of primary, igneous oxygen isotopic signatures, even through high-grade metamorphic events. This fact is evidenced by the preservation of sharp oxygen isotope gradients between igneous cores and metamorphic overgrowths in zircon grains that have undergone granulite-facies metamorphism (Peck and Valley, 2003). This same feature is seen in the zircons of Idiwhaa tonalite sample TC3, where the $\delta^{18}O$ values of metamorphic zircon growth Phases III and IV are markedly different than those of immediately adjacent Phase II igneous zircon. From this we conclude that zircon Phases I and II retain their original magmatic oxygen isotope compositions, which may therefore be used to make inferences about the igneous history of the Idiwhaa unit.

We analyzed oxygen isotopes from a total of 156 spots from 78 zircon grains extracted from ITG sample TC3. A subset of these grains was also analyzed for their U-Pb isotopic and trace-element compositions. The entire zircon oxygen isotope data set for Idiwhaa sample TC3 is summarized in Figure 2.15 and Table 1.3.

The main finding of this oxygen isotope study is a ~0.8‰ decrease in $\delta^{18}O$ values between Phase I and II zircon growth zones. We argued previously that this decrease must be linked to changes in the oxygen isotope composition of the magma throughout zircon crystallization, which in turn, most likely

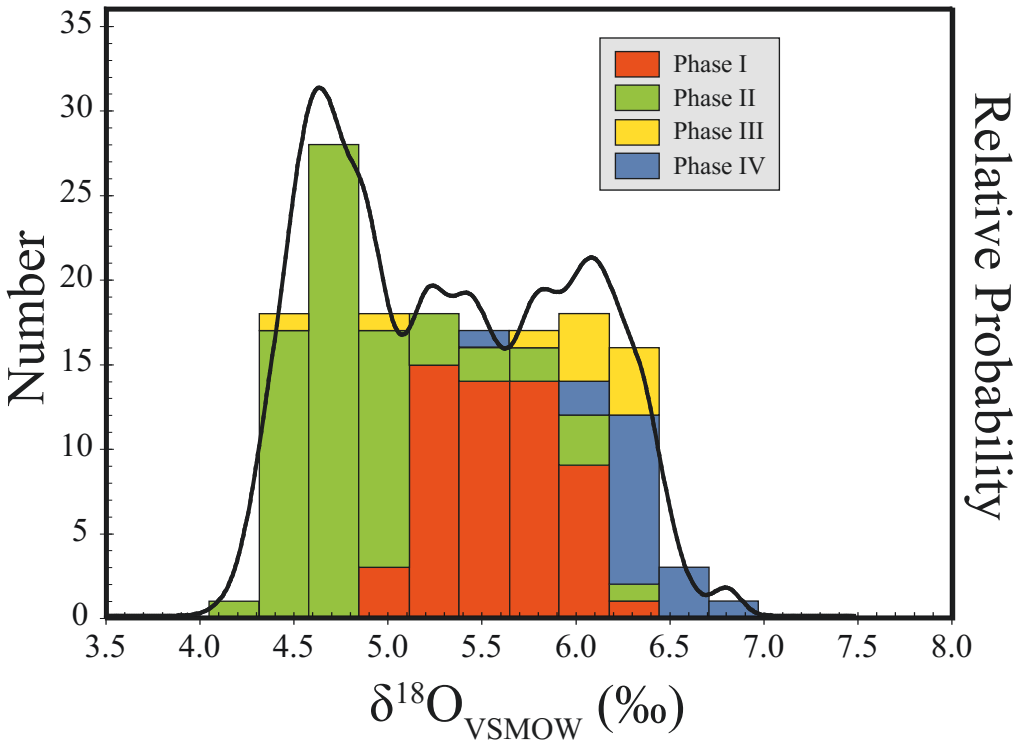

Figure 2.15: Probability density plot of zircon oxygen isotopic analyses. Plot includes all 155 oxygen isotopic analyses from ITG unit zircons (sample TC3) excluding one analysis of highly altered zircon material which is reported in Table 2.3. Histogram colors correspond to zircon growth phases. Note that this plot contains all the measured oxygen isotope compositions, whereas Fig. 2.1C only shows the data for analytical spots for which both oxygen and U-Pb isotopic compositions were determined.

resulted from assimilation of surface-water altered, low-$\delta^{18}O$ crustal material. Other potential explanations for the observed shift in $\delta^{18}O$ values from one igneous zircon growth domain to the next cannot adequately explain the direction or magnitude of the observed shift.

For example, several workers have noted that differences in the Hf content of zircons can have a small but detectable effect on the instrumental mass fractionation factor (IMF) used to correct oxygen isotope ratios measured by SIMS (Peck and Valley, 2003). Thus, in principle, the apparent differences in the $\delta^{18}O$ values of Phase I and II zircon could be an artifact of differences in their Hf contents. In this case, however, the Hf contents of Phase I and II zircon are nearly identical (~0.85 wt.% Hf) and thus cannot be the cause of the observed differences in their $\delta^{18}O$ values. Another explanation may be closed-system fractional crystallization, which can also cause a shift in magmatic $\delta^{18}O$ values, however, in this case the effect is usually small, and when it occurs, generally results in a small increase in $\delta^{18}O$ values of the residual magma (Eiler, 2001), rather than a decrease.

Additionally, it has been shown that radiation-damaged zircon material will preferentially react with fluids and could exchange enough oxygen to alter the measured oxygen isotopic ratios. Phase

II zircon material is slightly more discordant than Phase I material (see the zircon U-Pb discussion above), potentially suggesting that these areas may be more likely to have non-magmatic oxygen isotope ratios. However, Figure 2.16 indicates that Phase I material has higher concentrations of U+Th, indicating these areas would be more likely to accumulate radiation damage than Phase I. This corroborates with the textual evidence in which Phase I zircon is preferentially recrystallized by later metamorphic events. This may explain the higher scatter in the Phase I oxygen isotopic dataset (Fig. 2.2C). Additionally, though Phase II zircon is more discordant, the measured $\delta^{18}O$ values are consistent and not correlated with discordancy, indicating that no resetting of Phase II zircon oxygen isotopic ratios has occurred. We therefore conclude that the documented decrease in $\delta^{18}O$ values between Phase I and Phase II zircon growth in the ITG reflects assimilation of low $\delta^{18}O$ crustal material by the Idiwhaa magma.

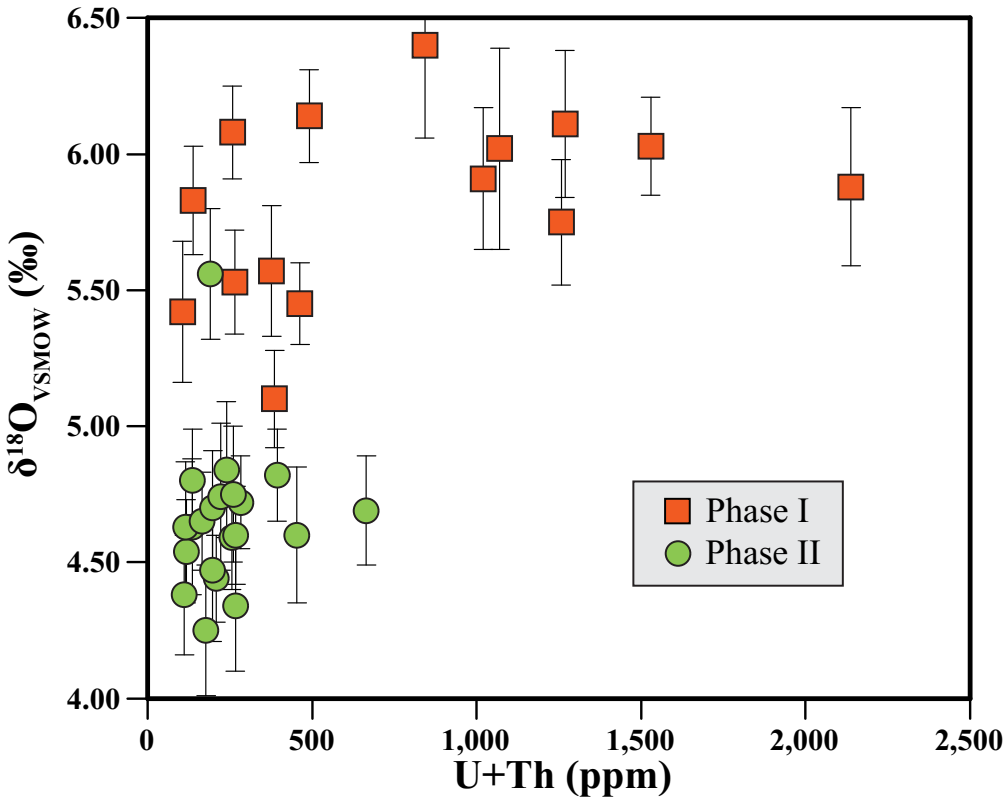

Figure 2.16: $\delta^{18}O$ versus U+Th contents in Phase I and II zircons. Overall, Phase I zircon contains significantly more U and Th than Phase II zircons. It follows that Phase I zircon would accumulate radiation damage more quickly than Phase II so that at the time of zircon recrystallization, ~3.2 Ga, Phase I cores were be more susceptible to overprinting. This is confirmed in the SEM and CL images of many Phase I zircons, and is highlighted in Fig. 2.2B. This later recrystallization may preferentially overprint the O-isotope ratio of some Phase I zircons. We suggest that some Phase I igneous cores may have been overprinted by later metamorphic fluids, causing their $\delta^{18}O$ values to be elevated above 6‰.

Intra-grain variations in $\delta^{18}O$ values of igneous zircons have been documented in a number of Phanerozoic volcanic centers (Bindeman and Valley, 2000; Bindeman, 2008; Bindeman et al., 2012).

These variations, along with phenocryst-melt disequilibrium from places such as Yellowstone, Iceland, and Kamchatka, are attributed to long phenocryst residence times in pre-eruptive magma chambers with varying oxygen isotopic compositions. Bindeman *et al.* (2012) documented Icelandic zircons with heterogeneous $\delta^{18}O$ characterized by mantle-like $\delta^{18}O$ values in cores overgrown by igneous rims with values down to +1.5‰. These variations were attributed to assimilation or partial melting of low $\delta^{18}O$ crustal material, whereas zircon material with mantle-like $\delta^{18}O$ simply did not re-equilibrate with changing magma oxygen isotope composition. Bindeman *et al.* (2000) attributed a core to rim decrease in $\delta^{18}O$ values of several per mil to a model of 'crustal cannibalism', whereby a magma chamber's heat flux into overlying rocks hydrothermally alters these rocks followed by caldera collapse and assimilation of low $\delta^{18}O$ material. Due to the similarity of U-Pb ages between the two igneous phases of zircon growth documented here for the ITG, we also interpret the corresponding shift in oxygen isotope values to reflect a significant (~0.8‰) change in magma oxygen isotopic composition during zircon crystallization, ultimately caused by a similar process of 'crustal cannibalism' at ~4.02 Ga. Interestingly, (Hiess et al., 2011) also invoked 'crustal cannibalism' to explain low $\delta^{18}O$ zircons from an early Archean gneiss terrane in West Greenland.

References:

Allen, R.M., 2002. Plume-driven plumbing and crustal formation in Iceland. Journal of Geophysical Research 107, 2163.

Balsley, S.D., Gregory, R.T., 1998. Low-18O silicic magmas: why are they so rare? Earth and Planetary Science Letters 162, 123–136.

Barker, F., Arth, J.G., 1976. Generation of trondhjemitic-tonalitic liquids and Archean bimodal trondhjemite-basalt suites. Geology 4, 596–600.

Bindeman, I., 2008. Oxygen isotopes in mantle and crustal magmas as revealed by single crystal analysis. Reviews in Mineralogy and Geochemistry 69, 445-478.

Bindeman, I.N., Valley, J.W., 2000. Formation of low-δ18O rhyolites after caldera collapse at Yellowstone, Wyoming, USA. Geology 28, 719–722.

Bindeman, I.N., Valley, J.W., 2001. Low-δ18O Rhyolites from Yellowstone: Magmatic Evolution Based on Analyses of Zircons and Individual Phenocrysts. Journal of Petrology 42, 1491–1517.

Bindeman, I., Gurenko, A., Carley, T., Miller, C., Martin, E., Sigmarsson, O., 2012. Silicic magma petrogenesis in Iceland by remelting of hydrothermally altered crust based on oxygen isotope diversity and disequilibria between zircon and magma with implications for MORB. Terra Nova 24, 227–232.

Black, L.P., Kamo, S.L., Allen, C.M., Davis, D.W., Aleinikoff, J.N., Valley, J.W., Mundil, R., Campbell, I.H., Korsch, R.J., Williams, I.S., Foudoulis, C., 2004. Improved 206Pb/238U microprobe geochronology by the monitoring of a trace-element-related matrix effect; SHRIMP, ID–TIMS, ELA–ICP–MS and oxygen isotope documentation for a series of zircon standards. Chemical Geology 205, 115–140.

Blundy, J., Wood, B., 1994. Prediction of crystalðmelt partition coefficients from elastic moduli. Nature 372, 452–454.

Bowring, S.A., Williams, I.S., 1999. Priscoan (4.00–4.03 Ga) orthogneisses from northwestern Canada. Contributions to Mineralogy and Petrology 134, 3–16.

Bowring, S.A., Williams, I.S., Compston, W., 1989. 3.96 Ga gneisses from the Slave province, Northwest Territories, Canada. Geology 17, 971–975.

Carmichael, I.S.E., 1964. The petrology of Thingmuli, a Tertiary volcano in eastern Iceland. Journal of

Petrology 5, 435–460.

Catling, D.C., Claire, M.W., 2005. How Earth's atmosphere evolved to an oxic state: A status report. Earth and Planetary Science Letters 237, 1–20.

Condie, K., 2007. Chapter 1.2 The Distribution of Paleoarchean Crust, in: Developments in Precambrian Geology. Elsevier, pp. 9–18.

Eiler, J.M., 2001. Oxygen isotope variations of basaltic lavas and upper mantle rocks. Reviews in Mineralogy and Geochemistry 43, 319–364.

Ferry, J.M., Watson, E.B., 2007. New thermodynamic models and revised calibrations for the Ti-in-zircon and Zr-in-rutile thermometers. Contributions to Mineralogy and Petrology 154, 429-437.

Geisler, T., Pidgeon, R.T., Van Bronswijk, W., Kurtz, R., 2002. Transport of uranium, thorium, and lead in metamict zircon under low-temperature hydrothermal conditions. Chemical Geology 191, 141–154.

Grove, T.L., Kinzler, R.J., 1986. Petrogenesis of andesites. Annual Review of Earth and Planetary Sciences 14, 417.

Hanchar, J.M., van Westrenen, W., 2007. Rare Earth Element Behavior in Zircon-Melt Systems. Elements.

Harrison, T.M., 2009. The hadean crust: Evidence from >4 ga zircons. Annual Review of Earth and Planetary Sciences 37, 479–505.

Harrison, T.M., Schmitt, A.K., McCulloch, M.T., Lovera, O.M., 2008. Early (≥ 4.5 Ga) formation of terrestrial crust: Lu-Hf, δ18O, and Ti thermometry results for Hadean zircons. Earth and Planetary Science Letters 268, 476–486.

Hiess, J., Bennett, V.C., Nutman, A.P., Williams, I.S., 2011. Archaean fluid-assisted crustal cannibalism recorded by low δ18O and negative εHf(T) isotopic signatures of West Greenland granite zircon. Contributions to Mineralogy and Petrology 161, 1027–1050.

Hinton, R.W., Upton, B.G.J., 1991. The chemistry of zircon: Variations within and between large crystals from syenite and alkali basalt xenoliths. Geochimica et Cosmochimica Acta 55, 3287–3302.

Hoskin, P.W.O., 2000. Patterns of chaos: fractal statistics and the oscillatory chemistry of zircon. Geochimica et Cosmochimica Acta 64, 1905–1923.

Hoskin, P.W.O., 2003. The Composition of Zircon and Igneous and Metamorphic Petrogenesis. Reviews

in Mineralogy and Geochemistry 53, 27–62.

Hoskin, P.W.O., Kinny, P.D., Wyborn, D., Chappell, B.W., 2000. Identifying Accessory Mineral Saturation during Differentiation in Granitoid Magmas: an Integrated Approach. Journal of Petrology 1–32.

Iizuka, T., Horie, K., Komiya, T., Maruyama, S., Hirata, T., Hidaka, H., Windley, B.F., 2006. 4.2 Ga zircon xenocryst in an Acasta gneiss from northwestern Canada: Evidence for early continental crust. Geology 34, 245–248.

Iizuka, T., Komiya, T., Ueno, Y., Katayama, I., Uehara, Y., Maruyama, S., Hirata, T., Johnson, S.P., Dunkley, D.J., 2007. Geology and zircon geochronology of the Acasta Gneiss Complex, northwestern Canada: New constraints on its tectonothermal history. Precambrian Res 153, 179–208.

Jaffey, A.H., Flynn, K.F., Glendenin, L.E., Bentley, W.C., Essling, A.M., 1971. Precision measurement of half-lives and specific activities of U235 and U238. Physical Review C 4, 1889–1906.

Jakobsson, S., Jonasson, K., Sigurdsson, I., 2008. The three igneous rock series of Iceland. Jokull 58, 1–22.

Johnson, D.M., Hooper, P.R., Conrey, R.M., 1999. XRF analysis of rocks and minerals for major and trace elements on a single low dilution Li-tetraborate fused bead. Advances in X-ray Analysis 41, 843–867.

Kasting, J., 1993. Earth's early atmosphere. Science 259, 920–926.

Knaack, C., Cornelius, S., Hooper, P.R., 1994. Trace element analyses of rocks and minerals by ICP-MS. Open File Report. Department of Geology.

Kroner, A., 1985. Evolution of the Archean Continental Crust. Annual Review of Earth and Planetary Sciences 13, 49–74.

Ludwig, K.R., 2001. Isoplot 3.75: A Geochronological Toolkit for Microsoft Excel. BGC Special Publications 5.

Ludwig, K.R., 2009. SQUID2: A User's Manual. Berkeley Geochronology Center Special Publication 110.

Martin, H., 1986. Effect of steeper Archean geothermal gradient on geochemistry of subduction-zone magmas. Geology 14, 753–756.

Martin, E., Martin, H., Sigmarsson, O., 2008. Could Iceland be a modern analogue for the Earth's early

continental crust? Terra Nova 20, 463–468.

Mattinson, J.M., 2005. Zircon U–Pb chemical abrasion ("CA-TIMS") method: Combined annealing and multi-step partial dissolution analysis for improved precision and accuracy of zircon ages. Chemical Geology 220, 47–66.

Moyen, J.-F., 2011. The composite Archaean grey gneisses: Petrological significance, and evidence for a non-unique tectonic setting for Archaean crustal growth. Lithos 123, 21–36.

Moyen, J.-F., Martin, H., 2012. Forty years of TTG research. Lithos 148, 312–336.

Muehlenbachs, K., Anderson, A.T., Sigvaldason, G.E., 1974. Low-O18 basalts from Iceland. Geochimica et Cosmochimica Acta 38, 577–588. doi:10.1016/0016-7037(74)90042-8

Nair, R., Chacko, T., 2008. Role of oceanic plateaus in the initiation of subduction and origin of continental crust. Geology 36, 583–586. doi:10.1130/G24773A.1

Nicholson, H., Condomines, M., Fitton, J.G., Fallick, A.E., Gronveld, K., Rogers, G., 1991. Geochemical and Isotopic Evidence for Crustal Assimilation Beneath Krafla, Iceland. Journal of Petrology 32, 1005–1020.

Onuma, N., Higuchi, H., Wakita, H., Nagasawa, H., 1968. Trace element partition between two pyroxenes and the host lava. Earth and Planetary Science Letters 5, 47–51.

Page, F.Z., Ushikubo, T., Kita, N.T., Riciputi, L.R., Valley, J.W., 2007. High-precision oxygen isotope analysis of picogram samples reveals 2 m gradients and slow diffusion in zircon. American Mineralogist 92, 1772–1775.

Peck, W., Valley, J., 2003. Slow oxygen diffusion rates in igneous zircons from metamorphic rocks. American Mineralogist 88, 1003-1014.

Prowatke, S., Klemme, S., 2005. Effect of melt composition on the partitioning of trace elements between titanite and silicate melt. Geochimica et Cosmochimica Acta 69, 695–709.

Rapp, R.P., Rapp, R., Watson, E.B., Miller, C.F., 1991. Partial melting of amphibolite/eclogite and the origin of Archean trondhjemites and tonalites. Precambrian Res 51, 1–25.

Sambridge, M.S., Compston, W., 1994. Mixture modeling of multi-component data sets with application to ion-probe zircon ages. Earth and Planetary Science Letters 128, 373–390.

Sano, Y., Terada, K., Fukuoka, T., 2002. High mass resolution ion microprobe analysis of rare earth elements in silicate glass, apatite and zircon: lack of matrix dependency. Chemical Geology 184,

Smithies, R.H., Champion, D.C., Van Kranendonk, M.J., 2009. Formation of Paleoarchean continental crust through infracrustal melting of enriched basalt. Earth and Planetary Science Letters 281, 298–306.

Stacey, J.S., Kramers, J.D., 1975. Approximation of terrestrial lead isotope evolution by a two-stage model. Earth and Planetary Science Letters 26, 207–221.

Stern, R.A., Amelin, Y., 2003. Assessment of errors in SIMS zircon U–Pb geochronology using a natural zircon standard and NIST SRM 610 glass. Chemical Geology 197, 111–142.

Stern, R., Bleeker, W., 1998. Age of the world“s oldest rocks refined using Canada”s SHRIMP: The Acasta Gneiss Complex, Northwest Territories, Canada. Geoscience Canada 25, 27–31.

Stern, R.A., Bodorkos, S., Kamo, S.L., Hickman, A.H., Corfu, F., 2009. Measurement of SIMS Instrumental Mass Fractionation of Pb Isotopes During Zircon Dating. Geostandards and Geoanalytical Research 33, 145–168.

Taylor, H.P., Sheppard, S.M.F., 1986. Igneous rocks; I Processes of isotopic fractionation and isotope systematics. Reviews in Mineralogy and Geochemistry 16, 227–271.

Trail, D., Watson, E.B., Tailby, N.D., 2011. The oxidation state of Hadean magmas and implications for early Earth’s atmosphere. Nature 480, 79–82.

Valley, J.W., Kinny, P.D., Schulze, D.J., Spicuzza, M.J., 1998. Zircon megacrysts from kimberlite: oxygen isotope variability among mantle melts. Contributions to Mineralogy and Petrology 133, 1–11.

Zegers, T.E., van Keken, P.E., 2001. Middle Archean continent formation by crustal delamination. Geology 29, 1083–1086.

Table 2.1. Whole-rock compositions of the Idiwhaa Tonalitic Gneiss

Sample Name	TC3-A*	TC3-B*	AC2I	AC2C	JR12-141	JR12-145	Idiwhaa Average	1SD
SiO_2 (wt.%)	58.78	57.94	66.89	61.95	60.13	60.73	61.07	3.19
TiO_2	1.22	1.24	0.82	1.08	1.12	1.06	1.09	0.15
Al_2O_3	13.84	13.88	13.87	14.02	14.13	13.82	13.93	0.12
$FeO_{(total)}$	14.51	15.25	8.57	11.71	12.53	13.13	12.62	2.36
MnO	0.17	0.17	0.12	0.16	0.16	0.18	0.16	0.02
MgO	1.26	1.26	0.95	1.48	1.43	1.20	1.26	0.19
CaO	4.54	4.61	2.84	4.70	4.93	4.27	4.31	0.75
Na_2O	2.99	2.98	3.39	3.35	3.06	2.92	3.12	0.20
K_2O	2.36	2.35	2.34	1.24	2.21	2.39	2.15	0.45
P_2O_5	0.34	0.33	0.19	0.31	0.30	0.29	0.29	0.05
Sum	100.00	100.00	100.00	100.00	100.00	100.00	100.00	
LOI	0.93	0.33	0.13	1.07	0.67	0.55	0.61	0.36
Mg#	13	13	17	18	17	14	15	4
XRF								
V (ppm)	2	5	4	3	5	4	4	1
Cr	1	1	1	1	1	1	1	0
Ni	2	1	18	3	3	1	5	7
Cu	85	20	242	160	111	120	123	74
Zn	85	81	106	95	111	120	100	15
Ga	23	25	24	24	24	24	24	1
Zr	312	317	348	286	293	380	323	35
Ba	727	712	642	279	599	753	619	176
ICP-MS								
Sc (ppm)	35.7	35.3	25.4	33.4	34.5	30.4	32.4	3.9
Rb	74.57	74.36	53.93	18.32	52.96	59.13	55.55	20.61
Sr	151	151	191	120	167	189	162	27
Y	69.99	72.86	70.74	78.02	86.40	82.59	76.77	6.72
Nb	21.52	21.34	26.45	20.29	23.07	22.69	22.56	2.15
Cs	2.07	2.00	1.70	0.58	1.64	1.84	1.64	0.54
Hf	7.77	8.02	8.86	7.19	7.18	9.26	8.05	0.86
Ta	1.25	1.31	1.76	1.24	1.41	1.54	1.42	0.20
Pb	4.79	4.75	7.48	4.89	5.72	6.74	5.73	1.15
Th	2.87	2.37	8.36	3.87	3.99	4.63	4.35	2.13
U	0.79	0.82	1.60	1.12	0.98	1.28	1.10	0.31
La	30.86	27.15	14.49	24.94	19.72	28.54	24.28	6.11

Sample Name	TC3-A*	TC3-B*	AC2I	AC2C	JR12-141	JR12-145	Average	1SD
Ce	77.58	71.39	40.71	65.49	55.38	70.08	63.44	13.37
Pr	11.10	10.42	6.56	9.82	8.54	10.09	9.42	1.63
Nd	49.20	47.48	32.59	45.36	40.24	45.48	43.39	6.09
Sm	12.69	12.63	9.99	12.31	11.87	12.74	12.04	1.05
Eu	3.00	3.10	2.10	2.80	2.92	2.95	2.81	0.36
Gd	13.54	13.75	11.32	13.35	14.11	14.59	13.44	1.13
Tb	2.31	2.34	2.09	2.40	2.56	2.58	2.38	0.18
Dy	13.92	14.52	13.35	15.41	16.72	16.24	15.03	1.32
Ho	2.83	2.94	2.86	3.23	3.49	3.34	3.12	0.28
Er	7.66	7.84	7.92	8.82	9.55	9.07	8.48	0.77
Tm	1.05	1.11	1.13	1.27	1.36	1.27	1.20	0.12
Yb	6.43	6.65	6.72	7.61	8.20	7.66	7.21	0.71
Lu	0.98	1.02	1.02	1.15	1.25	1.16	1.10	0.11
La_N/Yb_N[1]	3.26	2.77	1.47	2.23	1.63	2.53	2.29	0.69
Eu/Eu*[2]	0.70	0.72	0.61	0.67	0.69	0.66	0.68	0.04
La/Yb	4.80	4.08	2.16	3.28	2.40	3.73	3.37	

* TC3-A and TC3-B analyses are replicates of the same powder made from sample TC3

Mg# = 100*[MgO/(FeO+MgO)] calculated on a molar basis.

[1]normalization values from ref. [50]

[2]Eu/Eu* = $Eu_N/sqrt[(Sm_N * Gd_N)]$ normalized to ref. [50].

[3]Average icelandite calculated from data obtained from GeoRoc database with the following screens; 55-65 wt% SiO_2, <15 wt% Al_2O_3, >8 wt% FeO.

[4]N is the number of analyses used in computing the average.

[5]Data from ref. [3].

Sample Name	Icelandite Average[3]	N[4]	Average TTG[5] High HREE	Med HREE	Low HREE
SiO_2 (wt.%)	58.43	90	71.12	68.29	68.81
TiO_2	1.81	90	0.25	0.4	0.42
Al_2O_3	13.68	90	15.55	15.65	15.21
$FeO_{(total)}$	11.16	90	1.83	3.02	3.31
MnO	0.22	90	0.04	0.05	0.06
MgO	2.80	90	0.79	1.33	1.29
CaO	5.83	90	2.63	3.44	3.24
Na_2O	3.77	90	5.24	4.7	4.47
K_2O	1.59	90	1.71	1.64	1.76
P_2O_5	0.52	73	0.09	0.14	0.13
Sum					
LOI	0.25	31			
Mg#	31	90	43	44	41
XRF					
V (ppm)	197	30	23	36	42
Cr	15	49	42	38	28
Ni	14	52	86	22	15
Cu	41	34			
Zn	134	38			
Ga	24	2			
Zr	511	44	114	143	174
Ba	367	58	542	532	447
ICP-MS					
Sc (ppm)	28.4	28			
Rb	37.49	44	46.44	54.98	70.58
Sr	299	52	583	483	328
Y	61.77	37	5.44	8.31	18.24
Nb	57.19	36	2.91	5.25	8.07
Cs	0.46	22			
Hf	12.21	25	3.01	4.17	4.51
Ta	3.50	24	0.52	0.81	0.79
Pb	4.15	31			
Th	2.77	90	3.86	6.16	7.16
U	1.61	29	0.83	1.31	1.83
La	50.87	37	16.35	26.88	31.03

Sample Name	Average[3]	N[4]	High HREE	Med HREE	Low HREE
Ce	111.66	38	28.72	52.87	57.91
Pr	13.96	17			
Nd	63.13	30	11.64	19.31	22.51
Sm	12.08	40	1.82	3.18	3.76
Eu	4.31	34	0.59	0.91	0.95
Gd	12.56	31	1.24	2.43	3.15
Tb	2.17	33			
Dy	13.39	17	0.84	1.63	2.68
Ho	2.62	17			
Er	7.19	17	0.41	0.81	1.39
Tm	1.03	23			
Yb	6.55	27	0.38	0.70	1.18
Lu	1.01	34	0.07	0.13	0.19
La_N/Yb_N[1]	5.28	27	29.23	26.09	17.86
Eu/Eu*[2]	1.07	31	1.20	1.00	0.85

La/Yb

Table 2.2. U-Th-Pb analyses of TC3 (S1425) zircons by SIMS

Spot Name	Phase Type	sess	Session	U (ppm)	Th (ppm)	Th/U	$^{204}Pb/^{206}Pb$	±1σ (%)	% of ^{206}Pb that is common Pb	$^{232}Th/^{238}U$	±1σ (%)	$^{208}Pb^*/^{206}Pb^*$
S1425 33-5	I	1	1129	174.7	82.5	0.472	2.1E-05	12	0.02	0.488	0.23	0.140
S1425 33-6	II	1	1129	102.1	45.3	0.443	1.5E-05	18	0.02	0.458	0.28	0.127
S1425 34-5	I	1	1129	216.9	139.6	0.644	8.9E-06	18	0.01	0.665	1.62	0.180
S1425 34-7	II	4	13004	345.6	42262.0	0.923	5.4E-05	8	0.06	0.954	0.16	0.270
S1425 34-8	I	4	13004	91.7	45.8	0.500	1.0E-04	11	0.11	0.516	0.90	0.144
S1425 34-9	I	4	13004	206.2	133.5	0.647	4.3E-05	25	0.05	0.669	0.59	0.182
S1425 35-4	II	1	1129	251.7	176.5	0.701	8.4E-06	16	0.01	0.724	0.70	0.196
S1425 35-5	II	1	1129	206.5	171.6	0.831	2.2E-05	27	0.02	0.858	0.35	0.245
S1425 35-6	I	2	13003A	227.0	158.5	0.698	6.0E-05	15	0.07	0.721	0.27	0.193
S1425 35-7	II	4	13004	294.8	261.2	0.886	3.0E-05	12	0.03	0.915	0.18	0.252
S1425 36-3	II	1	1129	89.7	32.8	0.365	8.3E-05	13	0.09	0.377	0.59	0.106
S1425 36-5	II	2	13003A	149.4	58.3	0.390	9.1E-05	27	0.10	0.403	1.28	0.111
S1425 37-3	II	1	1129	80.8	33.6	0.416	2.6E-05	16	0.03	0.429	0.34	0.117
S1425 37-4	II	1	1129	106.7	46.7	0.437	2.3E-05	15	0.03	0.451	0.52	0.120
S1425 37-5	II	4	13004	94.9	40.5	0.427	1.7E-04	18	0.19	0.441	0.38	0.120
S1425 37-6	II	4	13004	126.9	75.1	0.592	2.6E-04	6	0.29	0.611	0.31	0.166
S1425 38-2	II	1	1129	214.7	154.3	0.719	1.6E-05	13	0.02	0.743	0.16	0.205
S1425 38-3	I	2	13003A	286.9	203.5	0.709	7.5E-05	37	0.08	0.733	0.40	0.191
S1425 38-4	IV	2	13003A	686.7	50.0	0.073	3.8E-05	33	0.04	0.075	2.67	0.019
S1425 38-6	II	4	13004	134.4	62.4	0.464	6.1E-05	21	0.07	0.480	0.33	0.131
S1425 39-2	II	1	1129	169.6	97.3	0.574	1.1E-05	16	0.01	0.593	0.19	0.161
S1425 39-3	I	1	1129	231.5	154.0	0.665	1.2E-05	13	0.01	0.687	0.16	0.188
S1425 39-4	II	4	13004	168.8	84.5	0.501	7.5E-05	10	0.08	0.517	0.29	0.141
S1425 41-3	II	1	1129	70.3	25.2	0.358	3.9E-05	14	0.04	0.370	0.65	0.103
S1425 41-4	II	4	13004	80.9	30.1	0.372	1.5E-04	27	0.17	0.385	0.45	0.108
S1425 41-5	I	4	13004	856.0	674.0	0.787	3.4E-05	41	0.04	0.813	0.83	0.230
S1425 42-3	II	3	13003B	229.5	163.4	0.712	5.0E-05	28	0.06	0.735	0.47	0.198
S1425 43-3	II	3	13003B	172.3	109.8	0.637	9.7E-05	18	0.11	0.658	0.25	0.174

Spot Name	Phase Type	sess	Session	U (ppm)	Th (ppm)	Th/U	$^{204}Pb/^{206}Pb$	±1σ (%)	% of ^{206}Pb that is common Pb	$^{232}Th/^{238}U$	±1σ (%)	$^{208}Pb^*/^{206}Pb^*$
S1425 44-3	III	1	1129	491.4	51.1	0.104	9.4E-06	12	0.01	0.107	0.26	0.030
S1425 46-4	I	1	1129	539.3	510.5	0.947	2.9E-06	23	0.00	0.978	0.34	0.269
S1425 46-7	II	4	13004	150.1	75.3	0.502	9.0E-05	27	0.10	0.518	0.30	0.141
S1425 47-5	III	1	1129	750.6	37.4	0.050	9.8E-06	10	0.01	0.052	0.37	0.014
S1425 47-6	I	4	13004	271.9	189.9	0.699	2.8E-05	22	0.03	0.722	0.21	0.198
S1425 47-7	II	4	13004	79.7	34.2	0.429	7.4E-05	18	0.08	0.443	0.44	0.112
S1425 48-1	I	9	13010B	570.7	499.3	0.875	2.7E-05	19	0.03	0.904	0.30	0.234
S1425 48-2	I	9	13010B	470.9	371.2	0.788	2.1E-05	24	0.02	0.814	0.33	0.218
S1425 49-2	II	3	13003B	142.4	79.0	0.555	6.4E-05	26	0.07	0.573	0.30	0.155
S1425 50-2	III	1	1129	398.6	376.8	0.945	4.7E-06	16	0.01	0.976	0.26	0.267
S1425 51-3	II	1	1129	125.4	70.4	0.562	1.2E-05	18	0.01	0.580	0.53	0.157
S1425 51-4	I	1	1129	193.1	121.1	0.627	2.3E-05	12	0.03	0.648	0.36	0.179
S1425 51-5	II	2	13003A	120.0	56.7	0.473	1.1E-04	22	0.12	0.488	0.33	0.131
S1425 51-5	II	9	13010B	98.7	42.9	0.435	1.6E-04	19	0.18	0.449	0.89	0.114
S1425 51-6	I	9	13010B	211.6	139.1	0.657	3.1E-04	21	0.35	0.679	0.54	0.187
S1425 51-7	I	9	13010B	145.3	90.0	0.620	1.3E-04	21	0.15	0.640	0.63	0.168
S1425 51-7	II	4	13004	140.7	78.1	0.556	5.4E-05	30	0.06	0.574	0.63	0.154
S1425 51-8	I	4	13004	252.9	176.4	0.697	5.3E-05	26	0.06	0.720	0.52	0.198
S1425 52-3	I	3	13003B	303.8	221.8	0.730	4.8E-05	21	0.05	0.754	0.31	0.204
S1425 52-3	IV	9	13010B	414.7	48.4	0.117	4.0E-05	21	0.05	0.120	0.72	0.035
S1425 52-4	II	3	13003B	110.3	52.3	0.474	7.3E-05	37	0.08	0.490	0.35	0.131
S1425 53-3	II	3	13003B	176.8	88.9	0.503	1.0E-04	23	0.11	0.519	0.28	0.144
S1425 53-4	I	3	13003B	556.6	464.1	0.834	1.3E-05	16	0.01	0.861	0.13	0.235
S1425 54-2	III	9	13010B	451.7	76.4	0.169	3.7E-05	20	0.04	0.175	0.58	0.041
S1425 54-3	II	9	13010B	154.1	84.3	0.547	1.3E-04	23	0.14	0.565	0.65	0.141
S1425 55-3	II	1	1129	81.8	31.9	0.390	1.5E-05	19	0.02	0.403	0.63	0.111
S1425 55-4	III	4	13004	137.2	51.0	0.372	5.9E-05	35	0.07	0.384	0.34	0.110
S1425 55-5	II	4	13004	127.7	58.0	0.454	6.1E-05	15	0.07	0.469	0.34	0.130
S1425 57-2	II	9	13010B	159.0	100.6	0.633	1.2E-04	20	0.13	0.653	0.61	0.165

Spot Name	Phase Type	sess	Session	U (ppm)	Th (ppm)	Th/U	$^{204}Pb/^{206}Pb$	±1σ (%)	% of ^{206}Pb that is common Pb	$^{232}Th/^{238}U$	±1σ (%)	$^{208}Pb^*/^{206}Pb^*$
S1425 57-3	II	4	13004	168.2	101.9	0.606	3.1E-05	29	0.03	0.626	0.26	0.175
S1425 57-3	IV	9	13010B	239.4	26.2	0.109	1.0E-04	18	0.12	0.113	1.00	0.029
S1425 57-4	III	9	13010B	699.9	118.5	0.169	2.4E-05	20	0.03	0.175	3.41	0.048
S1425 58-3	IV	1	1129	276.4	14.1	0.051	6.8E-06	18	0.01	0.053	0.49	0.016
S1425 58-5	I	4	13004	72.3	32.3	0.447	1.0E-04	14	0.12	0.462	0.74	0.126
S1425 58-5	IV	9	13010B	211.5	55.1	0.260	6.3E-05	22	0.07	0.269	0.72	0.072
S1425 58-6	III	9	13010B	194.8	116.6	0.599	5.5E-05	25	0.06	0.619	2.11	0.146
S1425 58-6	IV	4	13004	312.6	22.9	0.073	1.2E-04	13	0.14	0.076	0.46	0.020
S1425 59-3	IV	3	13003B	196.4	35.8	0.182	3.7E-04	16	0.42	0.188	1.33	0.048
S1425 60-2	I	1	1129	682.6	575.0	0.842	2.5E-06	22	0.00	0.870	0.20	0.235
S1425 61-2	I	3	13003B	225.8	150.8	0.668	5.7E-05	23	0.06	0.690	0.22	0.183
S1425 62-3	III	9	13010B	724.0	96.6	0.133	2.2E-05	21	0.03	0.138	1.17	0.033
S1425 62-3	IV	2	13003A	238.8	4.7	0.020	1.4E-04	27	0.17	0.020	1.26	0.005
S1425 62-4	IV	9	13010B	244.0	14.8	0.061	7.4E-05	22	0.09	0.063	1.31	0.016
S1425 62-5	IV	9	13010B	370.0	70.8	0.191	5.4E-05	19	0.06	0.198	1.89	0.048
S1425 63-3	III	1	1129	742.9	510.6	0.687	3.4E-06	18	0.00	0.710	1.00	0.201
S1425 64-2	II	8	13010A	138.2	77.7	0.562	2.5E-04	23	0.28	0.581	0.69	0.156
S1425 64-3	II	4	13004	135.9	58.8	0.433	4.9E-05	14	0.05	0.447	0.55	0.125
S1425 64-3	II	8	13010A	177.0	94.1	0.532	1.6E-04	25	0.18	0.549	1.01	0.156
S1425 64-4	II	8	13010A	68.1	30.1	0.442	6.3E-04	22	0.70	0.457	1.08	0.113
S1425 64-5	II	9	13010B	173.4	104.0	0.600	8.1E-05	20	0.09	0.620	0.61	0.161
S1425 64-6	II	9	13010B	199.2	111.7	0.561	1.3E-04	18	0.14	0.579	0.59	0.156
S1425 65-3	II	2	13003A	129.2	68.0	0.526	2.8E-04	30	0.31	0.544	0.44	0.161
S1425 66-3	I	1	1129	687.8	1093.9	1.590	3.9E-06	14	0.00	1.643	0.60	0.450
S1425 66-4	I	4	13004	783.0	1264.3	1.615	8.4E-06	26	0.01	1.668	0.75	0.457
S1425 66-5	IV	4	13004	190.5	32.8	0.172	6.7E-05	19	0.08	0.178	0.98	0.054
S1425 66-6	I	4	13004	677.6	1061.8	1.567	6.7E-06	19	0.01	1.619	0.11	0.433
S1425 67-2	II	9	13010B	85.9	35.6	0.415	3.7E-04	16	0.41	0.428	0.98	0.117
S1425 67-3	IV	9	13010B	177.4	25.8	0.146	1.4E-04	19	0.16	0.150	1.01	0.035

Spot Name	Phase Type	sess	Session	U (ppm)	Th (ppm)	Th/U	$^{204}Pb/^{206}Pb$	±1σ (%)	% of ^{206}Pb that is common Pb	$^{232}Th/^{238}U$	±1σ (%)	$^{208}Pb^*/^{206}Pb^*$
S1425 67-4	III	9	13010B	838.4	13.3	0.016	2.6E-05	22	0.03	0.016	1.32	0.004
S1425 68-1	II	9	13010B	107.2	56.6	0.528	1.8E-04	18	0.20	0.545	0.78	0.140
S1425 68-2	IV	9	13010B	241.7	9.7	0.040	9.1E-05	19	0.11	0.041	1.54	0.009
S1425 68-3	II	9	13010B	141.2	78.0	0.553	2.0E-04	16	0.23	0.571	0.67	0.151
S1425 69-2	III	4	13004	451.8	330.1	0.731	1.3E-05	14	0.01	0.755	0.61	0.211
S1425 70-2	I	4	13004	164.1	99.3	0.605	2.7E-05	35	0.03	0.625	0.42	0.172
S1425 72-1	II	9	13010B	166.4	88.6	0.533	1.0E-04	18	0.11	0.550	0.61	0.139
S1425 72-2	III	9	13010B	655.4	50.9	0.078	2.4E-05	21	0.03	0.080	0.68	0.021
S1425 73-2	II	1	1129	82.8	34.1	0.412	9.2E-05	8	0.10	0.426	0.34	0.123
S1425 75-1	I	9	13010B	816.4	1322.1	1.619	1.7E-05	20	0.02	1.673	0.21	0.434
S1425 75-3	II	9	13010B	94.7	40.2	0.425	1.6E-04	20	0.18	0.439	0.88	0.122
S1425 77-3	II	4	13004	253.2	200.2	0.791	2.7E-05	15	0.03	0.817	0.34	0.226
S1425 78-3	II	3	13003B	123.7	65.9	0.533	1.5E-04	20	0.17	0.551	0.32	0.152
S1425 78-4	I	4	13004	540.3	728.3	1.348	1.0E-05	38	0.01	1.393	0.19	0.378
S1425 80-1	II	1	1129	105.7	44.8	0.424	1.1E-05	20	0.01	0.438	0.31	0.118
S1425 80-2	II	4	13004	136.4	74.8	0.549	7.8E-05	21	0.09	0.567	0.61	0.157
S1425 81-1	II	1	1129	108.7	60.3	0.555	9.6E-06	21	0.01	0.573	0.59	0.155
S1425 81-4	I	4	13004	187.9	118.7	0.632	5.1E-05	12	0.06	0.653	0.24	0.180
S1425 82-1	II	1	1129	84.2	29.1	0.345	2.2E-05	18	0.02	0.357	0.37	0.099
S1425 82-2	I	4	13004	252.8	133.5	0.528	3.0E-05	23	0.03	0.545	0.23	0.148
S1425 82-3	IV	4	13004	153.3	52.0	0.339	1.1E-04	11	0.13	0.351	0.36	0.102
S1425 83-1	III	1	1129	369.1	47.7	0.129	6.1E-06	16	0.01	0.133	0.46	0.037
S1425 83-2	II	4	13004	133.3	66.6	0.500	5.0E-05	17	0.06	0.516	0.55	0.138
S1425 84-1	IV	1	1129	389.2	56.2	0.144	1.9E-06	28	0.00	0.149	1.52	0.042
S1425 85-1	IV	1	1129	189.1	0.6	0.003	1.1E-05	18	0.01	0.003	2.40	0.001
S1425 85-2	III	9	13010B	709.6	45.9	0.065	2.8E-05	20	0.03	0.067	3.39	0.020
S1425 85-3	IV	9	13010B	199.4	2.1	0.011	2.6E-04	15	0.33	0.011	3.36	0.004
S1425 86-1	IV	1	1129	285.1	3.8	0.013	4.4E-05	7	0.06	0.014	0.97	0.005
S1425 86-2	II	4	13004	255.1	164.9	0.646	4.1E-05	26	0.05	0.668	0.22	0.181

Spot Name	Phase Type	sess	Session	U (ppm)	Th (ppm)	Th/U	$^{204}Pb/^{206}Pb$	±1σ (%)	% of ^{206}Pb that is common Pb	$^{232}Th/^{238}U$	±1σ (%)	$^{208}Pb^*/^{206}Pb^*$
S1425 87-1	I	1	1129	223.2	149.5	0.670	7.6E-06	17	0.01	0.692	0.17	0.188
S1425 87-2	II	4	13004	128.8	61.8	0.480	5.9E-05	15	0.07	0.496	0.31	0.136
S1425 88-1	IV	4	13004	258.8	14.5	0.056	3.3E-05	14	0.04	0.058	3.90	0.018
S1425 89-1	II	2	13003A	330.1	289.8	0.878	7.6E-05	10	0.08	0.907	0.20	0.246
S1425 89-2	III	2	13003A	450.5	68.5	0.152	5.4E-05	28	0.06	0.157	0.33	0.044
S1425B 1-1	I	6	13005A	186.2	112.5	0.604	7.1E-06	32	0.01	0.624	0.22	0.172
S1425B 1-2	II	6	13005A	114.0	53.0	0.465	5.6E-06	45	0.01	0.480	0.30	0.130
S1425B 6-1	I	6	13005A	262.4	180.1	0.686	8.3E-06	24	0.01	0.709	0.17	0.193
S1425B 6-2	II	6	13005A	200.0	139.2	0.696	4.6E-06	38	0.01	0.719	0.32	0.195
S1425D 2-1	I	7	13005B	67.8	27.6	0.407	2.3E-05	29	0.03	0.420	0.41	0.112
S1425D 2-2	II	7	13005B	97.7	41.4	0.424	5.2E-06	50	0.01	0.438	0.33	0.119
S1425D 3-1	I	6	13005A	162.2	92.6	0.571	1.6E-05	22	0.02	0.590	0.47	0.164
S1425D 3-2	II	6	13005A	109.0	39.4	0.362	8.7E-06	38	0.01	0.374	0.34	0.101
S1425D 4-1	I	6	13005A	200.5	120.6	0.602	4.4E-06	38	0.00	0.622	0.21	0.169
S1425G 4-1	II	6	13005A	184.3	116.1	0.630	8.6E-06	29	0.01	0.651	0.22	0.180
S1425G 4-2	II	6	13005A	150.7	76.8	0.509	3.4E-06	50	0.00	0.526	0.26	0.144
S1425H 1-1	II	6	13005A	69.8	26.5	0.380	1.3E-05	35	0.01	0.392	0.49	0.105
S1425H 1-2	II	6	13005A	163.4	91.0	0.557	5.9E-06	38	0.01	0.575	0.24	0.160
S1425H 1-3	II	6	13005A	208.9	145.2	0.695	7.0E-06	30	0.01	0.718	0.20	0.195
S1425H 3-1	II	6	13005A	274.9	215.8	0.785	4.7E-06	30	0.01	0.811	0.20	0.220
S1425H 3-2	II	7	13005B	217.0	138.0	0.636	4.1E-06	38	0.00	0.657	0.20	0.179
S1425H 4-1	II	6	13005A	96.6	34.0	0.352	1.2E-05	33	0.01	0.364	0.37	0.101
S1425H 7-1	I	6	13005A	193.1	121.5	0.629	4.6E-06	38	0.01	0.650	0.21	0.178
S1425K 1-1	III	6	13005A	511.0	49.6	0.097	7.7E-06	20	0.01	0.100	0.27	0.028
S1425K 1-2	II	6	13005A	157.3	90.8	0.577	4.8E-06	41	0.01	0.596	0.44	0.164
S1425K 4-1	II	6	13005A	167.3	73.9	0.442	3.0E-06	50	0.00	0.457	0.25	0.125
S1425K 4-2	II	6	13005A	259.9	158.6	0.610	5.7E-06	29	0.01	0.630	0.18	0.174
S1425L 3-1	I	7	13005B	250.2	168.0	0.672	6.8E-06	27	0.01	0.694	0.18	0.191
S1425L 3-2	II	7	13005B	486.2	458.6	0.943	7.3E-06	19	0.01	0.974	0.27	0.268

Spot Name	Phase Type	sess	Session	U (ppm)	Th (ppm)	Th/U	$^{204}Pb/^{206}Pb$	±1σ (%)	% of ^{206}Pb that is common Pb	$^{232}Th/^{238}U$	±1σ (%)	$^{208}Pb^*/^{206}Pb^*$
S1425M 13-1	II	7	13005B	235.3	126.4	0.537	7.3E-06	27	0.01	0.555	0.37	0.153
S1425M 13-2	II	7	13005B	244.2	155.6	0.637	6.5E-06	28	0.01	0.658	0.70	0.183
S1425M 14-1	II	7	13005B	265.7	137.7	0.518	3.8E-06	35	0.00	0.535	0.80	0.149
S1425M 5-1	II	7	13005B	162.0	88.4	0.546	9.1E-06	29	0.01	0.564	0.23	0.156
S1425M 5-2	II	7	13005B	201.0	122.9	0.612	1.0E-05	25	0.01	0.632	0.21	0.171
S1425O 1-1	IV	6	13005A	452.3	24.3	0.054	3.8E-06	32	0.00	0.055	0.38	0.016
S1425O 1-2	IV	6	13005A	384.6	76.1	0.198	5.7E-06	27	0.01	0.205	0.23	0.058
S1425O 2-1	II	6	13005A	123.8	59.1	0.478	1.4E-05	28	0.02	0.493	0.28	0.138
S1425O 2-2	I	6	13005A	425.2	436.4	1.026	5.0E-06	25	0.01	1.060	0.23	0.292
S1425O 7-1	IV	7	13005B	260.6	44.7	0.172	1.1E-05	24	0.01	0.177	1.26	0.052
S1425O 7-2	IV	7	13005B	257.6	47.3	0.184	1.0E-05	25	0.01	0.190	1.45	0.046
S1425O 7-3	II	7	13005B	203.5	120.2	0.591	7.4E-06	29	0.01	0.610	0.20	0.170
S1425O 9-1	II	7	13005B	168.7	101.5	0.601	1.3E-05	24	0.01	0.621	0.46	0.171
S1425O 9-2	II	7	13005B	107.0	47.8	0.446	1.5E-05	28	0.02	0.461	0.31	0.130
S1425O 9-3	II	7	13005B	171.3	105.2	0.614	1.2E-05	27	0.01	0.634	0.23	0.171
S1425O 9-4	II	7	13005B	148.4	83.8	0.565	7.2E-06	41	0.01	0.583	0.27	0.156

Table 2.2. U-Th-I

Spot Name	±1σ (%)	$^{207}Pb^*/^{206}Pb^*$	±1σ (%)	$^{207}Pb^*/^{235}U$	±1σ (%)	$^{206}Pb^*/^{238}U$	±1σ (%)	Pb/U Error Correlation	$^{207}Pb/^{206}Pb$ Age (Ma)	±1σ (Ma)
S1425 33-5	0.68	0.4282	0.17	41.94	0.57	0.792	0.56	0.976	3849	2
S1425 33-6	0.91	0.4287	0.36	47.62	0.62	0.836	0.60	0.967	3958	2
S1425 34-5	1.26	0.4294	1.08	50.64	0.60	0.862	0.56	0.938	4004	3
S1425 34-7	0.38	0.4066	0.18	48.39	0.59	0.834	0.58	0.974	3986	2
S1425 34-8	1.00	0.4239	0.27	49.60	1.41	0.854	1.22	0.865	3987	11
S1425 34-9	1.11	0.4292	0.15	51.66	0.74	0.872	0.64	0.867	4016	5
S1425 35-4	0.96	0.4289	0.35	50.65	1.64	0.860	1.08	0.658	4007	18
S1425 35-5	0.46	0.4281	0.64	49.82	0.60	0.849	0.56	0.929	4001	3
S1425 35-6	0.7	0.4281	0.16	49.65	1.3	0.841	1.2	0.978	4012	4
S1425 35-7	0.64	0.3017	0.13	50.89	0.61	0.864	0.59	0.971	4008	2
S1425 36-3	1.22	0.4308	0.17	46.54	0.71	0.825	0.63	0.889	3942	5
S1425 36-5	1.7	0.4299	0.17	46.57	1.3	0.811	1.3	0.976	3970	4
S1425 37-3	1.07	0.4300	0.13	49.78	0.85	0.856	0.62	0.739	3988	9
S1425 37-4	0.94	0.4256	0.14	51.73	2.56	0.864	0.80	0.312	4033	36
S1425 37-5	1.30	0.4280	0.20	49.73	0.79	0.849	0.74	0.938	3999	4
S1425 37-6	0.85	0.4243	0.26	50.23	0.74	0.856	0.71	0.951	4003	3
S1425 38-2	0.49	0.4305	0.14	50.15	0.56	0.851	0.55	0.981	4009	2
S1425 38-3	1.3	0.4063	0.13	46.25	1.3	0.819	1.2	0.980	3945	4
S1425 38-4	2.5	0.4287	1.24	28.58	1.4	0.679	1.3	0.940	3497	7
S1425 38-6	0.91	0.4211	0.16	50.73	0.81	0.860	0.70	0.864	4009	6
S1425 39-2	0.61	0.2651	0.25	50.85	0.65	0.858	0.56	0.858	4017	5
S1425 39-3	0.49	0.3049	0.13	50.67	0.56	0.858	0.55	0.983	4012	2
S1425 39-4	0.77	0.4000	0.20	50.22	0.80	0.855	0.67	0.837	4003	7
S1425 41-3	1.29	0.4249	0.11	44.58	0.81	0.812	0.65	0.799	3902	7
S1425 41-4	1.65	0.2963	0.26	51.16	0.84	0.866	0.79	0.939	4012	4
S1425 41-5	0.75	0.2833	0.33	45.41	0.69	0.827	0.65	0.935	3902	4
S1425 42-3	0.56	0.4103	0.39	51.67	1.1	0.874	1.1	0.960	4013	5
S1425 43-3	0.70	0.4216	0.39	51.49	1.2	0.869	1.2	0.981	4017	4

Spot Name	±1σ (%)	$^{207}Pb^*/^{206}Pb^*$	±1σ (%)	$^{207}Pb^*/^{235}U$	±1σ (%)	$^{206}Pb^*/^{238}U$	±1σ (%)	Pb/U Error Correlation	$^{207}Pb/^{206}Pb$ Age (Ma)	±1σ (Ma)
S1425 44-3	0.96	0.4343	0.73	27.64	0.62	0.668	0.52	0.844	3470	5
S1425 46-4	0.28	0.4265	0.18	48.84	0.53	0.849	0.52	0.991	3972	1
S1425 46-7	1.66	0.4250	0.64	49.31	0.71	0.846	0.68	0.953	3993	3
S1425 47-5	1.27	0.2944	0.13	27.44	0.54	0.676	0.52	0.970	3441	2
S1425 47-6	0.51	0.4207	0.16	49.29	0.63	0.850	0.61	0.968	3985	2
S1425 47-7	1.30	0.4162	0.64	45.54	1.03	0.794	0.81	0.782	3969	10
S1425 48-1	1.2	0.4197	0.38	49.32	0.8	0.852	0.70	0.878	3981	6
S1425 48-2	0.9	0.4223	0.18	49.31	1.0	0.847	1.00	0.984	3990	3
S1425 49-2	0.85	0.4227	0.28	47.59	1.2	0.817	1.1	0.970	3992	4
S1425 50-2	0.32	0.4218	0.08	48.73	0.53	0.838	0.53	0.989	3989	1
S1425 51-3	0.79	0.4322	1.20	51.78	1.34	0.869	0.60	0.445	4025	18
S1425 51-4	0.60	0.4141	0.38	47.31	0.68	0.829	0.56	0.827	3961	6
S1425 51-5	1.1	0.4312	0.73	52.15	1.5	0.877	1.3	0.866	4022	11
S1425 51-5	2.6	0.4123	2.00	48.63	2.4	0.855	1.29	0.541	3955	30
S1425 51-6	1.7	0.4239	0.31	49.12	1.0	0.840	0.96	0.953	3996	5
S1425 51-7	1.7	0.4368	2.06	51.58	2.7	0.856	1.66	0.627	4041	31
S1425 51-7	2.03	0.4261	0.58	50.80	1.55	0.865	1.44	0.928	4004	9
S1425 51-8	0.85	0.4247	0.26	50.61	0.67	0.864	0.61	0.920	3999	4
S1425 52-3	0.47	0.4304	0.29	52.15	1.1	0.879	1.1	0.965	4019	4
S1425 52-3	2.5	0.2879	0.86	26.53	1.3	0.668	1.04	0.773	3407	13
S1425 52-4	1.12	0.4256	0.32	50.47	1.3	0.860	1.3	0.971	4002	5
S1425 53-3	0.88	0.4281	0.26	47.68	1.2	0.808	1.1	0.974	4011	4
S1425 53-4	0.31	0.4193	0.14	49.49	1.1	0.856	1.1	0.992	3980	2
S1425 54-2	2.1	0.3107	0.58	29.60	1.2	0.691	1.10	0.884	3525	9
S1425 54-3	2.0	0.4213	0.55	50.28	1.2	0.865	1.08	0.891	3987	8
S1425 55-3	2.04	0.4219	0.66	49.81	1.23	0.856	1.03	0.842	3989	10
S1425 55-4	1.14	0.3066	0.91	30.03	1.13	0.710	0.68	0.600	3504	14
S1425 55-5	0.92	0.4287	0.23	50.09	0.97	0.847	0.94	0.972	4013	3
S1425 57-2	1.7	0.4275	0.33	50.25	1.1	0.852	1.06	0.955	4009	5

Spot Name	±1σ (%)	$^{207}Pb^*/^{206}Pb^*$	±1σ (%)	$^{207}Pb^*/^{235}U$	±1σ (%)	$^{206}Pb^*/^{238}U$	±1σ (%)	Pb/U Error Correlation	$^{207}Pb/^{206}Pb$ Age (Ma)	±1σ (Ma)
S1425 57-3	0.67	0.4276	0.39	51.23	0.76	0.869	0.65	0.858	4009	6
S1425 57-3	4.0	0.2968	0.76	28.09	1.2	0.686	0.90	0.763	3454	12
S1425 57-4	5.4	0.3177	0.43	30.83	1.1	0.704	0.96	0.912	3559	7
S1425 58-3	1.84	0.2721	0.28	24.64	0.61	0.657	0.54	0.888	3318	4
S1425 58-5	1.21	0.4192	0.30	49.07	0.86	0.849	0.81	0.939	3980	4
S1425 58-5	2.3	0.3229	0.64	32.27	1.1	0.725	0.93	0.825	3583	10
S1425 58-6	1.6	0.4015	0.32	40.14	1.0	0.725	0.97	0.949	3915	5
S1425 58-6	3.70	0.2828	0.20	24.42	0.77	0.626	0.74	0.966	3378	3
S1425 59-3	6.47	0.3285	0.32	30.73	1.2	0.678	1.1	0.960	3610	5
S1425 60-2	0.28	0.4258	0.06	50.85	0.52	0.866	0.52	0.992	4003	1
S1425 61-2	0.59	0.4264	0.22	50.49	1.1	0.859	1.1	0.981	4005	3
S1425 62-3	3.4	0.3112	0.65	28.49	1.2	0.664	1.01	0.839	3527	10
S1425 62-3	35.5	0.2853	0.53	26.05	1.5	0.662	1.4	0.936	3392	8
S1425 62-4	6.5	0.2694	0.80	24.62	2.2	0.663	2.04	0.930	3303	13
S1425 62-5	2.2	0.3630	0.82	33.92	1.1	0.678	0.79	0.693	3762	12
S1425 63-3	0.86	0.3915	0.25	43.04	0.71	0.797	0.66	0.935	3877	4
S1425 64-2	2.0	0.3920	0.6	44.12	1.6	0.816	1.4	0.912	3879	10
S1425 64-3	0.88	0.4236	0.21	48.46	0.71	0.830	0.68	0.954	3995	3
S1425 64-3	1.7	0.3830	0.3	43.28	1.3	0.819	1.3	0.970	3844	5
S1425 64-4	5.9	0.4152	2.9	49.25	3.5	0.860	2.0	0.568	3965	43
S1425 64-5	2.6	0.4315	0.31	52.00	1.1	0.874	1.02	0.957	4023	5
S1425 64-6	1.7	0.3860	0.34	41.20	1.1	0.774	1.01	0.948	3856	5
S1425 65-3	3.2	0.4273	1.46	50.42	2.4	0.856	1.9	0.791	4008	22
S1425 66-3	0.49	0.4291	0.16	50.48	0.56	0.853	0.54	0.957	4014	2
S1425 66-4	0.78	0.4182	0.09	49.77	0.55	0.863	0.54	0.986	3976	1
S1425 66-5	1.49	0.2872	0.24	26.36	0.69	0.666	0.65	0.938	3403	4
S1425 66-6	0.22	0.4277	0.21	50.94	0.58	0.864	0.55	0.934	4010	3
S1425 67-2	3.1	0.4144	1.18	47.52	1.8	0.832	1.36	0.757	3962	18
S1425 67-3	4.5	0.2866	0.40	26.56	1.9	0.672	1.81	0.977	3399	6

Spot Name	±1σ (%)	$^{207}Pb^*/^{206}Pb^*$	±1σ (%)	$^{207}Pb^*/^{235}U$	±1σ (%)	$^{206}Pb^*/^{238}U$	±1σ (%)	Pb/U Error Correlation	$^{207}Pb/^{206}Pb$ Age (Ma)	±1σ (Ma)
S1425 67-4	7.0	0.3013	0.27	28.85	0.7	0.694	0.64	0.923	3477	4
S1425 68-1	2.2	0.4258	0.40	48.32	1.3	0.823	1.21	0.950	4003	6
S1425 68-2	9.5	0.2694	0.35	24.07	1.0	0.648	0.91	0.931	3303	6
S1425 68-3	2.0	0.4060	0.37	44.58	1.2	0.796	1.10	0.947	3931	6
S1425 69-2	0.36	0.4136	0.13	48.82	0.57	0.856	0.56	0.974	3959	2
S1425 70-2	1.18	0.4224	0.19	49.74	0.68	0.854	0.65	0.958	3991	3
S1425 72-1	1.7	0.4298	0.31	50.71	1.1	0.856	1.01	0.956	4017	5
S1425 72-2	2.5	0.3045	0.32	29.31	0.7	0.698	0.67	0.904	3493	5
S1425 73-2	1.07	0.4181	0.36	48.96	0.72	0.849	0.63	0.866	3975	5
S1425 75-1	0.4	0.4264	0.14	50.24	0.9	0.855	0.92	0.988	4005	2
S1425 75-3	2.5	0.4232	0.46	48.21	1.3	0.826	1.26	0.941	3993	7
S1425 77-3	0.46	0.4290	0.15	51.15	0.62	0.865	0.60	0.969	4014	2
S1425 78-3	1.03	0.4287	0.44	50.02	1.2	0.846	1.2	0.934	4013	7
S1425 78-4	0.65	0.4274	0.17	51.03	0.58	0.866	0.56	0.955	4008	3
S1425 80-1	0.97	0.4325	0.83	51.48	1.03	0.863	0.61	0.590	4026	12
S1425 80-2	0.86	0.4211	0.48	49.57	0.85	0.854	0.70	0.827	3986	7
S1425 81-1	0.83	0.4251	0.16	50.35	0.62	0.859	0.60	0.967	4000	2
S1425 81-4	0.61	0.4235	0.18	49.31	0.66	0.845	0.63	0.961	3995	3
S1425 82-1	1.18	0.4000	0.46	44.93	0.77	0.815	0.62	0.807	3909	7
S1425 82-2	0.62	0.4162	0.57	48.16	1.00	0.839	0.83	0.825	3969	9
S1425 82-3	1.11	0.3038	0.26	29.49	0.73	0.704	0.68	0.935	3490	4
S1425 83-1	1.01	0.3092	0.10	29.39	0.59	0.689	0.58	0.985	3517	2
S1425 83-2	0.93	0.4290	0.37	48.32	0.80	0.817	0.71	0.887	4014	5
S1425 84-1	3.11	0.3017	0.33	28.53	0.63	0.686	0.53	0.850	3479	5
S1425 85-1	13	0.2504	0.16	21.34	0.58	0.618	0.56	0.963	3187	2
S1425 85-2	4.7	0.2571	0.46	21.99	0.8	0.620	0.66	0.822	3229	7
S1425 85-3	35.7	0.2393	0.47	18.40	1.1	0.558	0.99	0.903	3116	8
S1425 86-1	4.51	0.2478	0.13	20.56	0.56	0.602	0.54	0.972	3171	2
S1425 86-2	0.58	0.4156	0.28	48.22	0.68	0.841	0.62	0.913	3967	4

Spot Name	±1σ (%)	$^{207}Pb^*/^{206}Pb^*$	±1σ (%)	$^{207}Pb^*/^{235}U$	±1σ (%)	$^{206}Pb^*/^{238}U$	±1σ (%)	Pb/U Error Correlation	$^{207}Pb/^{206}Pb$ Age (Ma)	±1σ (Ma)
S1425 87-1	0.52	0.4259	0.12	49.25	0.56	0.839	0.55	0.977	4003	2
S1425 87-2	0.85	0.4170	0.24	48.41	0.94	0.842	0.91	0.966	3972	4
S1425 88-1	4.21	0.2645	0.47	23.58	0.76	0.647	0.60	0.789	3274	7
S1425 89-1	0.7	0.4272	0.48	49.43	1.3	0.839	1.2	0.931	4008	7
S1425 89-2	2.2	0.2978	0.53	27.96	1.3	0.681	1.2	0.916	3459	8
S1425B 1-1	0.56	0.4147	0.27	47.96	0.67	0.839	0.61	0.913	3963	4
S1425B 1-2	0.81	0.4312	0.42	49.73	0.78	0.836	0.66	0.843	4022	6
S1425B 6-1	0.44	0.4277	0.14	50.69	0.59	0.860	0.58	0.974	4009	2
S1425B 6-2	0.50	0.4281	0.28	49.65	0.66	0.841	0.60	0.904	4011	4
S1425D 2-1	1.14	0.4312	0.98	51.18	1.63	0.861	1.30	0.797	4021	15
S1425D 2-2	0.90	0.4282	1.09	49.72	1.29	0.842	0.69	0.533	4011	16
S1425D 3-1	0.72	0.4062	0.62	45.87	0.91	0.819	0.66	0.729	3932	9
S1425D 3-2	0.96	0.4071	0.22	46.89	0.71	0.835	0.67	0.951	3936	3
S1425D 4-1	0.53	0.4293	0.15	50.93	0.62	0.860	0.60	0.969	4015	2
S1425G 4-1	0.55	0.4282	0.17	50.91	0.63	0.862	0.61	0.965	4011	2
S1425G 4-2	0.67	0.4287	0.36	51.14	0.73	0.865	0.63	0.868	4013	5
S1425H 1-1	1.33	0.4294	1.08	51.66	1.36	0.873	0.83	0.611	4015	16
S1425H 1-2	0.63	0.4066	0.18	46.44	0.65	0.828	0.62	0.961	3934	3
S1425H 1-3	0.50	0.4239	0.27	50.09	0.66	0.857	0.60	0.911	3996	4
S1425H 3-1	0.81	0.4292	0.15	51.09	0.62	0.863	0.60	0.969	4015	2
S1425H 3-2	0.50	0.4289	0.35	50.46	0.71	0.853	0.61	0.867	4014	5
S1425H 4-1	0.98	0.4281	0.64	50.53	0.95	0.856	0.69	0.733	4011	10
S1425H 7-1	0.53	0.4281	0.16	50.75	0.62	0.860	0.60	0.968	4011	2
S1425K 1-1	0.90	0.3017	0.13	28.86	0.56	0.694	0.54	0.973	3479	2
S1425K 1-2	0.60	0.4308	0.17	50.57	0.65	0.851	0.62	0.964	4020	3
S1425K 4-1	0.67	0.4299	0.17	51.04	0.64	0.861	0.62	0.964	4017	3
S1425K 4-2	0.46	0.4300	0.13	51.19	0.59	0.863	0.58	0.974	4018	2
S1425L 3-1	0.44	0.4256	0.14	50.42	0.59	0.859	0.58	0.974	4002	2
S1425L 3-2	0.27	0.4280	0.20	50.61	0.63	0.858	0.60	0.949	4010	3

Spot Name	±1σ (%)	$^{207}Pb^*/^{206}Pb^*$	±1σ (%)	$^{207}Pb^*/^{235}U$	±1σ (%)	$^{206}Pb^*/^{238}U$	±1σ (%)	Pb/U Error Correlation	$^{207}Pb/^{206}Pb$ Age (Ma)	±1σ (Ma)
S1425M 13-1	0.51	0.4243	0.26	50.39	0.64	0.861	0.58	0.916	3998	4
S1425M 13-2	0.45	0.4305	0.14	51.58	0.62	0.869	0.60	0.975	4019	2
S1425M 14-1	1.29	0.4063	0.13	46.76	0.76	0.835	0.75	0.984	3932	2
S1425M 5-1	1.23	0.4287	1.24	50.23	1.39	0.850	0.62	0.446	4013	19
S1425M 5-2	0.53	0.4211	0.16	49.37	0.62	0.850	0.60	0.968	3986	2
S1425O 1-1	1.33	0.2651	0.25	23.72	0.69	0.649	0.64	0.935	3277	4
S1425O 1-2	0.72	0.3049	0.13	29.37	0.57	0.698	0.55	0.972	3496	2
S1425O 2-1	0.76	0.4000	0.20	44.46	0.68	0.806	0.65	0.955	3909	3
S1425O 2-2	0.29	0.4249	0.11	50.25	0.63	0.858	0.62	0.985	4000	2
S1425O 7-1	1.01	0.2963	0.26	27.90	0.63	0.683	0.58	0.913	3451	4
S1425O 7-2	1.04	0.2833	0.33	25.89	0.67	0.663	0.58	0.869	3381	5
S1425O 7-3	1.00	0.4103	0.39	46.57	0.71	0.823	0.60	0.840	3947	6
S1425O 9-1	1.04	0.4216	0.39	49.38	0.73	0.849	0.62	0.845	3988	6
S1425O 9-2	0.82	0.4343	0.73	52.07	1.15	0.870	0.89	0.771	4032	11
S1425O 9-3	0.61	0.4265	0.18	49.85	0.65	0.848	0.62	0.962	4005	3
S1425O 9-4	0.76	0.4250	0.64	48.78	0.92	0.832	0.66	0.721	4000	10

Table 2.3. Oxygen isotopic analyses of TC3 (S1425) zircons by SIMS

Spot Number	Mount	Phase Type	Correlated U-Pb Spot	Session	δ18O (SMOW) (‰)	2σ (‰)
1-1	M1070	I		11019	6.02	0.27
1-2	M1070	II		11019	4.53	0.20
1-3	M1070	II		11019	4.60	0.21
1-4	M1070	I		11019	5.15	0.23
2-1	M1070	I		11019	5.66	0.23
2-2	M1070	I		11019	5.47	0.20
2-3	M1070	I		11019	5.40	0.18
2-4	M1070	I		11019	5.78	0.24
3-1	M1070	I		11019	5.15	0.24
3-2	M1070	I		11019	5.24	0.16
3-3	M1070	I		11019	5.82	0.20
3-4	M1070	IV		11019	6.47	0.24
4-1	M1070	I		11019	5.77	0.15
4-2	M1070	II		11019	4.91	0.18
4-3	M1070	II		11019	4.68	0.24
4-4	M1070	II		11019	4.49	0.23
5-1	M1070	I		11019	5.55	0.20
5-2	M1070	IV		11019	6.16	0.32
5-3	M1070	IV		11019	6.10	0.26
5-4	M1070	*		11019	9.22	0.25
6-1	M1070	II		11019	4.71	0.14
6-2	M1070	II		11019	4.86	0.23
7-1	M1070	I		11019	5.98	0.17
7-2	M1070	I		11019	6.24	0.19
8-1	M1070	II		11019	4.91	0.15
8-2	M1070	II		11019	5.21	0.20
9-1	M1070	II		11019	4.61	0.18
9-2	M1070	I		11019	5.11	0.33
10-1	M1070	II		11020	4.60	0.24
10-2	M1070	I		11020	5.39	0.25
10-3	M1070	IV		11020	6.18	0.29
11-1	M1070	I		11020	5.52	0.26
11-2	M1070	I		11020	5.75	0.24
12-1	M1070	II		11020	4.57	0.27
12-2	M1070	I		11020	5.41	0.25
13-1	M1070	IV		11020	6.34	0.24
12-2	M1070	IV		11020	6.52	0.25
14-1	M1070	I		11020	5.27	0.23
14-2	M1070	I		11020	5.62	0.25

Spot Number	Mount	Phase Type	U-Pb Spot	Session	δ18O (SMOW) (‰)	2σ (‰)
15-1	M1070	I		11020	5.30	0.24
15-2	M1070	IV		11020	6.40	0.25
16-1	M1070	I		11020	5.77	0.24
16-2	M1070	II		11020	4.56	0.27
17-1	M1070	II		11020	4.57	0.27
17-2	M1070	II		11020	4.79	0.24
17-3	M1070	I		11020	5.12	0.27
18-1	M1070	I		11020	5.61	0.24
19-1	M1070	II		11020	5.36	0.26
19-2	M1070	IV		11020	6.26	0.27
19-3	M1070	II		11020	5.88	0.27
19-4	M1070	III		11020	5.80	0.29
20-1	M1070	II		11020	4.44	0.28
20-2	M1070	I		11020	5.39	0.29
20-3	M1070	II		11020	4.72	0.28
22-1	M1070	II		11020	4.87	0.28
23-1	M1070	II		11020	4.98	0.27
23-2	M1070	II		11020	4.99	0.23
24-1	M1070	I		11020	5.20	0.24
24-2	M1070	II		11020	4.79	0.23
25-1	M1070	II		11020	4.53	0.27
25-2	M1070	II		11020	4.56	0.29
25-3	M1070	II		11020	4.41	0.25
26-1	M1070	II		11020	4.95	0.27
26-2	M1070	II		11020	4.95	0.26
27-1	M1070	II		11020	4.49	0.30
28-1	M1070	I		11020	5.95	0.29
29-1	M1070	I		11020	5.53	0.27
29-2	M1070	I		11020	5.35	0.30
30-1	M1070	I		11020	5.09	0.27
31-1	M1070	II		11020	4.86	0.25
31-2	M1070	III		11020	4.47	0.27
32-1	M1070	II		11020	4.82	0.27
32-2	M1070	I		11020	5.84	0.26
33-3	M1093	I	S1425 33-5	11094C	6.08	0.17
33-4	M1093	I		11094C	5.21	0.17
34-3	M1093	I	S1425 34-8	11094C	5.83	0.20
34-4	M1093	II	S1425 34-7	11094C	4.69	0.20
35-3	M1093	I	S1425 35-6	11094C	5.10	0.18
36-2	M1093	II	S1425 36-5	11094C	4.44	0.16
37-2	M1093	II	S1425 37-5	11094C	4.80	0.19

Spot Number	Mount	Phase Type	U-Pb Spot	Session	δ18O (SMOW) (‰)	2σ (‰)
38-1	M1093	I	S1425 38-3	11094C	6.14	0.17
39-1	M1093	II	S1425 39-2	11094C	4.60	0.18
40-1	M1093	I		11094C	4.92	0.20
40-2	M1093	I		11094C	5.21	0.16
40-3	M1093	I		11094C	5.30	0.21
41-1	M1093	II	S1425 41-4	11094C	4.38	0.22
41-2	M1093	I	S1425 41-5	11094C	6.03	0.18
42-1	M1093	II	S1425 42-3	11094C	4.82	0.17
42-2	M1093	II		11094C	5.01	0.19
43-1	M1093	II	S1425 43-3	11094C	4.72	0.17
43-2	M1093	II		11094C	5.40	0.19
44-1	M1093	III		11094C	6.20	0.23
44-2	M1093	II		11094C	4.48	0.21
45-1	M1093	II		11095	4.86	0.15
45-2	M1093	IV		11095	6.46	0.16
46-1	M1093	I	S1425 46-4	11095	5.88	0.18
46-2	M1093	II	S1425 46-7	11095	4.34	0.15
47-1	M1093	III	S1425 47-5	11095	6.38	0.14
47-2	M1093	I	S1425 47-6	11095	5.45	0.15
47-3	M1093	I		11095	5.87	0.19
47-4	M1093	IV		11095	6.81	0.15
48-1	M1093	I	S1425 48-1	11095B	6.02	0.37
48-2	M1093	I	S1425 48-2	11095B	6.40	0.34
49-1	M1093	II	S1425 49-2	11095B	4.74	0.27
50-1	M1093	III	S1425 50-2	11095B	6.08	0.28
51-1	M1093	II	S1425 51-5	11095B	4.25	0.24
51-2	M1093	II	S1425 51-3	11095B	4.47	0.26
52-1	M1093	II		11095B	4.93	0.25
52-2	M1093	IV	S1425 52-3	11095B	6.30	0.23
53-1	M1093	I	S1425 53-4	11095B	5.91	0.26
53-2	M1093	II	S1425 53-3	11095B	4.34	0.24
54-1	M1093	II	S1425 54-3	11095B	4.84	0.25
54-2	M1093	IV	S1425 54-2	11095B	6.35	0.24
55-1	M1093	III		11095B	4.94	0.26
55-2	M1093	II	S1425 55-3	11095B	4.63	0.24
56-1	M1093	II		11095B	4.60	0.24
56-2	M1093	I		11095B	5.66	0.25
57-1	M1093	III	S1425 57-4	11095B	6.11	0.25
57-2	M1093	II	S1425 57-2	11095B	4.75	0.25
58-1	M1093	I	S1425 58-5	11095B	5.42	0.26
58-2	M1093	IV	S1425 58-3	11095B	6.19	0.24

Spot Number	Mount	Phase Type	U-Pb Spot	Session	δ18O (SMOW) (‰)	2σ (‰)
59-1	M1093	I		11095B	6.01	0.24
59-2	M1093	II		11095B	5.21	0.26
60-1	M1093	I	S1425 60-2	11095B	5.75	0.23
61-1	M1093	I	S1425 61-2	11095B	5.57	0.24
62-1	M1093	I	S1425 62-3	11106	5.36	0.20
62-2	M1093	IV	S1425 62-4	11106	6.20	0.19
63-1	M1093	III	S1425 63-3	11106	6.07	0.18
64-1	M1093	II		11106	4.60	0.17
64-2	M1093	I		11106	6.07	0.19
65-1	M1093	II	S1425 65-3	11106	4.70	0.21
65-2	M1093	I		11106	5.67	0.24
66-1	M1093	I	S1425 66-3	11106	5.26	0.19
66-2	M1093	I		11106	5.92	0.23
67-1	M1093	II		11106	4.75	0.18
67-2	M1093	III		11106	6.29	0.20
68-1	M1093	I		11106	5.48	0.21
68-2	M1093	II	S1425 68-1	11106	4.65	0.18
69-1	M1093	IV	S1425 69-2	11106	6.22	0.18
70-1	M1093	I	S1425 70-2	11106	5.53	0.19
71-1	M1093	II		11106	4.93	0.21
72-1	M1093	II	S1425 72-1	11106	4.59	0.19
72-2	M1093	III	S1425 72-2	11106	6.35	0.16
73-1	M1093	II	S1425 73-2	11106	4.54	0.19
74-1	M1093	III		11107	6.22	0.25
74-2	M1093	II		11107	4.66	0.25
75-1	M1093	I	S1425 75-1	11107	5.88	0.29
75-2	M1093	II	S1425 75-3	11107	4.63	0.25
76-1	M1093	I		11107	5.76	0.24
76-2	M1093	II		11107	4.53	0.24
77-1	M1093	II	S1425 77-3	11107	4.60	0.25
77-2	M1093	I		11107	5.02	0.24
78-1	M1093	I	S1425 78-4	11107	6.11	0.27
78-2	M1093	II	S1425 78-3	11107	5.56	0.24
79-1	M1093	III		11107	6.04	0.26
79-2	M1093	II		11107	4.80	0.28

* heavily altered zircon material

Supplementary Table 4. Trace-element analyses of TC3 (S1425) zircons by SIMS

Spot Number	33-1	34-1	34-2	35-1	35-2	36-1	37-1	37-2	39-1	44-1	46-1
Correlated U-Pb Spot	S1425 33-5	S1425 34-8	S1425 34-7	S1425 35-6	S1425 35-5	S1425 36-5	S1425 37-3	S1425 37-4	S1425 39-2	S1425 44-3	S1425 46-4
Phase Type	I	I	II	I	II	II	II	II	II	III	I
P (ppm)	217.97	201.78	126.01	147.77	167.85	154.71	143.76	155.62	204.84	92.66	277.15
Ca	2.18	2.27	1.15	2.49	26.92	2.24	1.51	1.07	1.9	28.76	61.44
Ti	6.56	6.22	4.5	2.31	4.02	2.95	3.7	3.86	6.92	7.27	93.49
Y	3033	2699	739	2036	863	865	779	795	1265	331	4154
Zr	468769	467406	463070	476069	481673	471885	454708	452659	476851	449787	450701
Ba	0.31	0.2	0.2	0.03	1.09	0.25	0.3	0.19	0.27	0.86	11.97
La	0.05	0.04	0.02	0.01	10.01	0.01	0.01	0.02	0.03	1.9	12.96
Ce	4.22	4.04	3.44	3.38	30.39	3.24	3.29	3.27	4.45	11.23	92.44
Pr	0.21	0.25	0.02	0.14	3.77	0.03	0.04	0.05	0.08	1.43	13.69
Nd	3.6	3.54	0.58	2.6	16.8	0.99	0.5	0.7	1.16	8.37	94.26
Sm	8.14	7.26	1.24	5.87	8.34	1.7	1.24	1.22	2.8	4.76	69.85
Eu	1.39	1.16	0.15	1.04	1.31	0.26	0.19	0.2	0.35	1.2	15.28
Gd	58.15	53.64	11.17	39.74	20.8	13.26	11.56	12.14	18.67	9.65	163.55
Tb	21.46	18.7	4.01	14.26	7.36	4.85	4.69	4.5	7.14	2.75	46.85
Dy	254.78	231.46	55.71	170.94	76.24	65.11	60.68	60.62	96.55	28.05	448.6
Ho	100.59	89.1	23.35	67.42	29.44	28.25	25.63	24.41	41.25	9.84	149.8
Er	457.22	399.76	114.56	302.01	138.81	129.19	117.61	119.96	191.51	47.49	605.66
Tm	86.92	76.58	23.33	60.05	28.05	27.73	24.64	24.72	39.99	11.31	109.62
Yb	695.07	606.87	193.31	465.28	233.4	228.59	205.44	205.51	331.85	108.86	829.97
Lu	149.25	130.85	44.54	102.25	52.29	51.92	46.46	45.81	75.91	28.09	177.38
Sum (REE)	1841.05	1623.25	475.43	1234.99	657.01	555.13	501.98	503.13	811.74	274.93	2829.91
Hf	8660	8682	9441	9110	9818	9222	8838	8835	8837	11502	8137
Th	151.63	125.73	34.74	87.26	38.79	48.45	43.55	42.42	84.22	63.59	194.52
U	238.42	203.29	92.24	151.6	99.98	115.22	101.45	102.21	165.75	351.57	442.3
Ce/Ce*	9.96	9.77	41.61	21.85	1.20	45.26	39.80	25.02	21.98	1.65	1.68
Eu/Eu**	0.19	0.18	0.12	0.21	0.30	0.17	0.15	0.16	0.15	0.54	0.44

* calculated using the following equation: $Ce_N/sqrt(La_N*Pr_N)$ and normalization values from McDonough and Sun (1995)

** calculated using the following equation: $Eu_N/sqrt(Sm_N*Gd_N)$ and normalization values from McDonough and Sun (1995)

Spot Number	46-2	47-1	51-2	51-2	55-1	58-1	66-1	81-1	81-2	84-1	85-1
Correlated U-Pb Spot	S1425 46-7	S1425 47-5	S1425 51-3	S1425 51-4	S1425 55-4	S1425 58-3	S142 66-3	S1425 81-4	S1425 81-1	S1425 84-1	S1425 85-1
Phase Type	II	III	II	I	III	IV	I	I	II	IV	IV
P (ppm)	200.51	58.6	152.44	219	265.68	77.19	414.31	198.59	177.56	80.65	40.88
Ca	42.44	6.79	2.09	80.87	31.13	20.31	1.89	4.52	5.15	8.53	4.2
Ti	13.23	10.3	6.33	70.12	26.49	389.45	15.29	3.62	4.04	4.25	1.92
Y	1004	246	819	2331	3108	371	3973	2136	2250	236	143
Zr	443163	475793	480139	451813	447307	476431	480329	465233	462116	451845	451516
Ba	1.58	0.28	0.19	7.99	1.46	0.78	0.23	0.31	0.54	0.37	0.24
La	14.93	0.02	0.01	3.08	5.66	6.53	0.06	0.75	0.37	0.59	0.03
Ce	49.32	1.06	3.33	10.57	23.3	14.05	21.61	6.04	5.71	3.57	0.67
Pr	6.11	0.01	0.03	1.41	3.37	2.6	0.29	0.42	0.4	0.3	0.01
Nd	29.56	0.16	0.72	9.92	23.61	15.88	4.83	3.96	4.16	1.49	0.12
Sm	9.92	0.23	1.58	9.81	19.28	7.23	8.82	5.79	6.26	0.7	0.25
Eu	2.07	0.12	0.26	2.72	3.17	1.54	1.65	1	0.87	0.14	0.1
Gd	22.77	2.37	11.4	50.34	76.62	15.66	69.46	38.62	40.74	3.58	2.36
Tb	7.34	0.94	4.82	17.63	25.54	4.02	28.01	13.84	15.71	1.16	0.83
Dy	80.66	12.47	63.7	193.86	273.88	33.82	344.73	171.12	187.14	13.54	12.04
Ho	32.62	6.14	27.3	76.94	104.86	11.33	137.24	68.44	76.22	5.95	3.79
Er	152.64	38.27	128.47	341.41	452.92	47.98	598.41	313.02	339.43	33.96	13.81
Tm	31.01	10.28	26.52	67.1	83.08	9.18	114.14	61.83	64.59	8.37	2.24
Yb	251.42	113.24	219.27	523.1	630.72	75.19	885.76	491.41	506.44	80.41	16.73
Lu	56.12	32.15	49.47	115.58	133.51	16.63	180.42	113.47	110.53	21.34	3.09
Sum (REE)	746.49	217.46	536.88	1423.47	1859.52	261.64	2395.43	1289.71	1358.57	175.1	56.07
Hf	8296	12242	9745	8397	8436	11952	8664	8577	8868	11910	12237
Th	50.03	36.99	47.57	137.41	240.54	18.62	1333.14	91.31	98.49	60.26	0.79
U	116.9	893.55	116.81	219.53	385.14	257.82	840.29	185.46	178.34	410.38	245.84
Ce/Ce*	1.25	18.13	46.51	1.23	1.29	0.82	39.63	2.60	3.59	2.05	9.36
Eu/Eu**	0.42	0.50	0.19	0.37	0.25	0.44	0.20	0.20	0.17	0.27	0.40

* calculated using th

** calculated using t

Spot Number	85-2	87-1
Correlated U-Pb Spot	S1425 85-3	S1425 87-1
Phase Type	IV	I
P (ppm)	41.54	225.28
Ca	27.7	2.27
Ti	4.49	6.67
Y	337	3106
Zr	445633	449027
Ba	0.6	0.38
La	4.06	0.02
Ce	18.49	4.21
Pr	2.74	0.23
Nd	15.74	3.31
Sm	8.69	8.21
Eu	2.03	1.28
Gd	18.66	59.39
Tb	5.23	21.83
Dy	43.87	266.08
Ho	11.97	102.47
Er	40.12	447.53
Tm	6.63	87.22
Yb	46.15	673.4
Lu	10.2	145.94
Sum (REE)	234.58	1821.12
Hf	11492	8104
Th	1.86	152.51
U	213.06	238.46
Ce/Ce*	1.34	15.02
Eu/Eu**	0.49	0.18

* calculated using th

** calculated using t

Chapter 3: No evidence for Hadean continents within Earth's oldest evolved rock unit

Introduction:

An understanding of the amount of continental crust produced in the first 500 million years of Earth history, and the resulting chemical differentiation of the Hadean silicate Earth, are critical parameters for developing robust geodynamical and geochemical models of our planet. Recently, evidence that the silicate Earth experienced very early (~4.4 Ga) differentiation was discovered in the form of anomalous ^{142}Nd isotope signatures in ancient rocks (Caro et al., 2003; O'Neil et al., 2008; Rizo et al., 2012; Roth et al., 2014) as well as differences between bulk Earth and chondrites (Boyet and Carlson, 2005). These signatures, along with the recovery of zircon grains dated up to 4.4 Ga (Froude et al., 1983; Harrison, 2009; Valley et al., 2014), imply that some type of crust existed on the young Earth though the chemical nature of that crust, whether largely mafic, felsic, or some mixture, remains contentious (e.g., Bowring and Housh, 1995; Harrison, 2005; Kamber et al., 2005; Kemp et al., 2010; Kemp et al., 2015). To date, the rock and mineral record that represents Hadean crust consists of putative 4.4–4.3 Ga mafic rocks from northeastern Canada (O'Neil et al., 2008) and rare 4.0–4.4 Ga detrital zircon grains recovered from quartzites and conglomerates in western Australia (e.g., Froude et al., 1983; Valley et al., 2014). However, the age and composition of crystalline source rocks for Hadean detrital zircons remains controversial (e.g., Harrison, 2009; Kemp et al., 2010), as does the true age of the mafic rocks from Canada (Roth et al., 2013).

A variety of features preserved within Hadean detrital zircons motivated the uniformitarian view that the Hadean Earth contained voluminous amounts of nascent continental crust, possibly formed by tectonic processes similar to those that operate today (Mojzsis et al., 2001; Harrison, 2009). An opposing view contends that Hadean crust was dominantly composed of mafic rocks formed and recycled in a geodynamic environment distinct from the modern Earth (Kamber et al., 2003; 2005; O'Neill et al., 2007; Kemp et al., 2010). These endmember scenarios allow us to formulate a testable hypothesis. If large volumes of Hadean continental crust did indeed exist, that crust would be expected to have compositions comparable to that which dominates the Archean (2.5–4.0 Ga) crustal rock record, namely the tonalite-trondhjemite-granodiorite (TTG) suite of granitoids that are characterized by high

La/Yb ratios (Martin, 1986; Moyen and Martin, 2012). However, coherent units of Hadean rocks are extraordinarily rare, hence the difficulty in evaluating the true extent and composition of Hadean crust.

We have defined a new Hadean lithological unit—the Idiwhaa tonalitic gneiss—within the Acasta Gneiss Complex (AGC), Slave craton, Canada (Reimink et al., 2014), which represents the oldest precisely dated zircon-bearing Hadean rock suite known on Earth. We use whole rock compositions in concert with high precision dating and oxygen isotope, trace element, and U-Pb-Hf isotope analyses of well-characterized 4.02 Ga zircons to test the model of expansive amounts of nascent continental crust on the Hadean Earth.

The Idiwhaa unit

The Idiwhaa unit is dominated by tonalitic gneiss with a range of silica contents (~58–70 wt.% SiO_2). The major-, minor-, and trace-element systematics of these samples are consistent with derivation via fractional crystallization of primary basaltic magma (Reimink et al., 2014; Supplementary Materials; Figs. 3.9–3.11). All samples within the Idiwhaa unit share critical features including high FeO, relatively low Al_2O_3, and flat rare-earth-element (REE) patterns that are distinct from Archean TTGs (e.g., Moyen and Martin, 2012) and require high degrees of crystal fractionation of a water-poor basaltic magma at relatively shallow crustal levels (Grove and Kinzler, 1986). Notably, the Idiwhaa whole-rock REE patterns are in equilibrium with the REE patterns measured in >4.0 Ga igneous zircon extracted from the unit, indicating that whole-rock compositions can reliably be used to infer the petrogenetic history of this unit (Reimink et al., 2014). Additionally, the whole-rock Sm-Nd isotope systematics of the Idiwhaa unit samples are consistent with the zircon U-Pb crystallization age as well as zircon Hf isotope data (Figs. 3.14–3.16).

The petrogenetic history of the Idiwhaa unit involves partial melting of the Hadean mantle to generate a primary basaltic magma that underwent extensive crystal fractionation and possibly some degree of crustal assimilation prior to reaching zircon saturation. This iron-enriched magma then crystallized two phases (I and II) of igneous zircon. Phase I zircons are unzoned cores mantled by oscillatory-zoned Phase II mantles. Secondary ion mass spectrometric (SIMS) data indicate that both phases of zircon crystallized at ~4.02 Ga (Reimink et al., 2014). Using a novel technique for analyzing

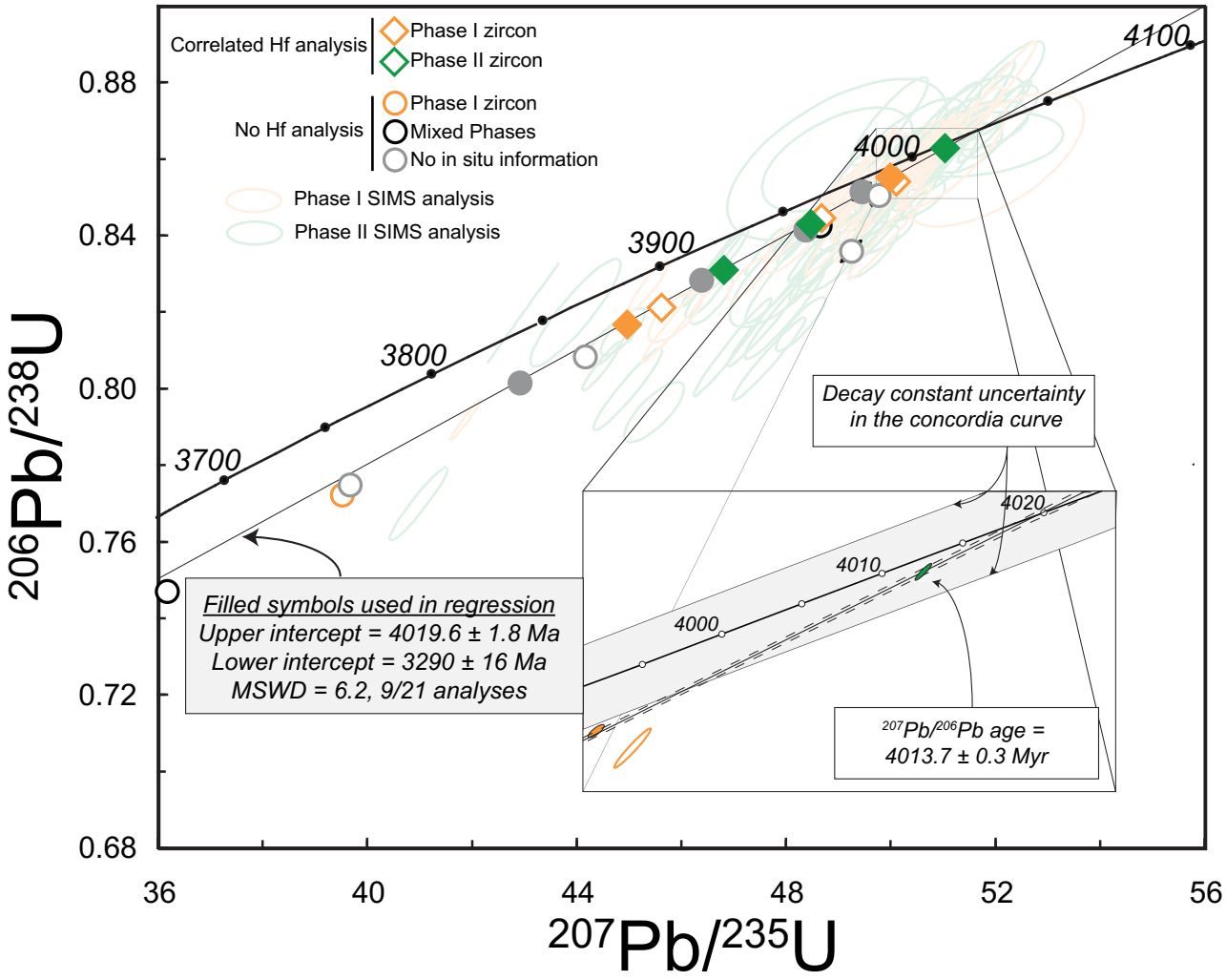

Figure 3.1: Concordia plot of CA-ID-TIMS U-Pb data from the TC3 zircons. Large, light-colored ellispes are previously reported SIMS U-Pb plotted at the 1σ level for clarity (Reimink et al., 2014). Symbols for the TIMS data correspond to zircon phases, as established by electron microprobe analysis of Y contents (Methods). Symbol sizes for TIMS data are much greater than the typical 2σ uncertainty ellipse. A regression line through the nine analyses containing the least amount of recent Pb-loss (shown with filled symbols) yields an upper intercept age of 4019.6 ± 1.8 Ma and a lower intercept age of 3290 ±16 Ma with an MSWD of 6.2. These ages are in excellent agreement with previously published SIMS data, and document the crystallization age of this unit. Inset shows one analysis that plots completely within the uncertainty band of concordia, and returns a $^{207}Pb/^{206}Pb$ age of 4013.7 ± 0.3 Ma, a minimum age of crystallization for the Idiwhaa unit.

complex zircons (Methods), we refine the crystallization age to a highly precise chemical abrasion, isotope dilution, thermal ionization mass spectrometric (CA-ID-TIMS) age of 4019.6 ± 1.8 Ma (Fig. 3.1). Phase I zircon records $\delta^{18}O$ values (5.6 ± 0.35‰; n = 62) indistinguishable from mantle zircon (5.3 ± 0.3‰; Valley et al., 1998) whereas Phase II has distinctly lower values (4.7 ± 0.3‰; n = 66; Reimink et al., 2014; Fig. 3.2B). This ~0.9‰ drop in $\delta^{18}O$ between two zircon phases with identical ages indicates that pre-existing crust was altered at high temperature by meteoric waters, and that this altered crust was assimilated shortly after the magma reached zircon saturation (Bindeman and Valley, 2001; Reimink et al., 2014).

Hf isotope analysis

The Hf isotope composition of igneous zircon in the 4.02 Ga Idiwhaa unit allows us to evaluate the pre-existing crust and mantle at the time of magma intrusion. Specifically, Phase I zircon, with its mantle-like oxygen isotope composition, allows us to appraise the nature of the mantle source region that gave rise to the parental Idiwhaa magma and attempt to evaluate any early-stage crustal assimilation that this magma may have undergone prior to zircon crystallization. In addition, a comparison of the Hf isotope compositions of Phase I and II zircon allows us to evaluate the nature of pre-existing AGC crust that the parent magma intruded and assimilated. The weighted mean of initial εHf values from Phase I zircon is -2.07 ± 0.51 (2SE, MSWD = 2), a value indistinguishable from that of Phase II (-1.88 ± 0.26 2SE MSWD = 0.96; Supplementary Information–Methods), despite their distinct oxygen isotope compositions (Fig. 3.2B). These Hf isotope data are in broad agreement with previous data from other, younger AGC rocks (3.5–3.9 Ga) that reveal unradiogenic Hf isotopic compositions (Amelin et al., 1999; Iizuka et al., 2009). However, given our detailed petrological knowledge of the Idiwhaa unit, its Hf isotopic compositions require distinctly different explanations to those previously derived from zircon Hf isotope data alone.

The Hf isotope data presented here indicate that the crustal assimilation process occurring between Phase I and II zircon crystallization could not have involved more ancient (e.g., >4.2 Ga) continental crust of TTG-like composition, characterized by low Lu/Hf and hence low εHf at 4.02 Ga. In such a scenario, the drop in $\delta^{18}O$ values observed in Phase II growth would have significantly

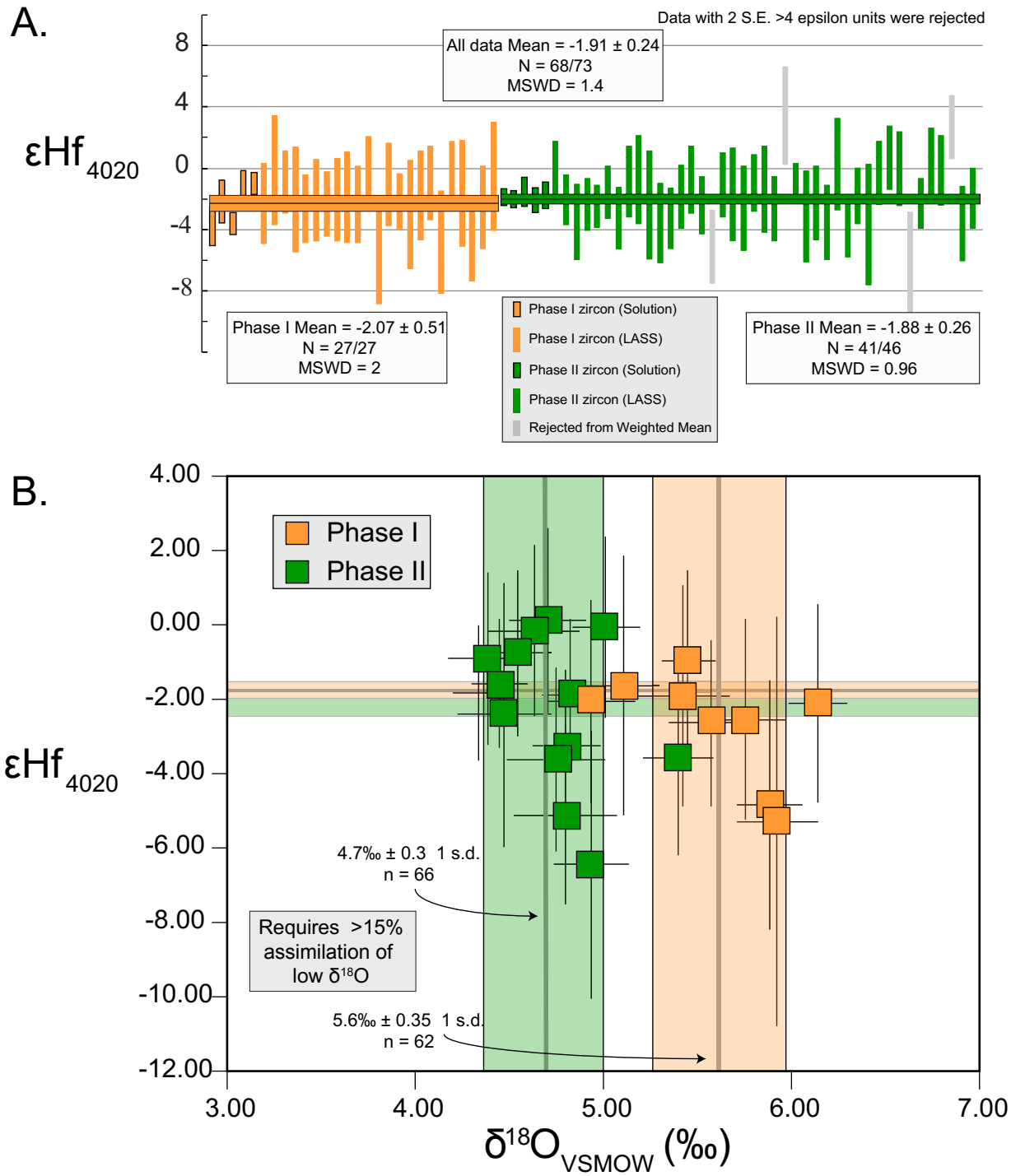

Figure 3.2: Hafnium isotope analysis from 4020 Ma zircon grains from Idiwhaa sample TC3. A. Epsilon Hf values for two igneous phases of TC3 zircon. There is no discernable difference be`tween Phase I and Phase II zircon material, suggesting the assimilant material was not significantly older evolved crust. B. Correlated Hf and O isotope data from TC3 zircon material are plotted by growth phase. Also shown are the weighted means and 1 s.d. for both εHf and $\delta^{18}O$ of both phases. The 0.9‰ shift in $\delta^{18}O$ requires ~35% assimilation between magmatic zircon growth stages. All uncertainties are fully propagated 2 sigma uncertainties including decay constant and age correction uncertainty. Solution Hf data comes from dissolved zircons while LASS refers to *in situ* laser-ablation split stream (Methods).

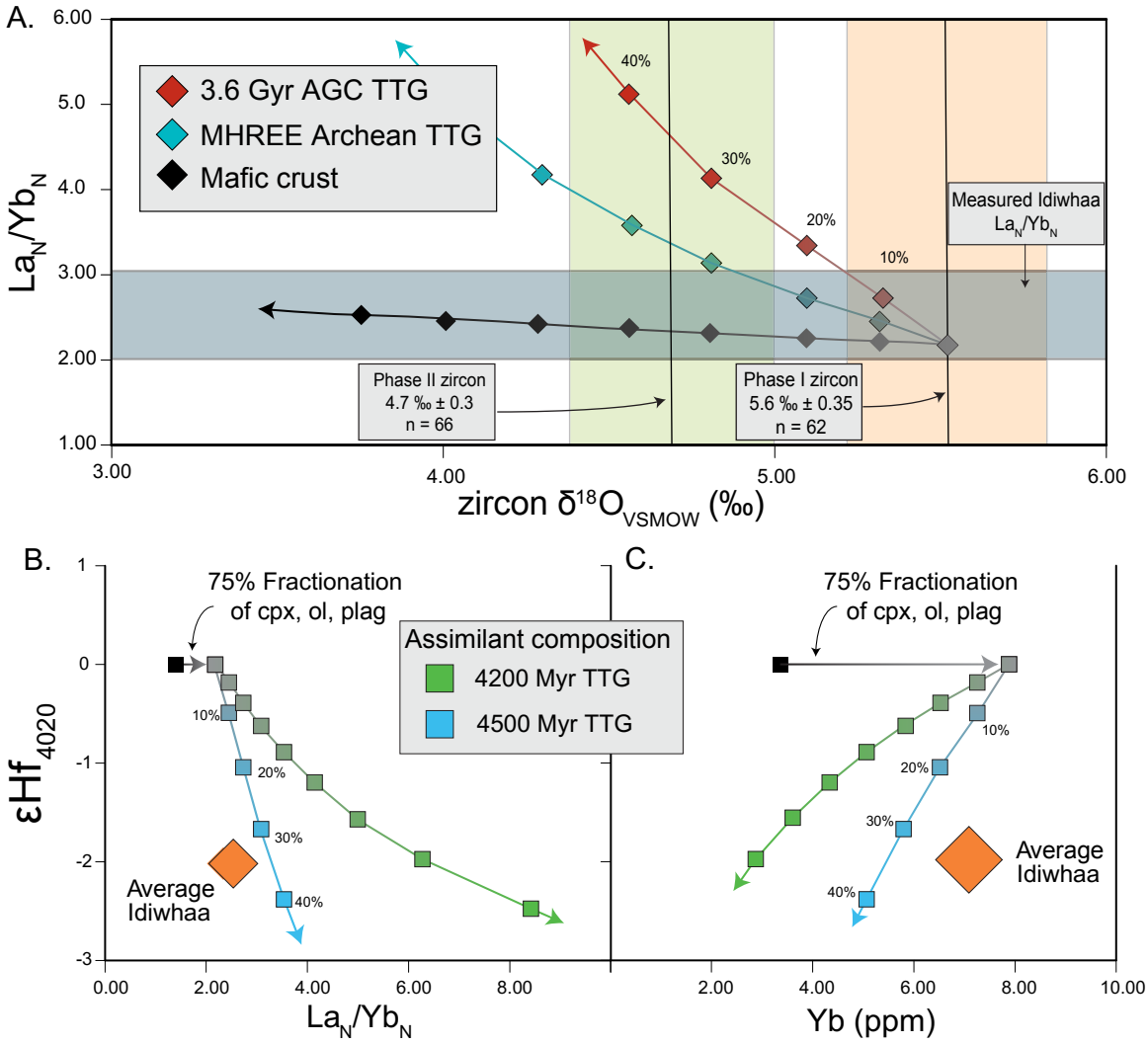

Figure 3.3: Modeling of REE systematics of the average Idiwhaa low SiO_2 unit samples in concert with zircon $\delta^{18}O$ and εHf. a, input parameters start with basaltic liquid with flat chondrite-normalized REE patterns that then undergoes fractionation of 10% olivine, 30% plagioclase, and 60% clinopyroxene. The resulting liquid is then mixed with various types of crust. The MHREE Archean TTG field is the average composition (Moyen and Martin, 2012) while the 3.6 Ga AGC TTG is the average composition of TTG-like rock units found within the Acasta Gneiss Complex that have crystallization ages ~3.6 Ga (Methods). Mafic crust is defined by an average basaltic andesite within an Icelandic volcanic center (Mancini et al., 2015). B, C. Modeling starting with the same modeled fractionated liquid compositions in an attempt to reconcile the measured -2 εHf value of Idiwhaa unit zircons with assimilation of MHREE Archean TTG (Moyen and Martin, 2012). Based on this analysis, we can rule out typical Archean continental crust as the assimilant in either the post-zircon assimilations step or any possible assimilation prior to zircon saturation. Idiwhaa unit symbols represent the mean and one standard deviation of the population.

decreased the εHf value for Phase II relative to Phase I zircon and generated much more fractionated whole-rock REE patterns than those observed in the Idiwhaa unit (Fig. 3.3A). Moreover, small differences in the slope of REE patterns in Phase I and Phase II zircons are opposite to that expected if the late-stage assimilant had a TTG-like composition, and are instead consistent with assimilation of pre-existing mafic, as opposed to felsic, crust (Fig. 3.12–13).

The subchondritic εHf value of -2 ± 0.5 recorded by Phase I zircon is surprising, particularly given that the whole-rock composition of the Idiwhaa unit and the mantle-like O-isotope composition of Phase I zircon can be accounted for by closed-system fractional crystallization of mantle-derived basaltic magma without assimilation of crustal rocks. Following the arguments outlined above for Phase II zircon, a -2 unit shift in εHf values (recorded in Phase I zircon) from an assumed primary chondritic value of 0 εHf for the Hadean mantle cannot be generated by assimilation of TTG-like crust prior to zircon saturation without significantly changing the REE systematics of the Idiwhaa unit (Fig. 3.3B-C).

Discussion

Hafnium isotope data presented here record a distinctly unradiogenic signature, but one that is not derived from interactions with putative Hadean continental crust. An enriched (i.e., low Lu/Hf) reservoir must have played a role in the petrogenesis of the Idiwhaa unit, though this reservoir cannot have been highly evolved (high SiO_2) because melting of an evolved composition is inconsistent with the major-element characteristics of the Idiwhaa unit. However, early-formed enriched mafic-ultramafic material, potentially analogous to the lunar KREEP source (Taylor et al., 2009), may be suitable. Assimilation of—or mantle interaction with—such a reservoir would lower the εHf value of the magma prior to Phase I zircon saturation while not significantly affecting the major- and trace-element characteristics of the Idiwhaa unit (Fig. 3.3). Our suggestion of an early Earth dominated by mafic crust may seem to contradict the presence of older Hadean zircons from both western Australia (Froude et al., 1983; Harrison, 2009) and Acasta (Iizuka et al., 2006). However, the source rock of these zircons remain enigmatic and contentious. Zircons with characterisitcs similar to detrital and xenocrystic grains so far identified from the Hadean may be formed by intracrustal reworking of Hadean mafic crust, forming small pockets of evolved material (Kamber et al., 2003; Kemp et al., 2010) markedly different

from modern (and Archean) continental crust.

The intermediate SiO_2 contents of most Idiwhaa unit samples combined with a lack of evidence for interaction with typical Archean continental crust indicates that negative εHf values can be produced on the early Earth without interactions with putative continental crust. The lack of significant Hadean continental crust suggested here is consistent with recent estimates for the composition of melts parental to the Jack Hills zircon suite (Kemp et al., 2010), the mafic composition of presumed 4.4 Ga rocks from Nuvvuaggituq (O'Neil et al., 2008), and a lack of evidence for significant Hadean continental crust in other ancient gneiss terranes (Kamber et al., 2005; Kemp et al., 2015). Collectively, available data support a vision of the Hadean Earth dominated by long-lived enriched mafic crustal and mantle reservoirs (Fig. 3.4). Such a setting, where evolved rock suites capable of producing zircon are formed by fractionation/assimilation and partial melting of much older mafic crust (Kamber et al., 2003; Kemp et al., 2010; Kamber, 2015), is not drastically different from processes forming evolved compositions on an Icelandic-like protocontinent (Kroner, 1985; Reimink et al., 2014). Additionally, the longevity of enriched Hadean crustal or mantle domains such as those documented here and in Greenland (Rizo et al., 2012), along with their depleted counterparts (Caro et al., 2003; Debaille et al., 2013; Roth et al., 2014), implies that processes operating on the earliest Earth were distinctly different from the modern paradigm of plate tectonics, and may suggest unique geodynamic settings (O'Neil et al., 2007).

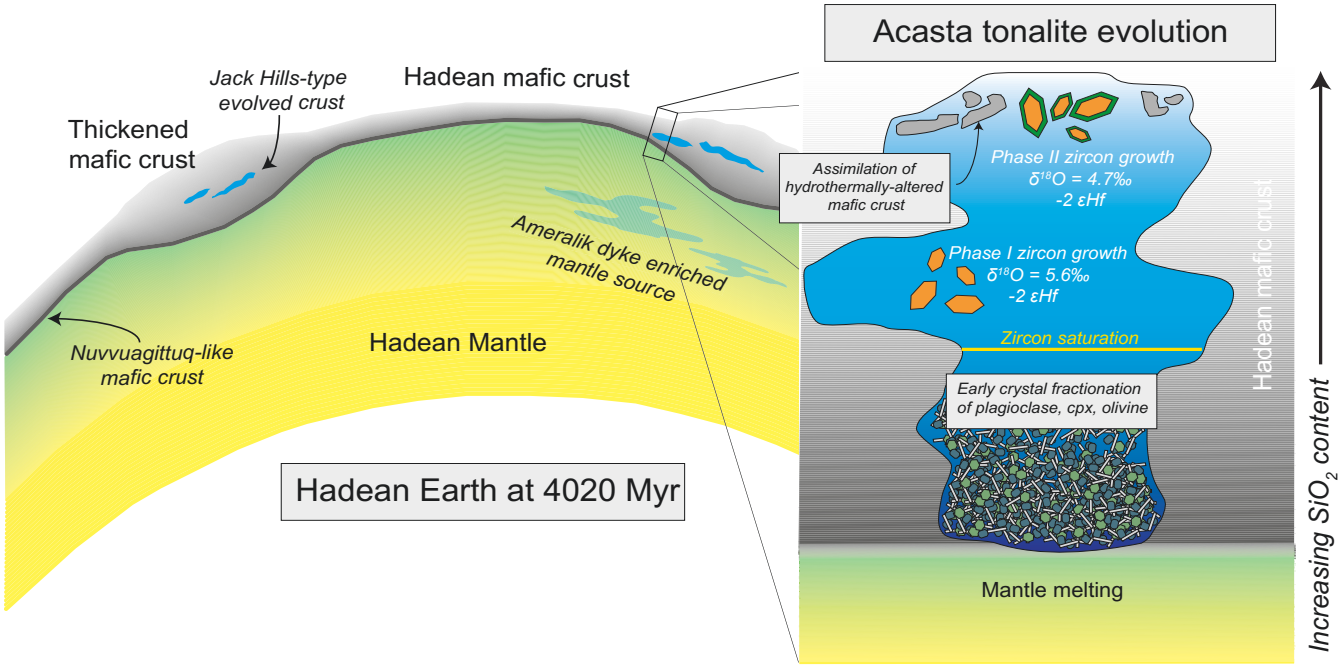

Figure 3.4: A schematic representation for the composition of the Hadean Earth at 4.02 Ga. The crustal budget is dominated by mafic compositions, except for small pockets that derive evolved components by reworking of mafic crust (Jack Hills; Kemp et al., 2010) and high degrees of crystal fractionation (Acasta). The inset shows our model for the petrogenesis of the Idiwhaa unit. Key points include mantle melting to form a mafic or ultramafic parental magma that then undergoes a significant amount of fractional crystallization producing a high FeO intermediate magma. Once zircon saturation is reached, igneous zircon with mantle-like oxygen isotope ratios, -2 εHf, and high REE contents is formed (Phase I). Following this, at least 15% assimilation of low $\delta^{18}O$ material occurs, lowering the magmatic oxygen isotope composition by ~0.9‰, but not detectably changing the εHf value. The -2 εHf value of both phases of zircon documented here may be formed by interactions with either long-lived mafic crust (Nuvvuagittuq; O'Neil et al., 2008) or and early-enriched mantle (Ameralik source; Rizo et al., 2012).

Methods:

Sample Descriptions:

All samples reported here were identified in the field and later geochemically as parts of the same 4.02 Ga rock unit, a unit we have previously identified and informally termed the Idiwhaa tonalitic gneiss (Reimink et al., 2014). These samples share the following key field characteristics; they are relatively melanocratic, containing significant biotite and amphibole, as well as some garnet, and have 2–3 modal % of magnetite. Some Idiwhaa samples have higher SiO_2, and in the field contain small, augen-like feldspar and quartz laths. Throughout the mapped area, higher silica Idiwhaa units are found a few meters to the west of the more mafic components, though the contact is often obscured (Chapters 2, 4). Sample locations are given in Table 3.1.

Whole-rock elemental analysis:

Whole-rock samples were cut into slabs, removing all obvious alteration and crosscutting veins. Slabs were then crushed using a combination of hand sledge and alumina shatterbox. Powders were at the Washington State University GeoAnalytical Laboratory using XRF (Johnson et al., 1999) and ICP-MS (Knaack et al., 1994). XRF analyses typically have limits of detection that are <0.2 wt.% for all major elements and <4 ppm for the trace elements measured using this method. Uncertainties in analyses for trace element by ICPMS are ~10% but closer to 5% for the rare-earth-elements.

Modeling of assimilation processes:

We employed petrogenetic modeling to evaluate changes in whole-rock and zircon geochemistry through differentiation and assimilation processes that may have influenced the Idiwhaa unit.

First, we used the MELTS software package (Gualda et al., 2012; Ghiorso and Gualda, 2015) in order to evaluate the effect of significant fractional crystallization on a primary basaltic magma. No unique scenario gives rise to compositions identical to the Idiwhaa unit, however, to model the potential assimilation process, we used 75% fractional crystallization of an assemblage consisting of 30% plagioclase, 10% olivine, and 60% clinopyroxene. This assemblage is broadly similar to those required to generate modern magmas with similar major-element compositions to the Idiwhaa unit (Wood, 1978; Jónasson and Jonasson, 2005; Mancini et al., 2015) using starting magma compositions

similar to those documented in primitive Icelandic basalts (e.g., Mancini et al., 2015). Significant plagioclase is required to generate the very high FeO, as well as the moderate negative Eu anomalies observed in the Idiwhaa unit, and some olivine is also likely required as the Ni contents of the Idiwhaa unit are low, even compared to modern icelandite magmas (Jónasson and Jonasson, 2005; Mancini et al., 2015). Using the partition coefficients for plagioclase, clinopyroxene, and olivine applicable to basaltic liquids (Rollinson, 1993) we can model the La, Yb, and Hf concentrations for residual liquids given the fractionating assemblage described above. We then used this resulting magma to assess the effect of possible assimilation of Archean TTG-like material.

The resulting modeled liquid composition evolved to ~55 wt% SiO_2, lower than the measured Idiwhaa unit, but leaving ample room for assimilation of more evolved Archean TTG-like crust to generate the observed Idiwhaa SiO_2 contents. The modeled liquid composition contained ~26 ppm La, ~8 ppm Yb, and ~9 ppm Hf. Using these parameters as one end member input, and various compositions of TTG-like material, we are able to perform simple mixing calculations to derive the elemental and isotopic composition of a potential magma-assimilant mixture. The Archean MHREE (Medium Heavy-Rare-Earth-Element) TTG composition was taken from (Moyen and Martin, 2012) and the average AGC TTG was taken from Chapter 4.

The 0.9‰ decrease in $\delta^{18}O$ between the two igneous zircon phases requires varying amounts of assimilation depending on the assumed assimilant composition. Even in Iceland, a location on the modern Earth that contains a high proportion of low $\delta^{18}O$ rocks, whole-rock and corresponding zircon $\delta^{18}O$ values lower than 3.0‰ are uncommon (e.g., Muehlenbachs et al., 1974; Eiler, 2001; Carley et al., 2014). Therefore, we use a $\delta^{18}O$ value of 3.0‰ as a reasonable estimate of the composition of the assimilant, derived from the peak in distribution of Icelandic zircon $\delta^{18}O$ values from Carley et al., (2014). Using a starting zircon composition of 5.7‰ and an assimilant value of 3.0‰, ~35% assimilation is required to generate the observed drop in $\delta^{18}O$ values. Using Archean MHREE TTG as an assimilant (Moyen and Martin, 2012), any amount of assimilation that is great enough to produce a 0.9‰ drop in the zircon $\delta^{18}O$ values will raise the resulting composition's La_N/Yb_N above those observed in the Idiwhaa unit.

The same input parameters noted above be used to model any assimilation occuring prior to the magma becoming saturated in zircon (i.e., prior to Phase I zircon crystallization). In this case, we

are interested in determining if the -2 εHf value of zircons with mantle-like oxygen isotope ratios can be produced by assimilation of Archean TTG-like rocks. Again using the REE and Hf concentrations of MHREE Archean TTGs (Moyen and Martin, 2012), we can model how the Hf isotope composition of this reservoir would change depending on the age of TTG extraction from a chondritic reservoir. When mixing with the magma's assumed chondritic Hf isotope composition, the amount of assimilation required to generate a -2 εHf change using a TTG assimilant creates a drop in Yb content and corresponding La_N/Yb_N outside of the range observed for the Idiwhaa unit (Figure 3.3B–C). In contrast, assimilation of mafic crust is able produce a -2 decrease in εHf without significantly altering the La_N/Yb_N of the resulting melt. However, based on our modeling procedure, only very ancient (>4400 Ma) mafic crust could produce this change with any petrologically reasonable amount of assimilation.

Sm-Nd isotopic analysis:

Rock powders were accurately weighed and totally spiked with a known amount of mixed ^{150}Nd-^{149}Sm tracer solution - this tracer was calibrated directly against the Caltech mixed Sm/Nd normal described by (Wasserburg et al., 1981). Dissolution occurred in mixed 24N HF + 16N HNO_3 media in sealed PFA Teflon vessels at 160 ºC for five days. The fluoride residue was converted to chloride with HCl, and Nd and Sm were separated by conventional cation and HDEHP-based chromatography. Chemical processing blanks are <200 picograms of either Sm or Nd, and were insignificant relative to the amount of Sm or Nd analyzed for any rock sample. Further details can be found in (Creaser et al., 1997) and (Unterschutz et al., 2002).

The isotopic composition of Nd was determined in static mode by Multi-Collector ICPMS (Schmidberger et al., 2007). All isotope ratios were normalized for variable mass fractionation to a value of $^{146}Nd/^{144}Nd = 0.7219$ using the exponential fractionation law. The $^{143}Nd/^{144}Nd$ ratio of samples were presented here relative to a value of 0.511850 for the La Jolla Nd isotopic standard, monitored by use of an in-house Alfa Nd isotope standard for each analytical session. Sm isotopic abundances are measured in static mode by Multi-Collector ICP- Mass Spectrometry, and are normalized for variable mass fractionation to a value of 1.17537 for $^{152}Sm/^{154}Sm$ also using the exponential law. Using the same isotopic analysis and normalization procedures above, we analyzed the Geological Survey of Japan Nd isotope standard "Shin Etsu: J-Ndi-1" (Tanaka et al., 2000) which has a $^{143}Nd/^{144}Nd$ value of 0.512107

± 7 relative to a LaJolla $^{143}Nd/^{144}Nd$ value of 0.511850, when normalized to $^{146}Nd/^{144}Nd = 0.7219$. The value of $^{143}Nd/^{144}Nd$ determined for the JNdi-1 standard conducted during the analysis of the 5 samples reported here was 0.512097 ± 8 (2SE); the long-term average value was 0.512098 ± 11; 1SD, n = 67, past six years). Using the mixed ^{150}Nd-^{149}Sm tracer, the measured $^{147}Sm/^{144}Nd$ ratios for the international rock standard BCR-1 range from 0.1380 to 0.1382, suggesting reproducibility for $^{147}Sm/^{144}Nd$ of ~ ± 0.1% for real rock powders. The value of $^{147}Sm/^{144}Nd$ determined for BCR-1 is within the range of reported literature values by isotope dilution methods.

LASS Hf methods:

Concurrent Hf and U-Pb isotope measurements using laser-ablation split stream (LASS) protocols broadly followed the methods of Fischer *et al.* (2014). Measurements were made in the Arctic Resources Laboratory at the University of Alberta. Laser ablation of zircon material was conducted using a Resonetics Excimer 193 nm laser operating with an energy fluence of 5 J/cm^2 and 10 Hz with a 33 µm diameter spot size. U-Pb isotope measurements were made on a Thermo Element-XR mass spectrometer using a single Secondary Electron Multiplier (SEM) detector in peak hopping mode while Hf isotope measurements were made on a Thermo Neptune *Plus* using multiple Faraday detectors with

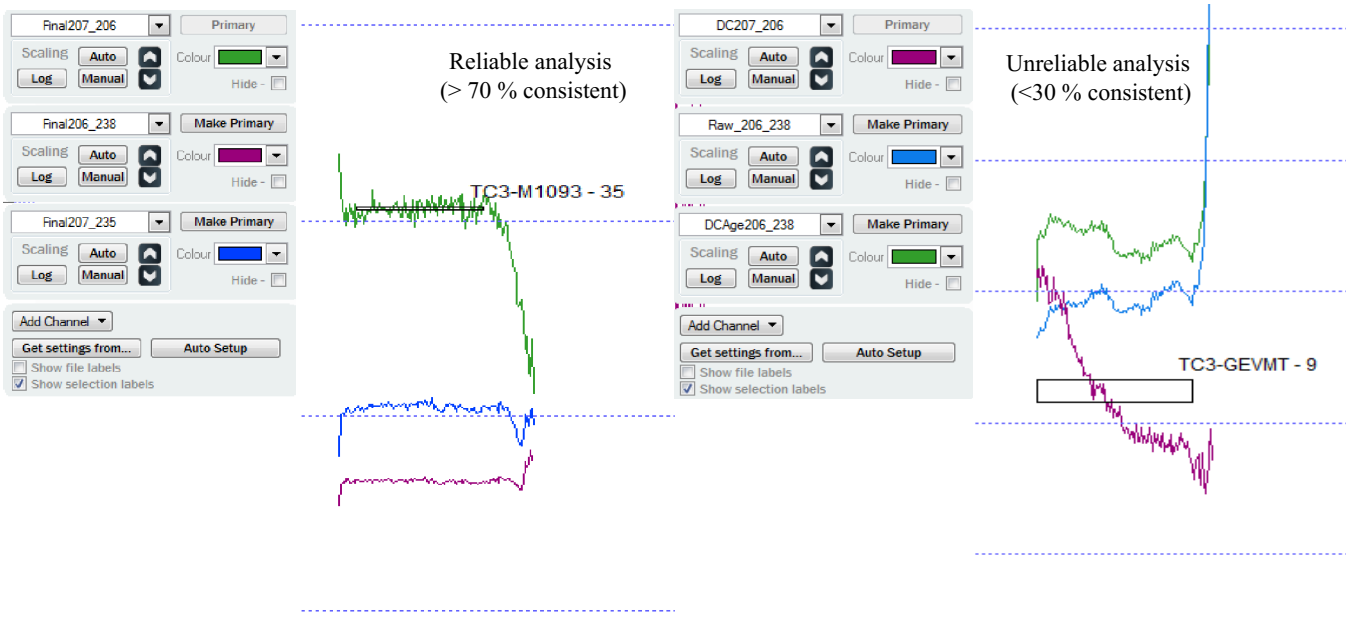

Figure 3.5: LASS U-Pb analyses from two examples showing the variability of isotope ratios throughout the run. Reliable analyses such as that on the left, had consistent U-Pb-Hf isotope systematics throughout >70% of the analysis time. Analyses where <30% had consistent isotopic, such as that on the right, were deemed unreliable and cut from future evaluation. Images were taken directly from the Iolite software package.

10^{11} Ω amplifiers operating in static mode. Analysis time was typically 90 seconds consisting of 20 second of background followed by 40 second of ablation and 30 second of washout. Both Hf and U-Pb data were processed offline using Iolite v3 software where integrations were chosen very carefully and trimmed, if necessary to remove portions with highly variable U-Pb or Hf isotope compositions.

Both Hf and U-Pb mass bias corrections were calibrated using Plesovîce zircon as a primary reference material (Sláma et al., 2008). Due to the large corrections necessary for the isobaric interference of ^{176}Yb on the ^{176}Hf signal combined with relatively low Yb contents in Plesovîce zircon (average ^{176}Yb/^{177}Hf = 0.006), it is absolutely essential to evaluate other reference materials with higher concentrations of Yb (Fisher et al., 2011). Without analysis of zircons with high and variable Yb contents, the accuracy of the Yb interference correction cannot be properly evaluated. Here we monitored the Yb interference correction by analysis of a variety of natural and synthetic zircons. FC1 and R33 are natural zircons with Yb contents in the range of most natural zircons (Fisher et al., 2014). Synthetic, Yb-doped zircons (MUN1 and MUN4; Fisher et al., 2011) were also evaluated, with MUN4 containing a much greater concentration of Yb than the TC3 zircon unknowns analyzed here. The measured ^{176}Yb/^{173}Yb ratio was iteratively calibrated to optimize the Yb-interference correction, monitored by five zircon reference materials with variable Yb contents (Plesovîce, FC1, R33, MUN1, MUN4) in the same manner as that of Fisher et al. (2014).

Due to the complexity of TC3 zircons, the quality of each analysis was evaluated by monitoring both U-Pb and Pb-Pb ratios throughout the length of the analysis. Consistent U-Pb and Pb-Pb ratios throughout each run indicated that the analysis volume likely consisted on one growth phase, and the Hf-isotope composition of the integration represents that of a particular domain. The relative reliability of each analysis was evaluated using the length of selected integration relative to the total ablation duration. Analyses where a substantial (>70%) portion of the analysis was retained were deemed highly reliable. Analyses where ~30–70% of the run was consistent in both U-Pb and Hf composition were deemed moderately reliable and retained while analyses with <30% of the ablation returning consistent data were deemed unreliable and cut from further evaluation (Fig. 3.5).

All εHf values and fully propagated uncertainties were calculated using the equations from Ickert (2013). All εHf values were calculated at 4020 Ma, the time of igneous crystallization determined by ID-TIMS analysis (Fig. 3.1). This method is valid for several reasons. First, although zircon material

with igneous zoning characteristics does contain small degrees of Pb-loss (Fig. S5–6 of Reimink et al., 2014), this Pb-loss likely does not affect the Hf-isotope composition of the zircon. Hf is incorporated into the zircon crystal structure during crystallization and is lattice bound (Hoskin, 2003) whereas Pb is created by decay of U. Heating or fluid interactions may mobilize Pb from the zircon structure while Hf should remain unaffected (Lenting et al., 2010; Amelin et al., 2011). Additionally, LASS U-Pb analyses have substantially lower precision than other methods reported here (ID-TIMS) and previously (SIMS; Reimink et al., 2014). Therefore, we deem both the ID-TIMS and SIMS U-Pb age more accurate and reliable than the U-Pb ages generated during LASS, which was collected only to monitor the heterogeneity of the zircon volume analyzed during laser ablation Hf analyses. Results for TC3 zircon that had fully propagated uncertainties in εHf exceeding 4 epsilon units were filtered out of all future calculations (n = 4).

CA-ID-TIMS U-Pb and solution Hf

An aggressive chemical abrasion procedure was applied to zircons extracted from the TC3 sample. In order to test the efficacy of the chemical abrasion technique on these very ancient zircons, we first applied a relatively simple chemical abrasion procedure comprising 48 hours annealing at 1000 ºC followed by 19 hours of chemical abrasion in full strength HF and trace HNO_3 at 190 ºC. These grains were analyzed for only their U-Pb systematics following the methods described below, with no *in situ* information collected from these samples (grey symbols in Fig. 3.1).

A second batch of TC3 zircons was first characterized using cathodoluminescence imaging and EPMA analyses of Y contents prior to solution work. This process entailed annealing at 1000 ºC for 48 hours in a muffle furnace, followed by 24 hours of chemical abrasion at 190 ºC in HF with trace HNO_3 in 200 µl Savillex microcapsules. Fragments of grains that survived the chemical abrasion procedure were mounted in epoxy and imaged using both CL and BSE to identify grains that were dominated by single growth zones. Previous SIMS trace-element measurements of Phase I and II zircon material identified a dramatic difference in Y contents (Phase I = 2000–3000 ppm Y; Phase II = 700–800 ppm Y; Reimink et al., 2014). This large difference is quantitatively detectable by EPMA analysis; therefore we analyzed the mounted and imaged grains for Y contents by EPMA (University of Alberta) to assist in identification of the two igneous growth zones. Major elements (Zr, Si) as well as a suite of trace

elements (Ca, Y, P, Yb) were analyzed on the JEOL 8900R EPMA using a 15 kV accelerating voltage and 50 nA of current. Using these data, grains with simple zoning patterns and consistent trace-element concentrations were plucked out of the mount and subjected to a further five hours of chemical abrasion in concentrated HF and trace HNO_3 at 190 ºC. This was performed to clean the abraded grains of any residual epoxy and attempt to further reduce discordance. The grain fragments were then ready for dissolution following the procedures of Wotzlaw et al. (2013) and Davies et al. (2014).

Prior to dissolution, all of the grain fragments were ultrasonically cleaned in 7 mol/L HNO_3 four times for 30 minutes each before being loaded into the 200 µl Savillex microcapsules and spiked with ~5 ml of EARTHTIME ^{202}Pb-^{205}Pb-^{233}U-^{235}U spike. The grains were dissolved in Parr bombs at 210 °C with ~70 µl of HF and trace HNO_3 for 48 hours. After dissolution, the samples were dried down on a hot plate and re-dissolved in 6 mol/L HCl. The capsules were then placed back in Parr bombs and back in to the oven at 180°C overnight to convert the solutions to a chloride form. After the final dissolution step, the microcapsules were dried down again and the samples were re-dissolved in 3 mol/L HCl before loading onto pre-cleaned and conditioned micro-columns. U and Pb were extracted from the dissolved zircons using a modified version of the HCl-based anion exchange column chemistry (Krogh, 1973) where the volumes of elutants are greatly reduced to minimize the blank. The Zr and Hf fractions were collected in cleaned TPX beakers for Hf isotope analysis (see below). The U-Pb fraction was dried down with 1 drop of 0.02 mol/L H_3PO_4 and then loaded onto outgassed Re filaments with a modified version of the Si-Gel emitter (Gerstenberger and Haase, 1997) with 0.02 mol/L H_3PO_4, 0.2 mol/L HBr and 3 ml per 50 ml solution of Merk colloidal silicic acid. The U and Pb isotopic measurements were conducted on a Thermo TRITON thermal ionization mass spectrometer. Pb and U were both measured in dynamic mode on a MassCom secondary electron multiplier. Pb fractionation was controlled using a $^{202}Pb/^{205}Pb$ of 0.99924 ± 0.00027 (1σ absolute; Condon et al., 2015). U was measured as an oxide and the interferences from $^{233}U^{18}O^{16}O$ on $^{235}U^{16}O_2$ were corrected using an $^{18}O/^{16}O$ of 0.00205. U-Pb ratios were calculated relative to a $^{235}U/^{205}Pb$ of 100.23 ± 0.023% (1σ abs) and the $^{238}U/^{235}U$ of the samples was assumed to be 137.818 ± 0.045 (2σ: Hiess et al., 2012). All common Pb was assumed to be procedural blank and was routinely low throughout the study. The blank isotopic composition was $^{206}Pb/^{204}Pb$ = 18.102 ± 0.377, $^{207}Pb/^{204}Pb$ = 14.452 ± 0.469 and $^{208}Pb/^{204}Pb$ = 38.011 ± 1.13 and was determined through an average of long-term blank measurements in the U-Pb lab at the University of Geneva. All

data reduction was performed using Tripoli and Redux software (Bowring et al., 2011), which utilizes the algorithms of McLean et al. (2011).

Solution Hf isotope analyses were performed at the University of Geneva using a Thermo Neptune plus MC-ICP-MS equipped with nickel cones (Thermo "X series") under dry plasma conditions using a Cetac "Aridus 2" desolvation unit and a Teflon nebulizer (~50 ml/min uptake rate). The 9 Faraday cups were configured to measure the following masses at low mass resolution (m/_m ~450): 172 (L4), 173 (L3), 175 (L2), 176 (L1), 177 (C), 178 (H1), 179 (H2), 180 (H3), 181 (H4). The Hf (plus Zr and trace element) fractions collected during anion column chemistry were re-dissolved in 2% HNO_3 and trace HF to minimize memory effects and were then transferred to clean autosampler PFA microtubes. The Plešovice zircon natural reference material (Sláma et al., 2008) was run throughout the campaign at a Hf concentration of ~10 ppb. A series of Plešovice stock solutions doped with variable amounts of Yb (ICP-MS standard solution, Merck KGaA, Germany) so that Yb concentrations range from 0.5 to 2 ppb (i.e. $0.001 < {}^{173}Yb/{}^{177}Hf < 0.5$), was prepared in order to optimize the ^{176}Yb interference correction (D'Abzac et al., in prep.) and to determine a normalization factor from the reference value of (Sláma et al., 2008). Several grains of Temora-2 (Wu et al., 2006) were also measured as secondary standards and normalized following the factor determined by the doped Plešovice.

After the extended chemical abrasion treatment applied to the zircons, the volume of Hf remaining for analysis was small. Therefore we employed short acquisition time measurements for the samples and bracketed each sample with a more concentrated Plešovice analysis measured over a longer time to determine the mass bias of the sample by standard bracketing (D'Abzac et al., in prep.). Sample measurements were made using a 50 x 1 second acquisition time and Plešovice measurements utilized a 60 x 3 second acquisition. The βYb and βHf mass bias coefficients were calculated using an exponential law (Albarede et al., 2004) from the measured $^{172}Yb/^{173}Yb$ and $^{179}Hf/^{177}Hf$ respectively and using natural abundances reference values: $^{172}Yb/^{173}Yb = 1.3534$ and $^{179}Hf/^{177}Hf = 0.7325$ (Blichert-Toft and Albarède, 1997). Mass bias correction on Lu was calculated using βYb (Yuan et al., 2008) and the isobaric interference of ^{176}Lu was removed using the natural abundances of ^{175}Lu (0.97416) and ^{176}Lu (0.02584). The isobaric interference of ^{176}Yb is the most significant and was evaluated from Yb-doped Plešovice solutions by calculating $^{176}Yb/^{173}Yb$ using βYb and using a reference value that is empirically determined for each run by minimizing the drift in corrected $^{176}Hf/^{177}Hf$ ratios for increasing $^{173}Yb/^{177}Yb$

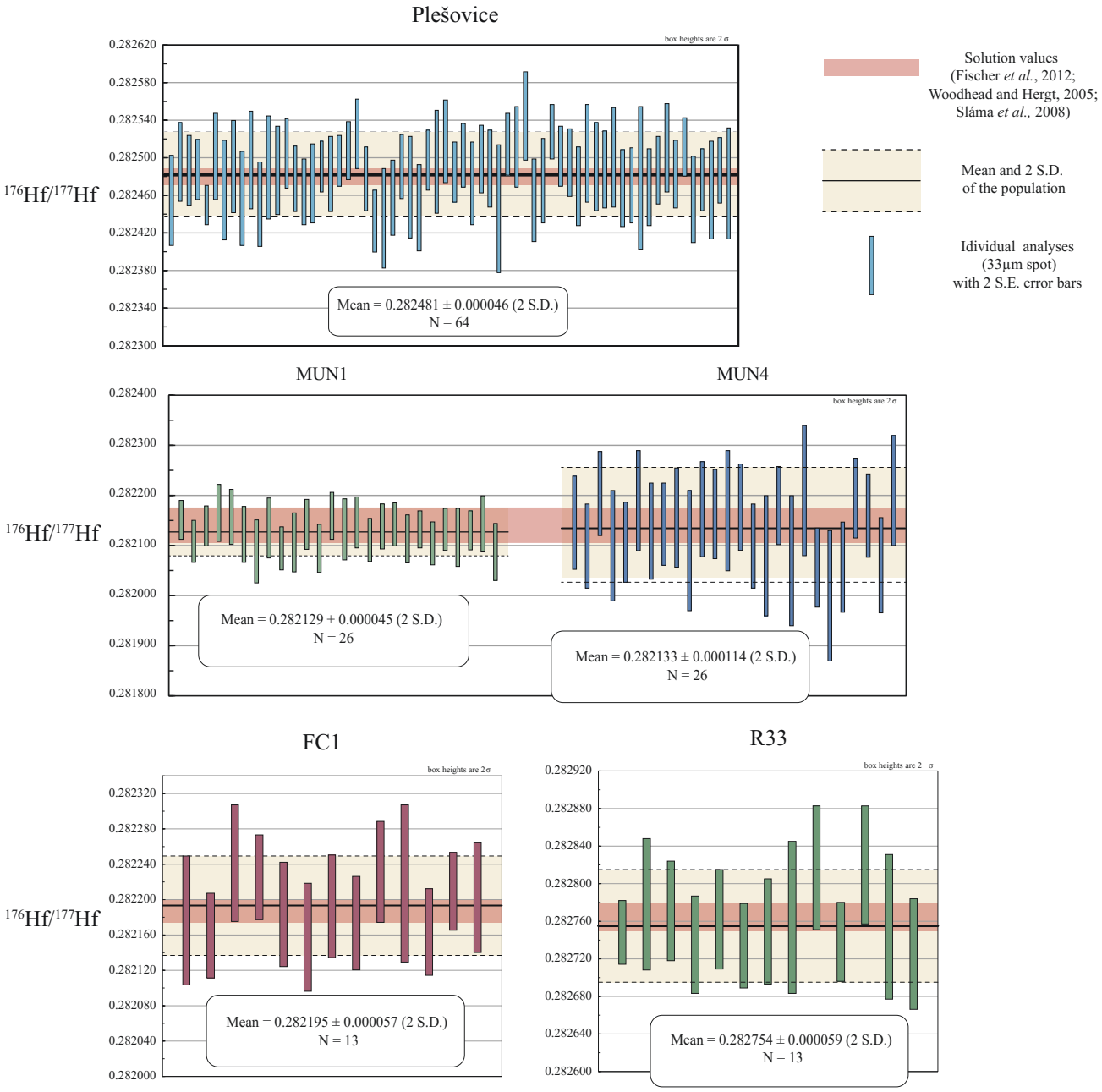

Figure 3.6: LASS Hf isotope results for reference materials analyzed during the LASS campaign. The method accurately and precisely reproduces the accepted solution Hf isotope compositions of each reference material, which contain zircons with a wide span of Yb/Hf ratios.

(D'Abzac et al., in prep.), as shown by Fisher et al. (2014). The efficiency of this correction method was verified by the results obtained with Yb doped Plešovice and Temora-2 zircons. The optimized value of $^{176}Yb/^{173}Yb$ is 0.787000, which is within 0.015% of the natural Yb isotope composition ($^{176}Yb/^{173}Yb$ = 0.786956; Thirlwall and Anczkiewicz, 2004). Correction for ^{176}Hf in-growth due to ^{176}Lu decay has been

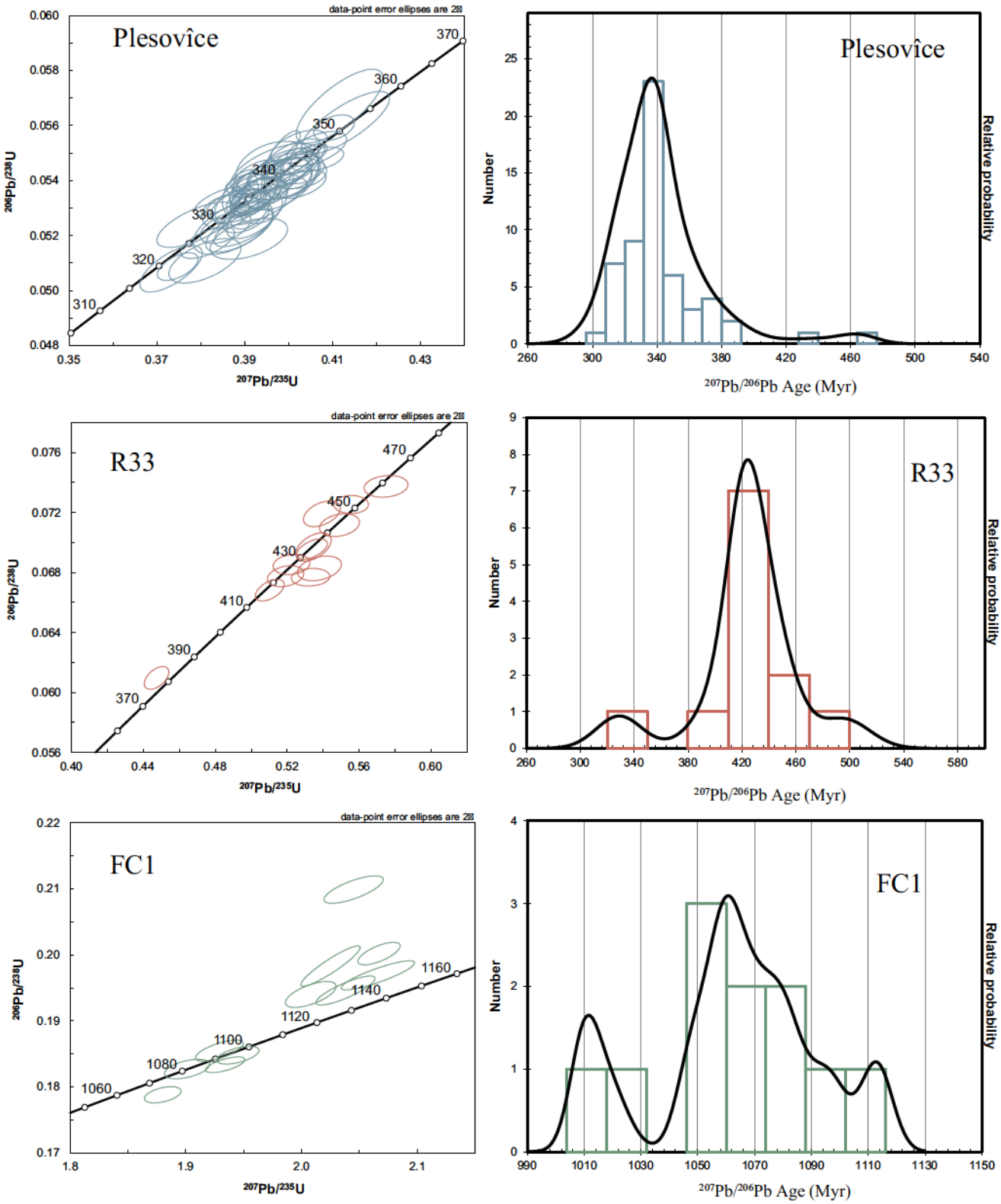

Figure 3.7: Compilation of U-Pb results from reference materials analyzed during the LASS campaign. U-Pb results show accurate reproduction of the U-Pb systematics of the reference materials. However, slight reverse discordance is generated in FC1 material, as well as calculation of younger $^{207}Pb/^{206}Pb$ ratios, indicating a 2-3% bias towards younger $^{207}Pb/^{206}Pb$ ages.

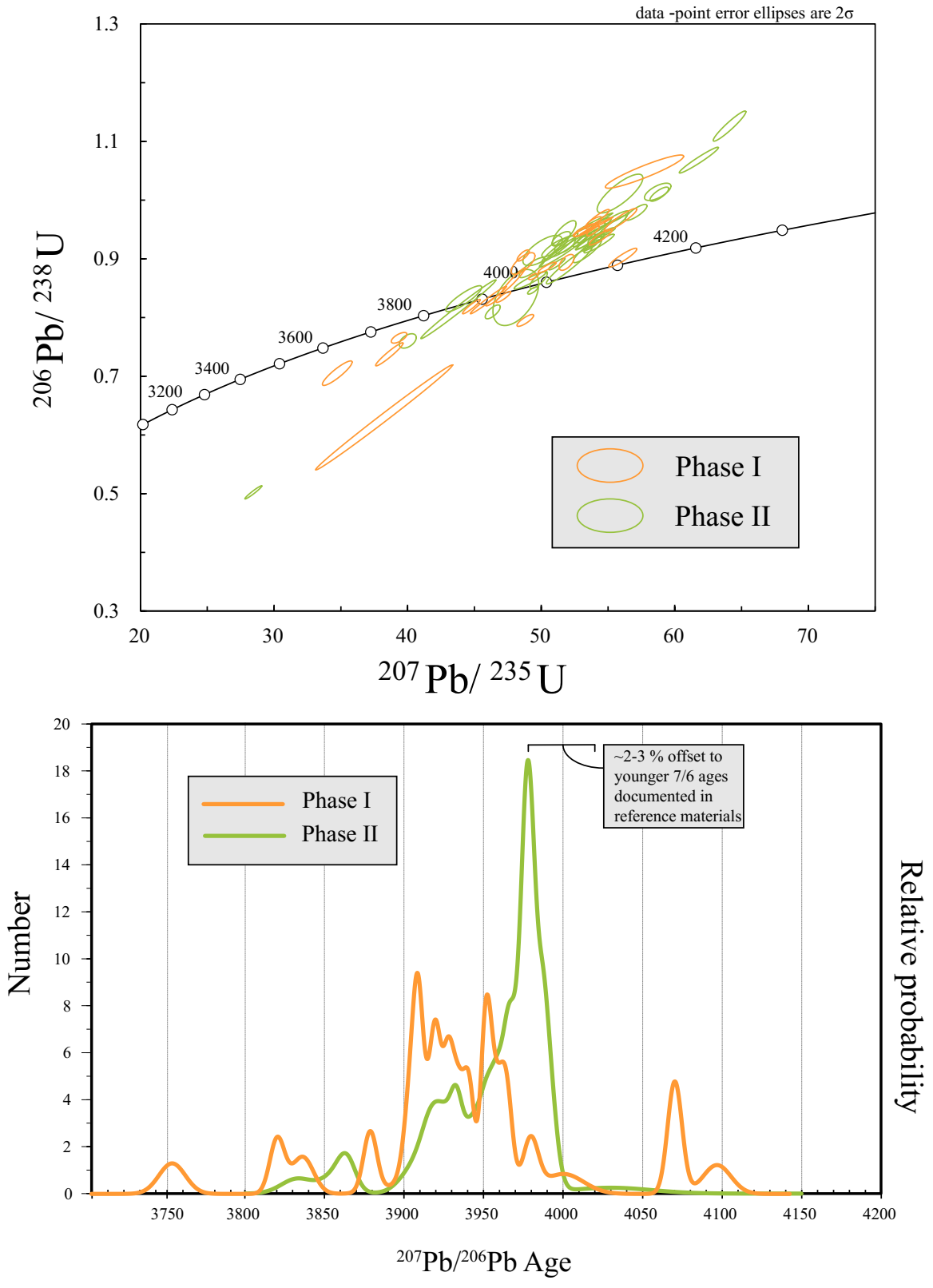

Figure 3.8: U-Pb systematics for TC3 zircon from the LASS method. Similar to FC1 zircon, significant reverse discordance is produced, as well as $^{207}Pb/^{206}Pb$ ages that are ~2-3% younger than those determined by SIMS and TIMS dating (Reimink et al., 2014). Once corrected, the $^{207}Pb/^{206}Pb$ ages of TC3 zircon measured by LASS matches well with the distributions obtained by SIMS analyses (Reimink et al., 2014).

calculated using $^{176}Lu = 1.87\times10^{-11}$ year^{-1} (Scherer, 2001; Söderlund et al., 2004) and the age determined by the ID-TIMS U-Pb dating. During the measurement session, the $^{176}Hf/^{177}Hf$ ratio for Plešovice was 0.282481 ± 40 (2 s.d., n = 11) and the normalized Temora-2 $^{176}Hf/^{177}Hf$ ratio was 0.282666 ± 62 (2 s.d., n = 7).

LASS Hf reference material results:

LASS Hf isotope results for reference materials are reported in Table 3.6. As is commonly seen in laser ablation Hf measurements (Fisher et al., 2014) measured Hf compositions were slightly lower than accepted solution values. A correction ($^{176}Hf/^{177}Hf = +0.000060$) was applied to the entire data set. Additionally, the Yb-interference correction is dependent on the Yb mass bias coefficient measured in each laboratory. We are able to accurately and precisely reproduce the accepted solution Hf isotopic compositions of zircons with a wide range in Yb contents (Fig. 3.6), bracketing the Yb contents of the unknown zircon (TC3).

LASS U-Pb reference material results:

U-Pb analyses of reference materials are reported in Table 3.5 and data for TC3 zircons are reported in Table 3.3. Though we are able to accurately reproduce the ages from young reference materials (Fig. 3.7) some reverse discordance was generated for TC3 zircons and the FC1 reference material (Figs. 3.7–3.8). The cause of this discordance is likely improper calibration of the downhole fractionation of U from Pb. As is typical in laser ablation U-Pb analyses, U and Pb were fractionated throughout each analysis. This factor was corrected for in the Iolite software package using Plesovîce zircon, a young zircon (337 Ma; Sláma et al., 2008) with moderate U contents. The ablation characteristics of Plesovice zircon, as well as other reference zircons used here (R33), are almost certainly different from the 4020 Ma TC3 zircons, which, given their ancient age, have accrued much more radiation damage, resulting in an improper in-run downhole U-Pb fractionation correction. This hypothesis is substantiated by some small reverse discordance imposed on the FC1 data set, a 1099 Ma reference material that likely has more radiation damage than Plesovîce, though not as much as TC3 zircons.

Additionally, there is a small bias (~1–3%) in the measured $^{207}Pb/^{206}Pb$ ages for both FC1

and TC3 zircons. The FC1 $^{207}Pb/^{206}Pb$ ages are all slightly younger than the magmatic age of these grains (1099 Ma; Paces and Miller, 1993) by about 1–3%. At 4020 Ma, this bias represents ~80–100 Ma, precisely the difference between $^{207}Pb/^{206}Pb$ ages measured by LASS reported here and the age distribution of TC3 grains determined by SIMS (Reimink et al., 2014) and TIMS (Fig. 3.1).

TIMS U-Pb Results

TIMS U-Pb results for both the well characterized zircon fragments (described above) and those for the grains that were chemically abraded for 19 hours without characterization are identical. Broadly speaking, all of the analyses (apart from z70 and 19h_z2) fall on a discordia chord with an upper intercept of ~4020 Ma and a lower intercept of ~3290 Ma. However, there is some complexity to this data set and not all points fall on the regression line. Despite our aggressive chemical abrasion, many of the analyses fall slightly below the regression chord reflecting some small degree of recent Pb loss. A regression chord through the analyses with the least recent Pb loss gives an upper intercept age of 4019 ± 1.8 Ma and a lower intercept of 3290 ± 16 Ma (n = 9, MSWD 6.2). We interpret the upper intercept age as the best estimate of the magmatic crystallization age of the Idiwhaa unit.

These upper and lower intercept ages agree well with previous estimates for rock other samples within the AGC (Stern and Bleeker, 1998; Bowring and Williams, 1999) as well as our previous age calculations from SIMS U-Pb analysis of the same zircon population (Reimink et al., 2014). The lower intercept age corresponds well to the ages of large bodies of granite-granodiorite intrusions found a few kilometers west of the Idiwhaa unit (Chapter 4), as well as the age of zircon overgrowths (Stern and Bleeker, 1998; Reimink et al., 2014).

Arguably the most significant aspect of this TIMS dataset is analysis TC3_z38, which lies fully within the uncertainty band of the Concordia curve and represents, as far as we are aware, the first fully concordant TIMS analysis of terrestrial Hadean zircon. Analyses from Phase 1 and Phase 2 grains are indistinguishable, and fall on the same discordia chord indicating that at the resolution of our data these two zircon growth events occurred simultaneously.

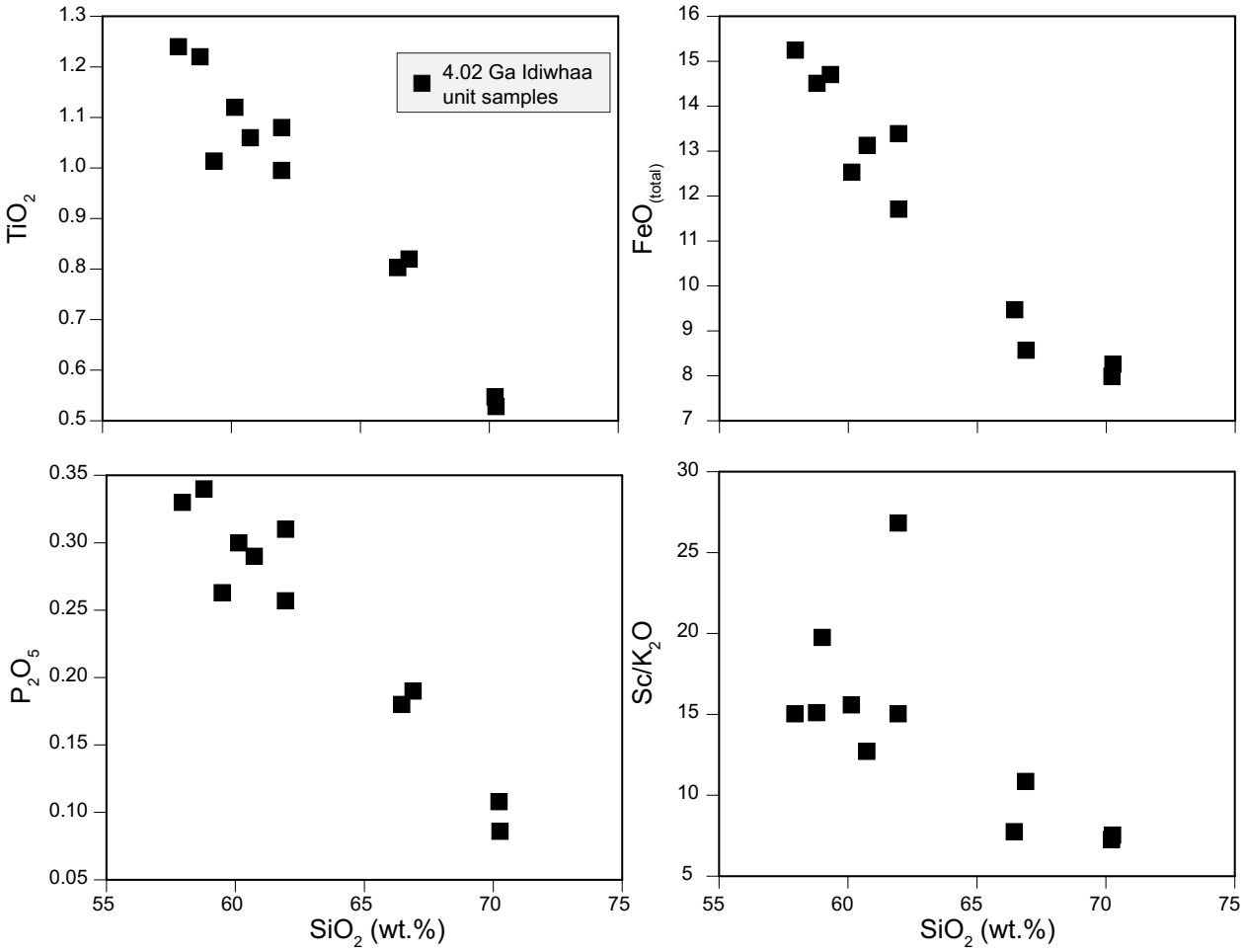

Figure 3.9: Plot of major element trends within the Idiwhaa unit samples. All samples broadly follow typical differentiation trends, with FeO, TiO_2, and P_2O_5 all decreasing with increasing SiO_2. A decrease in Sc/K_2O versus SiO_2 can be attributed to crystallization of a high Sc phase, such as amphibole or pyroxene. Note that even at high SiO_2, the FeO contents of Idiwhaa samples are still quite enriched (~8 wt.%).

Supplementary Discussion:

Whole-rock systematics of Idiwhaa unit samples:

The full suite of Idiwhaa samples contains a variety of SiO_2 contents ranging from 58 wt.% to 71 wt.%. Despite this variability, all samples share important similarities and are consistent with derivation via fractional crystallization (Figs. 3.9–3.11). Increases in most incompatible trace elements, including the high field strength elements with increasing SiO_2 is consistent with derivation by crystal fractionation (Fig. 3.9). Notably, high silica (~70 wt.%) Idiwhaa samples have significantly higher La_N/Yb_N values (7.13 and 6.82) than all other Idiwhaa samples (<3.8). This increase in La_N/Yb_N cannot be produced by assimilation of high La_N/Yb_N material such as Archean TTG, as increases

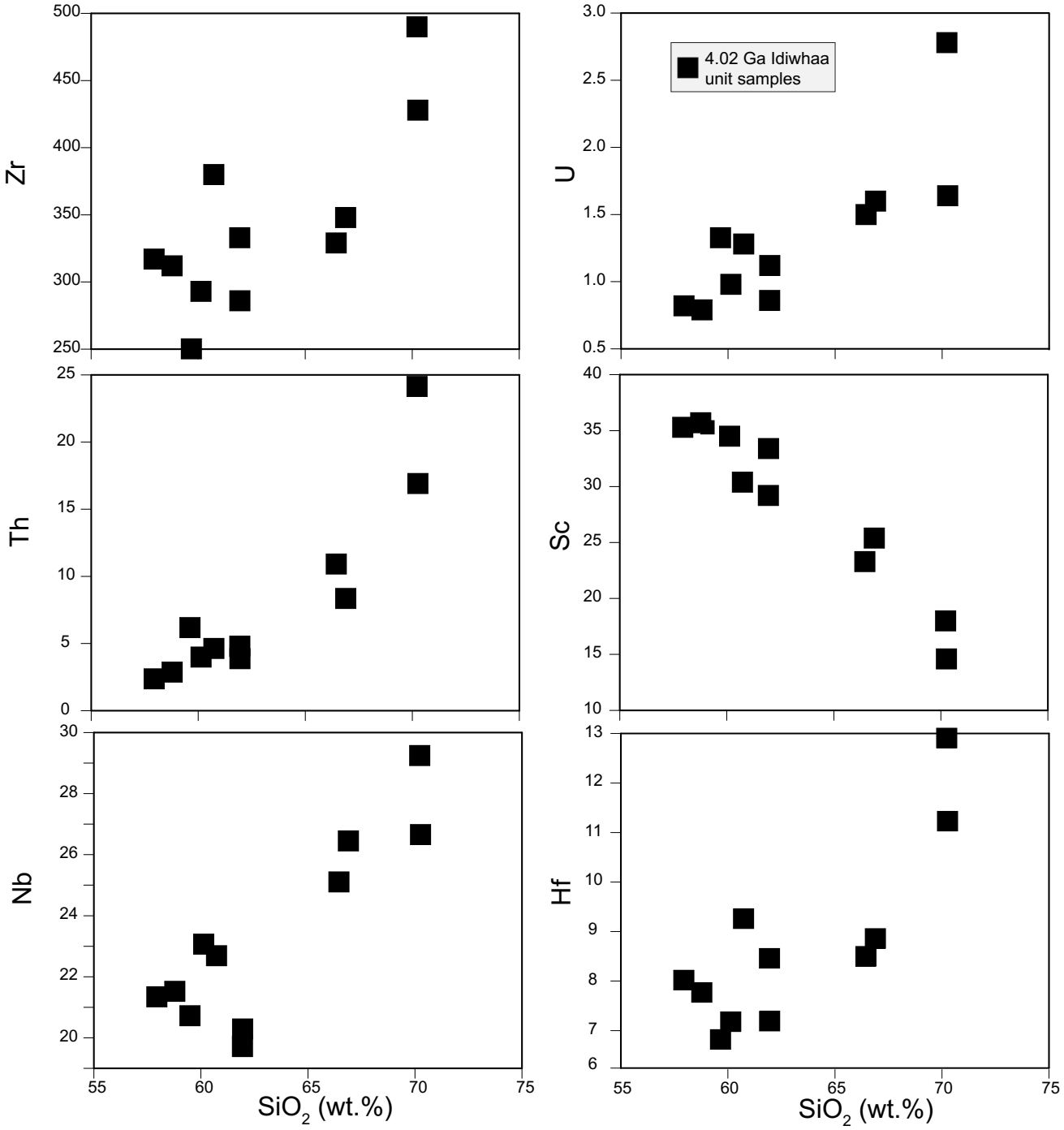

Figure 3.10: Plot showing trace-element systematics of Idiwhaa unit samples with increasing SiO_2. All incompatible trace elements, including the high field strength elements (Zr, Nb, Hf), increase with increasing SiO_2, apart from Sc, which is compatible in pyroxene and amphibole.

in most incompatible elements, including Hf, Nb, and Yb in the high SiO_2 samples rule out this scenario. Average Archean TTG has much lower concentrations of Hf, Nb, and Yb than even 60 wt.% SiO_2 Idiwhaa samples; therefore even a moderate amount of assimilation of TTG-like material would substantially lower the concentrations of these elements. Increases in the incompatible element concentrations are consistent with derivation by continued fractionation involving pyroxene or amphibole (Fig. 3.10). This is further evidenced by the decrease in Sc concentration with increasing SiO_2 as both amphibole and pyroxene have the ability to fractionate LREE from HREE and have Sc partition coefficients >1 (e.g., Rollinson, 1993). Indeed, our model for the petrogenesis of the intermediate Idiwhaa samples includes assimilation of hydrated mafic rocks, which may have served to raise the H_2O content of the magma enough to stabilize significant hornblende. Hornblende's greater ability to fractionate La from Yb than clinopyroxene (Rollinson, 1993; Tiepolo et al., 2007) may makes it a more suitable candidate for the fractionating assemblage that may have produced the highest SiO_2 samples.

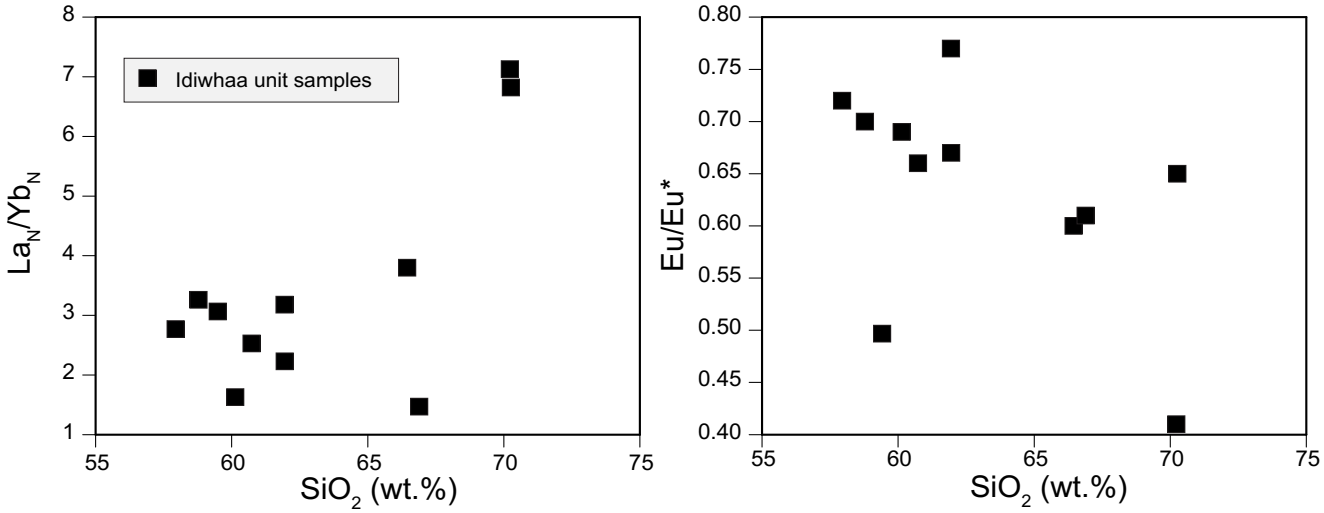

Figure 3.11: Chondrite-normalized(McDonough and Sun, 1995) La/Yb and degree of Eu anomaly versus SiO_2 for Idiwhaa samples. The increase in La_N/Yb_N in the high silica samples may be an indication of continued fractionation of a mineral assemblage dominated by pyroxene. Pyroxene fractionation can produce increases in the slope of the normalized REE pattern through the differentiation process without interactions with pre-existing crust (e.g., Mancini et al., 2015). The relatively consistent and low La_N/Yb_N in the lower silica units (>70 wt.%) suggests that pyroxene may not have played as significant as a role early in the differentiation process. The trend to more negative Eu-anomalies with increasing SiO_2 indicates that plagioclase was a major fractionating phase throughout the differentiation process.

In and attempt to evaluate the trace-element composition of a potential mantle source for the generation of the Idiwhaa unit, we modeled the REE systematics of the intermediate silica Idiwhaa samples. These samples have the following average concentrations: La = 29.2, Sm = 12.77, and Yb = 7.51. As noted above, an acceptable fractionating assemblage that can produce the high FeO, low MgO, and intermediate Al_2O_3 'icelandite' signature comprised 10% olivine, 30% plagioclase, and 60% clinopyroxene (determined using the MELTS software package; Gualda et al., 2012; Ghiorso and Gualda, 2015) with a typical Icelandic basalt starting composition (Mancini et al., 2015). Using this fractionating composition and standard melt/mineral distribution coefficients (Rollinson, 1993), we attempted to model the REE systematics of the Idiwhaa unit. Using starting N-MORB REE values (Niu et al., 2002) and the fractionating phases described above, the melt composition after removal of 80% of the starting mass has La contents (14.7 ppm) and resulting La_N/Yb_N (1.49) much lower than that of the measured intermediate Idiwhaa unit samples (La = 29.2, La_N/Yb_N = 2.64). In order to produce magmas with the REE contents and slightly elevated LREE/HREE of the Idiwhaa unit by fractionation crystallization processes, the primary basalt magma must be derived from a mantle source with higher LREE than modern NMORB. A suitable mantle source has La contents of ~8 ppm and corresponding flat chondrite normalized REE patterns (La_N/Yb_N = 1.6).

Felsic samples: Differentiates or partial melts?

Two felsic samples were analyzed that share geochemical similarities to the mafic Idiwhaa unit samples. These two samples (JR12-137 and JR12-146) were both collected a few meters northwest of other samples that are along strike, discussed above. This field relationship is robust and can be observed many hundreds of meters along strike. The petrogenesis of these more felsic samples, however, are not as straightforward. These two samples contain all the chemical features of lower SiO_2 Idiwhaa samples (high FeO, low Al_2O_3; Fig. 3.9) but have slightly higher LREE contents (Fig. 3.10). All Idiwhaa samples, including the two high SiO_2 samples, form major- and trace-element trends that are consistent with derivation via fractional crystallization from a common parental melt such as increasing trace-element abundances with increasing SiO_2 (Figs. 3.10–3.11). In this scenario, the higher La_N/Yb_N in these two samples may have been formed by further fractionation. This fractionation would likely have involved significant clinopyroxene or amphibole in order to drive the La_N/Yb_N up while removing Sc,

a trace element that preferentially partitions into clinopyroxene (Fig. 3.10). Amphibole may be a more likely fractionating phase, as it has slighty higher affinity for HREE than clinopyroxene. Additionally, the increase in Nb-anomaly in the two higher silica samples may be explained by signficant amphibole fractionation. This scenario is consistent with the whole-rock data presented here and elsewhere (Reimink 2014). However, the apparent absence of >4.0 Ga zircon material in these samples (presented in Chapter 4) precludes acceptance of this scenario without further evaluation.

Another possibility warrants further discussion; partial melting of Idiwhaa-like mafic rocks may have formed the higher SiO_2 samples. If Idiwhaa-like compositions were melted, either at ~4.02 Ga (age of sample TC3) or ~3.96 Ga (the minimum age of JR12-137; Chapter 4), they might form rhyolitic or dacitic compositions with the compositions documented in the felsic samples. If this were the case, the poorly preserved zircon may in fact record the crystallization age of these samples. However, if these samples are indeed formed by further fractionation as described above, and are directly related to the more mafic Idiwhaa unit samples, their relatively young minimum ages can be explained by more radiation-damaged and altered zircon material. Regardless of how these higher silica units were formed, partial melting or fractionation, they are genetically related to the mafic Idiwhaa unit samples and are therefore consistent with the petrologic settings suggested by analysis of those samples. Interestingly, the two scenarios discussed above are identical to the most commonly invoked

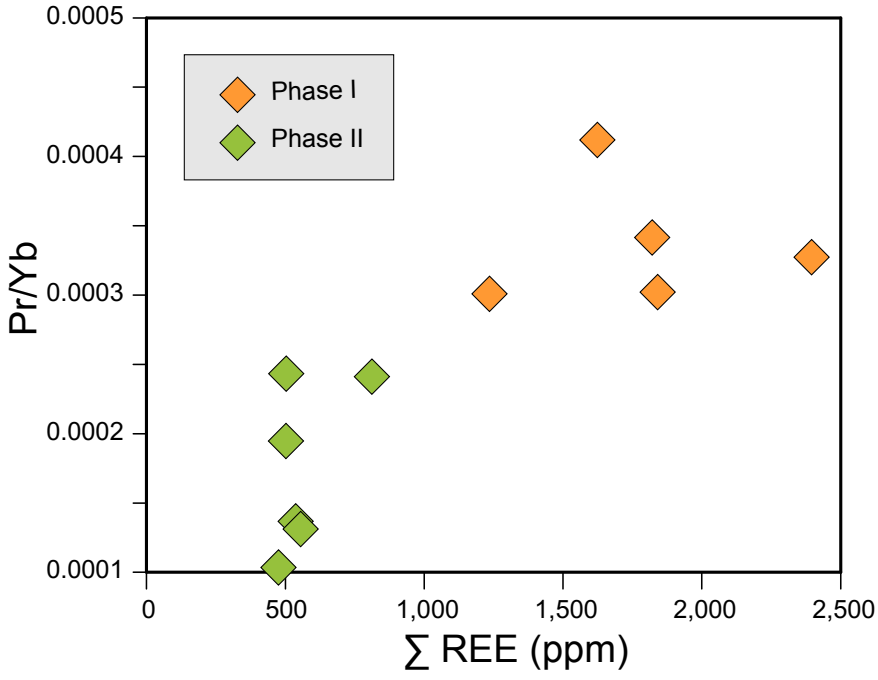

Figure 3.12: Trace element systematics from Phase I and Phase II zircon material from Reimink et al. (2014). The degree of LREE/HREE fractionation, here represented by Pr/Yb instead of La/Yb (see SI Discussion), decreases between Phase I and Phase II. This is inconsistent with assimilation of Archean TTG-like material. Combined with the drop in overall REE concentrations, a drop in Pr/Yb from Phase I to II is more in line with assimilation of mafic material that has relatively low REE concentrations and low Pr/Yb ratios.

processes for crust formation on modern Iceland (e.g., Wood, 1964; Nicholson et al., 1991; Jakobsson et al. 2008; Willibold et al., 2012; Mancini et al., 2015).

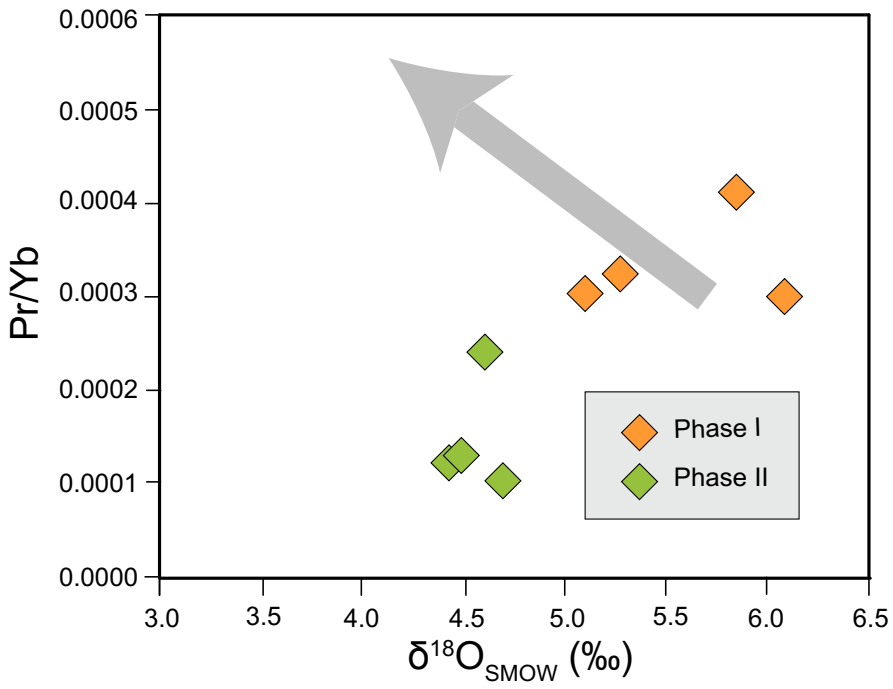

Figure 3.13: Trace-element compositions of TC3 zircons with correlated $\delta^{18}O$ values. If the magma had assimilated TTG-like compositions, the LREE/HREE ratio, represented here by Pr/Yb, would be expected to increase. A decrease in Pr/Yb from Phase I to Phase II with a correlated drop in $\delta^{18}O$ values is consistent with assimilation of mafic crust (i.e., low total REE, low Pr/Yb) that was hydrothermally altered by surface waters.

Zircon Trace Elements:

Trace-element contents of both Phase I and Phase II zircon was previously measured by SIMS (Reimink et al., 2014). These data show that measured Idiwhaa whole-rock REE patterns were in equilibrium with the zircon REE patterns, indicating that whole-rock REE systematics retain their primary magmatic signatures. Despite the similar overall shape of REE patterns from Phase I and II zircon, there are some small differences. First, Phase II zircon contains lower concentrations of most of the REE than Phase I (Fig. 3.12). Additionally, there is a small difference in the overall slope of the REE patterns, which is important to evaluate given our arguments regarding potential interactions between the Idiwhaa magma and Archean TTG-like rocks.

Zircon trace-element compositions may in fact be a more useful tracer of assimilation processes than whole rocks; at intermediate compositions, a rock such as the TC3 sample may have existed in a partially crystalline state during assimilation. If this were the case, assimilation would only impact the trace-element compositions of the melt fraction. In this scenario, measurement of the bulk-rock trace-element concentrations may mask a small melt fraction assimilation processes. However, zircon that clearly shows the effects of assimilation processes in its oxygen isotope compositions would be expected to show the effects of assimilation in trace-element patterns as well.

If ~35% assimilation of Archean TTG took place between the two phases of zircon growth (see above), a decrease in the La/Yb ratios would be expected. Here we use Pr as a tracer of LREE abundance because La exists in very low amounts in zircon making accurate and precise measurement difficult. The drop in Pr/Yb documented in Phase II zircon (Figs. 3.12–13) is opposite to what would be expected if the assimilant had Archean TTG-like compositions. In fact, the drop in Pr/Yb combined with the drop in total REE concentrations between Phase I and II zircon is more consistent with assimilation with broadly mafic rock in which the REE are substantially lower, though with only slight differences in the chondrite-normalized slope of the REE pattern.

Nd-isotope systematics within the AGC:

Whole-rock Nd-isotope analyses of Idiwhaa samples are reported in Table 3.2. Samples show a spread in $^{147}Sm/^{144}Nd$ from 0.10770 to 0.16620 and variable εNd (at 4020 Ma) between -3.4 and -0.1 epsilon units, calculated assuming a crystallization age of 4020 Ma and chondritic $^{143}Nd/^{144}Nd$ value of 0.512630 (Bouvier et al., 2008) and equations of Ickert (2013). However, when regressed together the Idiwhaa unit samples provide an errorchron age of 3824 ± 270 Ma with a large MSWD of 78, but within uncertainty of the zircon U-Pb crystallization age (Fig. 3.14).

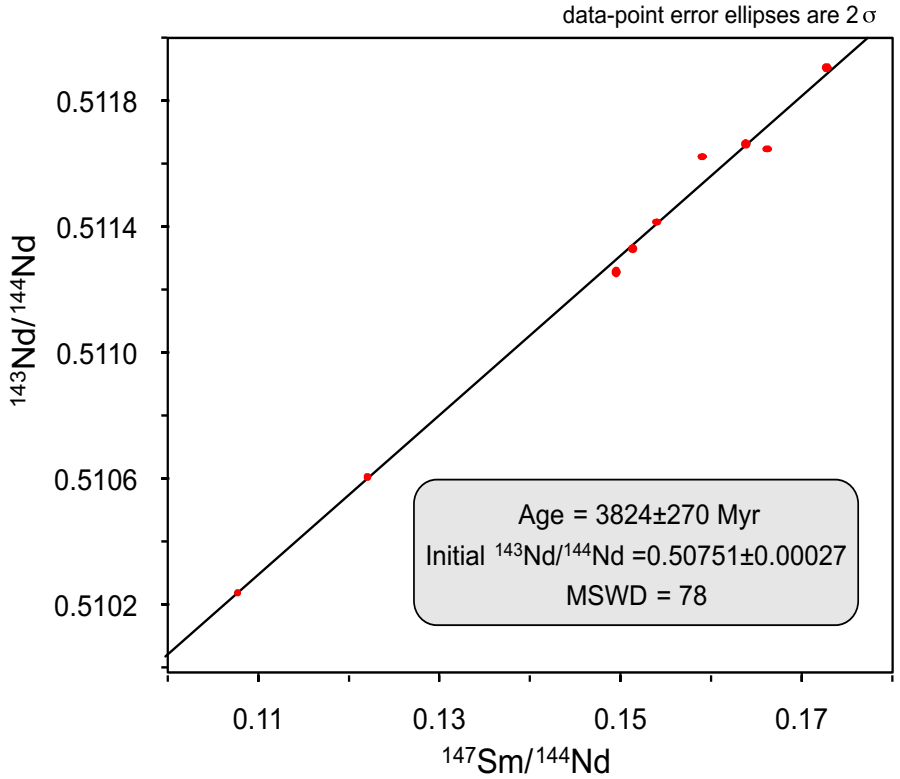

Figure 3.14: Sm-Nd isotope systematics from Idiwhaa unit samples. Though the data are not isochronous, the errorchron regression age is within uncertainty of the zircon U-Pb crystallization age, but outside of uncertainty of the potential AGC Sm-Nd resetting age (3390 ± 86 Myr; Figure 3.16) suggested by several authors (Moorbath et al., 1997; Mojzsis et al., 2014; Roth et al., 2014) indicating the Idiwhaa unit samples come from a well-preserved area of the AGC.

The validity of using

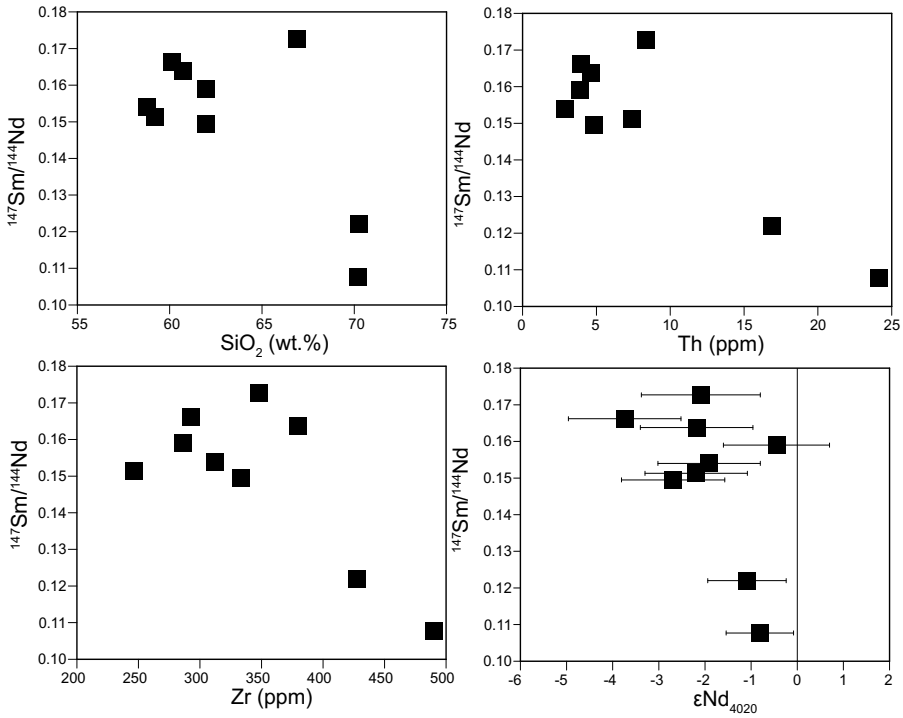

Figure 3.15: $^{147}Sm/^{144}Nd$ of Idiwhaa samples plotted againts standard indices of differentiation. These data suggest that variability in Sm/Nd ratios is consistent with fractionation processes, not alteration. Additionally, the increase in Ce/Pb in samples with low Sm/Nd and high SiO_2 suggests that assimilation of pre-existing crust was not a major factor. Nevertheless, a high degree of variability in the calculated εNd values, along with the non-isochronous relationships between the samples, calls into question the reliability of using calculated εNd values for the evaluation of source differentiation state.

Nd-isotope data in high-grade, poly-metamorphosed gneiss domains is contentious, particularly within the AGC (Moorbath et al., 1997; Bowring and Williams, 1999; Whitehouse et al., 2001). Indeed, the high degree of $^{147}Sm/^{144}Nd$ variability within the Idiwhaa unit is more than would be expected from igneous processes alone. However, there is relatively good correlation between measured $^{147}Sm/^{144}Nd$ and standard indices of fractionation (Fig. 3.15) potentially suggesting that the measured $^{147}Sm/^{144}Nd$ retains values close to those of the primary magmas.

Though the first Nd-isotope work performed on rock from the AGC showed highly variable initial $^{143}Nd/^{144}Nd$ (Bowring et al., 1989; Bowring and Housh, 1995), more recent work has suggested wholesale resetting of the Nd-isotope systematics within the AGC (Moorbath et al., 1997; Mojzsis et al., 2014; Roth et al., 2014). It remains difficult to evaluate much of the earlier work as no sample localities or rock descriptions were provided (Moorbath et al., 1997). However, data from samples which may be identified (Bowring et al., 1989; Bowring and Housh, 1995; Mojzsis et al., 2014; Roth et al., 2014) were typically collected from highly strained outcrops containing components with widely variable ages and inheritance. These samples define an errorchron corresponding to an age of 3390 ± 86 Ma (MSWD =

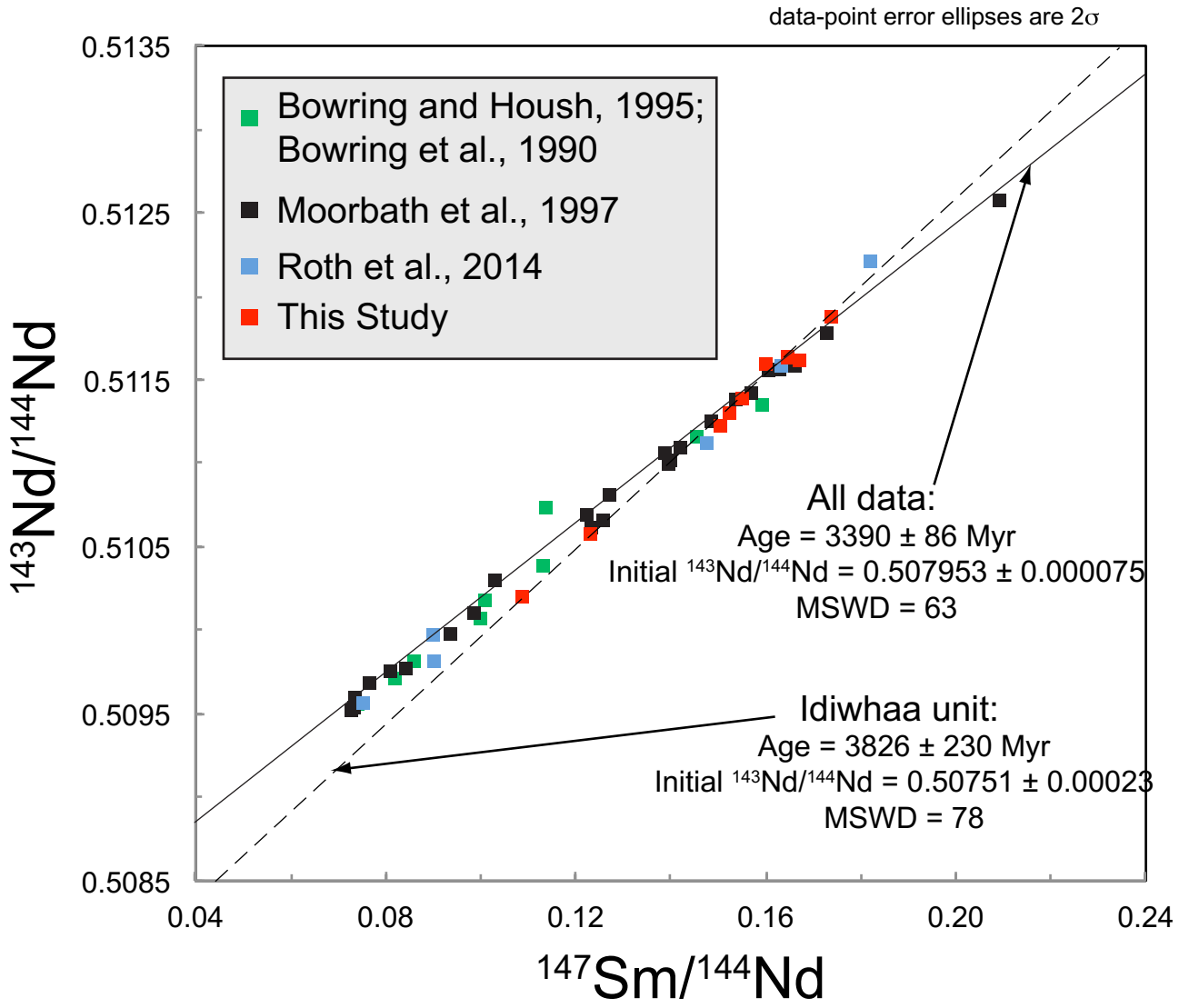

Figure 3.16: Sm-Nd systematics of all analyses from samples within the Acasta Gneiss Complex. Although many previous studies have suggested wholesale resetting of the Sm-Nd system within the AGC ca. 3370 Ma (Moorbath et al., 1997; Mojzsis et al., 2014; Roth et al., 2014), a regression of Idiwhaa unit samples indicates our previous assessment that the area surrounding the Idiwhaa unit exposures is better preserved than other areas (Reimink et al., 2014; Chapter 4).

63; Figure 3.16).

This potential resetting age is within uncertainty of the crystallization age of large granitic bodies found a few km from the discovery area (Chapter 4) as well as small granitic sheets of comparable age closer to the discovery outcrops (Bleeker and Stern, 1997). Additionally, the Idiwhaa unit itself records zircon U-Pb evidence for a fluid/metamorphic event of this age in the form of recrystallized zircon and metamorphic overgrowths with ca. 3.3 Ga ages (Reimink et al., 2014).

However, the Nd-isotope systematics of the Idiwhaa unit itself do not record the ~3.39 Ga

resetting event documented in the rest of the AGC (Fig. 3.16). This further substantiates our field analysis that the Idiwhaa unit and surrounding area are significantly better preserved than the majority of the previously studied areas within the AGC (Reimink et al., 2014; Chapter 4). Taken within the context of the large body of Nd-isotope work previously published for the AGC, our new data indicates that at least some areas within the AGC remained unaffected by a ~3.39 Ga resetting event, and previous conclusions suggesting that the entirety of the AGC experienced wholesale resetting of the Nd-isotope systematics at this time are unfounded (e.g., Moorbath et al., 1997; Roth et al., 2014). However, the non-isochronous relationship of the Sm-Nd systematics within the well-preserved Idiwhaa unit calls into question the use of measured $^{143}Nd/^{144}Nd$ ratios from single samples as primary signatures indicating very early differentiation events (Bowring et al., 1989; Bowring and Housh, 1995).

Difference between Phase I and Phase II Hf compositions:

We performed a Student's T-test on the εHf values of Phase I and Phase II zircon material in order to test the hypothesis that the mean εHf of the two populations were statistically the same. Using a two-sample t-test assuming equal variance (established by applying an f-test to the two populations) we derive a t-test statistic of -1.003 with 71 degrees of freedom. The two-tailed probability given these parameters is 0.319, indicating that we may not reject the null hypothesis that the two populations are equal. Put another way, the two populations are the same at the current resolution.

References:

Albarede, F., Telouk, P., Blichert-Toft, J., Boyet, M., Agranier, A., Nelson, B., 2004. Precise and accurate isotopic measurements using multiple-collector ICPMS. Geochimica et Cosmochimica Acta 68, 2725–2744.

Amelin, Y., Kamo, S.L., Lee, D.-C., 2011. Evolution of early crust in chondritic or non-chondritic Earth inferred from U–Pb and Lu–Hf data for chemically abraded zircon from the Itsaq Gneiss Complex, West GreenlandThis article is one of a series of papers published in this Special Issue on the theme of Geochronology in honour of Tom Krogh. Can. J. Earth Sci. 48, 141–160.

Amelin, Y., Lee, D.C., Halliday, A.N., Pidgeon, R.T., 1999. Nature of the Earth's earliest crust from hafnium isotopes in single detrital zircons. Nature. 399, 252-255.

Bindeman, I.N., Valley, J.W., 2001. Low-δ18O Rhyolites from Yellowstone: Magmatic Evolution Based on Analyses of Zircons and Individual Phenocrysts. Journal of Petrology 42, 1491–1517.

Bleeker, W., Stern, R.A., 1997. The Acasta Gneisses: An imperfect sample of Earth's oldest crust, in:. Presented at the Lithoprobe, pp. 1–5.

Blichert-Toft, J., Albarède, F., 1997. The Lu-Hf isotope geochemistry of chondrites and the evolution of the mantle-crust system. Earth and Planetary Science Letters 148, 243–258.

Bouvier, A., Vervoort, J.D., Patchett, P.J., 2008. The Lu–Hf and Sm–Nd isotopic composition of CHUR: Constraints from unequilibrated chondrites and implications for the bulk composition of terrestrial planets. Earth and Planetary Science Letters 273, 48–57.

Bowring, S.A., Housh, T., 1995. The Earth's early evolution. Science 269, 1535–1540.

Bowring, S.A., Williams, I.S., 1999. Priscoan (4.00–4.03 Ga) orthogneisses from northwestern Canada. Contributions to Mineralogy and Petrology 134, 3–16. Bowring, J.F., McLean, N.M., Bowring, S.A., 2011. Engineering cyber infrastructure for U-Pb geochronology: Tripoli and U-Pb_Redux. Geochem. Geophys. Geosyst. 12, 1-19.

Bowring, S.A., King, J.E., Housh, T.B., Isachsen, C.E., Podosek, F.A., 1989. Neodymium and lead isotope evidence for enriched early Archaean crust in North America. Nature 340, 222–225.

Boyet, M., Carlson, R.W., 2005. Geochemistry: 142Nd evidence for early (>4.53 Ga) global differentiation of the silicate earth. Science 309, 576–581.

Carley, T.L., Miller, C.F., Wooden, J.L., Padilla, A.J., Schmitt, A.K., Economos, R.C., Bindeman, I.N.,

Jordan, B.T., 2014. Iceland is not a magmatic analog for the Hadean: Evidence from the zircon record. Earth and Planetary Science Letters 405, 85–97.

Caro, G., Bourdon, B., Birck, J.-L., Moorbath, S., 2003. 146Sm-142Nd evidence from Isua metamorphosed sediments for early differentiation of the Earth's mantle. Nature 423, 428–432.

Condon, D.J., Schoene, B., McLean, N.M., Bowring, S.A., Parrish, R.R., 2015. Metrology and traceability of U–Pb isotope dilution geochronology (EARTHTIME Tracer Calibration Part I). Geochimica et Cosmochimica Acta 164, 464–480.

Creaser, R.A., Erdmer, P., Stevens, R.A., Grant, S.L., 1997. Tectonic affinity of Nisutlin and Anvil assemblage strata from the Teslin tectonic zone, northern Canadian Cordillera: Constraints from neodymium isotope and geochemical evidence. Tectonics 16, 107–121.

D'Abzac, F.X., Davies, J.H.F.L., Wotzlaw, J.-F., Schaltegger, U. Hafnium isotope analysis of Yb-doped zircon and JMC475 reference materials by solution MC-ICP-MS: Protocols and pitfalls, in:. Presented at the Goldschmidt Geochemistry Conference.

Davies, J.H.F.L., Wotzlaw, J.-F., Wolfe, A.P., Heaman, L.M., Arbour, V., 2014. Assessing the age of the Late Cretaceous Danek Bonebed with U–Pb geochronology 1. Can. J. Earth Sci. 51, 982–986.

Debaille, V., O'Neill, C., Brandon, A.D., Haenecour, P., 2013. Stagnant-lid tectonics in early Earth revealed by 142Nd variations in late Archean rocks. Earth and Planetary Science Letters 373, 83–92.

Eiler, J.M., 2001. Oxygen isotope variations of basaltic lavas and upper mantle rocks. Reviews in Mineralogy and Geochemistry 43, 319–364.

Fisher, C.M., Hanchar, J.M., Samson, S.D., Dhuime, B., Blichert-Toft, J., Vervoort, J.D., Lam, R., 2011. Synthetic zircon doped with hafnium and rare earth elements: A reference material for in situ hafnium isotope analysis. Chemical Geology 286, 32–47.

Fisher, C.M., Vervoort, J.D., DuFrane, S.A., 2014. Accurate Hf isotope determinations of complex zircons using the "laser ablation split stream" method. Geochem. Geophys. Geosyst. 15, 121–139.

Froude, D.O., Ireland, T.R., Kinny, P.D., Williams, I.S., Compston, W., Williams, I.R., Myers, J.S., 1983. Ion microprobe identification of 4,100–4,200 Ma-old terrestrial zircons. Nature 304, 616–618.

Gerstenberger, H., Haase, G., 1997. A highly effective emitter substance for mass spectrometric Pb isotope ratio determinations. Chemical Geology 136, 309–312.

Ghiorso, M.S., Gualda, G.A.R., 2015. An H2O–CO2 mixed fluid saturation model compatible with

rhyolite-MELTS. Contributions to Mineralogy and Petrology 169, 53–30.

Grove, T.L., Kinzler, R.J., 1986. Petrogenesis of andesites. Annual Review of Earth and Planetary Sciences 14, 417.

Gualda, G.A.R., Ghiorso, M.S., Lemons, R.V., Carley, T.L., 2012. Rhyolite-MELTS: a Modified Calibration of MELTS Optimized for Silica-rich, Fluid-bearing Magmatic Systems. Journal of Petrology 53, 875–890.

Harrison, T.M., 2005. Heterogeneous Hadean Hafnium: Evidence of Continental Crust at 4.4 to 4.5 Ga. Science 310, 1947–1950.

Harrison, T.M., 2009. The hadean crust: Evidence from >4 ga zircons. Annual Review of Earth and Planetary Sciences 37, 479–505.

Hiess, J., Condon, D.J., McLean, N., Noble, S.R., 2012. 238U/ 235U systematics in terrestrial uranium-bearing minerals. Science 335, 1610–1614.

Hoskin, P.W.O., 2003. The Composition of Zircon and Igneous and Metamorphic Petrogenesis. Reviews in Mineralogy and Geochemistry 53, 27–62.

Ickert, R.B., 2013. Algorithms for Estimating Uncertainties in Initial Radiogenic Isotope Ratios and Model Ages. Chemical Geology 1–43.

Iizuka, T., Horie, K., Komiya, T., Maruyama, S., Hirata, T., Hidaka, H., Windley, B.F., 2006. 4.2 Ga zircon xenocryst in an Acasta gneiss from northwestern Canada: Evidence for early continental crust. Geology 34, 245–248.

Iizuka, T., Komiya, T., Johnson, S.P., Kon, Y., Maruyama, S., Hirata, T., 2009. Reworking of Hadean crust in the Acasta gneisses, northwestern Canada: Evidence from in-situ Lu–Hf isotope analysis of zircon. Chemical Geology 259, 230–239.

Johnson, D.M., Hooper, P.R., Conrey, R.M., 1999. XRF analysis of rocks and minerals for major and trace elements on a single low dilution Li-tetraborate fused bead. Advances in X-ray Analysis 41, 843–867.

Jónasson, K., Jonasson, K., 2005. Magmatic evolution of the Heiðarsporður ridge, NE-Iceland. Journal of Volcanology and Geothermal Research 147, 109–124.

Kamber, B.S., 2015. The evolving nature of terrestrial crust from the Hadean, through the Archaean, into the Proterozoic. Precambrian Res 258, 48–82.

Kamber, B.S., Collerson, K.D., Moorbath, S., Whitehouse, M.J., 2003. Inheritance of early Archaean Pb-isotope variability from long-lived Hadean protocrust. Contributions to Mineralogy and Petrology 145, 25–46.

Kamber, B.S., Whitehouse, M.J., Bolhar, R., Moorbath, S., 2005. Volcanic resurfacing and the early terrestrial crust: zircon U–Pb and REE constraints from the Isua Greenstone Belt, southern West Greenland. Earth and Planetary Science Letters 240, 276–290.

Kemp, A.I.S., Hickman, A.H., Kirkland, C.L., Vervoort, J.D., 2015. Hf isotopes in detrital and inherited zircons of the Pilbara Craton provide no evidence for Hadean continents. Precambrian Res 261, 112–126.

Kemp, A.I.S., Wilde, S.A., Hawkesworth, C.J., Coath, C.D., Nemchin, A., Pidgeon, R.T., Vervoort, J.D., DuFrane, S.A., 2010. Hadean crustal evolution revisited: New constraints from Pb–Hf isotope systematics of the Jack Hills zircons. Earth and Planetary Science Letters 296, 45–56.

Knaack, C., Cornelius, S., Hooper, P.R., 1994. Trace element analyses of rocks and minerals by ICP-MS. Open File Report. Department of Geology.

Krogh, T.E., 1973. A low-contamination method for hydrothermal decomposition of zircon and extraction of U and Pb for isotopic age determinations. Geochimica et Cosmochimica Acta 37, 485–494.

Kroner, A., 1985. Evolution of the Archean Continental Crust. Annual Review of Earth and Planetary Sciences 13, 49–74.

Lenting, C., Geisler, T., Gerdes, A., Kooijman, E., Scherer, E.E., Zeh, A., 2010. The behavior of the Hf isotope system in radiation-damaged zircon during experimental hydrothermal alteration. American Mineralogist 95, 1343–1348.

Mancini, A., Mattsson, H.B., Bachmann, O., 2015. Origin of the compositional diversity in the basalt-to-dacite series erupted along the Heiðarsporður ridge, NE Iceland. Journal of Volcanology and Geothermal Research 301, 116–127.

Martin, H., 1986. Effect of steeper Archean geothermal gradient on geochemistry of subduction-zone magmas. Geology 14, 753–756.

McDonough, W.F., Sun, S.S., 1995. The composition of the Earth. Chemical Geology 120, 223–253.

McLean, N.M., Bowring, J.F., Bowring, S.A., 2011. An algorithm for U-Pb isotope dilution data

reduction and uncertainty propagation. Geochemistry, Geophysics, Geosystems 12, 1-26.

Mojzsis, S.J., Cates, N.L., Caro, G., Trail, D., Abramov, O., Guitreau, M., Blichert-Toft, J., Hopkins, M.D., Bleeker, W., 2014. Component geochronology in the polyphase ca. 3920Ma Acasta Gneiss. Geochimica et Cosmochimica Acta 133, 68–96.

Mojzsis, S.J., Harrison, T.M., Pidgeon, R.T., 2001. Oxygen-isotope evidence from ancient zircons for liquid water at the Earth's surface 4,300 Ma ago. Nature 409, 178–181.

Moorbath, S., Whitehouse, M.J., Kamber, B.S., 1997. Extreme Nd-isotope heterogeneity in the early Archaean - Fact or fiction? Case histories from northern Canada and West Greenland. Chemical Geology 135, 213–231.

Moyen, J.-F., Martin, H., 2012. Forty years of TTG research. Lithos 148, 312–336.

Muehlenbachs, K., Anderson, A.T., Sigvaldason, G.E., 1974. Low-O18 basalts from Iceland. Geochimica et Cosmochimica Acta 38, 577–588.

Niu, Y., Regelous, M., Wendt, I.J., Batiza, R., O'Hara, M.J., 2002. Geochemistry of near-EPR seamounts: importance of source vs. process and the origin of enriched mantle component. Earth and Planetary Science Letters 199, 327–345.

O'Neil, J., Carlson, R.W., Francis, D., Stevenson, R.K., 2008. Neodymium-142 evidence for Hadean mafic crust. Science 321, 1828–1831.

Paces, J.B., Miller, J.D., Jr., 1993. Precise U-Pb ages of Duluth Complex and related mafic intrusions, northeastern Minnesota: Geochronological insights to physical, petrogenetic, paleomagnetic, and tectonomagmatic processes associated with the 1.1 Ga Midcontinent Rift System. Journal of Geophysical Research 98, 13997.

Reimink, J.R., Chacko, T., Stern, R.A., Heaman, L.M., 2014. Earth's earliest evolved crust generated in an Iceland-like setting. Nature Geoscience 7, 529–533.

Rizo, H., Boyet, M., Blichert-Toft, J., O'Neil, J., Rosing, M.T., Paquette, J.-L., 2012. The elusive Hadean enriched reservoir revealed by 142Nd deficits in Isua Archaean rocks. Nature 491, 96–99.

Rollinson, H.R., 1993. Using Geochemical Data. Pearson Education Limited.

Roth, A.S.G., Bourdon, B., Mojzsis, S.J., Rudge, J.F., Guitreau, M., Blichert-Toft, J., 2014. Combined 147,146Sm- 143,142Nd constraints on the longevity and residence time of early terrestrial crust. Geochem. Geophys. Geosyst. 15, 2329–2345.

Roth, A.S.G., Bourdon, B., Mojzsis, S.J., Touboul, M., Sprung, P., Guitreau, M., Blichert-Toft, J., 2013. Inherited 142Nd anomalies in Eoarchean protoliths. Earth and Planetary Science Letters 361, 50–57.

Scherer, E., Munker, C., Mezger, K., 2001. Calibration of the Lutetium-Hafnium Clock. Science 293, 683–687.

Schmidberger, S.S., Simonetti, A., Heaman, L.M., Creaser, R.A., Whiteford, S., 2007. Lu–Hf, in-situ Sr and Pb isotope and trace element systematics for mantle eclogites from the Diavik diamond mine: Evidence for Paleoproterozoic subduction beneath the Slave craton, Canada. Earth and Planetary Science Letters 254, 55–68.

Sláma, J., Košler, J., Condon, D.J., Crowley, J.L., Gerdes, A., Hanchar, J.M., Horstwood, M.S.A., Morris, G.A., Nasdala, L., Norberg, N., Schaltegger, U., Schoene, B., Tubrett, M.N., Whitehouse, M.J., 2008. Plešovice zircon — A new natural reference material for U–Pb and Hf isotopic microanalysis. Chemical Geology 249, 1–35.

Söderlund, U., Patchett, P.J., Vervoort, J.D., Isachsen, C.E., 2004. The 176Lu decay constant determined by Lu–Hf and U–Pb isotope systematics of Precambrian mafic intrusions. Earth and Planetary Science Letters 219, 311–324.

Stern, R., Bleeker, W., 1998. Age of the world's oldest rocks refined using Canada's SHRIMP: The Acasta Gneiss Complex, Northwest Territories, Canada. Geosci Can 25, 27–31.

Tanaka, T., Togashi, S., Kamioka, H., Amakawa, H., Kagami, H., Hamamoto, T., Yuhara, M., Orihashi, Y., Yoneda, S., Shimizu, H., Kunimaru, T., Takahashi, K., Yanagi, T., Nakano, T., Fujimaki, H., Shinjo, R., Asahara, Y., Tanimizu, M., Dragusanu, C., 2000. JNdi-1: a neodymium isotopic reference in consistency with LaJolla neodymium. Chemical Geology 168, 279–281.

Taylor, D.J., McKeegan, K.D., Harrison, T.M., 2009. Lu–Hf zircon evidence for rapid lunar differentiation. Earth and Planetary Science Letters 279, 157–164.

Thirlwall, M.F., Anczkiewicz, R., 2004. Multidynamic isotope ratio analysis using MC–ICP–MS and the causes of secular drift in Hf, Nd and Pb isotope ratios. International Journal of Mass Spectrometry 235, 59–81.

Tiepolo, M., Oberti, R., Zanetti, A., Vannucci, R., Foley, S.F., 2007. Trace-Element Partitioning Between Amphibole and Silicate Melt. Reviews in Mineralogy and Geochemistry 67, 417–452.

Unterschutz, J.L., Creaser, R.A., Erdmer, P., Thompson, R.I., Daughtry, K.L., 2002. North American

margin origin of Quesnel terrane strata in the southern Canadian Cordillera: Inferences from geochemical and Nd isotopic characteristics of Triassic metasedimentary rocks. Geological Society of America Bulletin 114, 462–475.

Valley, J.W., Cavosie, A.J., Ushikubo, T., Reinhard, D.A., Lawrence, D.F., Larson, D.J., Clifton, P.H., Kelly, T.F., Wilde, S.A., Moser, D.E., Spicuzza, M.J., 2014. Hadean age for a post-magma-ocean zircon confirmed by atom-probe tomography. Nature Geoscience 7, 219-223.

Valley, J.W., Kinny, P.D., Schulze, D.J., Spicuzza, M.J., 1998. Zircon megacrysts from kimberlite: oxygen isotope variability among mantle melts. Contributions to Mineralogy and Petrology 133, 1–11.

Wasserburg, G.J., Jacousen, S.B., DePaolo, D.J., McCulloch, M.T., Wen, T., 1981. Precise determination of ratios, Sm and Nd isotopic abundances in standard solutions. Geochimica et Cosmochimica Acta 45, 2311–2323.

Whitehouse, M., Nagler, T., Moorbath, S., Kramers, J., Kamber, B., Frei, R., 2001. Priscoan (4.00-4.03 Ga) orthogneisses from northwestern Canada - by Samuel A. Bowring and Ian S. Williams: discussion. Contributions to Mineralogy and Petrology 141, 248–250.

Wood, D.A., 1978. Major and Trace Element Variations in the Tertiary Lavas of Eastern Iceland and their Significance with respect to the Iceland Geochemical Anomaly. Journal of Petrology 19, 393–436.

Wotzlaw, J.F., Schaltegger, U., Frick, D.A., Dungan, M.A., Gerdes, A., Günther, D., 2013. Tracking the evolution of large-volume silicic magma reservoirs from assembly to supereruption. Geology 41, 867–870.

Wu, F.-Y., Yang, Y.-H., Xie, L.-W., Yang, J.-H., Xu, P., 2006. Hf isotopic compositions of the standard zircons and baddeleyites used in U–Pb geochronology. Chemical Geology 234, 105–126.

Yuan, H., Gao, S., Dai, M., Zong, C., Günther, D., Fontaine, G., Liu, X., Diwu, C., 2008. Simultaneous determinations of U–Pb age, Hf isotopes and trace element compositions of zircon by excimer laser-ablation quadrupole and multiple-collector ICP-MS. Chemical Geology 247, 100–118.

Table 3.1 Whole rock elemental compositions of Idiwhaa unit samples

Sample Name	JR12-137	JR12-146	JR12-119**	AC2I*	TC3-A*	TC3-B*	AC2C*	JR12-141*	JR12-145*	JR13-108**	JR13-207
Northing	7228607	7228629	7229220	7228595	7228605	7228605	7228617	7228605	7228659	7228857	7228058
Easting	567758	567781	567883	567768	567763	567763	567774	567760	567786	568010	567536
SiO_2 (wt.%)	70.22	70.26	66.45	66.89	58.78	57.94	61.95	60.13	60.73	61.94	59.22
TiO_2	0.547	0.528	0.803	0.82	1.22	1.24	1.08	1.12	1.06	0.99	1.01
Al_2O_3	12.66	12.70	13.66	13.87	13.84	13.88	14.02	14.13	13.82	13.25	13.55
$FeO_{(total)}$	7.99	8.26	9.47	8.57	14.51	15.25	11.71	12.53	13.13	13.39	14.77
MnO	0.268	0.110	0.226	0.12	0.17	0.17	0.16	0.16	0.18	0.20	0.21
MgO	1.16	0.63	1.81	0.95	1.26	1.26	1.48	1.43	1.20	1.13	1.43
CaO	1.92	2.29	1.82	2.84	4.54	4.61	4.70	4.93	4.27	3.96	5.21
Na_2O	2.65	3.19	2.58	3.39	2.99	2.98	3.35	3.06	2.92	2.93	2.55
K_2O	2.48	1.94	3.01	2.34	2.36	2.35	1.24	2.21	2.39	1.94	1.79
P_2O_5	0.108	0.086	0.180	0.19	0.34	0.33	0.31	0.30	0.29	0.26	0.26
Sum	100.00	100.00	100.00	100.00	100.00	100.00	100.00	100.00	100.00	100.00	100.00
LOI				0.13	0.93	0.33	1.07	0.67	0.55		
Mg#	20.60	12.00	25.39	16.53	13.43	12.85	18.36	16.86	13.98	13.12	14.73
XRF											
V (ppm)	8	5	5	4	2	5	3	5	4	3	8
Cr	1	3	1	1	1	1	1	1	1	2	1
Ni	1	2	4	18	2	1	3	3	1	0	0
Cu	81	14	6	242	85	20	160	111	120	12	45
Zn	90	115	114	106	85	81	95	111	120	118	102
Ga	22	22	22	24	23	25	24	24	24	23	24
Zr	490	428	329	348	312	317	286	293	380	333	246
Ba	600	577	936	642	727	712	279	599	753	614	539
ICP-MS											
Sc (ppm)	18.0	14.6	23.3	25.4	35.7	35.3	33.4	34.5	30.4	29.2	35.4
Rb	76.8	51.2	81.1	53.93	74.57	74.36	18.32	52.96	59.13	60.10	39.67
Sr	132	138	114	191	151	151	120	167	189	103	168
Y	91.83	65.47	59.38	70.74	69.99	72.86	78.02	86.40	82.59	69.69	107.83
Nb	29.25	26.66	25.11	26.45	21.52	21.34	20.29	23.07	22.69	19.71	20.89
Cs	4.74	1.58	2.19	1.70	2.07	2.00	0.58	1.64	1.84	1.24	1.36
Hf	12.91	11.23	8.50	8.86	7.77	8.02	7.19	7.18	9.26	8.46	6.49

Table 3.1 Whole rock elemental compositions of Idiwhaa unit samples

Sample Name	JR12-137	JR12-146	JR12-119**	AC2I*	TC3-A*	TC3-B*	AC2C*	JR12-141*	JR12-145*	JR13-108**	JR13-207
Ta	2.39	1.70	1.36	1.76	1.25	1.31	1.24	1.41	1.54	1.26	1.32
Pb	7.94	8.05	5.10	7.48	4.79	4.75	4.89	5.72	6.74	6.00	6.04
Th	24.14	16.92	10.92	8.36	2.87	2.37	3.87	3.99	4.63	4.80	7.44
U	2.78	1.64	1.50	1.60	0.79	0.82	1.12	0.98	1.28	0.86	1.40
La	96.59	71.31	36.06	14.49	30.86	27.15	24.94	19.72	28.54	31.46	41.73
Ce	185.70	141.70	83.27	40.71	77.58	71.39	65.49	55.38	70.08	67.40	111.83
Pr	21.16	15.41	11.29	6.56	11.10	10.42	9.82	8.54	10.09	8.72	16.00
Nd	76.62	57.79	45.96	32.59	49.20	47.48	45.36	40.24	45.48	36.60	68.52
Sm	14.18	11.96	10.03	9.99	12.69	12.63	12.31	11.87	12.74	9.51	17.66
Eu	1.83	2.49	1.91	2.10	3.00	3.10	2.80	2.92	2.95	2.57	2.92
Gd	13.31	11.44	9.31	11.32	13.54	13.75	13.35	14.11	14.59	10.97	18.64
Tb	2.39	1.91	1.67	2.09	2.31	2.34	2.40	2.56	2.58	1.96	3.28
Dy	16.08	12.30	11.16	13.35	13.92	14.52	15.41	16.72	16.24	13.00	20.59
Ho	3.40	2.64	2.38	2.86	2.83	2.94	3.23	3.49	3.34	2.71	4.18
Er	9.72	7.62	6.79	7.92	7.66	7.84	8.82	9.55	9.07	7.52	11.26
Tm	1.43	1.14	1.01	1.13	1.05	1.11	1.27	1.36	1.27	1.09	1.58
Yb	9.21	7.10	6.45	6.72	6.43	6.65	7.61	8.20	7.66	6.71	9.33
Lu	1.42	1.10	0.98	1.02	0.98	1.02	1.15	1.25	1.16	1.04	1.34
La_N/Yb_N[1]	7.13	6.82	3.80	1.47	3.26	2.77	2.23	1.63	2.53	3.18	3.04
Eu/Eu[2]	0.41	0.65	0.60	0.61	0.70	0.72	0.67	0.69	0.66	0.77	0.49

* Data from Reimink et al., (2014)

** Data from Reimink et al., Submitted

Mg# = 100*[MgO/(FeO+MgO)] calculated on a molar basis.

[1]normalization values from McDonough and Sun (1995)

[2]$Eu/Eu = Eu_N/sqrt[(Sm_N * Gd_N)]$ normalized to ref. [50].

Table 3.2 Sm-Nd isotopic analyses of Idiwhaa whole-rock samples

Sample	Sm ppm	Nd ppm	147Sm/144Nd	0.2% uncertainty	143Nd/144Nd	2 sigma	Age (Ma)	Uncertainty	εNdT	2sigma
JR12-146	11.11	55.05	0.1220	0.0002	0.510605	0.000007	4020	10	-1.09	0.85
JR13-108	8.869	35.864	0.1495	0.0003	0.511256	0.000011	4020	10	-2.69	1.12
JR13-207	15.785	63.065	0.1513	0.0003	0.511330	0.000008	4020	10	-2.19	1.11
JR12-141	12.050	43.839	0.1662	0.0003	0.511647	0.000006	4020	10	-3.74	1.22
JR12-137	13.193	74.058	0.1077	0.0002	0.510238	0.000007	4020	10	-0.81	0.73
AC2I	9.343	32.702	0.1727	0.0003	0.511905	0.000009	4020	10	-2.09	1.29
TC3	11.8	46.2	0.1540	0.0003	0.511414	0.000006	4020	10	-1.91	1.11
AC2C	11.2	42.7	0.1590	0.0003	0.511622	0.000006	4020	10	-0.45	1.15
JR12-145	11.2	41.5	0.1638	0.0003	0.511662	0.000009	4020	10	-2.18	1.22

Table 3.3 LASS U-Pb and Hf data from TC3 zircons

Analysis	Date	Time	Duration (s)	Spot	Zircon Phase	Analysis Quality	Corrected 176/177 Hf	2SE	Lu176/Hf177	2SE
TC3/GEVMT/1	6/5/15	20:34:59	19.5	1	1	High	0.280339	0.000072	0.003140	0.000150
TC3/GEVMT/3	6/5/15	20:38:13	20.2	3	1	High	0.280541	0.000100	0.004950	0.000019
TC3/GEVMT/8	6/5/15	20:52:56	32.9	8	1	High	0.280381	0.000055	0.003170	0.000170
TC3/GEVMT/36	6/5/15	23:16:49	10.9	36	1	High	0.280269	0.000095	0.002150	0.000130
TC3/M1093/26	6/9/15	0:24:27	29.0	26	1	High	0.280205	0.000061	0.001540	0.000110
TC3/M1093/3	6/9/15	17:34:03	20.5	30	1	High	0.280283	0.000074	0.002347	0.000025
TC3/M1093/6	6/9/15	17:45:39	27.5	33	1	High	0.280174	0.000058	0.001038	0.000066
TC3/M1093/8	6/9/15	17:48:53	25.1	35	1	High	0.280348	0.000075	0.003166	0.000079
TC3/M1093/20	6/9/15	19:18:43	21.9	47	1	High	0.280189	0.000082	0.001071	0.000086
TC3/GEVMT/7	6/5/15	20:51:22	21.4	7	1	Good	0.280269	0.000069	0.002267	0.000080
TC3/GEVMT/31	6/5/15	23:02:04	16.6	31	1	Good	0.280226	0.000067	0.000983	0.000095
TC3/GEVMT/32	6/5/15	23:10:22	11.6	32	1	Good	0.280143	0.000087	0.001810	0.000330
TC3/GEVMT/41	6/5/15	23:47:38	17.6	41	1	Good	0.280299	0.000075	0.002179	0.000092
TC3/GEVMT/45	6/5/15	23:54:05	15.7	45	1	Good	0.280252	0.000050	0.001976	0.000080
TC3/GEVMT/47	6/6/15	0:19:04	14.6	47	1	Good	0.280363	0.000098	0.003711	0.000086
TC3/GEVMT/54	6/6/15	0:37:03	17.2	54	1	Good	0.280180	0.000081	0.000909	0.000061
TC3/M1093/9	6/8/15	22:54:36	13.3	9	1	Good	0.280295	0.000065	0.002090	0.000220
TC3/M1093/12	6/8/15	23:15:22	11.8	12	1	Good	0.280269	0.000091	0.003150	0.000280
TC3/M1093/2	6/9/15	17:32:26	13.2	29	1	Good	0.280391	0.000150	0.004880	0.000450
TC3/M1093/5	6/9/15	17:43:59	19.4	32	1	Good	0.280309	0.000051	0.001960	0.000150
TC3/M1093/10	6/9/15	18:08:55	10.4	37	1	Good	0.280259	0.000098	0.001870	0.000300
TC3/M1093/19	6/9/15	19:17:05	11.3	46	1	Good	0.280244	0.000074	0.002800	0.000170
TC3/M1093/31	6/9/15	20:09:27	13.0	58	1	Good	0.280336	0.000076	0.003187	0.000008
TC3/M1093/35	6/9/15	20:22:39	12.6	62	1	Good	0.280311	0.000100	0.002140	0.000240
TC3/GEVMT/5	6/5/15	20:48:07	14.7	5	2	High	0.280255	0.000051	0.001276	0.000093
TC3/GEVMT/11	6/5/15	21:12:26	25.2	11	2	High	0.280192	0.000045	0.001162	0.000033
TC3/GEVMT/24	6/5/15	22:00:58	25.2	24	2	High	0.280212	0.000066	0.001940	0.000250
TC3/GEVMT/28	6/5/15	22:57:13	25.5	28	2	High	0.280181	0.000046	0.001138	0.000013
TC3/GEVMT/42	6/5/15	23:49:14	16.1	42	2	High	0.280179	0.000037	0.001158	0.000075
TC3/M1093/3	6/8/15	22:38:11	12.6	3	2	High	0.280177	0.000047	0.000798	0.000018
TC3/M1093/4	6/8/15	22:39:49	13.5	4	2	High	0.280131	0.000056	0.000810	0.000007
TC3/M1093/7	6/8/15	22:51:23	13.5	7	2	High	0.280196	0.000064	0.000795	0.000047
TC3/M1093/13	6/8/15	23:16:57	14.9	13	2	High	0.280206	0.000080	0.000885	0.000023
TC3/M1093/14	6/8/15	23:25:16	13.2	14	2	High	0.280156	0.000099	0.000829	0.000018
TC3/M1093/17	6/8/15	23:30:09	17.1	17	2	High	0.280175	0.000072	0.001490	0.000100
TC3/M1093/27	6/9/15	0:26:07	13.3	27	2	High	0.280146	0.000055	0.001008	0.000013
TC3/M1093/12	6/9/15	18:12:10	22.9	39	2	High	0.280194	0.000057	0.001128	0.000013
TC3/M1093/14	6/9/15	18:22:07	25.8	41	2	High	0.280198	0.000061	0.000776	0.000063
TC3/M1093/17	6/9/15	18:26:59	22.9	44	2	High	0.280168	0.000051	0.000991	0.000012
TC3/M1093/34	6/9/15	20:21:00	17.2	61	2	High	0.280123	0.000065	0.001380	0.000200

Analysis	Date	Time	Duration (s)	Spot	Zircon Phase	Analysis Quality	Corrected 176/177 Hf	2SE	Lu176/Hf177	2SE
TC3/M1093/36	6/9/15	20:24:16	31.7	63	2	High	0.280197	0.000058	0.000888	0.000020
TC3/GEVMT/4	6/5/15	20:39:49	20.2	4	2	Good	0.280246	0.000084	0.001730	0.000170
TC3/GEVMT/12	6/5/15	21:14:04	12.5	12	2	Good	0.280193	0.000077	0.001376	0.000015
TC3/GEVMT/16	6/5/15	21:27:11	20.0	16	2	Good	0.280191	0.000051	0.000764	0.000022
TC3/GEVMT/20	6/5/15	21:47:49	18.1	20	2	Good	0.280221	0.000076	0.001290	0.000260
TC3/GEVMT/22	6/5/15	21:51:04	16.7	22	2	Good	0.280180	0.000058	0.001227	0.000036
TC3/GEVMT/25	6/5/15	22:02:32	42.6	25	2	Good	0.280345	0.000088	0.001170	0.000170
TC3/GEVMT/26	6/5/15	22:04:12	16.8	26	2	Good	0.280203	0.000033	0.000895	0.000015
TC3/GEVMT/37	6/5/15	23:34:32	14.3	37	2	Good	0.280271	0.000083	0.002570	0.000130
TC3/GEVMT/40	6/5/15	23:39:22	17.3	40	2	Good	0.280214	0.000067	0.001528	0.000078
TC3/GEVMT/43	6/5/15	23:50:51	9.0	43	2	Good	0.280228	0.000067	0.002160	0.000110
TC3/GEVMT/50	6/6/15	0:30:36	16.2	50	2	Good	0.280307	0.000083	0.001809	0.000083
TC3/M1093/10	6/8/15	23:12:07	12.3	10	2	Good	0.280258	0.000056	0.002637	0.000027
TC3/M1093/11	6/8/15	23:13:44	38.6	11	2	Good	0.280187	0.000050	0.001015	0.000053
TC3/M1093/21	6/9/15	0:09:39	11.5	21	2	Good	0.280228	0.000057	0.001007	0.000064
TC3/M1093/7	6/9/15	17:47:14	32.9	34	2	Good	0.280243	0.000057	0.000839	0.000039
TC3/M1093/13	6/9/15	18:13:48	19.8	40	2	Good	0.280250	0.000067	0.001187	0.000084
TC3/M1093/15	6/9/15	18:23:44	9.6	42	2	Good	0.280038	0.000100	0.000770	0.000062
TC3/M1093/18	6/9/15	18:28:38	19.5	45	2	Good	0.280146	0.000044	0.000666	0.000037
TC3/M1093/22	6/9/15	19:21:55	12.4	49	2	Good	0.280232	0.000070	0.000889	0.000018
TC3/M1093/25	6/9/15	19:33:29	16.4	52	2	Good	0.280213	0.000064	0.000751	0.000043
TC3/M1093/26	6/9/15	19:35:07	9.5	53	2	Good	0.280410	0.000058	0.002260	0.000350
TC3/M1093/27	6/9/15	19:36:44	10.4	54	2	Good	0.280164	0.000069	0.001367	0.000076
TC3/M1093/29	6/9/15	20:06:11	12.1	56	2	Good	0.280211	0.000056	0.001375	0.000075

Analysis	Yb176/Hf177	2SE	Hf178/177	2SE	Total Hf	Epsilon (0)	2SE	176Hf/177Hf (i)	Epsilon (i)	2SE	Assigned Age
TC3/GEVMT/1	0.1274	0.0072	1.46738	0.00007	8.3	-86.8	2.6	0.280094	-2.3	2.6	4020
TC3/GEVMT/3	0.2055	0.0024	1.46731	0.00006	9.3	-79.6	3.6	0.280155	-0.1	3.6	4020
TC3/GEVMT/8	0.1235	0.0057	1.46731	0.00006	7.5	-85.3	2.0	0.280134	-0.9	2.1	4020
TC3/GEVMT/36	0.0858	0.0035	1.46749	0.00010	9.8	-89.3	3.4	0.280101	-2.0	3.4	4020
TC3/M1093/26	0.0602	0.0052	1.46733	0.00006	7.8	-91.5	2.2	0.280085	-2.6	2.2	4020
TC3/M1093/3	0.0953	0.0020	1.46737	0.00007	9.5	-88.8	2.6	0.280100	-2.1	2.7	4020
TC3/M1093/6	0.0403	0.0027	1.46735	0.00007	8.5	-92.6	2.1	0.280093	-2.3	2.1	4020
TC3/M1093/8	0.1283	0.0038	1.46733	0.00008	8.3	-86.5	2.7	0.280101	-2.0	2.7	4020
TC3/M1093/20	0.0408	0.0032	1.46740	0.00007	8.9	-92.1	2.9	0.280106	-1.9	3.0	4020
TC3/GEVMT/7	0.0882	0.0040	1.46734	0.00005	8.0	-89.3	2.5	0.280092	-2.4	2.5	4020
TC3/GEVMT/31	0.0371	0.0039	1.46741	0.00010	9.6	-90.8	2.4	0.280149	-0.3	2.4	4020
TC3/GEVMT/32	0.0720	0.0140	1.46742	0.00013	9.6	-93.7	3.1	0.280002	-5.6	3.3	4020
TC3/GEVMT/41	0.0851	0.0032	1.46744	0.00011	8.6	-88.2	2.7	0.280129	-1.0	2.7	4020
TC3/GEVMT/45	0.0795	0.0043	1.46741	0.00009	8.9	-89.9	1.8	0.280098	-2.2	1.9	4020
TC3/GEVMT/47	0.1499	0.0056	1.46743	0.00010	8.8	-85.9	3.5	0.280074	-3.0	3.5	4020
TC3/GEVMT/54	0.0342	0.0023	1.46751	0.00010	8.7	-92.4	2.9	0.280109	-1.8	2.9	4020
TC3/M1093/9	0.0859	0.0099	1.46734	0.00010	9.9	-88.3	2.3	0.280132	-0.9	2.4	4020
TC3/M1093/12	0.1290	0.0130	1.46742	0.00010	9.4	-89.3	3.2	0.280023	-4.8	3.4	4020
TC3/M1093/2	0.2090	0.0240	1.46731	0.00008	9.8	-84.9	5.3	0.280011	-5.3	5.5	4020
TC3/M1093/5	0.0797	0.0065	1.46733	0.00007	10.4	-87.8	1.8	0.280156	-0.1	1.8	4020
TC3/M1093/10	0.0770	0.0140	1.46729	0.00008	10.2	-89.6	3.5	0.280113	-1.6	3.5	4020
TC3/M1093/19	0.1124	0.0085	1.46732	0.00009	10.3	-90.1	2.6	0.280026	-4.7	2.6	4020
TC3/M1093/31	0.1272	0.0013	1.46737	0.00007	10.3	-86.9	2.7	0.280088	-2.5	2.7	4020
TC3/M1093/35	0.0860	0.0100	1.46733	0.00006	10.6	-87.8	3.6	0.280144	-0.5	3.6	4020
TC3/GEVMT/5	0.0498	0.0030	1.46733	0.00008	9.2	-89.7	1.8	0.280156	-0.1	1.9	4020
TC3/GEVMT/11	0.0445	0.0010	1.46734	0.00008	8.7	-92.0	1.6	0.280101	-2.0	1.7	4020
TC3/GEVMT/24	0.0748	0.0094	1.46743	0.00007	7.8	-91.3	2.4	0.280061	-3.5	2.5	4020
TC3/GEVMT/28	0.0430	0.0006	1.46742	0.00008	8.1	-92.4	1.7	0.280092	-2.4	1.7	4020
TC3/GEVMT/42	0.0444	0.0030	1.46738	0.00008	8.9	-92.4	1.4	0.280089	-2.5	1.4	4020
TC3/M1093/3	0.0314	0.0002	1.46740	0.00008	10.8	-92.5	1.7	0.280115	-1.6	1.7	4020
TC3/M1093/4	0.0318	0.0006	1.46738	0.00007	10.4	-94.1	2.0	0.280068	-3.2	2.0	4020
TC3/M1093/7	0.0310	0.0022	1.46748	0.00004	10.0	-91.8	2.3	0.280134	-0.9	2.3	4020
TC3/M1093/13	0.0347	0.0014	1.46735	0.00006	10.3	-91.5	2.9	0.280137	-0.8	2.9	4020
TC3/M1093/14	0.0324	0.0012	1.46743	0.00011	10.8	-93.2	3.5	0.280091	-2.4	3.6	4020
TC3/M1093/17	0.0597	0.0047	1.46739	0.00007	9.4	-92.6	2.6	0.280059	-3.6	2.6	4020
TC3/M1093/27	0.0389	0.0009	1.46740	0.00008	9.1	-93.6	2.0	0.280067	-3.3	2.0	4020
TC3/M1093/12	0.0436	0.0007	1.46732	0.00008	9.0	-91.9	2.1	0.280106	-1.9	2.1	4020
TC3/M1093/14	0.0300	0.0023	1.46729	0.00007	8.8	-91.8	2.2	0.280138	-0.8	2.2	4020
TC3/M1093/17	0.0388	0.0007	1.46732	0.00006	9.6	-92.8	1.8	0.280091	-2.4	1.9	4020
TC3/M1093/34	0.0562	0.0095	1.46728	0.00009	9.4	-94.4	2.3	0.280015	-5.1	2.4	4020

Analysis	Yb176/Hf177	2SE	Hf178/177	2SE	Total Hf	Epsilon (0)	2SE	176Hf/177Hf (i)	Epsilon (i)	2SE	Assigned Age
TC3/M1093/36	0.0341	0.0009	1.46733	0.00007	8.2	-91.8	2.1	0.280128	-1.1	2.1	4020
TC3/GEVMT/4	0.0712	0.0089	1.46733	0.00007	8.8	-90.1	3.0	0.280111	-1.7	3.1	4020
TC3/GEVMT/12	0.0510	0.0009	1.46744	0.00010	9.3	-91.9	2.7	0.280086	-2.6	2.8	4020
TC3/GEVMT/16	0.0290	0.0004	1.46742	0.00008	9.7	-92.0	1.8	0.280131	-1.0	1.9	4020
TC3/GEVMT/20	0.0540	0.0120	1.46738	0.00009	9.6	-90.9	2.7	0.280120	-1.4	2.8	4020
TC3/GEVMT/22	0.0463	0.0013	1.46751	0.00009	8.7	-92.4	2.1	0.280084	-2.6	2.1	4020
TC3/GEVMT/25	0.0456	0.0064	1.46744	0.00008	7.0	-86.6	3.1	0.280254	3.4	3.2	4020
TC3/GEVMT/26	0.0343	0.0007	1.46750	0.00011	9.2	-91.6	1.2	0.280133	-0.9	1.3	4020
TC3/GEVMT/37	0.1016	0.0070	1.46752	0.00006	8.5	-89.2	3.0	0.280071	-3.1	3.0	4020
TC3/GEVMT/40	0.0601	0.0032	1.46747	0.00006	9.3	-91.2	2.4	0.280095	-2.3	2.4	4020
TC3/GEVMT/43	0.0885	0.0055	1.46748	0.00007	9.9	-90.7	2.4	0.280060	-3.5	2.5	4020
TC3/GEVMT/50	0.0704	0.0049	1.46750	0.00007	8.3	-87.9	3.0	0.280166	0.3	3.0	4020
TC3/M1093/10	0.1060	0.0021	1.46737	0.00007	9.5	-89.6	2.0	0.280052	-3.8	2.0	4020
TC3/M1093/11	0.0377	0.0022	1.46737	0.00007	6.7	-92.2	1.8	0.280108	-1.8	1.8	4020
TC3/M1093/21	0.0406	0.0018	1.46734	0.00016	10.8	-90.7	2.1	0.280150	-0.3	2.1	4020
TC3/M1093/7	0.0338	0.0014	1.46728	0.00006	8.6	-90.2	2.1	0.280178	0.7	2.1	4020
TC3/M1093/13	0.0482	0.0038	1.46731	0.00005	10.3	-89.9	2.4	0.280157	0.0	2.4	4020
TC3/M1093/15	0.0302	0.0037	1.46745	0.00016	10.7	-97.4	3.6	0.279978	-6.4	3.6	4020
TC3/M1093/18	0.0260	0.0017	1.46734	0.00006	10.3	-93.6	1.6	0.280094	-2.3	1.6	4020
TC3/M1093/22	0.0357	0.0005	1.46722	0.00014	11.4	-90.6	2.5	0.280163	0.1	2.5	4020
TC3/M1093/25	0.0293	0.0022	1.46740	0.00007	10.2	-91.2	2.3	0.280154	-0.1	2.3	4020
TC3/M1093/26	0.0910	0.0140	1.46737	0.00012	11.1	-84.3	2.1	0.280234	2.7	2.1	4020
TC3/M1093/27	0.0550	0.0035	1.46732	0.00009	10.8	-93.0	2.5	0.280057	-3.6	2.5	4020
TC3/M1093/29	0.0549	0.0020	1.46738	0.00005	11.5	-91.3	2.0	0.280104	-2.0	2.0	4020

Analysis	Pb204 (cps)	Pb206 (cps)	206/204	207/235	2SE	206/238	2SE	Rho	207/206	2SE	7/35 Age	2SE	6/38 Age	2SE	7/6 Age	2SE
TC3/GEVMT/1	403	2280000	5658	44.8	0.5	0.820	0.010	0.94	0.4035	0.0017	3885	12	3858	35	3922	7
TC3/GEVMT/3	423	5250000	12411	48.9	0.5	0.797	0.008	0.83	0.4470	0.0027	3969	11	3776	30	4075	9
TC3/GEVMT/8	446	2110000	4731	46.5	0.5	0.831	0.008	0.92	0.4005	0.0016	3918	10	3896	27	3911	6
TC3/GEVMT/36	310	1718000	5542	49.5	0.3	0.871	0.004	0.67	0.4094	0.0018	3982	6	4038	14	3944	7
TC3/M1093/26	269	1450000	5390	54.0	0.5	0.962	0.008	0.79	0.4070	0.0024	4067	10	4344	28	3934	9
TC3/M1093/3	484	1749000	3614	50.5	0.6	0.886	0.007	0.90	0.4160	0.0021	4002	11	4091	25	3968	8
TC3/M1093/6	424	1260000	2972	56.0	1.0	0.967	0.016	0.93	0.4203	0.0028	4102	18	4357	53	3983	10
TC3/M1093/8	444	2090000	4707	53.9	0.4	0.948	0.007	0.81	0.4124	0.0018	4067	7	4298	22	3955	7
TC3/M1093/20	371	790000	2129	54.5	0.7	0.938	0.011	0.89	0.4151	0.0024	4077	13	4263	35	3964	9
TC3/GEVMT/7	467	1790000	3833	47.2	0.5	0.836	0.008	0.89	0.4055	0.0018	3935	10	3917	27	3929	7
TC3/GEVMT/31	558	1059000	1898	38.7	0.8	0.739	0.016	0.96	0.3771	0.0024	3735	21	3565	58	3820	10
TC3/GEVMT/32	348	1760000	5057	48.0	0.7	0.865	0.017	0.97	0.4000	0.0026	3951	15	4014	58	3909	10
TC3/GEVMT/41	362	1648000	4552	46.1	1.1	0.831	0.019	0.98	0.4121	0.0018	3908	24	3892	69	3954	6
TC3/GEVMT/45	355	1317000	3710	54.3	0.7	0.970	0.012	0.92	0.4136	0.0021	4073	13	4369	39	3959	8
TC3/GEVMT/47	350	3207000	9163	48.7	0.4	0.907	0.008	0.76	0.3923	0.0022	3966	8	4160	26	3880	9
TC3/GEVMT/54	396	1056000	2667	39.4	0.5	0.767	0.007	0.67	0.3813	0.0035	3756	12	3669	27	3836	14
TC3/M1093/9	295	1840000	6237	53.3	0.7	0.950	0.009	0.88	0.3994	0.0024	4054	12	4304	29	3907	9
TC3/M1093/12	411	4650000	11314	52.0	0.5	0.895	0.011	0.60	0.4266	0.0071	4030	9	4119	36	4004	26
TC3/M1093/2	640	5130000	8016	38.3	4.2	0.632	0.073	1.00	0.4556	0.0054	3690	110	3120	290	4103	18
TC3/M1093/5	464	1957000	4218	34.8	0.9	0.707	0.017	0.90	0.3606	0.0041	3630	26	3444	64	3752	17
TC3/M1093/10	332	1400000	4217	57.8	2.4	1.049	0.023	0.92	0.4025	0.0092	4129	45	4620	72	3914	37
TC3/M1093/19	365	2640000	7233	53.4	0.7	0.950	0.009	0.89	0.4030	0.0028	4058	14	4303	29	3920	10
TC3/M1093/31	375	4850000	12933	56.2	0.9	0.903	0.013	0.92	0.4476	0.0027	4107	16	4146	44	4077	9
TC3/M1093/35	331	2090000	6314	54.2	1.0	0.957	0.012	0.99	0.4078	0.0025	4071	19	4329	41	3938	9
TC3/GEVMT/5	449	1563000	3481	49.4	0.3	0.846	0.005	0.78	0.4186	0.0017	3979	6	3951	18	3978	6
TC3/GEVMT/11	374	1256000	3358	54.2	0.4	0.934	0.007	0.86	0.4198	0.0017	4072	8	4249	24	3981	6
TC3/GEVMT/24	378	1526000	4037	54.0	0.4	0.929	0.008	0.90	0.4186	0.0016	4069	8	4234	27	3977	6
TC3/GEVMT/28	362	1284000	3547	53.6	0.5	0.920	0.006	0.88	0.4182	0.0017	4061	8	4206	20	3975	6
TC3/GEVMT/42	343	1186000	3458	53.0	0.5	0.930	0.008	0.91	0.4215	0.0016	4049	8	4238	28	3987	6
TC3/M1093/3	319	853700	2676	54.0	0.4	0.931	0.006	0.51	0.4193	0.0030	4069	8	4243	19	3979	11
TC3/M1093/4	395	863000	2185	49.3	0.8	0.885	0.014	0.82	0.4026	0.0038	3977	16	4086	46	3918	14
TC3/M1093/7	292	816000	2795	51.8	0.6	0.924	0.012	0.62	0.3996	0.0044	4026	12	4219	41	3906	17
TC3/M1093/13	418	1148000	2746	55.6	0.7	0.971	0.009	0.91	0.4230	0.0026	4098	13	4372	30	3993	9
TC3/M1093/14	322	986000	3062	54.8	0.6	0.944	0.007	0.91	0.4224	0.0022	4083	11	4286	24	3991	8
TC3/M1093/17	345	1104000	3200	54.5	0.9	0.954	0.011	1.00	0.4175	0.0021	4075	17	4316	37	3973	8
TC3/M1093/27	279	1112000	3986	53.2	0.5	0.935	0.006	0.83	0.4143	0.0020	4054	9	4253	20	3961	7
TC3/M1093/12	350	1059000	3026	58.8	0.6	1.010	0.010	0.78	0.4192	0.0027	4154	10	4500	32	3979	10
TC3/M1093/14	375	674000	1797	57.1	0.7	0.979	0.011	0.82	0.4225	0.0029	4123	12	4399	35	3990	10
TC3/M1093/17	429	1327000	3093	61.8	1.2	1.068	0.018	0.97	0.4192	0.0022	4201	20	4681	56	3979	8
TC3/M1093/34	343	1150000	3353	53.7	0.9	0.931	0.013	0.97	0.4133	0.0019	4060	17	4238	45	3958	7

Analysis	Pb204 (cps)	Pb206 (cps)	206/204	207/235	2SE	206/238	2SE	Rho	207/206	2SE	7/35 Age	2SE	6/38 Age	2SE	7/6 Age	2SE
TC3/M1093/36	303	775000	2558	53.5	0.9	0.913	0.016	0.89	0.4209	0.0034	4058	17	4178	54	3984	12
TC3/GEVMT/4	398	1983000	4982	46.4	0.5	0.810	0.010	0.72	0.4186	0.0035	3917	10	3822	34	3977	13
TC3/GEVMT/12	745	1056000	1417	51.0	0.8	0.919	0.013	0.86	0.4025	0.0032	4011	16	4200	44	3918	12
TC3/GEVMT/16	412	719000	1745	55.4	0.9	0.957	0.014	0.94	0.4194	0.0022	4092	15	4324	46	3980	8
TC3/GEVMT/20	482	1950000	4046	43.8	2.3	0.814	0.041	0.99	0.3885	0.0027	3844	50	3820	140	3864	11
TC3/GEVMT/22	348	1121000	3221	53.4	0.6	0.930	0.010	0.86	0.4155	0.0023	4057	10	4239	35	3966	8
TC3/GEVMT/25	390	1007000	2582	40.0	0.5	0.760	0.010	0.47	0.3805	0.0051	3770	13	3642	37	3833	20
TC3/GEVMT/26	376	861000	2290	49.2	1.0	0.863	0.012	0.93	0.4110	0.0035	3973	20	4008	43	3949	13
TC3/GEVMT/37	339	2600000	7670	28.5	0.5	0.502	0.009	0.97	0.4065	0.0019	3432	18	2621	40	3933	7
TC3/GEVMT/40	338	1370000	4053	54.2	0.8	0.954	0.013	0.90	0.4207	0.0029	4071	15	4318	42	3984	10
TC3/GEVMT/43	363	1645000	4532	51.5	0.6	0.934	0.010	0.69	0.4091	0.0035	4021	11	4251	35	3942	13
TC3/GEVMT/50	356	1407000	3952	51.4	1.1	0.919	0.020	0.97	0.4119	0.0023	4021	20	4198	69	3953	8
TC3/M1093/10	450	4270000	9489	51.7	0.7	0.944	0.017	0.76	0.4037	0.0047	4025	14	4283	55	3922	17
TC3/M1093/11	318	920000	2893	51.2	0.5	0.891	0.008	0.91	0.4153	0.0017	4014	10	4106	28	3966	6
TC3/M1093/21	292	1155000	3955	64.1	1.0	1.126	0.021	0.95	0.4119	0.0026	4238	16	4875	58	3953	10
TC3/M1093/7	448	649000	1449	44.2	1.1	0.832	0.018	0.88	0.3867	0.0046	3865	25	3892	63	3857	17
TC3/M1093/13	480	980000	2042	50.1	1.2	0.914	0.021	0.70	0.4026	0.0073	3993	25	4183	70	3917	27
TC3/M1093/15	520	1010000	1942	55.9	1.4	1.011	0.027	0.80	0.4065	0.0066	4102	25	4500	88	3932	24
TC3/M1093/18	394	733000	1860	58.7	0.8	1.014	0.012	0.66	0.4201	0.0045	4151	14	4511	39	3982	16
TC3/M1093/22	360	878000	2439	52.1	1.4	0.889	0.026	0.96	0.4180	0.0035	4030	28	4117	81	3974	13
TC3/M1093/25	410	732000	1785	54.3	0.9	0.926	0.013	0.94	0.4186	0.0025	4076	16	4224	44	3977	9
TC3/M1093/26	410	1977000	4822	51.9	1.0	0.921	0.015	0.94	0.4052	0.0027	4028	19	4206	51	3928	10
TC3/M1093/27	397	1083000	2728	51.7	1.5	0.914	0.023	0.97	0.4089	0.0031	4023	29	4182	77	3942	12
TC3/M1093/29	422	1800000	4265	49.8	0.5	0.864	0.012	0.78	0.4157	0.0036	3990	12	4013	40	3966	13

Analysis	Discordance	O isotope Session	Delta 18O	2sigma	Oxygen Spot
TC3/GEVMT/1	1.1				
TC3/GEVMT/3	8.8				
TC3/GEVMT/8	-0.5				
TC3/GEVMT/36	-4.2				
TC3/M1093/26	-15.5	IP11095B	5.57	0.23	S1425/61@1
TC3/M1093/3	-5.2	IP11094C	6.14	0.16	S1425/38@1
TC3/M1093/6	-14.2				
TC3/M1093/8	-13.1	IP11095B	4.93	0.24	S1425/52@1
TC3/M1093/20	-11.5	IP11095B	5.42	0.25	S1425/58@1
TC3/GEVMT/7	-0.6				
TC3/GEVMT/31	7.7				
TC3/GEVMT/32	-4.8				
TC3/GEVMT/41	0.9				
TC3/GEVMT/45	-15.5				
TC3/GEVMT/47	-10.9				
TC3/GEVMT/54	4.8				
TC3/M1093/9	-15.1	IP11095	5.45	0.15	S1425/47@2
TC3/M1093/12	-5.0	IP11095	5.88	0.17	S1425/46@1
TC3/M1093/2	28.3	IP11106	5.92	0.22	S1425/66@2
TC3/M1093/5	9.6				
TC3/M1093/10	-26.8	IP14076B	5.10	0.19	S1425/87@103
TC3/M1093/19	-14.6				
TC3/M1093/31	-3.4	IP11095B	5.75	0.22	S1425/60@1
TC3/M1093/35	-14.8				
TC3/GEVMT/5	-0.1				
TC3/GEVMT/11	-10.3				
TC3/GEVMT/24	-9.9				
TC3/GEVMT/28	-9.0				
TC3/GEVMT/42	-9.7				
TC3/M1093/3	-10.1	IP11094C	4.44	0.15	S1425/36@2
TC3/M1093/4	-6.8	IP11094C	4.80	0.18	S1425/37@2
TC3/M1093/7	-12.0	IP11094C	4.38	0.22	S1425/41@1
TC3/M1093/13	-14.3				
TC3/M1093/14	-11.3	IP11095B	4.47	0.25	S1425/51@2
TC3/M1093/17	-13.1	IP11094C	5.40	0.19	S1425/43@2
TC3/M1093/27	-11.2				
TC3/M1093/12	-19.5	IP11094C	4.82	0.16	S1425/42@1
TC3/M1093/14	-15.4	IP11106	4.54	0.18	S1425/73@1
TC3/M1093/17	-26.3				
TC3/M1093/34	-10.9	IP11107	4.80	0.27	S1425/79@2

Analysis	Discordance	O isotope Session	Delta 18O	2sigma	Oxygen Spot
TC3/M1093/36	-7.8				
TC3/GEVMT/4	4.2				
TC3/GEVMT/12	-11.0				
TC3/GEVMT/16	-13.2				
TC3/GEVMT/20	-0.1				
TC3/GEVMT/22	-10.5				
TC3/GEVMT/25	5.5				
TC3/GEVMT/26	-3.1				
TC3/GEVMT/37	39.7				
TC3/GEVMT/40	-12.6				
TC3/GEVMT/43	-11.9				
TC3/GEVMT/50	-9.7				
TC3/M1093/10	-13.8				
TC3/M1093/11	-5.8	IP11095	4.34	0.14	S1425/46@2
TC3/M1093/21	-34.4				
TC3/M1093/7	-2.6				
TC3/M1093/13	-10.4	IP11094C	5.01	0.18	S1425/42@2
TC3/M1093/15	-21.5	IP11106	4.93	0.20	S1425/71@1
TC3/M1093/18	-19.8				
TC3/M1093/22	-5.3	IP11106	4.70	0.20	S1425/65@1
TC3/M1093/25	-9.6	IP11107	4.63	0.24	S1425/75@2
TC3/M1093/26	-10.8				
TC3/M1093/27	-9.5	IP11095B	4.74	0.26	S1425/49@1
TC3/M1093/29	-2.6				

Table 3.4 TIMS U-Pb analyses of TC3 zircons

		Composition				Dates (Ma)								
Fraction	Zircon Phase	Th/ U (a)	Pb* (pg) (b)	Pbc (pg) (c)	Pb*/ Pbc (d)	206Pb/ 238U (e)	±2σ abs	207Pb/ 235U (e)	±2σ abs	207Pb/ 206Pb (e)	±2σ abs	Corr. coef.	% disc (f)	206Pb/ 204Pb (g)
TC3_19h_z1	**n/a**	0.44	301	0.54	558	3798.6	3.1	3841.8	1.1	3864.36	0.32	0.981	1.7	26692
TC3_19h_z2	**n/a**	0.5	23.2	0.94	25	3919	11	3977.2	4.1	4006.8	2.3	0.929	2.2	1152
TC3_19h_z3	**n/a**	0.53	44.5	0.06	742	3822.8	2.9	3870	1.1	3894.52	0.39	0.969	1.84	34771
TC3_19h_z4	**n/a**	0.39	60.8	0.05	1123	3703.3	2.5	3764.81	0.91	3797.73	0.33	0.971	2.49	54802
TC3_19h_z5	**n/a**	0.69	57.9	0.08	744	3972.1	6.1	3981.3	2.1	3985.97	0.5	0.987	0.35	33477
TC3_19h_z6	**n/a**	0.71	29	0.07	391	3968.8	8	3987.9	2.7	3997.55	0.55	0.991	0.72	17497
TC3_19h_z8	**n/a**	0.53	54.6	0.06	915	3940.1	1.5	3959.41	0.58	3969.22	0.35	0.917	0.73	42392
TC3_19h_z9	**n/a**	0.53	35	0.05	638	3892.4	1.3	3918.5	0.56	3931.86	0.42	0.868	1	29728
TC3_z1	**1**	0.6	38.7	0.12	333	3984	1.1	3992.09	0.51	3996.15	0.47	0.799	0.3	15188
TC3_z15	**mixed**	0.5	93.5	0.12	767	3942.1	1.2	3961.99	0.51	3972.1	0.35	0.893	0.76	35644
TC3_z16	**mixed**	0.34	136	0.25	544	3604.1	1.5	3673.91	0.66	3712.17	0.44	0.904	2.91	27183
TC3_z18	**mixed**	0.34	24.9	0.19	134	3693.7	1.6	3761.52	0.77	3797.83	0.69	0.812	2.74	6595
TC3_z19	**1**	0.55	24.9	0.11	221	3867.8	2.3	3902.38	0.93	3920.2	0.64	0.891	1.34	10301
TC3_z23	**1**	0.64	154	0.14	1122	3947.6	1.4	3966.11	0.55	3975.5	0.36	0.9	0.7	50938
TC3_z31	**1**	0.47	32.6	0.08	393	3852.1	3.5	3887.9	1.3	3906.45	0.52	0.963	1.39	18580
TC3_z38	**3**	0.53	216	0.12	1731	4010.3	1.4	4012.57	0.52	4013.72	0.3	0.924	0.09	79436
TC3_z41	**2**	0.5	50.8	0.5	102	3901.3	1.5	3927.36	0.78	3940.67	0.72	0.8	1	4769
TC3_z50	**metamporphic**	0.01	117	0.16	710	3180.6	2	3224.2	1	3251.42	0.81	0.875	2.18	40444
TC3_z67	**2**	0.51	43.3	0.17	251	3942.1	2.1	3960.68	0.79	3970.08	0.49	0.909	0.7	11682
TC3_z69	**1**	0.63	107	0.15	697	3981.2	3.3	3994.4	1.2	4001.02	0.45	0.966	0.5	31591
TC3_z70	**2**	0.55	115	0.16	694	2938.6	1.3	3590.38	0.6	3977.12	0.34	0.929	26.11	31834

a Th contents calculated from radiogenic 208Pb and the 230Th-corrected 206Pb/238U date of the sample assuming concordance between the U-Pb and Th-Pb systems

b Total mass of radiogenic Pb.

c Total mass of common Pb.

d Ratio of radiogenic Pb (including 208Pb) to common Pb.

e Isotopic dates calculated using the decay constants λ238 = 1.55125E-10 and λ235 = 9.8485E-10 (Jaffey et al. 1971).

f % discordance = 100 - (100 * (206Pb/238U date) / (207Pb/206Pb date))

g Measured ratio corrected for fractionation and spike contribution only.

h Measured ratios corrected for fractionation, tracer and blank.

	Isotopic Ratios					
Fraction	206Pb/ 238U (h)	±2σ %	207Pb/ 235U (h)	±2σ %	207Pb/ 206Pb (h)	±2σ %
TC3_19h_z1	0.80266	0.11	42.973	0.11	0.38847	0.016
TC3_19h_z2	0.8365	0.37	49.25	0.42	0.42714	0.15
TC3_19h_z3	0.80942	0.1	44.211	0.11	0.396325	0.022
TC3_19h_z4	0.77619	0.088	39.763	0.092	0.371713	0.017
TC3_19h_z5	0.8518	0.2	49.45	0.21	0.42123	0.03
TC3_19h_z6	0.8509	0.27	49.78	0.28	0.4245	0.034
TC3_19h_z8	0.84265	0.051	48.374	0.059	0.416544	0.018
TC3_19h_z9	0.82909	0.045	46.424	0.056	0.406294	0.024
TC3_z1	0.85525	0.036	49.989	0.052	0.42411	0.028
TC3_z15	0.84322	0.04	48.5	0.051	0.417343	0.019
TC3_z16	0.74908	0.055	36.272	0.066	0.351349	0.025
TC3_z18	0.77356	0.058	39.631	0.078	0.37174	0.043
TC3_z19	0.8221	0.08	45.677	0.093	0.40315	0.04
TC3_z23	0.8448	0.046	48.701	0.055	0.418293	0.019
TC3_z31	0.81767	0.12	45.017	0.13	0.39948	0.031
TC3_z38	0.86282	0.047	51.028	0.052	0.42912	0.014
TC3_z41	0.83161	0.053	46.84	0.078	0.40869	0.046
TC3_z50	0.63785	0.08	22.935	0.1	0.2609	0.049
TC3_z67	0.84324	0.07	48.436	0.079	0.41678	0.03
TC3_z69	0.85444	0.11	50.104	0.12	0.42549	0.026
TC3_z70	0.57752	0.054	33.329	0.061	0.418746	0.017

Table 3.5 ICPMS Solution Hf isotope data from the same dissolutions as TIMS U-Pb data

Analysis	Date	Time	Duration (s)	Zircon Phase	Analysis Quality (1-3)	Corrected 176/177 Hf	2SE	Lu176/Hf177	2SE
TC3_1	6/9/15	13:24:33	80	1	5	0.280187	0.000034	0.00171	0.00000
TC3_19	6/9/15	18:11:52	80	1	5	0.280260	0.000037	0.00208	0.00000
TC3_23	6/9/15	18:25:43	80	1	5	0.280301	0.000017	0.00312	0.00001
TC3_31	6/9/15	19:51:11	80	1	5	0.280263	0.000019	0.00169	0.00000
TC3_69	6/9/15	03:57:06	80	1	5	0.280334	0.000016	0.00261	0.00000
TC3_12	6/9/15	15:12:22	80	2	5	0.280230	0.000009	0.00160	0.00000
TC3_38	6/9/15	21:25:08	80	2	5	0.280197	0.000009	0.00121	0.00000
TC3_41	6/9/15	22:31:22	80	2	5	0.280274	0.000024	0.00204	0.00000
TC3_67	6/9/15	02:31:36	80	2	5	0.280217	0.000019	0.00150	0.00000
TC3_70	6/9/15	04:10:58	80	2	5	0.280338	0.000021	0.00293	0.00000

Analysis	Hf178/177	2SE	Epsilon (0)	2SE	176Hf/177Hf (i)	Epsilon (i)	2SE	Assigned Age
TC3_1	1.48764	0.00008	-92.2	1.3	0.280053	**-3.76**	1.28	4020
TC3_19	1.48766	0.00010	-89.6	1.4	0.280098	**-2.17**	1.39	4020
TC3_23	1.48758	0.00004	-88.1	0.7	0.280058	**-3.60**	0.74	4020
TC3_31	1.48813	0.00005	-89.5	0.8	0.280132	**-0.97**	0.81	4020
TC3_69	1.48867	0.00005	-87.0	0.7	0.280130	**-1.00**	0.71	4020
TC3_12	1.48772	0.00003	-90.6	0.5	0.280106	**-1.88**	0.55	4020
TC3_38	1.48821	0.00002	-91.8	0.5	0.280102	**-2.03**	0.55	4020
TC3_41	1.48825	0.00005	-89.1	0.9	0.280116	**-1.53**	0.96	4020
TC3_67	1.48855	0.00006	-91.1	0.8	0.280101	**-2.07**	0.81	4020
TC3_70	1.48863	0.00004	-86.8	0.8	0.280109	**-1.76**	0.87	4020

Table 3.6 LASS Hf isotope data from Reference Materials

Averages	Corrected 176/177Hf	2SD	Lu176/Hf177	2SD	Yb176/Hf177	2SD
FC1	0.282203	0.000057	0.001446	0.000513	0.057680	0.021665
MUN1	0.282136	0.000045	0.001724	0.001170	0.013048	0.009379
MUN4	0.282140	0.000114	0.009351	0.002429	0.360787	0.125953
R33	0.282761	0.000059	0.002127	0.001546	0.081212	0.065320
Plesovice	0.282489	0.000046	0.000124	0.000090	0.006540	0.004930

Analysis	Date	Time	Duration (s)	Comments	Standard	176Hf/177Hf	Corrected 176/177Hf	2SE
FC1_1	6/5/15	20:43:11	34.297	FC1 - 1	FC1	0.282116	**0.282184**	0.000073
FC1_2	6/5/15	21:19:01	34.963	FC1 - 2	FC1	0.282099	**0.282167**	0.000048
FC1_3	6/5/15	21:54:23	36.474	FC1 - 3	FC1	0.282181	**0.282249**	0.000066
FC1_4	6/5/15	23:05:23	26.935	FC1 - 4	FC1	0.282165	**0.282233**	0.000048
FC1_5	6/5/15	23:42:39	28.135	FC1 - 5	FC1	0.282123	**0.282191**	0.000059
FC1_6	6/6/15	0:12:30	33.912	FC1 - 6	FC1	0.282097	**0.282165**	0.000061
FC1_1	6/8/15	22:43:07	34.257	FC1 - 1	FC1	0.282132	**0.282200**	0.000058
FC1_2	6/8/15	23:20:17	31.895	FC1 - 2	FC1	0.282113	**0.282181**	0.000053
FC1_1	6/9/15	17:38:59	34.12	FC1 - 1	FC1	0.282171	**0.282239**	0.000057
FC1_2	6/9/15	18:17:09	11.117	FC1 - 2	FC1	0.282158	**0.282226**	0.000089
FC1_3	6/9/15	0:14:39	32.263	FC1 - 3	FC1	0.282103	**0.282171**	0.000049
FC1_3	6/9/15	19:25:18	30.776	FC1 - 3	FC1	0.282149	**0.282217**	0.000044
FC1_4	6/9/15	20:12:46	31.133	FC1 - 4	FC1	0.282142	**0.282210**	0.000062
MUN1_1	6/5/15	20:31:39	37.51	MUN1 - 1	MUN1	0.282093	**0.282161**	0.000039
MUN1_10	6/5/15	23:44:21	33.77	MUN1 - 10	MUN1	0.282050	**0.282118**	0.000042
MUN1_2	6/5/15	20:44:51	33.951	MUN1 - 2	MUN1	0.282081	**0.282149**	0.000040
MUN1_3	6/5/15	21:07:33	35.389	MUN1 - 3	MUN1	0.282107	**0.282175**	0.000057
MUN1_4	6/5/15	21:20:40	33.778	MUN1 - 4	MUN1	0.282099	**0.282167**	0.000055
MUN1_5	6/5/15	21:42:55	35.35	MUN1 - 5	MUN1	0.282064	**0.282132**	0.000056
MUN1_6	6/5/15	21:56:04	33.788	MUN1 - 6	MUN1	0.282030	**0.282098**	0.000063
MUN1_7	6/5/15	22:53:56	35.387	MUN1 - 7	MUN1	0.282077	**0.282145**	0.000060
MUN1_8	6/5/15	23:07:05	32.794	MUN1 - 8	MUN1	0.282036	**0.282104**	0.000043
MUN1_9	6/5/15	23:31:13	34.446	MUN1 - 9	MUN1	0.282048	**0.282116**	0.000059
MUN1_11	6/6/15	0:14:12	33.728	MUN1 - 11	MUN1	0.282084	**0.282152**	0.000050
MUN1_12	6/6/15	0:28:56	31.717	MUN1 - 12	MUN1	0.282036	**0.282104**	0.000048
MUN1_1	6/8/15	22:31:42	15.679	MUN1 - 1	MUN1	0.282101	**0.282169**	0.000047
MUN1_2	6/8/15	22:44:49	26.38	MUN1 - 2	MUN1	0.282074	**0.282142**	0.000061
MUN1_3	6/8/15	23:08:47	26.677	MUN1 - 3	MUN1	0.282088	**0.282156**	0.000051
MUN1_4	6/8/15	23:21:59	25.394	MUN1 - 4	MUN1	0.282053	**0.282121**	0.000043
MUN1_1	6/9/15	17:27:30	30.305	MUN1 - 1	MUN1	0.282080	**0.282148**	0.000045

Analysis	Date	Time	Duration (s)	Comments	Standard	176Hf/177Hf	Corrected 176/177Hf	2SE
MUN1_2	6/9/15	17:40:43	29.39	MUN1 - 2	MUN1	0.282084	**0.282152**	0.000043
MUN1_3	6/9/15	18:05:39	27.638	MUN1 - 3	MUN1	0.282055	**0.282123**	0.000048
MUN1_4	6/9/15	18:18:50	27.505	MUN1 - 4	MUN1	0.282074	**0.282142**	0.000037
MUN1_5	6/9/15	0:03:09	26.085	MUN1 - 5	MUN1	0.282046	**0.282114**	0.000043
MUN1_5	6/9/15	19:13:50	29.992	MUN1 - 5	MUN1	0.282074	**0.282142**	0.000042
MUN1_6	6/9/15	0:16:19	25.653	MUN1 - 6	MUN1	0.282058	**0.282126**	0.000058
MUN1_6	6/9/15	19:26:57	32.897	MUN1 - 6	MUN1	0.282072	**0.282140**	0.000039
MUN1_7	6/9/15	20:01:18	29.056	MUN1 - 7	MUN1	0.282085	**0.282153**	0.000056
MUN1_8	6/9/15	20:14:30	28.578	MUN1 - 8	MUN1	0.282029	**0.282097**	0.000057
MUN4_1	6/5/15	20:33:20	31.814	MUN4 - 1	MUN4	0.282086	**0.282154**	0.000093
MUN4_10	6/5/15	23:45:57	35.363	MUN4 - 10	MUN4	0.282039	**0.282107**	0.000084
MUN4_2	6/5/15	20:46:28	33.385	MUN4 - 2	MUN4	0.282144	**0.282212**	0.000084
MUN4_3	6/5/15	21:09:11	33.408	MUN4 - 3	MUN4	0.282040	**0.282108**	0.000110
MUN4_4	6/5/15	21:22:19	34.499	MUN4 - 4	MUN4	0.282047	**0.282115**	0.000080
MUN4_5	6/5/15	21:44:34	15.718	MUN4 - 5	MUN4	0.282130	**0.282198**	0.000100
MUN4_6	6/5/15	21:57:43	31.228	MUN4 - 6	MUN4	0.282069	**0.282137**	0.000096
MUN4_7	6/5/15	22:55:33	35.886	MUN4 - 7	MUN4	0.282083	**0.282151**	0.000082
MUN4_8	6/5/15	23:08:40	36.405	MUN4 - 8	MUN4	0.282096	**0.282164**	0.000099
MUN4_9	6/5/15	23:32:51	33.399	MUN4 - 9	MUN4	0.282030	**0.282098**	0.000120
MUN4_11	6/6/15	0:15:47	20.823	MUN4 - 11 - 1	MUN4	0.282113	**0.282181**	0.000095
MUN4_12	6/6/15	0:27:16	31.682	MUN4 - 12 - 1	MUN4	0.282103	**0.282171**	0.000089
MUN4_1	6/8/15	22:33:19	24.722	MUN4 - 1	MUN4	0.282110	**0.282178**	0.000120
MUN4_2	6/8/15	22:46:28	23.806	MUN4 - 2	MUN4	0.282117	**0.282185**	0.000086
MUN4_3	6/8/15	23:10:26	25.65	MUN4 - 3	MUN4	0.282039	**0.282107**	0.000084
MUN4_4	6/8/15	23:23:37	25.69	MUN4 - 4	MUN4	0.282020	**0.282088**	0.000120
MUN4_1	6/9/15	17:29:06	36.335	MUN4 - 1	MUN4	0.282120	**0.282188**	0.000078
MUN4_2	6/9/15	17:42:21	32.04	MUN4 - 2	MUN4	0.282010	**0.282078**	0.000130
MUN4_3	6/9/15	18:07:17	27.075	MUN4 - 3	MUN4	0.282150	**0.282218**	0.000130
MUN4_4	6/9/15	18:20:27	32.491	MUN4 - 4	MUN4	0.281996	**0.282064**	0.000079
MUN4_5	6/9/15	0:04:48	24.701	MUN4 - 5	MUN4	0.281940	**0.282008**	0.000130
MUN4_5	6/9/15	19:15:27	31.072	MUN4 - 5	MUN4	0.281997	**0.282065**	0.000090
MUN4_6	6/9/15	0:17:59	23.349	MUN4 - 6	MUN4	0.282134	**0.282202**	0.000079
MUN4_6	6/9/15	19:28:35	32.861	MUN4 - 6	MUN4	0.282100	**0.282168**	0.000083
MUN4_7	6/9/15	20:02:57	28.372	MUN4 - 7	MUN4	0.282001	**0.282069**	0.000095
MUN4_8	6/9/15	20:16:09	27.59	MUN4 - 8	MUN4	0.282150	**0.282218**	0.000110
Z_Plesovice_1	6/5/15	20:26:47	24.964	PLESOVICE - 1	PLE	0.282392	**0.282460**	0.000048
Z_Plesovice_10	6/5/15	21:33:43	28.819	PLESOVICE - 10	PLE	0.282433	**0.282501**	0.000042
Z_Plesovice_11	6/5/15	21:38:01	18.801	PLESOVICE - 11	PLE	0.282424	**0.282492**	0.000037

Analysis	Date	Time	Duration (s)	Comments	Standard	176Hf/177Hf	Corrected 176/177Hf	2SE
Z_Plesovice_12	6/5/15	21:39:38	27.906	PLESOVICE - 12	PLE	0.282425	**0.282493**	0.000032
Z_Plesovice_13	6/5/15	21:52:44	10.684	PLESOVICE - 13	PLE	0.282387	**0.282455**	0.000021
Z_Plesovice_14	6/5/15	22:07:32	21.515	PLESOVICE - 14	PLE	0.282439	**0.282507**	0.000046
Z_Plesovice_15	6/5/15	22:09:10	23.416	PLESOVICE - 15	PLE	0.282403	**0.282471**	0.000053
Z_Plesovice_16	6/5/15	22:49:03	31.114	PLESOVICE - 16	PLE	0.282428	**0.282496**	0.000049
Z_Plesovice_17	6/5/15	22:50:41	19.065	PLESOVICE - 17	PLE	0.282394	**0.282462**	0.000050
Z_Plesovice_18	6/5/15	23:03:47	27.924	PLESOVICE - 18	PLE	0.282435	**0.282503**	0.000052
Z_Plesovice_19	6/5/15	23:18:31	15.614	PLESOVICE - 19	PLE	0.282388	**0.282456**	0.000045
Z_Plesovice_2	6/5/15	20:28:19	17.207	PLESOVICE - 2	PLE	0.282427	**0.282495**	0.000055
Z_Plesovice_20	6/5/15	23:20:08	17.749	PLESOVICE - 20	PLE	0.282424	**0.282492**	0.000047
Z_Plesovice_21	6/5/15	23:26:17	34.517	PLESOVICE - 21	PLE	0.282442	**0.282510**	0.000037
Z_Plesovice_22	6/5/15	23:27:58	24.1	PLESOVICE - 22	PLE	0.282415	**0.282483**	0.000035
Z_Plesovice_23	6/5/15	23:41:01	16.281	PLESOVICE - 23	PLE	0.282401	**0.282469**	0.000035
Z_Plesovice_24	6/5/15	23:55:47	26.768	PLESOVICE - 24	PLE	0.282410	**0.282478**	0.000042
Z_Plesovice_25	6/5/15	23:57:24	27.865	PLESOVICE - 25	PLE	0.282428	**0.282496**	0.000027
Z_Plesovice_3	6/5/15	20:41:32	22.264	PLESOVICE - 3	PLE	0.282420	**0.282488**	0.000040
Z_Plesovice_4	6/5/15	20:56:15	34.406	PLESOVICE - 4	PLE	0.282434	**0.282502**	0.000027
Z_Plesovice_5	6/5/15	20:57:50	35.307	PLESOVICE - 5	PLE	0.282445	**0.282513**	0.000031
Z_Plesovice_6	6/5/15	21:02:38	30.615	PLESOVICE - 6	PLE	0.282463	**0.282531**	0.000037
Z_Plesovice_7	6/5/15	21:04:14	34.401	PLESOVICE - 7	PLE	0.282415	**0.282483**	0.000034
Z_Plesovice_8	6/5/15	21:17:22	17.993	PLESOVICE - 8	PLE	0.282370	**0.282438**	0.000033
Z_Plesovice_9	6/5/15	21:32:08	14.034	PLESOVICE - 9	PLE	0.282373	**0.282441**	0.000053
Z_Plesovice_26	6/6/15	0:09:15	20.961	PLESOVICE - 26	PLE	0.282395	**0.282463**	0.000040
Z_Plesovice_27	6/6/15	0:10:53	33.07	PLESOVICE - 27	PLE	0.282428	**0.282496**	0.000034
Z_Plesovice_28	6/6/15	0:24:01	26.605	PLESOVICE - 28	PLE	0.282406	**0.282474**	0.000054
Z_Plesovice_29	6/6/15	0:38:44	20.37	PLESOVICE - 29	PLE	0.282384	**0.282452**	0.000046
Z_Plesovice_30	6/6/15	0:40:19	18.398	PLESOVICE - 30	PLE	0.282435	**0.282503**	0.000032
Z_Plesovice_1	6/8/15	22:26:44	32.51	PLE - 1	PLE	0.282433	**0.282501**	0.000055
Z_Plesovice_10	6/8/15	23:35:02	34.007	PLE - 10	PLE	0.282455	**0.282523**	0.000044
Z_Plesovice_11	6/8/15	23:58:11	32.964	PLE - 11	PLE	0.282422	**0.282490**	0.000032
Z_Plesovice_12	6/8/15	23:59:47	38.514	PLE - 12	PLE	0.282440	**0.282508**	0.000034
Z_Plesovice_2	6/8/15	22:28:21	11.106	PLE - 2	PLE	0.282410	**0.282478**	0.000044
Z_Plesovice_3	6/8/15	22:41:29	19.349	PLE - 3	PLE	0.282436	**0.282504**	0.000036
Z_Plesovice_4	6/8/15	22:56:16	34.536	PLE - 4	PLE	0.282426	**0.282494**	0.000041
Z_Plesovice_5	6/8/15	22:57:54	14.786	PLE - 5	PLE	0.282383	**0.282451**	0.000068
Z_Plesovice_6	6/8/15	23:03:50	27.383	PLE - 6	PLE	0.282452	**0.282520**	0.000033
Z_Plesovice_7	6/8/15	23:05:27	19.412	PLE - 7	PLE	0.282449	**0.282517**	0.000043
Z_Plesovice_8	6/8/15	23:18:37	35.239	PLE - 8	PLE	0.282482	**0.282550**	0.000047

Analysis	Date	Time	Duration (s)	Comments	Standard	176Hf/177Hf	Corrected 176/177Hf	2SE
Z_Plesovice_9	6/8/15	23:33:26	31.881	PLE - 9	PLE	0.282392	**0.282460**	0.000044
Z_Plesovice_1	6/9/15	17:22:31	23.975	PLE - 1	PLE	0.282413	**0.282481**	0.000045
Z_Plesovice_10	6/9/15	18:31:53	31.295	PLE - 10	PLE	0.282465	**0.282533**	0.000029
Z_Plesovice_11	6/9/15	19:08:48	33.611	PLE - 11	PLE	0.282439	**0.282507**	0.000032
Z_Plesovice_12	6/9/15	19:10:25	34.504	PLE - 12	PLE	0.282432	**0.282500**	0.000036
Z_Plesovice_13	6/9/15	0:12:59	22.402	PLE - 13	PLE	0.282407	**0.282475**	0.000042
Z_Plesovice_13	6/9/15	19:23:36	7.4638	PLE - 13	PLE	0.282442	**0.282510**	0.000052
Z_Plesovice_14	6/9/15	0:27:45	22.74	PLE - 14	PLE	0.282428	**0.282496**	0.000047
Z_Plesovice_14	6/9/15	19:38:24	21.86	PLE - 14	PLE	0.282425	**0.282493**	0.000041
Z_Plesovice_15	6/9/15	0:29:22	20.623	PLE - 15	PLE	0.282438	**0.282506**	0.000053
Z_Plesovice_15	6/9/15	19:40:02	20.065	PLE - 15	PLE	0.282405	**0.282473**	0.000041
Z_Plesovice_16	6/9/15	19:56:18	19.162	PLE - 16	PLE	0.282408	**0.282476**	0.000040
Z_Plesovice_17	6/9/15	19:57:54	5.9513	PLE - 17	PLE	0.282416	**0.282484**	0.000076
Z_Plesovice_18	6/9/15	20:25:57	22.134	PLE - 19	PLE	0.282406	**0.282474**	0.000041
Z_Plesovice_2	6/9/15	17:24:07	33.509	PLE - 2	PLE	0.282424	**0.282492**	0.000036
Z_Plesovice_19	6/9/15	20:27:33	15.024	PLE - 20	PLE	0.282448	**0.282516**	0.000047
Z_Plesovice_3	6/9/15	17:37:20	33.032	PLE - 3	PLE	0.282420	**0.282488**	0.000036
Z_Plesovice_4	6/9/15	17:52:10	24.968	PLE - 4	PLE	0.282449	**0.282517**	0.000031
Z_Plesovice_5	6/9/15	17:53:48	14.837	PLE - 5	PLE	0.282393	**0.282461**	0.000046
Z_Plesovice_6	6/9/15	18:00:41	26.35	PLE - 6	PLE	0.282414	**0.282482**	0.000033
Z_Plesovice_7	6/9/15	18:02:17	22.639	PLE - 7	PLE	0.282403	**0.282471**	0.000052
Z_Plesovice_8	6/9/15	18:15:27	27.178	PLE - 8	PLE	0.282424	**0.282492**	0.000035
Z_Plesovice_9	6/9/15	18:30:19	5.8486	PLE - 9	PLE	0.282410	**0.282478**	0.000059
R33_1	6/5/15	20:30:01	27.405	R33 - 1	R33	0.282680	**0.282748**	0.000034
R33_2	6/5/15	21:05:54	27.851	R33 - 2	R33	0.282710	**0.282778**	0.000070
R33_3	6/5/15	21:41:16	31.131	R33 - 3	R33	0.282703	**0.282771**	0.000053
R33_4	6/5/15	22:52:16	29.51	R33 - 4	R33	0.282667	**0.282735**	0.000052
R33_5	6/5/15	23:29:32	31.697	R33 - 5	R33	0.282694	**0.282762**	0.000053
R33_6	6/6/15	0:25:37	31.245	R33 - 6	R33	0.282666	**0.282734**	0.000045
R33_1	6/8/15	22:30:00	31.572	R33 - 1	R33	0.282681	**0.282749**	0.000056
R33_2	6/8/15	23:07:08	32.441	R33 - 2	R33	0.282696	**0.282764**	0.000081
R33_1	6/9/15	17:25:49	29.488	R33 - 1	R33	0.282749	**0.282817**	0.000066
R33_2	6/9/15	18:03:56	29.397	R33 - 2	R33	0.282670	**0.282738**	0.000042
R33_3	6/9/15	0:01:28	30.595	R33 - 3	R33	0.282752	**0.282820**	0.000063
R33_3	6/9/15	19:12:08	30.298	R33 - 3	R33	0.282686	**0.282754**	0.000077
R33_4	6/9/15	19:59:34	15.545	R33 - 4	R33	0.282657	**0.282725**	0.000059

Averages	Hf178/177	2SD	Total Hf	Epsilon (0)	2SD	176Hf/177Hf (i)	Epsilon (i)	2SD	Assigned Age
FC1	1.46735	0.00007		-20.88	1.01		2.85	0.93	1099
MUN1	1.46734	0.00005							
MUN4	1.46735	0.00005							
R33	1.46736	0.00006		-1.13	1.05		7.68	1.02	419
Plesovice	1.46739	0.00006		-10.75	0.80		-3.23	0.80	337

Analysis	Lu176/Hf177	2SE	Yb176/Hf177	2SE	Hf178/177	2SE	Total Hf	Epsilon (0)	2SE
FC1_1	0.001517	0.000010	0.059860	0.000230	1.46738	0.00006	7.8	-21.54	2.61
FC1_2	0.001508	0.000010	0.059820	0.000290	1.46739	0.00006	8.0	-22.14	1.74
FC1_3	0.001890	0.000006	0.076290	0.000450	1.46738	0.00006	7.2	-19.24	2.37
FC1_4	0.001553	0.000009	0.062650	0.000900	1.46740	0.00008	8.4	-19.80	1.74
FC1_5	0.001366	0.000052	0.054500	0.002400	1.46744	0.00004	10.5	-21.29	2.12
FC1_6	0.001488	0.000012	0.058910	0.000230	1.46742	0.00005	8.3	-22.21	2.19
FC1_1	0.001558	0.000027	0.059420	0.000490	1.46731	0.00008	6.7	-20.97	2.09
FC1_2	0.000831	0.000008	0.031800	0.000430	1.46734	0.00007	7.2	-21.64	1.91
FC1_1	0.001631	0.000006	0.067310	0.000510	1.46725	0.00005	8.2	-19.59	2.05
FC1_2	0.001284	0.000004	0.052870	0.000530	1.46736	0.00007	15.6	-20.05	3.17
FC1_3	0.001132	0.000092	0.043900	0.003600	1.46741	0.00007	7.5	-21.99	1.78
FC1_3	0.001468	0.000062	0.058800	0.002500	1.46723	0.00006	9.2	-20.37	1.60
FC1_4	0.001566	0.000005	0.063710	0.000320	1.46728	0.00006	8.7	-20.62	2.23
MUN1_1	0.001520	0.000012	0.011780	0.000320	1.46736	0.00006	8.3		
MUN1_10	0.000923	0.000018	0.006580	0.000110	1.46743	0.00006	6.6		
MUN1_2	0.001611	0.000039	0.012300	0.000250	1.46737	0.00007	8.1		
MUN1_3	0.001722	0.000044	0.013240	0.000250	1.46731	0.00006	8.3		
MUN1_4	0.002018	0.000046	0.015720	0.000220	1.46741	0.00009	8.0		
MUN1_5	0.002249	0.000063	0.017600	0.000310	1.46745	0.00007	8.0		
MUN1_6	0.002569	0.000052	0.019970	0.000190	1.46741	0.00008	7.4		
MUN1_7	0.001933	0.000045	0.013550	0.000420	1.46733	0.00007	6.4		
MUN1_8	0.001966	0.000016	0.013720	0.000210	1.46737	0.00008	6.6		
MUN1_9	0.001791	0.000037	0.012480	0.000220	1.46738	0.00006	6.8		
MUN1_11	0.000836	0.000010	0.005773	0.000066	1.46734	0.00007	6.8		
MUN1_12	0.001892	0.000042	0.014690	0.000230	1.46741	0.00006	8.2		
MUN1_1	0.000697	0.000005	0.005075	0.000090	1.46737	0.00011	9.2		
MUN1_2	0.001056	0.000013	0.007720	0.000190	1.46732	0.00008	7.5		
MUN1_3	0.000975	0.000026	0.007280	0.000260	1.46729	0.00007	7.3		
MUN1_4	0.000830	0.000017	0.006130	0.000190	1.46736	0.00006	7.8		
MUN1_1	0.001536	0.000025	0.011420	0.000230	1.46733	0.00005	8.3		

Analysis	Lu176/Hf177	2SE	Yb176/Hf177	2SE	Hf178/177	2SE	Total Hf	Epsilon (0)	2SE
MUN1_2	0.001590	0.000023	0.011720	0.000230	1.46731	0.00006	8.4		
MUN1_3	0.002217	0.000029	0.017860	0.000340	1.46728	0.00008	9.4		
MUN1_4	0.002130	0.000038	0.017070	0.000450	1.46729	0.00005	10.2		
MUN1_5	0.001450	0.000045	0.010690	0.000450	1.46727	0.00008	7.7		
MUN1_5	0.002228	0.000020	0.017940	0.000140	1.46732	0.00005	9.6		
MUN1_6	0.001493	0.000023	0.010930	0.000240	1.46732	0.00007	7.9		
MUN1_6	0.002195	0.000019	0.017980	0.000140	1.46735	0.00004	10.2		
MUN1_7	0.002621	0.000073	0.019260	0.000750	1.46727	0.00006	7.4		
MUN1_8	0.002785	0.000016	0.020770	0.000220	1.46730	0.00008	7.7		
MUN4_1	0.007465	0.000024	0.265300	0.002000	1.46734	0.00005	8.6		
MUN4_10	0.009775	0.000025	0.362400	0.002800	1.46740	0.00006	9.0		
MUN4_2	0.007647	0.000027	0.272200	0.001200	1.46731	0.00006	8.5		
MUN4_3	0.007852	0.000024	0.281400	0.001800	1.46737	0.00006	8.6		
MUN4_4	0.008479	0.000027	0.305600	0.002000	1.46737	0.00008	8.3		
MUN4_5	0.009025	0.000015	0.338100	0.003100	1.46739	0.00009	10.4		
MUN4_6	0.008301	0.000014	0.299400	0.002300	1.46740	0.00007	8.6		
MUN4_7	0.008407	0.000003	0.303500	0.002900	1.46742	0.00007	8.6		
MUN4_8	0.008542	0.000004	0.309500	0.003300	1.46747	0.00006	8.5		
MUN4_9	0.008740	0.000010	0.318600	0.003200	1.46740	0.00006	8.7		
MUN4_11	0.009262	0.000014	0.356400	0.005200	1.46739	0.00004	10.6		
MUN4_12	0.008994	0.000006	0.335300	0.003700	1.46745	0.00005	10.3		
MUN4_1	0.010650	0.000240	0.432000	0.015000	1.46732	0.00006	9.6		
MUN4_2	0.007655	0.000009	0.290800	0.002600	1.46733	0.00006	10.4		
MUN4_3	0.007598	0.000012	0.292200	0.002300	1.46727	0.00006	11.0		
MUN4_4	0.010573	0.000033	0.424700	0.001900	1.46737	0.00005	9.9		
MUN4_1	0.010481	0.000052	0.427960	0.000890	1.46731	0.00005	10.0		
MUN4_2	0.010813	0.000086	0.442500	0.001500	1.46729	0.00005	9.5		
MUN4_3	0.010983	0.000059	0.444100	0.001300	1.46733	0.00006	9.3		
MUN4_4	0.011291	0.000065	0.458500	0.001000	1.46732	0.00005	9.6		
MUN4_5	0.010430	0.000170	0.417300	0.005800	1.46734	0.00007	9.3		
MUN4_5	0.010393	0.000061	0.419800	0.005400	1.46728	0.00007	10.2		
MUN4_6	0.009604	0.000044	0.382100	0.004500	1.46734	0.00006	9.8		
MUN4_6	0.010940	0.000140	0.436200	0.002100	1.46733	0.00006	9.3		
MUN4_7	0.009665	0.000057	0.384700	0.003900	1.46730	0.00005	9.8		
MUN4_8	0.009565	0.000063	0.379900	0.001800	1.46728	0.00006	9.5		
Z_Plesovice_1	0.000147	0.000001	0.007828	0.000057	1.46737	0.00005	9.2	-11.78	1.74
Z_Plesovice_10	0.000116	0.000007	0.005870	0.000290	1.46743	0.00005	11.6	-10.33	1.54
Z_Plesovice_11	0.000095	0.000010	0.004500	0.000410	1.46752	0.00007	11.9	-10.64	1.36

Analysis	Lu176/Hf177	2SE	Yb176/Hf177	2SE	Hf178/177	2SE	Total Hf	Epsilon (0)	2SE
Z_Plesovice_12	0.000073	0.000007	0.003540	0.000230	1.46745	0.00007	10.6	-10.61	1.20
Z_Plesovice_13	0.000068	0.000001	0.003614	0.000033	1.46747	0.00008	14.5	-11.95	0.84
Z_Plesovice_14	0.000065	0.000006	0.003260	0.000230	1.46751	0.00008	11.0	-10.11	1.67
Z_Plesovice_15	0.000139	0.000007	0.007320	0.000330	1.46745	0.00007	9.2	-11.39	1.91
Z_Plesovice_16	0.000091	0.000005	0.004640	0.000200	1.46743	0.00006	8.9	-10.50	1.78
Z_Plesovice_17	0.000155	0.000004	0.008100	0.000200	1.46736	0.00012	9.6	-11.70	1.81
Z_Plesovice_18	0.000247	0.000006	0.012460	0.000230	1.46741	0.00008	8.9	-10.25	1.88
Z_Plesovice_19	0.000076	0.000002	0.003890	0.000140	1.46744	0.00006	10.3	-11.92	1.64
Z_Plesovice_2	0.000117	0.000003	0.006200	0.000290	1.46739	0.00011	13.6	-10.54	1.98
Z_Plesovice_20	0.000081	0.000001	0.004128	0.000092	1.46744	0.00008	10.2	-10.64	1.71
Z_Plesovice_21	0.000098	0.000002	0.004920	0.000130	1.46744	0.00006	10.4	-10.01	1.36
Z_Plesovice_22	0.000082	0.000007	0.003820	0.000300	1.46739	0.00005	9.8	-10.96	1.30
Z_Plesovice_23	0.000057	0.000000	0.003027	0.000060	1.46742	0.00010	13.2	-11.46	1.30
Z_Plesovice_24	0.000053	0.000001	0.002782	0.000036	1.46740	0.00006	10.6	-11.14	1.54
Z_Plesovice_25	0.000053	0.000001	0.002747	0.000043	1.46739	0.00005	10.3	-10.50	1.03
Z_Plesovice_3	0.000159	0.000005	0.008320	0.000390	1.46738	0.00006	11.0	-10.79	1.47
Z_Plesovice_4	0.000163	0.000002	0.008490	0.000200	1.46733	0.00006	10.5	-10.29	1.03
Z_Plesovice_5	0.000177	0.000001	0.009223	0.000073	1.46734	0.00006	10.8	-9.90	1.16
Z_Plesovice_6	0.000171	0.000003	0.008817	0.000089	1.46735	0.00006	10.7	-9.26	1.36
Z_Plesovice_7	0.000160	0.000001	0.008390	0.000110	1.46732	0.00007	10.6	-10.96	1.26
Z_Plesovice_8	0.000093	0.000005	0.004750	0.000170	1.46745	0.00009	12.2	-12.55	1.23
Z_Plesovice_9	0.000124	0.000000	0.006368	0.000074	1.46760	0.00011	12.8	-12.45	1.91
Z_Plesovice_26	0.000083	0.000009	0.003940	0.000310	1.46745	0.00006	11.3	-11.67	1.47
Z_Plesovice_27	0.000121	0.000007	0.006230	0.000330	1.46741	0.00006	9.2	-10.50	1.26
Z_Plesovice_28	0.000238	0.000006	0.012200	0.000290	1.46740	0.00007	8.5	-11.28	1.95
Z_Plesovice_29	0.000144	0.000023	0.007900	0.001300	1.46745	0.00007	10.3	-12.06	1.67
Z_Plesovice_30	0.000096	0.000011	0.004610	0.000480	1.46746	0.00007	12.9	-10.25	1.20
Z_Plesovice_1	0.000132	0.000004	0.007010	0.000280	1.46734	0.00006	9.4	-10.33	1.98
Z_Plesovice_10	0.000133	0.000001	0.007308	0.000094	1.46737	0.00004	9.8	-9.55	1.60
Z_Plesovice_11	0.000147	0.000002	0.007704	0.000082	1.46736	0.00005	10.0	-10.71	1.20
Z_Plesovice_12	0.000149	0.000002	0.007950	0.000120	1.46732	0.00006	9.8	-10.08	1.26
Z_Plesovice_2	0.000140	0.000005	0.007640	0.000380	1.46737	0.00011	12.6	-11.14	1.60
Z_Plesovice_3	0.000149	0.000004	0.007900	0.000300	1.46740	0.00008	11.4	-10.22	1.33
Z_Plesovice_4	0.000138	0.000002	0.007280	0.000190	1.46736	0.00006	9.9	-10.57	1.50
Z_Plesovice_5	0.000081	0.000003	0.004340	0.000110	1.46738	0.00008	12.0	-12.09	2.44
Z_Plesovice_6	0.000102	0.000000	0.005528	0.000060	1.46734	0.00006	10.4	-9.65	1.23
Z_Plesovice_7	0.000136	0.000001	0.007277	0.000081	1.46742	0.00008	11.9	-9.76	1.57
Z_Plesovice_8	0.000115	0.000004	0.006320	0.000180	1.46733	0.00005	9.7	-8.59	1.71

Analysis	Lu176/Hf177	2SE	Yb176/Hf177	2SE	Hf178/177	2SE	Total Hf	Epsilon (0)	2SE
Z_Plesovice_9	0.000113	0.000005	0.006250	0.000230	1.46733	0.00006	10.0	-11.78	1.60
Z_Plesovice_1	0.000204	0.000001	0.011516	0.000071	1.46735	0.00006	11.0	-11.03	1.64
Z_Plesovice_10	0.000125	0.000001	0.006534	0.000059	1.46735	0.00006	11.5	-9.19	1.10
Z_Plesovice_11	0.000085	0.000002	0.004381	0.000088	1.46728	0.00005	11.1	-10.11	1.20
Z_Plesovice_12	0.000144	0.000004	0.007550	0.000250	1.46733	0.00006	11.3	-10.36	1.33
Z_Plesovice_13	0.000088	0.000001	0.004622	0.000089	1.46741	0.00007	11.1	-11.24	1.54
Z_Plesovice_13	0.000122	0.000001	0.006510	0.000150	1.46750	0.00020	15.1	-10.01	1.88
Z_Plesovice_14	0.000139	0.000017	0.007260	0.000810	1.46738	0.00006	11.2	-10.50	1.71
Z_Plesovice_14	0.000150	0.000001	0.007960	0.000120	1.46731	0.00007	12.1	-10.61	1.50
Z_Plesovice_15	0.000203	0.000001	0.011310	0.000150	1.46738	0.00008	10.6	-10.15	1.91
Z_Plesovice_15	0.000141	0.000001	0.007470	0.000120	1.46742	0.00008	12.7	-11.32	1.50
Z_Plesovice_16	0.000078	0.000002	0.004057	0.000063	1.46735	0.00008	12.8	-11.21	1.47
Z_Plesovice_17	0.000141	0.000002	0.007790	0.000340	1.46740	0.00025	15.5	-10.93	2.72
Z_Plesovice_18	0.000160	0.000012	0.008320	0.000650	1.46737	0.00005	11.2	-11.28	1.50
Z_Plesovice_2	0.000210	0.000001	0.011871	0.000069	1.46732	0.00005	10.2	-10.64	1.33
Z_Plesovice_19	0.000145	0.000010	0.007680	0.000570	1.46741	0.00011	13.7	-9.80	1.71
Z_Plesovice_3	0.000200	0.000000	0.011270	0.000150	1.46732	0.00005	10.4	-10.79	1.33
Z_Plesovice_4	0.000063	0.000000	0.003435	0.000054	1.46729	0.00005	11.1	-9.76	1.16
Z_Plesovice_5	0.000063	0.000003	0.003437	0.000098	1.46738	0.00008	12.3	-11.74	1.67
Z_Plesovice_6	0.000063	0.000001	0.003391	0.000063	1.46737	0.00006	11.1	-11.00	1.23
Z_Plesovice_7	0.000130	0.000002	0.006864	0.000057	1.46734	0.00007	11.3	-11.39	1.88
Z_Plesovice_8	0.000080	0.000005	0.004220	0.000230	1.46737	0.00006	11.5	-10.64	1.30
Z_Plesovice_9	0.000125	0.000001	0.006730	0.000110	1.46736	0.00013	14.5	-11.14	2.12
R33_1	0.001807	0.000073	0.065000	0.001900	1.46731	0.00006	10.2	-1.59	1.26
R33_2	0.001974	0.000080	0.072800	0.003600	1.46738	0.00008	8.9	-0.53	2.51
R33_3	0.002281	0.000071	0.082500	0.003100	1.46741	0.00004	10.0	-0.78	1.91
R33_4	0.001338	0.000016	0.049610	0.000230	1.46736	0.00005	9.4	-2.05	1.88
R33_5	0.001525	0.000005	0.057700	0.000900	1.46740	0.00007	9.4	-1.10	1.91
R33_6	0.001883	0.000046	0.070600	0.002600	1.46748	0.00005	8.9	-2.09	1.64
R33_1	0.001910	0.000022	0.076300	0.001700	1.46729	0.00006	8.5	-1.56	2.02
R33_2	0.004500	0.000100	0.182600	0.005800	1.46737	0.00006	7.3	-1.03	2.89
R33_1	0.002064	0.000068	0.082000	0.002100	1.46729	0.00008	8.3	0.85	2.37
R33_2	0.002080	0.000054	0.077300	0.002700	1.46733	0.00004	10.6	-1.94	1.54
R33_3	0.002527	0.000019	0.097270	0.000270	1.46728	0.00007	8.3	0.95	2.26
R33_3	0.001956	0.000026	0.073870	0.000980	1.46731	0.00007	8.2	-1.38	2.75
R33_4	0.001811	0.000011	0.068200	0.001500	1.46742	0.00008	11.5	-2.40	2.12

Analysis	176Hf/177Hf (i)	Epsilon (i)	2SE	Assigned Age
FC1_1	0.282153	2.14	2.62	1099
FC1_2	0.282136	1.54	1.75	1099
FC1_3	0.282210	4.17	2.38	1099
FC1_4	0.282201	3.85	1.75	1099
FC1_5	0.282163	2.49	2.13	1099
FC1_6	0.282134	1.48	2.20	1099
FC1_1	0.282168	2.67	2.10	1099
FC1_2	0.282164	2.53	1.93	1099
FC1_1	0.282205	4.00	2.06	1099
FC1_2	0.282199	3.80	3.18	1099
FC1_3	0.282148	1.96	1.79	1099
FC1_3	0.282187	3.34	1.62	1099
FC1_4	0.282178	3.02	2.24	1099
MUN1_1	0.282161			
MUN1_10	0.282118			
MUN1_2	0.282149			
MUN1_3	0.282175			
MUN1_4	0.282167			
MUN1_5	0.282132			
MUN1_6	0.282098			
MUN1_7	0.282145			
MUN1_8	0.282104			
MUN1_9	0.282116			
MUN1_11	0.282152			
MUN1_12	0.282104			
MUN1_1	0.282169			
MUN1_2	0.282142			
MUN1_3	0.282156			
MUN1_4	0.282121			
MUN1_1	0.282148			

Analysis	176Hf/177Hf (i)	Epsilon (i)	2SE	Assigned Age
MUN1_2	0.282152			
MUN1_3	0.282123			
MUN1_4	0.282142			
MUN1_5	0.282114			
MUN1_5	0.282142			
MUN1_6	0.282126			
MUN1_6	0.282140			
MUN1_7	0.282153			
MUN1_8	0.282097			
MUN4_1	0.282154			
MUN4_10	0.282107			
MUN4_2	0.282212			
MUN4_3	0.282108			
MUN4_4	0.282115			
MUN4_5	0.282198			
MUN4_6	0.282137			
MUN4_7	0.282151			
MUN4_8	0.282164			
MUN4_9	0.282098			
MUN4_11	0.282181			
MUN4_12	0.282171			
MUN4_1	0.282178			
MUN4_2	0.282185			
MUN4_3	0.282107			
MUN4_4	0.282088			
MUN4_1	0.282188			
MUN4_2	0.282078			
MUN4_3	0.282218			
MUN4_4	0.282064			
MUN4_5	0.282008			
MUN4_5	0.282065			
MUN4_6	0.282202			
MUN4_6	0.282168			
MUN4_7	0.282069			
MUN4_8	0.282218			
Z_Plesovice_1	0.282459	-4.27	1.74	337
Z_Plesovice_10	0.282500	-2.81	1.53	337
Z_Plesovice_11	0.282491	-3.12	1.36	337

Analysis	176Hf/177Hf (i)	Epsilon (i)	2SE	Assigned Age
Z_Plesovice_12	0.282493	-3.08	1.19	337
Z_Plesovice_13	0.282455	-4.43	0.83	337
Z_Plesovice_14	0.282507	-2.59	1.67	337
Z_Plesovice_15	0.282470	-3.88	1.91	337
Z_Plesovice_16	0.282495	-2.98	1.77	337
Z_Plesovice_17	0.282461	-4.20	1.81	337
Z_Plesovice_18	0.282501	-2.77	1.88	337
Z_Plesovice_19	0.282456	-4.39	1.64	337
Z_Plesovice_2	0.282494	-3.02	1.98	337
Z_Plesovice_20	0.282491	-3.12	1.71	337
Z_Plesovice_21	0.282509	-2.49	1.36	337
Z_Plesovice_22	0.282482	-3.44	1.30	337
Z_Plesovice_23	0.282469	-3.93	1.30	337
Z_Plesovice_24	0.282478	-3.61	1.53	337
Z_Plesovice_25	0.282496	-2.97	1.03	337
Z_Plesovice_3	0.282487	-3.28	1.47	337
Z_Plesovice_4	0.282501	-2.78	1.03	337
Z_Plesovice_5	0.282512	-2.40	1.16	337
Z_Plesovice_6	0.282530	-1.76	1.36	337
Z_Plesovice_7	0.282482	-3.46	1.26	337
Z_Plesovice_8	0.282437	-5.03	1.23	337
Z_Plesovice_9	0.282440	-4.93	1.91	337
Z_Plesovice_26	0.282462	-4.15	1.47	337
Z_Plesovice_27	0.282495	-2.99	1.26	337
Z_Plesovice_28	0.282473	-3.79	1.95	337
Z_Plesovice_29	0.282451	-4.55	1.67	337
Z_Plesovice_30	0.282502	-2.73	1.19	337
Z_Plesovice_1	0.282500	-2.81	1.98	337
Z_Plesovice_10	0.282522	-2.04	1.60	337
Z_Plesovice_11	0.282489	-3.21	1.19	337
Z_Plesovice_12	0.282507	-2.57	1.26	337
Z_Plesovice_2	0.282477	-3.63	1.60	337
Z_Plesovice_3	0.282503	-2.71	1.33	337
Z_Plesovice_4	0.282493	-3.06	1.50	337
Z_Plesovice_5	0.282450	-4.57	2.44	337
Z_Plesovice_6	0.282519	-2.13	1.23	337
Z_Plesovice_7	0.282516	-2.25	1.57	337
Z_Plesovice_8	0.282549	-1.08	1.71	337

Analysis	176Hf/177Hf (i)	Epsilon (i)	2SE	Assigned Age
Z_Plesovice_9	0.282459	-4.26	1.60	337
Z_Plesovice_1	0.282480	-3.54	1.64	337
Z_Plesovice_10	0.282532	-1.68	1.09	337
Z_Plesovice_11	0.282506	-2.59	1.19	337
Z_Plesovice_12	0.282499	-2.85	1.33	337
Z_Plesovice_13	0.282474	-3.72	1.53	337
Z_Plesovice_13	0.282509	-2.49	1.88	337
Z_Plesovice_14	0.282495	-2.99	1.71	337
Z_Plesovice_14	0.282492	-3.10	1.50	337
Z_Plesovice_15	0.282505	-2.65	1.91	337
Z_Plesovice_15	0.282472	-3.81	1.50	337
Z_Plesovice_16	0.282476	-3.69	1.47	337
Z_Plesovice_17	0.282483	-3.42	2.72	337
Z_Plesovice_18	0.282473	-3.78	1.50	337
Z_Plesovice_2	0.282491	-3.15	1.33	337
Z_Plesovice_19	0.282515	-2.29	1.71	337
Z_Plesovice_3	0.282487	-3.29	1.33	337
Z_Plesovice_4	0.282517	-2.23	1.16	337
Z_Plesovice_5	0.282461	-4.21	1.67	337
Z_Plesovice_6	0.282482	-3.47	1.23	337
Z_Plesovice_7	0.282470	-3.87	1.88	337
Z_Plesovice_8	0.282491	-3.12	1.30	337
Z_Plesovice_9	0.282477	-3.63	2.12	337
R33_1	0.282734	7.30	1.26	419
R33_2	0.282762	8.32	2.51	419
R33_3	0.282753	7.98	1.91	419
R33_4	0.282724	6.97	1.88	419
R33_5	0.282750	7.87	1.91	419
R33_6	0.282719	6.78	1.64	419
R33_1	0.282734	7.31	2.02	419
R33_2	0.282729	7.12	2.89	419
R33_1	0.282801	9.67	2.37	419
R33_2	0.282722	6.87	1.53	419
R33_3	0.282800	9.65	2.26	419
R33_3	0.282739	7.47	2.75	419
R33_4	0.282711	6.49	2.12	419

Table 3.7 LASS U-Pb data from Reference Materials

								Ratios				
Analysis	**Date**	**Time**	**Duration**	**Sample**	**204 cps**	**206 cps**	**206/204**	**207Pb/235U**	**2SE**	**206Pb/235U**	**2SE**	**Rho**
FC1 1	6/5/15	20:43:22	29.03	FC1 - 1	102	554000	5431	1.880	0.013	0.179	0.001	0.456
FC1 1	6/8/15	22:43:26	34.083	FC1 - 1	62	543000	8758	2.038	0.021	0.195	0.002	0.838
FC1 1	6/9/15	17:39:22	29.632	FC1 - 1	100	587000	5870	1.934	0.014	0.183	0.001	0.657
FC1 2	6/5/15	21:19:07	26.67	FC1 - 2	64	652000	10188	2.067	0.015	0.200	0.001	0.689
FC1 2	6/8/15	23:20:33	36.233	FC1 - 2	44	427000	9705	2.066	0.026	0.197	0.002	0.864
FC1 2	6/9/15	18:17:23	10.277	FC1 - 2	46	2052000	44609	2.045	0.021	0.210	0.002	0.728
FC1 3	6/5/15	21:54:41	22.108	FC1 - 3	84	773000	9202	1.929	0.017	0.186	0.001	0.692
FC1 3	6/9/15	19:25:36	23.283	FC1 - 3	97	1139000	11742	2.025	0.021	0.198	0.003	0.921
FC1 4	6/5/15	23:05:42	19.104	FC1 - 4	55	652000	11855	1.901	0.016	0.183	0.001	0.488
FC1 4	6/9/15	20:13:12	26.965	FC1 - 4	45	487000	10822	1.945	0.015	0.185	0.001	0.551
FC1 5	6/6/15	0:12:40	34.912	FC1 - 6	84	542000	6452	2.008	0.018	0.194	0.002	0.631
Plesovice 1	6/9/15	17:22:51	19.488	PLE - 1	78	1090000	13974	0.396	0.003	0.054	0.000	0.629
Plesovice 8	6/8/15	23:35:20	32.351	PLE - 10	47	383000	8149	0.390	0.004	0.053	0.000	0.375
Plesovice 10	6/9/15	18:32:10	27.428	PLE - 10	38	249300	6561	0.393	0.004	0.054	0.000	0.522
Plesovice 11	6/9/15	19:09:07	34.013	PLE - 11	58	173000	2983	0.382	0.005	0.052	0.000	0.631
Plesovice 9	6/9/15	0:00:04	32.963	PLE - 12	62	318000	5129	0.403	0.005	0.054	0.000	0.518
Plesovice 12	6/9/15	19:10:44	17.783	PLE - 12	67	335400	5006	0.406	0.005	0.055	0.000	0.424
Plesovice 13	6/9/15	19:23:56	5.3975	PLE - 13	72	261400	3631	0.397	0.008	0.054	0.001	0.600
Plesovice 10	6/9/15	0:28:01	19.181	PLE - 14	48	276300	5756	0.393	0.005	0.054	0.001	0.641
Plesovice 14	6/9/15	19:38:43	14.408	PLE - 14	25	306100	12244	0.401	0.006	0.054	0.001	0.439
Plesovice 15	6/9/15	19:40:21	13.914	PLE - 15	60	305200	5087	0.402	0.006	0.054	0.000	0.186
Plesovice 16	6/9/15	19:56:34	17.256	PLE - 16	18	208800	11600	0.373	0.006	0.051	0.001	0.680
Plesovice 17	6/9/15	19:58:10	7.2434	PLE - 17	78	231000	2962	0.397	0.009	0.054	0.001	0.909
Plesovice 18	6/9/15	20:11:24	8.7834	PLE - 18	12	360000	30000	0.398	0.007	0.054	0.001	0.488
Plesovice 19	6/9/15	20:26:12	12.985	PLE - 19	0	360000	#DIV/0!	0.398	0.006	0.054	0.001	0.633
Plesovice 1	6/8/15	22:28:38	10.418	PLE - 2	104	329000	3163	0.393	0.006	0.054	0.000	0.518
Plesovice 2	6/9/15	17:24:23	38.068	PLE - 2	51	996700	19543	0.390	0.003	0.053	0.000	0.690
Plesovice 20	6/9/15	20:27:49	13.18	PLE - 20	30	292000	9733	0.393	0.006	0.054	0.000	0.351
Plesovice 2	6/8/15	22:41:45	13.679	PLE - 3	62	347000	5597	0.402	0.005	0.054	0.000	0.230
Plesovice 3	6/9/15	17:37:39	32.705	PLE - 3	36	1031000	28639	0.399	0.003	0.055	0.001	0.757
Plesovice 4	6/9/15	17:52:25	11.562	PLE - 4	116	249000	2147	0.397	0.008	0.054	0.001	0.225
Plesovice 3	6/8/15	22:58:10	12.678	PLE - 5	60	235200	3920	0.381	0.007	0.051	0.001	0.577
Plesovice 5	6/9/15	17:54:02	11.061	PLE - 5	-13	231000	-17769	0.396	0.007	0.054	0.000	0.126
Plesovice 4	6/8/15	23:04:08	33.658	PLE - 6	65	258200	3972	0.392	0.004	0.053	0.000	0.554
Plesovice 6	6/9/15	18:00:53	27.442	PLE - 6	43	220000	5116	0.390	0.004	0.053	0.000	0.498

Analysis	Date	Time	Duration	Sample	204 cps	206 cps	206/204	207Pb/235U	2SE	206Pb/235U	2SE	Rho
Plesovice 5	6/8/15	23:05:45	16.327	PLE - 7	49	312800	6384	0.389	0.006	0.053	0.001	0.585
Plesovice 7	6/9/15	18:02:31	27.021	PLE - 7	39	231000	5923	0.393	0.005	0.053	0.001	0.566
Plesovice 6	6/8/15	23:18:57	27.435	PLE - 8	31	336400	10852	0.401	0.004	0.054	0.000	0.467
Plesovice 8	6/9/15	18:15:44	19.52	PLE - 8	34	206400	6071	0.393	0.005	0.054	0.001	0.483
Plesovice 7	6/8/15	23:33:42	22.64	PLE - 9	48	358200	7463	0.391	0.003	0.054	0.000	0.328
Plesovice 9	6/9/15	18:30:32	7.516	PLE - 9	56	261100	4663	0.394	0.009	0.054	0.001	0.628
Plesovice 9	6/5/15	21:33:50	27.868	PLESOVICE - 10	71	256300	3610	0.386	0.005	0.052	0.000	0.522
Plesovice 10	6/5/15	21:38:03	21.641	PLESOVICE - 11	70	219600	3137	0.394	0.006	0.054	0.001	0.693
Plesovice 11	6/5/15	21:39:43	26.875	PLESOVICE - 12	88	203000	2307	0.401	0.006	0.055	0.001	0.660
Plesovice 12	6/5/15	21:52:51	12.977	PLESOVICE - 13	54	219000	4056	0.387	0.007	0.052	0.001	0.553
Plesovice 13	6/5/15	22:07:35	18.353	PLESOVICE - 14	115	291100	2531	0.391	0.004	0.053	0.001	0.505
Plesovice 14	6/5/15	22:09:09	29.444	PLESOVICE - 15	72	502000	6972	0.403	0.004	0.055	0.000	0.755
Plesovice 15	6/5/15	22:49:11	35.06	PLESOVICE - 16	68	246100	3619	0.375	0.004	0.051	0.000	0.566
Plesovice 16	6/5/15	22:50:51	31.646	PLESOVICE - 17	66	359000	5439	0.410	0.004	0.056	0.000	0.394
Plesovice 17	6/5/15	23:03:57	28.6	PLESOVICE - 18	79	436000	5519	0.392	0.003	0.053	0.000	0.367
Plesovice 18	6/5/15	23:18:41	16.948	PLESOVICE - 19	62	205600	3316	0.413	0.008	0.056	0.001	0.782
Plesovice 1	6/5/15	20:28:30	15.717	PLESOVICE - 2	154	403000	2617	0.390	0.006	0.052	0.001	0.687
Plesovice 19	6/5/15	23:20:19	14.612	PLESOVICE - 20	57	234200	4109	0.399	0.007	0.054	0.001	0.573
Plesovice 20	6/5/15	23:28:05	18.798	PLESOVICE - 22	58	236400	4076	0.406	0.006	0.055	0.001	0.556
Plesovice 21	6/5/15	23:41:13	14.531	PLESOVICE - 23	110	219000	1991	0.391	0.007	0.052	0.001	0.474
Plesovice 22	6/5/15	23:56:00	30.236	PLESOVICE - 24	86	223700	2601	0.384	0.005	0.053	0.000	0.707
Plesovice 23	6/5/15	23:57:41	26.25	PLESOVICE - 25	49	209800	4282	0.387	0.005	0.053	0.000	0.569
Plesovice 24	6/6/15	0:09:26	14.869	PLESOVICE - 26	65	330000	5077	0.394	0.005	0.053	0.001	0.307
Plesovice 25	6/6/15	0:11:03	30.213	PLESOVICE - 27	67	394000	5881	0.401	0.004	0.055	0.000	0.613
Plesovice 26	6/6/15	0:38:55	20.609	PLESOVICE - 29	99	458000	4626	0.412	0.008	0.057	0.001	0.751
Plesovice 2	6/5/15	20:41:41	22.03	PLESOVICE - 3	94	668000	7106	0.396	0.003	0.054	0.000	0.452
Plesovice 27	6/6/15	0:40:28	19.107	PLESOVICE - 30	71	232000	3268	0.379	0.007	0.052	0.001	0.681
Plesovice 3	6/5/15	20:56:25	30.56	PLESOVICE - 4	83	373000	4494	0.392	0.005	0.053	0.001	0.618
Plesovice 4	6/5/15	20:57:59	25.201	PLESOVICE - 5	96	416000	4333	0.401	0.003	0.054	0.000	0.317
Plesovice 5	6/5/15	21:02:45	17.829	PLESOVICE - 6	73	411000	5630	0.386	0.004	0.053	0.001	0.244
Plesovice 6	6/5/15	21:04:17	26.055	PLESOVICE - 7	63	412000	6540	0.390	0.004	0.054	0.001	0.356
Plesovice 7	6/5/15	21:17:26	20.51	PLESOVICE - 8	117	225000	1923	0.389	0.006	0.052	0.001	0.654
Plesovice 8	6/5/15	21:32:08	15.294	PLESOVICE - 9	84	259000	3083	0.402	0.005	0.055	0.001	0.530
R33 1	6/5/15	20:30:07	29.784	R33 - 1	57	143900	2525	0.447	0.006	0.061	0.001	0.510
R33 1	6/8/15	22:30:16	35.642	R33 - 1	104	64900	624	0.549	0.009	0.071	0.001	0.253
R33 1	6/9/15	17:26:05	32.441	R33 - 1	75	55760	743	0.533	0.009	0.068	0.000	0.109
R33 2	6/5/15	21:05:58	27.07	R33 - 2	101	110400	1093	0.535	0.008	0.070	0.001	0.488

Analysis	Date	Time	Duration	Sample	204 cps	206 cps	206/204	207Pb/235U	2SE	206Pb/235U	2SE	Rho
R33 2	6/8/15	23:07:25	34.925	R33 - 2	51	147300	2888	0.510	0.007	0.067	0.001	0.525
R33 2	6/9/15	18:04:22	26.958	R33 - 2	53	94600	1785	0.556	0.008	0.073	0.000	0.005
R33 3	6/5/15	21:41:20	27.897	R33 - 3	81	238000	2938	0.534	0.007	0.070	0.001	0.542
R33 3	6/9/15	0:01:47	27.378	R33 - 3	78	105400	1351	0.539	0.008	0.072	0.001	0.435
R33 3	6/9/15	19:12:31	25.702	R33 - 3	52	60100	1156	0.575	0.010	0.074	0.001	0.163
R33 4	6/5/15	22:52:30	29.558	R33 - 4	74	62400	843	0.522	0.008	0.069	0.001	0.162
R33 4	6/9/15	19:59:53	21.426	R33 - 4	63	77900	1237	0.538	0.010	0.068	0.001	0.331
R33 5	6/6/15	0:25:48	34.469	R33 - 6	73	88500	1212	0.519	0.008	0.068	0.001	0.276

			Ages (Myr)					
Analysis	**207Pb/206Pb**	**2SE**	**FinalAge207 235**	**2SE**	**FinalAge206 238**	**2SE**	**FinalAge207 206**	**2SE**
FC1 1	0.0755	0.0005	1074	5	1060	6	1081	13
FC1 1	0.0743	0.0004	1128	7	1146	10	1048	11
FC1 1	0.0766	0.0004	1093	5	1085	5	1113	11
FC1 2	0.0747	0.0004	1138	5	1176	7	1059	11
FC1 2	0.0761	0.0005	1137	9	1158	10	1096	13
FC1 2	0.0707	0.0005	1130	7	1228	9	949	14
FC1 3	0.0747	0.0005	1091	6	1097	7	1059	13
FC1 3	0.0729	0.0004	1123	7	1166	14	1010	10
FC1 4	0.0748	0.0006	1081	6	1082	6	1063	16
FC1 4	0.0751	0.0005	1096	5	1093	6	1069	13
FC1 5	0.0754	0.0006	1119	6	1143	8	1078	15
Plesovice 1	0.0534	0.0003	339	2	337	2	344	14
Plesovice 8	0.0533	0.0005	335	3	334	2	339	22
Plesovice 10	0.0531	0.0005	336	3	336	3	329	22
Plesovice 11	0.0529	0.0005	328	4	325	3	325	24
Plesovice 9	0.0533	0.0006	343	3	338	3	335	23
Plesovice 12	0.0535	0.0006	346	4	344	2	346	25
Plesovice 13	0.0537	0.0014	339	6	342	5	354	56
Plesovice 10	0.0533	0.0005	336	4	338	4	337	23
Plesovice 14	0.0533	0.0007	342	4	340	4	336	31
Plesovice 15	0.0533	0.0008	343	4	341	3	340	33
Plesovice 16	0.0526	0.0006	322	4	319	4	310	26
Plesovice 17	0.0537	0.0005	340	7	339	7	358	21
Plesovice 18	0.0534	0.0009	340	5	339	6	341	40
Plesovice 19	0.0531	0.0006	340	4	340	3	331	25
Plesovice 1	0.0533	0.0007	337	4	339	2	337	31
Plesovice 2	0.0532	0.0003	334	2	336	3	338	14
Plesovice 20	0.0533	0.0007	337	4	336	3	339	31
Plesovice 2	0.0532	0.0007	343	3	342	3	336	29
Plesovice 3	0.0529	0.0004	341	2	346	4	320	16
Plesovice 4	0.0541	0.0012	340	6	341	5	371	48
Plesovice 3	0.0533	0.0008	328	5	321	4	340	33
Plesovice 5	0.0543	0.0009	339	5	338	2	380	39
Plesovice 4	0.0533	0.0004	335	3	334	2	338	18
Plesovice 6	0.0538	0.0005	334	3	331	3	361	23

Analysis	207Pb/206Pb	2SE	FinalAge207 235	2SE	FinalAge206 238	2SE	FinalAge207 206	2SE
Plesovice 5	0.0531	0.0007	334	4	334	4	336	31
Plesovice 7	0.0533	0.0005	336	3	336	3	341	24
Plesovice 6	0.0533	0.0004	342	3	342	2	338	18
Plesovice 8	0.0526	0.0006	337	3	340	3	309	25
Plesovice 7	0.0532	0.0005	335	2	338	2	335	19
Plesovice 9	0.0542	0.0010	337	7	336	6	375	41
Plesovice 9	0.0532	0.0006	331	3	329	3	331	24
Plesovice 10	0.0532	0.0006	337	4	336	4	337	26
Plesovice 11	0.0527	0.0006	342	4	344	4	313	24
Plesovice 12	0.0536	0.0009	332	5	329	5	350	38
Plesovice 13	0.0533	0.0005	335	3	333	4	340	23
Plesovice 14	0.0531	0.0004	344	3	344	3	333	16
Plesovice 15	0.0530	0.0005	323	3	320	3	325	20
Plesovice 16	0.0529	0.0005	349	3	351	2	321	20
Plesovice 17	0.0527	0.0003	336	2	335	2	314	15
Plesovice 18	0.0531	0.0007	351	6	352	6	336	26
Plesovice 1	0.0564	0.0006	334	4	328	3	465	23
Plesovice 19	0.0530	0.0007	341	5	341	3	324	31
Plesovice 20	0.0536	0.0006	346	4	346	3	353	26
Plesovice 21	0.0558	0.0009	335	5	326	4	438	37
Plesovice 22	0.0530	0.0005	330	3	334	3	328	18
Plesovice 23	0.0535	0.0006	332	4	334	3	349	25
Plesovice 24	0.0539	0.0008	337	3	335	4	371	37
Plesovice 25	0.0533	0.0004	342	3	343	3	339	18
Plesovice 26	0.0544	0.0008	350	6	356	7	381	31
Plesovice 2	0.0527	0.0004	339	2	341	2	313	17
Plesovice 27	0.0539	0.0008	326	5	329	4	360	32
Plesovice 3	0.0533	0.0006	336	4	331	4	339	26
Plesovice 4	0.0533	0.0005	343	2	340	2	340	19
Plesovice 5	0.0526	0.0007	331	3	332	3	308	30
Plesovice 6	0.0526	0.0007	334	3	336	4	307	31
Plesovice 7	0.0539	0.0007	333	5	328	4	368	30
Plesovice 8	0.0528	0.0006	343	4	347	3	316	26
R33 1	0.0552	0.0006	375	4	382	4	420	24
R33 1	0.0558	0.0009	444	6	443	4	441	36
R33 1	0.0574	0.0010	434	6	422	3	496	38
R33 2	0.0554	0.0008	435	5	434	5	426	32

Analysis	207Pb/206Pb	2SE	FinalAge207 235	2SE	FinalAge206 238	2SE	FinalAge207 206	2SE
R33 2	0.0554	0.0006	418	4	417	4	423	25
R33 2	0.0554	0.0009	448	5	451	3	419	35
R33 3	0.0552	0.0006	434	5	434	3	422	26
R33 3	0.0530	0.0008	439	6	448	4	329	34
R33 3	0.0558	0.0010	461	7	459	4	434	39
R33 4	0.0549	0.0009	427	6	427	3	398	37
R33 4	0.0558	0.0010	437	7	426	4	435	40
R33 5	0.0561	0.0009	424	6	423	3	444	35

Chapter 4: The birth of a cratonic nucleus: Lithogeochemical evolution of the 4.02–2.94 Ga Acasta Gneiss Complex

Introduction:

The overall paucity of terrestrial rock and mineral samples older than 3.7 Ga has led to development of many divergent theories regarding crust formation during the Hadean and Eoarchean. The available information regarding processes operating on the planet at this time come from rare locations where >3.7 Ga crust is preserved (e.g., Condie, 2007) as well as Hadean-age detrital zircons from western Australia (e.g., Froude et al., 1983; Harrison, 2009 and references therein). However, valuable information retained in these samples may be challenging to extract as early crust localities typically consist of poly-deformed and metamorphosed gneiss terranes containing a wide variety of lithological and age components interlayered on a variety of scales (e.g., Bowring et al., 1989b; Moorbath et al., 1997; Mojzsis et al. 2014). Particularly within the most ancient terranes, additional geological complexity may have been induced by large-scale events such as the proposed late bombardment of Earth by meteoritic material at ~3.8 Ga (e.g., Tera, 1987; Norman, 2009), which has been suggested to have had a significant impact on the deformational history and preservation of ancient gneiss complexes (e.g., Mojzsis et al., 2014).

The complexity typical of ancient gneiss terranes make mapping and identifying specific units within these rocks difficult, and can obscure the interpretation of whole-rock geochemical and isotopic data (e.g., Bowring and Housh, 1995; Moorbath and Whitehouse, 1996; Moorbath et al., 1997). Due to intricacies in mapping and sampling within ancient gneiss complexes, it remains of utmost importance to identify areas where individual lithological components are relatively well preserved, and therefore more likely to retain their original composition.

Careful investigation of ancient gneiss terranes worldwide indicates they are dominated by the tonalite-trondhjemite-granodiorite (TTG) suite of rocks (e.g., Barker and Arth, 1976; Martin, 1986; Moyen, 2011; Moyen and Martin, 2012). Diagnostic geochemical characteristics of Archean TTGs include elevated Na_2O and Sr/Y, negative Nb anomalies, and pronounced HREE depletion. Some of these signatures, namely the fractionated REE patterns (low HREE relative to LREE) and high Sr/Y, indicate the presence of considerable quantities of garnet in the residue, implying deep-seated melting

of a hydrated basaltic precursor (e.g., Moyen and Stevens, 2006 and references therein), potentially in a setting broadly analogous to modern subduction zones (e.g., Martin, 1986; Nair and Chacko, 2008).

One of the most well-known ancient gneiss terranes is the Acasta Gneiss Complex (AGC), which comprises the westernmost exposure of the basement to the Slave Craton, Northwest Territories, Canada. The AGC contains the oldest known zircon-bearing rocks on Earth (Bowring et al., 1989b; Stern and Bleeker, 1998; Bowring and Williams, 1999; Reimink et al., 2014), and is composed of a wide variety of rock types, ranging from metagabbros to granitic gneisses, with a range in crystallization ages from 4.02 Ga to <3.4 Ga (Iizuka et al., 2007). Although early studies suggested that the oldest components within this terrane are chemically similar to Archean TTG suites, more recent work indicates that some of the oldest rocks of the AGC (>4.0 Ga) are unlike typical Archean TTGs in that they are characterized by intermediate silica contents (~60 wt.% SiO_2), high FeO contents (>10 wt.%), low Mg-numbers and relatively flat REE patterns (Reimink et al., 2014). Reimink et al. (2014) proposed that these rocks formed by distinct petrogenetic processes and likely in a tectonic environment differing from typical Archean TTGs. The present study aims to document the transition from crust-forming processes responsible for generation of the >4.0 Ga rocks to that of younger, Archean TTG-like rocks present within the AGC. The study targets well-preserved samples with formation ages spanning >1 billion years, that were identified during an intermediate-scale mapping and sampling campaign conducted over multiple field seasons.

The foundation of the study is an updated intermediate-scale geologic map of key areas within the AGC in which map units are separated based on age and composition, something not accomplished previously. We also present new whole-rock geochemical and zircon U-Pb and O-isotope data for samples spanning a range of crystallization ages from 4.02 to 2.94 Ga. These data are used to show a gradual transition in crust generation processes from a proposed Iceland-like setting (Reimink et al., 2014) at 4.02 Ga, to a classic Archean TTG subduction-like setting at 3.6–3.5 Ga. By ~3.6 Ga, a cratonic nucleus composed of newly formed, evolved rock types derived from a deep-seated source had been formed.

Geologic Setting:

The Slave Province

The Slave Province in the Northwest Territories, Canada is a well-exposed Archean craton that occupies the northwestern portion of the Canadian Shield (Fig. 4.1A) (Hoffman, 1988; Padgham and Fyson, 1992). Essential components of the Slave Province include a 4.02–2.8 Ga basement complex formed by multiple episodes of magmatic activity that is overlain by a ~2.9 Ga cover sequence (Bleeker et al., 1999; Sircombe et al., 2001; Ketchum et al., 2004). Neoarchean rocks consist of 2.72-2.60 Ga supracrustal packages of the Yellowknife Supergroup (Green et al., 1968; Jenner et al., 1981; Isachsen et al., 1991). The final stage of craton stabilization is represented by voluminous 2.62–2.58 Ga intrusion of tonalites to granites (van Breemen et al., 1992), which comprise ~50% of the exposed craton (Padgham and Fyson, 1992) and define an east-west boundary between granitoids that interacted with older evolved crust to the West and those that had not to the East (Davis and Hegner, 1992).

The Acasta Gneiss Complex (AGC), located on the western margin of the Slave Craton (Fig. 4.1), is a large block of basement gneisses of variable composition, age, and degree of deformation that is exposed in a series of structural culminations along the Acasta River (St Onge et al., 1988). Discovery of the extreme age of some rock units within the AGC (Bowring et al., 1989b) led to many studies that, until very recently, focused mainly on mapping and dating individual components within this complex gneiss terrane. Key discoveries from those studies pertinent to the present work are outlined below.

Previous mapping within the Acasta Gneiss Complex

The entire basement window of the AGC has an area >1300 km^2 (Fig. 4.1B; St Onge et al., 1988), however, the vast majority of published work has come from a ~30 km^2 area near the originally described ‘discovery’ outcrops (Fig. 4.1C). Many geologic maps of the area surrounding the discovery outcrops have been published with varying degrees of detail (Bowring et al., 1989b; Bowring and Housh, 1995; Iizuka et al., 2007; Iizuka et al., 2010) with Iizuka et al. (2007; 2010) publishing the most detailed regional maps thus far. The difficult logistics of working in such a remote location, as well as significant glacial and lichen cover, limits the success of mapping such locations. Additionally, the inherent complexity of mapping in a poly-deformed gneiss terrane such as this, as well as the difficulty in obtaining meaningful ages from complex outcrops, has led all previous workers to separate map units

on the basis of broad compositional differences without knowledge of their formation ages.

In general, the local region around the discovery outcrops has been subdivided into two main lithological assemblages; 1) an eastern domain where distinct rock units are banded on a decimeter- to meter-scale, and subdivided into felsic and mafic gneiss packages, and 2) a western domain comprising highly deformed gneisses banded on a centimeter-scale, typically containing both felsic and mafic

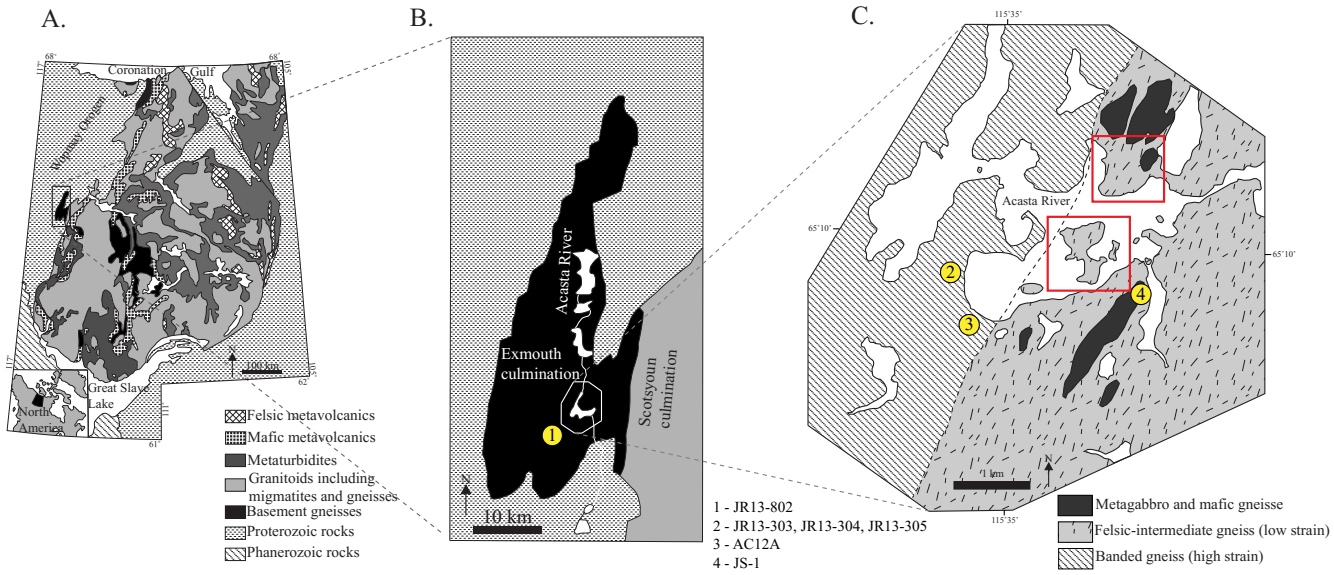

Figure 4.1: A: Simplified map of the Slave Province showing the location of the Acasta Gneiss Complex on the western margin of the craton. Modified after St. Onge et al., (1988) and Bleeker (2000). B: A closer view of the ~1300 km^2 basement exposure that comprises the broader Acasta Gneiss Complex. C: Simplified map of the area immediately surround the discovery outcrops along the Acasta River. Modified after Iizuka et al., (2007).

components (Bowring and Williams, 1999; Iizuka et al., 2007). Large bodies of ~3.6 Ga foliated granite to granodiorite intrude both the eastern and western domains (Bowring et al., 1989b; Iizuka et al., 2007).

Geochronology within the AGC

Bowring et al. (1989 a,b) reported zircon U-Pb ages of up to 3.96 Ga, obtained using both thermal ionization and secondary ion mass spectrometry. The crystallization age of the oldest components within the AGC was later refined to 4.02–4.03 Ga (Stern and Bleeker, 1998; Bowring and Williams, 1999). Although many of the samples within the AGC are Eoarchean-Paleoarchean in age, heretofore, much of the research focus in the region had naturally been directed towards the oldest

components and the information they contain regarding the origin and nature of the Hadean Earth.

Further exploration and dating of individual components was aided by the advent of laser ablation inductively coupled plasma mass spectrometry (LA-ICPMS), which provided a rapid tool for dating zircons in a larger number of samples. This procedure, supplemented by traditional U-Pb dating of apatite and titanite (Davidek et al., 1997; Sano et al., 1999) as well as $^{40}Ar/^{39}Ar$ dating of hornblende and biotite (Hodges et al.,1995) allowed further refinement of maps of the AGC as well as assembly of a detailed tectonothermal history of the complex (Iizuka et al., 2007). Predictably, the AGC has a complex history, with multiple pulses of magmatic activity from 4.03 to 3.3 Ga (e.g., Iizuka et al., 2007; Bleeker and Stern, 1997) as well as thermal and structural overprinting associated with younger tectonic events, including development of the nearby 1.8–1.9 Ga Wopmay Orogen (Davidek et al., 1997; Sano et al., 1999). Paleoproterozoic mafic dykes have also intruded this complex, and while there is reliable field evidence (dyke orientation, magnetic susceptibility etc.) for the presence of dykes associated with the ca. 1270 Ma Mackenzie dyke swarm (LeCheminant and Heaman, 1989), no direct dating of these samples has been undertaken.

Whole-rock geochemistry of AGC rocks

Relatively little basic petrological and geochemical information has been reported from the AGC, and whole-rock data that has been published (Bowring et al., 1990; Iizuka et al., 2010; Mojzsis et al., 2014) is difficult to interpret, in part due to the inherent lithological heterogeneity at the hand sample scale. For example, it was proposed that even the ancient components of the AGC were dominated by rocks similar to Archean TTGs (Bowring et al., 1990), though many of these analyses come from samples taken from the highly deformed and finely banded western portion of the AGC where ages are difficult to establish (Mojzsis et al., 2014). Mojzsis et al. (2014) provided whole-rock elemental data from a more substantial sample suite, though the main focus and conclusions of their study consisted of a detailed investigation of a single large sample coming again from the western, highly strained portion of the AGC. This sample suite has been investigated for the Hf isotope composition of zircon (Guitreau et al., 2012) as well as a variety of whole-rock tracer isotopes analyses (Roth et al., 2014; Guitreau et al., 2014; Willibold et al., 2015). These studies, while potentially informative of the pre-history of these important rocks, do not address in detail the petrogenesis of the investigated samples.

Despite the protracted history and extensive reworking experienced by some components within the AGC, areas of lower strain and significantly better preservation may still be found. Reimink et al. (2014) documented the existence of a mappable 4.02 Ga tonalitic unit that occurs in a relatively low-strain zone near a sample locality described by Stern and Bleeker (1998). This unit is relatively well preserved and retains significant information regarding its petrogenesis and therefore the state of the early Earth at the time of crystallization. The specific rock unit, informally called the Idiwhaa tonalitic gneiss (Reimink et al., 2014), is compositionally similar to intermediate high-Fe rocks from Iceland termed 'icelandites' (Carmichael, 1964; Nicholson et al., 1991). Notably, the whole-rock composition of the Idiwhaa unit is unlike typical Archean TTG.

Geologic map and sample descriptions

In light of our discovery of a relatively well-preserved area within the mapped region near the discovery outcrops, we have created a geologic map in the ACG discovery area that divides rock units by age as well as composition. We have focused on a relatively low-strain zone described previously by Reimink et al. (2014) but have further expanded the mapping to cover an area of ~1 km^2 (Map Area 1; Fig. 4.2A). The rock units from this map area are less deformed than in most other areas within a few kilometers of the discovery outcrops, and homogeneous rock units commonly occur on the meter, or larger, scale. We have also re-mapped and sampled the discovery (and camp) island (Map Area 2), using map units derived from the low-strain peninsula immediately to the north (Fig. 4.2B). The island has been mapped and sampled in great detail by the majority of previous investigators because of the relatively good exposure (outcrops are barren of lichen) and ease of access.

Figure 4.2 shows the maps produced for small, well-preserved areas within the AGC and broken into map units based on age as well as composition. Figure 4.2A shows Map Area 1 immediately surrounding the ~4.02 Ga tonalitic gneiss described by Reimink et al. (2014) which represents an area of lower strain than the majority of the areas previously investigated. Figure 4.2B shows Map Area 2, our map of the original discovery island that has been mapped in some detail by previous workers. We have broken both Map Areas into four main rock units as described below.

1) A banded unit in which tonalitic- to granodioritic-composition gneisses are interlayered on the

decimeter- to meter-scale. This unit includes the Idiwhaa tonalitic gneiss described by Reimink et al. (2014). The Idiwhaa gneiss is a garnet-hornblende-biotite tonalitic gneiss that is more melanocratic than adjacent rocks and contains significant (2–3 modal %) magnetite. Also, present are zircon, allanite, apatite, and titanite as accessory minerals. Other rock types within the banded gneiss unit include somewhat more leucocratic tonalitic to granodioritic gneisses that contain varying amounts of the major constituents amphibole, biotite, quartz, plagioclase, with accessory zircon, allanite, titanite, and minor garnet.

2) The amphibolitic gneiss unit comprises a fine-grained, foliated amphibolite with some portions containing variable amounts of garnet.
3) A relatively undeformed metagabbro that typically forms broad hills within the complex and, in places, preserves igneous textures. Note that we refer to this unit, which comprises mainly amphibole and plagioclase, as a metagabbro on the assumption that the amphibole presently in the rock replaced primary igneous pyroxene. Various other authors have called this rock type either metadiorite or metagabbro.
4) A group of granodioritic to granitic gneisses that are deformed with the previously mentioned units, and are in places inter-banded with Unit 1.

Samples were collected from each of these units (sample locations shown in Fig. 4.1C and Fig. 4.2). Detailed descriptions of each of the investigated samples are given in the Results.

Methods:

Whole-rock geochemistry:

Samples were collected over a three-year interval during the 2011–2013 field seasons. Key samples were identified and samples with the least deformation and alteration were selected for further investigation. Areas of visible alteration or crosscutting leucocratic material were removed before samples were crushed using an alumina shatterbox, which were pre-cleaned with quartz sand, producing between 0.5–2 kg of powder. Powders were homogenized and separate aliquots were taken from the bulk sample. Whole-rock powders were analyzed at Washington State University's GeoAnalytical Laboratory using XRF (Johnson et al., 1999) and ICP-MS (Knaack et al. 1994) techniques. Typical

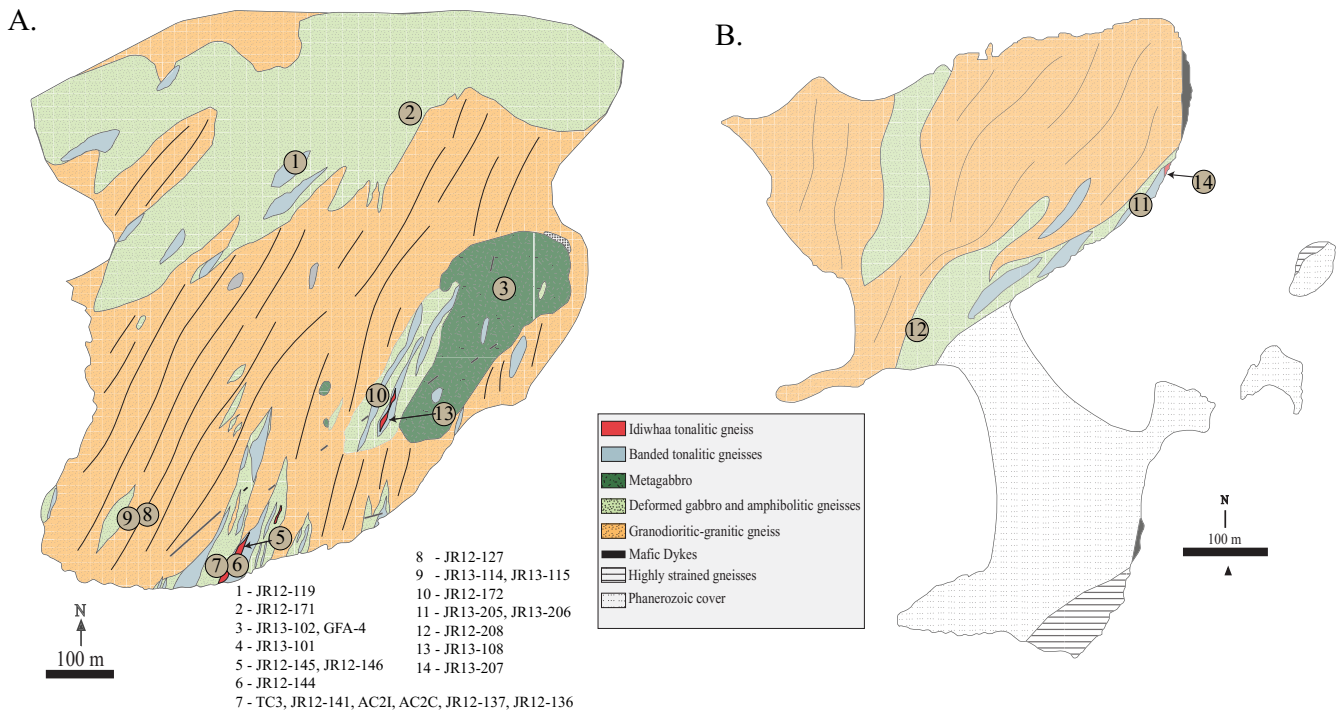

Figure 4.2: Results from our intermediate scale mapping campaign whereby we separate maps units based on age as well as composition. A: Map of the peninsula area immediately surrounding the Idiwhaa tonalitic gneiss unit. B: Map of the camp island using map units derived from the peninsula area. See text for a detailed description of map units. Sample locations are marked on each map.

limits of detection for XRF analyses are <0.2 wt.% for all major elements and <4 ppm for the trace elements analyzed using XRF. Uncertainties in the ICP-MS analyses used here to measure most trace elements are ~10% but closer to 5% for the rare-earth-elements.

Zircon separation:

Between 0.5–1 kg of sample aliquots were taken from the sample powders described above. Zircons were extracted using standard Wilfley table, magnetic, and heavy-liquid separation techniques. Zircons were picked for quality and mounted in epoxy. Internal growth zones were identified using a Zeiss EVO MA15 SEM with a broadband cathodoluminescence (CL) detector in the Canadian Centre for Isotopic Microanalysis at the University of Alberta.

LA-ICPMS U-Pb analysis of zircon:

U-Pb isotope data were collected using LA-ICP-MS and SIMS techniques at the University of

Alberta. For LA-ICP-MS data, most zircons were mounted and internal growth zones were identified by CL imaging. A few samples, with high-quality zircons, were analyzed in thin section using the methods outlined by Simonetti et al. (2005; 2006).

Zircons analyzed by ICP-MS in both mounts and thin sections were ablated using a Nu Wave Research 213 nm laser using spot sizes of 20 μm or 30 μm. Ablated material was mixed with thallium solution to correct for instrumental mass fractionation and transported in a He carrier gas to the torch of a Nu Plasma MC-ICP-MS. An in-house zircon standard (LH94-15, Ashton et al., 1999; Heaman, unpublished data) was used as the primary reference material. A secondary reference material was used to monitor the accuracy of the correction applied to unknown analyses (OG1, Stern et al*.,* 2009). LA-ICP-MS analyses took place over 14 analytical sessions between November 2011 and October 2014. Both the primary (LH94-15) and secondary (OG1) reference materials were analyzed throughout each analytical session with one analysis of both reference materials bracketing every 6-10 unknowns. A total of 163 analyses of OG1 zircon yielded a weighted mean $^{207}Pb/^{206}Pb$ age of 3456.8 ± 1.4 Ma with an MSWD of 1.6, which is outside uncertainty of the accepted age for OG1 (3465.4 ± 0.6 Ma, Stern et al*.,* 2009), indicating a slight bias towards younger ages in our analyses. Therefore, the true ages of analyzed samples may be ~10 myr older than those we have reported, however, a correction as small as this does not affect the conclusions of this paper.

Each analytical spot was investigated using CL imagery and categorized as either igneous, metamorphic, or undefined based on the presence of diagnostic characteristics such as oscillatory zoning or rim growth (Corfu, 2003). These were classified as one of the following: 1) oscillatory, where the presence of fine-scale oscillatory zoning indicates a magmatic origin or broader-scale zoning that may be indicative of derivation from more mafic magmas; 2) metamorphic rims without oscillatory zoning that can be clearly identified as overgrowths on igneous zircon; 3) irregularly-shaped zones of metamorphic recrystallization within igneous zircon. Due to the poor preservation of many zircon populations present within the samples documented here another category of zircon morphology that was difficult to confidently categorize into one of the above groups was created, called uncertain. These grains or grain portions often occured within or surrounded by highly metamict domains and very little information could be derived from CL or backscatter electron imaging. These classifications are presented with the U-Pb data in Appendix 1 and example images detailed in Appendix 5.

A few analyses showed a large change in isotopic composition during the course of an analysis, implying the laser beam has drilled through the main zircon growth phase and into a new phase, or had hit an inclusion. Analyses with these characteristics were either filtered to only contain data from the primary portion of the analyses, or discarded altogether.

Due to inherent uncertainty in estimating the common-lead isotopic composition in such complex zircons, no ^{204}Pb correction was applied to the LA-ICP-MS data. Instead, a simple filter using the measured $^{206}Pb/^{204}Pb$ ratio was applied to filter out analyses with a high proportion of common lead. Analyses with a $^{206}Pb/^{204}Pb < 500$ were omitted, leaving a total of 517 analyses.

SIMS U-Th-Pb analyses of zircon:

A small subset of samples with complex zircon growth features were analyzed for U-Th-Pb isotopic composition on the Cameca IMS1280 Ion Microprobe at the University of Alberta following the methods outlined in Reimink et al. (2014). Unknown samples were analyzed using a 20 μm spot diameter O-beam during two analytical sessions over one day. The primary reference material used for U-Pb calibration was Temora zircon (Black et al., 2004) while zircon OG1 (Stern et al., 2009) was monitored as a secondary reference material to assess accuracy of the Pb-Pb ages. Every four unknown analyses were bracketed with reference materials to track any potential changes in instrumental mass fractionation bias.

U-Th-Pb results for samples analyzed by SIMS are reported in Appendix 2. Analytical spots were classified into igneous or metamorphic phases using high-resolution imaging in a similar manner to the LA-ICPMS data. Ages for individual samples were calculated in a similar manner using weighted mean of $^{207}Pb/^{206}Pb$ of the oldest suite of analyses from igneous material. These data are also reported in Appendix 2. Table 4.1 presents the assigned ages for each sample reported here, along with the method for calculating the assigned age, as well as any information regarding inherited zircons or metamorphic history of the sample.

Oxygen isotope analysis of zircon:

We obtained $^{18}O/^{16}O$ analyses of a subset of zircons using the Cameca 1280 ion microprobe at the University of Alberta following the methods outlined in Reimink et al. (2014). Zircons were mounted,

imaged, and classified in a similar manner to the U-Pb analyses discussed above, but on separate grain mounts to those used for LA-ICPMS and SIMS U-Pb isotope measurements. Data were collected from zircons in three different mounts over four separate analytical sessions. Oxygen isotope measurements were made using a Cs^+ primary beam, and reference materials used to monitor instrumental mass fractionation were TEM2 (S0022; Black et al., 2004) and an in house reference material, zircon UAMT1 (S0081; R. Stern unpublished data). A single analysis lasted 4.5 minutes including pre-analysis rastering, automatic secondary ion tuning, and 100 seconds of isotope measurements. Oxygen isotope analyses were conducted on different mounts than those used for LA-ICP-MS U-Pb analyses; therefore the analytical spots are not strictly correlated. However, the only samples used for oxygen isotope analyses were those with the simplest U-Pb systematics, and only oxygen isotope data taken from igneous portions of grains is used here. Therefore, we are confident that the measured oxygen isotope ratios reflect that of the magmatic protolith to the metaigneous rocks . All oxygen isotope data were assigned U-Pb ages based on the calculated U-Pb age returned from igneous zircon of a particular sample.

Results:

Description of U-Pb results:

All analyses are reported in Appendix 1, while concordia plots for each sample are shown in Appendix 4. Representative images of zircons analyzed here are shown in Appendix 5.

Idiwhaa unit samples:

JR12-119

Zircons from JR12-119 are typically poorly preserved, with many of textural characteristics obscured. Some clear metamorphic rims were preserved and analyzed here. Eight analyses from seven zircons in a grain mount, and 13 analyses from six zircons found in thin section were analyzed from sample JR12-119. Of the 21 total analyses, two were from metamorphic rim material, one of which records near-concordant U-Pb data of ~3.4 Ga. Radiation damage in the zircons limited the data quality returned from many grains. One discordant analysis returned a $^{207}Pb/^{206}Pb$ age of 4000 ± 16 Ma. This

single analysis may present a more reliable estimate of the minimum crystallization age, and is similar to that returned by Idiwhaa unit sample TC3 that was investigated in detail using SIMS and TIMS techniques (Reimink et al., 2014; Chapter 3).

JR13-108

Zircons from JR13-108 are well preserved and plentiful. Morphologies in these grains are similar to grains extracted from sample TC3 (Reimink et al., 2014) and contain four main growth zones. These zones include an inner, unzoned igneous growth zone, and outer, oscillartory-zoned growth phase, a recrystallized growth zone and finally metamorphic rims that surround most grains. Thirteen analyses from six zircon grains were analyzed from sample JR13-108 in a grain mount. Of these analyses, two came from metamorphic zircons, and three from oscillatory-zoned areas. Many analyses are discordant, however a high proportion (8 analyses) have $^{207}Pb/^{206}Pb$ ages > 3900 Ma. A weighted mean of the seven analyses with the oldest $^{207}Pb/^{206}Pb$ ages yields an age of 3997 ± 6 Ma, interpreted as a minimum crystallization age. All zircon material from this sample closely shares zoning characteristics with zircon extracted from Idiwhaa tonalite sample TC3.

JR12-141

Zircons from sample JR12-141 are moderately well preserved and plentiful in thin section. Morphologies are typically uncertain, with a few metamorphic rims. Some grains preserve cryptic zoning patterns likely indicative of igneous zircon growth. A total of 25 analyses were obtained from six zircons found in a thin section of sample JR12-141. Four of these analyses were from metamorphic rims with the rest coming from zircon areas of uncertain origin using CL imaging. Analyses from metamorphic rims suggests that growth and/or recrystallization took place ~3370 Ma, while a weighted mean of the five analyses with the oldest $^{207}Pb/^{206}Pb$ ages yields an age of 3971 ± 29 Ma, interpreted to be a minimum crystallization age.

JR12-145

Zircons in sample JR12-145 are large and moderately preserved. Most have large areas that are very metamict with only small portions of well-preserved zircon, some of which contains portions that

have oscillatory-zoned igneous features. A total of 17 analyses from six zircons in thin section were analyzed from sample JR12-145. Of these analyses, three were from metamorphic zircon material and four from oscillatory-zoned portions. One analysis, from a zircon with oscillatory zoning patterns, returned a $^{207}Pb/^{206}Pb$ age of 3968 ± 14 Ma, giving a minimum crystallization age of the sample.

JR12-146

Of the 17 analyses from eight zircons in thin section from JR12-146, only four were from areas that did not have clear metamorphic morphologies. One analysis returned a $^{207}Pb/^{206}Pb$ age of 3996 ± 20 Ma, interpreted to be the minimum estimate for the crystallization age of the sample. All other analyses of metamorphic zircon material returned ages from 3977–3243 Ma, indicating partial resetting of pre-existing zircon or metamorphic zircon growth at ~3250 Ma.

JR13-207

Very few zircons were recovered from sample JR13-207, all of which were poorly preserved and had zoning patterns that were could not be confidently classified. Twelve spots from seven zircons were analyzed in grain mount, all displaying broad, dark, zoning patterns of unclear origin. Of these, four record $^{207}Pb/^{206}Pb$ ages > 3900 Ma, with one recording a $^{207}Pb/^{206}Pb$ age of 4003 ± 23 Ma, interpreted to represent the minimum age of crystallization. Two analyses record near-concordant analyses with $^{207}Pb/^{206}Pb$ ages of 3274 ± 17 and 3260 ± 19 Ma, suggesting zircon recrystallization and or metamorphic growth near this time.

JR12-137

JR12-137 yielded a moderate amount of zircon material, all of which could not be confidently classified on morphology alone. A total of 16 spots from eight zircon grains were analyzed in a grain mount from sample JR12-137. All of these analyses came from zircon that was of unclear origin and form a scattered discordia array. Of these, most record $^{207}Pb/^{206}Pb$ ages > 3800 Ma with the oldest analysis yielding a $^{207}Pb/^{206}Pb$ age of 3958 ± 22 Ma, interpreted to be a minimum crystallization age of this sample. Three analyses record much younger $^{207}Pb/^{206}Pb$ ages and may represent recrystallization during metamorphism ~3400 Ma.

Highly-strained gneiss sample:

AC12A

Zircons extracted from sample AC12A are extremely well preserved, particularly in comparison to other very ancient (>3.7 Ga) samples investigated here. Many zircons show strong oscillatory zoning patterns and some xenocrystic cores are present. Most grains have thin metamorphic rims. Twenty-three were obtained from 14 grains by secondary ion mass spectrometry at the University of Alberta's Canadian Centre for Isotopic Microanalysis using the Cameca 1280 Ion Microprobe. Of these analyses, six were from metamorphic rims, five from recrystallized portions of grains, three from igneous growth phases, and nine from oscillatory-zoned growth zones. The results define a discordia array that intersects the concordia curve at a shallow angle, with the lower end anchored by metamorphic rims. One metamorphic rim analysis is concordant and records an age of 3427±1 Ma, interpreted to be an age of metamorphism. A minimum magmatic age was determined by two concordant analyses with very precise $^{207}Pb/^{206}Pb$ ages of 3989 ± 6 Ma and 3984 ± 2 Ma. This calculation excludes one metamorphic zircon analysis, identified in CL as having 'fir-tree' zoning patterns characteristic of metamorphic zircon, and showing significant reverse discordance as well as another, less precise analysis that is slightly reversely discordant.

Banded gneiss map unit samples:

JR13-206

Grains extracted from JR13-206 were relatively low quality, although the zircon yield was good. All analyzed spots show morphological characteristics that are of uncertain origin. Twenty analyses from 17 zircons were determined in a grain mount. All of these analyses were from igneous material, yet returned a wide range of $^{207}Pb/^{206}Pb$ ages. Most analyses are discordant and form a broad discordia array. A minimum crystallization age was determined by taking a weighted mean of the three analyses with the oldest $^{207}Pb/^{206}Pb$ ages, yielding an age of 3962 ± 29 Ma (MSWD = 3.6).

JR13-101

Zircons extracted from JR13-101 were plentiful and moderately well presereved, with some

grains preserving clear oscillatory-zoning patterns. A total of 19 analyses from ten zircon grains were obtained in thin section from sample JR13-101, in addition to 16 analyses from nine grains in a mount. Four of these analyses were from metamorphic zircon, one of them a rim. Two metamorphic rims record near-concordant U-Pb dates near ~3300 Ma, suggesting this as a time of metamorphic zircon growth. Eighteen analyses plot as a cluster, and a weighted mean of their $^{207}Pb/^{206}Pb$ ages yields an age of 3739 ± 6 Ma (MSWD = 1.8), interpreted to be the igneous crystallization age. All other analyses plot in a field defined by this upper age, the lower metamorphic age, and a recent Pb-loss event.

Metagabbro map unit sample:

JR12-136

Twenty-three analyses from 15 grains were collected from zircon in thin section and grain mount from metagabbro sample JR12-136. Most of these zircons display zoning characteristics suggestive of a metamorphic origin and all but two analyses returned $^{207}Pb/^{206}Pb$ ages <3600 Ma. Most analyses fall along a broad discordia array with an upper intercept of ~3.3 Ga and a lower intercept at the origin. We interpret most of these grains to have formed during metamorphism ~3300-3400 Ma, though two grains with $^{207}Pb/^{206}Pb$ ages >3600 Ma contain older radiogenic Pb, possibly from incomplete Pb-loss during recrystallization. No unambiguous igneous or xenocrystic zircons were analyzed from this sample.

Granite-granodiorite map unit samples:

JR13-205

JR13-205 yielded many zircon grains, many showing clear fine-scale oscillatory-zoning patterns. Eighteen analyses were obtained from 16 zircons in grain mount from JR13-205. Sixteen of these analyses came from oscillatory-zoned zircons. One analysis, interpreted to be xenocrystic, returned a near-concordant U-Pb analysis with a $^{207}Pb/^{206}Pb$ age of 3834 ± 23 Ma, while a majority of oscillatory-zoned grains yielded ages near the estimated crystallization age of the sample, 3588 ± 8 Ma (MSWD = 0.35). This minimum age was determined by taking the weighted mean of seven analyses yielding the oldest $^{207}Pb/^{206}Pb$ ages, excluding the one xenocrystic zircon analysis.

JR13-305

JR13-305 yielded zircon grains with a wide range of preservation quality. Many grains seemed to contain xenocrystic cores and some grains were dominated by metamorphic growth. However, many grains contained areas defined by fine- and broad-scale oscillatory zoning. Twenty-four analyses were obtained from 20 grains in a mount. Four of these came from zircon cores, three from metamorphic rims, and the rest from either oscillatory-zoned zircon or zircon of uncertain origin. The best estimate for the crystallization age of this unit comes from a weighted mean of the oldest four $^{207}Pb/^{206}Pb$ ages, yielding an age of 3596 ± 13 Ma (MSWD = 1.6). This calculation excludes two analyses of xenocrystic material that returned $^{207}Pb/^{206}Pb$ ages >3600 Ma, and two analyses from zircon of uncertain origin returning $^{207}Pb/^{206}Pb$ ages >3600 Ma. Many analyses plot along a scattered discordia array extending along the concordia line towards ~3300 Ma, interpreted to be a time of metamorphic Pb-loss or recrystallization.

JR13-208

JR13-208 yielded many high-quality zircon grains that display fin-scale oscillatory zoning patterns. The vast majority of zircon grains have small metamorphic rims. Nineteen analyses were obtained from 18 grains in a mount. One of these analyses was from a metamorphic rim, while 13 came from oscillatory-zoned zircons. Most of the analyses presented here cluster near the calculated crystallization age of 3569 ± 12 Ma, determined by taking the weighted mean of the nine analyses recording the oldest $^{207}Pb/^{206}Pb$ ages (MSWD = 1.9). The one analysis of a metamorphic rim yielded a $^{207}Pb/^{206}Pb$ age of 3501±23 Ma, suggesting this as a potential time of recrystallization.

JR13-303

JR13-303 yielded zircons that are typically less well preserved than other ~3.6 Ga samples. These grains are dominated by CL-dark regions and contain many areas of uncertain morphology. Twelve analyses were obtained from eight zircon grains in a mount. Of these analyses, four were from apparently xenocrystic cores, all yielding $^{207}Pb/^{206}Pb$ ages >3700 Ma. Of these four analyses, one yielded a very old $^{207}Pb/^{206}Pb$ age of 3946 ± 24 Ma. The rest of the zircon analyses came from oscillatory-zoned zircon or zircon of uncertain origin. These analyses cluster around the calculated crystallization age of the sample, 3512 ± 43 Ma (MSWD = 3.7), determined by taking the weighted mean of the

oldest four $^{207}Pb/^{206}Pb$ ages.

JR12-144

JR12-144 yielded many small grains that contained well-preserved oscillatory-zoning patterns. Most grains are elongate and surrounded by small metamorphic rims. A total of 25 analyses from 19 grains (11 in grain mount and eight in thin section) were analyzed from sample JR12-144. All of these analyses were taken from igneous zircon material, and they form a scattered discordia line. The seven analyses with the oldest $^{207}Pb/^{206}Pb$ ages yield a weighted mean of 3596 ± 13 Ma (MSWD = 1.7), interpreted to be the minimum crystallization age of the unit.

JR13-114

JR13-114 yielded many zircons with diverse zoning patterns. Grains contain oscillatory-zoned regions that were both CL-bright and CL-dark. Almost all grains contain small portions that are metamict, and are surrounded by small metamorphic rims. Eighteen analyses were obtained from 12 grains from sample JR13-114 were analyzed. Of these spots, one came from metamorphic zircon and nine from oscillatory-zoned material. The one metamorphic analysis yielded a concordant age of 3301±17 Ma whereas the remaining data is mostly discordant, with some analyses showing significant recent Pb-loss. The best estimate of the crystallization age for this sample is given by a weighted mean of the five oldest $^{207}Pb/^{206}Pb$ ages, 3589 ± 18 Ma (MSWD = 2.9).

JR12-127

JR12-127 yielded zircon grains that have CL-dark oscillatory zoning patterns and most contain metamorphic rims. A total of 28 analyses coming from 16 zircons were collected in both thin section and grain mount from sample JR12-127. Of these analyses, 12 came from oscillatory-zoned graines. The full data set forms a loose discordia array between an upper crystallization age and recent Pb-loss. The upper age, interpreted to be the minimum crystallization age, is 3590 ± 6 Ma (MSWD = 0.86), calculated by a weighted mean of the $^{207}Pb/^{206}Pb$ ages of the oldest eight analyses.

JR12-171

JR12-171 yielded many zircons with well-preserved oscillatory-zoning patterns surrounded by metamorphic rims of varying size. Twenty-one analyses were obtained from 12 zircons in a grain mount. All of these analyses came from zircon displaying oscillatory zoning patterns and provides a relatively simple Pb-loss pattern on the concordia diagram. A weighted mean of the $^{207}Pb/^{206}Pb$ ages from the 14 oldest analyses gives an age of 3581 ± 6 Ma (MSWD = 0.23), interpreted to be the minimum crystallization age of this sample.

JR13-115

JR13-115 yielded zircons with widely varying preservation states. Most contain some portion of CL-bright oscillatory zoning while some display metamict interior zones. Seventeen spots coming from 14 grains were analyzed in a grain mount from sample JR13-115. Of these analyses,12 came from oscillatory-zoned areas. Many of the analyses coming from this oscillatory-zoned zircon plot near the best estimate for the igneous crystallization age, 3572 ± 10 Ma. This ages was derived by taking the weighted mean of the 10 oldest $^{207}Pb/^{206}Pb$ ages (MSWD = 1.3). Two analyses coming from portions of zircon with uncertain morphological characteristics are near concordant with $^{207}Pb/^{206}Pb$ ages of 3285 ± 27 and 3323 ± 23 Ma, suggesting this as a time of zircon metamorphism/recrystallization.

JR13-802

JR13-802 contained abundant zircons in thin section that preserve fine-scale oscillatory-zoning patterns. Nine zircons from sample JR13-802 were analyzed 20 times in thin section. Two of these analyses originally appeared to be xenocrystic, however the ages returned from these portions of grains were not distinguishable from the rest of the population. Therefore, they are interpreted to represent magmatic dissolution and may be antecrystic. Two other analyses came from metamorphic zircon, but again returned U-Pb analyses indistinguishable from the rest of the population. No analyses returned concordant data, however, all data fall on a simple discordia array with an upper intercept age of 3358 ± 17 Ma (MSWD = 11) and a recent lower intercept. The upper intercept of this line is interpreted to be the best estimate for the crystallization age of the sample.

JR13-304

JR13-304 yielded many zircons with CL-dark oscillatory-zoned patterns surrounded by small metamorphic rims. Seventeen analyses were obtained from 13 zircons in a grain mount. One of these analyses came from metamorphic rim zircon, and the other 16 from either oscillatory zoned zircon or zircon of uncertain origin. The analysis of a metamorphic rim returned a concordant $^{207}Pb/^{206}Pb$ age of 2874 ± 24 Ma, while the minimum crystallization age of the sample comes from a concordia age calculated by analysis of 14 concordant analyses at 2935 ± 9 Ma and incorporates 14/17 of the total analyses (MSWD = 0.97).

Summary of U-Pb Zircon Geochronology

The U-Pb isotopic data obtained by LA-ICPMS and SIMS are reported in Appendix 1 and Appendix 2, respectively. The key features of the U-Pb data are described within the context of the map units and summarized in Table 4.1. The U-Pb results for many samples are somewhat complex, with a high proportion of discordant analyses. Reported ages (Table 4.1) were determined in two ways. Samples that contain chemical similarities to the Idiwhaa unit (high FeO, flat REE patterns) and also contained zircons >3.95 Ga have reported ages that represent a minimum age, based on the oldest $^{207}Pb/^{206}Pb$ age recorded in zircon from that sample. A further discussion of the true magmatic age of these samples is found in Section 6.1 and 6.2. All other samples have reported ages determined by taking the weighted mean of a cluster of analyses with the oldest $^{207}Pb/^{206}Pb$ ages, excluding any analyses determined to be xenocrystic or metamorphic on the basis of textural criteria. The number of analyses included in the weighted mean calculation, as well as the reported uncertainties and any further information regarding the U-Pb systematics of the sample, are also reported in Table 4.1.

First, samples belonging to the Idiwhaa tonalitic gneiss unit returned a restricted range of ages. The youngest minimum age estimate from any Idiwhaa unit sample is 3958 ± 22 Ma (sample JR12-137) though the majority of samples return minimum ages of >3.99 Ga. Non-Idiwhaa unit samples are also found in the banded gneiss map unit. One sample records U-Pb zircon ages approaching 4.0 Ga (JR13-206), while a few samples from this map unit have distinctly younger igneous crystallization ages of ~3.75 Ga (e.g., JR13-101; Appendices 4–5).

As might be expected of mafic rocks, the mafic samples processed from the mapped area (amphibolite and metagabbro map units) yielded very few zircon grains despite large quantities of

material processed (1–2 kg). The one exception is metagabbro sample JR12-136, which yielded many small, rounded zircon grains. However, CL imaging revealed these grains to be dominated by metamorphic zircon growth, and the U-Pb analyses of this metamorphic zircon show a recrystallization/growth event ca. 3.55 Ga, providing a minimum crystallization age for the metagabbros.

Metamorphic zircon growth at 3.55 Ga fits well with the crystallization ages of the volumetrically dominant suite of rocks within our mapped areas, the granite-granodiorite map unit. All of the samples from this unit have well-defined U-Pb crystallization ages between 3.55 and 3.6 Ga. This fits well with our field analysis suggesting that these represent a younger, less deformed suite of potentially related granitoids.

Outside of Map Area 1, U-Pb ages become more complex, despite broad correlation in lithochemistry. First, one other ~3.75 Ga sample was identified (JS-1), while analysis of the high-quality zircon extracted from highly strained gneiss sample AC12A shows complex U-Pb patterns, but a significant portion of the analyses indicate igneous crystallization at ~3.98 Ga. Additionally, two younger granites were identified outside of both map areas; (JR13-304) is a ~2.93 Ga granite body that cross-cuts the main foliated gneisses in the western portion of the AGC while JR13-802 was collected from a large body of ~3.37 Ga foliated granite, located ~5 km to the west of the main mapped area (Fig. 4.1).

Notably, a large proportion of the samples described above contain metamorphic zircon overgrowths, most of which return U-Pb ages consistent with zircon growth and/or recrystallization during a 3.2–3.4 Ga metamorphic event. This is consistent with previous estimates of a large-scale metamorphic/fluid event within the AGC (Moorbath et al., 1997; Stern and Bleeker, 1998; Roth et al., 2014; Reimink et al., 2014).

Whole-rock Geochemistry:

The whole rock major-, minor-, and trace-element geochemistry of selected samples are presented in Table 4.2. Within the geochemical and age data there are some important trends to note and are discussed by map unit from oldest to youngest below.

Within the banded gneiss map unit, the 4.02 Ga Idiwhaa tonalitic gneiss mostly displays low SiO_2 contents (58–67 wt.%) although two samples (JR12-137, JR12-146) have higher SiO_2 contents

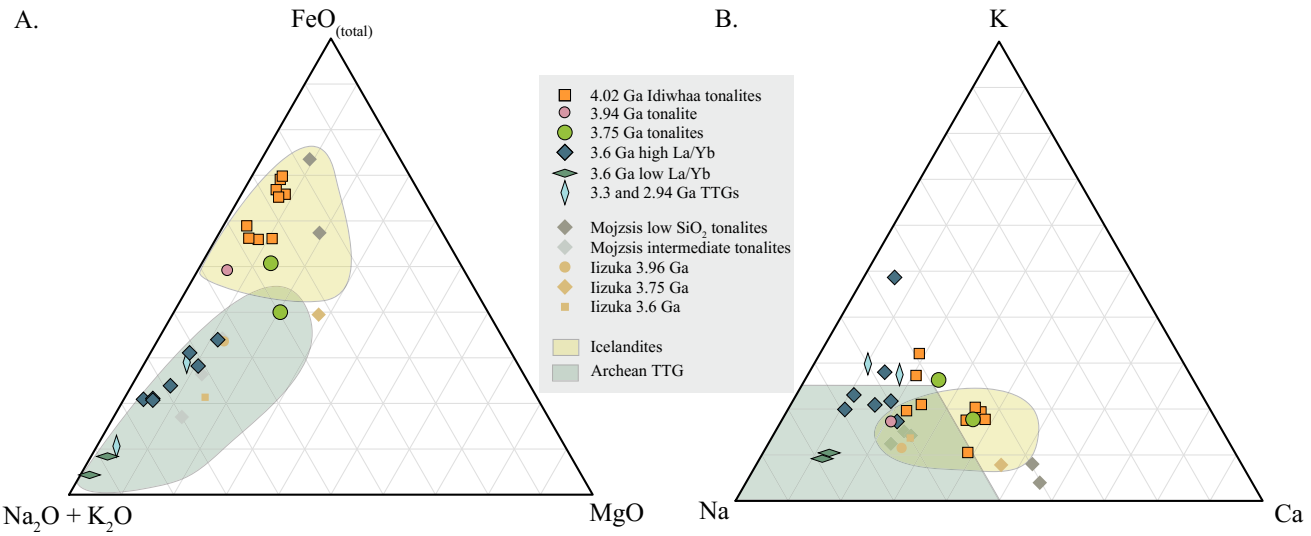

Figure 4.3: Major element data from the samples discussed in this chapter. A: Traditional AFM plot showing the evolution of granitoids within the AGC from highly Fe-enriched at 4.02 Ga to a more typical calc-alkaline rocks at 3.6 Ga. Also shown for comparison are icelandites (rocks from Iceland via the Georoc database defined as having 55–65 wt.% SiO_2, <14 wt.% Al_2O_3, and >8 wt.% total FeO) and Archean TTGs (Moyen, 2011). B: An elemental K-Na-Ca ternary plot showing the relatively Na rich character of the 3.96–3.6 Ga rocks from the AGC, suggesting derivation via partial melting of hydrated basalt. Also shown are the fields for Archean TTG (Martin, 1999) and icelandites from the GEOROC database described in Figure 2.1.

(~70 wt.%). Other diagnostic features of the Idiwhaa unit include high-FeO contents (8–15 wt.%) and low Mg# (<21; Fig. 4.3A). The Idiwhaa unit samples also have flat REE patterns (La_N/Yb_N < 3.8) although the high-silica Idiwhaa samples have significantly higher La_N/Yb_N of 7.1 and 6.8. All Idiwhaa samples are high in Zr (280–490 ppm) and Hf (7–13 ppm; Figs. 4.4–6). These rocks all lack the characteristically high Na_2O contents (Fig. 4.3), negative Nb anomalies, and high La_N/Yb_N of typical Archean TTGs.

Other samples from the banded gneiss map unit include 3.94–3.75 Ga tonalite samples. These have broadly similar range of SiO_2 contents (64–72 wt.%) to the Idiwhaa tonalite gneiss. However, these samples have lower FeO contents (6–7 wt.%) and higher Mg# (17–47) when compared to the ITG samples with similar SiO_2. Additionally, these younger tonalites have similarly high Zr contents (260–470 ppm) but more variable and fractionated REE patterns (La_N/Yb_N = 5.6–19) and significant negative Nb anomalies compared to the ITG samples.

One amphibolite and three metagabbro samples were analyzed and are compared here. The three metagabbro samples have similar compositions and also compare well with the amphibolite sample

(JR12-172) taken from the same map area. The amphibolite and metagabbros contain intermediate SiO_2 contents (~55 wt.%), moderate FeO (~9–13 wt.%), high MgO (~7 wt.%) with correspondingly high Mg# (41–58). These samples also have moderate Cr and Ni contents (18–149 and 14–49 ppm, respectively), with relatively flat REE patterns (La_N/Yb_N = 2–5).

The younger (3.6–2.9 Ga), and volumetrically dominant (Fig. 4.2) suite of granitoid rocks in the AGC, comprising the granite-granodiorite map unit, is much more typical of classic Archean TTGs, and clearly geochemically distinct from the >3.75 Ga suite described above. The samples have generally higher SiO_2 contents (>65 wt%) than older tonalites and most have Na_2O > 4 wt.% (Fig. 4.3B), as well as La_N/Yb_N > 40. This granite-granodiorite sample suite contains some significant variability; one small group, consisting of two samples, has significantly higher Na_2O/K_2O (4–5) and lower La_N/Yb_N (20–30) than the other samples in this suite (<2 and >30, respectively). All samples in this age group have significant negative Nb-anomalies (Figs. 4.4, 4.6) and most exhibit either negative or positive Eu-anomalies (Figs. 4.5, 4.7; Table 4.2).

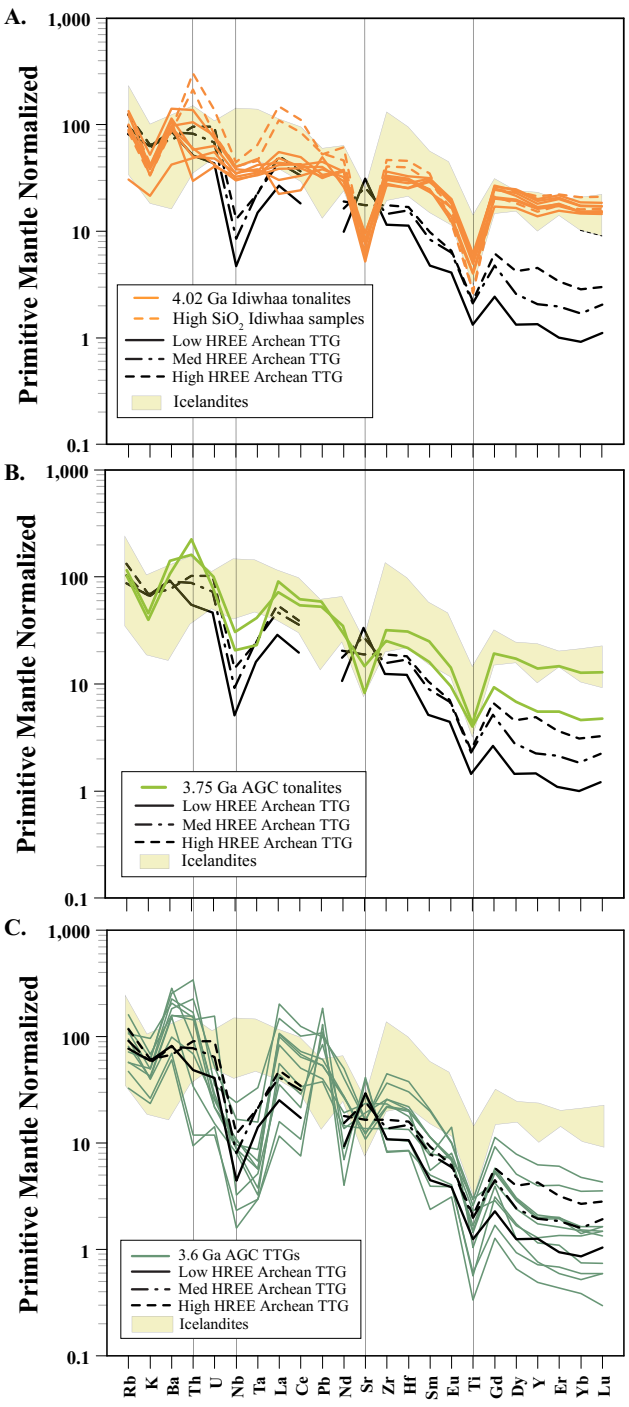

O-isotope analysis of zircon

A total of 317 $^{18}O/^{16}O$ analyses of zircons were conducted on 15 samples. Each analytical spot was investigated first using high-resolution imagery and categorized as either igneous or metamorphic in the

Figure 4.4: Primitive-mantle normalized (McDonough and Sun, 1995) trace-element plots for different ages of AGC granitoids. Note the evolution to lower HREE, Nb, Ta, Zr, and Hf with age. Icelandites and average Archean TTGs (Moyen and Martin, 2012) are shown for comparison.

same manner as the U-Pb analyses mentioned above. The results are reported in Appendix 3 along with the phase of zircon growth identified from images. Crystallization ages (Table 4.1) were assigned to igneous oxygen isotope data using the ages calculated from LA-ICPMS U-Pb data collected on separate zircons from each sample. The average oxygen-isotope composition of igneous zircon material from each sample, reported in $\delta^{18}O_{VSMOW}$, along with their standard deviation is given in Table 4.3 and plotted in Figure 8.

Magmatic zircons in the oldest samples (JR13-108, JR12-206, TC3) have $\delta^{18}O$ values ranging from +6.4 to +4.2‰. In the well-preserved zircon grains extracted from sample TC3, Reimink et al. (2014) documented two chemically distinct phases of igneous zircon growth, the first with mantle-like oxygen isotope compositions (mean $\delta^{18}O$ of +5.6‰) surrounded by a second phase of zircon growth with lower than mantle $\delta^{18}O$ values (mean of +4.7‰). This result is confirmed in this study with a second sample of the Idiwhaa gneiss JR13-108 (Fig. 4.8), collected a few hundred meters away from the TC3 locality (Fig. 4.2). Zircons extracted from this sample have identical zoning patterns to those of TC3 zircons (Phase I and II) and similar $\delta^{18}O$ values, ranging from +6.36 to +4.32‰. A different sample taken from the camp island outcrops, JR13-205, contains lower quality zircon that displays a similar range in igneous $\delta^{18}O$ (+4.2 to +6.3‰) though the generally more damaged nature of zircon grains in this sample inhibits our ability to compare zoning patterns to those present in sample (TC3).

Metagabbro sample JR13-102, containing dominately metamorphic zircon was the only amphibolite or metagabbro sample conducive to oxygen isotope analysis. In CL imaging, only three analytical spots from this sample were placed on zircon material that had igneous characteristics such as oscillatory zoning and yield a mean $\delta^{18}O$ of +5.6‰.

We also analyzed well-preserved zircon grains extracted from a highly strained ~3.94 Ga gneiss sample AC12A. These zircons show a narrow range of igneous $\delta^{18}O$ values between +6.0 and +6.8‰, very similar to the range in igneous $\delta^{18}O$ values (+5.6 to +7.0‰) recorded in virtually all of the zircons extracted from the other post-3.9 Ga granitoid suites investigated here. The one exception to this is a single analysis (5.0‰) obtained from the 3.37 Ga granodiorite sample JR13-802. Sample JR13-304, a 2.94 Ga granodioritic body that cross-cuts the highly deformed gneisses in the western portion of the AGC, has a slightly lower range of igneous $\delta^{18}O$ values than the ~3.6 Ga suite, from +5.6 to +6.3‰.

Although our main focus was on the oxygen isotope compositions of zircons of igneous origin,

we did perform a few analyses of metamorphic zircon. These analyses showed a wide range in $\delta^{18}O$ values from +5.0 to +7.5‰. The variation within the metamorphic zircon oxygen isotope composition does not correlate with age or other geochemical parameters.

Discussion:

Hadean (>4.0 Ga) ages of the AGC

We have previously documented the existence of a mappable unit, which we termed the Idiwhaa tonalitic gneiss, with an igneous crystallization age of ~4.02 Ga (Reimink et al., 2014). The morphologies of zircons found in this unit are similar to >4.0 Ga zircons previously documented in other rocks from the AGC (Stern and Bleeker 1998; Bowring and Williams 1999) although the U-Pb isotope systematics in our samples are generally simpler than those reported in other studies. Given the limited number of samples that have returned >4.0 Ga ages in nearly 25 years of research, it would appear that this most ancient unit of the AGC is rarely exposed at surface, or more likely is a volumetrically minor component within the complex (Fig. 4.2). In the present study, we have obtained U-Pb zircon age information from two additional samples of the Idiwhaa unit (JR12-141, JR13-108). Unfortunately, the quality of zircons in these new samples is not as good as in the original Idiwhaa sample, TC3, investigated by Reimink et al. (2014), potentially due

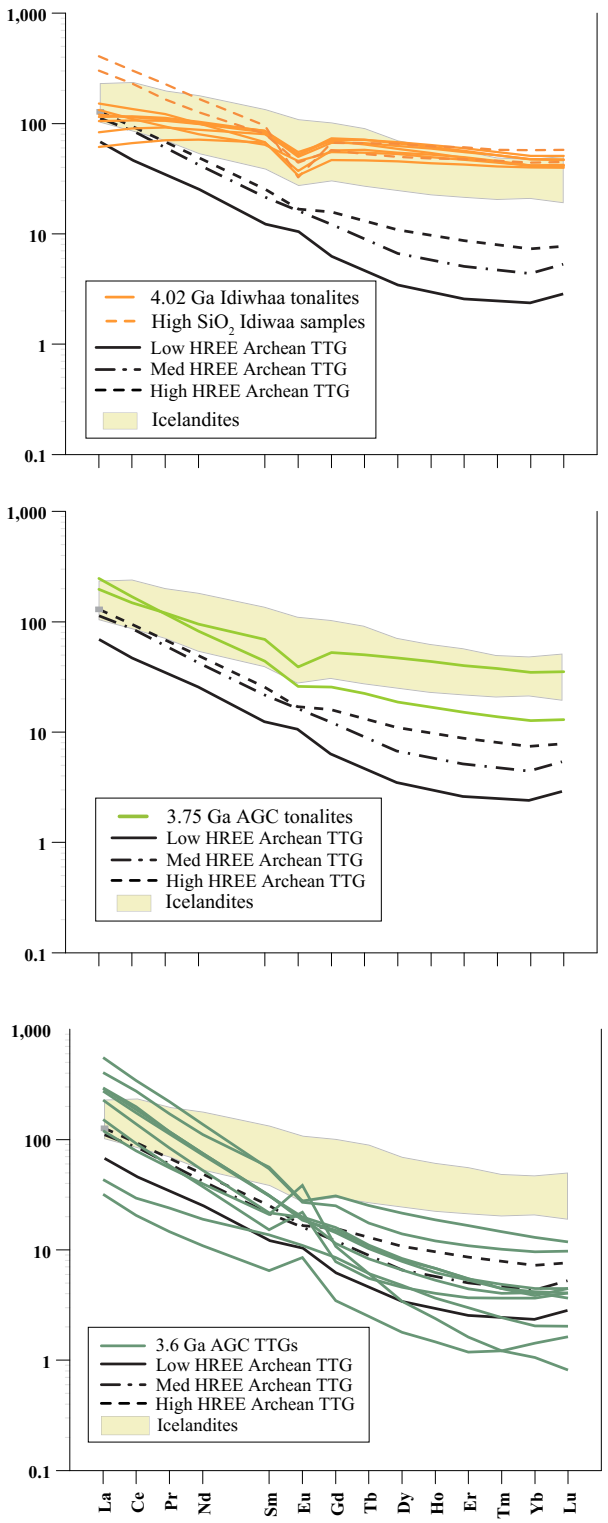

Figure 4.5: Chondrite normalized (McDonough and Sun, 1995) REE plots for different ages of AGC granitoids. Note the evolution to lower HREE with age. Icelandites and average Archean TTGs (Moyen and Martin, 2012) are shown for comparison.

to more significant radiation damage, caused by higher U and Th contents in the zircons. One other potential explanation is that sample TC3 was serendipitously preserved from later fluid alteration that affected other samples, leading to higher Pb-loss in other Idiwhaa unit zircon material. However, as in the original sample, zircons from new samples yielded numerous analyses with $^{207}Pb/^{206}Pb$ ages >4.0 Ga as well as ca. 3.3 Ga metamorphic overgrowths. The similarity of the U-Pb isotope systematics combined with shared lithological and geochemical features (see discussion below) indicate all these

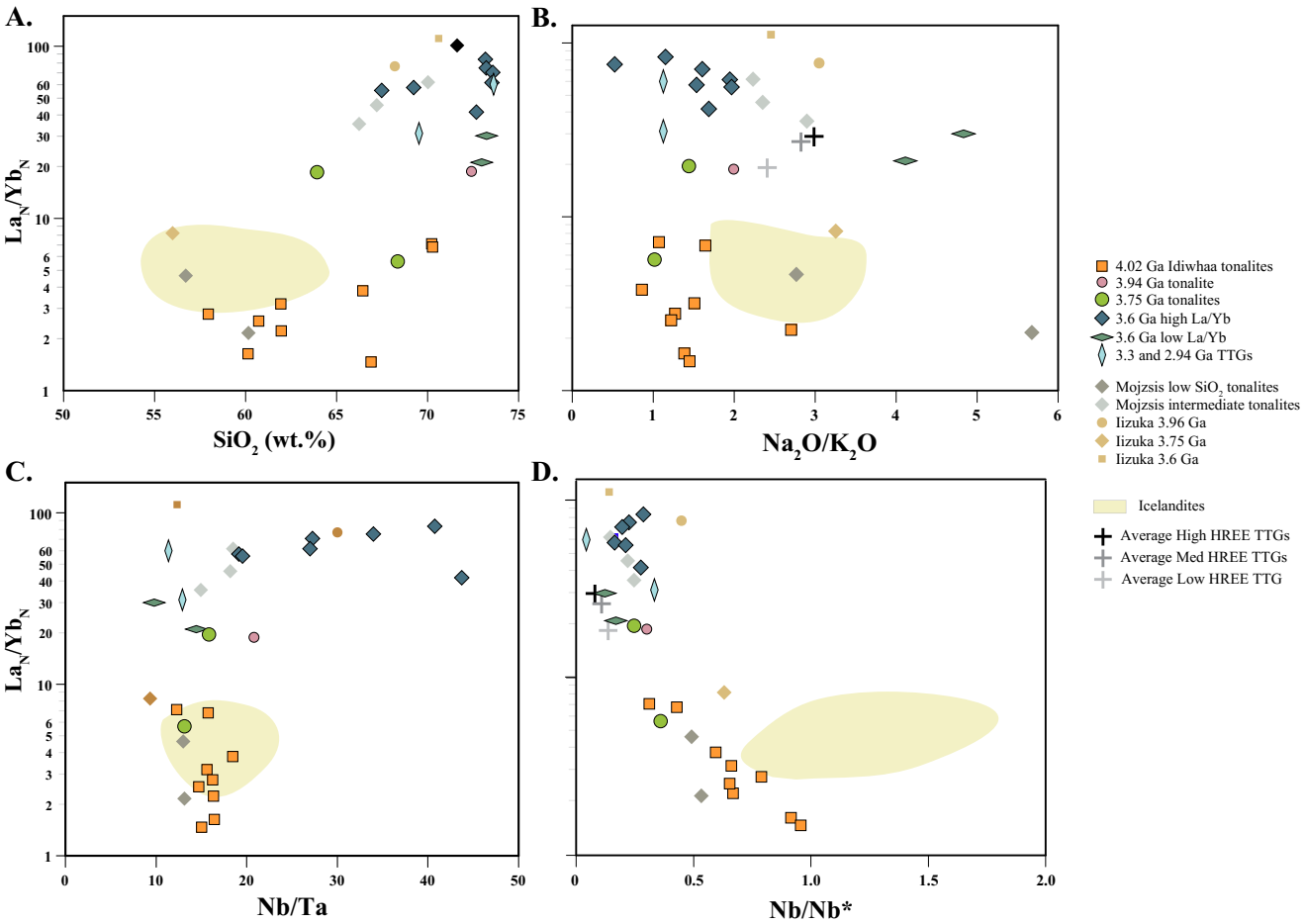

Figure 4.6: Various geochemical parameters discussed in the text plotted against normalized La/Yb. A. La_N/Yb_N versus SiO_2 showing the trend to more evolved components, generated at progressively deeper depths, with age. B. La_N/Yb_N versus Na_2O/K_2O shows the trend from derivation via fractional crystallization in the 4.02 Ga components to derivation via partial melting at changing depths post 3.94 Ga. C. Normalized La/Yb versus Nb/Ta anomaly. The trend to high Nb/Ta in some rocks with high La_N/Yb_N suggests melting in the presence of both rutile and significant garnet. D. La_N/Yb_N versus normalized Nb anomaly. Rocks with higher La_N/Yb_N also contain a significant negative Nb anomaly, an indication of formation by partial melting. Primitive mantle normalized (McDonough and Sun, 1995) Nb/Nb* is calculated in the following manner:

$$\frac{Nb}{Nb*} = \frac{\frac{Nb}{0.658}}{\sqrt{\left(\frac{U}{0.0203}\right)*\left(\frac{La}{0.648}\right)}}$$

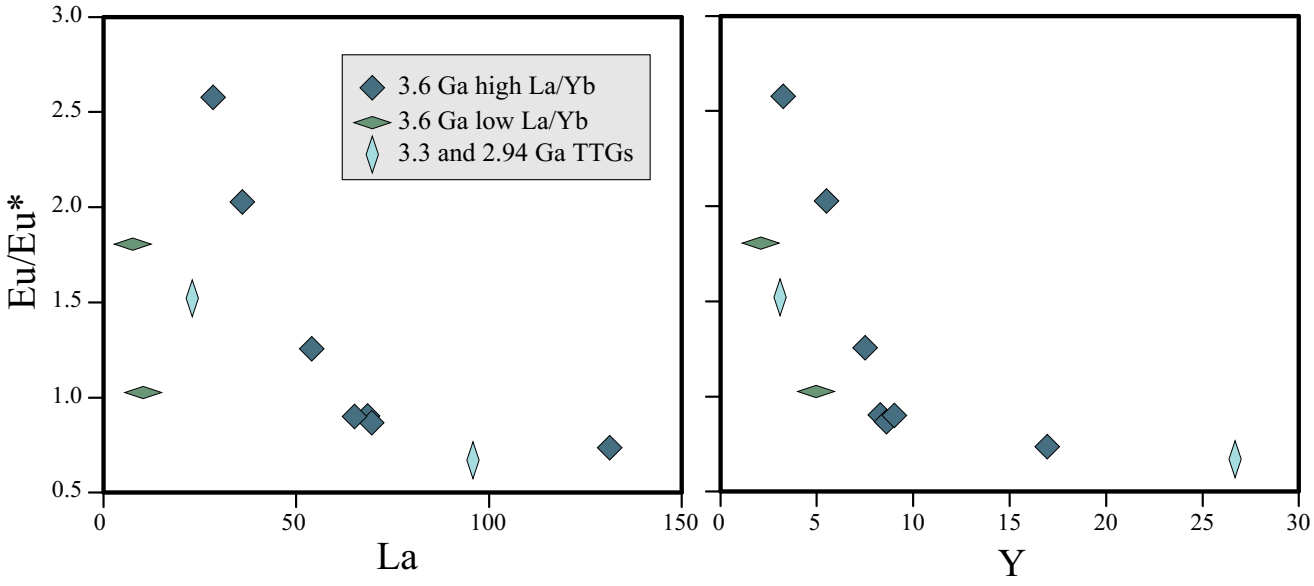

Figure 4.7: Broad correlation of Eu/Eu* with incompatible element contents of ~3.6 Ga AGC granitoids. This can be explained by development of Eu anomalies via fractionation processes, where rocks that had experienced significant plagioclase fractionation (negative Eu anomalies) are enriched in incompatible elements.

samples belong to a single unit.

Given our findings regarding the Idiwhaa tonalitic gneiss, it is important to respond to the claim of Mojzsis et al. (2014) that the oldest rocks in the complex are ~ 3.92–3.96 Ga and that all pre-4.0 Ga zircons in the AGC are xenocrystic in origin. They base this claim on a detailed study of one, banded gneiss sample from the highly strained western portion of the AGC. Specifically, they used whole-rock major- minor- and trace-element geochemistry and Lu-Hf and Sm-Nd isotope analyses of this sample as well as zircon REE partition modeling and Ti-thermometry, to conclude that the oldest components of the AGC were no more than 3.96 Ga and that they were emplaced as migmatites; they conclude that any pre-3.96 Ga zircon found in AGC samples are xenocrysts derived from rocks no longer present in the complex.

For a number of reasons, we believe Mojzsis et al.'s (2014) assertions regarding the absence of pre-3.96 Ga rocks in the AGC to be overstated. Their conclusions were based on a single, mixed sample, with a variety of components interlayered at the cm-scale. Mojzsis et al. (2014) interpreted this compositional banding to be migmatitic in origin (i.e., the result of in-situ partial melting) but there is no compelling evidence from metamorphic mineral assemblages that the grade of metamorphism in the presently exposed AGC was ever sufficiently high to engender partial melting of these rocks. A possi-

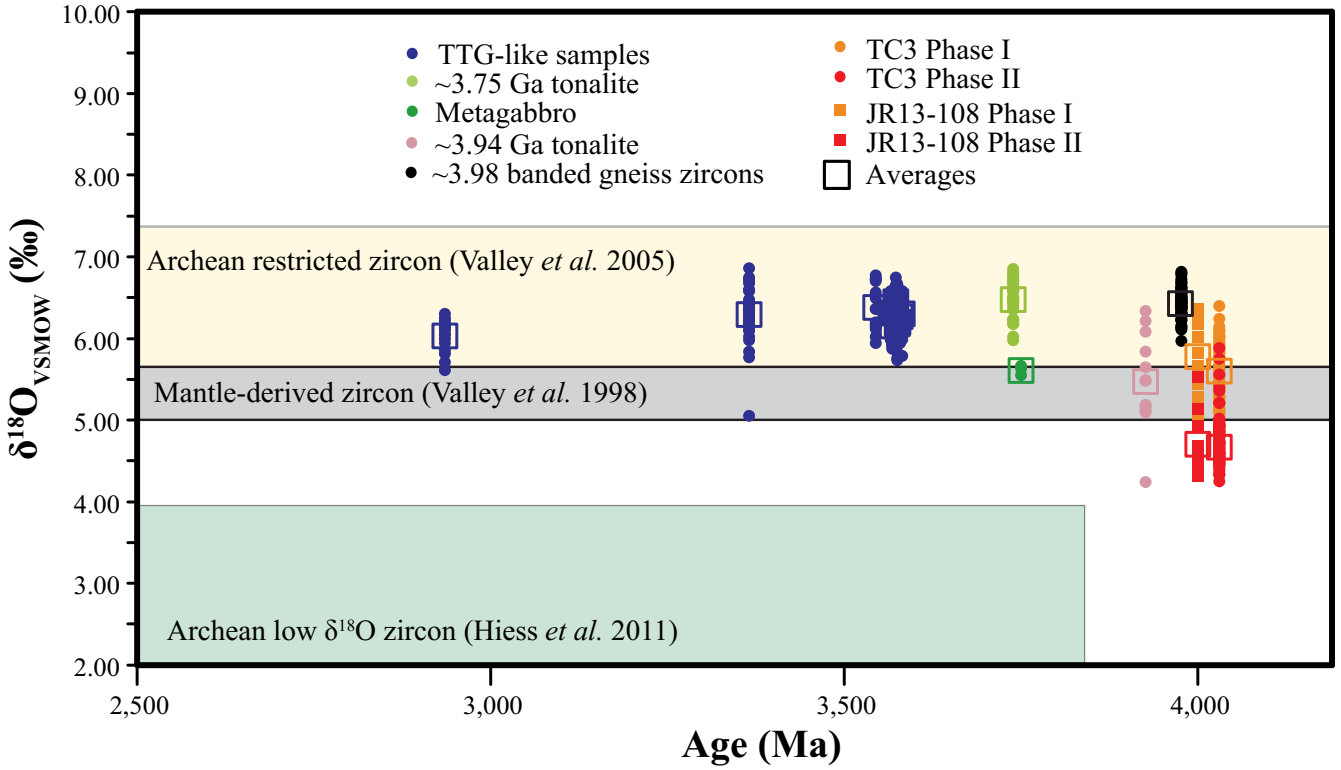

Figure 4.8: Zircon oxygen isotope systematics from over a billion years of magmatism from the AGC. The oldest components (4.02 Ga) have mantle like and lower oxygen isotope compositions, while very soon thereafter (3.94 Ga) zircons acquire an elevated above mantle signature, which persists for the duration of magmatism in the AGC.

ble alternative interpretation is that the banding is tectonic in origin such that rocks of disparate age and composition were interlayered on the cm-scale as a result of high strain in the western AGC. Regardless of the true source of the banding in the sample selected by Mojzsis et al., their choice of a highly strained, multi-component sample for study predictably led to complicated zircon U-Pb systematics with many age peaks (see their Fig. 4.7). The Idiwhaa gneiss, in contrast, is a single component sample collected from a lower strain portion of the AGC that is mappable over a distance of at least several hundred meters. The relative simplicity of the Idiwhaa unit manifests itself in more straightforward zircon U-Pb systematics characterized by a single dominant > 4.0 Ga peak in $^{207}Pb/^{206}Pb$ ages in zircon with igneous zoning characteristics and a well-defined discordia array with a lower intercept around 3.3 Ga (Figs. 4.S5–6, Reimink et al., 2014).

Importantly, only a small proportion of analyses (14 of 198 total) obtained from three Idiwhaa unit samples return $^{207}Pb/^{206}Pb$ ages between 3.92–3.96 Ga, the oldest age of AGC rocks suggested by Mojzsis et al. (2014). Given the shallow angle of the discordia array that would be generated on >4.0

Ga zircon grains that experienced a metamorphic event at ~3.3 Ga, we argue that this small proportion of analyses with $^{207}Pb/^{206}Pb$ ages in the 3.92–3.96 Ga range carry no geological age significance but merely represent partial Pb-loss from the >4.0 Ga grains produced by the 3.3 Ga metamorphism.

Additionally, in Chapter 3 we applied the chemical abrasion isotope dilution thermal ionization mass spectrometry (CA-ID-TIMS) technique to zircons from one sample of Idiwhaa unit zircons (TC3). In combination with *in situ* trace element analysis, these data show a simple Pb-loss trend exactly matching the SIMS U-Pb data of Reimink et al., (2014), with no data indicative of a ~3.92–3.96 Ga age.

Finally, Reimink et al. (2014) demonstrated that the REE compositions of >4.0 Ga magmatic zircons in the Idiwhaa gneiss are broadly in equilibrium with the whole-rock REE compositions of the gneiss (Figs. 2.13–2.14; Reimink et al., 2014). This finding is distinctly unlike the sample investigated by Mojzsis et al. (2014), in which the REE patterns of ca. 4.0 Ga zircons conflicted with measured whole-rock REE patterns. Indeed, this inconsistency between measured and calculated REE patterns (using zircon REE compositions and lattice strain theory) was a key line of evidence used by Mojzsis et al. to conclude that the 4.0 Ga zircons in their sample were xenocrysts. Interestingly, on the basis of the REE patterns of ca. 4.0 Ga zircons in their sample, Mojzsis et al. speculated that these xenocrystic zircons originally crystallized in a "… a mafic to intermediate rock with only moderate LREE/HREE enrichment…" (Page 87, Section 5.1.3, Mojzsis et al. 2014). These are precisely the characteristics of the 4.02 Ga Idiwhaa unit. Thus, we would propose that the xenocrystic zircons in the sample investigated by Mojzsis et al. were derived from rocks equivalent to the Idiwhaa unit.

In summary, the data from a range of samples and methods show that rocks with crystallization ages older than 4.0 Ga are indeed present in the AGC (Stern and Bleeker, 1998; Bowring and Williams, 1999; Reimink et al., 2014).

Petrogenesis of the 4.02 Ga Idiwhaa unit:

Idiwhaa samples

The geochemical and isotopic features of the mafic samples of the Idiwhaa unit offer insight into crust formation processes on the Hadean Earth. These samples have variable silica (58–66 wt.%), relatively low Al_2O_3 (~13 wt.%) and high FeO (8–15 wt.%), and follow an iron-enrichment trend on an AFM diagram (Fig. 4.3A). This high FeO signature, along with negative Eu-anomalies and flat

REE patterns (Figs. 4.4–6, 4.9), can be explained by extensive shallow-level fractional crystallization of a relatively low-H_2O parental basalt magma in which plagioclase is a major constituent of the fractionating assemblage (Wood, 1978; Grove and Kinzler 1986; Nicholson et al., 1991; Reimink et al., 2014). There is also evidence from the low $\delta^{18}O$ values (<+5‰) of one phase of magmatic zircon in the Idiwhaa unit samples (e.g., sample TC3, Reimink et al., 2014; sample JR13-108 from this study) that assimilation of country rocks that had previously been altered at high temperature by surface water played a role in magma evolution.

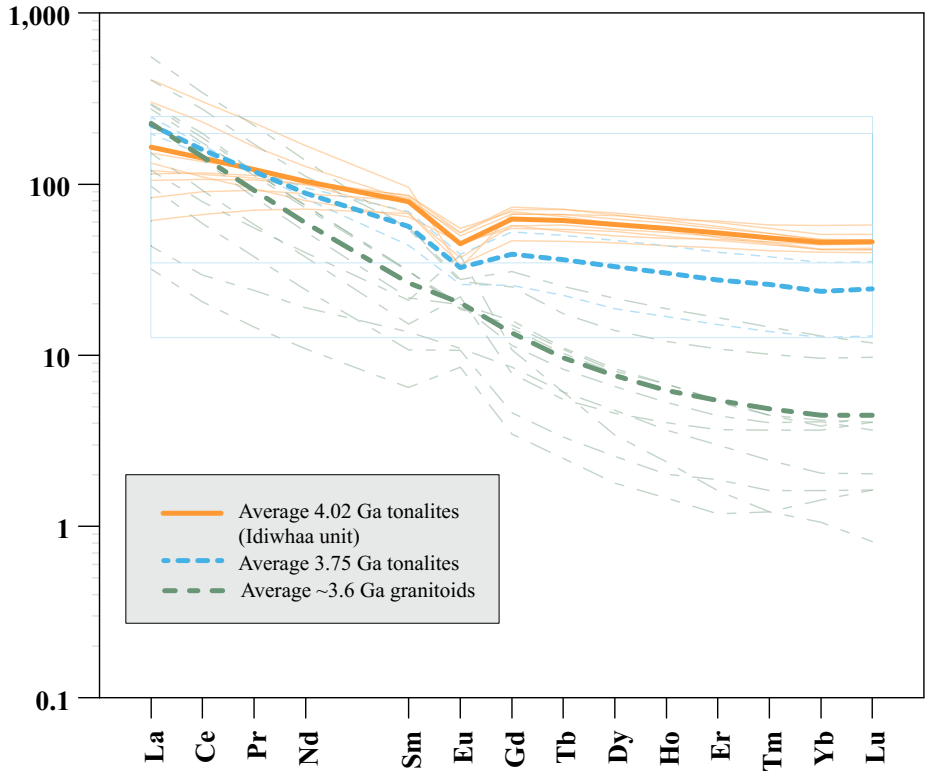

Figure 4.9: Chondrite-normalized (McDonough and Sun, 1995) REE plot showing the steepening of REE patterns in average AGC granitoids with age. Light colored lines represent individual samples while bold lines are averages of each age group.

It has been suggested that the degree to which a magma's $\delta^{18}O$ value may be changed by assimilation-fractional crystallization (AFC) processes is controlled by the water content of the original magma (Balsley and Gregory, 1998). For example, a relatively hydrous magma is more likely to erupt explosively or quench in the subsurface before extensive assimilation of country rocks can occur. In contrast, water-undersaturated magmas experience a wider crystallization interval before reaching water saturation, which in turn allows greater assimilation of country rocks and associated changes to magmatic $\delta^{18}O$ values (e.g., Bindeman et al., 2000). Though lowering in magmatic $\delta^{18}O$ values documented in the 4.02 Ga tonalite is small (~0.9‰), it still requires significant assimilation, which would be favored by a relatively dry primary basaltic magma. This interpretation is consistent with the constraints imposed by the whole-rock elemental data, namely the low Al_2O_3 and high FeO contents and

flat REE patterns of the Idiwhaa rocks.

Significantly, other early Archean zircons were shown to have crystallized from magmas that had lower-than-mantle $\delta^{18}O$ (Hiess et al., 2009; 2011). Hiess et al. (2011) invoked a model of crustal cannibalism, similar to that described above, to account for the low $\delta^{18}O$ values. It should be noted that low-$\delta^{18}O$ magmas are relatively rare in the Phanerozoic rock record but, where present, have most commonly been reported for rocks formed in rift- or plume-related settings (e.g., Yellowstone, Iceland, Skye). Given the paucity of low $\delta^{18}O$ magmas on the modern Earth (Balsley and Gregory, 1998; Valley et al., 2005), it is striking that there are two documented cases of low-^{18}O magmatic rocks among the few currently known locales worldwide with preserved Eoarchean or Hadean crust. This observation suggests that assimilation of surface water altered country rocks in shallow level magma chambers may have been a more widespread process on the early Earth than at present and also that tectonic settings conducive to the operation of this process may have been favorable sites for early crust formation.

The full range of Idiwhaa unit compositions includes some samples with SiO_2 > 70 wt.% (Figs. 3.9–3.11). As discussed in Chapter 3, these samples, although consistent with formation by continued fractional crystallization involving clinopyroxene or amphibole, may also be derived by partial melting of Idiwhaa samples with intermediate silica contents. Ultimately, the potential partial melting event would have to take place relatively close to the crystallization age of the intermediate Idiwhaa unit samples (~4020 Ma) as even the felsic Idiwhaa unit samples contain very ancient zircons with crystallization ages near 4.0 Ga.

Due to petrogenetic and geochemical similarities between the Idiwhaa unit and intermediate rocks from modern Iceland such as high FeO, flat REE patterns, lower than mantle $\delta^{18}O$ values, Reimink et al., (2014) invoked an Iceland-like model for the generation of the >4.0 Ga Idiwhaa tonalite gniess. The Icelandic analogy is fitting as the higher proportion of evolved rocks in Iceland relative to other oceanic plateaus (e.g., Jakobsson et al. 2008) make it unique on the modern Earth. This, as well as high heat flow associated with the confluence of a mid-ocean ridge and a long-lived mantle plume forms the basis for the analogy with primary crust formation on the ancient Earth (Kröner, 1985). We discuss this further in a later section.

Petrogenesis of the 3.94 – 3.75 Ga suite

A number of samples from the AGC, including the original discovery samples, record zircon crystallization ages that are 60–100 m.y. younger than the oldest known (ca. 4.02 Ga) components in the complex (Bowring et al*.,* 1989; Iizuka et al*.,* 2007; 2009; Mojzsis et al*.,* 2014). In our sample set, this includes sample JR13-206 collected from near Bowring et al.'s (1989) original discovery site (Fig. 4.2B) and which records a crystallization age of ~3.94 Ga, and strongly banded gneiss sample AC12A, which records an age of ~3.94 Ga. We present whole-rock geochemical data for sample JR13-206 but, because of its inherent lithological heterogeneity, did not attempt a whole-rock analysis for sample AC12A.

Like the 4.02 Ga Idiwhaa unit, sample JR13-206 has a low Mg# but, unlike that unit, has a steeper REE pattern (La_N/Yb_N = 19), negative Nb anomaly, and a positive Eu-anomaly. These geochemical traits are similar to those reported in some layers of the 3.92 Ga banded sample that Mojzsis et al. (2014) studied in detail, as well as two other samples identified in their study as 'low SiO_2 tonalites'. In particular the fractionated REE pattern, negative Nb anomaly, and positive Eu anomaly of JR13-206 compares well to Lithology 1 of Mojzsis et al. (2014).

The fractionated REE, high silica, and high Na_2O/K_2O of JR12-206 suggest derivation by partial melting of a mafic precursor with some small amount of residual garnet present (Fig. 4.10). Given the very high Fe/Mg ratio of the Idiwhaa unit, garnet may be expected to stabilize at lower pressures during partial melting of Idiwhaa-like mafic material than during melting of more typical mafic rocks. Given this, it is plausible that JR13-206 formed by partial melting of Idiwhaa-like mafic rocks (i.e. as yet unidentified mafic components parental to the Idiwhaa unit) at mid-crustal levels. This hypothesis is in line with the documentation by Mojzsis et al*.,* (2014) of xenocrystic zircon material, which compares very well with Idiwhaa unit zircons, found within a sample that is chemically similar to JR13-206 and likely the same age. Additionally, certain rare dacites found on modern Iceland contain geochemical signatures very similar to JR13-206 and have been attributed to partial melting of basaltic crust followed by crystal fractionation (Willibold et al*.,* 2009). This model is in agreement with our previous assessment that the early stages of evolved crust generation within the AGC involved processes similar to that of modern Iceland (Reimink et al*.,* 2014).

Two samples from the banded gneiss unit (JR13-101, JS-1), which have crystallization ages of ~3.75 Ga, share some of the characteristics of the 3.94 Ga sample. Specifically, these samples share

significant negative Nb anomalies (Figs. 4.4, 4.6), which likely formed by partial melting of source rocks with residual Fe-Ti phases (e.g., Moyen and Stevens, 2006; Moyen et al., 2012). However, the 3.75 Ga samples have higher Mg#'s and lower SiO_2 contents than the 3.94 Ga sample.

The average $\delta^{18}O$ values of zircons in the two 3.75 Ga samples, AC12A and JS-1 are 6.4 and 6.5‰, respectively, which are above the range of values for typical mantle zircon (Valley et al., 1998; Page et al., 2007; Grimes et al., 2010). This indicates that the magmatic protoliths of these samples either assimilated rocks that had a prior history of relatively low-temperature surface water-rock interaction or were derived directly from partial melting of source rocks that had undergone such a process.

The generally more silicic nature of the 3.75 Ga samples compared to the 4.02 Ga Idiwhaa unit along with the high Na_2O/K_2O ratio (Fig. 4.3B) and zircon $\delta^{18}O$ values above those of pristine mantle are consistent with derivation of these samples via dehydration melting of an originally hydrated mafic source rock (e.g., an amphibolite).

The REE patterns of the two samples in this age group are variable (Fig. 4.5), ranging from relatively unfractionated patterns (JR13-101), similar to the Idiwhaa unit, to moderately fractionated patterns in which there is significant enrichment of LREE over HREE (JS-1). These differences can be explained in several ways. One possibility is that the mafic source rocks from which these granitoids were derived differed in their REE patterns. Alternatively, the differences in the REE patterns may be due to differences in the depth of melting wherein relatively low-pressure partial melting would generate a two-pyroxene granulite residue comprising clinopyroxene-orthopyroxene-plagioclase ± hornblende and an associated REE unfractionated melt; moderate-pressure melting would produce a garnet granulite residue of clinopyroxene-hornblende-plagioclase with minor garnet and a melt with a more fractionated REE pattern (e.g., Nair and Chacko, 2008). It should be noted that high-pressure melting of mafic bulk compositions would produce larger amounts of garnet in the residue and in turn a more strongly fractionated REE pattern than observed in any of 3.94–3.75 Ga AGC samples (e.g., Moyen and Stevens, 2006).

Overall, the 3.75 Ga suite of tonalites have some similarities to the high HREE Archean TTG suite defined by Moyen and Martin (2012), most significantly in the moderate La_N/Yb_N and high Na_2O/K_2O. Interestingly, similar rocks have been also been documented on modern Iceland (Willibold et al.,

2009) that share many characteristics (moderate La_N/Yb_N, high Na_2O/K_2O) of the low pressure Archean TTG suite (Moyen and Stevens, 2006; Moyen, 2011; Moyen and Martin, 2012) with lower La_N/Yb_N than classically defined, high-pressure Archean TTGs, as well as the ~3.75 Ga suite documented here.

Petrogenesis of the ≤3.6 Ga and younger rocks:

Depth of melting

The most abundant rock suite within the AGC is the 3.56–3.60 Ga granodiorites to granites (Fig. 4.2). These rocks have geochemical signatures comparable to classic Archean TTG (Barker and Arth, 1976; Martin, 1986). Specifically, they are sodic (>4 wt.% Na_2O), high silica rocks with highly fractionated REE patterns and strong HREE depletion. There is a general consensus that rocks of this nature were produced by partial melting of hydrated basalt at considerable depth (e.g., Beard and Lofgren, 1991; Rapp et al., 1991; Moyen and Stevens, 2006; Moyen and Martin, 2012). Various attempts have been made to calibrate the depth of melting of TTG magmas (e.g., Moyen and Stevens, 2006; Foley et al., 2002; Rapp et al., 2003; Nair and Chacko, 2008), and although results are somewhat dependent upon starting composition, we may utilize these studies to gain insight on the genesis of the 3.6 Ga TTGs from the AGC.

One geochemical parameter that has been used to infer the depth of melting is based on the occurrence of rutile as a residual phase during high-pressure melting ($P \geq 15$ kbar) of mafic bulk composition rocks (Foley et al., 2002; Rapp et al., 2003; Moyen and Stevens, 2006; Hoffmann et al., 2011). As rutile has an ability to fractionate Ta from Nb, melts produced in the presence of rutile acquire a higher Nb/Ta than lower-pressure melts without rutile in the residue (Foley et al., 2002). The Nb/Ta ratios in the 3.6 Ga AGC granitoid suite span a wide range (Fig. 4.6C) with two samples (JR13-303, JR13-305) having somewhat lower values (9–14) whereas all others possess high Nb/Ta (19–43) suggesting the presence of residual rutile and a minimum depth of melting of 15 kbar (e.g., Moyen and Stevens, 2006).

Another geochemical parameter useful for appraising depth of melting relies on the depletion of HREE due to presence of increasing proportions of garnet in the melt residue with increasing pressure (Moyen and Stevens, 2006; Nair and Chacko, 2008). Garnet-in curves are relatively temperature independent and therefore, despite some reliance on starting composition (Moyen and Stevens, 2006),

provide rough estimates for depth of melting. The TTG-like rocks documented here may be separated into two groups based on La_N/Yb_N, one low La_N/Yb_N group (with two samples) with values between 20–30 and another high La_N/Yb_N group with values between 40 and 75. Rough estimates suggest ~15–20 modal percent garnet in the residue for the low La_N/Yb_N samples and >30 modal percent garnet for the high La_N/Yb_N samples (Nair and Chacko, 2008). These garnet proportions correspond to, respectively, pressures of ~14 kbar and >18 kbar, consistent with pressures inferred from Nb/Ta ratios (Fig. 4.6C).

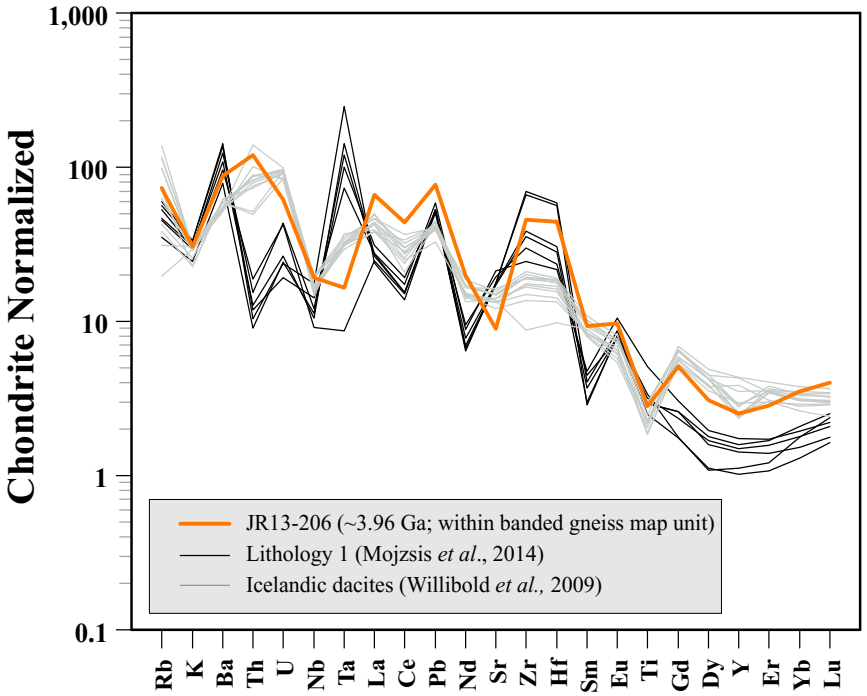

Figure 4.10: Comparison of a 3.94 Ga tonalite (JR13-206) with Lithology 1 of Mojzsis et al. (2014) and dacites from modern Iceland (Willibold et al., 2009). We suggest that JR13-206 formed by partial melting of Idiwhaa-like mafic rocks, consistent with the observations though not interpretations of Mojzsis et al. (2014).

Both depth of melting calibrations broadly agree and together suggest that two samples (JR13-305 and JR13-303) having higher Al_2O_3 and Na_2O/K_2O than other samples in this suite, melted at shallower depth, likely in the garnet granulite stability field (clinopyroxene-plagioclase-garnet ± hornblende). Higher La_N/Yb_N samples likely formed in the presence of rutile-bearing eclogite at greater depths, though there is no discernable difference in ages between these two groups.

Petrogenetic comparisons:

One difference between the ~3.6 Ga AGC granitoids and typical Archean TTGs, which are commonly characterized by a lack of significant Eu-anomaly, is the presence of both positive and negative Eu-anomalies in the AGC granitoids (Fig. 4.7). The presence of these anomalies implies the involvment of plagioclase at some point during the magma generation or crystallization. Two

possible explanations exist; first, melting may not have occurred in the presence of residual eclogite but rather plagioclase-bearing garnet granulite, which would produce negative Eu anomalies in the melt. Secondly, negative Eu anomalies could also be produced in magmas generated in the ecologite stability field if the magmas underwent plagioclase fractionation once they rose into the plagioclase stability field. In contrast, positive Eu anomalies would require plagioclase accumulation, possibly at the site of magma emplacement.

Previous workers have published a limited amount of whole-rock geochemical data from samples inferred to be from the ~3.6 Ga suites (Iizuka et al., 2010; Mojzsis et al., 2014). The geochemical features in these four samples (three from Mojzsis et al., 2014 and one from Iizuka et al., 2010) are generally consistent with the interpretations presented here (Fig. 4.11). However, two of the samples of Mojzsis et al. (2014) do not have direct age constraints; the third sample, AG09014, has a reported age of ca. 3.6 Ga (Roth et al., 2014) but no documentation has been provided as to how this age was obtained. Therefore, we have placed these samples within the 3.6 suite based on geochemical similarity as well as consistency between their sample locations and our mapped units. One geochemical distinction is the very high La_N/Yb_N in sample AY066 (111; Iizuka et al., 2010) that does not correspond to a high Nb/Ta ratio as documented in other 3.6 Ga samples. Additionally, sample AG09016 of Mojzsis et al. (2014) has characteristics that are transitional between our lower La_N/Yb_N and high La_N/Yb_N suites.

Source composition:

Many of the ~3.6 Ga AGC granitoids have higher K_2O contents than typical Archean TTG (>2 wt.%). Possible explanations for this discrepancy include melting from a basaltic source composition that had higher K_2O contents, formation by lower degrees of partial melting, or interactions with a pre-existing crustal component during emplacement. Guitreau et al. (2012; 2014) analyzed a small set of rocks similar in composition and age to our 3.6 Ga suite for their Lu-Hf isotope systematics. They concluded, based on the broadly chondritic to slightly sub-chondriditic initial Hf-isotope composition as well as a lack of correlation between $\varepsilon Hf_{(t)}$ and Ce/Pb, that there was little room for involvement of pre-existing crustal components. Chemical similarities between the samples investigated by Guitreau et al. (2012; 2014) and our suite of 3.6 Ga granitoids allows us suggest no significant crustal contamination

of the 3.6 Ga suite, implying that higher K_2O/Na_2O of these rocks may more likely reflect the source composition (i.e., melting of a basaltic source with higher K_2O). This, however, remains somewhat uncertain, as xenocrystic zircons have been reported in some samples of this age (Bowring and Williams, 1999; Iizuka et al., 2007). Additionally, we identified some xenocrystic zircons present within samples of ~3.6 Ga crystallization ages (JR13-205; 305; 303) indicating interaction with older (~3.75 Ga) crustal material.

The oxygen-isotope compositions of igneous zircons from the 3.6 Ga suite are remarkably homogeneous, with mean $\delta^{18}O$ values for each sample only ranging from 6.1 to 6.3‰ (Table 4.3, Fig. 4.8). These values are outside the pristine mantle field, again requiring some interaction of the magma source rocks or country rock assimilants with surface waters. The oxygen isotope systematics are consistent with the model derived from other geochemical parameters above, suggesting that these granitoids formed by partial melting of a mafic precursor that had been previously altered by low-temperature surface waters.

It may be possible that the above-mantle oxygen isotope compositions of zircons in the ~3.6 Ga suite were produced by direct incorporation of sedimentary material. However, the only moderately elevated average zircon $\delta^{18}O$ value of ~6.2‰ for this suite of granitoids indicate that metasediments were not extensively involved in the genesis of these magmas. Incorporation of a high proportion of sedimentary material into the magma would likely raise zircon $\delta^{18}O$ values above +7.5‰ (e.g., Kemp et al., 2007). Moderately elevated oxygen isotope compositions, such as those documented here, can be formed by partial melting of the altered upper portion of oceanic crust, which commonly has $\delta^{18}O$ values between 6 and 9 ‰ (e.g., Muehlenbachs, 1986)

3.37 and 2.94 Ga events:

One sample coming from a broad expanse of granitic-granodioritic rocks a few km west of the main study area (Fig. 4.1C) was analyzed here (JR13-802) and has a well-defined U-Pb crystallization age of 3.37 Ga. The igneous crystallization age for this suite is coincident with a metamorphic event at approximately that time inferred from metamorphic zircon overgrowths (Stern and Bleeker 1998; Reimink et al., 2014) and whole-rock Sm-Nd data (Moorbath and Whitehouse, 1996; Moorbath et al., 1997; Whitehouse et al., 2001; Roth et al., 2014). Additionally, within the granite-granodiorite map

unit, we have documented the existence of a ~2.94 Ga granitic unit (JR13-304) that crosscuts ~3.6 Ga units (JR13-303, JR13-305) at a high angle. The 2.94 Ga crystallization age is meaningful in that, in combination with the 3.37 Ga granitoid, it links magmatic events in the AGC region at the westernmost margin of the Slave craton with previously documented magmatic events further to the east in the Central Slave Basement Complex (Sircombe et al., 2001; Bleeker and Stern, 1997; Bleeker et al., 1999; Ketchum et al., 2004).

The geochemical characteristics of the 3.37 and 2.94 Ga granitic samples broadly align with those of the ~3.6 Ga TTG suite of the AGC. Sample JR13-304, the ~2.94 Ga granodioritic sample, shares many similarities with the lower La_N/Yb_N samples (La_N/Yb_N = 31, Nb/Ta = 13). Sample JR13-802, with an age of 3.37 Ga, has a higher La_N/Yb_N (60) and shares similar features to the higher La_N/Yb_N suite, apart from a low Nb/Ta ratio (11). Additionally, oxygen isotope systematics in magmatic zircons extracted from these two units record identical $\delta^{18}O$ values to the 3.6 Ga suite (+6.30‰ and +6.03‰ for JR13-802 and JR13-304, respectively). Overall these similarities suggest that melting of hydrated basalt occurred episodically after the initial generation of a deeply sourced crust at 3.6 Ga. These samples, as with some of the 3.6 Ga suite, contain higher K_2O contents than is typical for Archean TTG. As discussed above the cause of this enrichment is not clear and may be caused by partial melting of mafic or intermediate composition source rock with higher K_2O contents than a typical basalt, or potentially by interactions with pre-existing felsic crust during emplacement.

An oceanic plateau setting for generation of the Acasta Gneiss Complex?

The data presented here indicate that there was a change in the geochemical character of AGC granitoid magmatism from 4.02–2.94 Ga, as a result of changes in the petrogenetic processes responsible for crust generation over that time period. Specifically, the data here suggest a gradual shift from shallow-level processes involving fractional crystallization of parental basaltic magma at 4.02 Ga to processes dominated by partial melting of hydrated basalt at progressively deeper levels. Rocks that had been hydrothermally altered by surface waters played a role in magma generation or evolution in both the shallow- and deeper-level processes.

In this section, we discuss the geodynamic implications of these changes in petrogenetic processes through time in the AGC. For the earliest rocks (≥3.9 Ga) present in the AGC we favor a

geodynamic model broadly similar to those proposed for the 3.5–3.1 Ga Pilbara craton (e.g. Champion et al., 2007), the 3.5–3.2 Ga Barberton granitoids (e.g. Moyen et al., 2007), the 3.7–3.8 Ga Isua Greenstone Belt (e.g. Kamber et al., 2005), and the 4.0–4.4 Ga source to the Jack Hills zircons (Kemp et al., 2010). Although significant differences exist in these various models, they all involve felsic crust generation that initiated over an extended history first by internal reworking of a thickened mafic pile in some way analogous to modern oceanic plateaus. This model manifests itself within the ≥3.9 Ga portion of the AGC in the following way. First, a long-lived volcanic edifice produced significant quantities of mafic to intermediate crust at 4.02 Ga, producing intermediate-felsic components by fractionation and assimilation of the parental mafic components. The thickened and partially hydrated mafic- to intermediate-composition pile was episodically melted ca. 3.95 and 3.75 at moderate depths to produce tonalitic magmas.

It must be noted that the geochemical signatures of rock types in this interval are distinctly different from broadly defined Archean TTG (Moyen and Martin, 2012) and compare better with a particular suite of Icelandic dacites (Willibold et al., 2009). These Icelandic dacites differ from typical Icelandic felsic crust in that they have relative depletions in Nb and Ti and enrichments in Pb and La. However, these rocks are not directly comparable to typical Archean TTG as they do not share the moderate to extreme depletion in Yb and correspondingly high La/Yb that is diagnostic of Archean TTG and the presence of residual garnet (Martin et al., 2010). Therefore, we suggest that the 3.94–3.75 Ga AGC suite was formed by similar processes to the Icelandic dacites documented by Willibold et al. (2009) such as partial melting of hydrated basalt at moderate depths. This interpretation implies that between 3.94–3.75 Ga the core of the AGC was potentially stabilized by partial melting of a thickened basaltic crust, but at shallower depths than typical Archean TTG (<10 kbar).

Once a thickened and buoyant evolved continental nucleus was stabilized, additional formation of evolved crust was made possible by partial melting at greater depth beneath the buoyant nucleus possibly driven by horizontal plate motions (e.g., Martin, 1986; Drummond and Defant, 1990; Smithies et al., 2003; Moyen et al., 2007; Nair and Chacko, 2008). The >50–60 km depth required to form enough garnet to create the high La_N/Yb_N ratios in some of the ~3.6 Ga TTG rocks present within the AGC may preclude formation by burial at the base of an oceanic plateau. Deep burial of hydrated rocks that had formerly been hydrated at shallow depths by surface waters seems unlikely in a plateau setting

and is more likely to require tectonic underthrusting associated with horizontal plate movements (e.g., Boher et al., 1992; Moyen and Stevens, 2006; Nair and Chacko, 2008). Differing La_N/Yb_N in the ~3.6 Ga samples is consistent with the variable depth of melting associated with initiation of subduction-related magmatism, while the similarities in ages between these samples is consistent with a large pulse of magmatism at broadly similar times. At the age resolution presented here, it remains difficult to evaluate whether the ~3.6 Ga voluminous magmatism is more consistent with episodic subduction suggested by geodynamical modeling (e.g., O'Neill et al., 2007; O'Neill and Debaille, 2014), or modern-style convergent magmatism that is periodically active at longer length (e.g., Silva et al., 2015).

An evolving oceanic plateau model for crust formation on the early Earth is far from a new concept (e.g., Kroner, 1985). One modern oceanic plateau, Iceland, has served as a commonly invoked modern analog for early terrestrial crust formation. The high geothermal gradient on Iceland induced by the confluence of a mid-ocean ridge and mantle plume has generated a crust averaging ~30 km in thickness (Allen et al., 2002), which in turn has promoted the formation of a higher proportion of evolved rocks than in other oceanic plateau (Jakobsson et al., 2008).

As previously discussed (Reimink et al. 2014), the oldest rocks in the AGC share many key geochemical features with a group of high FeO, intermediate rocks termed 'icelandites' (Carmichael, 1964; Nicholson et al., 1991). Within the AGC, petrologic processes progress to shallow partial melting of hydrated mafic rocks between 3.94–3.75 Ga. Compositions within this suite compare well with the Kroksfjördur eruptive sequences on Iceland (Willibold et al., 2009). Though these Icelandic rocks have a La_N/Yb_N too low (11–20) to be classified as Archean TTG *sensu stricto* (Moyen et al., 2010), they share many geochemical characteristics with the intermediate-aged (3.75–3.94 Ga) tonalites documented here and likely formed via partial melting of a hydrated mafic source (Willibold et al., 2009). Therefore early felsic crust generation within the AGC may have occurred by similar petrogenetic processes as those operating on modern Iceland.

Of particular relevance to the data from the oldest samples (≥3.75 Ga) presented here are the models from Kamber et al. (2005) and Kemp et al. (2010). Based in part on the paucity of zircons found within ~3.74 Ga mica schists from southwest Greenland (Kamber et al., 2005) and Hf-isotope compositions of 3.9–4.4 Ga detrital zircons from Australia (Kemp et al., 2010), these models both invoke some form of burial and partial melting of early basaltic protocrust to generate evolved

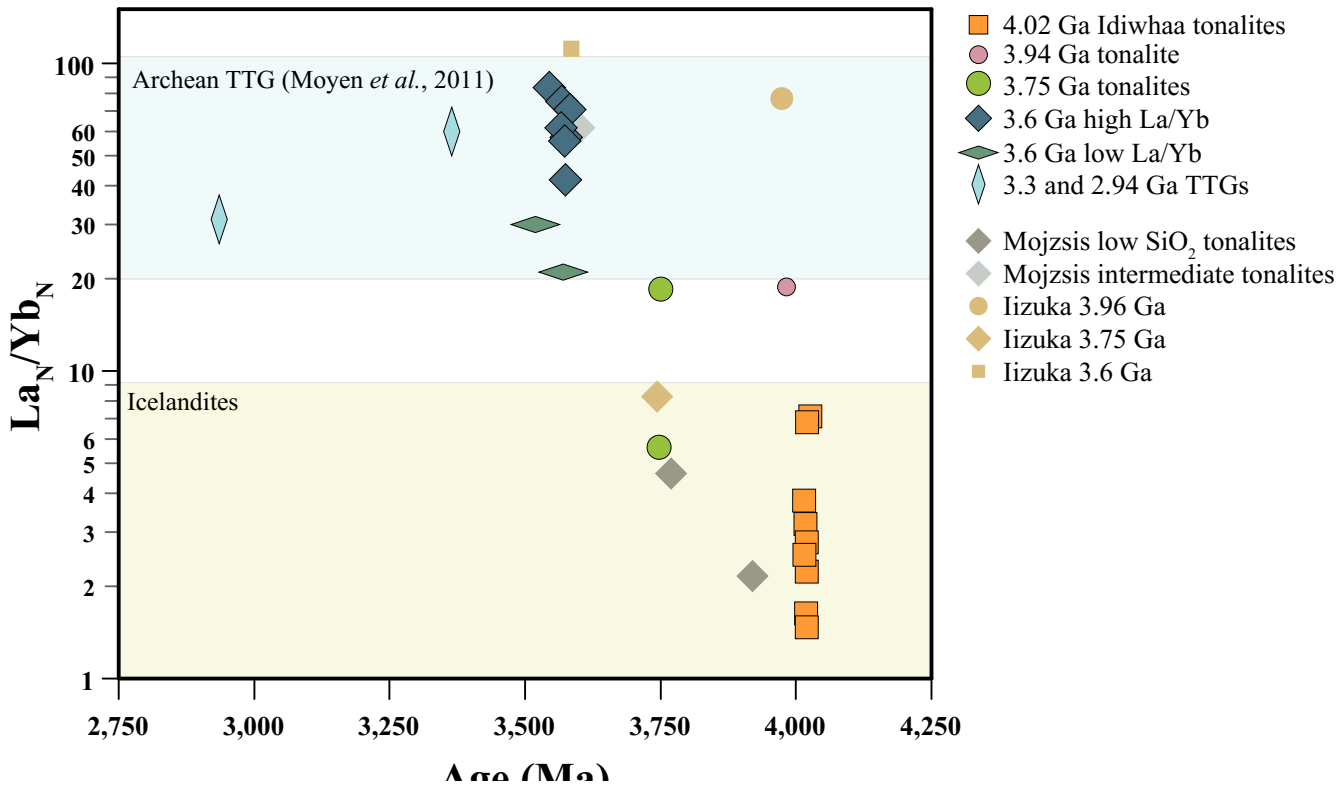

Figure 4.11: Chondrite-normalized (McDonough and Sun, 1995) La/Yb versus crystallization age within AGC rocks showing the trend from low La_N/Yb_N at 4.02 Ga to progressively higher through 3.94–3.75 Ga until finally reaching La_N/Yb_N typical of Archean TTGs at 3.6 Ga.

magmatism. The generation of the 4020 Ma Idiwhaa unit via assimilation and fractional crystallization from basaltic parental magma, along with interactions with surface waters, are similar to processes described by the previously mentioned authors. However, we note that as Zr behaves incompatibly during the early stages of mafic magma crystallization, zircon-saturated magmas intermediate magmas can be produced by AFC processes without requiring partial melting and the generation of felsic rocks (Kamber et al., 2005). Additionally, intermediate magmas, akin to those documented here, may provide the ideal magma composition for the formation and preservation of zircon. Intermediate magmas that reach zircon saturation, but are still relatively low in U and Th, may more readily produce zircons low in U and Th (such as documented in the Idiwhaa unit zircons). These low U and Th grains will sustain less radiation damage and be less susceptible to overprinting and recrystallization, likely an important consideration when dealing four billion year old grains.

Despite broad agreement between the models proposed by Kamber et al. (2005), Kemp et al. (2010), and the processes involved in crust formation within the AGC documented here, significant

differences exist. First, the model proposed by Kamber et al. (2005) to explain a lack of ancient zircon material present in ~3.71 Ga mica schists from the Isua Supracrustal belt includes heavy volcanic resurfacing (continuous eruption, effectively burying hydrated rocks) of dominantly mafic lithologies thereby thickening and hydrating the crust allowing for partial melting to internally differentiate itself. This portion of the model is wholly consistent with the composition of >3.75 Ga tonalites of the AGC. However, as with SW Greenland TTGs, the high La_N/Yb_N present in the ~3.6 Ga AGC granitoids requires a much greater proportion of residual garnet, and corresponding depth of melting (>50 km), than is realistic for burying hydrated crust in oceanic plateaus. Therefore, some form of horizontal plate motions is likely required to bury hydrated mafic crust to such depths (e.g., Boher et al., 1992; Niu et al., 2003; Smithies et al., 2003; Kamber et al., 2005; Nair and Chacko, 2008).

The transition in the AGC from magmatism controlled by shallow-level to deep-seated processes took place over a time interval of approximately 400 m.y. (4.02–3.55 Ga). Such a transition has not yet occurred in Iceland. However, once generated, an Iceland-like oceanic plateau may be an ideal setting for later generation of deeply sourced magmas, potentially via a process broadly akin to modern subduction in which hydrated mafic crust is tectonically underthrust to significant depths beneath the plateau (e.g., Smithies et al., 2003; Nair and Chacko, 2008), serving to stabilize the protocratonic nucleus.

It must be noted that we invoke the Icelandic analogy for generation of the earliest (>3.94 Ga) crust in the AGC on petrologic grounds, namely evolved crust generation induced by shallow-level fractionation of basaltic magma and partial melting of hydrated basaltic crust are present in both locations. This does not necessarily imply that the tectonic setting of modern Iceland, which involves the interactions of a mid-ocean ridge and a mantle plume, were required for evolved crust generation on the Early Earth. Indeed, higher heat production in the Hadean may create a geothermal gradient sufficient to produce Iceland-like petrologic processes in any long lived thermal upwelling (Reimink et al., 2014; Kamber, 2015).

Similar models and transitions in petrogenetic processes have been invoked for other ancient terranes. For example, a transitional plateau-to-subduction scenario has been suggested for the Pilbara Craton (e.g. Smithies et al., 2005; Van Kranendonk 2007; Van Kranendonk 2010) as well as for granitoids of the Barberton greenstone belt (Moyen et al., 2007). Interestingly, this transition has been

suggested to occur over broadly the same time interval as documented in the AGC: roughly 300 m.y. in the Barberton terrane (3.55–3.25 Ga; Moyen et al., 2007) and ca. 300–400 m.y. in the East Pilbara terrane (> 3.45–3.12 Ga; e.g., Smithies et al., 2005; Smithies et al., 2007; Van Kranendonk, 2010).

Our documentation of an early (4.0–3.94 Ga) Acasta Gneiss Complex dominated by mafic-intermediate rocks formed by shallow crustal processes is in line with recent hypotheses suggesting the equal, if not greater, importance of oceanic plateaus relative to more felsic composition micro-continents on the Hadean and Eoarchean Earth (e.g., Kamber et al., 2005, 2010; Smithies et al., 2005; Kemp et al., 2015). The significance of this duality of Archean evolved crust has been emphasized in recent discussions of Archean geodynamics (Kamber, 2010, 2015; Van Kranendonk, 2010), as has the potential for oceanic plateaus to be involved in subduction and production of TTG-like magmas (Nair and Chacko, 2008; Martin et al., 2014). Our work here documenting the importance of long-lived mafic-intermediate magmatism early in the evolution of the AGC fits well with these models suggesting that oceanic plateaus formed proto-continental crust that was began as dominantly mafic in composition but evolved to contain a moderate proportion of intermediate to felsic rocks. These proto-continental blocks then became a nucleus for later subduction- or underthrusting-related felsic magmatism produced by partial melting of hydrated mafic precursors at great depth (e.g., Smithies et al., 2003; Nair and Chacko, 2008; Martin et al., 2014).

Conclusions:

Here we presented the results of detailed field mapping, using lithochemical data and U-Pb geochronology to define map units in a relatively well-preserved portion of the Acasta Gneiss Complex. On the basis of U-Pb dating of zircon in representative samples of the various rock units, we identified six major episodes of granitoid magmatism in the AGC: 4.02 Ga, 3.96 Ga, 3.75 Ga, 3.55–3.60 Ga, 3.37 Ga, and 2.94 Ga. Whole-rock geochemical and zircon oxygen isotope data obtained for these granitoid suites indicates a gradual change in the processes responsible for forming the granitoid magmas.

The earliest granitoids (ca. 4.02 Ga), which are intermediate in composition, formed by shallow-level fractional crystallization of a basaltic magma combined with assimilation of country rocks that had been hydrothermally altered by surface waters at relatively high temperatures. Later granitoids

(3.96–2.94 Ga), which are generally more silica-rich, formed by partial melting of mafic composition rocks that originally had been hydrated by surface waters at low temperature. The dehydration melting process that generated these magmas occurred at progressively deeper levels such that garnet only became increasingly abundant as a residual phase in the melting process at ~3.6 Ga. Only the volumetrically most extensive granitoid suite in the field area, the 3.55–3.60 Ga suite, has major- and trace-element composition comparable to average Archean TTG. In particular, the granitoids are characterized by strong LREE/HREE fractionation, indicative of melt generation at considerable depth and significant garnet in the melt residue. The youngest granitoids in the field area (3.3 and 2.9 Ga) are compositionally similar to the ca. 3.6 Ga suite, albeit with somewhat higher K_2O contents. As such, these younger granitoids likely formed by similar processes as the 3.6 Ga suite but may also reflect the incorporation of larger amounts of earlier-formed felsic crust or derivation from enriched basaltic precursors.

To account for the geochemical and petrological observations noted above, we propose that the earliest rocks (>3.94 Ga) in the AGC formed in an oceanic plateau setting broadly similar to modern-day Iceland. The development of a relatively thick crust (~30 km) enabled fractional crystallization and assimilation processes to form a significant proportion of intermediate to felsic composition rocks. This nucleus then transitioned over ~400 m.y. to more evolved TTG-like compositions as hydrated mafic rocks were under-thrust beneath the nucleus to undergo partial at significant depths to generate TTG magmas producing relatively voluminous TTG-like magmatism ~3.6 Ga. This transition from an oceanic plateau to a subduction-like setting has been proposed previously for the Pilbara (e.g., Smithies et al., 2005; Smithies et al., 2007; Van Kranendonk, 2010) and Kaapvaal cratons (Moyen et al., 2007). We suggest that the Acasta Gneiss Complex underwent a similar process much earlier in Earth history.

References:

Allen, R.M., 2002. Plume-driven plumbing and crustal formation in Iceland. Journal of Geophysical Research 107, 2163.

Ashton, K.E., Heaman, L.M., Lewry, J.F., Hartlaub, R.P., Shi, R., 1999. Age and origin of the Jan Lake Complex: a glimpse at the buried Archean craton of the Trans-Hudson Orogen. Can. J. Earth Sci. 36, 185–208.

Balsley, S.D., Gregory, R.T., 1998. Low-18O silicic magmas: why are they so rare? Earth and Planetary Science Letters 162, 123–136.

Barker, F., Arth, J.G., 1976. Generation of trondhjemitic-tonalitic liquids and Archean bimodal trondhjemite-basalt suites. Geology 4, 596–600.

Beard, J.S., Lofgren, G.E., 1991. Dehydration Melting and Water-Saturated Melting of Basaltic and Andesitic Greenstones and Amphibolites at 1, 3, and 6. 9 kb. Journal of Petrology 32, 365–401.

Bindeman, I.N., Valley, J.W., 2000. Formation of low-δ18O rhyolites after caldera collapse at Yellowstone, Wyoming, USA. Geology 28, 719–722.

Black, L.P., Kamo, S.L., Allen, C.M., Davis, D.W., Aleinikoff, J.N., Valley, J.W., Mundil, R., Campbell, I.H., Korsch, R.J., Williams, I.S., Foudoulis, C., 2004. Improved 206Pb/238U microprobe geochronology by the monitoring of a trace-element-related matrix effect; SHRIMP, ID–TIMS, ELA–ICP–MS and oxygen isotope documentation for a series of zircon standards. Chemical Geology 205, 115–140.

Bleeker, W., Stern, R.A., 1997. The Acasta Gneisses: An imperfect sample of Earth's oldest crust, in:. Presented at the Lithoprobe, pp. 1–5.

Bleeker, W., Stern, R., 2000. Why the Slave Province, Northwest Territories, got a little bigger, Geological Survey of Canada Current Research.

Bleeker, W., Ketchum, J.W., Davis, W.J., 1999. The Central Slave Basement Complex, Part II: age and tectonic significance of high-strain zones along the basement-cover contact. Can. J. Earth Sci. 36, 1111–1130.

Boher, M., Abouchami, W., Michard, A., Albarede, F., Arndt, N. 1992. Crustal Growth in West Africa at 2.1 Ga. Journal of Geophysical Research 97, 345–369

Bowring, S.A., Housh, T., 1995. The Earth's early evolution. Science 269, 1535–1540.

Bowring, S.A., Williams, I.S., 1999. Priscoan (4.00–4.03 Ga) orthogneisses from northwestern Canada. Contributions to Mineralogy and Petrology 134, 3–16.

Bowring, S.A., Housh, T.B., Isachsen, C.E., 1990. The Acasta Gneisses: Remnant of Earth's Early Crust. In: Origin of the Earth 1–25.

Bowring, S.A., King, J.E., Housh, T.B., Isachsen, C.E., 1989a. Neodymium and lead isotope evidence for enriched early Archaean crust in North America. Nature 340, 222–225.

Bowring, S.A., Williams, I.S., Compston, W., 1989b. 3.96 Ga gneisses from the Slave province, Northwest Territories, Canada. Geology 17, 971–975.

Breemen, O.V., Davis, W.J., King, J.E., 1992. Temporal distribution of granitoid plutonic rocks in the Archean Slave Province, northwest Canadian Shield. Can. J. Earth Sci. 29, 2186–2199.

Carmichael, I.S.E., 1964. The petrology of Thingmuli, a Tertiary volcano in eastern Iceland. Journal of Petrology 5, 435–460.

Champion, D.C., Smithies, R.H., 2007. Chapter 4.3 Geochemistry of Paleoarchean Granites of the East Pilbara Terrane, Pilbara Craton, Western Australia: Implications for Early Archean Crustal Growth, in: Developments in Precambrian Geology, Elsevier, pp. 369–409.

Condie, K., 2007. Chapter 1.2 The Distribution of Paleoarchean Crust, in: Developments in Precambrian Geology. Elsevier, pp. 9–18.

Corfu, F., 2003. Atlas of Zircon Textures. Reviews in Mineralogy and Geochemistry 53, 469–500.

Davidek, K.L., A Bowring, S., Williams, I.S., 1997. Conventional U-Pb geochronology of the Acasta gneisses using single grain zircon fragmentation techniques. American Geophysical Union Annual Meeting A–75.

Davis, W.J., Hegner, E., 1992. Neodymium isotopic evidence for the tectonic assembly of Late Archean crust in the Slave Province, northwest Canada. Contrib Mineral Petrol 111, 493–504

Froude, D.O., Ireland, T.R., Kinny, P.D., Williams, I.S., Compston, W., Williams, I.R., Myers, J.S., 1983. Ion microprobe identification of 4,100–4,200 Myr-old terrestrial zircons. Nature 304, 616–618.

Foley, S., Tiepolo, M., Vannucci, R., 2002. Growth of early continental crust controlled by melting of amphibolite in subduction zones. Nature 417, 837–840.

Green, D.C., Baadsgaard, H., Cumming, G.L., 1968. Geochronology of the Yellowknife area, Northwest Territories, Canada. Can. J. Earth Sci. 5, 725–735.

Grimes, C.B., Ushikubo, T., John, B.E., Valley, J.W., 2010. Uniformly mantle-like $\delta^{18}O$ in zircons from oceanic plagiogranites and gabbros. Contributions to Mineralogy and Petrology 161, 13–33.

Grove, T.L., Kinzler, R.J., 1986. Petrogenesis of andesites. Annual Review of Earth and Planetary Sciences 14, 417.

Guitreau, M., Blichert-Toft, J., Martin, H., Mojzsis, S.J., 2012. Hafnium isotope evidence from Archean granitic rocks for deep-mantle origin of continental crust. Earth and Planetary Science Letters 337-338, 211–223.

Guitreau, M., Blichert-Toft, J., Mojzsis, S.J., Roth, A.S.G., Bourdon, B., Cates, N.L., Bleeker, W., 2014. Lu–Hf isotope systematics of the Hadean–Eoarchean Acasta Gneiss Complex (Northwest Territories, Canada). Geochimica et Cosmochimica Acta 135, 251–269.

Harrison, T.M., 2009. The hadean crust: Evidence from >4 ga zircons. Annual Review of Earth and Planetary Sciences 37, 479–505.

Hiess, J., Bennett, V.C., Nutman, A.P., Williams, I.S., 2009. In situ U–Pb, O and Hf isotopic compositions of zircon and olivine from Eoarchaean rocks, West Greenland: New insights to making old crust. Geochimica et Cosmochimica Acta 73, 4489–4516.

Hiess, J., Bennett, V.C., Nutman, A.P., Williams, I.S., 2011. Archaean fluid-assisted crustal cannibalism recorded by low $\delta^{18}O$ and negative $\varepsilon Hf(T)$ isotopic signatures of West Greenland granite zircon. Contributions to Mineralogy and Petrology 161, 1027–1050.

Hodges, K.V., A Bowring, S., 1995. Multi-Stage Thermal History of the 4.0 Ga Acasta Gneisses, in:. Presented at the American Geophysical Union Annual Meeting, p. F708.

Hoffmann, J.E., Münker, C., Næraa, T., Rosing, M.T., Herwartz, D., Garbe-Schönber, D., Svahnberg, H., 2011. Geochimica et Cosmochimica Acta 75, 4157–4178.

Iizuka, T., Komiya, T., Johnson, S.P., Kon, Y., Maruyama, S., 2009. Reworking of Hadean crust in the Acasta gneisses, northwestern Canada: Evidence from in-situ Lu–Hf isotope analysis of zircon. Chemical Geology 259, 230–239.

Iizuka, T., Komiya, T., Ueno, Y., Katayama, I., Uehara, Y., Maruyama, S., Hirata, T., Johnson, S.P., Dunkley, D.J., 2007. Geology and zircon geochronology of the Acasta Gneiss Complex, northwestern Canada: New constraints on its tectonothermal history. Precambrian Res 153, 179–208.

Iizuka, T., Nakai, S., Sahoo, Y.V., Takamasa, A., Hirata, T., Maruyama, S., 2010. The tungsten isotopic composition of Eoarchean rocks: Implications for early silicate differentiation and core–mantle interaction on Earth. Earth and Planetary Science Letters 291, 189–200.

Isachsen, C.E., Bowring, S.A., Padgham, W.A., 1991. U-Pb Zircon Geochronology of the Yellowknife Volcanic Belt, NWT, Canada: New Constraints on the Timing and Duration of Greenstone Belt Magmatism. The Journal of Geology 99, 55–67.

Jakobsson, S., Jonasson, K., Sigurdsson, I., 2008. The three igneous rock series of Iceland. Jokull 58, 1–22.

Jenner, G.A., Fryer, B.J., McLennan, S.M., 1981. Geochemistry of the Archean Yellowknife Supergroup. Geochimica et Cosmochimica Acta 45, 1111–1129.

Johnson, D.M., Hooper, P.R., Conrey, R.M., 1999. XRF analysis of rocks and minerals for major and trace elements on a single low dilution Li-tetraborate fused bead. Advances in X-ray Analysis 41, 843–867.

Kamber, B.S., 2010. Archean mafic–ultramafic volcanic landmasses and their effect on ocean–atmosphere chemistry. Chemical Geology 274, 19–28.

Kamber, B.S., 2015. The evolving nature of terrestrial crust from the Hadean, through the Archaean, into the Proterozoic. Precambrian Res 258, 48–82.

Kemp, A.I.S., Hawkesworth, C.J., Foster, G.L., Paterson, B.A., Woodhead, J.D., Hergt, J.M., Gray, C.M., Whitehouse, M.J., 2007. Magmatic and crustal differentiation history of granitic rocks from Hf-O isotopes in zircon. Science 315, 980–983.

Ketchum, J., Bleeker, W., Stern, R.A., 2004. Evolution of an Archean basement complex and its autochthonous cover, southern Slave Province, Canada. Precambrian Res 135, 149–176.

Kroner, A., 1985. Evolution of the Archean Continental Crust. Annual Review of Earth and Planetary Sciences 13, 49–74.

LeCheminant, A.N., Heaman, L.M., 1989. Mackenzie igneous events, Canada: Middle Proterozoic hotspot magmatism associated with ocean opening. Earth and Planetary Science Letters 96, 38–48.

Martin, E., Martin, H., Sigmarsson, O., 2010. Comment on “Continental geochemical signatures in dacites from Iceland and implications for models of early Archaean crust formation” by Willbold, M., Hegner, E., Stracke A. and Rocholl A. Earth and Planetary Science Letters 293, 218–219.

Martin, H., 1986. Effect of steeper Archean geothermal gradient on geochemistry of subduction-zone magmas. Geology 14, 753–756.

Martin, H., 1987. Petrogenesis of Archaean Trondhjemites, Tonalites, and Granodiorites from Eastern Finland: Major and Trace Element Geochemistry. Journal of Petrology 28, 921–953.

Martin, H., 1999. Adakitic magmas: modern analogues of Archaean granitoids. Lithos 46, 411–429.

Martin, H., Moyen, J.-F., Guitreau, M., Blichert-Toft, J., 2014. Why Archaean TTG cannot be generated by MORB melting in subduction zones. Lithos 198-199, 1–13.

McDonough, W.F., Sun, S.S., 1995. The composition of the Earth. Chemical Geology 120, 223–253.

Mojzsis, S.J., Cates, N.L., Caro, G., Trail, D., Abramov, O., Guitreau, M., Blichert-Toft, J., Hopkins, M.D., Bleeker, W., 2014. Component geochronology in the polyphase ca. 3920Ma Acasta Gneiss. Geochimica et Cosmochimica Acta 133, 68–96.

Moorbath, S., Whitehouse, M.J., 1996. Comment: Sm-Nd Isotopic Data and Earth's Evolution. Science 273, 1878b–1879b.

Moorbath, S., Whitehouse, M.J., Kamber, B.S., 1997. Extreme Nd-isotope heterogeneity in the early Archaean - Fact or fiction? Case histories from northern Canada and West Greenland. Chemical Geology 135, 213–231.

Moyen, J.-F., 2011. The composite Archaean grey gneisses: Petrological significance, and evidence for a non-unique tectonic setting for Archaean crustal growth. Lithos 123, 21–36.

Moyen, J.-F., Martin, H., 2012. Forty years of TTG research. Lithos 148, 312–336.

Moyen, J.-F., Stevens, G., 2006. Experimental constraints on TTG petrogenesis: Implications for Archean geodynamics, in: Archean Geodynamics and Environments, Geophysical Monograph Series. American Geophysical Union, Washington, D. C., pp. 149–175.

Moyen, J.-F., Stevens, G., Kisters, A.F.M., Belcher, R.W., 2007. TTG Plutons of the Barberton Granitoid-Greenstone Terrain, South Africa, in: Developments in Precambrian Geology, Developments in Precambrian Geology. Elsevier, pp. 607–667.

Nair, R., Chacko, T., 2008. Role of oceanic plateaus in the initiation of subduction and origin of continental crust. Geology 36, 583–586.

Nicholson, H., Condomines, M., Fitton, J.G., Fallick, A.E., Gröveld, K., Rogers, G., 1991. Geochemical and Isotopic Evidence for Crustal Assimilation Beneath Krafla, Iceland. Journal of Petrology 32,

1005–1020.

Norman, M.D., 2009. The Lunar Cataclysm: Reality or "Mythconception"? Elements 5, 23–28.

Padgham, W.A., Fyson, W.K., 1992. The Slave Province: a distinct Archean craton. Can. J. Earth Sci. 29, 2072–2086.

Page, F.Z., Fu, B., Kita, N.T., Fournelle, J., Spicuzza, M.J., Schulze, D.J., Viljoen, F., Basei, M.A.S., Valley, J.W., 2007. Zircons from kimberlite: New insights from oxygen isotopes, trace elements, and Ti in zircon thermometry. Geochimica et Cosmochimica Acta 71, 3887–3903.

Rapp, R.P., Watson, E.B., Miller, C.F., 1991. Partial melting of amphibolite/eclogite and the origin of Archean trondhjemites and tonalites. Precambrian Res 51, 1–25.

Rapp, R.P., Shimizu, N., Norman, M.D., 2003. Growth of early continental crust by partial melting of eclogite. Nature 425, 605–609.

Reimink, J.R., Chacko, T., Stern, R.A., Heaman, L.M., 2014. Earth's earliest evolved crust generated in an Iceland-like setting. Nature Geoscience 7, 529–533.

Roth, A.S.G., Bourdon, B., Mojzsis, S.J., Rudge, J.F., Guitreau, M., Blichert-Toft, J., 2014. Combined ^{147,146}Sm-^{143,142}Nd constraints on the longevity and residence time of early terrestrial crust. Geochem. Geophys. Geosyst. 15, 2329–2345.

Sano, Y., Terada, K., Hidaka, H., Yokoyama, K., Nutman, A.P., 1999. Palaeoproterozoic thermal events recorded in the ~4.0 Ga Acasta gneiss, Canada: evidence from SHRIMP U-Pb dating of apatite and zircon. Geochimica et Cosmochimica Acta 63, 899–905.

Simonetti, A., Heaman, L.M., Chacko, T., Banerjee, N.R., 2006. In situ petrographic thin section U-Pb dating of zircon, monazite, and titanite using laser ablation-MC-ICP-MS. International Journal of Mass Spectrometry 253, 87–97.

Simonetti, A., Heaman, L.M., Hartlaub, R.P., Creaser, R.A., MacHattie, T.G., Böhm, C., 2005. U-Pb zircon dating by laser ablation-MC-ICP-MS using a new multiple ion counting Faraday collector array. Journal of Analytical Atomic Spectrometry 20, 677–686.

Sircombe, K.N., Bleeker, W., Stern, R.A., 2001. Detrital zircon geochronology and grain-size analysis of a ~2800 Ma Mesoarchean proto-cratonic cover succession, Slave Province, Canada. Earth and Planetary Science Letters 189, 207–220.

Smithies, R.H., Champion, D.C., Cassidy, K.F., 2003. Formation of Earth’s early Archaean continental

crust. Precambrian Res 127, 89–101.

Smithies, R.H., Van Kranendonk, M.J., Champion, D.C., 2005. It started with a plume - Early Archaean basaltic proto-continental crust. Earth and Planetary Science Letters 238, 284–297.

St Onge, M.R., King, J.E., Lalonde, A.E., 1988. Geology, east-central Wopmay Orogen, District of Mackenzie, Northwest Territories (No. 1923), Geological Survey of Canada Open-File Report.

Stern, R., Bleeker, W., 1998. Age of the world's oldest rocks refined using Canada's SHRIMP: The Acasta Gneiss Complex, northwest territories, Canada 25, 27–31.

Stern, R.A., Bodorkos, S., Kamo, S.L., Hickman, A.H., Corfu, F., 2009. Measurement of SIMS Instrumental Mass Fractionation of Pb Isotopes During Zircon Dating. Geostandards and Geoanalytical Research 33, 145–168.

Tera, F., Papanastassiou, D.A., Wasserburg, G.J., 1974. Isotopic evidence for a terminal lunar cataclysm. Earth and Planetary Science Letters 22, 1–21.

Valley, J.W., Kinny, P.D., Schulze, D.J., Spicuzza, M.J., 1998. Zircon megacrysts from kimberlite: oxygen isotope variability among mantle melts. Contributions to Mineralogy and Petrology 133, 1–11.

Valley, J.W., Lackey, J.S., Cavosie, A.J., Clechenko, C.C., Spicuzza, M.J., Basei, M.A.S., Bindeman, I.N., Ferreira, V.P., Sial, A.N., Peck, W.H., Sinha, A.K., Wei, C.S., 2005. 4.4 billion years of crustal maturation: oxygen isotope ratios of magmatic zircon. Contributions to Mineralogy and Petrology 150, 561–580.

Van Kranendonk, M.J., 2007. Chapter 8.6 Tectonics of Early Earth, Developments in Precambrian Geology, Elsevier.

Van Kranendonk, M.J., 2010. Two types of Archean continental crust: Plume and plate tectonics on early Earth. American Journal of Science 310, 1187–1209.

Whitehouse, M., Nagler, T., Moorbath, S., Kramers, J., Kamber, B., Frei, R., 2001. Priscoan (4.00-4.03 Ga) orthogneisses from northwestern Canada - by Samuel A. Bowring and Ian S. Williams: discussion. Contributions to Mineralogy and Petrology 141, 248–250.

Willbold, M., Hegner, E., Stracke, A., Rocholl, A., 2009. Continental geochemical signatures in dacites from Iceland and implications for models of early Archaean crust formation. Earth and Planetary Science Letters 279, 218–219.

Willbold, M., Mojzsis, S.J., Chen, H.W., Elliott, T., 2015. Tungsten isotope composition of the Acasta Gneiss Complex. Earth and Planetary Science Letters 419, 168–177.

Wood, D.A., 1978. Major and Trace Element Variations in the Tertiary Lavas of Eastern Iceland and their Significance with respect to the Iceland Geochemical Anomaly. Journal of Petrology 19, 393–436

Table 4.1 U-Pb summary of individual samples

Sample	Northing*	Easting*	Age (Ma)	2σ	Method	Metamorphism
JR12-141	7228605	567760	≥ 4001	23	Minimum age from oldest 207Pb/206Pb age	~3350 Ma
JR13-108	7228857	568010	≥ 3997	6	Minimum age from oldest 207Pb/206Pb age	N/A
JR12-145	7228659	567786	≥ 3973	18	Minimum age from oldest 207Pb/206Pb age	N/A
JR12-146	7228629	567781	≥ 3996	20	Minimum age from oldest 207Pb/206Pb age	~3250 Ma
JR12-207	7228058	567536	≥ 4003	23	Minimum age from oldest 207Pb/206Pb age	
JR12-137	7228607	567758	≥ 3958	22	Minimum age from oldest 207Pb/206Pb age	
JR12-119	7229220	567883	≥ 4000	16	Minimum age from oldest 207Pb/206Pb age	~3300 Ma
AC12A	7228635	565829	3977	10	WM of oldest 8 igneous analyses (SIMS 7/6 ages)	~3400 Ma
JR13-206	7228016	567519	3926	30	WM of 8 oldest igneous analyses (7/6 ages)	N/A
JR13-101	7228928	568045	3739	6	WM of 18 oldest analyses (7/6 ages)	~3300 Ma
JR12-144	7228607	567767	3545	20	WM of oldest 12 analayses (7/6 ages)	N/A
JR12-171	7229281	568078	3575	8	WM of oldest 16 analyses (7/6 ages)	N/A
JR13-114	7228676	567663	3568	21	WM of oldest 9 igneous analyses (7/6 ages)	N/A
JR13-115	7228676	567663	3566	14	WM of oldest 10 analyses (7/6 ages)	~3300 Ma
JR13-127	7228669	567638	3582	9	WM of oldest 13 analyses (7/6 ages)	N/A
JR13-205	7228016	567519	3576	14	WM of 12 oldest igneous analyses (7/6 ages)	N/A
JR13-208	7227867	567233	3573	11	WM of 8 oldest igneous analyses (7/6 ages)	~3250 Ma
JR13-303	7227459	565559	3519	56	WM of oldest 3 igneous analyses (7/6 ages)	N/A
JR13-305	7227553	565575	3571	38	WM of oldest 6 igneous analyses (7/6 ages)	N/A
JR13-802	7224438	562184	3365	13	Regression of all data (N=20)	N/A
JR13-304	7227553	565575	2935	9	Concordia age of oldest 14 concordant analyses	N/A

***UTM coordinates are in Zone 11W and using WGS 84 projection**

Sample	Method	Inheritance
JR12-141	close to concordant analyses of rims and ambiguous grains	N/A
JR13-108		N/A
JR12-145		N/A
JR12-146	Concordant analyses of metamorphic rims	N/A
JR12-207		N/A
JR12-137		N/A
JR12-119	qualitiative analysis of rim analyses	N/A
AC12A	qualitative analysis of rim analyses	N/A
JR13-206		N/A
JR13-101	concordant analyses of metamorphic grains	N/A
JR12-144		N/A
JR12-171		N/A
JR13-114		N/A
JR13-115	concordant analyses of metamorphic grains	N/A
JR13-127		N/A
JR13-205		3800 Ma
JR13-208	concordant analyses of metamorphic grains	N/A
JR13-303		signifificant 3700 Ma
JR13-305		3700 Ma
JR13-802		N/A
JR13-304		N/A

***UTM coorc**

Table 4.2 Whole-rock geochemistry for samples within the AGC

Group	Idiwhaa unit									
Sample Name	**TC-3***	**AC2C***	**JR12-145***	**JR12-141***	**AC2I***	**JR13-108**	**JR12-137**	**JR12-146**	**JR12-119**	**JR13-207**
Northing	7228606	7229030	7228659	7228605	7228595	7228857	7228607	7228629	7229220	7228058
Easting	567760	568174	567786	567760	567768	568010	567758	567781	567883	567536
SiO_2 (wt.%)	57.94	61.95	60.73	60.13	66.89	61.94	70.22	70.26	66.45	59.22
TiO_2	1.237	1.083	1.064	1.122	0.823	0.995	0.547	0.528	0.803	1.013
Al_2O_3	13.88	14.02	13.82	14.13	13.87	13.25	12.66	12.70	13.66	13.55
$FeO_{(total)}$	15.25	11.71	13.13	12.53	8.57	13.39	7.99	8.26	9.47	14.77
MnO	0.168	0.163	0.180	0.159	0.123	0.201	0.268	0.110	0.226	0.208
MgO	1.26	1.48	1.20	1.43	0.95	1.13	1.16	0.63	1.81	1.43
CaO	4.61	4.70	4.27	4.93	2.84	3.96	1.92	2.29	1.82	5.21
Na_2O	2.98	3.35	2.92	3.06	3.39	2.93	2.65	3.19	2.58	2.55
K_2O	2.35	1.24	2.39	2.21	2.34	1.94	2.48	1.94	3.01	1.79
P_2O_5	0.335	0.307	0.295	0.299	0.194	0.257	0.108	0.086	0.180	0.256
Sum	100.00	100.00	100.00	100.00	100.00	100.00	100.00	100.00	100.00	100.00
Mg#* **	12.8	18.4	14.0	16.9	16.5	13.1	20.6	12.0	25.4	14.7
Na2O/K2O	1.3	2.7	1.2	1.4	1.4	1.5	1.1	1.6	0.9	1.4
XRF										
V (ppm)	5	3	4	5	4	3	8	5	5	8
Cr	1	1	1	1	1	2	1	3	1	1
Ni	1	3	1	3	18	0	1	2	4	0
Cu	20	160	28	31	242	12	81	14	6	45
Zn	81	95	120	111	106	118	90	115	114	102
Ga	25	24	24	24	24	23	22	22	22	24
Zr	317	286	380	293	348	333	490	428	329	246
Ba	712	279	753	599	642	614	600	577	936	539
ICP-MS										
Sc (ppm)	35.3	33.4	30.4	34.5	25.4	29.2	18.0	14.6	23.3	35.4282
Rb	74.4	18.3	59.1	53.0	53.9	60.1	76.8	51.2	81.1	39.7
Sr	151	120	189	167	191	103	132	138	114	168
Y	72.86	78.02	82.59	86.40	70.74	69.69	91.83	65.47	59.38	107.83
Nb	21.34	20.29	22.69	23.07	26.45	19.71	29.25	26.66	25.11	20.89
Cs	2.00	0.58	1.84	1.64	1.70	1.24	4.74	1.58	2.19	1.36
Hf	8.02	7.19	9.26	7.18	8.86	8.46	12.91	11.23	8.50	6.49
Ta	1.31	1.24	1.54	1.41	1.76	1.26	2.39	1.70	1.36	1.32

Table 4.2 Whole-rock geochemistry for samples within the AGC

Group	Idiwhaa unit									
Sample Name	**TC-3***	**AC2C***	**JR12-145***	**JR12-141***	**AC2I***	**JR13-108**	**JR12-137**	**JR12-146**	**JR12-119**	**JR13-207**
Pb	4.75	4.89	6.74	5.72	7.48	6.00	7.94	8.05	5.10	6.04
Th	2.37	3.87	4.63	3.99	8.36	4.80	24.14	16.92	10.92	7.44
U	0.82	1.12	1.28	0.98	1.60	0.86	2.78	1.64	1.50	1.40
La	27.15	24.94	28.54	19.72	14.49	31.46	96.59	71.31	36.06	41.73
Ce	71.39	65.49	70.08	55.38	40.71	67.40	185.70	141.70	83.27	111.83
Pr	10.42	9.82	10.09	8.54	6.56	8.72	21.16	15.41	11.29	16.00
Nd	47.48	45.36	45.48	40.24	32.59	36.60	76.62	57.79	45.96	68.52
Sm	12.63	12.31	12.74	11.87	9.99	9.51	14.18	11.96	10.03	17.66
Eu	3.10	2.80	2.95	2.92	2.10	2.57	1.83	2.49	1.91	2.92
Gd	13.75	13.35	14.59	14.11	11.32	10.97	13.31	11.44	9.31	18.64
Tb	2.34	2.40	2.58	2.56	2.09	1.96	2.39	1.91	1.67	3.28
Dy	14.52	15.41	16.24	16.72	13.35	13.00	16.08	12.30	11.16	20.59
Ho	2.94	3.23	3.34	3.49	2.86	2.71	3.40	2.64	2.38	4.18
Er	7.84	8.82	9.07	9.55	7.92	7.52	9.72	7.62	6.79	11.26
Tm	1.11	1.27	1.27	1.36	1.13	1.09	1.43	1.14	1.01	1.58
Yb	6.65	7.61	7.66	8.20	6.72	6.71	9.21	7.10	6.45	9.33
Lu	1.02	1.15	1.16	1.25	1.02	1.04	1.42	1.10	0.98	1.34
La_N/Yb_N[1]	2.77	2.23	2.53	1.63	1.47	3.18	7.13	6.82	3.80	3.04
Eu/Eu*[2]	0.72	0.67	0.66	0.69	0.61	0.77	0.41	0.65	0.60	0.49

UTM coordinates are in Zone 11W and using WGS 84 projection
* Whole rock data from Reimink et al., (2014)
Mg# = 100*[MgO/(FeO+MgO)] calculated on a molar basis.

[1]normalization values from McDonough and Sun (1995)
[2]$Eu/Eu = Eu_N/sqrt[(Sm_N * Gd_N)]$ normalized to McDonough and Sun (1995).

Group	Metagabbro			Amphibolite	3.94 Ga tonalite	3.75 Ga tonalite				
Sample Name	**JR13-102**	**JR12-136**	**GFA-4**	**JR12-172**	**JR13-206**	**JR13-101**	**JS-1**	**JR12-144**	**JR13-205**	**JR13-114**
Northing	7229030	7228607	7229030	7228962	7228016	7228928	7227385	7228607	7228016	7228676
Easting	568174	567756	568170	568151	567519	568045	568068	567767	567519	567663
SiO_2 (wt.%)	52.90	53.89	55.16	53.26	72.41	68.35	63.93	73.17	69.24	73.21
TiO_2	0.694	0.552	0.739	1.158	0.568	0.867	0.801	0.209	0.515	0.289
Al_2O_3	15.18	15.52	15.49	13.85	12.99	13.30	16.01	14.86	15.77	14.20
$FeO_{(total)}$	10.41	9.09	10.09	13.33	5.76	7.43	5.70	2.07	3.66	2.43
MnO	0.172	0.194	0.179	0.229	0.056	0.093	0.079	0.012	0.044	0.020
MgO	6.81	7.06	6.31	5.27	0.65	1.87	2.86	0.37	0.88	0.63
CaO	9.20	8.79	7.66	8.96	2.22	2.60	4.80	1.82	2.52	0.69
Na_2O	3.20	3.27	3.09	2.70	3.52	2.70	3.32	3.99	4.39	2.91
K_2O	1.36	1.57	1.19	1.11	1.76	2.65	2.31	3.47	2.86	5.56
P_2O_5	0.076	0.061	0.090	0.139	0.061	0.143	0.185	0.046	0.120	0.066
Sum	100.00	100.00	100.00	100.00	100.00	100.00	100.00	100.00	100.00	100.00
Mg#* **	53.8	58.1	52.7	41.3	16.8	30.9	47.25	24.1	30.1	31.7
Na2O/K2O	2.4	2.1	2.6	2.4	2.0	1.0	1.4	1.2	1.5	0.5
XRF										
V (ppm)	144	128	125	315	2	24	88	14	36	20
Cr	53	149	114	18	1	8	47	3	7	5
Ni	20	26	14	49	0	5	23	3	4	3
Cu	43	49	29	83	196	40	33	1	35	2
Zn	94	109	106	99	78	78	66	37	44	33
Ga	17	18	18	20	21	22	19	19	21	17
Zr	96	92	143	162	478	336	265	143	386	228
Ba	341	211	343	175	578	930	706	1879	1203	1368
ICP-MS										
Sc (ppm)	22.7	20.1	20.7	43.2	9.1	14.5	11.9	2.8	5.5	3.8
Rb	19.6	16.3	19.0	14.2	43.8	69.2	61.5	42.9	66.5	63.9
Sr	293	214	185	136	178	164	291	273	328	216
Y	16.90	19.32	25.89	49.38	10.81	60.24	23.73	3.26	16.96	8.30
Nb	4.84	4.98	9.67	8.62	12.65	20.06	13.53	5.81	11.04	7.12
Cs	0.56	0.34	0.86	0.29	1.00	3.02	2.16	0.37	1.48	0.86
Hf	2.45	2.37	3.66	4.37	12.56	8.76	6.13	3.80	8.52	5.60
Ta	0.35	0.41	1.28	0.60	0.61	1.53	0.85	0.14	0.58	0.21

Group	Metagabbro			Amphibolite	3.94 Ga tonalite	3.75 Ga tonalite				
Sample Name	**JR13-102**	**JR12-136**	**GFA-4**	**JR12-172**	**JR13-206**	**JR13-101**	**JS-1**	**JR12-144**	**JR13-205**	**JR13-114**
Pb	8.35	6.12	4.23	6.03	11.59	7.94	8.85	12.60	14.88	7.97
Th	1.76	2.25	4.33	2.52	9.55	12.80	17.95	7.38	17.97	11.97
U	0.32	0.57	1.14	0.64	1.25	2.04	1.55	0.44	1.06	0.44
La	12.17	11.44	17.95	15.08	42.90	46.69	58.63	28.52	131.33	68.53
Ce	23.22	22.86	34.29	34.03	73.74	91.13	103.63	48.37	209.93	114.19
Pr	2.85	2.83	4.27	4.68	7.55	11.14	10.93	5.15	20.43	10.92
Nd	11.34	11.59	17.10	20.84	24.82	43.62	37.49	18.17	62.78	34.27
Sm	2.83	2.91	4.20	5.88	3.80	10.20	6.52	3.11	8.03	4.62
Eu	1.15	1.04	1.37	1.58	1.50	2.20	1.46	2.17	1.52	1.07
Gd	3.07	3.28	4.44	7.25	2.77	10.49	5.08	2.14	5.00	2.86
Tb	0.53	0.58	0.76	1.35	0.38	1.81	0.81	0.22	0.63	0.37
Dy	3.37	3.68	4.82	8.90	2.07	11.58	4.61	0.84	3.43	1.93
Ho	0.69	0.77	1.00	1.94	0.43	2.38	0.92	0.13	0.66	0.34
Er	1.81	2.11	2.73	5.43	1.24	6.40	2.42	0.26	1.75	0.85
Tm	0.26	0.30	0.41	0.81	0.21	0.93	0.34	0.03	0.25	0.11
Yb	1.62	1.92	2.56	5.11	1.55	5.59	2.04	0.23	1.55	0.62
Lu	0.25	0.30	0.39	0.81	0.27	0.87	0.32	0.04	0.24	0.11
La_N/Yb_N[1]	5.10	4.06	4.77	2.00	18.76	5.68	19.57	83.24	57.50	75.12
Eu/Eu^*[2]	1.20	1.03	0.97	0.74	1.41	0.65	0.78	2.58	0.73	0.90

Group	~3.6 Ga grantoids						~3.4 Ga granitoid	~2.9 Ga granitoid
Sample Name	JR12-127	JR13-115	JR13-208	JR12-171	JR13-305	JR13-303	JR13-304	JR13-802
Northing	7228669	7228676	7227867	7229281	7227553	7227459	7227553	7224438
Easting	567638	567663	567233	568078	565575	565559	565575	562184
SiO_2 (wt.%)	73.59	73.54	67.47	72.69	72.98	73.25	69.53	73.63
TiO_2	0.335	0.299	0.604	0.461	0.113	0.067	0.590	0.122
Al_2O_3	14.40	14.21	16.21	14.48	16.21	16.41	15.22	15.00
$FeO_{(total)}$	2.11	2.51	4.23	2.93	0.73	0.36	3.51	1.04
MnO	0.022	0.025	0.042	0.029	0.010	0.006	0.038	0.016
MgO	0.57	0.78	1.43	1.10	0.28	0.15	0.97	0.37
CaO	1.40	1.36	3.00	1.86	1.87	1.81	2.34	1.39
Na_2O	4.62	4.77	4.52	4.00	6.25	6.57	4.04	4.44
K_2O	2.88	2.45	2.30	2.37	1.52	1.36	3.59	3.95
P_2O_5	0.072	0.068	0.192	0.081	0.026	0.018	0.173	0.040
Sum	100.00	100.00	100.00	100.00	100.00	100.00	100.00	100.00
Mg#***	32.3	35.6	37.7	40.2	40.2	42.6	33.0	38.7
Na2O/K2O	1.6	1.9	2.0	1.7	4.1	4.8	1.1	1.1
XRF								
V (ppm)	20	21	48	28	11	4	39	12
Cr	5	5	16	3	7	3	15	4
Ni	2	3	9	2	3	1	9	0
Cu	1	1	3	2	0	9	20	0
Zn	26	27	42	41	28	8	64	36
Ga	19	18	20	19	20	20	18	17
Zr	269	233	245	271	86	88	469	114
Ba	1489	1041	652	1005	458	400	1683	1044
ICP-MS								
Sc (ppm)	3.1	2.6	4.2	4	3.3	0.5	4.4	0.7
Rb	34.2	34.6	57.2	48.7	28.2	19.6	72.0	95.9
Sr	240	249	466	384	820	791	322	556
Y	8.62	9.03	7.50	5.50	4.96	2.10	26.68	3.08
Nb	6.93	5.79	6.34	5.27	1.53	1.04	15.73	2.13
Cs	0.48	0.64	1.60	0.65	0.33	0.22	0.79	1.21
Hf	6.18	5.80	5.03	5.78	2.38	2.42	10.64	2.94
Ta	0.25	0.21	0.32	0.12	0.11	0.11	1.22	0.19

Group	~3.6 Ga grantoids						~3.4 Ga granitoid	~2.9 Ga granitoid
Sample Name	JR12-127	JR13-115	JR13-208	JR12-171	JR13-305	JR13-303	JR13-304	JR13-802
Pb	9.21	8.04	6.03	5.68	16.58	19.52	16.23	27.84
Th	13.42	12.40	5.47	2.70	0.94	0.75	27.11	11.39
U	0.54	0.59	0.51	0.31	0.24	0.29	0.71	3.17
La	69.52	65.09	53.98	36.05	10.27	7.55	95.80	23.06
Ce	121.56	107.15	84.93	56.31	18.10	12.62	168.80	36.15
Pr	10.95	10.43	7.81	5.40	2.23	1.36	15.89	3.49
Nd	34.17	33.09	23.99	17.13	8.69	4.98	50.57	11.03
Sm	4.60	4.58	3.21	2.25	2.02	0.96	8.31	1.59
Eu	1.05	1.12	1.11	1.24	0.62	0.48	1.56	0.60
Gd	2.99	3.17	2.28	1.56	1.70	0.69	6.14	0.92
Tb	0.39	0.40	0.30	0.20	0.22	0.09	0.91	0.12
Dy	1.99	2.06	1.62	1.13	1.17	0.44	5.30	0.63
Ho	0.37	0.37	0.29	0.22	0.20	0.08	1.02	0.11
Er	0.88	0.87	0.71	0.59	0.48	0.19	2.66	0.30
Tm	0.11	0.12	0.10	0.09	0.06	0.03	0.36	0.04
Yb	0.67	0.72	0.66	0.59	0.33	0.17	2.09	0.26
Lu	0.10	0.11	0.09	0.10	0.05	0.02	0.29	0.04
La_N/Yb_N[1]	70.67	61.59	55.83	41.82	20.97	29.94	31.15	59.95
Eu/Eu*[2]	0.87	0.90	1.26	2.03	1.03	1.81	0.67	1.51

Table 4.3 Summary of O-isotope data from samples within the AGC

Sample	Average δ18O (SMOW)	Standard Error	N
JR13-102	5.79	0.18	4
TC3 Phase I*	5.58	0.04	72
TC3 Phase II*	4.74	0.03	91
JR13-108 Phase I	5.78	0.12	13
JR13-108 Phase II	4.70	0.12	10
AC12A	6.44	0.02	65
JR13-206	5.47	0.16	13
JR13-101	6.48	0.04	37
JR12-127	6.33	0.05	18
JR13-205	6.2	0.03	13
JR12-171	6.18	0.03	44
JR13-208	6.45	0.05	15
JR13-114	6.15	0.02	30
JR13-115	6.31	0.04	19
JR12-144	6.38	0.08	14
JR13-802	6.29	0.06	36
JR13-304	6.03	0.05	16

*** includes data from Reimink *et al.*, (2014)**
**** see discussion of age in Section*******

Chapter 5: Conclusions

This thesis set out to accomplish two main objectives. The first was to use Hadean rocks preserved in the Acasta Gneiss Complex (AGC) to gain insight into the petrogenesis of Hadean crust on Earth. The second objective was to evaluate the compositions of rock units formed in the AGC over the following billion years (4.0–2.9 Ga), and to use these data to assess changes in crust-formation processes with time.

In Chapter 2, the discovery of the only mappable, zircon-bearing Hadean (> 4.0 Ga) rock unit known on Earth was presented. The whole-rock geochemical characteristics of this meta-igneous rock unit, (called the Idiwhaa unit) specifically its high iron content, low Mg#, flat rare-earth-element pattern, and negative Eu anomaly are markedly different from the tonalite-trondhjemite-granodiorite suite, the rocks that dominate the Archean (2.5–4.0 Ga) crustal record (Martin, 1986; Moyen and Martin, 2012). These distinctions imply a different mode of formation. Specifically, these signatures suggest a petrogenesis that is strikingly similar to modern Icelandic crust formation in that they were dominated by shallow-level fractionation of a mineral assemblage containing significant plagioclase. This shallow-level crust-forming process wsa distinct from later, deep-seated Archean crust formation (represented by TTG magmatism). Well-preserved zircons in this 4.02 Ga Idiwhaa unit allow us to further investigate its geochemical evolution. Specifically, changes in the oxygen isotope ratio between two phases of zircon growth present in these grains can be formed by magmatic assimilation of pre-existing rocks altered by high-temperature surface waters.

Taken together, the whole-rock and mineral geochemical features of this unit compare well with rocks formed on modern Iceland. Icelandic crust, having a higher geothermal gradient than most other places on Earth, has long been suggested to be analogous to settings that formed evolved crust on the early Earth (Kroner, 1985). Therefore, I suggest that the Idiwhaa unit provides the first direct evidence that a petrologic setting analogous to modern Iceland existed on the Hadean Earth, and may have served to initiate evolved crust production on our young planet.

Chapter 3 elaborates on the findings in Chapter 2 by refining the Idiwhaa unit crystallization age using high-precision zircon U-Pb dating by ID-TIMS and obtaining Hf isotope analyses of the ~4.02 Ga zircon by both solution and laser ablation ICP-MS. These new data, in concert with the whole-rock elemental compositions, provide constraints on the composition of pre-existing crust of the AGC into

which the Idiwhaa magma intruded as well as the differentiation state of the early Earth. More specifically, I refined the crystallization age of the Idiwhaa unit to 4019.7 ± 1.8 Ma as well as measured, to my knowledge, the oldest concordant TIMS U-Pb analysis of a terrestrial sample ever reported, with a $^{207}Pb/^{206}Pb$ age of 4013.7 ± 0.3 Ma. Hf isotope analyses of igneous zircon show no signs for much older (>4.2 Ga) evolved crust in the AGC despite suggestions that such a crust was widespread on the early Earth (Harrison et al., 2008). In addition, unradiogenic Hf isotope compositions in the earliest zircon growth zones, which have oxygen isotope ratios identical to that of pristine mantle composition, suggest that an early-enriched reservoir played a role in generation of the Idiwhaa magma. This provides the first direct evidence that the oldest known evolved crust on Earth interacted with, or was derived from, a long-lived enriched reservoir.

Chapter 4 uses many of the same geochemical techniques applied to the ca. 4.02 Ga Idiwhaa unit (whole-rock elemental chemistry, zircon U-Pb and oxygen isotope analyses) to investigate the younger and volumetrically more abundant igneous rocks suites present in the AGC. A steepening of the REE patterns of younger samples suggests a progressive increase in the depth of melting over ~400 myr. Using our previous analysis of the 4.02 Ga Idiwhaa unit (Chapters 2 and 3) as a starting point, I envision a model of crustal evolution in the AGC in which it transitions from a thickened and internally differentiated oceanic plateau dominated by mafic material prior to ~3.9 Ga, to being intruded by voluminous Archean TTG-like magmas at 3.6 Ga, probably in a subduction-like environment. The REE patterns of the ~3.6 Ga rock suite suggest that magmatic activity at that time was generated at great depth and likely served to stabilize the proto-cratonic nucleus.

In terms of the two competing models for the early Earth noted in Chapter 1, the largely uniformitarian versus the markedly non-uniformitarian models, my own view at the culmination of this thesis is that the *modus operandi* of our young planet was significantly different from the modern day. Specifically, my data on the ca. 4.02 Ga Idiwhaa unit of the AGC suggests that the Hadean Earth was dominated by mafic crust, with small components of evolved material formed by high degrees of fractional crystallization, combined perhaps with partial melting of hydrated mafic material at shallow depth. These data and interpretations align well with what seems to be a paradigm shift regarding the early Earth. This shift may be more accurately described as a tempering of uniformitarian theories that are largely based on data from the Jack Hills suite of detrital zircons. As noted by others (Cavosie et al.,

2006; Kemp et al., 2010; Rasmussen et al., 2011; Nebel et al., 2013), although the Jack Hills datasets can be interpreted in a uniformitarian framework to indicate the presence of large amounts of continental crust in the Hadean Earth, these interpretations are not unequivocal. Rather, these same data are also consistent with small amounts of evolved crust forming within a dominantly mafic early crust (Kemp et al., 2010).

Analysis of younger rock suites of the AGC indicates that partial melting of mafic material progressed to greater depths until voluminous magmatism at 3.6 Ga, formed by deep-seated melting of basaltic precursors. Chemical signatures present in the ca 3.6 Ga AGC rocks suggest a depth of melting that is similar to modern subduction processes (>50–60 km) and may require some form of horizontal tectonics for their production. This model, whereby an evolved mafic plateau initiates subduction of hydrated mafic rocks, validates previous suggestions (Nair and Chacko, 2008) and aligns well with detailed analysis of other ancient gneiss localities (Smithies et al., 2005; Moyen et al., 2007; Van Kranendonk, 2007).

Future Directions:

Although I believe this thesis has improved our understanding of the AGC, a great many questions remain unanswered concerning the complex as well as the early Earth in general. One such question is the real distribution of rock ages and compositions within the broader AGC. As indicated above, the AGC represents >1300 km^2 of exposed pre-2.8 Ga basement, of which <30 km^2 have been studied in any detail. Therefore, trends in age and composition documented here may not be representative of the broader AGC. Our mapping and dating presented in Chapter 4 suggests that >4.0 Ga rocks are volumetrically minor in the small area that I mapped in detail. Rather, the map area is dominated by ~3.6 Ga TTG-like rocks. Some preliminary regional work conducted during the 2013 field season, indicates that the broader AGC contains a surprising amount of >3.7 Ga rocks, as well as large swaths of ~3.4 Ga units (Ketchum et al., 2013). The distribution and proportion of various igneous rock suites within the broader AGC could be evaluated by mapping and sampling, detrital zircon age spectra, or other complex geochemical tracing methods using glacial till geochemistry. Such information would provide valuable insights into the age and compositional variability of Paleoarchean–Hadean crust within the AGC,

allowing for further evaluation of the processes of crust formation on the ancient Earth.

Additionally, I believe this thesis has demonstrated the importance of field observations and mapping, conducted over multiple field seasons and supported by U-Pb geochronology, in unraveling the complex history of ancient gneiss terranes. Though it may seem silly to highlight such a simple and fundamental procedure, too much of the published early-Earth geochemical data appears to come from samples with poorly constrained ages that lack a fundamental understanding or discussion of primary chemical signatures. Even within highly deformed, multiply metamorphosed gneiss terranes such as the AGC, I have documented a small region of lower strain that was studied in detail, providing a fuller understanding of the primary processes involved in crust formation. A 'layering' of correlated datasets from well-preserved rock samples creates a very powerful tool for investigating the origins of the studied samples. For instance, once the whole-rock geochemistry is be deemed reliable (for example the Idiwhaa unit in Chapter 2), whole-rock isotopic tracers may then be investigated, providing a more robust data set than those taken from less well constrained samples (the comparison of Idiwhaa unit Sm-Nd systematics with previously published Sm-Nd data from the AGC in Chapter 3). In Chapter 4, I have identified a large, well-preserved sample suite with crystallization ages spanning over one billion years. Given our analysis of the basic petrologic information of these samples (whole-rock elemental chemistry, zircon U-Pb and oxygen isotope analyses), more complex analyses will build upon the framework of this fundamental information. Information such as zircon Hf isotope composition, zircon trace-element analyses, whole-rock Nd isotope data (both ^{143}Nd and ^{142}Nd), as well as whole rock Lu-Hf data would provide more robust constraints on the processes and timescales involved in production of the Acasta Gneiss Complex than previous studies that lack this basic information.

Our identification of the Idiwhaa unit has provided a great deal of information regarding the earliest evolution of the AGC and the Hadean Earth. Detailed mapping and sampling in other ancient gneiss locations may provide equally provocative samples to investigate. Indeed, this has arguably been accomplished with the detailed study of the Nuvvuaggituq Supracrustal Belt in Quebec (O'Neil et al., 2008; O'Neil et al., 2012) and the Isua area of western Greenland (e.g., Moorbath et al., 1973). However, identification of such rare samples likely relies as much on serendipity as skill. While it remains possible and even likely that older and more informative samples will be discovered, possibly in the AGC itself, such discoveries require the fortuitous identification of the right samples. Such is the inherent

challenge of searching for the ‘needle in a haystack’ that very ancient rocks represent. However, future work in ancient gneiss localities will almost certainly uncover new and important samples that can lend insight into the earliest evolution of our planet. Therefore, I need to keep searching.

Full Reference List:

Adam, J., Rushmer, T., O'Neil, J., Francis, D., 2012. Hadean greenstones from the Nuvvuagittuq fold belt and the origin of the Earth's early continental crust. Geology 40, 363–366.

Albarede, F., Telouk, P., Blichert-Toft, J., Boyet, M., Agranier, A., Nelson, B., 2004. Precise and accurate isotopic measurements using multiple-collector ICPMS. Geochimica et Cosmochimica Acta 68, 2725–2744.

Allen, R.M., 2002. Plume-driven plumbing and crustal formation in Iceland. Journal of Geophysical Research 107, 2163.

Amelin, Y., Kamo, S.L., Lee, D.-C., 2011. Evolution of early crust in chondritic or non-chondritic Earth inferred from U–Pb and Lu–Hf data for chemically abraded zircon from the Itsaq Gneiss Complex, West GreenlandThis article is one of a series of papers published in this Special Issue on the theme of Geochronology in honour of Tom Krogh. Can. J. Earth Sci. 48, 141–160.

Amelin, Y., Lee, D.C., Halliday, A.N., 2000. Early-middle Archaean crustal evolution deduced from Lu-Hf and U-Pb isotopic studies of single zircon grains. Geochimica et Cosmochimica Acta.

Amelin, Y., Lee, D.C., Halliday, A.N., Pidgeon, R.T., 1999. Nature of the Earth's earliest crust from hafnium isotopes in single detrital zircons. Nature.

Ashton, K.E., Heaman, L.M., Lewry, J.F., Hartlaub, R.P., Shi, R., 1999. Age and origin of the Jan Lake Complex: a glimpse at the buried Archean craton of the Trans-Hudson Orogen. Can. J. Earth Sci. 36, 185–208.

Balsley, S.D., Gregory, R.T., 1998. Low-18O silicic magmas: why are they so rare? Earth and Planetary Science Letters 162, 123–136.

Barker, F., Arth, J.G., 1976. Generation of trondhjemitic-tonalitic liquids and Archean bimodal trondhjemite-basalt suites. Geology 4, 596–600.

Beard, J.S., Lofgren, G.E., 1991. Dehydration Melting and Water-Saturated Melting of Basaltic and Andesitic Greenstones and Amphibolites at 1, 3, and 6. 9 kb. Journal of Petrology 32, 365–401.

Bedard, J. H., 2006. A catalytic delamination-driven model for coupled genesis of Archaean crust and sub-continental lithospheric mantle. Geochimica et Cosmochimica Acta 70, 1188–1214.

Bell, E.A., Harrison, T.M., Kohl, I.E., Young, E.D., 2014. Eoarchean crustal evolution of the Jack Hills zircon source and loss of Hadean crust. Geochimica et Cosmochimica Acta 146, 27–42.

Bindeman, I., 2008. Oxygen isotopes in mantle and crustal magmas as revealed by single crystal analysis. Reviews in Mineralogy and Geochemistry 69, 445-478.

Bindeman, I.N., Valley, J.W., 2000. Formation of low-δ18O rhyolites after caldera collapse at Yellowstone, Wyoming, USA. Geology 28, 719–722.

Bindeman, I.N., Valley, J.W., 2001. Low-δ18O Rhyolites from Yellowstone: Magmatic Evolution Based on Analyses of Zircons and Individual Phenocrysts. Journal of Petrology 42, 1491–1517.

Bindeman, I., Gurenko, A., Carley, T., Miller, C., Martin, E., Sigmarsson, O., 2012. Silicic magma petrogenesis in Iceland by remelting of hydrothermally altered crust based on oxygen isotope diversity and disequilibria between zircon and magma with implications for MORB. Terra Nova 24, 227–232.

Black, L.P., Kamo, S.L., Allen, C.M., Davis, D.W., Aleinikoff, J.N., Valley, J.W., Mundil, R., Campbell, I.H., Korsch, R.J., Williams, I.S., Foudoulis, C., 2004. Improved 206Pb/238U microprobe geochronology by the monitoring of a trace-element-related matrix effect; SHRIMP, ID–TIMS, ELA–ICP–MS and oxygen isotope documentation for a series of zircon standards. Chemical Geology 205, 115–140.

Bleeker, W., Stern, R., 2000. Why the Slave Province, Northwest Territories, got a little bigger, Geological Survey of Canada Current Research.

Blichert-Toft, J., Gleason, J.D., Telouk, P., Albarède, F., 1997. The Lu–Hf isotope geochemistry of shergottites and the evolution of the Martian mantle–crust system. Earth and Planetary Science Letters 173, 25–39.

Blundy, J., Wood, B., 1994. Prediction of crystalðmelt partition coefficients from elastic moduli. Nature

372, 452–454.
Boher, M., Abouchami, W., Michard, A., Albarede, F., Arndt, N. 1992. Crustal Growth in West Africa at 2.1 Ga. Journal of Geophysical Research 97, 345–369
Bouvier, A., Vervoort, J.D., Patchett, P.J., 2008. The Lu–Hf and Sm–Nd isotopic composition of CHUR: Constraints from unequilibrated chondrites and implications for the bulk composition of terrestrial planets. Earth and Planetary Science Letters 273, 48–57.
Bowring, S.A., Housh, T., 1995. The Earth's early evolution. Science 269, 1535–1540.
Bowring, S.A., Williams, I.S., 1999. Priscoan (4.00–4.03 Ga) orthogneisses from northwestern Canada. Contributions to Mineralogy and Petrology 134, 3–16.
Bowring, S.A., Housh, T.B., Isachsen, C.E., 1990. The Acasta Gneisses: Remnant of Earth's Early Crust. In: Origin of the Earth 1–25.
Bowring, S.A., King, J.E., Housh, T.B., C.E., Isachsen, C.E., Podosek, F.A., 1989a. Neodymium and lead isotope evidence for enriched early Archaean crust in North America. Nature 340, 222–225.
Bowring, S.A., Williams, I.S., Compston, W., 1989b. 3.96 Ga gneisses from the Slave province, Northwest Territories, Canada. Geology 17, 971–975.
Boyet, M., Carlson, R.W., 2005. Geochemistry: 142Nd evidence for early (>4.53 Ga) global differentiation of the silicate earth. Science 309, 576–581.
Breemen, O.V., Davis, W.J., King, J.E., 1992. Temporal distribution of granitoid plutonic rocks in the Archean Slave Province, northwest Canadian Shield. Can. J. Earth Sci. 29, 2186–2199.
Carley, T.L., Miller, C.F., Wooden, J.L., Padilla, A.J., Schmitt, A.K., Economos, R.C., Bindeman, I.N., Jordan, B.T., 2014. Iceland is not a magmatic analog for the Hadean: Evidence from the zircon record. Earth and Planetary Science Letters 405, 85–97.
Carmichael, I.S.E., 1964. The petrology of Thingmuli, a Tertiary volcano in eastern Iceland. Journal of Petrology 5, 435–460.
Caro, G., Bourdon, B., Birck, J.-L., Moorbath, S., 2003. 146Sm-142Nd evidence from Isua metamorphosed sediments for early differentiation of the Earth's mantle. Nature 423, 428–432.
Catling, D.C., Claire, M.W., 2005. How Earth's atmosphere evolved to an oxic state: A status report. Earth and Planetary Science Letters 237, 1–20.
Cavosie, A.J., Valley, J.W., Wilde, S.A., 2006. Correlated microanalysis of zircon: Trace element, δ 18O, and U-Th-Pb isotopic constraints on the igneous origin of complex >3900 Ma detrital grains. Geochimica et Cosmochimica Acta 70, 5601–5616.
Champion, D.C., Smithies, R.H., 2007. Chapter 4.3 Geochemistry of Paleoarchean Granites of the East Pilbara Terrane, Pilbara Craton, Western Australia: Implications for Early Archean Crustal Growth, in: Developments in Precambrian Geology, Elsevier, pp. 369–409.
Condie, K., 2007. Chapter 1.2 The Distribution of Paleoarchean Crust, in: Developments in Precambrian Geology. Elsevier, pp. 9–18.
Condon, D.J., Schoene, B., McLean, N.M., Bowring, S.A., Parrish, R.R., 2015. Metrology and traceability of U–Pb isotope dilution geochronology (EARTHTIME Tracer Calibration Part I). Geochimica et Cosmochimica Acta 164, 464–480.
Corfu, F., 2003. Atlas of Zircon Textures. Reviews in Mineralogy and Geochemistry 53, 469–500.
Creaser, R.A., Erdmer, P., Stevens, R.A., Grant, S.L., 1997. Tectonic affinity of Nisutlin and Anvil assemblage strata from the Teslin tectonic zone, northern Canadian Cordillera: Constraints from neodymium isotope and geochemical evidence. Tectonics 16, 107–121.
D'Abzac, F.X., Davies, J.H.F.L., Wotzlaw, J.-F., Schaltegger, U. Hafnium isotope analysis of Yb-doped zircon and JMC475 reference materials by solution MC-ICP-MS: Protocols and pitfalls, in:. Presented at the Goldschmidt Geochemistry Conference.
Davidek, K.L., A Bowring, S., Williams, I.S., 1997. Conventional U-Pb geochronology of the Acasta gneisses using single grain zircon fragmentation techniques. American Geophysical Union Annual Meeting A–75.
David, J., Godin, L., Stevenson, R.K., O'Neil, J., Francis, D., 2009. U-Pb ages (3.8–2.7 Ga) and Nd

isotope data from the newly identified Eoarchean Nuvvuagittuq supracrustal belt, Superior Craton, Canada. Geological Society of America Bulletin 121, 150–163.
Davies, J.H.F.L., Wotzlaw, J.-F., Wolfe, A.P., Heaman, L.M., Arbour, V., 2014. Assessing the age of the Late Cretaceous Danek Bonebed with U–Pb geochronology 1. Can. J. Earth Sci. 51, 982–986.
Davis, W.J., Hegner, E., 1992. Neodymium isotopic evidence for the tectonic assembly of Late Archean crust in the Slave Province, northwest Canada. Contrib Mineral Petrol 111, 493–504
Debaille, V., O'Neill, C., Brandon, A.D., Haenecour, P., 2013. Stagnant-lid tectonics in early Earth revealed by 142Nd variations in late Archean rocks. Earth and Planetary Science Letters 373, 83–92
Eiler, J.M., 2001. Oxygen isotope variations of basaltic lavas and upper mantle rocks. Reviews in Mineralogy and Geochemistry 43, 319–364.
Fisher, C.M., Hanchar, J.M., Samson, S.D., Dhuime, B., Blichert-Toft, J., Vervoort, J.D., Lam, R., 2011. Synthetic zircon doped with hafnium and rare earth elements: A reference material for in situ hafnium isotope analysis. Chemical Geology 286, 32–47.
Fisher, C.M., Vervoort, J.D., DuFrane, S.A., 2014. Accurate Hf isotope determinations of complex zircons using the "laser ablation split stream" method. Geochem. Geophys. Geosyst. 15, 121–139.
Ferry, J.M., Watson, E.B., 2007. New thermodynamic models and revised calibrations for the Ti-in-zircon and Zr-in-rutile thermometers. Contributions to Mineralogy and Petrology 154, 429-437.
Foley, S., Tiepolo, M., Vannucci, R., 2002. Growth of early continental crust controlled by melting of amphibolite in subduction zones. Nature 417, 837–840.
Friend, C.R.L., Nutman, A.P., 2005. Complex 3670–3500 Ma Orogenic Episodes Superimposed on Juvenile Crust Accreted between 3850 and 3690 Ma, Itsaq Gneiss Complex, Southern West Greenland. The Journal of Geology 113, 375–397.
Froude, D.O., Ireland, T.R., Kinny, P.D., Williams, I.S., Compston, W., Williams, I.R., Myers, J.S., 1983. Ion microprobe identification of 4,100–4,200 Myr-old terrestrial zircons. Nature 304, 616–618.
Geisler, T., Pidgeon, R.T., Van Bronswijk, W., Kurtz, R., 2002. Transport of uranium, thorium, and lead in metamict zircon under low-temperature hydrothermal conditions. Chemical Geology 191, 141–154.
Gerstenberger, H., Haase, G., 1997. A highly effective emitter substance for mass spectrometric Pb isotope ratio determinations. Chemical Geology 136, 309–312.
Ghiorso, M.S., Gualda, G.A.R., 2015. An H2O–CO2 mixed fluid saturation model compatible with rhyolite-MELTS. Contributions to Mineralogy and Petrology 169, 53–30.
Glikson, A.Y., 1979. Early Precambrian Tonalite-Trondhjemite Sialic Nuclei. Earth Science Reviews 1–73.
Green, D.C., Baadsgaard, H., Cumming, G.L., 1968. Geochronology of the Yellowknife area, Northwest Territories, Canada. Can. J. Earth Sci. 5, 725–735.
Grimes, C.B., Ushikubo, T., John, B.E., Valley, J.W., 2010. Uniformly mantle-like $\delta^{18}O$ in zircons from oceanic plagiogranites and gabbros. Contributions to Mineralogy and Petrology 161, 13–33.
Grove, T.L., Kinzler, R.J., 1986. Petrogenesis of andesites. Annual Review of Earth and Planetary Sciences 14, 417.
Gualda, G.A.R., Ghiorso, M.S., Lemons, R.V., Carley, T.L., 2012. Rhyolite-MELTS: a Modified Calibration of MELTS Optimized for Silica-rich, Fluid-bearing Magmatic Systems. Journal of Petrology 53, 875–890.
Guitreau, M., Blichert-Toft, J., Martin, H., Mojzsis, S.J., 2012. Hafnium isotope evidence from Archean granitic rocks for deep-mantle origin of continental crust. Earth and Planetary Science Letters 337-338, 211–223.
Guitreau, M., Guitreau, M., Guitreau, M., Blichert-Toft, J., Blichert-Toft, J., Blichert-Toft, J., Mojzsis, S.J., Mojzsis, S.J., Mojzsis, S.J., Roth, A., Roth, A.S.G., Roth, A.S.G., Bourdon, B., Bourdon, B., Cates, N.L., Cates, N.L., Bleeker, W., Bleeker, W., 2014. Lu–Hf isotope systematics of the Hadean–Eoarchean Acasta Gneiss Complex (Northwest Territories, Canada). Geochimica et Cosmochimica Acta 135, 251–269.

Hanchar, J.M., van Westrenen, W., 2007. Rare Earth Element Behavior in Zircon-Melt Systems. Elements.
Harrison, T.M., 2005. Heterogeneous Hadean Hafnium: Evidence of Continental Crust at 4.4 to 4.5 Ga. Science 310, 1947–1950.
Harrison, T.M., 2009. The hadean crust: Evidence from >4 ga zircons. Annual Review of Earth and Planetary Sciences 37, 479–505.
Harrison, T.M., Schmitt, A.K., McCulloch, M.T., Lovera, O.M., 2008. Early (≥ 4.5 Ga) formation of terrestrial crust: Lu-Hf, $\delta^{18}O$, and Ti thermometry results for Hadean zircons. Earth and Planetary Science Letters 268, 476–486.
Hiess, J., Bennett, V.C., Nutman, A.P., Williams, I.S., 2009. In situ U–Pb, O and Hf isotopic compositions of zircon and olivine from Eoarchaean rocks, West Greenland: New insights to making old crust. Geochimica et Cosmochimica Acta 73, 4489–4516.
Hiess, J., Bennett, V.C., Nutman, A.P., Williams, I.S., 2011. Archaean fluid-assisted crustal cannibalism recorded by low δ18O and negative εHf(T) isotopic signatures of West Greenland granite zircon. Contributions to Mineralogy and Petrology 161, 1027–1050.
Hiess, J., Condon, D.J., McLean, N., Noble, S.R., 2012. 238U/ 235U systematics in terrestrial uranium-bearing minerals. Science 335, 1610–1614.
Hinton, R.W., Upton, B.G.J., 1991. The chemistry of zircon: Variations within and between large crystals from syenite and alkali basalt xenoliths. Geochimica et Cosmochimica Acta 55, 3287–3302.
Hodges, K.V., A Bowring, S., 1995. Multi-Stage Thermal History of the 4.0 Ga Acasta Gneisses, in:. Presented at the American Geophysical Union Annual Meeting, p. F708.
Hoffmann, J.E., Münker, C., Næraa, T., Rosing, M.T., Herwartz, D., Garbe-Schönber, D., Svahnberg, H., 2011. Geochimica et Cosmochimica Acta 75, 4157–4178.
Hopkins, M., Harrison, T.M., Manning, C.E., 2008. Low heat flow inferred from >4 Gyr zircons suggests Hadean plate boundary interactions. Nature 456, 493–496.
Hopkins, M.D., Harrison, T.M., Manning, C.E., 2010. Constraints on Hadean geodynamics from mineral inclusions in >4Ga zircons. Earth and Planetary Science Letters 298, 367–376.
Hoskin, P.W.O., 2000. Patterns of chaos: fractal statistics and the oscillatory chemistry of zircon. Geochimica et Cosmochimica Acta 64, 1905–1923.
Hoskin, P.W.O., 2003. The Composition of Zircon and Igneous and Metamorphic Petrogenesis. Reviews in Mineralogy and Geochemistry 53, 27–62.
Hoskin, P.W.O., Kinny, P.D., Wyborn, D., Chappell, B.W., 2000. Identifying Accessory Mineral Saturation during Differentiation in Granitoid Magmas: an Integrated Approach. Journal of Petrology 1–32.
Ickert, R.B., 2013. Algorithms for Estimating Uncertainties in Initial Radiogenic Isotope Ratios and Model Ages. Chemical Geology 1–43.
Iizuka, T., Hirata, T., 2005. Improvements of precision and accuracy in in situ Hf isotope microanalysis of zircon using the laser ablation-MC-ICPMS technique. Chemical Geology.
Iizuka, T., Horie, K., Komiya, T., Maruyama, S., Hirata, T., Hidaka, H., Windley, B.F., 2006. 4.2 Ga zircon xenocryst in an Acasta gneiss from northwestern Canada: Evidence for early continental crust. Geology 34, 245–248.
Iizuka, T., Komiya, T., Johnson, S.P., Kon, Y., Maruyama, S., Hirata, T., 2009. Reworking of Hadean crust in the Acasta gneisses, northwestern Canada: Evidence from in-situ Lu–Hf isotope analysis of zircon. Chemical Geology 259, 230–239.
Iizuka, T., Komiya, T., Ueno, Y., Katayama, I., Uehara, Y., Maruyama, S., Hirata, T., Johnson, S.P., Dunkley, D.J., 2007. Geology and zircon geochronology of the Acasta Gneiss Complex, northwestern Canada: New constraints on its tectonothermal history. Precambrian Res 153, 179–208.
Iizuka, T., Nakai, S., Sahoo, Y.V., Takamasa, A., Hirata, T., Maruyama, S., 2010. The tungsten isotopic composition of Eoarchean rocks: Implications for early silicate differentiation and core–mantle

interaction on Earth. Earth and Planetary Science Letters 291, 189–200.
Isachsen, C.E., Bowring, S.A., Padgham, W.A., 1991. U-Pb Zircon Geochronology of the Yellowknife Volcanic Belt, NWT, Canada: New Constraints on the Timing and Duration of Greenstone Belt Magmatism. The Journal of Geology 99, 55–67.
Jaffey, A.H., Flynn, K.F., Glendenin, L.E., Bentley, W.C., Essling, A.M., 1971. Precision measurement of half-lives and specific activities of U235 and U238. Physical Review C 4, 1889–1906.
Jakobsson, S., Jonasson, K., Sigurdsson, I., 2008. The three igneous rock series of Iceland. Jokull 58, 1–22.
Jenner, G.A., Fryer, B.J., McLennan, S.M., 1981. Geochemistry of the Archean Yellowknife Supergroup. Geochimica et Cosmochimica Acta 45, 1111–1129.
Johnson, D.M., Hooper, P.R., Conrey, R.M., 1999. XRF analysis of rocks and minerals for major and trace elements on a single low dilution Li-tetraborate fused bead. Advances in X-ray Analysis 41, 843–867.
Jónasson, K., Jonasson, K., 2005. Magmatic evolution of the Heiðarsporður ridge, NE-Iceland. Journal of Volcanology and Geothermal Research 147, 109–124.
Kamber, B.S., 2007. Chapter 2.4 The Enigma of the Terrestrial Protocrust: Evidence for Its Former Existence and the Importance of Its Complete Disappearance, in: Developments in Precambrian Geology, Developments in Precambrian Geology. Elsevier, pp. 75–89.
Kamber, B.S., 2010. Archean mafic–ultramafic volcanic landmasses and their effect on ocean–atmosphere chemistry. Chemical Geology 274, 19–28.
Kamber, B.S., 2015. The evolving nature of terrestrial crust from the Hadean, through the Archaean, into the Proterozoic. Precambrian Res 258, 48–82.
Kamber, B.S., Collerson, K.D., Moorbath, S., Whitehouse, M.J., 2003. Inheritance of early Archaean Pb-isotope variability from long-lived Hadean protocrust. Contributions to Mineralogy and Petrology 145, 25–46.
Kamber, B.S., Greig, A., Collerson, K.D., 2005. A new estimate for the composition of weathered young upper continental crust from alluvial sediments, Queensland, Australia. Geochimica et Cosmochimica Acta 69, 1041–1058.
Kasting, J., 1993. Earth's early atmosphere. Science 259, 920–926.
Knaack, C., Cornelius, S., Hooper, P.R., 1994. Trace element analyses of rocks and minerals by ICP-MS. Open File Report. Department of Geology.
Kroner, A., 1985. Evolution of the Archean Continental Crust. Annual Review of Earth and Planetary Sciences 13, 49–74.
Kemp, A.I.S., Hickman, A.H., Kirkland, C.L., Vervoort, J.D., 2015. Hf isotopes in detrital and inherited zircons of the Pilbara Craton provide no evidence for Hadean continents. Precambrian Res 261, 112–126.
Kemp, A.I.S., Wilde, S.A., Hawkesworth, C.J., Coath, C.D., Nemchin, A., Pidgeon, R.T., Vervoort, J.D., DuFrane, S.A., 2010. Hadean crustal evolution revisited: New constraints from Pb–Hf isotope systematics of the Jack Hills zircons. Earth and Planetary Science Letters 296, 45–56.
Ketchum, J., Bleeker, W., Stern, R.A., 2004. Evolution of an Archean basement complex and its autochthonous cover, southern Slave Province, Canada. Precambrian Res 135, 149–176.
Ketchum, J., Reimink, J.R., Chacko, T., Bauer, A., Reimink, R., Regional Investigation of the Acasta Gneiss Complex, western Slave Craton. Northwest Territories Geoscience Forum, 2013, Oral Presentation.
Krogh, T.E., 1973. A low-contamination method for hydrothermal decomposition of zircon and extraction of U and Pb for isotopic age determinations. Geochimica et Cosmochimica Acta 37, 485–494.
Kroner, A., 1985. Evolution of the Archean Continental Crust. Annual Review of Earth and Planetary Sciences 13, 49–74.
LeCheminant, A.N., Heaman, L.M., 1989. Mackenzie igneous events, Canada: Middle Proterozoic

hotspot magmatism associated with ocean opening. Earth and Planetary Science Letters 96, 38–48.
Lenting, C., Geisler, T., Gerdes, A., Kooijman, E., Scherer, E.E., Zeh, A., 2010. The behavior of the Hf isotope system in radiation-damaged zircon during experimental hydrothermal alteration. American Mineralogist 95, 1343–1348.
Ludwig, K.R., 2001. Isoplot 3.75: A Geochronological Toolkit for Microsoft Excel. BGC Special Publications 5.
Ludwig, K.R., 2009. SQUID2: A User's Manual. Berkeley Geochronology Center Special Publication 110.
Mancini, A., Mattsson, H.B., Bachmann, O., 2015. Origin of the compositional diversity in the basalt-to-dacite series erupted along the Heiðarsporður ridge, NE Iceland. Journal of Volcanology and Geothermal Research 301, 116–127.
McDonough, W.F., Sun, S.S., 1995. The composition of the Earth. Chemical Geology 120, 223–253.
McLean, N.M., Bowring, J.F., Bowring, S.A., 2011. An algorithm for U□Pb isotope dilution data reduction and uncertainty propagation. Geochemistry, Geophysics, Geosystems 12, 1-26.
Martin, H., 1986. Effect of steeper Archean geothermal gradient on geochemistry of subduction-zone magmas. Geology 14, 753–756.
Martin, H., 1987. Petrogenesis of Archaean Trondhjemites, Tonalites, and Granodiorites from Eastern Finland: Major and Trace Element Geochemistry. Journal of Petrology 28, 921–953.
Martin, H., 1999. Adakitic magmas: modern analogues of Archaean granitoids. Lithos 46, 411–429.
Martin, H., Moyen, J.-F., Guitreau, M., Blichert-Toft, J., 2014. Why Archaean TTG cannot be generated by MORB melting in subduction zones. Lithos 198-199, 1–13.
Martin, E., Martin, H., Sigmarsson, O., 2008. Could Iceland be a modern analogue for the Earth's early continental crust? Terra Nova 20, 463–468.
Martin, E., Martin, H., Sigmarsson, O., 2010. Comment on "Continental geochemical signatures in dacites from Iceland and implications for models of early Archaean crust formation" by Willbold, M., Hegner, E., Stracke A. and Rocholl A. Earth and Planetary Science Letters 293, 218–219.
Mattinson, J.M., 2005. Zircon U–Pb chemical abrasion ("CA-TIMS") method: Combined annealing and multi-step partial dissolution analysis for improved precision and accuracy of zircon ages. Chemical Geology 220, 47–66.
Mojzsis, S.J., Cates, N.L., Caro, G., Trail, D., Abramov, O., Guitreau, M., Blichert-Toft, J., Hopkins, M.D., Bleeker, W., 2014. Component geochronology in the polyphase ca. 3920Ma Acasta Gneiss. Geochimica et Cosmochimica Acta 133, 68–96.
Mojzsis, S.J., Harrison, T.M., Pidgeon, R.T., 2001. Oxygen-isotope evidence from ancient zircons for liquid water at the Earth's surface 4,300 Myr ago. Nature 409, 178–181.
Moorbath, S., O'Nions, R. K., Pankhurst, R. J., 1973 Early Archaean Age for the Isua Iron Formation, West Greenland. Nature 245, 138–139.
Moorbath, S., Whitehouse, M.J., Kamber, B.S., 1997. Extreme Nd-isotope heterogeneity in the early Archaean - Fact or fiction? Case histories from northern Canada and West Greenland. Chemical Geology 135, 213–231.
Moyen, J.-F., 2011. The composite Archaean grey gneisses: Petrological significance, and evidence for a non-unique tectonic setting for Archaean crustal growth. Lithos 123, 21–36.
Moyen, J.-F., Martin, H., 2012. Forty years of TTG research. Lithos 148, 312–336.
Moyen, J.-F., Stevens, G., 2006. Experimental constraints on TTG petrogenesis: Implications for Archean geodynamics, Geophysical Monograph Series.
Moyen, J.-F., Stevens, G., Kisters, A.F.M., Belcher, R.W., 2007. TTG Plutons of the Barberton Granitoid-Greenstone Terrain, South Africa, in: Developments in Precambrian Geology, Developments in Precambrian Geology. Elsevier, pp. 607–667.
Muehlenbachs, K., Anderson, A.T., Sigvaldason, G.E., 1974. Low-O18 basalts from Iceland. Geochimica et Cosmochimica Acta 38, 577–588. doi:10.1016/0016-7037(74)90042-8
Nair, R., Chacko, T., 2008. Role of oceanic plateaus in the initiation of subduction and origin of

continental crust. Geology 36, 583–586.
Nebel, O., Rapp, R.P., Yaxley, G.M., 2013. The role of detrital zircons in Hadean crustal research. Lithos 190-191, 313–327.
Nemchin, A.A., Pidgeon, R.T., Whitehouse, M.J., 2006. Re-evaluation of the origin and evolution of >4.2 Ga zircons from the Jack Hills metasedimentary rocks. Earth and Planetary Science Letters 244, 218–233.
Nicholson, H., Condomines, M., Fitton, J.G., Fallick, A.E., Gronveld, K., Rogers, G., 1991. Geochemical and Isotopic Evidence for Crustal Assimilation Beneath Krafla, Iceland. Journal of Petrology 32, 1005–1020.
Niu, Y., Regelous, M., Wendt, I.J., Batiza, R., O'Hara, M.J., 2002. Geochemistry of near-EPR seamounts: importance of source vs. process and the origin of enriched mantle component. Earth and Planetary Science Letters 199, 327–345.
Norman, M.D., 2009. The Lunar Cataclysm: Reality or "Mythconception"? Elements 5, 23–28.
Nutman, A.P., Friend, C.R.L., Horie, K., Hidaka, H., 2007. Chapter 3.3 The Itsaq Gneiss Complex of Southern West Greenland and the Construction of Eoarchaean Crust at Convergent Plate Boundaries, Developments in Precambrian Geology, Developments in Precambrian Geology. Elsevier.
Nutman, A.P., McGregor, V.R., Shiraishi, K., Friend, C.R.L., Bennett, V.C., Kinny, P.D., 2002. □3850 Ma BIF and mafic inclusions in the early Archaean Itsaq Gneiss Complex around Akilia, southern West Greenland? The difficulties of precise dating of zircon-free protoliths in migmatites. Precambrian Res 117, 185–224.
O'Neil, J., Carlson, R.W., Francis, D., Stevenson, R.K., 2008. Neodymium-142 evidence for Hadean mafic crust. Science 321, 1828–1831.
O'Neill, C., Debaille, V., 2014. The evolution of Hadean–Eoarchaean geodynamics. Earth and Planetary Science Letters 406, 49–58.
O'Neil, J., Boyet, M., Carlson, R.W., Paquette, J.-L., 2013. Half a billion years of reworking of Hadean mafic crust to produce the Nuvvuagittuq Eoarchean felsic crust. Earth and Planetary Science Letters 379, 13–25.
O'Neil, J., Carlson, R.W., Paquette, J.-L., Francis, D., 2012. Formation age and metamorphic history of the Nuvvuagittuq Greenstone Belt. Precambrian Res 220-221, 23–44.
O'Neill, C., Lenardic, A., Moresi, L., Torsvik, T.H., 2007. Episodic Precambrian subduction. Earth and Planetary Science Letters.
Onuma, N., Higuchi, H., Wakita, H., Nagasawa, H., 1968. Trace element partition between two pyroxenes and the host lava. Earth and Planetary Science Letters 5, 47–51.
Paces, J.B., Miller, J.D., Jr., 1993. Precise U-Pb ages of Duluth Complex and related mafic intrusions, northeastern Minnesota: Geochronological insights to physical, petrogenetic, paleomagnetic, and tectonomagmatic processes associated with the 1.1 Ga Midcontinent Rift System. Journal of Geophysical Research 98, 13997.
Padgham, W.A., Fyson, W.K., 1992. The Slave Province: a distinct Archean craton. Can. J. Earth Sci. 29, 2072–2086.
Page, F.Z., Ushikubo, T., Kita, N.T., Riciputi, L.R., Valley, J.W., 2007. High-precision oxygen isotope analysis of picogram samples reveals 2 m gradients and slow diffusion in zircon. American Mineralogist 92, 1772–1775.
Peck, W., Valley, J., 2003. Slow oxygen diffusion rates in igneous zircons from metamorphic rocks. American Mineralogist 88, 1003-1014.
Prowatke, S., Klemme, S., 2005. Effect of melt composition on the partitioning of trace elements between titanite and silicate melt. Geochimica et Cosmochimica Acta 69, 695–709.
Rapp, R.P., Rapp, R., Watson, E.B., Miller, C.F., 1991. Partial melting of amphibolite/eclogite and the origin of Archean trondhjemites and tonalites. Precambrian Res 51, 1–25.
Rasmussen, B., Fletcher, I.R., Muhling, J.R., Gregory, C.J., Wilde, S.A., 2011. Metamorphic

replacement of mineral inclusions in detrital zircon from Jack Hills, Australia: Implications for the Hadean Earth. Geology 39, 1143–1146.
Reimink, J.R., Chacko, T., Stern, R.A., Heaman, L.M., 2014. Earth's earliest evolved crust generated in an Iceland-like setting. Nature Geoscience 7, 529–533.
Rizo, H., Boyet, M., Blichert-Toft, J., O'Neil, J., Rosing, M.T., Paquette, J.-L., 2012. The elusive Hadean enriched reservoir revealed by 142Nd deficits in Isua Archaean rocks. Nature 491, 96–99.
Rollinson, H.R., 1993. Using Geochemical Data. Pearson Education Limited.
Roth, A.S.G., Bourdon, B., Mojzsis, S.J., Rudge, J.F., Guitreau, M., Blichert-Toft, J., 2014. Combined 147,146Sm- 143,142Nd constraints on the longevity and residence time of early terrestrial crust. Geochem. Geophys. Geosyst. 15, 2329–2345.
Roth, A.S.G., Bourdon, B., Mojzsis, S.J., Touboul, M., Sprung, P., Guitreau, M., Blichert-Toft, J., 2013. Inherited 142Nd anomalies in Eoarchean protoliths. Earth and Planetary Science Letters 361, 50–57.
Sambridge, M.S., Compston, W., 1994. Mixture modeling of multi-component data sets with application to ion-probe zircon ages. Earth and Planetary Science Letters 128, 373–390.
Sano, Y., Terada, K., Fukuoka, T., 2002. High mass resolution ion microprobe analysis of rare earth elements in silicate glass, apatite and zircon: lack of matrix dependency. Chemical Geology 184,
Scherer, E., Munker, C., Mezger, K., 2001. Calibration of the Lutetium-Hafnium Clock. Science 293, 683–687.
Schmidberger, S.S., Simonetti, A., Heaman, L.M., Creaser, R.A., Whiteford, S., 2007. Lu–Hf, in-situ Sr and Pb isotope and trace element systematics for mantle eclogites from the Diavik diamond mine: Evidence for Paleoproterozoic subduction beneath the Slave craton, Canada. Earth and Planetary Science Letters 254, 55–68.
Simonetti, A., Heaman, L.M., Chacko, T., Banerjee, N.R., 2006. In situ petrographic thin section U-Pb dating of zircon, monazite, and titanite using laser ablation-MC-ICP-MS. International Journal of Mass Spectrometry 253, 87–97.
Simonetti, A., Heaman, L.M., Hartlaub, R.P., Creaser, R.A., MacHattie, T.G., Böhm, C., 2005. U-Pb zircon dating by laser ablation-MC-ICP-MS using a new multiple ion counting Faraday collector array. Journal of Analytical Atomic Spectrometry 20, 677–686.
Sircombe, K.N., Bleeker, W., Stern, R.A., 2001. Detrital zircon geochronology and grain-size analysis of a □2800 Ma Mesoarchean proto-cratonic cover succession, Slave Province, Canada. Earth and Planetary Science Letters 189, 207–220.
Sláma, J., Košler, J., Condon, D.J., Crowley, J.L., Gerdes, A., Hanchar, J.M., Horstwood, M.S.A., Morris, G.A., Nasdala, L., Norberg, N., Schaltegger, U., Schoene, B., Tubrett, M.N., Whitehouse, M.J., 2008. Plešovice zircon — A new natural reference material for U–Pb and Hf isotopic microanalysis. Chemical Geology 249, 1–35.
Smithies, R.H., Van Kranendonk, M.J., Champion, D.C., 2005. It started with a plume - Early Archaean basaltic proto-continental crust. Earth and Planetary Science Letters 238, 284–297.
Smithies, R.H., Champion, D.C., Van Kranendonk, M.J., 2009. Formation of Paleoarchean continental crust through infracrustal melting of enriched basalt. Earth and Planetary Science Letters 281, 298–306.
Söderlund, U., Patchett, P.J., Vervoort, J.D., Isachsen, C.E., 2004. The 176Lu decay constant determined by Lu–Hf and U–Pb isotope systematics of Precambrian mafic intrusions. Earth and Planetary Science Letters 219, 311–324.
Stacey, J.S., Kramers, J.D., 1975. Approximation of terrestrial lead isotope evolution by a two-stage model. Earth and Planetary Science Letters 26, 207–221.
Stern, R.A., Amelin, Y., 2003. Assessment of errors in SIMS zircon U–Pb geochronology using a natural zircon standard and NIST SRM 610 glass. Chemical Geology 197, 111–142.
Stern, R., Bleeker, W., 1998. Age of the world's oldest rocks refined using Canada's SHRIMP: The Acasta Gneiss Complex, Northwest Territories, Canada. Geosci Can 25, 27–31.
Stern, R.A., Bodorkos, S., Kamo, S.L., Hickman, A.H., Corfu, F., 2009. Measurement of SIMS

Instrumental Mass Fractionation of Pb Isotopes During Zircon Dating. Geostandards and Geoanalytical Research 33, 145–168.
St Onge, M.R., King, J.E., Lalonde, A.E., 1988. Geology, east-central Wopmay Orogen, District of Mackenzie, Northwest Territories (No. 1923), Geological Survey of Canada Open-File Report.
Tanaka, T., Togashi, S., Kamioka, H., Amakawa, H., Kagami, H., Hamamoto, T., Yuhara, M., Orihashi, Y., Yoneda, S., Shimizu, H., Kunimaru, T., Takahashi, K., Yanagi, T., Nakano, T., Fujimaki, H., Shinjo, R., Asahara, Y., Tanimizu, M., Dragusanu, C., 2000. JNdi-1: a neodymium isotopic reference in consistency with LaJolla neodymium. Chemical Geology 168, 279–281.
Taylor, H.P., Sheppard, S.M.F., 1986. Igneous rocks; I Processes of isotopic fractionation and isotope systematics. Reviews in Mineralogy and Geochemistry 16, 227–271.
Taylor, D.J., McKeegan, K.D., Harrison, T.M., 2009. Lu–Hf zircon evidence for rapid lunar differentiation. Earth and Planetary Science Letters 279, 157–164.
Tera, F., Papanastassiou, D.A., Wasserburg, G.J., 1974. Isotopic evidence for a terminal lunar cataclysm. Earth and Planetary Science Letters 22, 1–21.
Thirlwall, M.F., Anczkiewicz, R., 2004. Multidynamic isotope ratio analysis using MC–ICP–MS and the causes of secular drift in Hf, Nd and Pb isotope ratios. International Journal of Mass Spectrometry 235, 59–81.
Tiepolo, M., Oberti, R., Zanetti, A., Vannucci, R., Foley, S.F., 2007. Trace-Element Partitioning Between Amphibole and Silicate Melt. Reviews in Mineralogy and Geochemistry 67, 417–452.
Trail, D., Watson, E.B., Tailby, N.D., 2011. The oxidation state of Hadean magmas and implications for early Earth's atmosphere. Nature 480, 79–82.
Unterschutz, J.L., Creaser, R.A., Erdmer, P., Thompson, R.I., Daughtry, K.L., 2002. North American margin origin of Quesnel terrane strata in the southern Canadian Cordillera: Inferences from geochemical and Nd isotopic characteristics of Triassic metasedimentary rocks. Geological Society of America Bulletin 114, 462–475.
Valley, J.W., Kinny, P.D., Schulze, D.J., Spicuzza, M.J., 1998. Zircon megacrysts from kimberlite: oxygen isotope variability among mantle melts. Contributions to Mineralogy and Petrology 133, 1–11.
Valley, J.W., Lackey, J.S., Cavosie, A.J., Clechenko, C.C., Spicuzza, M.J., Basei, M.A.S., Bindeman, I.N., Ferreira, V.P., Sial, A.N., Peck, W.H., Sinha, A.K., Wei, C.S., 2005. 4.4 billion years of crustal maturation: oxygen isotope ratios of magmatic zircon. Contributions to Mineralogy and Petrology 150, 561–580.
Valley, J.W., Cavosie, A.J., Ushikubo, T., Reinhard, D.A., Lawrence, D.F., Larson, D.J., Clifton, P.H., Kelly, T.F., Wilde, S.A., Moser, D.E., Spicuzza, M.J., 2014. Hadean age for a post-magma-ocean zircon confirmed by atom-probe tomography. Nature Geoscience.
Van Kranendonk, M.J., 2007. Chapter 8.6 Tectonics of Early Earth, Developments in Precambrian Geology.
Van Kranendonk, M.J., 2010. Two types of Archean continental crust: Plume and plate tectonics on early Earth. American Journal of Science 310, 1187–1209.
Wasserburg, G.J., Jacousen, S.B., DePaolo, D.J., McCulloch, M.T., Wen, T., 1981. Precise determination of ratios, Sm and Nd isotopic abundances in standard solutions. Geochimica et Cosmochimica Acta 45, 2311–2323.
Whitehouse, M., Nagler, T., Moorbath, S., Kramers, J., Kamber, B., Frei, R., 2001. Priscoan (4.00-4.03 Ga) orthogneisses from northwestern Canada - by Samuel A. Bowring and Ian S. Williams: discussion. Contributions to Mineralogy and Petrology 141, 248–250.
Wood, D.A., 1978. Major and Trace Element Variations in the Tertiary Lavas of Eastern Iceland and their Significance with respect to the Iceland Geochemical Anomaly. Journal of Petrology 19, 393–436.
Wotzlaw, J.F., Schaltegger, U., Frick, D.A., Dungan, M.A., Gerdes, A., Günther, D., 2013. Tracking the evolution of large-volume silicic magma reservoirs from assembly to supereruption. Geology 41,

867–870.
Wilde, S.A., Valley, J.W., Peck, W.H., Graham, C.M., 2001. Evidence from detrital zircons for the existence of continental crust and oceans on the Earth 4.4 Gyr ago. Nature 409, 175–178.
Willbold, M., Hegner, E., Stracke, A., Rocholl, A., 2009. Continental geochemical signatures in dacites from Iceland and implications for models of early Archaean crust formation. Earth and Planetary Science Letters 279, 218–219.
Willbold, M., Mojzsis, S.J., Chen, H.W., Elliott, T., 2015. Tungsten isotope composition of the Acasta Gneiss Complex. Earth and Planetary Science Letters 419, 168–177.
Wood, D.A., 1978. Major and Trace Element Variations in the Tertiary Lavas of Eastern Iceland and their Significance with respect to the Iceland Geochemical Anomaly. Journal of Petrology 19, 393–436
Wu, F.-Y., Yang, Y.-H., Xie, L.-W., Yang, J.-H., Xu, P., 2006. Hf isotopic compositions of the standard zircons and baddeleyites used in U–Pb geochronology. Chemical Geology 234, 105–126.
Yuan, H., Gao, S., Dai, M., Zong, C., Günther, D., Fontaine, G., Liu, X., Diwu, C., 2008. Simultaneous determinations of U–Pb age, Hf isotopes and trace element compositions of zircon by excimer laser-ablation quadrupole and multiple-collector ICP-MS. Chemical Geology 247, 100–118.
Zegers, T.E., van Keken, P.E., 2001. Middle Archean continent formation by crustal delamination. Geology 29, 1083–1086.

Appenidix Table 1. LA-ICPMS zircon U-Pb data

Spot Name	Sample Name	Date	Method	Zircon Phase	206Pb (cps)	204Pb (cps)	206Pb/204Pb	207Pb/206Pb	2σ	207Pb/235U
137-1A	JR12-137	15-Oct-14	MOUNT	ign	206023	1	206023	0.35916	0.00554	32.36087
137-1B	JR12-137	15-Oct-14	MOUNT	ign	392335	19	20347	0.33534	0.00526	26.70790
137-1C	JR12-137	15-Oct-14	MOUNT	ign	227813	16	13812	0.40170	0.00598	46.00084
137-1D	JR12-137	15-Oct-14	MOUNT	ign	242981	42	5781	0.38454	0.00578	38.52678
137-2A	JR12-137	15-Oct-14	MOUNT	ign	390888	15	25692	0.41326	0.00615	48.95564
137-2B	JR12-137	15-Oct-14	MOUNT	ign	318538	32	9911	0.39078	0.00584	47.10558
137-2C	JR12-137	15-Oct-14	MOUNT	ign	354157	15	23505	0.41273	0.00626	51.88219
137-2D	JR12-137	15-Oct-14	MOUNT	ign	455530	22	21085	0.41026	0.00599	49.36877
137-2E	JR12-137	15-Oct-14	MOUNT	ign	305741	15	20767	0.37015	0.00551	40.04805
137-3A	JR12-137	15-Oct-14	MOUNT	ign	297334	36	8203	0.29071	0.00723	29.27679
137-4A	JR12-137	15-Oct-14	MOUNT	ign	244824	29	8575	0.28985	0.00439	26.07288
137-4B	JR12-137	15-Oct-14	MOUNT	ign	525236	23	22945	0.38978	0.00610	40.92828
137-5A	JR12-137	15-Oct-14	MOUNT	ign	310627	25	12447	0.35448	0.00527	35.28936
137-6A	JR12-137	15-Oct-14	MOUNT	ign	318585	23	13841	0.37827	0.00556	39.74581
137-7A	JR12-137	15-Oct-14	MOUNT	ign	322455	27	11827	0.38466	0.00597	43.15509
137-8A	JR12-137	15-Oct-14	MOUNT	ign	340240	32	10509	0.25514	0.00383	21.80569
141-1A	JR12-141	16-Oct-12	Thin Section	ign	1056529	25	41750	0.28837	0.00439	24.55456
141-1B	JR12-141	16-Oct-12	Thin Section	rim	1329326	67	19877	0.42157	0.00621	46.60808
141-1C	JR12-141	16-Oct-12	Thin Section	rim	1027270	40	25888	0.28998	0.00443	24.73139
141-1D	JR12-141	16-Oct-12	Thin Section	ign	998693	99	10081	0.38903	0.00644	38.30191
141-1E	JR12-141	16-Oct-12	Thin Section	rim	1209377	52	23054	0.28119	0.00422	23.07215
141-1F	JR12-141	16-Oct-12	Thin Section	ign	94725	151	627	0.37655	0.00583	29.04981
141-1G	JR12-141	16-Oct-12	Thin Section	ign	882550	47	18929	0.35090	0.00559	34.56209
141-1H	JR12-141	16-Oct-12	Thin Section	ign	720421	44	16420	0.28068	0.00424	23.88699
141-1I	JR12-141	16-Oct-12	Thin Section	ign	1064600	109	9771	0.28619	0.00460	24.84144
141-2A	JR12-141	16-Oct-12	Thin Section	ign	671589	53	12759	0.29837	0.00442	27.39431
141-2B	JR12-141	16-Oct-12	Thin Section	ign	531776	37	14542	0.29379	0.00446	25.33353
141-2C	JR12-141	16-Oct-12	Thin Section	ign	599790	102	5908	0.23985	0.00424	13.19223
141-3A	JR12-141	16-Oct-12	Thin Section	ign	899703	91	9893	0.37852	0.00671	31.94672
141-4A	JR12-141	16-Oct-12	Thin Section	ign	174998	80	2186	0.41209	0.00652	39.07181
141-4B	JR12-141	16-Oct-12	Thin Section	ign	91219	62	1478	0.42528	0.00654	44.49082
141-4C	JR12-141	16-Oct-12	Thin Section	ign	328119	69	4774	0.25882	0.00400	21.18241
141-4D	JR12-141	16-Oct-12	Thin Section	ign	98860	118	839	0.39941	0.00750	35.76383
141-5A1	JR12-141	16-Oct-12	Thin Section	ign	1120697	97	11543	0.38241	0.00585	42.05148
141-5A2	JR12-141	16-Oct-12	Thin Section	ign	860254	71	12187	0.31082	0.00769	29.84709
141-5A3	JR12-141	16-Oct-12	Thin Section	ign	1257461	83	15149	0.28732	0.00447	28.69365

Appenidix Table 1. LA-ICPMS zircon U-Pb data

Spot Name	Sample Name	Date	Method	Zircon Phase	206Pb (cps)	204Pb (cps)	206Pb/204Pb	207Pb/206Pb	2σ	207Pb/235U
141-5B1	JR12-141	16-Oct-12	Thin Section	rim	1433588	65	22054	0.29352	0.00459	26.52513
141-5B2	JR12-141	16-Oct-12	Thin Section	ign	923236	83	11189	0.27637	0.00424	25.42168
141-6A	JR12-141	16-Oct-12	Thin Section	ign	709171	83	8558	0.41025	0.00607	47.22931
141-6B	JR12-141	16-Oct-12	Thin Section	ign	788730	34	23326	0.41525	0.00666	44.81336
141-6C	JR12-141	16-Oct-12	Thin Section	ign	443432	42	10509	0.31470	0.00510	26.82534
145-11A	JR12-145	17-Oct-12	Thin Section	ign	522403	139	3755	0.40664	0.00367	48.15662
145-11B	JR12-145	17-Oct-12	Thin Section	ign	1123245	170	6617	0.35397	0.00599	38.55384
145-11C	JR12-145	17-Oct-12	Thin Section	osc	383250	107	3598	0.41590	0.00389	47.98766
145-11D	JR12-145	17-Oct-12	Thin Section	ign	910214	136	6702	0.37504	0.00571	30.39107
145-11E	JR12-145	17-Oct-12	Thin Section	ign	377727	76	4973	0.40997	0.00362	47.61636
145-12A	JR12-145	17-Oct-12	Thin Section	osc	408984	131	3119	0.40991	0.00385	45.65104
145-12B	JR12-145	17-Oct-12	Thin Section	ign	1351629	190	7125	0.24434	0.00406	17.03302
145-2A	JR12-145	17-Oct-12	Thin Section	ign	227678	122	1861	0.34793	0.00416	27.95777
145-2B	JR12-145	17-Oct-12	Thin Section	ign	475286	147	3235	0.30774	0.00559	26.81675
145-3A	JR12-145	17-Oct-12	Thin Section	ign	1031979	126	8159	0.41743	0.00513	45.26472
145-3B	JR12-145	17-Oct-12	Thin Section	osc	883863	106	8364	0.41078	0.00439	43.37430
145-3C	JR12-145	17-Oct-12	Thin Section	ign	775214	132	5854	0.30394	0.00278	26.39465
145-3D	JR12-145	17-Oct-12	Thin Section	osc	439924	132	3338	0.40924	0.00444	46.56198
145-7A	JR12-145	17-Oct-12	Thin Section	meta	1908045	214	8935	0.34670	0.00318	29.85153
145-7B	JR12-145	17-Oct-12	Thin Section	meta	1092582	200	5454	0.30786	0.00402	29.53644
145-7C	JR12-145	17-Oct-12	Thin Section	meta	700615	205	3423	0.37442	0.00656	35.90080
145-9A	JR12-145	17-Oct-12	Thin Section	ign	560816	172	3256	0.40333	0.00452	45.21037
146-10A	JR12-146	15-Oct-12	Thin Section	rim	959817	78	12374	0.25946	0.00353	21.87200
146-10B	JR12-146	15-Oct-12	Thin Section	rim	691833	86	8018	0.30149	0.00417	25.39622
146-1A	JR12-146	15-Oct-12	Thin Section	ign	1236723	1	1197276	0.42390	0.00570	48.26570
146-1B	JR12-146	15-Oct-12	Thin Section	ign	2163524	27	79368	0.36444	0.00543	30.14301
146-1C	JR12-146	15-Oct-12	Thin Section	ign	1887392	35	53721	0.27247	0.00427	16.93558
146-2A	JR12-146	15-Oct-12	Thin Section	rim	1101364	8	129685	0.29089	0.00395	25.94285
146-5A	JR12-146	15-Oct-12	Thin Section	rim	1503730	11	134617	0.30975	0.00446	25.63512
146-5B	JR12-146	15-Oct-12	Thin Section	rim	1265387	1	1265387	0.30519	0.00414	29.17759
146-5C	JR12-146	15-Oct-12	Thin Section	rim	2097571	5	395242	0.38170	0.00526	44.13488
146-6A	JR12-146	15-Oct-12	Thin Section	rim	844702	62	13557	0.26282	0.00370	23.61268
146-6B	JR12-146	15-Oct-12	Thin Section	rim	870021	160	5428	0.26205	0.00385	21.18489
146-7A	JR12-146	15-Oct-12	Thin Section	rim	819850	79	10386	0.41858	0.00561	49.38608
146-7B	JR12-146	15-Oct-12	Thin Section	rim	1209626	134	9022	0.41506	0.00585	43.26004
146-7C	JR12-146	15-Oct-12	Thin Section	rim	410414	71	5745	0.28351	0.00391	25.12843

Appenidix Table 1. LA-ICPMS zircon U-Pb data

Spot Name	Sample Name	Date	Method	Zircon Phase	206Pb (cps)	204Pb (cps)	206Pb/204Pb	207Pb/206Pb	2σ	207Pb/235U
146-8A	JR12-146	15-Oct-12	Thin Section	rim	888659	60	14770	0.27419	0.00380	23.31890
146-8B	JR12-146	15-Oct-12	Thin Section	rim	1106760	86	12837	0.29105	0.00392	25.95059
146-9A	JR12-146	15-Oct-12	Thin Section	ign	973396	63	15536	0.40974	0.00556	41.70728
207-1A	JR13-207	21-May-14	Mount	ign	1957845	112	17496	0.42572	0.00662	45.58285
207-2A	JR13-207	21-May-14	Mount	ign	935632	38	24845	0.41935	0.00461	48.18029
207-2B	JR13-207	21-May-14	Mount	ign	851161	82	10398	0.39514	0.00416	43.93910
207-3A	JR13-207	21-May-14	Mount	ign	676815	69	9875	0.26191	0.00271	23.40135
207-4A	JR13-207	21-May-14	Mount	ign	500558	37	13519	0.30378	0.00315	28.08854
207-4B	JR13-207	21-May-14	Mount	ign	637666	43	14969	0.30378	0.00316	29.41905
207-4C	JR13-207	21-May-14	Mount	ign	572831	64	8895	0.28913	0.00365	18.52863
207-5A	JR13-207	21-May-14	Mount	ign	662313	58	11335	0.28682	0.00297	24.88703
207-6A	JR13-207	21-May-14	Mount	ign	941996	98	9644	0.41340	0.00436	44.08835
207-6B	JR13-207	21-May-14	Mount	ign	948598	96	9918	0.41968	0.00458	47.00428
207-7A	JR13-207	21-May-14	Mount	ign	1100662	77	14363	0.26457	0.00292	23.19574
207-7B	JR13-207	21-May-14	Mount	ign	941617	61	15355	0.26216	0.00324	23.16205
119-1A	JR12-119	20-May-14	Mount	ign	1204809	28	43712	0.39931	0.00440	42.49243
119-2A	JR12-119	20-May-14	Mount	ign	2006902	138	14569	0.38828	0.00428	41.47271
119-3A	JR12-119	20-May-14	Mount	ign	3239523	2	1533983	0.42504	0.00445	46.73913
119-4A	JR12-119	20-May-14	Mount	ign	1965254	27	71527	0.28148	0.00312	25.93332
119-5A	JR12-119	21-May-14	Mount	rim	1012501	62	16462	0.27239	0.00296	24.71731
119-6A	JR12-119	21-May-14	Mount	ign	857076	35	24597	0.42002	0.00475	45.50357
119-6B	JR12-119	21-May-14	Mount	ign	1187280	49	24179	0.41711	0.00471	52.21457
119-7A	JR12-119	21-May-14	Mount	ign	1016563	75	13537	0.28768	0.00305	26.74740
119-2A	JR12-119	16-Oct-12	Thin Section	ign	1278091	103	12444	0.30915	0.00481	23.05598
119-3A	JR12-119	16-Oct-12	Thin Section	ign	1202120	30	39868	0.30005	0.00463	26.73105
119-3B	JR12-119	16-Oct-12	Thin Section	ign	961526	14	67246	0.26507	0.00415	20.50969
119-4A1	JR12-119	16-Oct-12	Thin Section	rim	1107346	41	27007	0.36449	0.00548	39.48241
119-4A2	JR12-119	16-Oct-12	Thin Section	ign	1366937	111	12276	0.25968	0.00437	18.56872
119-4B1	JR12-119	16-Oct-12	Thin Section	ign	1428394	94	15122	0.33978	0.00697	35.14026
119-5A	JR12-119	16-Oct-12	Thin Section	ign	1654501	60	27656	0.36351	0.00749	35.94642
119-6A	JR12-119	16-Oct-12	Thin Section	ign	471492	11	42650	0.41774	0.00618	49.68779
119-6B	JR12-119	16-Oct-12	Thin Section	ign	808166	30	26878	0.38532	0.00604	39.92432
119-6C	JR12-119	16-Oct-12	Thin Section	ign	382399	35	10990	0.37274	0.00574	39.02651
119-6D	JR12-119	16-Oct-12	Thin Section	ign	681830	57	11920	0.37374	0.00576	42.76715
119-6E	JR12-119	16-Oct-12	Thin Section	ign	876391	42	20998	0.29573	0.00497	26.71379
119-7A	JR12-119	16-Oct-12	Thin Section	ign	1072177	42	25539	0.28182	0.00443	23.40717

Spot Name	Sample Name	Date	Method	Zircon Phase	206Pb (cps)	204Pb (cps)	206Pb/204Pb	207Pb/206Pb	2σ	207Pb/235U
127-10A	JR12-127	20-May-14	Mount	ign	113752	46	2473	0.32577	0.00353	32.01454
127-10B	JR12-127	20-May-14	Mount	ign	185878	44	4241	0.32651	0.00346	32.35265
127-1A	JR12-127	20-May-14	Mount	osc	285798	4	66611	0.30515	0.00328	27.88082
127-1B	JR12-127	20-May-14	Mount	osc	266655	1	266655	0.31217	0.00354	28.80816
127-2A	JR12-127	20-May-14	Mount	osc	539079	9	61905	0.30512	0.00351	24.36657
127-3A	JR12-127	20-May-14	Mount	osc	555996	1	555996	0.31885	0.00338	30.38501
127-3B	JR12-127	20-May-14	Mount	osc	523315	27	19737	0.32232	0.00339	31.07083
127-4A	JR12-127	20-May-14	Mount	ign	214108	5	46796	0.32505	0.00344	32.64361
127-5A	JR12-127	20-May-14	Mount	osc	157684	229	687	0.32197	0.00348	32.26667
127-6A	JR12-127	20-May-14	Mount	osc	63799	1	63799	0.31847	0.00395	28.94923
127-7A	JR12-127	20-May-14	Mount	osc	381470	1	381470	0.32480	0.00344	30.67275
127-8A	JR12-127	20-May-14	Mount	ign	189943	92	2061	0.32483	0.00347	28.98722
127-8B	JR12-127	20-May-14	Mount	ign	445897	66	6756	0.31920	0.00353	32.40708
127-9A	JR12-127	20-May-14	Mount	osc	244994	87	2807	0.32367	0.00342	32.23229
127-9B	JR12-127	20-May-14	Mount	osc	366947	62	5948	0.31442	0.00341	30.83372
127-1A	JR12-127	15-Oct-12	Thin Section	ign	502536	6	79868	0.30631	0.00428	24.49136
127-1B	JR12-127	15-Oct-12	Thin Section	ign	747660	39	19042	0.25639	0.00377	12.00178
127-1C	JR12-127	15-Oct-12	Thin Section	ign	823003	27	30225	0.26189	0.00537	14.19331
127-2A	JR12-127	15-Oct-12	Thin Section	ign	1755943	1268	1384	0.24099	0.00401	10.88959
127-4A	JR12-127	15-Oct-12	Thin Section	ign	1258008	169	7440	0.30030	0.00419	25.88181
127-4B	JR12-127	15-Oct-12	Thin Section	ign	1003214	120	8378	0.24993	0.00352	17.68768
127-5A	JR12-127	15-Oct-12	Thin Section	osc	830666	176	4713	0.31882	0.00440	32.78116
127-6A	JR12-127	15-Oct-12	Thin Section	ign	942137	214	4409	0.31232	0.00486	30.43686
127-6B	JR12-127	15-Oct-12	Thin Section	ign	755320	241	3132	0.27960	0.00383	21.28507
127-7A	JR12-127	15-Oct-12	Thin Section	osc	647868	206	3145	0.31861	0.00436	31.48330
127-8A	JR12-127	15-Oct-12	Thin Section	ign	647575	198	3275	0.28723	0.00492	27.39288
127-8B	JR12-127	15-Oct-12	Thin Section	ign	2545706	1634	1558	0.19207	0.01116	8.36413
127-8C	JR12-127	15-Oct-12	Thin Section	ign	716627	271	2644	0.28910	0.00392	26.73763
136-10A	JR12-136	22-May-14	Mount	ign	456596	111	4128	0.27762	0.00511	20.08483
136-1A	JR12-136	21-May-14	Mount	meta	1089005	72	15197	0.29935	0.00249	26.47056
136-2A	JR12-136	21-May-14	Mount	meta	1423190	93	15283	0.29868	0.00244	28.26868
136-2B	JR12-136	21-May-14	Mount	meta	2052283	110	18654	0.27920	0.00244	24.98789
136-3A	JR12-136	21-May-14	Mount	meta	952719	146	6542	0.29887	0.00325	28.11351
136-4A	JR12-136	21-May-14	Mount	meta	1047613	126	8323	0.34231	0.00490	30.27473
136-4B	JR12-136	21-May-14	Mount	meta	972320	181	5382	0.35623	0.00283	33.59005
136-7A	JR12-136	22-May-14	Mount	meta	552188	152	3623	0.31031	0.00548	22.15274

Spot Name	Sample Name	Date	Method	Zircon Phase	206Pb (cps)	204Pb (cps)	206Pb/204Pb	207Pb/206Pb	2σ	207Pb/235U
136-8A	JR12-136	22-May-14	Mount	meta	500908	120	4179	0.25889	0.00442	7.66852
136-8B	JR12-136	22-May-14	Mount	meta	536708	122	4385	0.25907	0.00446	6.46676
136-9A	JR12-136	22-May-14	Mount	meta	432555	142	3052	0.30418	0.00625	12.07369
136-2B	JR12-136	16-Oct-12	Thin Section	meta	2052283	110	18654	0.28306	0.00432	24.35659
136-2B	JR12-136	23-May-14	Thin Section	meta	2052283	110	18654	0.26984	0.00474	23.28334
136-6A	JR12-136	16-Oct-12	Thin Section	meta	1646249	130	12659	0.31049	0.00464	27.08210
136-6A	JR12-136	23-May-14	Thin Section	meta	1646249	130	12659	0.29599	0.00512	25.88875
136-6B	JR12-136	16-Oct-12	Thin Section	meta	1904713	129	14718	0.30834	0.00464	26.62370
136-6B	JR12-136	23-May-14	Thin Section	meta	1904713	129	14718	0.29394	0.00511	25.45055
136-12A	JR12-136	22-May-14	Mount	meta	267282	129	2074	0.28958	0.00519	24.08767
136-12B	JR12-136	22-May-14	Mount	meta	315440	130	2434	0.29478	0.00503	21.57252
136-3B	JR12-136	21-May-14	Mount	meta	1553705	139	11163	0.30243	0.00355	27.63981
136-5A	JR12-136	21-May-14	Mount	meta	1430004	96	14961	0.29630	0.00267	27.11841
136-6A	JR12-136	21-May-14	Mount	meta	1646249	130	12659	0.30626	0.00252	27.78404
136-6B	JR12-136	21-May-14	Mount	meta	1904713	129	14718	0.30414	0.00256	27.31376
136-11A	JR12-136	22-May-14	Mount	meta	610025	140	4363	0.30124	0.00537	22.20455
141-1A	JR12-141	16-Oct-12	Thin Section	ign	1056529	25	41750	0.28837	0.00439	24.55456
141-1B	JR12-141	16-Oct-12	Thin Section	rim	1329326	67	19877	0.42157	0.00621	46.60808
141-1C	JR12-141	16-Oct-12	Thin Section	rim	1027270	40	25888	0.28998	0.00443	24.73139
141-1D	JR12-141	16-Oct-12	Thin Section	ign	998693	99	10081	0.38903	0.00644	38.30191
141-1E	JR12-141	16-Oct-12	Thin Section	rim	1209377	52	23054	0.28119	0.00422	23.07215
141-1F	JR12-141	16-Oct-12	Thin Section	ign	94725	151	627	0.37655	0.00583	29.04981
141-1G	JR12-141	16-Oct-12	Thin Section	ign	882550	47	18929	0.35090	0.00559	34.56209
141-1H	JR12-141	16-Oct-12	Thin Section	ign	720421	44	16420	0.28068	0.00424	23.88699
141-1I	JR12-141	16-Oct-12	Thin Section	ign	1064600	109	9771	0.28619	0.00460	24.84144
141-2A	JR12-141	16-Oct-12	Thin Section	ign	671589	53	12759	0.29837	0.00442	27.39431
141-2B	JR12-141	16-Oct-12	Thin Section	ign	531776	37	14542	0.29379	0.00446	25.33353
141-2C	JR12-141	16-Oct-12	Thin Section	ign	599790	102	5908	0.23985	0.00424	13.19223
141-3A	JR12-141	16-Oct-12	Thin Section	ign	899703	91	9893	0.37852	0.00671	31.94672
141-4A	JR12-141	16-Oct-12	Thin Section	ign	174998	80	2186	0.41209	0.00652	39.07181
141-4B	JR12-141	16-Oct-12	Thin Section	ign	91219	62	1478	0.42528	0.00654	44.49082
141-4C	JR12-141	16-Oct-12	Thin Section	ign	328119	69	4774	0.25882	0.00400	21.18241
141-4D	JR12-141	16-Oct-12	Thin Section	ign	98860	118	839	0.39941	0.00750	35.76383
141-5A1	JR12-141	16-Oct-12	Thin Section	ign	1120697	97	11543	0.38241	0.00585	42.05148
141-5A2	JR12-141	16-Oct-12	Thin Section	ign	860254	71	12187	0.31082	0.00769	29.84709
141-5A3	JR12-141	16-Oct-12	Thin Section	ign	1257461	83	15149	0.28732	0.00447	28.69365

Spot Name	Sample Name	Date	Method	Zircon Phase	206Pb (cps)	204Pb (cps)	206Pb/204Pb	207Pb/206Pb	2σ	207Pb/235U
141-5B1	JR12-141	16-Oct-12	Thin Section	rim	1433588	65	22054	0.29352	0.00459	26.52513
141-5B2	JR12-141	16-Oct-12	Thin Section	ign	923236	83	11189	0.27637	0.00424	25.42168
141-6A	JR12-141	16-Oct-12	Thin Section	ign	709171	83	8558	0.41025	0.00607	47.22931
141-6B	JR12-141	16-Oct-12	Thin Section	ign	788730	34	23326	0.41525	0.00666	44.81336
141-6C	JR12-141	16-Oct-12	Thin Section	ign	443432	42	10509	0.31470	0.00510	26.82534
144-10A	JR12-144	21-May-14	Mount	ign	1919441	638	3006	0.29961	0.00453	21.61264
144-11A	JR12-144	21-May-14	Mount	ign	1712267	295	5807	0.28041	0.00441	21.13582
144-1A	JR12-144	21-May-14	Mount	ign	1222586	340	3591	0.31827	0.00487	27.72101
144-1B	JR12-144	21-May-14	Mount	ign	953588	278	3425	0.30044	0.00466	24.68238
144-1C	JR12-144	21-May-14	Mount	ign	1211369	222	5457	0.30603	0.00461	27.25834
144-2A	JR12-144	21-May-14	Mount	ign	771626	240	3215	0.31782	0.00479	30.75560
144-3A	JR12-144	21-May-14	Mount	ign	1656328	499	3321	0.32310	0.00502	29.01654
144-4A	JR12-144	21-May-14	Mount	ign	1019200	197	5170	0.32328	0.00482	30.99548
144-5A	JR12-144	21-May-14	Mount	ign	993045	270	3677	0.31056	0.00475	29.85929
144-6A	JR12-144	21-May-14	Mount	ign	739526	421	1756	0.32256	0.00481	31.48422
144-7A	JR12-144	21-May-14	Mount	ign	779106	535	1455	0.30898	0.00511	25.02028
144-8A	JR12-144	21-May-14	Mount	ign	1233828	458	2696	0.30909	0.00476	26.52445
144-9A	JR12-144	21-May-14	Mount	ign	728072	172	4245	0.31356	0.00464	29.26890
144C-2A1	JR12-144	16-Oct-12	Thin Section	ign	961028	562	1709	0.16959	0.00336	8.70732
144C-2A2	JR12-144	16-Oct-12	Thin Section	ign	814348	315	2584	0.27809	0.00374	23.74631
144C-2B1	JR12-144	16-Oct-12	Thin Section	ign	1219300	231	5278	0.24168	0.00303	17.62117
144C-2B2	JR12-144	16-Oct-12	Thin Section	ign	753884	758	995	0.22701	0.00354	15.36660
144C-3A	JR12-144	16-Oct-12	Thin Section	ign	695209	36	19233	0.30615	0.00373	34.15690
144C-3B	JR12-144	16-Oct-12	Thin Section	ign	2375867	495	4801	0.18599	0.00328	9.16039
144C-4A	JR12-144	16-Oct-12	Thin Section	ign	1192254	749	1591	0.26638	0.00413	18.70159
144C-4B	JR12-144	16-Oct-12	Thin Section	ign	612183	378	1620	0.29844	0.00475	26.12279
144C-5A	JR12-144	16-Oct-12	Thin Section	ign	1237119	223	5536	0.29874	0.00374	26.75441
144C-6A	JR12-144	16-Oct-12	Thin Section	ign	676389	355	1903	0.31616	0.00391	31.43899
144C-6B	JR12-144	16-Oct-12	Thin Section	ign	358593	408	878	0.31910	0.00394	29.94375
144C-6D	JR12-144	16-Oct-12	Thin Section	ign	1733673	324	5358	0.29180	0.00485	26.03015
145-11A	JR12-145	17-Oct-12	Thin Section	ign	522403	139	3755	0.40664	0.00367	48.15662
145-11B	JR12-145	17-Oct-12	Thin Section	ign	1123245	170	6617	0.35397	0.00599	38.55384
145-11C	JR12-145	17-Oct-12	Thin Section	osc	383250	107	3598	0.41590	0.00389	47.98766
145-11D	JR12-145	17-Oct-12	Thin Section	ign	910214	136	6702	0.37504	0.00571	30.39107
145-11E	JR12-145	17-Oct-12	Thin Section	ign	377727	76	4973	0.40997	0.00362	47.61636
145-12A	JR12-145	17-Oct-12	Thin Section	osc	408984	131	3119	0.40991	0.00385	45.65104

Spot Name	Sample Name	Date	Method	Zircon Phase	206Pb (cps)	204Pb (cps)	206Pb/204Pb	207Pb/206Pb	2σ	207Pb/235U
145-12B	JR12-145	17-Oct-12	Thin Section	ign	1351629	190	7125	0.24434	0.00406	17.03302
145-2A	JR12-145	17-Oct-12	Thin Section	ign	227678	122	1861	0.34793	0.00416	27.95777
145-2B	JR12-145	17-Oct-12	Thin Section	ign	475286	147	3235	0.30774	0.00559	26.81675
145-3A	JR12-145	17-Oct-12	Thin Section	ign	1031979	126	8159	0.41743	0.00513	45.26472
145-3B	JR12-145	17-Oct-12	Thin Section	osc	883863	106	8364	0.41078	0.00439	43.37430
145-3C	JR12-145	17-Oct-12	Thin Section	ign	775214	132	5854	0.30394	0.00278	26.39465
145-3D	JR12-145	17-Oct-12	Thin Section	osc	439924	132	3338	0.40924	0.00444	46.56198
145-7A	JR12-145	17-Oct-12	Thin Section	meta	1908045	214	8935	0.34670	0.00318	29.85153
145-7B	JR12-145	17-Oct-12	Thin Section	meta	1092582	200	5454	0.30786	0.00402	29.53644
145-7C	JR12-145	17-Oct-12	Thin Section	meta	700615	205	3423	0.37442	0.00656	35.90080
145-9A	JR12-145	17-Oct-12	Thin Section	ign	560816	172	3256	0.40333	0.00452	45.21037
146-10A	JR12-146	15-Oct-12	Thin Section	rim	959817	78	12374	0.25946	0.00353	21.87200
146-10B	JR12-146	15-Oct-12	Thin Section	rim	691833	86	8018	0.30149	0.00417	25.39622
146-1A	JR12-146	15-Oct-12	Thin Section	ign	1236723	1	1197276	0.42390	0.00570	48.26570
146-1B	JR12-146	15-Oct-12	Thin Section	ign	2163524	27	79368	0.36444	0.00543	30.14301
146-1C	JR12-146	15-Oct-12	Thin Section	ign	1887392	35	53721	0.27247	0.00427	16.93558
146-2A	JR12-146	15-Oct-12	Thin Section	rim	1101364	8	129685	0.29089	0.00395	25.94285
146-5A	JR12-146	15-Oct-12	Thin Section	rim	1503730	11	134617	0.30975	0.00446	25.63512
146-5B	JR12-146	15-Oct-12	Thin Section	rim	1265387	1	1265387	0.30519	0.00414	29.17759
146-5C	JR12-146	15-Oct-12	Thin Section	rim	2097571	5	395242	0.38170	0.00526	44.13488
146-6A	JR12-146	15-Oct-12	Thin Section	rim	844702	62	13557	0.26282	0.00370	23.61268
146-6B	JR12-146	15-Oct-12	Thin Section	rim	870021	160	5428	0.26205	0.00385	21.18489
146-7A	JR12-146	15-Oct-12	Thin Section	rim	819850	79	10386	0.41858	0.00561	49.38608
146-7B	JR12-146	15-Oct-12	Thin Section	rim	1209626	134	9022	0.41506	0.00585	43.26004
146-7C	JR12-146	15-Oct-12	Thin Section	rim	410414	71	5745	0.28351	0.00391	25.12843
146-8A	JR12-146	15-Oct-12	Thin Section	rim	888659	60	14770	0.27419	0.00380	23.31890
146-8B	JR12-146	15-Oct-12	Thin Section	rim	1106760	86	12837	0.29105	0.00392	25.95059
146-9A	JR12-146	15-Oct-12	Thin Section	ign	973396	63	15536	0.40974	0.00556	41.70728
171-10A	JR12-171	21-May-14	Mount	ign	1317519	595	2214	0.28240	0.00435	18.36075
171-10B	JR12-171	21-May-14	Mount	ign	985475	283	3485	0.30384	0.00453	28.54980
171-11A	JR12-171	21-May-14	Mount	ign	415919	231	1797	0.32177	0.00478	32.25122
171-11B	JR12-171	21-May-14	Mount	ign	359533	235	1531	0.32345	0.00482	32.47982
171-12A	JR12-171	21-May-14	Mount	ign	587158	551	1066	0.32440	0.00498	32.77973
171-12B	JR12-171	21-May-14	Mount	ign	637832	340	1878	0.32097	0.00477	32.34591
171-1A	JR12-171	21-May-14	Mount	ign	687555	470	1464	0.30034	0.00716	26.22055
171-1B	JR12-171	21-May-14	Mount	ign	568798	260	2190	0.31789	0.00471	31.10051

Spot Name	Sample Name	Date	Method	Zircon Phase	206Pb (cps)	204Pb (cps)	206Pb/204Pb	207Pb/206Pb	2σ	207Pb/235U
171-2A	JR12-171	21-May-14	Mount	ign	341485	273	1250	0.32430	0.00483	32.66996
171-2B	JR12-171	21-May-14	Mount	ign	2468602	343	7200	0.32294	0.00478	31.35231
171-3A	JR12-171	21-May-14	Mount	ign	502110	361	1392	0.32142	0.00477	30.52971
171-4A	JR12-171	21-May-14	Mount	ign	482987	274	1763	0.32335	0.00478	32.10087
171-4B	JR12-171	21-May-14	Mount	ign	402720	281	1435	0.32161	0.00476	34.06310
171-5A	JR12-171	21-May-14	Mount	ign	480215	296	1625	0.31772	0.00474	32.30984
171-5B	JR12-171	21-May-14	Mount	ign	889429	292	3044	0.29234	0.00461	25.17068
171-6A	JR12-171	21-May-14	Mount	ign	618837	271	2282	0.32197	0.00477	33.18963
171-6B	JR12-171	21-May-14	Mount	ign	563874	270	2090	0.32192	0.00477	33.41674
171-7A	JR12-171	21-May-14	Mount	ign	677728	275	2465	0.31217	0.00479	29.92856
171-8A	JR12-171	21-May-14	Mount	ign	355628	256	1390	0.32089	0.00478	33.34826
171-9A	JR12-171	21-May-14	Mount	ign	440939	256	1722	0.32268	0.00478	32.49462
171-9B	JR12-171	21-May-14	Mount	ign	482759	233	2068	0.32168	0.00478	32.49576
101-1A	JR13-101	20-May-14	Mount	ign	770873	1	770873	0.36104	0.00388	35.04184
101-1B	JR13-101	20-May-14	Mount	ign	881742	1	608016	0.35799	0.00380	33.33405
101-2A	JR13-101	20-May-14	Mount	ign	415952	32	12990	0.35352	0.00427	37.07730
101-2B	JR13-101	20-May-14	Mount	ign	458509	18	26148	0.35617	0.00382	37.23709
101-3A	JR13-101	20-May-14	Mount	ign	363295	364	998	0.30437	0.00466	13.90464
101-3B	JR13-101	20-May-14	Mount	ign	857781	4	204157	0.31131	0.00332	29.36809
101-4A	JR13-101	20-May-14	Mount	meta	834241	1	834241	0.36164	0.00380	37.71826
101-4B	JR13-101	20-May-14	Mount	meta	1281729	410	3124	0.35805	0.00376	39.58008
101-5A	JR13-101	20-May-14	Mount	ign	1953967	113	17349	0.35573	0.00375	38.72175
101-6A	JR13-101	20-May-14	Mount	ign	1620439	149	10844	0.30964	0.00643	28.91109
101-7A	JR13-101	20-May-14	Mount	ign	696293	10	71240	0.34630	0.00399	33.90777
101-7B	JR13-101	20-May-14	Mount	ign	1875709	44	42166	0.30518	0.00343	29.31943
101-8A	JR13-101	20-May-14	Mount	ign	788048	337	2337	0.35464	0.00384	34.59848
101-8B	JR13-101	20-May-14	Mount	ign	1032588	349	2957	0.34336	0.00408	32.90594
101-9A	JR13-101	20-May-14	Mount	ign	1402384	105	13370	0.35591	0.00383	35.16130
101-9B	JR13-101	20-May-14	Mount	ign	1475307	69	21340	0.35660	0.00377	38.77041
101-10A1	JR13-101	15-Oct-12	Thin Section	rim	310223	75	4132	0.26229	0.00356	23.28784
101-10A2	JR13-101	15-Oct-12	Thin Section	ign	531329	74	7216	0.33013	0.00451	33.94792
101-10B1	JR13-101	15-Oct-12	Thin Section	ign	979386	90	10920	0.35717	0.00482	36.58966
101-10B2	JR13-101	15-Oct-12	Thin Section	ign	261079	85	3077	0.34751	0.00472	37.48479
101-1A	JR13-101	15-Oct-12	Thin Section	ign	660066	45	14650	0.34053	0.00493	36.35368
101-1B	JR13-101	15-Oct-12	Thin Section	ign	917194	51	18058	0.35813	0.00484	37.65447
101-2A	JR13-101	15-Oct-12	Thin Section	ign	2065102	103	20083	0.36499	0.00583	31.84481

Spot Name	Sample Name	Date	Method	Zircon Phase	206Pb (cps)	204Pb (cps)	206Pb/204Pb	207Pb/206Pb	2σ	207Pb/235U
101-3A	JR13-101	15-Oct-12	Thin Section	ign	868553	85	10218	0.33480	0.00752	32.78359
101-3B	JR13-101	15-Oct-12	Thin Section	ign	732964	11	64659	0.35937	0.00483	37.82055
101-4A	JR13-101	15-Oct-12	Thin Section	ign	976165	56	17446	0.30599	0.00417	25.75433
101-4B	JR13-101	15-Oct-12	Thin Section	ign	668499	20	33607	0.35293	0.00475	36.41597
101-4C	JR13-101	15-Oct-12	Thin Section	ign	914560	12	74942	0.35559	0.00480	35.68580
101-5A	JR13-101	15-Oct-12	Thin Section	ign	413671	95	4364	0.35507	0.00477	35.94290
101-6A	JR13-101	15-Oct-12	Thin Section	ign	461874	52	8920	0.29997	0.00408	27.37202
101-6B	JR13-101	15-Oct-12	Thin Section	ign	463168	39	11820	0.29522	0.00405	26.06898
101-7A	JR13-101	15-Oct-12	Thin Section	ign	622945	59	10561	0.34413	0.00653	32.86200
101-8A	JR13-101	15-Oct-12	Thin Section	ign	944086	34	28163	0.36076	0.00487	39.74881
101-8B	JR13-101	15-Oct-12	Thin Section	meta	523725	108	4836	0.27811	0.00378	25.54486
101-9A	JR13-101	15-Oct-12	Thin Section	ign	1026460	65	15790	0.34744	0.00470	37.36068
102-10B	JR13-102	16-Oct-14	MOUNT	rim	177810	191	930	0.19913	0.00261	15.38989
102-11A	JR13-102	16-Oct-14	MOUNT	rim	269344	231	1166	0.31422	0.00358	30.41401
102-12B	JR13-102	16-Oct-14	MOUNT	rim	819877	148	5529	0.25922	0.00229	23.21068
102-13A	JR13-102	16-Oct-14	MOUNT	ign	510052	233	2185	0.34651	0.00313	35.96760
102-14B	JR13-102	16-Oct-14	MOUNT	osc	225027	221	1020	0.33466	0.00352	26.82804
102-15B	JR13-102	16-Oct-14	MOUNT	ign	307671	212	1450	0.30617	0.00295	29.19733
102-1A	JR13-102	16-Oct-14	MOUNT	rim	380571	129	2946	0.30944	0.00370	29.81154
102-1B	JR13-102	16-Oct-14	MOUNT	ign	685228	162	4234	0.30343	0.00270	28.11653
102-2A	JR13-102	16-Oct-14	MOUNT	ign	482259	170	2842	0.29504	0.00288	27.10872
102-2B	JR13-102	16-Oct-14	MOUNT	ign	737455	243	3040	0.31296	0.00284	29.15785
102-3A	JR13-102	16-Oct-14	MOUNT	ign	500355	185	2705	0.34902	0.00351	37.28435
102-4A	JR13-102	16-Oct-14	MOUNT	ign	563045	166	3391	0.31260	0.00281	30.54324
102-4B	JR13-102	16-Oct-14	MOUNT	ign	264346	146	1810	0.30617	0.00282	29.49718
102-5A	JR13-102	16-Oct-14	MOUNT	rim	582475	274	2127	0.25856	0.00245	22.82555
102-6A	JR13-102	16-Oct-14	MOUNT	core	583187	189	3078	0.31118	0.00291	30.79080
102-7A	JR13-102	16-Oct-14	MOUNT	rim	428876	199	2158	0.30030	0.00273	26.61269
102-8A	JR13-102	16-Oct-14	MOUNT	ign	568347	225	2527	0.30196	0.00288	28.45048
102-8B	JR13-102	16-Oct-14	MOUNT	ign	542204	228	2377	0.30999	0.00278	30.24145
102-9A	JR13-102	16-Oct-14	MOUNT	ign	586166	461	1271	0.30736	0.00275	29.09305
102-9B	JR13-102	16-Oct-14	MOUNT	rim	560683	201	2786	0.30213	0.00277	28.89670
108-1A	JR13-108	20-May-14	Mount	ign	450341	9	48231	0.42475	0.00447	46.47587
108-1B	JR13-108	20-May-14	Mount	ign	558147	11	50175	0.42266	0.00446	48.69431
108-2A	JR13-108	20-May-14	Mount	osc	1054303	17	60924	0.42534	0.00447	47.80700
108-2B	JR13-108	20-May-14	Mount	meta	641531	24	26195	0.30995	0.00331	27.66284

Spot Name	Sample Name	Date	Method	Zircon Phase	206Pb (cps)	204Pb (cps)	206Pb/204Pb	207Pb/206Pb	2σ	207Pb/235U
108-3A	JR13-108	20-May-14	Mount	meta	636436	31	20470	0.42238	0.00448	45.92344
108-3B	JR13-108	20-May-14	Mount	ign	197002	7	27442	0.35806	0.00401	27.68925
108-3C	JR13-108	20-May-14	Mount	ign	610629	41	14773	0.30197	0.00391	24.39465
108-4A	JR13-108	20-May-14	Mount	ign	575147	4	150050	0.42090	0.00441	46.40228
108-4B	JR13-108	20-May-14	Mount	ign	768917	1	898806	0.41206	0.00435	44.13535
108-5A	JR13-108	20-May-14	Mount	ign	549065	1	421973	0.42624	0.00450	47.13826
108-5B	JR13-108	20-May-14	Mount	osc	518517	5	109606	0.29554	0.00331	23.75786
108-6A	JR13-108	20-May-14	Mount	osc	329836	1	554611	0.42668	0.00453	47.82478
108-6B	JR13-108	20-May-14	Mount	ign	772537	1	772537	0.39622	0.00492	38.75672
114-10A	JR13-114	20-May-14	Mount	ign	815360	311	2623	0.26530	0.00301	9.87026
114-11A	JR13-114	20-May-14	Mount	osc	357051	9	39759	0.32404	0.00342	31.73154
114-12A	JR13-114	20-May-14	Mount	ign	822551	13	65346	0.27508	0.00287	25.22732
114-12B	JR13-114	20-May-14	Mount	ign	1937638	29	66263	0.20680	0.00713	10.93349
114-1A	JR13-114	20-May-14	Mount	osc	381887	3	134034	0.32552	0.00351	32.41759
114-1B	JR13-114	20-May-14	Mount	osc	191559	36	5273	0.32814	0.00386	34.07705
114-2A	JR13-114	20-May-14	Mount	ign	495459	98	5042	0.31542	0.00341	28.37777
114-3A	JR13-114	20-May-14	Mount	osc	928231	16	59307	0.31622	0.00333	31.32949
114-4A	JR13-114	20-May-14	Mount	ign	1015025	12	87524	0.31984	0.00338	31.03772
114-4B	JR13-114	20-May-14	Mount	ign	1059563	20	51971	0.31363	0.00337	25.67391
114-5A	JR13-114	20-May-14	Mount	osc	973894	5	179911	0.32321	0.00343	32.57481
114-5B	JR13-114	20-May-14	Mount	ign	2045143	71	28817	0.27103	0.00287	18.77541
114-6A	JR13-114	20-May-14	Mount	ign	701235	15	46528	0.30216	0.00356	26.36874
114-7A	JR13-114	20-May-14	Mount	osc	187781	7	26487	0.35565	0.00384	36.17626
114-8A	JR13-114	20-May-14	Mount	osc	503783	50	10069	0.31227	0.00349	28.73644
114-8B	JR13-114	20-May-14	Mount	meta	686438	14	49727	0.26906	0.00295	24.58655
114-9A	JR13-114	20-May-14	Mount	osc	509522	8	67160	0.27772	0.00294	24.82767
114-9B	JR13-114	20-May-14	Mount	osc	617027	3	229277	0.30053	0.00437	28.56859
115-11A	JR13-115	15-Oct-14	MOUNT	ign	464130	41	11364	0.31648	0.00461	30.94878
115-2A	JR13-115	15-Oct-14	MOUNT	ign	843519	117	7191	0.25183	0.00421	17.51234
115-2B	JR13-115	15-Oct-14	MOUNT	ign	739672	63	11669	0.26639	0.00463	23.70680
115-5A	JR13-115	15-Oct-14	MOUNT	ign	1182648	89	13219	0.26405	0.00604	16.73872
115-9A	JR13-115	15-Oct-14	MOUNT	ign	505428	55	9131	0.27298	0.00403	25.03461
115-10A	JR13-115	15-Oct-14	MOUNT	osc	667046	544	1226	0.32351	0.00515	33.23476
115-10B	JR13-115	15-Oct-14	MOUNT	osc	637631	99	6443	0.31785	0.00473	32.03024
115-12A	JR13-115	15-Oct-14	MOUNT	osc	177571	84	2122	0.31887	0.00472	30.19616
115-13A	JR13-115	15-Oct-14	MOUNT	osc	172302	59	2923	0.32494	0.00476	32.71790

Spot Name	Sample Name	Date	Method	Zircon Phase	206Pb (cps)	204Pb (cps)	206Pb/204Pb	207Pb/206Pb	2σ	207Pb/235U
115-14A	JR13-115	15-Oct-14	MOUNT	osc	162639	41	3943	0.31297	0.00470	30.66259
115-14B	JR13-115	15-Oct-14	MOUNT	osc	98883	65	1522	0.32097	0.00533	24.09926
115-1A	JR13-115	15-Oct-14	MOUNT	osc	138077	51	2707	0.31952	0.00487	30.34422
115-3A	JR13-115	15-Oct-14	MOUNT	osc	150033	32	4755	0.31965	0.00471	32.97032
115-4A	JR13-115	15-Oct-14	MOUNT	osc	188370	54	3520	0.31358	0.00580	28.43483
115-4B	JR13-115	15-Oct-14	MOUNT	osc	211849	39	5398	0.29281	0.00589	23.03863
115-7A	JR13-115	15-Oct-14	MOUNT	osc	145545	58	2529	0.32245	0.00473	30.72932
115-8A	JR13-115	15-Oct-14	MOUNT	osc	610388	104	5895	0.29936	0.00516	26.86959
119-11A	JR13-119	15-Oct-14	MOUNT	ign	661749	76	8698	0.29319	0.00485	24.48222
119-12A	JR13-119	15-Oct-14	MOUNT	ign	657360	65	10070	0.31009	0.00458	29.61146
119-3A	JR13-119	15-Oct-14	MOUNT	ign	378059	42	9097	0.32092	0.00467	31.73080
119-4A	JR13-119	15-Oct-14	MOUNT	ign	267394	82	3278	0.32453	0.00523	28.05017
119-10A	JR13-119	15-Oct-14	MOUNT	osc	526862	43	12145	0.32292	0.00473	33.01385
119-13A	JR13-119	15-Oct-14	MOUNT	osc	282578	30	9381	0.31276	0.00474	29.91050
119-13B	JR13-119	15-Oct-14	MOUNT	osc	327423	70	4673	0.30942	0.00479	28.39394
119-14A	JR13-119	15-Oct-14	MOUNT	osc	543908	52	10434	0.29660	0.01230	23.80584
119-14B	JR13-119	15-Oct-14	MOUNT	osc	524254	40	13227	0.29930	0.00543	24.66551
119-1A	JR13-119	15-Oct-14	MOUNT	osc	299429	76	3950	0.32664	0.00478	31.32342
119-1B	JR13-119	15-Oct-14	MOUNT	osc	246741	66	3749	0.32545	0.00476	31.68649
119-1C	JR13-119	15-Oct-14	MOUNT	osc	243435	69	3538	0.32547	0.00478	31.42861
119-2A	JR13-119	15-Oct-14	MOUNT	osc	381452	46	8361	0.32328	0.00472	34.21642
119-6A	JR13-119	15-Oct-14	MOUNT	osc	334132	45	7485	0.31971	0.00479	31.95066
119-7A	JR13-119	15-Oct-14	MOUNT	osc	367224	64	5777	0.31152	0.00464	29.91528
119-7B	JR13-119	15-Oct-14	MOUNT	osc	379660	62	6095	0.31848	0.00481	31.15937
119-8A	JR13-119	15-Oct-14	MOUNT	osc	299460	60	4980	0.30811	0.00471	30.14069
119-8B	JR13-119	15-Oct-14	MOUNT	osc	267028	58	4598	0.31947	0.00478	31.66066
119-9A	JR13-119	15-Oct-14	MOUNT	osc	600976	27	22183	0.31769	0.00507	31.83649
205-10A	JR13-205	15-Oct-14	MOUNT	osc	1154581	187	6175	0.29833	0.00453	25.61804
205-10B	JR13-205	15-Oct-14	MOUNT	osc	508007	113	4508	0.31822	0.00479	31.22761
205-11A	JR13-205	15-Oct-14	MOUNT	osc	660062	113	5826	0.31955	0.00467	33.22376
205-12A	JR13-205	15-Oct-14	MOUNT	osc	228479	81	2835	0.32459	0.00475	31.30669
205-12B	JR13-205	15-Oct-14	MOUNT	osc	254040	104	2435	0.32528	0.00477	30.79493
205-14A	JR13-205	15-Oct-14	MOUNT	osc	459040	128	3593	0.32244	0.00489	32.40425
205-15A	JR13-205	15-Oct-14	MOUNT	osc	430156	327	1316	0.32254	0.00494	31.87018
205-16A	JR13-205	15-Oct-14	MOUNT	osc	749344	138	5427	0.38057	0.00592	41.27991
205-1A	JR13-205	15-Oct-14	MOUNT	osc	282088	168	1679	0.31033	0.00495	27.84399

Spot Name	Sample Name	Date	Method	Zircon Phase	206Pb (cps)	204Pb (cps)	206Pb/204Pb	207Pb/206Pb	2σ	207Pb/235U
205-2A	JR13-205	15-Oct-14	MOUNT	ign	477964	113	4230	0.30921	0.00627	20.22470
205-3A	JR13-205	15-Oct-14	MOUNT	osc	247579	117	2116	0.32396	0.00474	30.98673
205-4A	JR13-205	15-Oct-14	MOUNT	osc	657899	219	3007	0.31733	0.00484	32.25142
205-4B	JR13-205	15-Oct-14	MOUNT	osc	830492	208	3988	0.31773	0.00470	31.95264
205-5A	JR13-205	15-Oct-14	MOUNT	osc	581839	122	4752	0.32249	0.00470	31.00070
205-6A	JR13-205	15-Oct-14	MOUNT	osc	188321	291	648	0.32584	0.00495	31.20545
205-7A	JR13-205	15-Oct-14	MOUNT	ign	699102	128	5441	0.27668	0.00475	23.38783
205-8A	JR13-205	15-Oct-14	MOUNT	osc	2106764	249	8466	0.26668	0.00419	19.75571
205-9A	JR13-205	15-Oct-14	MOUNT	ign	1085570	157	6908	0.31923	0.00468	31.20943
206-10A	JR13-206	16-Oct-14	MOUNT	ign	1372741	227	6036	0.28692	0.00481	23.46297
206-10B	JR13-206	16-Oct-14	MOUNT	ign	1392122	186	7469	0.29674	0.00468	27.53857
206-11A	JR13-206	16-Oct-14	MOUNT	ign	1216033	90	13524	0.40273	0.00376	44.95582
206-12A	JR13-206	16-Oct-14	MOUNT	ign	1480157	124	11903	0.34319	0.00405	32.34034
206-13A	JR13-206	16-Oct-14	MOUNT	ign	1172624	128	9138	0.36958	0.00423	35.69398
206-14A	JR13-206	16-Oct-14	MOUNT	ign	856520	181	4741	0.39993	0.00426	41.92230
206-15A	JR13-206	16-Oct-14	MOUNT	ign	1719591	161	10676	0.39502	0.00409	40.40278
206-16A	JR13-206	16-Oct-14	MOUNT	ign	1633230	136	11999	0.35768	0.00493	33.08236
206-16B	JR13-206	16-Oct-14	MOUNT	ign	1846913	172	10754	0.36670	0.00356	36.01141
206-17A	JR13-206	16-Oct-14	MOUNT	ign	717445	138	5200	0.41049	0.00379	47.39241
206-1A	JR13-206	16-Oct-14	MOUNT	ign	233081	24	9906	0.27022	0.00288	21.22470
206-2A	JR13-206	16-Oct-14	MOUNT	ign	119473	48	2498	0.39749	0.00322	44.96773
206-2B	JR13-206	16-Oct-14	MOUNT	ign	102848	43	2413	0.35104	0.00331	35.34617
206-3A	JR13-206	16-Oct-14	MOUNT	ign	161048	51	3136	0.36119	0.00304	39.02721
206-4A	JR13-206	16-Oct-14	MOUNT	ign	172881	38	4600	0.39278	0.00330	41.80282
206-5A	JR13-206	16-Oct-14	MOUNT	ign	226367	50	4521	0.33981	0.00304	34.41723
206-6A	JR13-206	16-Oct-14	MOUNT	ign	156186	24	6607	0.41732	0.00340	44.70488
206-7A	JR13-206	16-Oct-14	MOUNT	ign	174185	51	3420	0.41458	0.00318	47.13483
206-8A	JR13-206	16-Oct-14	MOUNT	ign	2001212	95	21084	0.36560	0.00388	35.61354
206-9A	JR13-206	16-Oct-14	MOUNT	ign	1556577	109	14261	0.38451	0.00412	42.54376
208-10A	JR13-208	15-Oct-14	MOUNT	osc	292143	3	115816	0.30492	0.00454	27.36722
208-10B	JR13-208	15-Oct-14	MOUNT	rim	428947	22	19871	0.30602	0.00456	27.70608
208-11A	JR13-208	15-Oct-14	MOUNT	osc	177558	3	67039	0.31315	0.00461	28.70678
208-12A	JR13-208	15-Oct-14	MOUNT	osc	304969	10	29863	0.32453	0.00475	31.04940
208-13A	JR13-208	15-Oct-14	MOUNT	osc	463254	1	463254	0.31047	0.00454	32.90780
208-14A	JR13-208	15-Oct-14	MOUNT	osc	393548	3	123736	0.32294	0.00471	31.93645
208-15A	JR13-208	15-Oct-14	MOUNT	osc	115691	1	146881	0.31467	0.00470	29.50364

Spot Name	Sample Name	Date	Method	Zircon Phase	206Pb (cps)	204Pb (cps)	206Pb/204Pb	207Pb/206Pb	2σ	207Pb/235U
208-16A	JR13-208	15-Oct-14	MOUNT	ign	339915	4	93919	0.31978	0.00471	31.25051
208-18A	JR13-208	15-Oct-14	MOUNT	ign	885935	3	339084	0.26974	0.00394	24.18878
208-1A	JR13-208	15-Oct-14	MOUNT	osc	315296	1	315296	0.32046	0.00473	29.70285
208-2A	JR13-208	15-Oct-14	MOUNT	osc	313997	8	40578	0.32274	0.00471	32.19305
208-3A	JR13-208	15-Oct-14	MOUNT	ign	512690	9	58785	0.30192	0.00443	30.09299
208-4A	JR13-208	15-Oct-14	MOUNT	osc	243111	10	23479	0.31896	0.00468	31.55330
208-5A	JR13-208	15-Oct-14	MOUNT	osc	194251	1	135663	0.31618	0.00510	30.04108
208-6A	JR13-208	15-Oct-14	MOUNT	osc	220045	5	48358	0.31296	0.00468	29.65585
208-6B	JR13-208	15-Oct-14	MOUNT	osc	279916	11	25958	0.31779	0.00467	30.79414
208-7A	JR13-208	15-Oct-14	MOUNT	ign	626507	3	239677	0.26282	0.00406	22.63177
208-8A	JR13-208	15-Oct-14	MOUNT	ign	1050187	51	20708	0.28104	0.00567	23.04657
208-9A	JR13-208	15-Oct-14	MOUNT	osc	664880	8	83991	0.30644	0.00460	28.27914
303-10A	JR13-303	15-Oct-14	MOUNT	ign	89522	48	1854	0.30633	0.00481	28.48466
303-14A	JR13-303	15-Oct-14	MOUNT	osc	419986	480	875	0.30086	0.00686	28.98853
303-15A	JR13-303	15-Oct-14	MOUNT	core	424463	338	1255	0.36485	0.00566	37.56550
303-1A	JR13-303	15-Oct-14	MOUNT	core	698626	1251	559	0.41008	0.00650	44.73368
303-2A	JR13-303	15-Oct-14	MOUNT	osc	418170	4	101148	0.30067	0.00467	29.13168
303-2B	JR13-303	15-Oct-14	MOUNT	osc	568998	2	324168	0.31493	0.00564	31.71787
303-5B	JR13-303	15-Oct-14	MOUNT	ign	167045	136	1233	0.30861	0.00601	29.33534
303-6A	JR13-303	15-Oct-14	MOUNT	ign	971836	378	2568	0.28133	0.00511	25.13411
303-6B	JR13-303	15-Oct-14	MOUNT	core	869888	1115	780	0.38235	0.00651	40.29472
303-7A	JR13-303	15-Oct-14	MOUNT	core	435470	322	1353	0.37308	0.00638	40.81933
303-8A	JR13-303	15-Oct-14	MOUNT	ign	669319	43	15487	0.29299	0.00461	27.84323
303-9A	JR13-303	15-Oct-14	MOUNT	ign	22316	13	1775	0.28896	0.00493	29.63637
304-10A	JR13-304	15-Oct-14	MOUNT	osc	504048	3	161698	0.21235	0.00310	16.52519
304-11A	JR13-304	15-Oct-14	MOUNT	osc	235146	2	99565	0.21425	0.00313	17.09187
304-11B	JR13-304	15-Oct-14	MOUNT	osc	294891	24	12176	0.21659	0.00316	17.46217
304-12A	JR13-304	15-Oct-14	MOUNT	osc	201436	119	1698	0.21664	0.00327	16.77436
304-13A	JR13-304	15-Oct-14	MOUNT	osc	399671	2	183028	0.21299	0.00314	17.06310
304-1A	JR13-304	15-Oct-14	MOUNT	ign	495019	35	14024	0.21115	0.00311	17.16105
304-2A	JR13-304	15-Oct-14	MOUNT	osc	516588	93	5541	0.19923	0.00320	14.16623
304-3A	JR13-304	15-Oct-14	MOUNT	osc	317687	61	5233	0.21554	0.00314	17.40848
304-3B	JR13-304	15-Oct-14	MOUNT	osc	280974	28	9863	0.21526	0.00321	17.41455
304-4A	JR13-304	15-Oct-14	MOUNT	osc	614004	168	3661	0.21305	0.00331	15.62982
304-5A	JR13-304	15-Oct-14	MOUNT	osc	470365	87	5385	0.21628	0.00315	17.08962
304-6A	JR13-304	15-Oct-14	MOUNT	osc	354196	24	14558	0.21196	0.00311	16.59017

Spot Name	Sample Name	Date	Method	Zircon Phase	206Pb (cps)	204Pb (cps)	206Pb/204Pb	207Pb/206Pb	2σ	207Pb/235U
304-6B	JR13-304	15-Oct-14	MOUNT	rim	639978	2	337621	0.20597	0.00302	15.97923
304-7A	JR13-304	15-Oct-14	MOUNT	osc	323577	39	8283	0.21246	0.00310	16.69381
304-8A	JR13-304	15-Oct-14	MOUNT	osc	149639	5	30067	0.21465	0.00313	16.87304
304-8B	JR13-304	15-Oct-14	MOUNT	ign	663861	53	12521	0.21219	0.00311	17.22106
304-9A	JR13-304	15-Oct-14	MOUNT	osc	381577	7	55195	0.21228	0.00312	16.96337
305-11A	JR13-305	15-Oct-14	MOUNT	ign	29780	60	500	0.26812	0.00248	23.47075
305-14B	JR13-305	15-Oct-14	MOUNT	rim	812756	126	6455	0.27738	0.00143	25.97358
305-13A	JR13-305	15-Oct-14	MOUNT	ign	1737746	130	13325	0.28089	0.00133	25.11861
305-6A	JR13-305	15-Oct-14	MOUNT	ign	299402	203	1472	0.28657	0.00259	26.19600
305-7A	JR13-305	15-Oct-14	MOUNT	ign	2047750	210	9734	0.28676	0.00165	27.13436
305-8B	JR13-305	15-Oct-14	MOUNT	rim	1000766	988	1013	0.29447	0.00204	28.37624
305-12A	JR13-305	15-Oct-14	MOUNT	ign	222810	195	1143	0.29660	0.00161	27.42820
305-14A	JR13-305	15-Oct-14	MOUNT	core	632356	80	7886	0.30780	0.00147	30.24599
305-20A	JR13-305	15-Oct-14	MOUNT	ign	804704	110	7343	0.30810	0.00148	30.84929
305-4A	JR13-305	15-Oct-14	MOUNT	core	24533	4	5841	0.30883	0.00492	27.87919
305-9C	JR13-305	15-Oct-14	MOUNT	ign	157397	78	2011	0.30888	0.00161	29.81294
305-18A	JR13-305	15-Oct-14	MOUNT	ign	65994	57	1155	0.30903	0.00175	29.29365
305-18B	JR13-305	15-Oct-14	MOUNT	ign	47563	40	1194	0.30960	0.00194	29.20560
305-9B	JR13-305	15-Oct-14	MOUNT	ign	142597	76	1888	0.31004	0.00181	30.14156
305-9A	JR13-305	15-Oct-14	MOUNT	osc	102647	85	1203	0.31112	0.00186	29.98491
305-2B	JR13-305	15-Oct-14	MOUNT	osc	96876	5	20017	0.31394	0.00466	29.46150
305-2A	JR13-305	15-Oct-14	MOUNT	osc	33430	15	2296	0.32216	0.00510	28.58783
305-1A	JR13-305	15-Oct-14	MOUNT	ign	133383	167	797	0.32267	0.00517	30.50068
305-19A	JR13-305	15-Oct-14	MOUNT	ign	312417	567	551	0.32440	0.00324	30.63827
305-8A	JR13-305	15-Oct-14	MOUNT	ign	512859	99	5190	0.32645	0.00169	34.19173
305-15B	JR13-305	15-Oct-14	MOUNT	rim	110499	201	551	0.32882	0.00359	33.83169
305-15A	JR13-305	15-Oct-14	MOUNT	core	164693	216	762	0.33299	0.00207	32.59270
305-3A	JR13-305	15-Oct-14	MOUNT	core	12303	22	549	0.34301	0.00567	21.54492
305-16A	JR13-305	15-Oct-14	MOUNT	ign	340469	370	921	0.34636	0.00251	37.60483
802-1A	JR13-802	12-Nov-13	Thin Section	ign	1686788	129	13057	0.27723	0.00238	24.12030
802-2A	JR13-802	12-Nov-13	Thin Section	ign	3492590	4447	785	0.28305	0.00337	19.85533
802-2B	JR13-802	12-Nov-13	Thin Section	ign	1444155	43	33651	0.28384	0.00252	25.81475
802-2C	JR13-802	12-Nov-13	Thin Section	ign	2204079	656	3358	0.28180	0.00310	24.03612
802-2D	JR13-802	12-Nov-13	Thin Section	core	2007932	2406	834	0.28287	0.00504	19.18508
802-3A	JR13-802	12-Nov-13	Thin Section	core	2175344	84	25894	0.28130	0.00263	24.44225
802-3B	JR13-802	12-Nov-13	Thin Section	ign	1170002	70	16757	0.27862	0.00234	23.36514

Spot Name	Sample Name	Date	Method	Zircon Phase	206Pb (cps)	204Pb (cps)	206Pb/204Pb	207Pb/206Pb	2σ	207Pb/235U
802-3C	JR13-802	12-Nov-13	Thin Section	ign	857450	92	9272	0.27773	0.00237	23.21052
802-3D	JR13-802	12-Nov-13	Thin Section	ign	919293	62	14735	0.28019	0.00237	24.39670
802-4B	JR13-802	12-Nov-13	Thin Section	ign	1513299	1187	1275	0.28706	0.00272	24.14974
802-4C	JR13-802	12-Nov-13	Thin Section	ign	2253068	1275	1767	0.27922	0.00259	16.20350
802-5A	JR13-802	12-Nov-13	Thin Section	ign	1092078	1214	900	0.28628	0.00290	17.22444
802-6A	JR13-802	12-Nov-13	Thin Section	rim	1961005	738	2657	0.27927	0.00233	21.32587
802-6B	JR13-802	12-Nov-13	Thin Section	ign	2718991	823	3305	0.27811	0.00232	20.96135
802-7A	JR13-802	12-Nov-13	Thin Section	core	1471980	243	6054	0.27419	0.00262	22.72057
802-8A	JR13-802	12-Nov-13	Thin Section	ign	1308789	17	75127	0.27755	0.00241	23.62381
802-8B	JR13-802	12-Nov-13	Thin Section	ign	1358156	1134	1198	0.28009	0.00247	11.65481
802-8C	JR13-802	12-Nov-13	Thin Section	ign	1085247	544	1995	0.28064	0.00295	14.25316
802-9A	JR13-802	12-Nov-13	Thin Section	ign	1329184	1308	1016	0.28790	0.00273	19.35671
802-9B	JR13-802	12-Nov-13	Thin Section	ign	1762425	1324	1331	0.28273	0.00249	21.78784

Spot Name	2σ	206Pb/238U	2σ	r	207Pb/206Pb age (Ma)	2σ error (Ma)	207Pb/235U age (Ma)	2σ error (Ma)	206Pb/238U age (Ma)
137-1A	2.16252	0.65348	0.04249	0.973	3746	23	3561	64	3242
137-1B	1.92908	0.57763	0.04073	0.976	3642	24	3373	68	2939
137-1C	3.31623	0.83055	0.05859	0.978	3915	22	3909	69	3898
137-1D	3.06253	0.72665	0.05672	0.982	3850	22	3734	76	3521
137-2A	3.07393	0.85917	0.05241	0.971	3958	22	3971	61	3998
137-2B	3.39084	0.87426	0.06156	0.978	3874	22	3933	69	4050
137-2C	3.77412	0.91170	0.06486	0.978	3956	23	4029	70	4177
137-2D	2.97611	0.87276	0.05105	0.970	3947	22	3980	58	4045
137-2E	2.31735	0.78470	0.04388	0.966	3792	22	3772	56	3734
137-3A	2.08853	0.73040	0.04884	0.937	3421	38	3463	68	3535
137-4A	1.63594	0.65239	0.03972	0.970	3417	23	3349	60	3238
137-4B	3.02322	0.76156	0.05498	0.977	3870	23	3793	71	3650
137-5A	2.40655	0.72202	0.04805	0.976	3726	22	3647	65	3504
137-6A	2.18914	0.76206	0.04045	0.964	3825	22	3764	53	3652
137-7A	2.51555	0.81369	0.04572	0.964	3850	23	3846	56	3838
137-8A	1.55641	0.61985	0.04325	0.978	3217	24	3175	67	3109
141-1A	1.39626	0.61757	0.03383	0.963	3409	23	3291	54	3100
141-1B	3.21236	0.80184	0.05399	0.977	3988	22	3922	66	3796
141-1C	1.31528	0.61855	0.03151	0.958	3418	24	3298	51	3104
141-1D	2.18285	0.71407	0.03894	0.957	3867	25	3728	55	3474
141-1E	1.35022	0.59510	0.03366	0.966	3370	23	3230	55	3010
141-1F	1.50946	0.55953	0.02775	0.955	3818	23	3455	50	2865
141-1G	1.68560	0.71436	0.03293	0.945	3711	24	3626	47	3475
141-1H	1.33952	0.61723	0.03333	0.963	3367	23	3264	53	3099
141-1I	1.45532	0.62953	0.03546	0.962	3397	25	3302	56	3148
141-2A	1.35029	0.66590	0.03130	0.954	3462	23	3398	47	3290
141-2B	1.18191	0.62539	0.02759	0.946	3438	23	3321	45	3131
141-2C	0.60744	0.39892	0.01696	0.923	3119	28	2694	43	2164
141-3A	1.70942	0.61213	0.03090	0.943	3826	27	3549	51	3079
141-4A	2.01580	0.68765	0.03377	0.952	3954	24	3747	50	3374
141-4B	2.13172	0.75874	0.03443	0.947	4001	23	3876	47	3640
141-4C	1.06814	0.59357	0.02849	0.952	3240	24	3147	48	3004
141-4D	1.81858	0.64942	0.03069	0.929	3907	28	3660	49	3226
141-5A1	1.98152	0.79753	0.03555	0.946	3841	23	3820	46	3780
141-5A2	2.12004	0.69645	0.04637	0.937	3525	38	3482	67	3407
141-5A3	1.71982	0.72429	0.04192	0.966	3403	24	3443	57	3512

Spot Name	2σ	206Pb/238U	2σ	r	207Pb/206Pb age (Ma)	2σ error (Ma)	207Pb/235U age (Ma)	2σ error (Ma)	206Pb/238U age (Ma)
141-5B1	1.26179	0.65542	0.02944	0.944	3436	24	3366	46	3249
141-5B2	1.34649	0.66712	0.03382	0.957	3343	24	3325	50	3295
141-6A	2.32853	0.83495	0.03927	0.954	3947	22	3936	48	3913
141-6B	2.32103	0.78270	0.03855	0.951	3965	24	3883	50	3727
141-6C	1.37408	0.61822	0.03004	0.949	3544	25	3377	49	3103
145-11A	2.29969	0.85890	0.04028	0.982	3934	13	3955	46	3997
145-11B	1.80744	0.78995	0.03454	0.933	3724	26	3734	45	3753
145-11C	2.45807	0.83683	0.04215	0.983	3968	14	3951	50	3920
145-11D	1.62151	0.58771	0.03006	0.958	3812	23	3500	51	2980
145-11E	2.10850	0.84238	0.03655	0.980	3946	13	3944	43	3939
145-12A	1.99299	0.80772	0.03444	0.977	3946	14	3902	42	3817
145-12B	0.79318	0.50559	0.02200	0.934	3148	26	2937	44	2638
145-2A	1.23783	0.58278	0.02484	0.963	3698	18	3418	43	2960
145-2B	1.46813	0.63200	0.03264	0.943	3510	28	3377	52	3158
145-3A	2.09395	0.78646	0.03507	0.964	3973	18	3893	45	3740
145-3B	2.04258	0.76581	0.03512	0.974	3949	16	3851	46	3665
145-3C	1.13094	0.62983	0.02636	0.977	3490	14	3361	41	3149
145-3D	2.23171	0.82518	0.03852	0.974	3943	16	3921	47	3879
145-7A	1.20864	0.62448	0.02463	0.974	3693	14	3482	39	3128
145-7B	1.40079	0.69583	0.03173	0.961	3510	20	3472	46	3405
145-7C	1.52018	0.69541	0.02681	0.910	3809	26	3664	41	3403
145-9A	3.66946	0.81297	0.06535	0.990	3922	17	3892	78	3835
146-10A	1.39712	0.61140	0.03816	0.977	3243	21	3178	60	3076
146-10B	1.84809	0.61094	0.04365	0.982	3478	21	3324	69	3074
146-1A	3.24137	0.82580	0.05434	0.980	3996	20	3957	65	3881
146-1B	1.89994	0.59987	0.03674	0.972	3768	22	3491	60	3029
146-1C	1.14756	0.45079	0.02972	0.973	3320	24	2931	63	2399
146-2A	1.67503	0.64683	0.04083	0.978	3422	21	3344	61	3216
146-5A	1.81691	0.60023	0.04166	0.979	3520	22	3333	67	3031
146-5B	1.96739	0.69338	0.04580	0.980	3497	21	3460	64	3396
146-5C	2.88885	0.83860	0.05366	0.978	3839	21	3868	63	3926
146-6A	1.53899	0.65161	0.04147	0.976	3264	22	3253	62	3235
146-6B	1.51620	0.58633	0.04107	0.979	3259	23	3147	67	2975
146-7A	2.96011	0.85571	0.04999	0.975	3977	20	3980	58	3986
146-7B	2.61385	0.75591	0.04441	0.972	3965	21	3848	58	3629
146-7C	1.57671	0.64283	0.03935	0.976	3382	21	3313	59	3200

Spot Name	2σ	206Pb/238U	2σ	r	207Pb/206Pb age (Ma)	2σ error (Ma)	207Pb/235U age (Ma)	2σ error (Ma)	206Pb/238U age (Ma)
146-8A	1.65560	0.61681	0.04295	0.981	3330	22	3240	67	3097
146-8B	1.99613	0.64667	0.04897	0.985	3423	21	3345	73	3215
146-9A	2.86806	0.73826	0.04977	0.980	3945	20	3812	66	3564
207-1A	1.90115	0.77656	0.03006	0.928	4003	23	3900	41	3705
207-2A	1.99916	0.83328	0.03334	0.964	3980	16	3955	40	3907
207-2B	1.77681	0.80650	0.03149	0.966	3891	16	3864	39	3812
207-3A	0.99177	0.64803	0.02663	0.970	3258	16	3244	40	3220
207-4A	1.16610	0.67060	0.02696	0.968	3490	16	3422	40	3308
207-4B	1.07555	0.70237	0.02462	0.959	3490	16	3468	35	3430
207-4C	0.96274	0.46478	0.02343	0.970	3413	19	3018	49	2461
207-5A	1.19256	0.62931	0.02945	0.976	3400	16	3304	46	3147
207-6A	2.01871	0.77348	0.03446	0.973	3959	16	3867	44	3693
207-6B	1.96051	0.81231	0.03270	0.965	3981	16	3931	41	3833
207-7A	0.89787	0.63587	0.02359	0.959	3274	17	3235	37	3173
207-7B	0.88275	0.64077	0.02310	0.946	3260	19	3234	36	3192
119-1A	1.86757	0.77178	0.03283	0.968	3906	16	3831	43	3687
119-2A	2.12099	0.77467	0.03869	0.977	3864	17	3807	49	3698
119-3A	1.79010	0.79754	0.02938	0.962	4000	16	3925	37	3780
119-4A	1.08273	0.66820	0.02690	0.964	3371	17	3344	40	3299
119-5A	1.06653	0.65813	0.02748	0.968	3320	17	3297	41	3260
119-6A	2.13048	0.78574	0.03570	0.970	3982	17	3899	45	3738
119-6B	2.42763	0.90789	0.04095	0.970	3972	17	4035	45	4164
119-7A	1.08797	0.67432	0.02648	0.965	3405	16	3374	39	3323
119-2A	1.18401	0.54089	0.02647	0.953	3517	24	3229	49	2787
119-3A	1.48020	0.64613	0.03436	0.960	3470	24	3374	53	3213
119-3B	1.01424	0.56118	0.02632	0.948	3277	24	3116	47	2872
119-4A1	1.93615	0.78563	0.03667	0.952	3769	23	3758	47	3737
119-4A2	0.92259	0.51862	0.02425	0.941	3245	26	3020	47	2693
119-4B1	2.21100	0.75008	0.04462	0.945	3662	31	3643	60	3608
119-5A	2.01093	0.71719	0.03730	0.930	3765	31	3665	54	3486
119-6A	2.62058	0.86266	0.04367	0.960	3974	22	3986	51	4010
119-6B	2.15712	0.75148	0.03886	0.957	3853	23	3769	52	3613
119-6C	1.97976	0.75936	0.03671	0.953	3803	23	3746	49	3642
119-6D	2.20374	0.82993	0.04081	0.954	3807	23	3837	50	3895
119-6E	1.51666	0.65515	0.03553	0.955	3448	26	3373	54	3248
119-7A	1.25849	0.60238	0.03097	0.956	3373	24	3244	51	3039

Spot Name	2σ	206Pb/238U	2σ	r	207Pb/206Pb age (Ma)	2σ error (Ma)	207Pb/235U age (Ma)	2σ error (Ma)	206Pb/238U age (Ma)
127-10A	1.55639	0.71274	0.03378	0.975	3597	17	3551	47	3469
127-10B	1.99575	0.71865	0.04367	0.985	3601	16	3561	59	3491
127-1A	1.21973	0.66266	0.02810	0.969	3497	17	3415	42	3277
127-1B	1.39796	0.66931	0.03158	0.972	3532	17	3447	47	3303
127-2A	1.27138	0.57919	0.02948	0.975	3496	18	3283	50	2945
127-3A	1.34525	0.69114	0.02971	0.971	3564	16	3499	43	3387
127-3B	1.25904	0.69914	0.02736	0.966	3581	16	3521	39	3417
127-4A	1.31887	0.72837	0.02840	0.965	3594	16	3570	39	3527
127-5A	1.32759	0.72684	0.02885	0.965	3579	17	3558	40	3522
127-6A	1.47779	0.65928	0.03265	0.970	3562	19	3452	49	3264
127-7A	1.35664	0.68492	0.02941	0.971	3593	16	3509	43	3363
127-8A	1.54416	0.64722	0.03378	0.980	3593	16	3453	51	3217
127-8B	2.17933	0.73634	0.04884	0.986	3566	17	3563	64	3557
127-9A	1.62603	0.72224	0.03563	0.978	3587	16	3557	49	3504
127-9B	1.41919	0.71123	0.03181	0.972	3543	17	3514	44	3463
127-1A	1.78386	0.57990	0.04145	0.981	3502	21	3288	69	2948
127-1B	0.74888	0.33950	0.02059	0.972	3225	23	2605	57	1884
127-1C	1.15981	0.39306	0.03109	0.968	3258	32	2763	75	2137
127-2A	0.76150	0.32773	0.02226	0.971	3126	26	2514	63	1827
127-4A	1.94139	0.62509	0.04607	0.983	3472	21	3342	71	3130
127-4B	1.21292	0.51327	0.03445	0.979	3184	22	2973	64	2671
127-5A	2.11204	0.74571	0.04693	0.977	3564	21	3574	62	3592
127-6A	1.84482	0.70680	0.04140	0.966	3532	24	3501	58	3446
127-6B	1.28318	0.55213	0.03242	0.974	3361	21	3152	57	2834
127-7A	2.13994	0.71668	0.04772	0.980	3563	21	3534	65	3484
127-8A	1.78878	0.69167	0.04359	0.965	3403	26	3398	62	3389
127-8B	0.85643	0.31584	0.02663	0.823	2760	92	2271	89	1769
127-8C	2.06976	0.67077	0.05112	0.985	3413	21	3374	73	3309
136-10A	1.66704	0.52471	0.04247	0.975	3350	28	3095	77	2719
136-1A	0.67326	0.64134	0.01542	0.945	3467	13	3364	25	3194
136-2A	1.11999	0.68644	0.02661	0.978	3463	13	3428	38	3369
136-2B	0.77846	0.64910	0.01941	0.960	3358	14	3308	30	3225
136-3A	0.76852	0.68224	0.01711	0.917	3464	17	3423	26	3353
136-4A	1.07655	0.64145	0.02088	0.915	3673	22	3496	34	3195
136-4B	1.10829	0.68389	0.02190	0.971	3734	12	3598	32	3359
136-7A	1.47653	0.51776	0.03327	0.964	3522	27	3190	63	2690

Spot Name	2σ	206Pb/238U	2σ	r	207Pb/206Pb age (Ma)	2σ error (Ma)	207Pb/235U age (Ma)	2σ error (Ma)	206Pb/238U age (Ma)
136-8A	0.87861	0.21483	0.02434	0.989	3240	27	2193	98	1254
136-8B	0.60160	0.18104	0.01655	0.983	3241	27	2041	79	1073
136-9A	0.75147	0.28787	0.01691	0.944	3492	31	2610	57	1631
136-2B	1.18837	0.62408	0.02892	0.950	3380	24	3283	47	3126
136-2B	1.51218	0.62581	0.03913	0.963	3305	27	3239	61	3133
136-6A	1.37368	0.63261	0.03066	0.956	3523	23	3386	48	3160
136-6A	1.71930	0.63436	0.04067	0.965	3449	27	3342	63	3167
136-6B	1.25820	0.62624	0.02805	0.948	3513	23	3370	45	3135
136-6B	1.62385	0.62797	0.03855	0.962	3439	27	3326	60	3142
136-12A	2.09567	0.60328	0.05136	0.979	3415	28	3272	81	3043
136-12B	1.98659	0.53076	0.04803	0.983	3443	26	3165	86	2745
136-3B	0.88808	0.66283	0.01983	0.931	3483	18	3406	31	3278
136-5A	0.90593	0.66379	0.02135	0.963	3451	14	3388	32	3282
136-6A	0.94745	0.65797	0.02178	0.971	3502	13	3412	33	3259
136-6B	0.78378	0.65133	0.01787	0.956	3491	13	3395	28	3233
136-11A	1.31094	0.53460	0.03009	0.953	3477	27	3193	56	2761
141-1A	1.39626	0.61757	0.03383	0.963	3409	23	3291	54	3100
141-1B	3.21236	0.80184	0.05399	0.977	3988	22	3922	66	3796
141-1C	1.31528	0.61855	0.03151	0.958	3418	24	3298	51	3104
141-1D	2.18285	0.71407	0.03894	0.957	3867	25	3728	55	3474
141-1E	1.35022	0.59510	0.03366	0.966	3370	23	3230	55	3010
141-1F	1.50946	0.55953	0.02775	0.955	3818	23	3455	50	2865
141-1G	1.68560	0.71436	0.03293	0.945	3711	24	3626	47	3475
141-1H	1.33952	0.61723	0.03333	0.963	3367	23	3264	53	3099
141-1I	1.45532	0.62953	0.03546	0.962	3397	25	3302	56	3148
141-2A	1.35029	0.66590	0.03130	0.954	3462	23	3398	47	3290
141-2B	1.18191	0.62539	0.02759	0.946	3438	23	3321	45	3131
141-2C	0.60744	0.39892	0.01696	0.923	3119	28	2694	43	2164
141-3A	1.70942	0.61213	0.03090	0.943	3826	27	3549	51	3079
141-4A	2.01580	0.68765	0.03377	0.952	3954	24	3747	50	3374
141-4B	2.13172	0.75874	0.03443	0.947	4001	23	3876	47	3640
141-4C	1.06814	0.59357	0.02849	0.952	3240	24	3147	48	3004
141-4D	1.81858	0.64942	0.03069	0.929	3907	28	3660	49	3226
141-5A1	1.98152	0.79753	0.03555	0.946	3841	23	3820	46	3780
141-5A2	2.12004	0.69645	0.04637	0.937	3525	38	3482	67	3407
141-5A3	1.71982	0.72429	0.04192	0.966	3403	24	3443	57	3512

Spot Name	2σ	206Pb/238U	2σ	r	207Pb/206Pb age (Ma)	2σ error (Ma)	207Pb/235U age (Ma)	2σ error (Ma)	206Pb/238U age (Ma)
141-5B1	1.26179	0.65542	0.02944	0.944	3436	24	3366	46	3249
141-5B2	1.34649	0.66712	0.03382	0.957	3343	24	3325	50	3295
141-6A	2.32853	0.83495	0.03927	0.954	3947	22	3936	48	3913
141-6B	2.32103	0.78270	0.03855	0.951	3965	24	3883	50	3727
141-6C	1.37408	0.61822	0.03004	0.949	3544	25	3377	49	3103
144-10A	0.87571	0.52317	0.01966	0.928	3468	23	3166	39	2713
144-11A	1.08568	0.54666	0.02673	0.952	3365	24	3145	49	2811
144-1A	1.21398	0.63170	0.02592	0.937	3562	23	3409	42	3156
144-1B	1.08420	0.59583	0.02449	0.936	3473	24	3296	42	3013
144-1C	1.43573	0.64600	0.03260	0.958	3501	23	3393	50	3213
144-2A	1.43562	0.70185	0.03101	0.947	3559	23	3511	45	3428
144-3A	1.44903	0.65135	0.03091	0.950	3585	24	3454	48	3233
144-4A	1.35767	0.69537	0.02864	0.940	3586	23	3519	42	3403
144-5A	1.42877	0.69732	0.03162	0.948	3524	23	3482	46	3410
144-6A	1.43608	0.70791	0.03051	0.945	3582	23	3534	44	3451
144-7A	1.39245	0.58730	0.03121	0.955	3516	25	3309	53	2978
144-8A	1.21767	0.62238	0.02692	0.942	3516	24	3366	44	3119
144-9A	1.30061	0.67698	0.02836	0.943	3539	23	3463	43	3333
144C-2A1	0.44169	0.37239	0.01739	0.921	2554	33	2308	45	2041
144C-2A2	1.09045	0.61930	0.02719	0.956	3352	21	3258	44	3107
144C-2B1	0.78515	0.52881	0.02261	0.960	3131	20	2969	42	2736
144C-2B2	0.98865	0.49094	0.03065	0.970	3031	25	2838	60	2575
144C-3A	1.48395	0.80917	0.03374	0.960	3502	19	3615	42	3822
144C-3B	0.42808	0.35721	0.01546	0.926	2707	29	2354	42	1969
144C-4A	1.14829	0.50919	0.03025	0.968	3285	24	3027	58	2653
144C-4B	1.81512	0.63484	0.04294	0.973	3462	24	3351	66	3169
144C-5A	1.19608	0.64954	0.02787	0.960	3464	19	3375	43	3226
144C-6A	1.43717	0.72121	0.03174	0.963	3551	19	3533	44	3501
144C-6B	1.78828	0.68058	0.03977	0.978	3565	19	3485	57	3347
144C-6D	1.53168	0.64699	0.03652	0.959	3427	26	3348	56	3216
145-11A	2.29969	0.85890	0.04028	0.982	3934	13	3955	46	3997
145-11B	1.80744	0.78995	0.03454	0.933	3724	26	3734	45	3753
145-11C	2.45807	0.83683	0.04215	0.983	3968	14	3951	50	3920
145-11D	1.62151	0.58771	0.03006	0.958	3812	23	3500	51	2980
145-11E	2.10850	0.84238	0.03655	0.980	3946	13	3944	43	3939
145-12A	1.99299	0.80772	0.03444	0.977	3946	14	3902	42	3817

Spot Name	2σ	206Pb/238U	2σ	r	207Pb/206Pb age (Ma)	2σ error (Ma)	207Pb/235U age (Ma)	2σ error (Ma)	206Pb/238U age (Ma)
145-12B	0.79318	0.50559	0.02200	0.934	3148	26	2937	44	2638
145-2A	1.23783	0.58278	0.02484	0.963	3698	18	3418	43	2960
145-2B	1.46813	0.63200	0.03264	0.943	3510	28	3377	52	3158
145-3A	2.09395	0.78646	0.03507	0.964	3973	18	3893	45	3740
145-3B	2.04258	0.76581	0.03512	0.974	3949	16	3851	46	3665
145-3C	1.13094	0.62983	0.02636	0.977	3490	14	3361	41	3149
145-3D	2.23171	0.82518	0.03852	0.974	3943	16	3921	47	3879
145-7A	1.20864	0.62448	0.02463	0.974	3693	14	3482	39	3128
145-7B	1.40079	0.69583	0.03173	0.961	3510	20	3472	46	3405
145-7C	1.52018	0.69541	0.02681	0.910	3809	26	3664	41	3403
145-9A	3.66946	0.81297	0.06535	0.990	3922	17	3892	78	3835
146-10A	1.39712	0.61140	0.03816	0.977	3243	21	3178	60	3076
146-10B	1.84809	0.61094	0.04365	0.982	3478	21	3324	69	3074
146-1A	3.24137	0.82580	0.05434	0.980	3996	20	3957	65	3881
146-1B	1.89994	0.59987	0.03674	0.972	3768	22	3491	60	3029
146-1C	1.14756	0.45079	0.02972	0.973	3320	24	2931	63	2399
146-2A	1.67503	0.64683	0.04083	0.978	3422	21	3344	61	3216
146-5A	1.81691	0.60023	0.04166	0.979	3520	22	3333	67	3031
146-5B	1.96739	0.69338	0.04580	0.980	3497	21	3460	64	3396
146-5C	2.88885	0.83860	0.05366	0.978	3839	21	3868	63	3926
146-6A	1.53899	0.65161	0.04147	0.976	3264	22	3253	62	3235
146-6B	1.51620	0.58633	0.04107	0.979	3259	23	3147	67	2975
146-7A	2.96011	0.85571	0.04999	0.975	3977	20	3980	58	3986
146-7B	2.61385	0.75591	0.04441	0.972	3965	21	3848	58	3629
146-7C	1.57671	0.64283	0.03935	0.976	3382	21	3313	59	3200
146-8A	1.65560	0.61681	0.04295	0.981	3330	22	3240	67	3097
146-8B	1.99613	0.64667	0.04897	0.985	3423	21	3345	73	3215
146-9A	2.86806	0.73826	0.04977	0.980	3945	20	3812	66	3564
171-10A	0.87316	0.47155	0.02122	0.946	3376	24	3009	45	2490
171-10B	1.29322	0.68148	0.02915	0.944	3490	23	3438	43	3350
171-11A	1.37889	0.72695	0.02915	0.938	3578	23	3558	41	3522
171-11B	1.36334	0.72830	0.02858	0.935	3586	23	3565	41	3527
171-12A	1.46722	0.73286	0.03081	0.939	3591	23	3574	43	3544
171-12B	1.37392	0.73089	0.02908	0.937	3574	23	3561	41	3537
171-1A	1.18790	0.63318	0.02439	0.850	3472	36	3355	43	3162
171-1B	1.37475	0.70955	0.02955	0.942	3560	23	3522	43	3457

Spot Name	2σ	206Pb/238U	2σ	r	207Pb/206Pb age (Ma)	2σ error (Ma)	207Pb/235U age (Ma)	2σ error (Ma)	206Pb/238U age (Ma)
171-2A	1.65562	0.73063	0.03539	0.956	3590	23	3571	49	3536
171-2B	1.67607	0.70413	0.03617	0.961	3584	23	3530	51	3436
171-3A	2.13726	0.68889	0.04713	0.977	3577	23	3504	67	3378
171-4A	1.44315	0.72001	0.03057	0.944	3586	23	3553	43	3496
171-4B	1.64432	0.76816	0.03529	0.952	3578	23	3612	47	3674
171-5A	1.49318	0.73754	0.03226	0.947	3559	23	3560	45	3561
171-5B	1.06769	0.62445	0.02459	0.928	3430	24	3315	41	3128
171-6A	1.40763	0.74762	0.02971	0.937	3579	23	3586	41	3599
171-6B	1.66051	0.75285	0.03571	0.955	3579	23	3593	48	3618
171-7A	1.45255	0.69533	0.03202	0.949	3532	23	3484	47	3403
171-8A	1.41900	0.75374	0.03004	0.937	3574	23	3591	41	3621
171-9A	1.51612	0.73036	0.03231	0.948	3583	23	3565	45	3535
171-9B	1.58204	0.73266	0.03397	0.952	3578	23	3565	47	3543
101-1A	1.74753	0.70393	0.03428	0.977	3754	16	3640	48	3436
101-1B	1.37155	0.67533	0.02685	0.966	3741	16	3591	40	3326
101-2A	2.46791	0.76066	0.04979	0.983	3722	18	3696	64	3647
101-2B	2.05642	0.75827	0.04108	0.981	3734	16	3700	53	3638
101-3A	1.12896	0.33133	0.02642	0.982	3493	23	2743	74	1845
101-3B	1.80988	0.68419	0.04153	0.985	3527	16	3466	59	3360
101-4A	2.09046	0.75643	0.04116	0.982	3757	16	3713	53	3631
101-4B	1.79785	0.80173	0.03543	0.973	3742	16	3760	44	3795
101-5A	1.90208	0.78946	0.03788	0.977	3732	16	3739	47	3751
101-6A	1.82603	0.67718	0.04040	0.944	3519	32	3451	60	3334
101-7A	1.84954	0.71014	0.03786	0.977	3691	17	3607	52	3459
101-7B	1.27715	0.69679	0.02932	0.966	3497	17	3464	42	3408
101-8A	1.68751	0.70756	0.03365	0.975	3727	16	3627	47	3449
101-8B	1.63008	0.69506	0.03343	0.971	3678	18	3578	48	3402
101-9A	1.29229	0.71651	0.02518	0.956	3732	16	3643	36	3483
101-9B	1.48611	0.78852	0.02905	0.961	3735	16	3740	37	3748
101-10A1	1.02354	0.64395	0.02692	0.951	3260	21	3239	42	3205
101-10A2	1.53697	0.74581	0.03219	0.953	3618	21	3609	44	3592
101-10B1	1.46185	0.74299	0.02794	0.941	3738	20	3683	39	3582
101-10B2	1.57086	0.78233	0.03102	0.946	3696	21	3706	41	3726
101-1A	1.67611	0.77426	0.03390	0.950	3665	22	3676	45	3696
101-1B	1.73690	0.76257	0.03363	0.956	3742	20	3711	45	3654
101-2A	1.97081	0.63279	0.03783	0.966	3771	24	3546	59	3161

Spot Name	2σ	206Pb/238U	2σ	r	207Pb/206Pb age (Ma)	2σ error (Ma)	207Pb/235U age (Ma)	2σ error (Ma)	206Pb/238U age (Ma)
101-3A	1.45647	0.71018	0.02722	0.863	3639	34	3574	43	3459
101-3B	1.45349	0.76327	0.02748	0.937	3747	20	3715	37	3656
101-4A	1.08034	0.61043	0.02422	0.946	3501	21	3337	40	3072
101-4B	1.43022	0.74834	0.02761	0.940	3720	20	3678	38	3601
101-4C	1.30400	0.72786	0.02471	0.929	3731	20	3658	35	3525
101-5A	1.44232	0.73417	0.02776	0.942	3729	20	3665	39	3549
101-6A	1.20765	0.66180	0.02777	0.951	3470	21	3397	42	3274
101-6B	1.09791	0.64043	0.02550	0.946	3445	21	3349	40	3191
101-7A	1.31529	0.69258	0.02441	0.881	3681	29	3576	39	3392
101-8A	1.78314	0.79912	0.03419	0.954	3753	20	3764	43	3786
101-8B	1.00600	0.66616	0.02462	0.939	3352	21	3329	38	3291
101-9A	1.79525	0.77989	0.03596	0.960	3696	20	3703	46	3717
102-10B	1.05153	0.56054	0.03759	0.981	2819	21	2840	63	2869
102-11A	1.44654	0.70201	0.03242	0.971	3542	17	3500	46	3428
102-12B	1.11889	0.64940	0.03078	0.983	3242	14	3236	46	3226
102-13A	1.86198	0.75282	0.03837	0.985	3692	14	3666	50	3618
102-14B	2.05408	0.58141	0.04409	0.991	3639	16	3377	72	2955
102-15B	1.45148	0.69165	0.03373	0.981	3502	15	3460	48	3389
102-1A	1.44949	0.69873	0.03293	0.969	3518	18	3481	47	3416
102-1B	1.40099	0.67205	0.03295	0.984	3488	14	3423	48	3314
102-2A	1.46218	0.66639	0.03535	0.983	3444	15	3387	51	3292
102-2B	1.50403	0.67572	0.03431	0.984	3536	14	3459	49	3328
102-3A	1.64400	0.77476	0.03326	0.974	3703	15	3701	43	3698
102-4A	1.71123	0.70863	0.03919	0.987	3534	14	3504	54	3453
102-4B	1.42325	0.69875	0.03309	0.982	3502	14	3470	46	3416
102-5A	1.23929	0.64027	0.03423	0.985	3238	15	3220	51	3190
102-6A	1.63678	0.71764	0.03755	0.984	3527	14	3512	51	3487
102-7A	1.42044	0.64273	0.03381	0.985	3472	14	3369	51	3200
102-8A	1.55199	0.68334	0.03670	0.985	3480	15	3435	52	3357
102-8B	1.72165	0.70754	0.03978	0.987	3521	14	3495	54	3449
102-9A	1.33977	0.68651	0.03101	0.981	3508	14	3457	44	3369
102-9B	1.42659	0.69368	0.03365	0.983	3481	14	3450	47	3397
108-1A	2.56573	0.79358	0.04301	0.982	3999	16	3920	53	3766
108-1B	2.11691	0.83557	0.03524	0.970	3992	16	3966	42	3915
108-2A	2.57147	0.81518	0.04300	0.981	4001	16	3948	52	3843
108-2B	1.48877	0.64729	0.03415	0.980	3521	16	3407	51	3218

Spot Name	2σ	206Pb/238U	2σ	r	207Pb/206Pb age (Ma)	2σ error (Ma)	207Pb/235U age (Ma)	2σ error (Ma)	206Pb/238U age (Ma)
108-3A	2.52341	0.78856	0.04251	0.981	3991	16	3908	53	3748
108-3B	1.54760	0.56086	0.03071	0.980	3742	17	3408	53	2870
108-3C	1.08891	0.58591	0.02503	0.957	3480	20	3284	43	2973
108-4A	2.31908	0.79957	0.03907	0.978	3985	16	3918	48	3788
108-4B	2.36549	0.77682	0.04082	0.980	3954	16	3868	52	3706
108-5A	2.64681	0.80208	0.04424	0.982	4004	16	3934	54	3797
108-5B	1.39537	0.58303	0.03361	0.982	3447	17	3259	56	2961
108-6A	2.13566	0.81292	0.03526	0.971	4006	16	3948	43	3835
108-6B	2.35271	0.70944	0.04215	0.979	3895	19	3739	58	3456
114-10A	0.51729	0.26983	0.01381	0.976	3278	18	2423	47	1540
114-11A	1.34573	0.71021	0.02917	0.969	3589	16	3542	41	3459
114-12A	1.24262	0.66514	0.03202	0.977	3335	16	3317	47	3287
114-12B	0.56346	0.38346	0.01469	0.743	2881	55	2517	47	2092
114-1A	1.37458	0.72227	0.02962	0.967	3596	16	3563	41	3505
114-1B	1.59723	0.75318	0.03417	0.968	3608	18	3612	45	3619
114-2A	1.20440	0.65251	0.02678	0.967	3548	17	3432	41	3238
114-3A	1.34058	0.71856	0.02980	0.969	3552	16	3529	41	3491
114-4A	1.71134	0.70382	0.03809	0.981	3569	16	3520	53	3435
114-4B	1.02789	0.59371	0.02290	0.963	3539	16	3334	38	3004
114-5A	1.41080	0.73097	0.03069	0.969	3585	16	3568	42	3537
114-5B	0.86277	0.50243	0.02247	0.973	3312	17	3030	43	2624
114-6A	1.07062	0.63291	0.02459	0.957	3481	18	3360	39	3161
114-7A	1.61305	0.73773	0.03192	0.970	3731	16	3671	43	3562
114-8A	1.42422	0.66743	0.03223	0.974	3532	17	3445	48	3296
114-8B	1.25600	0.66275	0.03307	0.977	3301	17	3292	49	3278
114-9A	1.12778	0.64838	0.02864	0.972	3350	16	3301	43	3222
114-9B	1.33231	0.68945	0.03055	0.950	3473	22	3439	45	3381
115-11A	1.47955	0.70924	0.03229	0.952	3553	22	3517	46	3456
115-2A	0.97122	0.50436	0.02667	0.954	3196	26	2963	52	2633
115-2B	1.22162	0.64544	0.03131	0.941	3285	27	3256	49	3210
115-5A	1.25052	0.45976	0.03270	0.952	3271	35	2920	69	2438
115-9A	1.17395	0.66513	0.02961	0.949	3323	23	3310	45	3287
115-10A	2.05354	0.74509	0.04448	0.966	3587	24	3588	59	3589
115-10B	1.63007	0.73085	0.03557	0.956	3559	23	3551	49	3537
115-12A	1.55539	0.68681	0.03389	0.958	3564	23	3493	49	3370
115-13A	1.49096	0.73027	0.03151	0.947	3593	22	3572	44	3534

Spot Name	2σ	206Pb/238U	2σ	r	207Pb/206Pb age (Ma)	2σ error (Ma)	207Pb/235U age (Ma)	2σ error (Ma)	206Pb/238U age (Ma)
115-14A	2.04401	0.71058	0.04615	0.974	3536	23	3508	64	3461
115-14B	1.41429	0.54455	0.03065	0.959	3574	25	3272	56	2802
115-1A	1.72227	0.68877	0.03766	0.963	3568	23	3498	54	3378
115-3A	1.76044	0.74808	0.03839	0.961	3568	22	3580	51	3600
115-4A	1.61444	0.65766	0.03530	0.945	3539	28	3434	54	3258
115-4B	1.92299	0.57064	0.04623	0.971	3433	31	3229	78	2910
115-7A	1.85261	0.69117	0.04042	0.970	3582	22	3510	58	3387
115-8A	1.61234	0.65097	0.03742	0.958	3467	26	3379	57	3232
119-11A	1.34737	0.60563	0.03179	0.954	3435	25	3288	52	3052
119-12A	1.73952	0.69258	0.03938	0.968	3521	23	3474	56	3392
119-3A	1.71031	0.71710	0.03721	0.963	3574	22	3542	52	3485
119-4A	1.83790	0.62688	0.03981	0.969	3591	25	3421	62	3137
119-10A	1.50399	0.74148	0.03198	0.947	3584	22	3581	44	3576
119-13A	1.71016	0.69361	0.03824	0.964	3535	23	3484	55	3396
119-13B	1.52395	0.66555	0.03420	0.957	3518	24	3433	51	3289
119-14A	1.71210	0.58211	0.03420	0.817	3453	63	3260	68	2957
119-14B	1.84002	0.59770	0.04325	0.970	3467	28	3295	70	3021
119-1A	1.45693	0.69550	0.03070	0.949	3601	22	3529	45	3404
119-1B	1.78328	0.70614	0.03838	0.966	3596	22	3541	54	3444
119-1C	1.44782	0.70036	0.03058	0.948	3596	22	3533	44	3422
119-2A	1.81295	0.76764	0.03910	0.961	3585	22	3616	51	3672
119-6A	1.56412	0.72480	0.03378	0.952	3568	23	3549	47	3514
119-7A	1.41270	0.69648	0.03121	0.949	3528	23	3484	45	3407
119-7B	1.65557	0.70960	0.03615	0.959	3562	23	3524	51	3457
119-8A	1.70233	0.70949	0.03857	0.963	3511	23	3491	54	3457
119-8B	1.55672	0.71876	0.03366	0.952	3567	23	3540	47	3491
119-9A	1.93475	0.72680	0.04262	0.965	3559	24	3545	58	3521
205-10A	1.46474	0.62280	0.03433	0.964	3462	23	3332	54	3121
205-10B	1.93603	0.71173	0.04280	0.970	3561	23	3526	59	3465
205-11A	1.84108	0.75406	0.04030	0.965	3568	22	3587	53	3622
205-12A	1.53136	0.69952	0.03265	0.954	3592	22	3529	47	3419
205-12B	1.89304	0.68662	0.04099	0.971	3595	22	3513	59	3370
205-14A	1.64183	0.72888	0.03524	0.954	3582	23	3563	49	3529
205-15A	1.87147	0.71663	0.04063	0.965	3582	23	3546	56	3483
205-16A	2.29363	0.78669	0.04196	0.960	3834	23	3802	54	3741
205-1A	1.83027	0.65074	0.04150	0.970	3523	24	3414	62	3231

Spot Name	2σ	206Pb/238U	2σ	r	207Pb/206Pb age (Ma)	2σ error (Ma)	207Pb/235U age (Ma)	2σ error (Ma)	206Pb/238U age (Ma)
205-2A	2.30783	0.47439	0.05327	0.984	3517	31	3102	105	2503
205-3A	1.66062	0.69371	0.03576	0.962	3589	22	3519	51	3397
205-4A	1.75037	0.73712	0.03840	0.960	3557	23	3558	52	3560
205-4B	1.78094	0.72936	0.03920	0.964	3559	23	3549	53	3531
205-5A	1.63550	0.69719	0.03535	0.961	3582	22	3519	51	3410
205-6A	1.75035	0.69458	0.03751	0.963	3598	23	3526	54	3400
205-7A	1.79763	0.61308	0.04593	0.975	3344	27	3243	72	3082
205-8A	1.03993	0.53729	0.02699	0.954	3287	24	3079	50	2772
205-9A	1.82653	0.70906	0.04017	0.968	3566	22	3526	56	3455
206-10A	1.28247	0.59309	0.03086	0.952	3401	26	3246	52	3002
206-10B	1.95847	0.67308	0.04668	0.975	3453	24	3403	67	3318
206-11A	2.34391	0.80960	0.04153	0.984	3919	14	3887	51	3823
206-12A	1.62232	0.68345	0.03332	0.972	3677	18	3561	48	3358
206-13A	2.51136	0.70047	0.04863	0.987	3790	17	3658	67	3422
206-14A	2.31023	0.76025	0.04111	0.981	3909	16	3817	53	3645
206-15A	2.11852	0.74180	0.03813	0.980	3890	15	3781	51	3577
206-16A	1.77247	0.67081	0.03473	0.966	3740	21	3583	51	3309
206-16B	1.87193	0.71223	0.03637	0.982	3778	15	3667	50	3467
206-17A	2.51054	0.83735	0.04368	0.985	3948	14	3939	51	3922
206-1A	1.19811	0.56967	0.03158	0.982	3307	17	3149	53	2906
206-2A	2.66729	0.82049	0.04821	0.991	3900	12	3887	57	3862
206-2B	1.92457	0.73026	0.03916	0.985	3712	14	3648	52	3534
206-3A	2.77962	0.78366	0.05542	0.993	3755	13	3746	68	3730
206-4A	2.45346	0.77190	0.04484	0.990	3882	13	3814	57	3688
206-5A	2.18928	0.73458	0.04626	0.990	3662	14	3622	61	3550
206-6A	3.27704	0.77693	0.05660	0.994	3973	12	3881	70	3706
206-7A	2.73015	0.82457	0.04734	0.991	3963	11	3934	56	3877
206-8A	1.85733	0.70649	0.03608	0.979	3773	16	3656	50	3445
206-9A	2.06759	0.80248	0.03804	0.975	3850	16	3832	47	3798
208-10A	1.55780	0.65095	0.03576	0.965	3495	23	3397	54	3232
208-10B	1.41031	0.65663	0.03196	0.956	3501	23	3409	49	3254
208-11A	1.46293	0.66485	0.03244	0.957	3537	23	3444	49	3286
208-12A	1.83277	0.69389	0.03968	0.969	3591	22	3521	56	3397
208-13A	1.60682	0.76874	0.03581	0.954	3523	22	3578	47	3676
208-14A	1.98101	0.71724	0.04324	0.972	3584	22	3548	59	3486
208-15A	1.36281	0.68001	0.02972	0.946	3544	23	3470	44	3344

Spot Name	2σ	206Pb/238U	2σ	r	207Pb/206Pb age (Ma)	2σ error (Ma)	207Pb/235U age (Ma)	2σ error (Ma)	206Pb/238U age (Ma)
208-16A	2.00023	0.70877	0.04415	0.973	3569	22	3527	61	3454
208-18A	1.48541	0.65037	0.03879	0.971	3305	23	3276	58	3230
208-1A	1.82031	0.67224	0.03998	0.971	3572	23	3477	58	3315
208-2A	1.93147	0.72345	0.04210	0.970	3583	22	3556	57	3509
208-3A	1.87841	0.72290	0.04386	0.972	3480	23	3490	60	3507
208-4A	1.83500	0.71747	0.04038	0.968	3565	22	3536	56	3487
208-5A	1.45017	0.68910	0.03135	0.943	3551	25	3488	46	3379
208-6A	1.80633	0.68727	0.04058	0.969	3536	23	3475	58	3372
208-6B	1.44368	0.70280	0.03129	0.950	3559	22	3512	45	3431
208-7A	1.09193	0.62453	0.02855	0.947	3264	24	3211	46	3128
208-8A	1.66298	0.59475	0.04120	0.960	3369	31	3229	68	3009
208-9A	1.83724	0.66931	0.04231	0.973	3503	23	3429	62	3303
303-10A	1.41347	0.67440	0.03174	0.949	3503	24	3436	48	3323
303-14A	1.45586	0.69881	0.03127	0.891	3475	35	3453	48	3416
303-15A	2.01046	0.74674	0.03825	0.957	3770	23	3709	52	3595
303-1A	3.29964	0.79117	0.05700	0.977	3946	24	3882	71	3757
303-2A	1.79357	0.70270	0.04186	0.968	3474	24	3458	59	3431
303-2B	1.54855	0.73046	0.03317	0.930	3545	27	3542	47	3535
303-5B	1.67385	0.68941	0.03698	0.940	3514	30	3465	55	3380
303-6A	1.40858	0.64795	0.03436	0.946	3370	28	3313	53	3220
303-6B	1.97653	0.76434	0.03516	0.938	3841	25	3778	47	3660
303-7A	2.26077	0.79353	0.04180	0.951	3804	26	3791	53	3766
303-8A	1.45710	0.68923	0.03440	0.954	3434	24	3414	50	3380
303-9A	2.18614	0.74385	0.05338	0.973	3412	26	3475	70	3585
304-10A	0.80469	0.56441	0.02622	0.954	2924	23	2908	46	2885
304-11A	0.93983	0.57857	0.03067	0.964	2938	23	2940	51	2943
304-11B	0.97723	0.58474	0.03159	0.965	2955	23	2961	52	2968
304-12A	0.90995	0.56158	0.02926	0.960	2956	24	2922	51	2873
304-13A	0.84605	0.58104	0.02751	0.955	2928	24	2938	46	2953
304-1A	1.11482	0.58944	0.03729	0.974	2914	24	2944	60	2987
304-2A	0.89790	0.51571	0.03162	0.967	2820	26	2761	58	2681
304-3A	0.91589	0.58577	0.02962	0.961	2948	23	2958	49	2972
304-3B	0.96680	0.58674	0.03138	0.963	2946	24	2958	52	2976
304-4A	1.01523	0.53206	0.03356	0.971	2929	25	2854	60	2750
304-5A	0.88428	0.57307	0.02845	0.959	2953	23	2940	48	2920
304-6A	0.85879	0.56766	0.02818	0.959	2921	24	2911	48	2898

238

Spot Name	2σ	206Pb/238U	2σ	r	207Pb/206Pb age (Ma)	2σ error (Ma)	207Pb/235U age (Ma)	2σ error (Ma)	206Pb/238U age (Ma)
304-6B	0.79402	0.56266	0.02672	0.956	2874	24	2876	46	2878
304-7A	0.80264	0.56987	0.02611	0.953	2924	23	2917	45	2907
304-8A	0.74580	0.57011	0.02379	0.944	2941	23	2928	42	2908
304-8B	0.87087	0.58861	0.02849	0.957	2922	23	2947	47	2984
304-9A	0.85424	0.57956	0.02792	0.957	2923	24	2933	47	2947
305-11A	0.97731	0.63489	0.02578	0.975	3295	14	3247	40	3169
305-14B	0.71840	0.67913	0.01845	0.982	3348	8	3346	27	3341
305-13A	1.22053	0.64858	0.03137	0.995	3368	7	3313	46	3223
305-6A	1.17823	0.66298	0.02921	0.980	3399	14	3354	43	3279
305-7A	0.99098	0.68628	0.02475	0.988	3400	9	3388	35	3368
305-8B	0.84215	0.69891	0.02017	0.972	3441	11	3432	29	3417
305-12A	1.17563	0.67069	0.02852	0.992	3453	8	3399	41	3309
305-14A	0.98118	0.71269	0.02287	0.989	3510	7	3495	31	3469
305-20A	1.35346	0.72619	0.03167	0.994	3511	7	3514	42	3519
305-4A	1.70621	0.65473	0.03869	0.965	3515	24	3415	58	3247
305-9C	1.15414	0.70003	0.02685	0.991	3515	8	3481	37	3421
305-18A	1.22139	0.68749	0.02840	0.991	3516	9	3463	40	3373
305-18B	1.10166	0.68417	0.02545	0.986	3519	10	3460	36	3360
305-9B	1.32805	0.70510	0.03079	0.991	3521	9	3491	42	3440
305-9A	1.21860	0.69899	0.02810	0.989	3526	9	3486	39	3417
305-2B	1.50461	0.68063	0.03326	0.957	3540	23	3469	49	3347
305-2A	1.73596	0.64359	0.03773	0.965	3580	24	3439	58	3203
305-1A	1.97485	0.68556	0.04301	0.969	3583	24	3503	62	3366
305-19A	1.31636	0.68500	0.02862	0.973	3591	15	3508	41	3364
305-8A	1.16695	0.75964	0.02562	0.988	3600	8	3616	33	3643
305-15B	1.20664	0.74621	0.02533	0.952	3612	17	3605	35	3594
305-15A	1.15998	0.70989	0.02488	0.985	3631	10	3568	34	3458
305-3A	1.40322	0.45555	0.02870	0.967	3676	25	3163	61	2420
305-16A	1.58388	0.78745	0.03267	0.985	3691	11	3710	41	3744
802-1A	0.97155	0.63102	0.02483	0.977	3347	13	3273	39	3154
802-2A	0.77032	0.50876	0.01879	0.952	3380	18	3084	37	2651
802-2B	0.89058	0.65962	0.02199	0.966	3384	14	3340	33	3266
802-2C	0.78506	0.61863	0.01903	0.942	3373	17	3270	31	3104
802-2D	1.46524	0.49191	0.03653	0.972	3379	28	3051	71	2579
802-3A	1.08860	0.63019	0.02744	0.978	3370	15	3286	43	3150
802-3B	0.85979	0.60822	0.02179	0.974	3355	13	3242	35	3063

Spot Name	2σ	206Pb/238U	2σ	r	207Pb/206Pb age (Ma)	2σ error (Ma)	207Pb/235U age (Ma)	2σ error (Ma)	206Pb/238U age (Ma)
802-3C	0.93829	0.60612	0.02395	0.977	3350	13	3236	39	3054
802-3D	0.72767	0.63151	0.01806	0.959	3364	13	3284	29	3156
802-4B	0.77508	0.61014	0.01871	0.955	3402	15	3274	31	3071
802-4C	0.70037	0.42088	0.01777	0.977	3359	14	2889	41	2264
802-5A	0.52770	0.43637	0.01262	0.944	3398	16	2947	29	2334
802-6A	0.72239	0.55384	0.01818	0.969	3359	13	3154	32	2841
802-6B	0.66510	0.54664	0.01673	0.965	3352	13	3137	30	2811
802-7A	0.93284	0.60100	0.02400	0.973	3330	15	3215	39	3034
802-8A	0.78014	0.61732	0.01967	0.965	3349	14	3253	32	3099
802-8B	0.43617	0.30179	0.01098	0.972	3363	14	2577	34	1700
802-8C	0.84088	0.36834	0.02138	0.984	3367	16	2767	54	2022
802-9A	1.11644	0.48762	0.02774	0.986	3406	15	3060	54	2560
802-9B	0.83733	0.55891	0.02091	0.973	3378	14	3174	37	2862

Spot Name	2σ error (Ma)	discordance	238U/206Pb	2σ	207Pb/206Pb	2σ
137-1A	164	17.1	1.53027	0.09950	0.35916	0.00554
137-1B	164	23.9	1.73120	0.12206	0.33534	0.00526
137-1C	203	0.6	1.20402	0.08493	0.40170	0.00598
137-1D	208	11.1	1.37619	0.10742	0.38454	0.00578
137-2A	179	-1.3	1.16391	0.07100	0.41326	0.00615
137-2B	208	-6.1	1.14383	0.08054	0.39078	0.00584
137-2C	215	-7.6	1.09686	0.07804	0.41273	0.00626
137-2D	173	-3.3	1.14579	0.06702	0.41026	0.00599
137-2E	157	2.0	1.27437	0.07126	0.37015	0.00551
137-3A	179	-4.3	1.36912	0.09155	0.29071	0.00723
137-4A	153	6.7	1.53282	0.09333	0.28985	0.00439
137-4B	198	7.4	1.31310	0.09480	0.38978	0.00610
137-5A	177	7.7	1.38501	0.09218	0.35448	0.00527
137-6A	146	5.9	1.31222	0.06965	0.37827	0.00556
137-7A	160	0.4	1.22897	0.06906	0.38466	0.00597
137-8A	170	4.2	1.61330	0.11257	0.25514	0.00383
141-1A	133	11.4	1.61925	0.08871	0.28837	0.00439
141-1B	190	6.4	1.24713	0.08397	0.42157	0.00621
141-1C	124	11.5	1.61668	0.08236	0.28998	0.00443
141-1D	145	13.1	1.40042	0.07637	0.38903	0.00644
141-1E	135	13.3	1.68040	0.09504	0.28119	0.00422
141-1F	114	30.8	1.78721	0.08864	0.37655	0.00583
141-1G	123	8.2	1.39986	0.06452	0.35090	0.00559
141-1H	132	10.0	1.62015	0.08749	0.28068	0.00424
141-1I	139	9.3	1.58848	0.08949	0.28619	0.00460
141-2A	120	6.3	1.50174	0.07059	0.29837	0.00442
141-2B	109	11.2	1.59900	0.07054	0.29379	0.00446
141-2C	78	35.9	2.50677	0.10656	0.23985	0.00424
141-3A	122	24.5	1.63365	0.08247	0.37852	0.00671
141-4A	128	18.8	1.45422	0.07141	0.41209	0.00652
141-4B	125	11.8	1.31798	0.05981	0.42528	0.00654
141-4C	114	9.1	1.68471	0.08087	0.25882	0.00400
141-4D	119	22.1	1.53984	0.07277	0.39941	0.00750
141-5A1	126	2.1	1.25387	0.05589	0.38241	0.00585
141-5A2	174	4.3	1.43584	0.09560	0.31082	0.00769
141-5A3	155	-4.2	1.38066	0.07991	0.28732	0.00447

Spot Name	2σ error (Ma)	discordance	238U/206Pb	2σ	207Pb/206Pb	2σ
141-5B1	114	6.9	1.52575	0.06854	0.29352	0.00459
141-5B2	129	1.8	1.49897	0.07599	0.27637	0.00424
141-6A	137	1.1	1.19768	0.05633	0.41025	0.00607
141-6B	138	7.9	1.27763	0.06292	0.41525	0.00666
141-6C	119	15.6	1.61754	0.07861	0.31470	0.00510
145-11A	138	-2.1	1.16428	0.05460	0.40664	0.00367
145-11B	123	-1.0	1.26591	0.05535	0.35397	0.00599
145-11C	146	1.6	1.19498	0.06018	0.41590	0.00389
145-11D	121	27.1	1.70153	0.08702	0.37504	0.00571
145-11E	127	0.2	1.18712	0.05151	0.40997	0.00362
145-12A	122	4.3	1.23806	0.05279	0.40991	0.00385
145-12B	94	19.7	1.97788	0.08606	0.24434	0.00406
145-2A	100	24.8	1.71592	0.07315	0.34793	0.00416
145-2B	128	12.7	1.58227	0.08172	0.30774	0.00559
145-3A	125	7.7	1.27151	0.05671	0.41743	0.00513
145-3B	127	9.4	1.30581	0.05989	0.41078	0.00439
145-3C	103	12.3	1.58774	0.06646	0.30394	0.00278
145-3D	135	2.2	1.21186	0.05658	0.40924	0.00444
145-7A	97	19.2	1.60134	0.06315	0.34670	0.00318
145-7B	119	3.9	1.43713	0.06553	0.30786	0.00402
145-7C	101	13.7	1.43800	0.05544	0.37442	0.00656
145-9A	228	2.9	1.23005	0.09888	0.40333	0.00452
146-10A	151	6.5	1.63560	0.10208	0.25946	0.00353
146-10B	172	14.6	1.63683	0.11694	0.30149	0.00417
146-1A	189	3.8	1.21095	0.07968	0.42390	0.00570
146-1B	146	24.5	1.66702	0.10209	0.36444	0.00543
146-1C	131	33.1	2.21832	0.14623	0.27247	0.00427
146-2A	158	7.7	1.54599	0.09759	0.29089	0.00395
146-5A	166	17.4	1.66602	0.11562	0.30975	0.00446
146-5B	172	3.7	1.44220	0.09526	0.30519	0.00414
146-5C	185	-3.0	1.19247	0.07630	0.38170	0.00526
146-6A	160	1.1	1.53465	0.09766	0.26282	0.00370
146-6B	165	10.9	1.70551	0.11947	0.26205	0.00385
146-7A	171	-0.3	1.16862	0.06827	0.41858	0.00561
146-7B	161	11.0	1.32290	0.07773	0.41506	0.00585
146-7C	153	6.8	1.55563	0.09522	0.28351	0.00391

Spot Name	2σ error (Ma)	discordance	238U/206Pb	2σ	207Pb/206Pb	2σ
146-8A	169	8.8	1.62125	0.11289	0.27419	0.00380
146-8B	189	7.7	1.54637	0.11711	0.29105	0.00392
146-9A	182	12.5	1.35454	0.09131	0.40974	0.00556
207-1A	108	9.8	1.28774	0.04984	0.42572	0.00662
207-2A	116	2.4	1.20008	0.04801	0.41935	0.00461
207-2B	111	2.7	1.23993	0.04841	0.39514	0.00416
207-3A	103	1.5	1.54315	0.06343	0.26191	0.00271
207-4A	103	6.6	1.49119	0.05994	0.30378	0.00315
207-4B	93	2.2	1.42375	0.04990	0.30378	0.00316
207-4C	102	33.4	2.15156	0.10845	0.28913	0.00365
207-5A	115	9.4	1.58905	0.07435	0.28682	0.00297
207-6A	124	8.8	1.29286	0.05760	0.41340	0.00436
207-6B	115	4.9	1.23106	0.04956	0.41968	0.00458
207-7A	92	3.9	1.57264	0.05835	0.26457	0.00292
207-7B	90	2.6	1.56062	0.05627	0.26216	0.00324
119-1A	118	7.4	1.29570	0.05512	0.39931	0.00440
119-2A	139	5.7	1.29087	0.06447	0.38828	0.00428
119-3A	105	7.3	1.25385	0.04619	0.42504	0.00445
119-4A	103	2.7	1.49657	0.06024	0.28148	0.00312
119-5A	106	2.3	1.51947	0.06345	0.27239	0.00296
119-6A	128	8.1	1.27269	0.05782	0.42002	0.00475
119-6B	137	-6.6	1.10145	0.04967	0.41711	0.00471
119-7A	101	3.1	1.48297	0.05823	0.28768	0.00305
119-2A	110	25.4	1.84881	0.09047	0.30915	0.00481
119-3A	133	9.4	1.54767	0.08231	0.30005	0.00463
119-3B	108	15.3	1.78195	0.08358	0.26507	0.00415
119-4A1	131	1.1	1.27287	0.05941	0.36449	0.00548
119-4A2	102	20.7	1.92820	0.09015	0.25968	0.00437
119-4B1	162	1.9	1.33320	0.07930	0.33978	0.00697
119-5A	139	9.6	1.39433	0.07252	0.36351	0.00749
119-6A	149	-1.2	1.15921	0.05868	0.41774	0.00618
119-6B	141	8.1	1.33070	0.06881	0.38532	0.00604
119-6C	133	5.5	1.31689	0.06366	0.37274	0.00574
119-6D	142	-3.1	1.20492	0.05925	0.37374	0.00576
119-6E	137	7.4	1.52636	0.08277	0.29573	0.00497
119-7A	123	12.4	1.66009	0.08535	0.28182	0.00443

Spot Name	2σ error (Ma)	discordance	238U/206Pb	2σ	207Pb/206Pb	2σ
127-10A	126	4.6	1.40304	0.06650	0.32577	0.00353
127-10B	162	3.9	1.39149	0.08456	0.32651	0.00346
127-1A	108	8.0	1.50906	0.06399	0.30515	0.00328
127-1B	121	8.3	1.49407	0.07050	0.31217	0.00354
127-2A	119	19.6	1.72654	0.08787	0.30512	0.00351
127-3A	112	6.4	1.44688	0.06220	0.31885	0.00338
127-3B	103	5.9	1.43033	0.05597	0.32232	0.00339
127-4A	105	2.4	1.37294	0.05353	0.32505	0.00344
127-5A	107	2.1	1.37583	0.05461	0.32197	0.00348
127-6A	126	10.6	1.51679	0.07511	0.31847	0.00395
127-7A	112	8.2	1.46002	0.06269	0.32480	0.00344
127-8A	131	13.2	1.54506	0.08063	0.32483	0.00347
127-8B	179	0.3	1.35806	0.09008	0.31920	0.00353
127-9A	132	3.0	1.38458	0.06830	0.32367	0.00342
127-9B	119	2.9	1.40602	0.06289	0.31442	0.00341
127-1A	167	19.6	1.72443	0.12327	0.30631	0.00428
127-1B	98	47.7	2.94548	0.17862	0.25639	0.00377
127-1C	142	40.2	2.54416	0.20124	0.26189	0.00537
127-2A	107	47.5	3.05127	0.20725	0.24099	0.00401
127-4A	180	12.4	1.59978	0.11790	0.30030	0.00419
127-4B	145	19.7	1.94830	0.13076	0.24993	0.00352
127-5A	171	-1.0	1.34100	0.08440	0.31882	0.00440
127-6A	155	3.1	1.41482	0.08288	0.31232	0.00486
127-6B	133	19.3	1.81118	0.10634	0.27960	0.00383
127-7A	177	2.9	1.39533	0.09290	0.31861	0.00436
127-8A	164	0.5	1.44577	0.09111	0.28723	0.00492
127-8B	129	40.9	3.16615	0.26694	0.19207	0.01116
127-8C	194	3.9	1.49082	0.11362	0.28910	0.00392
136-10A	177	23.0	1.90582	0.15425	0.27762	0.00511
136-1A	60	10.0	1.55924	0.03748	0.29935	0.00249
136-2A	101	3.5	1.45679	0.05648	0.29868	0.00244
136-2B	75	5.1	1.54061	0.04607	0.27920	0.00244
136-3A	65	4.1	1.46576	0.03676	0.29887	0.00325
136-4A	81	16.5	1.55897	0.05075	0.34231	0.00490
136-4B	83	12.8	1.46223	0.04683	0.35623	0.00283
136-7A	140	28.8	1.93139	0.12412	0.31031	0.00548

Spot Name	2σ error (Ma)	discordance	238U/206Pb	2σ	207Pb/206Pb	2σ
136-8A	128	67.1	4.65490	0.52738	0.25889	0.00442
136-8B	90	72.3	5.52376	0.50499	0.25907	0.00446
136-9A	84	60.0	3.47374	0.20407	0.30418	0.00625
136-2B	114	9.5	1.60235	0.07426	0.28306	0.00432
136-2B	153	6.6	1.59794	0.09992	0.26984	0.00474
136-6A	120	13.0	1.58075	0.07662	0.31049	0.00464
136-6A	158	10.3	1.57639	0.10108	0.29599	0.00512
136-6B	110	13.6	1.59684	0.07153	0.30834	0.00464
136-6B	151	10.9	1.59244	0.09776	0.29394	0.00511
136-12A	203	13.6	1.65759	0.14112	0.28958	0.00519
136-12B	199	24.8	1.88407	0.17050	0.29478	0.00503
136-3B	76	7.5	1.50867	0.04513	0.30243	0.00355
136-5A	82	6.2	1.50649	0.04846	0.29630	0.00267
136-6A	84	8.8	1.51983	0.05030	0.30626	0.00252
136-6B	69	9.4	1.53531	0.04213	0.30414	0.00256
136-11A	125	25.2	1.87056	0.10527	0.30124	0.00537
141-1A	133	11.4	1.61925	0.08871	0.28837	0.00439
141-1B	190	6.4	1.24713	0.08397	0.42157	0.00621
141-1C	124	11.5	1.61668	0.08236	0.28998	0.00443
141-1D	145	13.1	1.40042	0.07637	0.38903	0.00644
141-1E	135	13.3	1.68040	0.09504	0.28119	0.00422
141-1F	114	30.8	1.78721	0.08864	0.37655	0.00583
141-1G	123	8.2	1.39986	0.06452	0.35090	0.00559
141-1H	132	10.0	1.62015	0.08749	0.28068	0.00424
141-1I	139	9.3	1.58848	0.08949	0.28619	0.00460
141-2A	120	6.3	1.50174	0.07059	0.29837	0.00442
141-2B	109	11.2	1.59900	0.07054	0.29379	0.00446
141-2C	78	35.9	2.50677	0.10656	0.23985	0.00424
141-3A	122	24.5	1.63365	0.08247	0.37852	0.00671
141-4A	128	18.8	1.45422	0.07141	0.41209	0.00652
141-4B	125	11.8	1.31798	0.05981	0.42528	0.00654
141-4C	114	9.1	1.68471	0.08087	0.25882	0.00400
141-4D	119	22.1	1.53984	0.07277	0.39941	0.00750
141-5A1	126	2.1	1.25387	0.05589	0.38241	0.00585
141-5A2	174	4.3	1.43584	0.09560	0.31082	0.00769
141-5A3	155	-4.2	1.38066	0.07991	0.28732	0.00447

Spot Name	2σ error (Ma)	discordance	238U/206Pb	2σ	207Pb/206Pb	2σ
141-5B1	114	6.9	1.52575	0.06854	0.29352	0.00459
141-5B2	129	1.8	1.49897	0.07599	0.27637	0.00424
141-6A	137	1.1	1.19768	0.05633	0.41025	0.00607
141-6B	138	7.9	1.27763	0.06292	0.41525	0.00666
141-6C	119	15.6	1.61754	0.07861	0.31470	0.00510
144-10A	83	26.6	1.91142	0.07184	0.29961	0.00453
144-11A	110	20.2	1.82929	0.08945	0.28041	0.00441
144-1A	102	14.4	1.58304	0.06496	0.31827	0.00487
144-1B	98	16.5	1.67833	0.06897	0.30044	0.00466
144-1C	126	10.4	1.54799	0.07813	0.30603	0.00461
144-2A	116	4.8	1.42481	0.06295	0.31782	0.00479
144-3A	120	12.4	1.53528	0.07286	0.32310	0.00502
144-4A	108	6.5	1.43809	0.05923	0.32328	0.00482
144-5A	119	4.1	1.43407	0.06502	0.31056	0.00475
144-6A	114	4.7	1.41261	0.06089	0.32256	0.00481
144-7A	126	19.0	1.70271	0.09048	0.30898	0.00511
144-8A	106	14.2	1.60673	0.06948	0.30909	0.00476
144-9A	108	7.4	1.47714	0.06189	0.31356	0.00464
144C-2A1	81	23.4	2.68539	0.12539	0.16959	0.00336
144C-2A2	107	9.2	1.61472	0.07089	0.27809	0.00374
144C-2B1	95	15.4	1.89105	0.08085	0.24168	0.00303
144C-2B2	131	18.2	2.03693	0.12715	0.22701	0.00354
144C-3A	119	-12.2	1.23584	0.05153	0.30615	0.00373
144C-3B	73	31.6	2.79950	0.12117	0.18599	0.00328
144C-4A	128	23.4	1.96392	0.11668	0.26638	0.00413
144C-4B	167	10.7	1.57519	0.10654	0.29844	0.00475
144C-5A	108	8.7	1.53954	0.06607	0.29874	0.00374
144C-6A	118	1.8	1.38656	0.06103	0.31616	0.00391
144C-6B	151	7.9	1.46933	0.08585	0.31910	0.00394
144C-6D	141	7.8	1.54563	0.08725	0.29180	0.00485
145-11A	138	-2.1	1.16428	0.05460	0.40664	0.00367
145-11B	123	-1.0	1.26591	0.05535	0.35397	0.00599
145-11C	146	1.6	1.19498	0.06018	0.41590	0.00389
145-11D	121	27.1	1.70153	0.08702	0.37504	0.00571
145-11E	127	0.2	1.18712	0.05151	0.40997	0.00362
145-12A	122	4.3	1.23806	0.05279	0.40991	0.00385

Spot Name	2σ error (Ma)	discordance	238U/206Pb	2σ	207Pb/206Pb	2σ
145-12B	94	19.7	1.97788	0.08606	0.24434	0.00406
145-2A	100	24.8	1.71592	0.07315	0.34793	0.00416
145-2B	128	12.7	1.58227	0.08172	0.30774	0.00559
145-3A	125	7.7	1.27151	0.05671	0.41743	0.00513
145-3B	127	9.4	1.30581	0.05989	0.41078	0.00439
145-3C	103	12.3	1.58774	0.06646	0.30394	0.00278
145-3D	135	2.2	1.21186	0.05658	0.40924	0.00444
145-7A	97	19.2	1.60134	0.06315	0.34670	0.00318
145-7B	119	3.9	1.43713	0.06553	0.30786	0.00402
145-7C	101	13.7	1.43800	0.05544	0.37442	0.00656
145-9A	228	2.9	1.23005	0.09888	0.40333	0.00452
146-10A	151	6.5	1.63560	0.10208	0.25946	0.00353
146-10B	172	14.6	1.63683	0.11694	0.30149	0.00417
146-1A	189	3.8	1.21095	0.07968	0.42390	0.00570
146-1B	146	24.5	1.66702	0.10209	0.36444	0.00543
146-1C	131	33.1	2.21832	0.14623	0.27247	0.00427
146-2A	158	7.7	1.54599	0.09759	0.29089	0.00395
146-5A	166	17.4	1.66602	0.11562	0.30975	0.00446
146-5B	172	3.7	1.44220	0.09526	0.30519	0.00414
146-5C	185	-3.0	1.19247	0.07630	0.38170	0.00526
146-6A	160	1.1	1.53465	0.09766	0.26282	0.00370
146-6B	165	10.9	1.70551	0.11947	0.26205	0.00385
146-7A	171	-0.3	1.16862	0.06827	0.41858	0.00561
146-7B	161	11.0	1.32290	0.07773	0.41506	0.00585
146-7C	153	6.8	1.55563	0.09522	0.28351	0.00391
146-8A	169	8.8	1.62125	0.11289	0.27419	0.00380
146-8B	189	7.7	1.54637	0.11711	0.29105	0.00392
146-9A	182	12.5	1.35454	0.09131	0.40974	0.00556
171-10A	92	31.5	2.12066	0.09541	0.28240	0.00435
171-10B	111	5.1	1.46739	0.06277	0.30384	0.00453
171-11A	108	2.0	1.37561	0.05515	0.32177	0.00478
171-11B	106	2.1	1.37307	0.05388	0.32345	0.00482
171-12A	114	1.7	1.36452	0.05737	0.32440	0.00498
171-12B	107	1.4	1.36819	0.05444	0.32097	0.00477
171-1A	96	11.3	1.57932	0.06083	0.30034	0.00716
171-1B	110	3.7	1.40934	0.05870	0.31789	0.00471

Spot Name	2σ error (Ma)	discordance	238U/206Pb	2σ	207Pb/206Pb	2σ
171-2A	130	2.0	1.36868	0.06629	0.32430	0.00483
171-2B	135	5.3	1.42019	0.07296	0.32294	0.00478
171-3A	177	7.1	1.45161	0.09931	0.32142	0.00477
171-4A	114	3.2	1.38888	0.05897	0.32335	0.00478
171-4B	127	-3.5	1.30182	0.05981	0.32161	0.00476
171-5A	119	-0.1	1.35586	0.05931	0.31772	0.00474
171-5B	97	11.1	1.60141	0.06305	0.29234	0.00461
171-6A	109	-0.7	1.33758	0.05316	0.32197	0.00477
171-6B	130	-1.4	1.32828	0.06300	0.32192	0.00477
171-7A	121	4.7	1.43818	0.06622	0.31217	0.00479
171-8A	110	-1.7	1.32672	0.05288	0.32089	0.00478
171-9A	119	1.7	1.36918	0.06057	0.32268	0.00478
171-9B	125	1.3	1.36488	0.06327	0.32168	0.00478
101-1A	128	10.9	1.42059	0.06918	0.36104	0.00388
101-1B	102	14.2	1.48077	0.05887	0.35799	0.00380
101-2A	180	2.7	1.31465	0.08605	0.35352	0.00427
101-2B	149	3.4	1.31880	0.07145	0.35617	0.00382
101-3A	127	53.9	3.01816	0.24067	0.30437	0.00466
101-3B	157	6.1	1.46158	0.08872	0.31131	0.00332
101-4A	149	4.4	1.32200	0.07194	0.36164	0.00380
101-4B	126	-1.9	1.24730	0.05512	0.35805	0.00376
101-5A	135	-0.7	1.26669	0.06077	0.35573	0.00375
101-6A	153	6.7	1.47671	0.08809	0.30964	0.00643
101-7A	141	8.1	1.40817	0.07508	0.34630	0.00399
101-7B	110	3.2	1.43516	0.06040	0.30518	0.00343
101-8A	126	9.6	1.41331	0.06721	0.35464	0.00384
101-8B	126	9.6	1.43872	0.06919	0.34336	0.00408
101-9A	94	8.6	1.39565	0.04905	0.35591	0.00383
101-9B	104	-0.4	1.26820	0.04672	0.35660	0.00377
101-10A1	105	2.2	1.55292	0.06491	0.26229	0.00356
101-10A2	118	0.9	1.34082	0.05787	0.33013	0.00451
101-10B1	103	5.4	1.34591	0.05062	0.35717	0.00482
101-10B2	111	-1.0	1.27823	0.05068	0.34751	0.00472
101-1A	122	-1.1	1.29156	0.05654	0.34053	0.00493
101-1B	122	3.1	1.31136	0.05783	0.35813	0.00484
101-2A	148	20.4	1.58030	0.09448	0.36499	0.00583

Spot Name	2σ error (Ma)	discordance	238U/206Pb	2σ	207Pb/206Pb	2σ
101-3A	102	6.4	1.40809	0.05397	0.33480	0.00752
101-3B	100	3.2	1.31015	0.04717	0.35937	0.00483
101-4A	96	15.4	1.63819	0.06499	0.30599	0.00417
101-4B	101	4.1	1.33629	0.04931	0.35293	0.00475
101-4C	92	7.1	1.37390	0.04665	0.35559	0.00480
101-5A	102	6.3	1.36208	0.05150	0.35507	0.00477
101-6A	107	7.2	1.51103	0.06341	0.29997	0.00408
101-6B	99	9.4	1.56145	0.06218	0.29522	0.00405
101-7A	92	10.1	1.44387	0.05089	0.34413	0.00653
101-8A	121	-1.2	1.25138	0.05354	0.36076	0.00487
101-8B	95	2.3	1.50114	0.05549	0.27811	0.00378
101-9A	129	-0.7	1.28224	0.05912	0.34744	0.00470
102-10B	153	-2.2	1.78399	0.11963	0.19913	0.00261
102-11A	122	4.1	1.42448	0.06578	0.31422	0.00358
102-12B	119	0.6	1.53989	0.07298	0.25922	0.00229
102-13A	140	2.6	1.32834	0.06771	0.34651	0.00313
102-14B	177	23.3	1.71996	0.13044	0.33466	0.00352
102-15B	127	4.1	1.44583	0.07052	0.30617	0.00295
102-1A	124	3.7	1.43118	0.06745	0.30944	0.00370
102-1B	126	6.4	1.48798	0.07295	0.30343	0.00270
102-2A	135	5.6	1.50062	0.07960	0.29504	0.00288
102-2B	131	7.5	1.47990	0.07515	0.31296	0.00284
102-3A	120	0.2	1.29072	0.05541	0.34902	0.00351
102-4A	146	2.9	1.41117	0.07804	0.31260	0.00281
102-4B	124	3.2	1.43113	0.06778	0.30617	0.00282
102-5A	133	1.9	1.56184	0.08350	0.25856	0.00245
102-6A	139	1.5	1.39345	0.07292	0.31118	0.00291
102-7A	131	9.9	1.55586	0.08183	0.30030	0.00273
102-8A	139	4.5	1.46339	0.07860	0.30196	0.00288
102-8B	148	2.6	1.41335	0.07946	0.30999	0.00278
102-9A	117	5.1	1.45665	0.06580	0.30736	0.00275
102-9B	127	3.1	1.44159	0.06993	0.30213	0.00277
108-1A	153	7.7	1.26011	0.06829	0.42475	0.00447
108-1B	123	2.6	1.19678	0.05048	0.42266	0.00446
108-2A	151	5.2	1.22673	0.06471	0.42534	0.00447
108-2B	132	10.9	1.54491	0.08150	0.30995	0.00331

Spot Name	2σ error (Ma)	discordance	238U/206Pb	2σ	207Pb/206Pb	2σ
108-3A	151	8.0	1.26814	0.06837	0.42238	0.00448
108-3B	126	28.7	1.78299	0.09763	0.35806	0.00401
108-3C	101	18.1	1.70674	0.07291	0.30197	0.00391
108-4A	138	6.6	1.25068	0.06112	0.42090	0.00441
108-4B	146	8.2	1.28730	0.06765	0.41206	0.00435
108-5A	156	6.9	1.24676	0.06876	0.42624	0.00450
108-5B	135	17.5	1.71518	0.09889	0.29554	0.00331
108-6A	124	5.6	1.23013	0.05336	0.42668	0.00453
108-6B	157	14.5	1.40957	0.08376	0.39622	0.00492
114-10A	70	59.3	3.70605	0.18961	0.26530	0.00301
114-11A	109	4.7	1.40803	0.05783	0.32404	0.00342
114-12A	123	1.8	1.50345	0.07237	0.27508	0.00287
114-12B	68	31.9	2.60786	0.09992	0.20680	0.00713
114-1A	110	3.3	1.38452	0.05678	0.32552	0.00351
114-1B	124	-0.4	1.32770	0.06024	0.32814	0.00386
114-2A	104	11.1	1.53254	0.06289	0.31542	0.00341
114-3A	111	2.2	1.39168	0.05772	0.31622	0.00333
114-4A	143	4.8	1.42082	0.07689	0.31984	0.00338
114-4B	92	18.8	1.68433	0.06496	0.31363	0.00337
114-5A	113	1.7	1.36805	0.05744	0.32321	0.00343
114-5B	96	25.2	1.99033	0.08900	0.27103	0.00287
114-6A	96	11.6	1.58000	0.06140	0.30216	0.00356
114-7A	117	5.9	1.35552	0.05865	0.35565	0.00384
114-8A	123	8.5	1.49829	0.07235	0.31227	0.00349
114-8B	127	0.9	1.50887	0.07529	0.26906	0.00295
114-9A	111	4.9	1.54230	0.06813	0.27772	0.00294
114-9B	116	3.4	1.45044	0.06427	0.30053	0.00437
115-11A	121	3.5	1.40996	0.06420	0.31648	0.00461
115-2A	113	21.4	1.98272	0.10485	0.25183	0.00421
115-2B	122	2.9	1.54932	0.07515	0.26639	0.00463
115-5A	143	30.4	2.17506	0.15470	0.26405	0.00604
115-9A	114	1.4	1.50348	0.06693	0.27298	0.00403
115-10A	162	-0.1	1.34212	0.08013	0.32351	0.00515
115-10B	131	0.8	1.36826	0.06659	0.31785	0.00473
115-12A	128	7.0	1.45601	0.07184	0.31887	0.00472
115-13A	116	2.1	1.36935	0.05908	0.32494	0.00476

Spot Name	2σ error (Ma)	discordance	238U/206Pb	2σ	207Pb/206Pb	2σ
115-14A	172	2.7	1.40731	0.09140	0.31297	0.00470
115-14B	127	26.5	1.83637	0.10336	0.32097	0.00533
115-1A	142	6.8	1.45185	0.07938	0.31952	0.00487
115-3A	140	-1.2	1.33675	0.06861	0.31965	0.00471
115-4A	136	10.1	1.52055	0.08161	0.31358	0.00580
115-4B	187	18.8	1.75242	0.14197	0.29281	0.00589
115-7A	152	7.0	1.44683	0.08461	0.32245	0.00473
115-8A	144	8.6	1.53616	0.08830	0.29936	0.00516
119-11A	126	13.9	1.65118	0.08667	0.29319	0.00485
119-12A	148	4.7	1.44389	0.08209	0.31009	0.00458
119-3A	138	3.2	1.39450	0.07237	0.32092	0.00467
119-4A	156	15.9	1.59520	0.10131	0.32453	0.00523
119-10A	117	0.3	1.34865	0.05817	0.32292	0.00473
119-13A	144	5.0	1.44173	0.07948	0.31276	0.00474
119-13B	131	8.3	1.50251	0.07721	0.30942	0.00479
119-14A	138	17.8	1.71789	0.10094	0.29660	0.01230
119-14B	172	16.1	1.67307	0.12106	0.29930	0.00543
119-1A	116	7.1	1.43782	0.06347	0.32664	0.00478
119-1B	143	5.4	1.41615	0.07697	0.32545	0.00476
119-1C	115	6.2	1.42785	0.06235	0.32547	0.00478
119-2A	141	-3.2	1.30269	0.06635	0.32328	0.00472
119-6A	125	2.0	1.37969	0.06430	0.31971	0.00479
119-7A	118	4.4	1.43580	0.06434	0.31152	0.00464
119-7B	135	3.8	1.40925	0.07179	0.31848	0.00481
119-8A	144	2.0	1.40947	0.07663	0.30811	0.00471
119-8B	125	2.8	1.39129	0.06516	0.31947	0.00478
119-9A	157	1.4	1.37589	0.08068	0.31769	0.00507
205-10A	135	12.4	1.60566	0.08851	0.29833	0.00453
205-10B	159	3.5	1.40503	0.08450	0.31822	0.00479
205-11A	146	-2.0	1.32615	0.07088	0.31955	0.00467
205-12A	123	6.2	1.42954	0.06673	0.32459	0.00475
205-12B	155	8.0	1.45641	0.08694	0.32528	0.00477
205-14A	130	1.9	1.37197	0.06633	0.32244	0.00489
205-15A	151	3.6	1.39541	0.07911	0.32254	0.00494
205-16A	150	3.2	1.27115	0.06780	0.38057	0.00592
205-1A	160	10.5	1.53670	0.09799	0.31033	0.00495

Spot Name	2σ error (Ma)	discordance	238U/206Pb	2σ	207Pb/206Pb	2σ
205-2A	229	34.6	2.10799	0.23671	0.30921	0.00627
205-3A	135	6.9	1.44152	0.07432	0.32396	0.00474
205-4A	141	-0.1	1.35663	0.07066	0.31733	0.00484
205-4B	144	1.0	1.37107	0.07368	0.31773	0.00470
205-5A	133	6.2	1.43434	0.07273	0.32249	0.00470
205-6A	141	7.1	1.43973	0.07774	0.32584	0.00495
205-7A	181	9.8	1.63111	0.12220	0.27668	0.00475
205-8A	112	19.2	1.86120	0.09350	0.26668	0.00419
205-9A	150	4.0	1.41032	0.07991	0.31923	0.00468
206-10A	124	14.6	1.68609	0.08772	0.28692	0.00481
206-10B	177	5.0	1.48571	0.10303	0.29674	0.00468
206-11A	146	3.2	1.23517	0.06336	0.40273	0.00376
206-12A	126	11.1	1.46317	0.07134	0.34319	0.00405
206-13A	182	12.5	1.42761	0.09911	0.36958	0.00423
206-14A	149	8.8	1.31535	0.07112	0.39993	0.00426
206-15A	140	10.5	1.34807	0.06930	0.39502	0.00409
206-16A	133	14.7	1.49074	0.07718	0.35768	0.00493
206-16B	136	10.6	1.40403	0.07170	0.36670	0.00356
206-17A	151	0.9	1.19424	0.06229	0.41049	0.00379
206-1A	128	15.0	1.75539	0.09731	0.27022	0.00288
206-2A	168	1.3	1.21879	0.07161	0.39749	0.00322
206-2B	144	6.2	1.36937	0.07343	0.35104	0.00331
206-3A	197	0.9	1.27607	0.09025	0.36119	0.00304
206-4A	161	6.6	1.29551	0.07525	0.39278	0.00330
206-5A	170	4.0	1.36132	0.08573	0.33981	0.00304
206-6A	202	8.8	1.28711	0.09377	0.41732	0.00340
206-7A	165	2.9	1.21275	0.06962	0.41458	0.00318
206-8A	135	11.2	1.41545	0.07228	0.36560	0.00388
206-9A	135	1.8	1.24614	0.05907	0.38451	0.00412
208-10A	138	9.6	1.53623	0.08440	0.30492	0.00454
208-10B	123	9.0	1.52292	0.07412	0.30602	0.00456
208-11A	124	9.0	1.50409	0.07338	0.31315	0.00461
208-12A	149	6.9	1.44114	0.08241	0.32453	0.00475
208-13A	129	-5.7	1.30083	0.06060	0.31047	0.00454
208-14A	160	3.5	1.39423	0.08406	0.32294	0.00471
208-15A	113	7.2	1.47057	0.06428	0.31467	0.00470

Spot Name	2σ error (Ma)	discordance	238U/206Pb	2σ	207Pb/206Pb	2σ
208-16A	164	4.2	1.41089	0.08788	0.31978	0.00471
208-18A	150	2.9	1.53759	0.09171	0.26974	0.00394
208-1A	152	9.2	1.48757	0.08848	0.32046	0.00473
208-2A	156	2.7	1.38227	0.08044	0.32274	0.00471
208-3A	162	-1.0	1.38331	0.08393	0.30192	0.00443
208-4A	150	2.8	1.39379	0.07844	0.31896	0.00468
208-5A	119	6.2	1.45117	0.06603	0.31618	0.00510
208-6A	153	5.9	1.45503	0.08591	0.31296	0.00468
208-6B	117	4.6	1.42287	0.06335	0.31779	0.00467
208-7A	112	5.2	1.60121	0.07319	0.26282	0.00406
208-8A	164	13.3	1.68139	0.11648	0.28104	0.00567
208-9A	161	7.3	1.49408	0.09445	0.30644	0.00460
303-10A	121	6.6	1.48281	0.06980	0.30633	0.00481
303-14A	118	2.2	1.43101	0.06404	0.30086	0.00686
303-15A	140	6.0	1.33915	0.06860	0.36485	0.00566
303-1A	202	6.3	1.26396	0.09106	0.41008	0.00650
303-2A	157	1.6	1.42308	0.08478	0.30067	0.00467
303-2B	122	0.4	1.36901	0.06217	0.31493	0.00564
303-5B	140	4.9	1.45052	0.07780	0.30861	0.00601
303-6A	133	5.7	1.54334	0.08183	0.28133	0.00511
303-6B	127	6.2	1.30832	0.06018	0.38235	0.00651
303-7A	149	1.3	1.26019	0.06638	0.37308	0.00638
303-8A	130	2.0	1.45090	0.07242	0.29299	0.00461
303-9A	194	-6.6	1.34436	0.09648	0.28896	0.00493
304-10A	107	1.6	1.77175	0.08229	0.21235	0.00310
304-11A	124	-0.2	1.72839	0.09162	0.21425	0.00313
304-11B	127	-0.5	1.71015	0.09238	0.21659	0.00316
304-12A	120	3.5	1.78070	0.09278	0.21664	0.00327
304-13A	111	-1.0	1.72107	0.08149	0.21299	0.00314
304-1A	150	-3.1	1.69652	0.10734	0.21115	0.00311
304-2A	133	6.0	1.93909	0.11890	0.19923	0.00320
304-3A	119	-1.0	1.70716	0.08631	0.21554	0.00314
304-3B	126	-1.3	1.70433	0.09115	0.21526	0.00321
304-4A	140	7.5	1.87948	0.11854	0.21305	0.00331
304-5A	116	1.4	1.74498	0.08663	0.21628	0.00315
304-6A	115	1.0	1.76162	0.08746	0.21196	0.00311

Spot Name	2σ error (Ma)	discordance	238U/206Pb	2σ	207Pb/206Pb	2σ
304-6B	109	-0.2	1.77727	0.08439	0.20597	0.00302
304-7A	106	0.7	1.75478	0.08039	0.21246	0.00310
304-8A	97	1.4	1.75405	0.07318	0.21465	0.00313
304-8B	115	-2.6	1.69893	0.08224	0.21219	0.00311
304-9A	113	-1.0	1.72546	0.08312	0.21228	0.00312
305-11A	101	4.8	1.57508	0.06395	0.26812	0.00248
305-14B	70	0.3	1.47247	0.04001	0.27738	0.00143
305-13A	121	5.5	1.54184	0.07456	0.28089	0.00133
305-6A	112	4.5	1.50835	0.06646	0.28657	0.00259
305-7A	94	1.2	1.45712	0.05256	0.28676	0.00165
305-8B	76	0.9	1.43081	0.04129	0.29447	0.00204
305-12A	109	5.3	1.49100	0.06339	0.29660	0.00161
305-14A	86	1.5	1.40314	0.04502	0.30780	0.00147
305-20A	117	-0.3	1.37705	0.06005	0.30810	0.00148
305-4A	149	9.7	1.52735	0.09025	0.30883	0.00492
305-9C	101	3.5	1.42852	0.05480	0.30888	0.00161
305-18A	108	5.2	1.45457	0.06008	0.30903	0.00175
305-18B	97	5.8	1.46162	0.05436	0.30960	0.00194
305-9B	115	3.0	1.41824	0.06193	0.31004	0.00181
305-9A	106	4.0	1.43063	0.05751	0.31112	0.00186
305-2B	126	7.0	1.46923	0.07179	0.31394	0.00466
305-2A	146	13.3	1.55377	0.09109	0.32216	0.00510
305-1A	162	7.8	1.45867	0.09150	0.32267	0.00517
305-19A	109	8.1	1.45986	0.06101	0.32440	0.00324
305-8A	93	-1.5	1.31641	0.04441	0.32645	0.00169
305-15B	93	0.7	1.34011	0.04550	0.32882	0.00359
305-15A	93	6.1	1.40866	0.04936	0.33299	0.00207
305-3A	126	40.7	2.19516	0.13829	0.34301	0.00567
305-16A	117	-1.9	1.26993	0.05269	0.34636	0.00251
802-1A	97	7.3	1.58473	0.06237	0.27723	0.00238
802-2A	80	26.2	1.96558	0.07258	0.28305	0.00337
802-2B	85	4.5	1.51603	0.05054	0.28384	0.00252
802-2C	75	10.0	1.61649	0.04972	0.28180	0.00310
802-2D	156	28.6	2.03291	0.15097	0.28287	0.00504
802-3A	108	8.2	1.58684	0.06910	0.28130	0.00263
802-3B	87	10.9	1.64415	0.05890	0.27862	0.00234

Spot Name	2σ error (Ma)	discordance	238U/206Pb	2σ	207Pb/206Pb	2σ
802-3C	95	11.1	1.64985	0.06519	0.27773	0.00237
802-3D	71	7.8	1.58351	0.04528	0.28019	0.00237
802-4B	74	12.2	1.63896	0.05026	0.28706	0.00272
802-4C	80	38.4	2.37598	0.10031	0.27922	0.00259
802-5A	56	37.1	2.29166	0.06627	0.28628	0.00290
802-6A	75	19.0	1.80559	0.05927	0.27927	0.00233
802-6B	69	19.9	1.82934	0.05600	0.27811	0.00232
802-7A	96	11.1	1.66390	0.06644	0.27419	0.00262
802-8A	78	9.4	1.61990	0.05160	0.27755	0.00241
802-8B	54	55.9	3.31356	0.12053	0.28009	0.00247
802-8C	100	46.3	2.71485	0.15760	0.28064	0.00295
802-9A	119	30.0	2.05078	0.11668	0.28790	0.00273
802-9B	86	18.9	1.78919	0.06692	0.28273	0.00249

Appendix Table 2. SIMS zircon U-Pb data from sample AC12A

Spot Name	Sample Name	Phase Type	Session	U (ppm)	Th (ppm)	Th/U	$^{204}Pb/^{206}Pb$	±1σ (%)	$^{232}Th/^{238}U$	±1σ (%)	$^{208}Pb^*/^{206}Pb^*$	±1σ (%)
S1768_69@1	AC12A	ign	IP13011A	83	18	0.21	4.5E-5	19	0.22	0.46	0.056	1.43
S1768_96@2	AC12A	ign	IP13011A	304	67	0.22	2.0E-5	14	0.23	0.23	0.059	0.67
S1768_96@1	AC12A	ign	IP13011A	468	125	0.27	8.9E-6	17	0.27	0.17	0.071	0.48
S1768_88@4	AC12A	meta	IP13011B	98	15	0.15	3.4E-5	25	0.16	0.66	0.042	2.0
S1768_88@2	AC12A	meta	IP13011A	91	15	0.16	3.2E-5	20	0.17	0.48	0.043	1.51
S1768_88@3	AC12A	meta	IP13011B	99	29	0.29	4.4E-5	21	0.30	0.50	0.077	2.5
S1768_88@5	AC12A	meta	IP13011B	100	31	0.31	2.5E-5	28	0.32	0.79	0.082	1.3
S1768_88@1	AC12A	meta	IP13011A	71	16	0.22	5.3E-5	19	0.23	0.48	0.056	1.44
S1768_99@2	AC12A	osc	IP13011A	330	55	0.17	1.0E-5	18	0.17	0.25	0.044	0.77
S1768_99@1	AC12A	osc	IP13011A	301	55	0.18	1.1E-5	18	0.19	0.25	0.048	0.74
S1768_100@1	AC12A	osc	IP13011A	449	201	0.45	7.8E-5	10	0.46	0.60	0.118	0.44
S1768_13@1	AC12A	osc	IP13011A	175	68	0.39	2.6E-5	16	0.40	0.60	0.103	1.12
S1768_96@3	AC12A	osc	IP13011A	369	70	0.19	1.1E-5	29	0.20	0.22	0.051	0.67
S1768_90@1	AC12A	osc	IP13011A	319	66	0.21	9.1E-6	19	0.21	0.23	0.055	0.66
S1768_69@2	AC12A	osc	IP13011A	266	65	0.24	1.5E-5	18	0.25	0.24	0.065	0.68
S1768_75@1	AC12A	osc	IP13011A	164	58	0.35	4.4E-5	13	0.37	0.27	0.093	0.74
S1768_74@1	AC12A	osc	IP13011A	1345	533	0.40	3.0E-6	17	0.41	0.20	0.105	0.23
S1768_100@2	AC12A	rim	IP13011A	166	23	0.14	9.8E-5	18	0.15	0.77	0.046	1.74
S1768_73@1	AC12A	rim	IP13011A	159	32	0.20	4.4E-5	15	0.21	0.34	0.057	1.10
S1768_7@2	AC12A	rim	IP13011A	55	27	0.49	4.0E-4	8	0.50	0.41	0.136	1.39
S1768_62@4	AC12A	rim	IP13011A	39	25	0.64	9.0E-5	21	0.66	0.44	0.170	1.22
S1768_74@2	AC12A	rim	IP13011A	41	57	1.39	7.5E-5	20	1.43	0.36	0.365	0.80
S1768_59@1	AC12A	rim	IP13011A	38	45	1.18	5.8E-5	22	1.22	0.38	0.311	0.87

Spot Name	$^{207}Pb^*/^{206}Pb^*$	±1σ (%)	$^{207}Pb^*/^{235}U$	±1σ (%)	$^{206}Pb^*/^{238}U$	±1σ (%)	Pb/U Error Correlation	$^{207}Pb/^{206}Pb$ Age (Ma)	±1σ (Ma)	% Discordance to origin
S1768_69@1	0.385	0.83	41.4	1.06	0.780	0.65	0.62	3851	13	+5
S1768_96@2	0.417	0.19	48.1	0.57	0.836	0.54	0.94	3972	3	+2
S1768_96@1	0.422	0.20	49.8	0.56	0.856	0.52	0.93	3989	3	+0
S1768_88@4	0.349	0.30	36.4	0.70	0.757	0.63	0.91	3702	5	+2
S1768_88@2	0.377	0.84	41.5	1.04	0.799	0.62	0.59	3819	13	+1
S1768_88@3	0.413	1.09	47.2	1.26	0.831	0.63	0.50	3956	16	+2
S1768_88@5	0.426	0.44	50.8	0.77	0.865	0.64	0.82	4005	7	-0
S1768_88@1	0.463	0.22	58.5	0.68	0.917	0.65	0.95	4126	3	-2
S1768_99@2	0.373	0.12	39.0	0.55	0.759	0.53	0.98	3803	2	+6
S1768_99@1	0.401	0.37	45.0	0.65	0.814	0.54	0.82	3913	6	+3
S1768_100@1	0.401	0.33	44.8	0.62	0.810	0.53	0.84	3915	5	+3
S1768_13@1	0.408	1.67	47.5	1.97	0.844	1.04	0.53	3940	25	-0
S1768_96@3	0.412	0.24	47.2	0.58	0.831	0.53	0.91	3954	4	+2
S1768_90@1	0.413	0.20	47.8	0.57	0.839	0.54	0.94	3958	3	+1
S1768_69@2	0.417	0.31	47.9	0.63	0.835	0.54	0.87	3971	5	+2
S1768_75@1	0.419	0.16	48.5	0.60	0.839	0.57	0.97	3979	2	+2
S1768_74@1	0.420	0.10	49.8	0.54	0.859	0.53	0.98	3984	1	-0
S1768_100@2	0.244	0.23	19.9	0.61	0.592	0.57	0.93	3146	4	+6
S1768_73@1	0.292	0.65	28.1	3.55	0.699	3.49	0.98	3427	10	+0
S1768_7@2	0.310	0.36	29.5	1.00	0.694	0.93	0.93	3523	5	+5
S1768_62@4	0.317	0.37	31.5	0.83	0.722	0.74	0.90	3554	6	+2
S1768_74@2	0.344	0.35	35.9	0.82	0.757	0.74	0.91	3680	5	+2
S1768_59@1	0.364	0.34	39.2	0.82	0.781	0.75	0.91	3766	5	+2

Appendix Table 3. SIMS zircon oxygen isotope analyses

Spot Name	Sample Name	Phase	Session	$^{18}O/^{16}O$	1σ (%) inter-session	δ18O (SMOW)	2σ (‰) inter-session	Xpos (µm)	Ypos (µm)
S3051_1@1	JR13-101	ign	IP14071	0.0020177	0.0120	6.21	0.24	1860	-3131
S3051_2@1	JR13-101	ign	IP14071	0.0020172	0.0100	5.98	0.20	1698	-3107
S3051_4@1	JR13-101	osc	IP14071	0.0020176	0.0109	6.18	0.22	1099	-3515
S3051_4@2	JR13-101	ign	IP14071	0.0020179	0.0109	6.35	0.22	1783	-3420
S3051_5@1	JR13-101	ign	IP14071	0.0020184	0.0118	6.57	0.24	1098	-3410
S3051_5@2	JR13-101	ign	IP14071	0.0020189	0.0124	6.85	0.25	1060	-3404
S3051_6@1	JR13-101	ign	IP14071	0.0020176	0.0142	6.18	0.28	1006	-3281
S3051_7@1	JR13-101	ign	IP14071	0.0020182	0.0114	6.50	0.23	966	-3204
S3051_8@1	JR13-101	osc	IP14071	0.0020177	0.0107	6.23	0.21	1353	-3225
S3051_9@1	JR13-101	osc	IP14071	0.0020177	0.0105	6.23	0.21	1756	-2722
S3051_10@1	JR13-101	osc	IP14071	0.0020184	0.0112	6.59	0.22	1342	-2825
S3051_10@2	JR13-101	ign	IP14071	0.0020181	0.0076	6.45	0.15	1336	-2798
S3051_11@1	JR13-101	osc	IP14071	0.0020176	0.0101	6.19	0.20	1846	-2992
S3051_12@1	JR13-101	ign	IP14071	0.0020184	0.0105	6.61	0.21	1672	-2812
S3051_12@2	JR13-101	rim	IP14071	0.0020182	0.0100	6.49	0.20	1634	-2831
S3051_13@1	JR13-101	rim	IP14071	0.0020179	0.0089	6.32	0.18	1738	-2911
S3051_14@1	JR13-101	osc	IP14071	0.0020181	0.0099	6.44	0.20	1145	-2771
S3051_14@2	JR13-101	osc	IP14071	0.0020173	0.0104	6.02	0.21	1190	-2801
S3051_15@1	JR13-101	osc	IP14071	0.0020184	0.0125	6.59	0.25	803	-3114
S3051_16@1	JR13-101	osc	IP14071	0.0020184	0.0102	6.59	0.20	1190	-3010
S3050_1@1	JR12-171	ign	IP14071	0.0020177	0.0091	6.22	0.18	2025	-2058
S3050_1@2	JR12-171	osc	IP14071	0.0020176	0.0092	6.18	0.18	1994	-2084
S3050_1@3	JR12-171	ign	IP14071	0.0020176	0.0106	6.18	0.21	1972	-2065
S3050_2@1	JR12-171	ign	IP14071	0.0020175	0.0130	6.14	0.26	2014	-1931
S3050_2@2	JR12-171	ign rim	IP14071	0.0020167	0.0121	5.73	0.24	2082	-1943
S3050_3@1	JR12-171	osc	IP14071	0.0020176	0.0111	6.20	0.22	1823	-2022
S3050_3@2	JR12-171	osc	IP14071	0.0020169	0.0086	5.83	0.17	1766	-2095
S3050_4@1	JR12-171	osc	IP14071	0.0020172	0.0130	5.97	0.26	1856	-1845
S3050_5@1	JR12-171	ign	IP14071	0.0020171	0.0103	5.91	0.21	1643	-1963
S3050_6@1	JR12-171	ign	IP14071	0.0020177	0.0124	6.21	0.25	1561	-2149
S3050_7@1	JR12-171	osc	IP14071	0.0020186	0.0123	6.67	0.25	1399	-1956
S3050_8@1	JR12-171	osc	IP14071	0.0020175	0.0121	6.11	0.24	1266	-1998
S3050_9@1	JR12-171	osc	IP14071	0.0020176	0.0104	6.17	0.21	1263	-2093

Appendix Table 3. SIMS zircon oxygen isotope analyses

Spot Name	Sample Name	Phase	Session	$^{18}O/^{16}O$	1σ (%) inter-session	δ18O (SMOW)	2σ (‰) inter-session	Xpos (µm)	Ypos (µm)
S3050_9@2	JR12-171	ign	IP14071	0.0020173	0.0133	6.05	0.27	1193	-2076
S3050_9@3	JR12-171	osc	IP14071	0.0020178	0.0141	6.31	0.28	1208	-2124
S3050_10@1	JR12-171	osc	IP14071	0.0020177	0.0113	6.21	0.23	1112	-2225
S3050_11@1	JR12-171	osc	IP14071	0.0020177	0.0095	6.21	0.19	1009	-2126
S3050_11@2	JR12-171	ign	IP14071	0.0020176	0.0081	6.17	0.16	1006	-2101
S3050_11@3	JR12-171	ign	IP14071	0.0020167	0.0096	5.76	0.19	956	-2111
S3050_12@1	JR12-171	osc	IP14071	0.0020180	0.0103	6.40	0.21	886	-2049
S3050_12@2	JR12-171	osc	IP14071	0.0020179	0.0130	6.32	0.26	851	-2051
S3050_13@1	JR12-171	osc	IP14071	0.0020176	0.0112	6.18	0.22	631	-2235
S3050_13@2	JR12-171	rim	IP14071	0.0020169	0.0111	5.85	0.22	668	-2180
S3050_14@1	JR12-171	ign	IP14071	0.0020171	0.0101	5.95	0.20	772	-1969
S3058_1@1	JR13-206	meta	IP14071	0.0020190	0.0114	6.87	0.23	-2975	-1715
S3058_1@2	JR13-206	meta	IP14071	0.0020188	0.0138	6.78	0.28	-2997	-1732
S3058_2@1	JR13-206	ign	IP14071	0.0020155	0.0152	5.16	0.30	-3107	-1814
S3058_2@2	JR13-206	ign	IP14071	0.0020156	0.0131	5.18	0.26	-3132	-1818
S3058_3@1	JR13-206	ign	IP14071	0.0020154	0.0085	5.10	0.17	-3120	-1583
S3058_3@2	JR13-206	rim	IP14071	0.0020179	0.0112	6.35	0.22	-3163	-1570
S3058_4@1	JR13-206	ign	IP14071	0.0020176	0.0107	6.21	0.21	-3206	-1684
S3058_5@1	JR13-206	rim	IP14071	0.0020157	0.0127	5.25	0.25	-3220	-1783
S3058_5@2	JR13-206	ign	IP14071	0.0020155	0.0114	5.11	0.23	-3279	-1804
S3058_6@1	JR13-206	ign	IP14071	0.0020165	0.0110	5.65	0.22	-3356	-1790
S3058_7@1	JR13-206	ign	IP14071	0.0020169	0.0134	5.84	0.27	-3532	-1723
S3058_8@1	JR13-206	ign	IP14071	0.0020137	0.0109	4.24	0.22	-4033	-1789
S3058_9@1	JR13-206	ign	IP14071	0.0020174	0.0104	6.08	0.21	-3971	-1714
S3058_9@2	JR13-206	ign	IP14071	0.0020163	0.0115	5.54	0.23	-3997	-1715
S3058_10@1	JR13-206	ign	IP14071	0.0020179	0.0093	6.34	0.19	-3990	-1635
S3058_11@1	JR13-206	ign	IP14071	0.0020162	0.0115	5.49	0.23	-4059	-1736
S3058_12@1	JR13-206	rim	IP14071	0.0020178	0.0116	6.29	0.23	-4140	-1707
S3058_12@2	JR13-206	ign	IP14071	0.0020156	0.0118	5.18	0.24	-4132	-1692
S3058_13@1	JR13-206	ign	IP14071	0.0020162	0.0086	5.48	0.17	-4099	-1578
S3061_1@1	JR13-304	osc	IP14071	0.0020177	0.0079	6.25	0.16	-1594	-1737
S3061_1@2	JR13-304	osc	IP14071	0.0020175	0.0122	6.12	0.24	-1650	-1729
S3061_2@1	JR13-304	ign	IP14071	0.0020176	0.0134	6.16	0.27	-1688	-1558

Appendix Table 3. SIMS zircon oxygen isotope analyses

Spot Name	Sample Name	Phase	Session	$^{18}O/^{16}O$	1σ (%) inter-session	δ18O (SMOW)	2σ (‰) inter-session	Xpos (µm)	Ypos (µm)
S3061_2@2	JR13-304	ign	IP14071	0.0020173	0.0129	6.05	0.26	-1719	-1564
S3061_3@1	JR13-304	ign	IP14071	0.0020173	0.0117	6.06	0.23	-1562	-1478
S3061_3@2	JR13-304	ign	IP14071	0.0020175	0.0113	6.14	0.23	-1626	-1483
S3061_4@1	JR13-304	osc	IP14071	0.0020178	0.0064	6.30	0.13	-1990	-1671
S3061_5@1	JR13-304	osc	IP14071	0.0020175	0.0083	6.11	0.17	-2338	-1857
S3061_6@1	JR13-304	osc	IP14071	0.0020176	0.0071	6.17	0.14	-2283	-1587
S3061_6@2	JR13-304	osc	IP14071	0.0020176	0.0093	6.21	0.19	-2310	-1589
S3061_7@1	JR13-304	meta	IP14071	0.0020170	0.0106	5.87	0.21	-2512	-1429
S3061_7@2	JR13-304	meta	IP14071	0.0020167	0.0112	5.74	0.22	-2564	-1444
S3061_7@3	JR13-304	meta	IP14071	0.0020168	0.0132	5.77	0.26	-2594	-1453
S3061_8@1	JR13-304	rim	IP14071	0.0020167	0.0111	5.73	0.22	-1657	-1302
S3061_9@1	JR13-304	osc	IP14071	0.0020169	0.0105	5.86	0.21	-1745	-1189
S3061_10@1	JR13-304	osc	IP14071	0.0020172	0.0144	6.00	0.29	-1876	-1006
S3061_10@2	JR13-304	rim	IP14071	0.0020168	0.0115	5.77	0.23	-1899	-935
S3061_11@1	JR13-304	ign	IP14071	0.0020171	0.0094	5.94	0.19	-2113	-1212
S3061_11@2	JR13-304	ign	IP14071	0.0020166	0.0096	5.71	0.19	-2155	-1242
S3061_12@1	JR13-304	osc	IP14071	0.0020169	0.0108	5.81	0.22	-2086	-1122
S3061_13@1	JR13-304	osc	IP14071	0.0020164	0.0147	5.61	0.29	-2406	-1134
S3062_1@1	JR13-802	osc	IP14071	0.0020172	0.0117	5.98	0.23	4076	-3341
S3062_2@1	JR13-802	ign	IP14071	0.0020178	0.0132	6.29	0.26	3910	-3313
S3062_2@2	JR13-802	ign	IP14071	0.0020179	0.0139	6.35	0.28	3885	-3290
S3062_3@1	JR13-802	osc	IP14071	0.0020176	0.0115	6.17	0.23	3766	-2926
S3062_3@2	JR13-802	osc	IP14071	0.0020168	0.0126	5.77	0.25	3725	-2999
S3062_4@1	JR13-802	rim	IP14071	0.0020180	0.0125	6.36	0.25	3604	-3114
S3062_4@2	JR13-802	ign	IP14071	0.0020179	0.0130	6.36	0.26	3565	-3090
S3062_5@1	JR13-802	rim	IP14071	0.0020174	0.0103	6.09	0.21	3419	-3133
S3062_6@1	JR13-802	ign	IP14071	0.0020181	0.0108	6.42	0.22	3358	-3381
S3062_6@2	JR13-802	ign	IP14071	0.0020184	0.0108	6.60	0.22	3312	-3413
S3062_7@1	JR13-802	osc	IP14071	0.0020174	0.0109	6.10	0.22	2874	-3287
S3062_8@1	JR13-802	ign	IP14071	0.0020179	0.0087	6.33	0.17	2505	-3480
S3062_8@2	JR13-802	ign	IP14071	0.0020181	0.0116	6.45	0.23	2445	-3476
S3062_8@3	JR13-802	ign	IP14071	0.0020184	0.0126	6.59	0.25	2373	-3475
S3062_8@4	JR13-802	osc	IP14071	0.0020186	0.0125	6.68	0.25	2293	-3458

Appendix Table 3. SIMS zircon oxygen isotope analyses

Spot Name	Sample Name	Phase	Session	$^{18}O/^{16}O$	1σ (%) inter-session	δ18O (SMOW)	2σ (‰) inter-session	Xpos (µm)	Ypos (µm)
S3062_9@1	JR13-802	ign	IP14071	0.0020184	0.0099	6.58	0.20	2839	-2948
S3062_10@1	JR13-802	rim	IP14071	0.0020176	0.0142	6.20	0.28	2432	-3028
S3062_11@1	JR13-802	ign	IP14071	0.0020187	0.0108	6.75	0.22	2261	-2849
S3062_12@1	JR13-802	osc	IP14071	0.0020174	0.0135	6.10	0.27	3446	-2622
S3062_13@1	JR13-802	osc	IP14071	0.0020178	0.0130	6.29	0.26	2569	-2504
S3062_13@2	JR13-802	osc	IP14071	0.0020176	0.0152	6.21	0.30	2549	-2477
S3052_1@1	JR13-102	rim	IP14071	0.0020180	0.0132	6.37	0.26	-1506	-2554
S3052_2@1	JR13-102	ign	IP14071	0.0020176	0.0092	6.19	0.18	-1669	-2656
S3052_2@2	JR13-102	rim	IP14071	0.0020179	0.0090	6.34	0.18	-1701	-2628
S3052_3@1	JR13-102	ign	IP14071	0.0020182	0.0178	6.47	0.36	-1792	-2658
S3052_4@1	JR13-102	rim	IP14071	0.0020183	0.0134	6.52	0.27	-1592	-2421
S3052_4@2	JR13-102	ign	IP14071	0.0020179	0.0082	6.33	0.16	-1609	-2411
S3052_5@1	JR13-102	ign	IP14071	0.0020176	0.0094	6.18	0.19	-1697	-2403
S3052_5@2	JR13-102	ign	IP14071	0.0020178	0.0142	6.31	0.28	-1682	-2390
S3052_6@1	JR13-102	ign	IP14071	0.0020178	0.0148	6.30	0.30	-2050	-2607
S3052_7@1	JR13-102	ign	IP14071	0.0020180	0.0136	6.41	0.27	-1974	-2474
S3052_8@1	JR13-102	rim	IP14071	0.0020181	0.0106	6.44	0.21	-2165	-2458
S3052_9@1	JR13-102	ign	IP14071	0.0020179	0.0124	6.32	0.25	-2270	-2381
S3052_10@1	JR13-102	ign	IP14071	0.0020177	0.0136	6.22	0.27	-2538	-2384
S3052_11@1	JR13-102	rim	IP14071	0.0020182	0.0144	6.49	0.29	-2668	-2338
S3052_12@1	JR13-102	ign	IP14071	0.0020178	0.0139	6.30	0.28	-2707	-2504
S3052_13@1	JR13-102	osc	IP14071	0.0020166	0.0162	5.66	0.32	-1393	-2210
S3052_13@2	JR13-102	osc	IP14071	0.0020163	0.0115	5.55	0.23	-1385	-2186
S3052_13@3	JR13-102	osc	IP14071	0.0020165	0.0111	5.63	0.22	-1405	-2184
S3052_14@1	JR13-102	osc	IP14071	0.0020179	0.0097	6.32	0.19	-1896	-2314
S3052_14@2	JR13-102	rim	IP14071	0.0020183	0.0159	6.52	0.32	-1895	-2202
S3045_1@1	JR12-127	osc	IP14071	0.0020182	0.0161	6.47	0.32	2266	-462
S3045_2@1	JR12-127	ign	IP14071	0.0020176	0.0132	6.19	0.26	2329	-269
S3045_2@2	JR12-127	ign	IP14071	0.0020176	0.0145	6.20	0.29	2312	-287
S3045_3@1	JR12-127	osc	IP14071	0.0020181	0.0106	6.41	0.21	2090	-532
S3045_4@1	JR12-127	rim	IP14071	0.0020173	0.0169	6.01	0.34	2018	-310
S3045_5@1	JR12-127	osc	IP14071	0.0020173	0.0092	6.02	0.18	2034	-220
S3045_6@1	JR12-127	ign	IP14071	0.0020183	0.0110	6.55	0.22	1851	-157

Appendix Table 3. SIMS zircon oxygen isotope analyses

Spot Name	Sample Name	Phase	Session	$^{18}O/^{16}O$	1σ (%) inter-session	δ18O (SMOW)	2σ (‰) inter-session	Xpos (µm)	Ypos (µm)
S3045_6@2	JR12-127	osc	IP14071	0.0020182	0.0137	6.49	0.27	1840	-131
S3045_7@1	JR12-127	osc	IP14071	0.0020172	0.0107	5.99	0.21	1793	-457
S3045_7@2	JR12-127	osc	IP14071	0.0020173	0.0129	6.03	0.26	1727	-494
S3045_8@1	JR12-127	core?	IP14071	0.0020168	0.0166	5.79	0.33	1656	-330
S3045_9@1	JR12-127	osc	IP14071	0.0020182	0.0140	6.49	0.28	1601	-185
S3045_10@1	JR12-127	osc	IP14071	0.0020184	0.0138	6.58	0.28	1264	-373
S3045_11@1	JR12-127	osc	IP14071	0.0020180	0.0149	6.40	0.30	1023	-41
S3045_11@2	JR12-127	osc	IP14071	0.0020179	0.0094	6.32	0.19	993	-98
S3045_12@1	JR12-127	ign	IP14071	0.0020184	0.0126	6.56	0.25	652	-469
S3045_13@1	JR12-127	osc	IP14071	0.0020179	0.0134	6.32	0.27	607	-526
S3045_13@2	JR12-127	osc	IP14071	0.0020177	0.0140	6.21	0.28	559	-548
S3045_14@1	JR12-127	osc	IP14071	0.0020179	0.0126	6.33	0.25	486	-338
S3044_1@1	JR12-119	osc	IP14071	0.0020173	0.0134	6.04	0.27	-1305	-4084
S3044_1@2	JR12-119	osc	IP14071	0.0020184	0.0123	6.59	0.25	-1330	-4065
S3044_2@1	JR12-119	rim	IP14071	0.0020170	0.0159	5.90	0.32	-1520	-4132
S3044_3@1	JR12-119	ign	IP14071	0.0020178	0.0122	6.28	0.24	-1434	-3822
S3044_3@2	JR12-119	ign	IP14071	0.0020179	0.0130	6.32	0.26	-1470	-3816
S3044_4@1	JR12-119	ign	IP14071	0.0020176	0.0103	6.19	0.21	-1684	-4007
S3044_5@1	JR12-119	osc	IP14071	0.0020176	0.0107	6.17	0.21	-1828	-4156
S3044_5@2	JR12-119	osc	IP14071	0.0020176	0.0125	6.21	0.25	-1858	-4161
S3044_6@1	JR12-119	osc	IP14071	0.0020182	0.0122	6.50	0.24	-1864	-4032
S3044_7@1	JR12-119	osc	IP14071	0.0020174	0.0130	6.09	0.26	-1895	-3952
S3044_7@2	JR12-119	osc	IP14071	0.0020174	0.0164	6.06	0.33	-1917	-3946
S3044_8@1	JR12-119	osc	IP14073	0.0020178	0.0116	6.28	0.23	-2338	-4132
S3044_9@1	JR12-119	osc	IP14073	0.0020180	0.0103	6.37	0.21	-2346	-3990
S3044_9@2	JR12-119	rim	IP14073	0.0020180	0.0178	6.40	0.36	-2356	-3971
S3044_10@1	JR12-119	osc	IP14073	0.0020180	0.0119	6.37	0.24	-2532	-3868
S3044_10@2	JR12-119	osc	IP14073	0.0020180	0.0132	6.39	0.26	-2559	-3861
S3044_10@3	JR12-119	osc	IP14073	0.0020183	0.0129	6.52	0.26	-2598	-3866
S3044_11@1	JR12-119	osc	IP14073	0.0020182	0.0146	6.48	0.29	-2701	-3999
S3044_11@2	JR12-119	osc	IP14073	0.0020182	0.0141	6.49	0.28	-2746	-3976
S3044_12@1	JR12-119	osc	IP14073	0.0020177	0.0110	6.22	0.22	-1945	-3713
S3044_13@1	JR12-119	ign	IP14073	0.0020171	0.0093	5.94	0.19	-2076	-3772

Appendix Table 3. SIMS zircon oxygen isotope analyses

Spot Name	Sample Name	Phase	Session	$^{18}O/^{16}O$	1σ (%) inter-session	δ18O (SMOW)	2σ (‰) inter-session	Xpos (µm)	Ypos (µm)
S3044_13@2	JR12-119	ign	IP14073	0.0020172	0.0108	5.96	0.22	-2101	-3783
S3049_1@1	JR12-144	osc	IP14073	0.0020184	0.0117	6.56	0.23	271	-5312
S3049_2@1	JR12-144	osc	IP14073	0.0020173	0.0132	6.02	0.26	247	-4906
S3049_3@1	JR12-144	ign	IP14073	0.0020171	0.0135	5.94	0.27	29	-5045
S3049_3@2	JR12-144	ign	IP14073	0.0020175	0.0108	6.12	0.22	-27	-5084
S3049_4@1	JR12-144	core	IP14073	0.0020176	0.0130	6.20	0.26	-103	-4946
S3049_5@1	JR12-144	core	IP14073	0.0020186	0.0094	6.70	0.19	-225	-4893
S3049_6@1	JR12-144	osc	IP14073	0.0020176	0.0105	6.17	0.21	-126	-5185
S3049_7@1	JR12-144	osc	IP14073	0.0020182	0.0110	6.49	0.22	-209	-5296
S3049_7@2	JR12-144	rim	IP14073	0.0020169	0.0088	5.84	0.18	-161	-5277
S3049_8@1	JR12-144	ign	IP14073	0.0020187	0.0137	6.73	0.27	-319	-5128
S3049_9@1	JR12-144	osc	IP14073	0.0020175	0.0107	6.14	0.21	-559	-5175
S3049_10@2	JR12-144	osc	IP14073	0.0020187	0.0109	6.73	0.22	-734	-5093
S3049_13@2	JR12-144	osc	IP14073	0.0020180	0.0097	6.36	0.19	-359	-4535
S3049_14@1	JR12-144	osc	IP14073	0.0020180	0.0102	6.36	0.20	-347	-4468
S3049_15@1	JR12-144	osc	IP14073	0.0020188	0.0085	6.77	0.17	-578	-4627
S3055_1@2	JR13-115	osc	IP14073	0.0020172	0.0103	5.99	0.21	42	-274
S3055_2@1_altered	JR13-115	meta	IP14073	0.0020203	0.0137	7.54	0.27	-104	-218
S3055_2@2	JR13-115	core	IP14073	0.0020181	0.0091	6.42	0.18	-128	-239
S3055_2@3	JR13-115	osc	IP14073	0.0020184	0.0130	6.56	0.26	-148	-274
S3055_3@1	JR13-115	osc	IP14073	0.0020178	0.0096	6.27	0.19	-220	-227
S3055_4@1	JR13-115	osc	IP14073	0.0020178	0.0086	6.31	0.17	-203	-35
S3055_1@3	JR13-115	rim	IP14073	0.0020174	0.0091	6.06	0.18	72	-217
S3055_4@2	JR13-115	osc	IP14073	0.0020179	0.0075	6.35	0.15	-225	-43
S3055_5@1	JR13-115	osc	IP14073	0.0020172	0.0097	5.99	0.19	-112	38
S3055_6@1	JR13-115	rim	IP14073	0.0020175	0.0104	6.15	0.21	-385	-88
S3055_7@1	JR13-115	osc	IP14073	0.0020176	0.0119	6.20	0.24	-517	-252
S3055_7@2	JR13-115	osc	IP14073	0.0020184	0.0070	6.58	0.14	-536	-276
S3055_8@1	JR13-115	osc	IP14073	0.0020179	0.0077	6.33	0.15	-723	-299
S3055_8@2	JR13-115	osc	IP14073	0.0020180	0.0087	6.39	0.17	-756	-311
S3055_9@1	JR13-115	osc	IP14073	0.0020182	0.0087	6.47	0.17	-821	-243
S3055_10@1	JR13-115	osc	IP14073	0.0020181	0.0094	6.45	0.19	-891	-150
S3055_10@2	JR13-115	osc	IP14073	0.0020178	0.0082	6.29	0.16	-903	-163

Appendix Table 3. SIMS zircon oxygen isotope analyses

Spot Name	Sample Name	Phase	Session	$^{18}O/^{16}O$	1σ (%) inter-session	δ18O (SMOW)	2σ (‰) inter-session	Xpos (µm)	Ypos (µm)
S3055_10@3	JR13-115	osc	IP14073	0.0020177	0.0096	6.23	0.19	-901	-188
S3055_11@1	JR13-115	osc	IP14073	0.0020179	0.0101	6.35	0.20	-717	-37
S3055_11@2	JR13-115	osc	IP14073	0.0020177	0.0093	6.25	0.19	-729	-17
S3055_11@3	JR13-115	osc	IP14073	0.0020179	0.0105	6.32	0.21	-720	5
S3055_12@1	JR13-115	osc	IP14073	0.0020175	0.0083	6.13	0.17	-975	-252
S3054_1@1	JR13-114	core	IP14073	0.0020171	0.0126	5.91	0.25	98	-810
S3054_1@2	JR13-114	osc	IP14073	0.0020173	0.0087	6.05	0.17	100	-843
S3054_1@3	JR13-114	osc	IP14073	0.0020177	0.0073	6.22	0.15	69	-833
S3054_2@1	JR13-114	meta	IP14073	0.0020176	0.0092	6.19	0.18	-85	-801
S3054_2@2	JR13-114	meta	IP14073	0.0020178	0.0097	6.29	0.19	-111	-816
S3054_3@1	JR13-114	osc	IP14073	0.0020170	0.0097	5.87	0.19	-30	-1013
S3054_3@2	JR13-114	osc	IP14073	0.0020176	0.0074	6.20	0.15	-54	-1017
S3054_4@1	JR13-114	core	IP14073	0.0020180	0.0100	6.40	0.20	-486	-987
S3054_5@1	JR13-114	rim	IP14073	0.0020174	0.0086	6.07	0.17	-596	-958
S3054_6@1	JR13-114	osc	IP14073	0.0020177	0.0083	6.22	0.17	-721	-932
S3054_7@1	JR13-114	osc	IP14073	0.0020175	0.0091	6.15	0.18	-788	-1191
S3054_8@1	JR13-114	core	IP14073	0.0020177	0.0083	6.23	0.17	-868	-1178
S3054_8@2	JR13-114	osc	IP14073	0.0020174	0.0094	6.07	0.19	-885	-1217
S3054_9@1	JR13-114	osc	IP14073	0.0020173	0.0113	6.03	0.23	-1042	-1102
S3054_10@1	JR13-114	osc	IP14073	0.0020173	0.0093	6.04	0.19	359	-685
S3054_10@2	JR13-114	osc	IP14073	0.0020176	0.0125	6.17	0.25	324	-716
S3054_11@1	JR13-114	rim	IP14073	0.0020173	0.0084	6.04	0.17	-658	-738
S3054_11@2	JR13-114	meta	IP14073	0.0020175	0.0092	6.14	0.18	-687	-738
S3054_12@1	JR13-114	osc	IP14073	0.0020176	0.0102	6.18	0.20	-673	-589
S3060_1@1	JR13-208	osc	IP14073	0.0020179	0.0100	6.31	0.20	-1524	-3268
S3060_2@1	JR13-208	osc	IP14073	0.0020180	0.0082	6.39	0.16	-1615	-3266
S3060_2@2	JR13-208	osc	IP14073	0.0020180	0.0104	6.38	0.21	-1647	-3264
S3060_3@1	JR13-208	osc	IP14073	0.0020184	0.0108	6.58	0.22	-1573	-3154
S3060_4@1	JR13-208	osc	IP14073	0.0020182	0.0113	6.49	0.23	-1640	-3097
S3060_4@2	JR13-208	osc	IP14073	0.0020175	0.0098	6.12	0.20	-1642	-3067
S3060_5@1	JR13-208	osc	IP14073	0.0020184	0.0090	6.58	0.18	-1743	-3172
S3060_5@2	JR13-208	osc	IP14073	0.0020176	0.0121	6.19	0.24	-1792	-3217
S3060_6@1	JR13-208	osc	IP14073	0.0020178	0.0100	6.26	0.20	-1833	-3358

Appendix Table 3. SIMS zircon oxygen isotope analyses

Spot Name	Sample Name	Phase	Session	$^{18}O/^{16}O$	1σ (%) inter-session	δ18O (SMOW)	2σ (‰) inter-session	Xpos (µm)	Ypos (µm)
S3060_7@1	JR13-208	osc	IP14073	0.0020187	0.0087	6.75	0.17	-2100	-3400
S3060_8@1	JR13-208	osc	IP14073	0.0020185	0.0098	6.62	0.20	-2159	-3322
S3060_13@1	JR13-208	osc	IP14073	0.0020179	0.0084	6.35	0.17	-1961	-3137
S3060_13@2	JR13-208	osc	IP14073	0.0020181	0.0124	6.43	0.25	-2036	-3128
S3060_9@1	JR13-208	meta	IP14073	0.0020175	0.0101	6.11	0.20	-2351	-3221
S3060_9@2	JR13-208	meta	IP14073	0.0020174	0.0072	6.06	0.14	-2379	-3238
S3060_10@1	JR13-208	meta	IP14073	0.0020179	0.0100	6.31	0.20	-2547	-3207
S3060_11@1	JR13-208	osc	IP14073	0.0020185	0.0092	6.65	0.18	-2648	-3237
S3060_11@2	JR13-208	rim	IP14073	0.0020182	0.0073	6.49	0.15	-2721	-3215
S3060_12@1	JR13-208	osc	IP14073	0.0020185	0.0090	6.63	0.18	-2700	-3109
S3059_2@1	JR13-207	meta	IP14073	0.0020169	0.0115	5.81	0.23	1716	-981
S3059_3@1	JR13-207	meta	IP14073	0.0020172	0.0113	5.99	0.23	1753	-889
S3059_4@1	JR13-207	meta	IP14073	0.0020169	0.0123	5.82	0.25	1670	-850
S3059_4@2	JR13-207	meta	IP14073	0.0020167	0.0107	5.72	0.21	1641	-868
S3059_4@3	JR13-207	meta	IP14073	0.0020168	0.0117	5.78	0.23	1623	-865
S3059_5@1	JR13-207	meta	IP14073	0.0020166	0.0096	5.69	0.19	1218	-742
S3059_6@1	JR13-207	meta	IP14073	0.0020166	0.0125	5.67	0.25	1131	-746
S3059_6@2	JR13-207	meta	IP14073	0.0020166	0.0123	5.69	0.25	1100	-767
S3059_7@1	JR13-207	meta	IP14073	0.0020169	0.0117	5.86	0.23	1124	-1026
S3059_7@2	JR13-207	meta	IP14073	0.0020170	0.0108	5.88	0.22	1099	-1022
S3059_8@1	JR13-207	meta	IP14073	0.0020173	0.0129	6.02	0.26	857	-1161
S3059_9@1	JR13-207	meta	IP14073	0.0020165	0.0104	5.63	0.21	678	-1165
S3059_10@1	JR13-207	meta	IP14073	0.0020167	0.0108	5.74	0.22	628	-778
S3059_10@2	JR13-207	meta	IP14073	0.0020166	0.0113	5.68	0.23	604	-800
S3057_1@1	JR13-205	osc	IP14073	0.0020176	0.0105	6.19	0.21	-3078	-2535
S3057_1@2	JR13-205	osc	IP14073	0.0020171	0.0099	5.94	0.20	-3099	-2539
S3057_2@1	JR13-205	osc	IP14073	0.0020174	0.0087	6.10	0.17	-3169	-2500
S3057_3@1	JR13-205	osc	IP14073	0.0020176	0.0097	6.19	0.19	-3387	-2412
S3057_4@1	JR13-205	osc	IP14073	0.0020176	0.0090	6.18	0.18	-3398	-2362
S3057_5@1	JR13-205	meta	IP14073	0.0020176	0.0109	6.16	0.22	-3450	-2653
S3057_6@1	JR13-205	osc	IP14073	0.0020179	0.0094	6.34	0.19	-3513	-2702
S3057_6@2	JR13-205	osc	IP14073	0.0020178	0.0112	6.29	0.22	-3546	-2706
S3057_6@3	JR13-205	meta	IP14073	0.0020174	0.0093	6.07	0.19	-3591	-2728

Appendix Table 3. SIMS zircon oxygen isotope analyses

Spot Name	Sample Name	Phase	Session	$^{18}O/^{16}O$	1σ (%) inter-session	δ18O (SMOW)	2σ (‰) inter-session	Xpos (µm)	Ypos (µm)
S3057_6@4	JR13-205	osc	IP14073	0.0020178	0.0101	6.27	0.20	-3624	-2715
S3057_7@1	JR13-205	meta	IP14073	0.0020176	0.0094	6.16	0.19	-3510	-2420
S3057_7@2	JR13-205	osc	IP14073	0.0020174	0.0077	6.08	0.15	-3514	-2447
S3057_7@3	JR13-205	osc	IP14073	0.0020177	0.0093	6.23	0.19	-3540	-2434
S3057_7@4	JR13-205	meta	IP14073	0.0020176	0.0080	6.17	0.16	-3561	-2460
S3057_7@5	JR13-205	osc	IP14073	0.0020178	0.0093	6.29	0.19	-3597	-2442
S3057_7@6	JR13-205	osc	IP14073	0.0020179	0.0104	6.34	0.21	-3612	-2467
S3057_8@1	JR13-205	meta	IP14073	0.0020174	0.0071	6.09	0.14	-3900	-2517
S3057_9@1	JR13-205	core	IP14073	0.0020177	0.0086	6.21	0.17	-3939	-2711
S3057_9@2	JR13-205	rim	IP14073	0.0020175	0.0116	6.15	0.23	-3979	-2722
S3056_1@1	JR13-119	rim	IP14073	0.0020178	0.0110	6.28	0.22	-1346	-5252
S3056_1@2	JR13-119	rim	IP14073	0.0020180	0.0100	6.36	0.20	-1406	-5238
S3056_2@1	JR13-119	rim	IP14073	0.0020176	0.0122	6.16	0.24	-1375	-5115
S3056_3@1	JR13-119	ign	IP14073	0.0020158	0.0139	5.26	0.28	-1371	-4949
S3056_4@1	JR13-119	rim	IP14073	0.0020177	0.0092	6.22	0.18	-1542	-5002
S3056_5@1	JR13-119	rim	IP14073	0.0020178	0.0092	6.30	0.18	-1606	-4882
S3056_5@2	JR13-119	rim	IP14073	0.0020175	0.0074	6.16	0.15	-1580	-4836
S3056_6@1	JR13-119	rim	IP14073	0.0020174	0.0115	6.09	0.23	-1680	-5029
S3056_7@1	JR13-119	rim	IP14073	0.0020177	0.0118	6.22	0.24	-2321	-5224
S3056_8@1	JR13-119	rim	IP14073	0.0020177	0.0120	6.21	0.24	-2359	-4921
S3056_8@2	JR13-119	ign	IP14073	0.0020150	0.0110	4.88	0.22	-2399	-4928
S3056_8@3	JR13-119	rim	IP14073	0.0020177	0.0110	6.25	0.22	-2452	-4932
S3056_11@1	JR13-119	rim	IP14073	0.0020172	0.0103	6.01	0.21	-1886	-4814
S3056_11@2	JR13-119	rim	IP14073	0.0020172	0.0113	5.99	0.23	-1949	-4773
S3056_9@1	JR13-119	osc	IP14073	0.0020146	0.0079	4.71	0.16	-2652	-5029
S3056_9@2	JR13-119	osc	IP14073	0.0020151	0.0098	4.96	0.20	-2670	-5015
S3056_9@3	JR13-119	osc	IP14073	0.0020172	0.0104	5.97	0.21	-2687	-5026
S3056_10@1	JR13-119	ign	IP14073	0.0020148	0.0096	4.77	0.19	-2737	-4821
S3056_10@2	JR13-119	ign	IP14073	0.0020149	0.0084	4.86	0.17	-2752	-4838
S3053_2@2	JR13-108	ign 1	IP14073	0.0020153	0.0097	5.06	0.19	4068	-1769
S3053_4@1	JR13-108	ign 1	IP14073	0.0020155	0.0093	5.14	0.19	3717	-1803
S3053_9@1	JR13-108	ign 1	IP14073	0.0020158	0.0090	5.29	0.18	2920	-1143
S3053_7@2	JR13-108	ign 1	IP14073	0.0020161	0.0106	5.45	0.21	2664	-2070

Appendix Table 3. SIMS zircon oxygen isotope analyses

Spot Name	Sample Name	Phase	Session	$^{18}O/^{16}O$	1σ (%) inter-session	δ18O (SMOW)	2σ (‰) inter-session	Xpos (µm)	Ypos (µm)
S3053_2@1	JR13-108	ign 1	IP14073	0.0020164	0.0105	5.58	0.21	4122	-1790
S3053_3@1	JR13-108	ign 1	IP14073	0.0020165	0.0104	5.66	0.21	3691	-2056
S3053_5@1	JR13-108	ign 1	IP14073	0.0020169	0.0099	5.82	0.20	2857	-1782
S3053_7@3	JR13-108	ign 1	IP14073	0.0020173	0.0097	6.02	0.19	2648	-2108
S3053_8@1	JR13-108	ign 1	IP14073	0.0020176	0.0093	6.18	0.19	3161	-1152
S3053_11@1	JR13-108	ign 1	IP14073	0.0020176	0.0112	6.19	0.22	3427	-816
S3053_7@1	JR13-108	ign 1	IP14073	0.0020177	0.0088	6.22	0.18	2681	-2024
S3053_1@2	JR13-108	ign 1	IP14073	0.0020178	0.0121	6.26	0.24	4050	-1981
S3053_1@1	JR13-108	ign 1	IP14073	0.0020179	0.0101	6.36	0.20	4080	-1996
S3053_10@1	JR13-108	ign 2	IP14073	0.0020139	0.0097	4.32	0.19	3905	-769
S3053_4@2	JR13-108	ign 2	IP14073	0.0020139	0.0108	4.33	0.22	3688	-1730
S3053_8@2	JR13-108	ign 2	IP14073	0.0020142	0.0085	4.48	0.17	3104	-1210
S3053_12@1	JR13-108	ign 2	IP14073	0.0020143	0.0112	4.54	0.22	2913	-1372
S3053_9@2	JR13-108	ign 2	IP14073	0.0020146	0.0098	4.68	0.20	2864	-1086
S3053_6@1	JR13-108	ign 2	IP14073	0.0020151	0.0104	4.93	0.21	2661	-1815
S3053_9@3	JR13-108	ign 2	IP14073	0.0020163	0.0105	5.52	0.21	2836	-1085
S3053_12@2	JR13-108	ign 2	IP14073	0.0020139	0.0103	4.35	0.21	2909	-1352
S3053_13@1	JR13-108	ign 2	IP14073	0.0020146	0.0099	4.67	0.20	3238	-1355
S3053_13@2	JR13-108	ign 2	IP14073	0.0020155	0.0116	5.13	0.23	3187	-1370
S3053_13@3	JR13-108	meta	IP14073	0.0020179	0.0116	6.35	0.23	3143	-1436

Appendix 4: Concordia plots of U-Pb data for samples discussed in Chapter 4

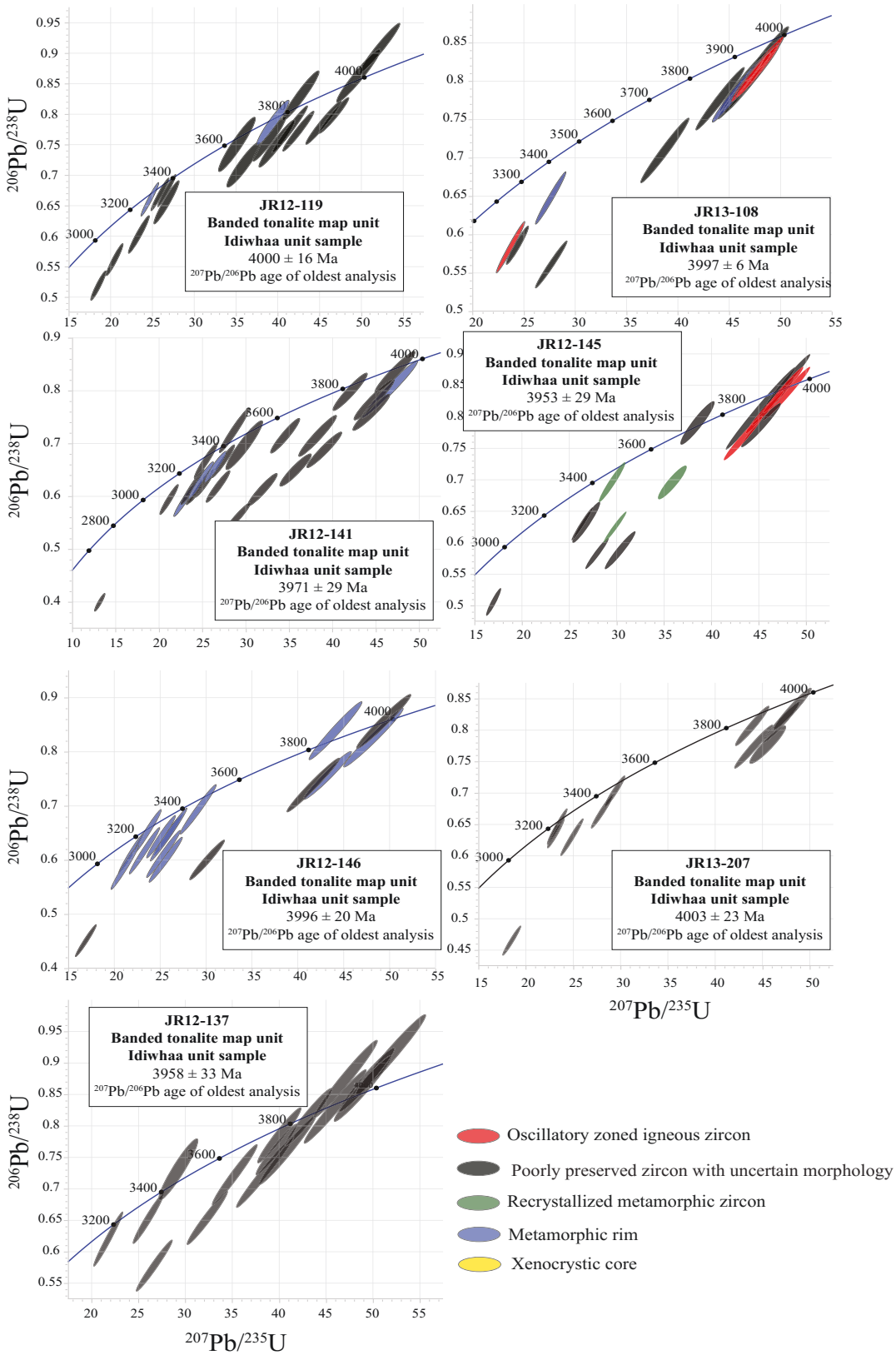

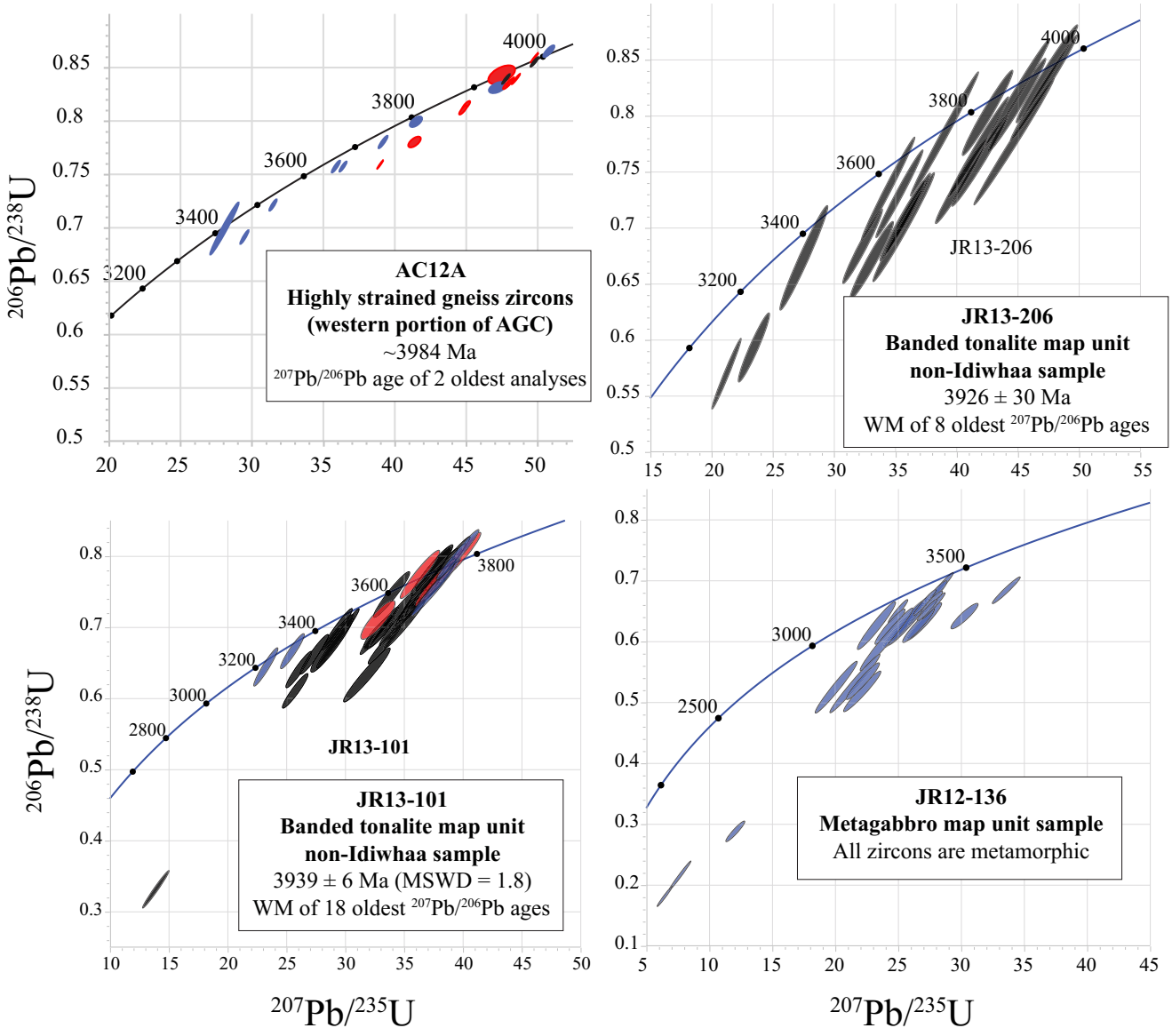
AC12A
Highly strained gneiss zircons
(western portion of AGC)
~3984 Ma
207Pb/206Pb age of 2 oldest analyses
JR13-206
JR13-206
Banded tonalite map unit
non-Idiwhaa sample
3926 ± 30 Ma
WM of 8 oldest 207Pb/206Pb ages
JR13-101
JR13-101
Banded tonalite map unit
non-Idiwhaa sample
3939 ± 6 Ma (MSWD = 1.8)
WM of 18 oldest 207Pb/206Pb ages
JR12-136
Metagabbro map unit sample
All zircons are metamorphic
206Pb/238U
207Pb/235U
Oscillatory zoned igneous zircon
Poorly preserved zircon with uncertain morphology
Recrystallized metamorphic zircon
Metamorphic rim
Xenocrystic core

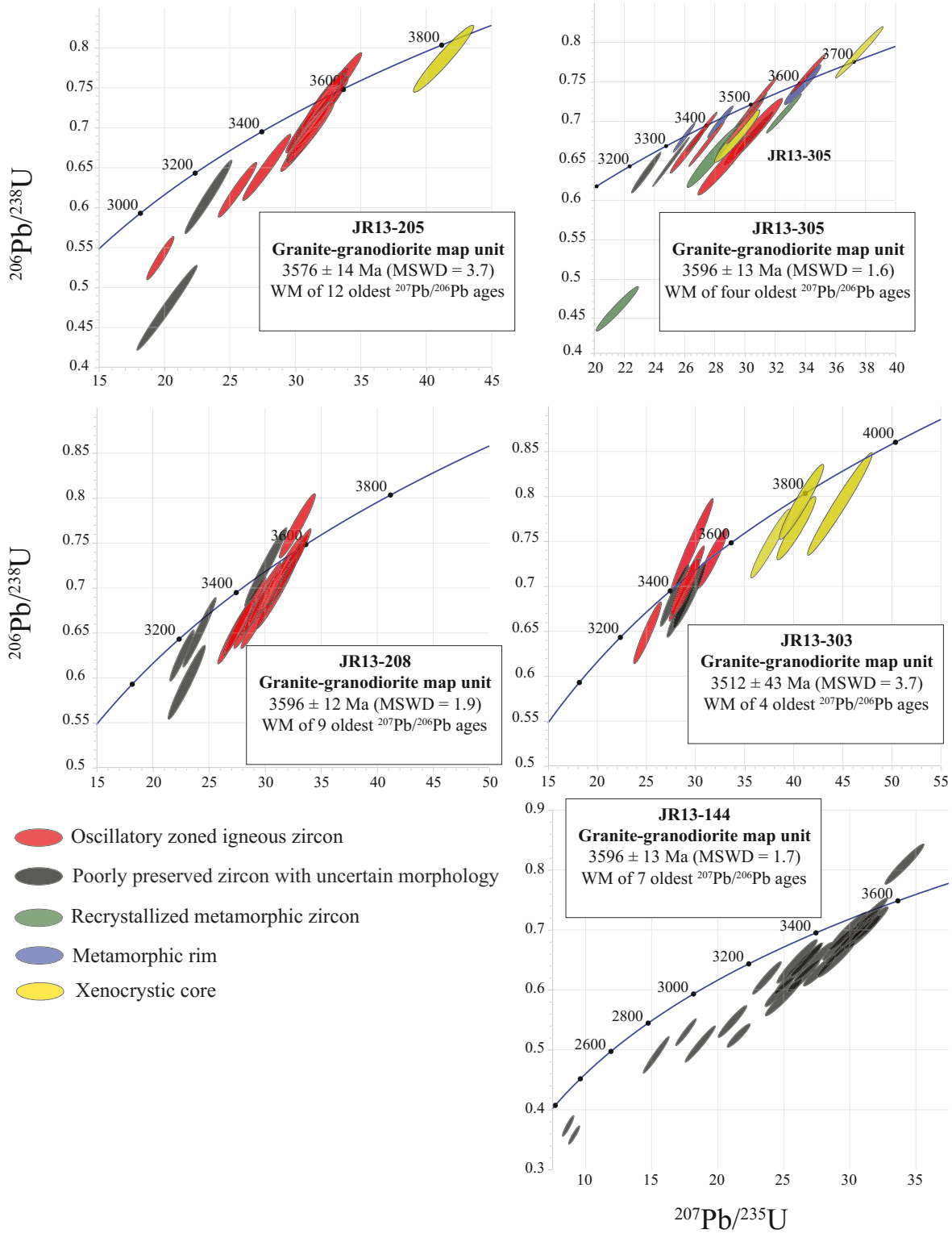
$^{206}Pb/^{238}U$
JR13-205
Granite-granodiorite map unit
3576 ± 14 Ma (MSWD = 3.7)
WM of 12 oldest $^{207}Pb/^{206}Pb$ ages
JR13-305
Granite-granodiorite map unit
3596 ± 13 Ma (MSWD = 1.6)
WM of four oldest $^{207}Pb/^{206}Pb$ ages
JR13-208
Granite-granodiorite map unit
3596 ± 12 Ma (MSWD = 1.9)
WM of 9 oldest $^{207}Pb/^{206}Pb$ ages
JR13-303
Granite-granodiorite map unit
3512 ± 43 Ma (MSWD = 3.7)
WM of 4 oldest $^{207}Pb/^{206}Pb$ ages
JR13-144
Granite-granodiorite map unit
3596 ± 13 Ma (MSWD = 1.7)
WM of 7 oldest $^{207}Pb/^{206}Pb$ ages
Oscillatory zoned igneous zircon
Poorly preserved zircon with uncertain morphology
Recrystallized metamorphic zircon
Metamorphic rim
Xenocrystic core
$^{207}Pb/^{235}U$

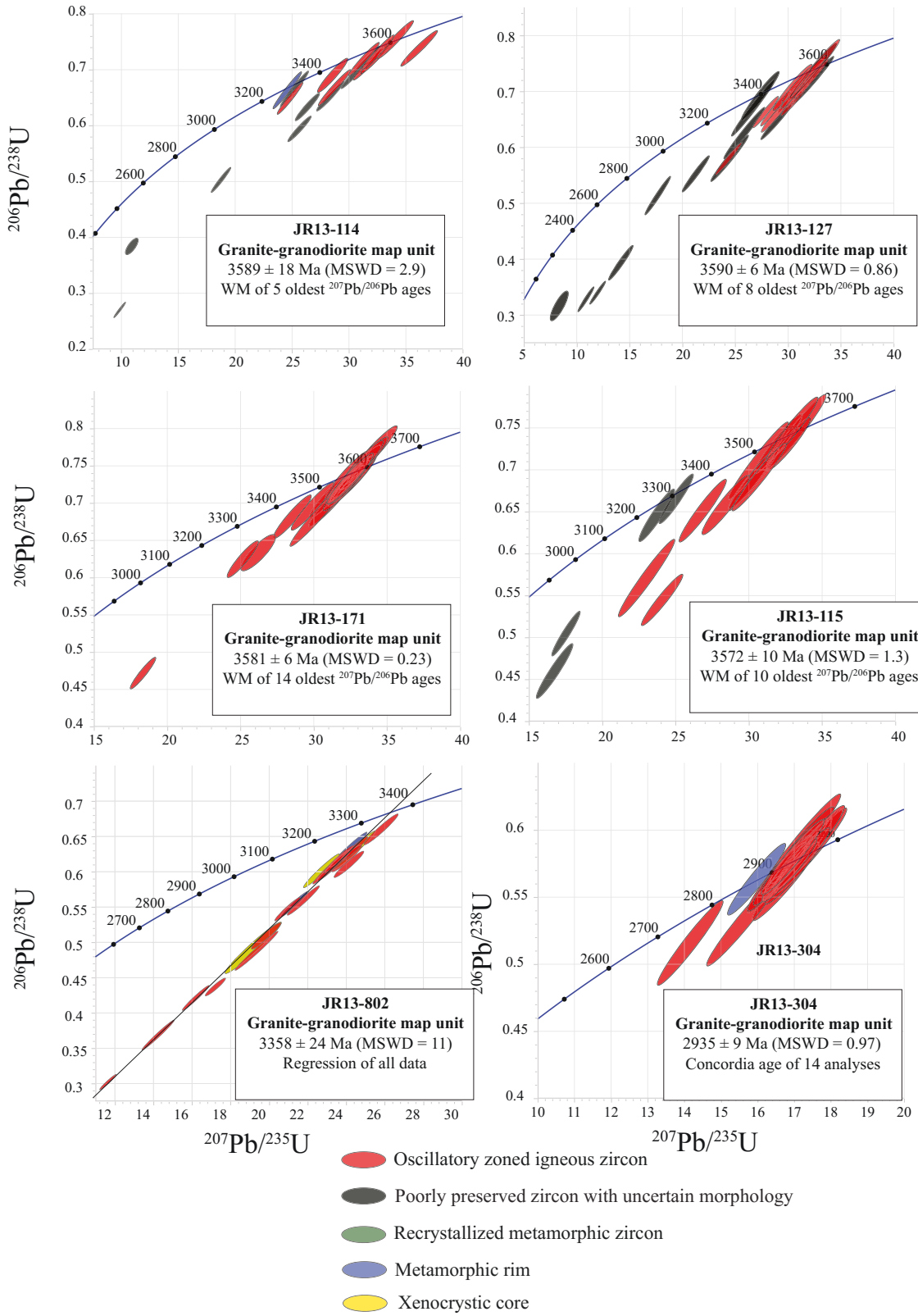
JR13-114
Granite-granodiorite map unit
3589 ± 18 Ma (MSWD = 2.9)
WM of 5 oldest 207Pb/206Pb ages
JR13-127
Granite-granodiorite map unit
3590 ± 6 Ma (MSWD = 0.86)
WM of 8 oldest 207Pb/206Pb ages
JR13-171
Granite-granodiorite map unit
3581 ± 6 Ma (MSWD = 0.23)
WM of 14 oldest 207Pb/206Pb ages
JR13-115
Granite-granodiorite map unit
3572 ± 10 Ma (MSWD = 1.3)
WM of 10 oldest 207Pb/206Pb ages
JR13-802
Granite-granodiorite map unit
3358 ± 24 Ma (MSWD = 11)
Regression of all data
JR13-304
JR13-304
Granite-granodiorite map unit
2935 ± 9 Ma (MSWD = 0.97)
Concordia age of 14 analyses
206Pb/238U
207Pb/235U
Oscillatory zoned igneous zircon
Poorly preserved zircon with uncertain morphology
Recrystallized metamorphic zircon
Metamorphic rim
Xenocrystic core

Appendix 5: Zircon images from samples discussed in Chapter 4

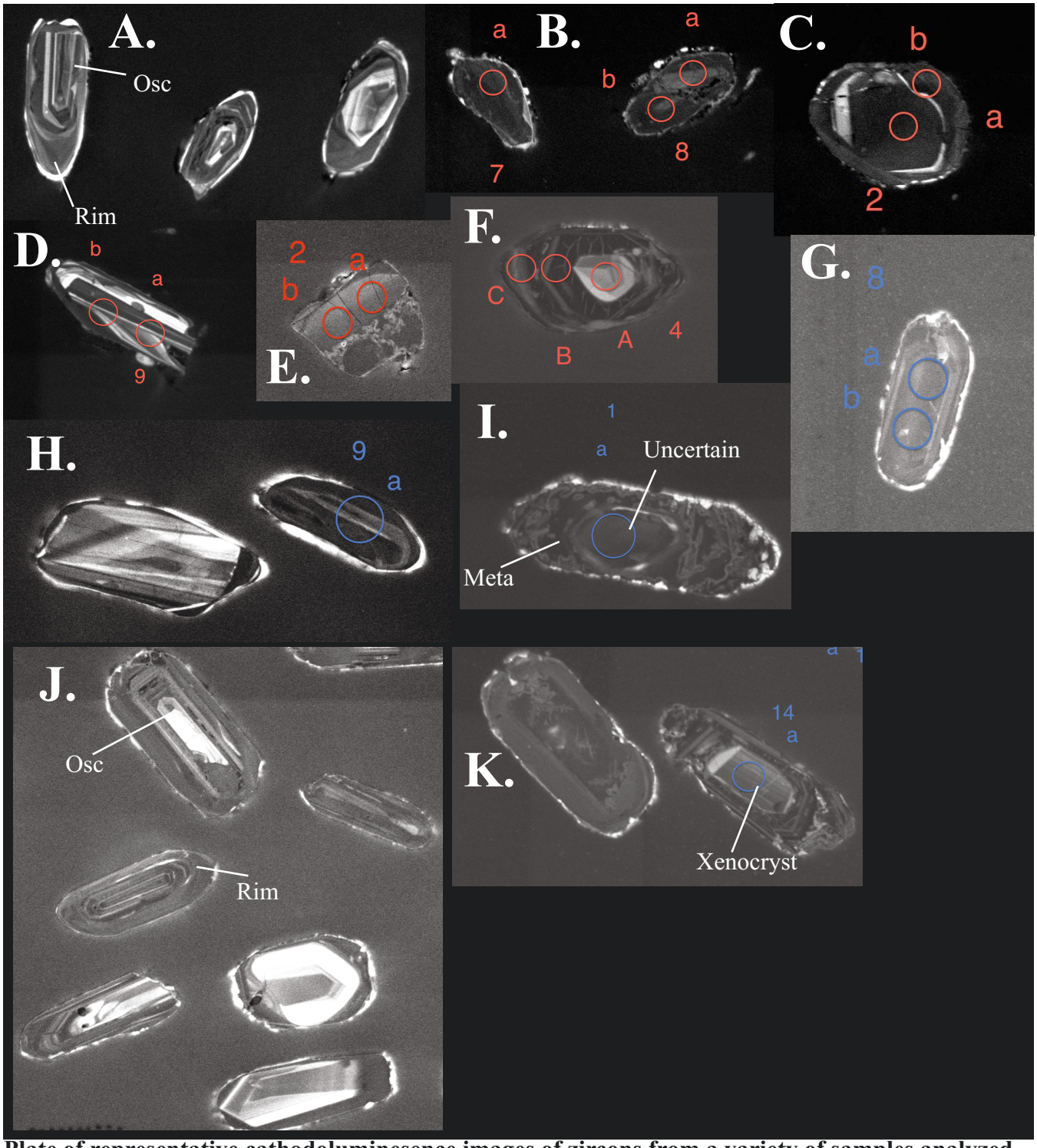

Plate of representative cathodoluminesence images of zircons from a variety of samples analyzed in this study. Red and blue circles represent analytical pits of 25 and 30 μm, respectively. **A**. Three oscillatory-zoned zircon grains extracted from sample JR12-171. The grain on the right has a small, dark, metamorphic rim growing around the oscillatory-zoned central portion. **B**. Poorly preserved zircon material from sample JR12-136. The grain on the left is dominated by metamorphic growth, while the upper portion of the right-hand grain (analysis 8a) displays some cryptic zoning patterns potentially representing igneous growth. **C.** Typical zircon from JR13-108 showing an unzoned core,

surrounded by high CL response igneous growth, that is in turn overgrown by a metamorphic rim (analysis 2b). **D.** Beautifully zoned zircon extracted from JR13-127. **E.** Another zircon from JR13-108 showing cryptic igneous zoning, with a lower portion that is poorly preserved. **F.** Example of a zircon from sample JR13-305 showing an apparently inherited core (analysis 4a) surrounded by a darkly banded zone (4b and 4c). **G.** Zircon from sample JR12-119 displaying a dark, igneous center with and oscillatory-zoned mantle, surrounded by a thin metamorphic rim. These characteristics are similar to those documented in JR13-108. **H.** Oscillatory-zoned zircons typical of sample JR13-208. **I.** Poorly preserved zircon from JR13-303. A dark igneous core is surrounded by a heavily radiation damaged and altered rim. **J.** A suite of nicely preserved and oscillatory-zoned zircons from JR13-205. These grains show a wide range of CL response but all show well-preserved oscillatory zoning patterns. **K.** More typical zircon from sample JR13-303. The left-hand grain has an altered core surrounded by a metamorphic rim while the grain on the right has a well-preserved and zoned igneous core surrounded by heavily damaged outer rim.

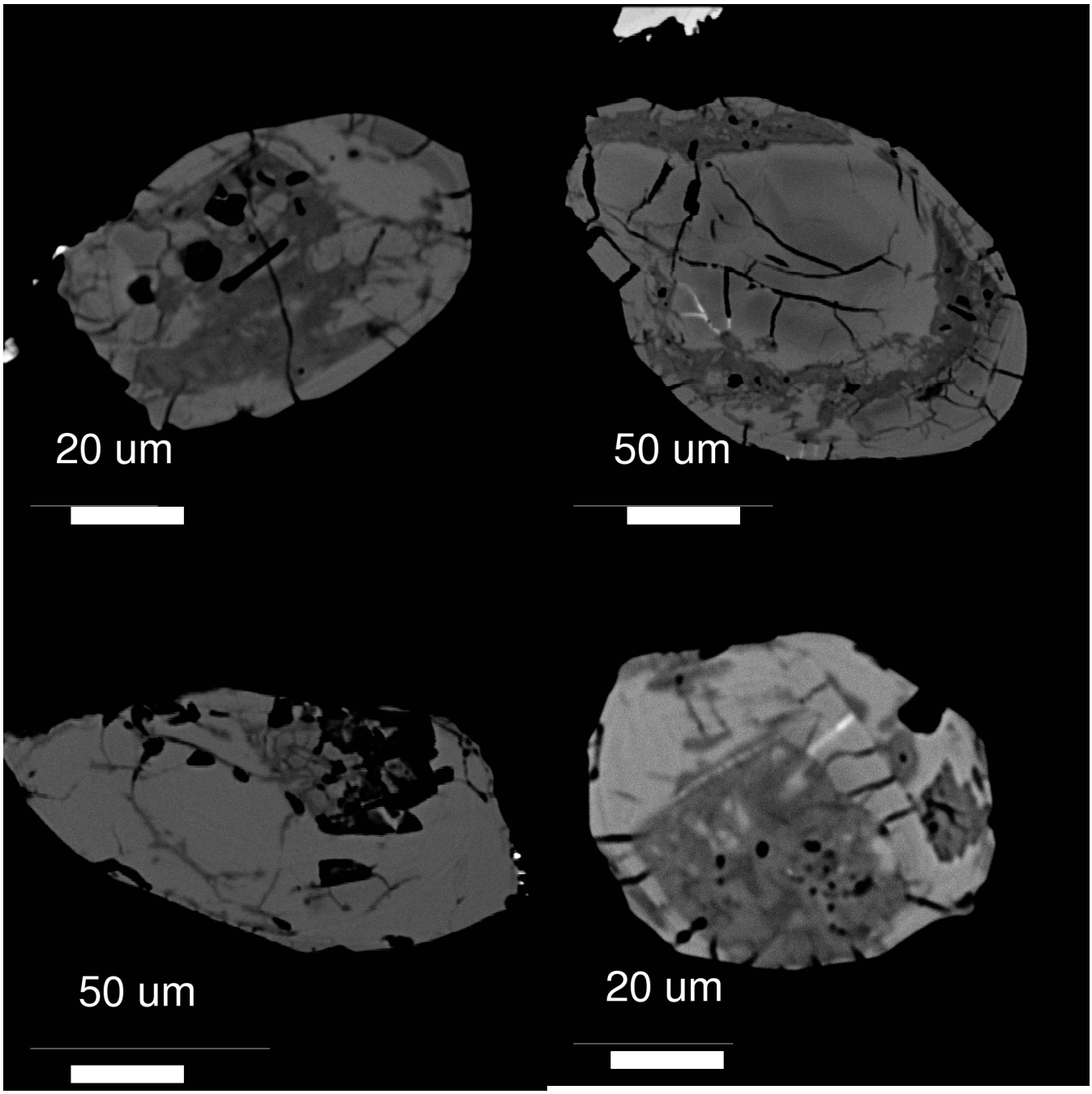

Backscatter electron images of example zircon grains from sample JR12-119 in thin section. Idiwhaa unit sample >4.0 Ga

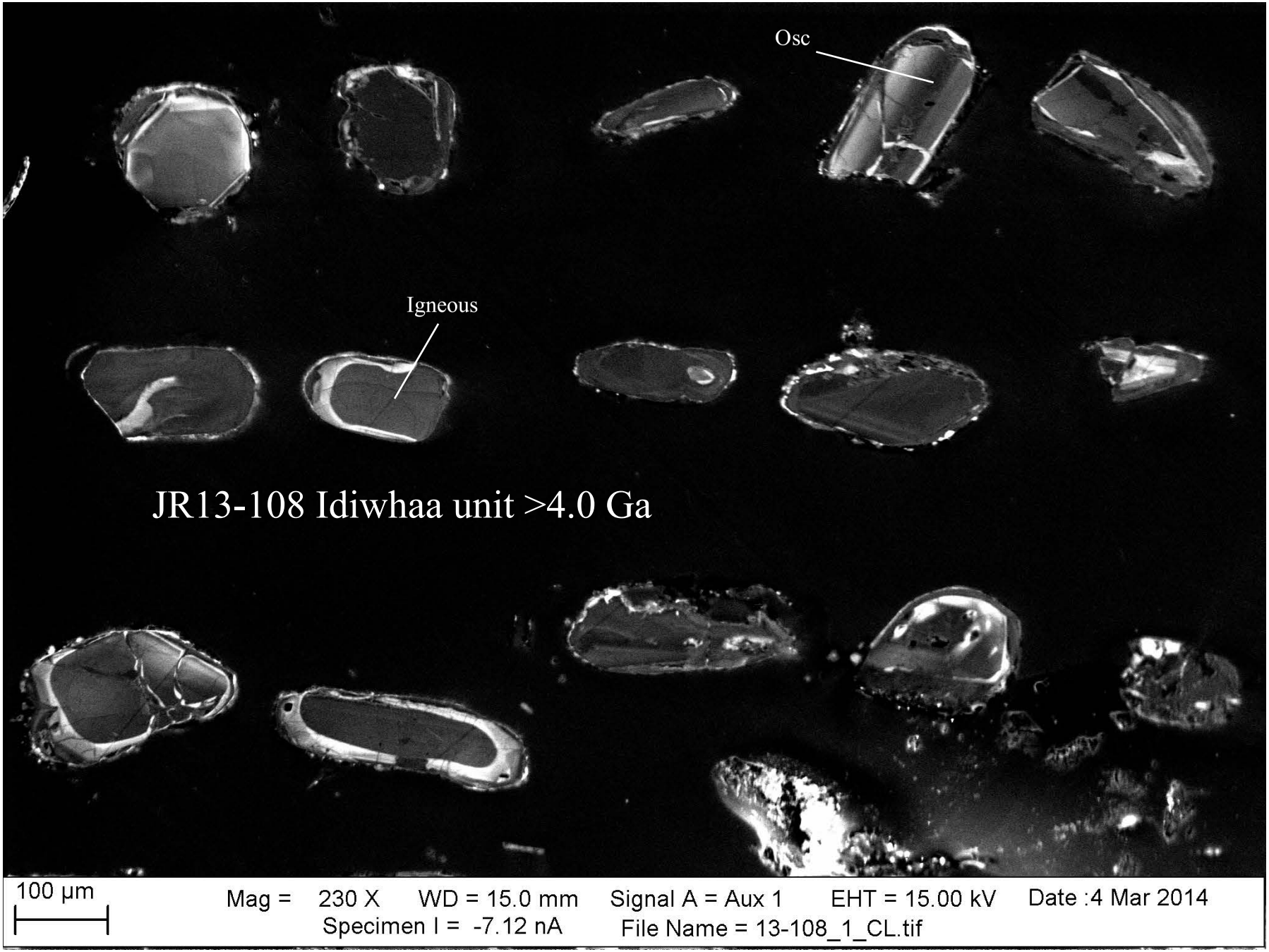
Osc
Igneous
JR13-108 Idiwhaa unit >4.0 Ga
100 µm
Mag = 230 X WD = 15.0 mm Signal A = Aux 1 EHT = 15.00 kV Date :4 Mar 2014
Specimen I = -7.12 nA File Name = 13-108_1_CL.tif

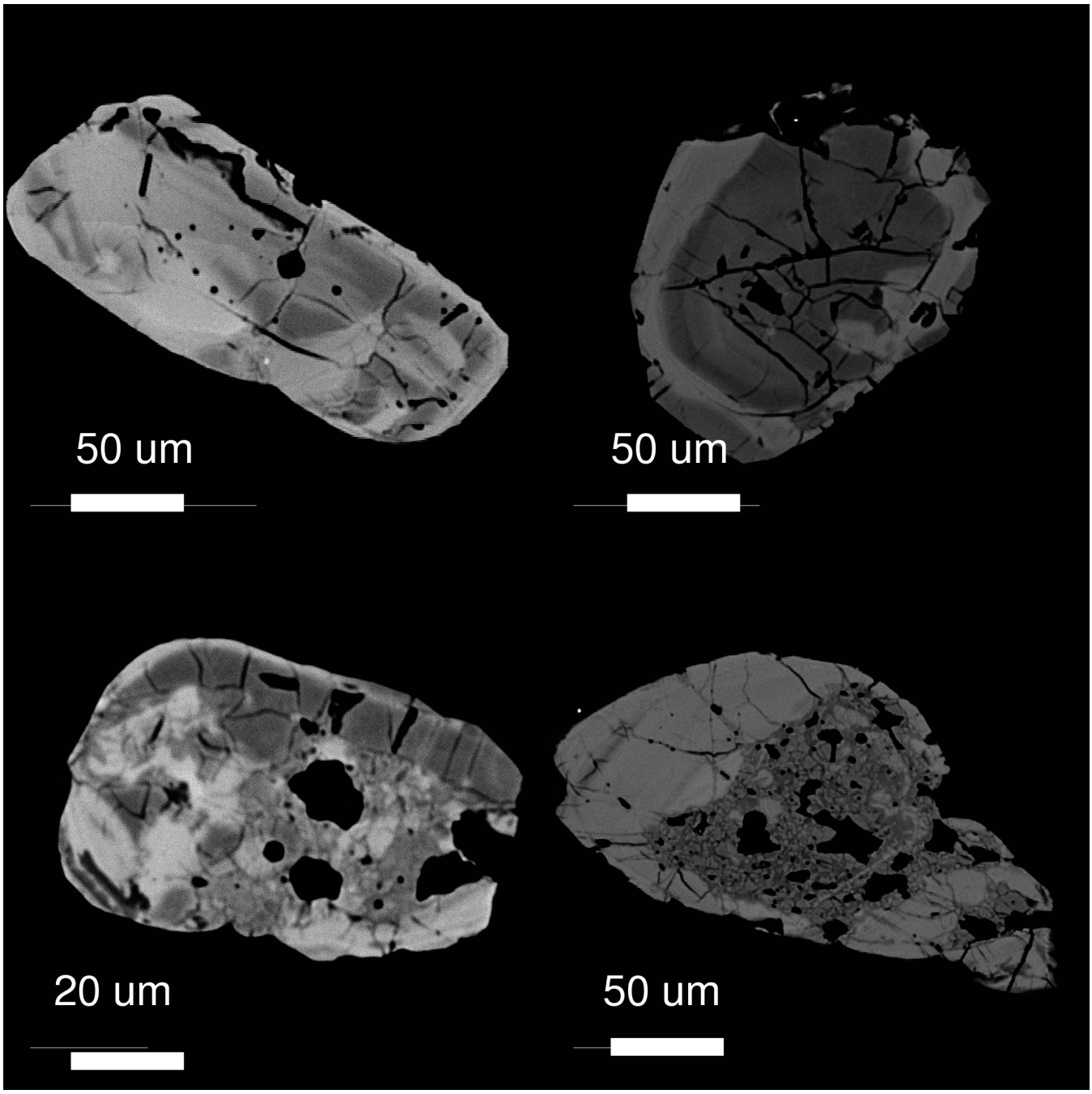

Backscatter electron images of example zircon grains from sample JR12-141 in thin section. Idiwhaa unit sample >4.0 Ga

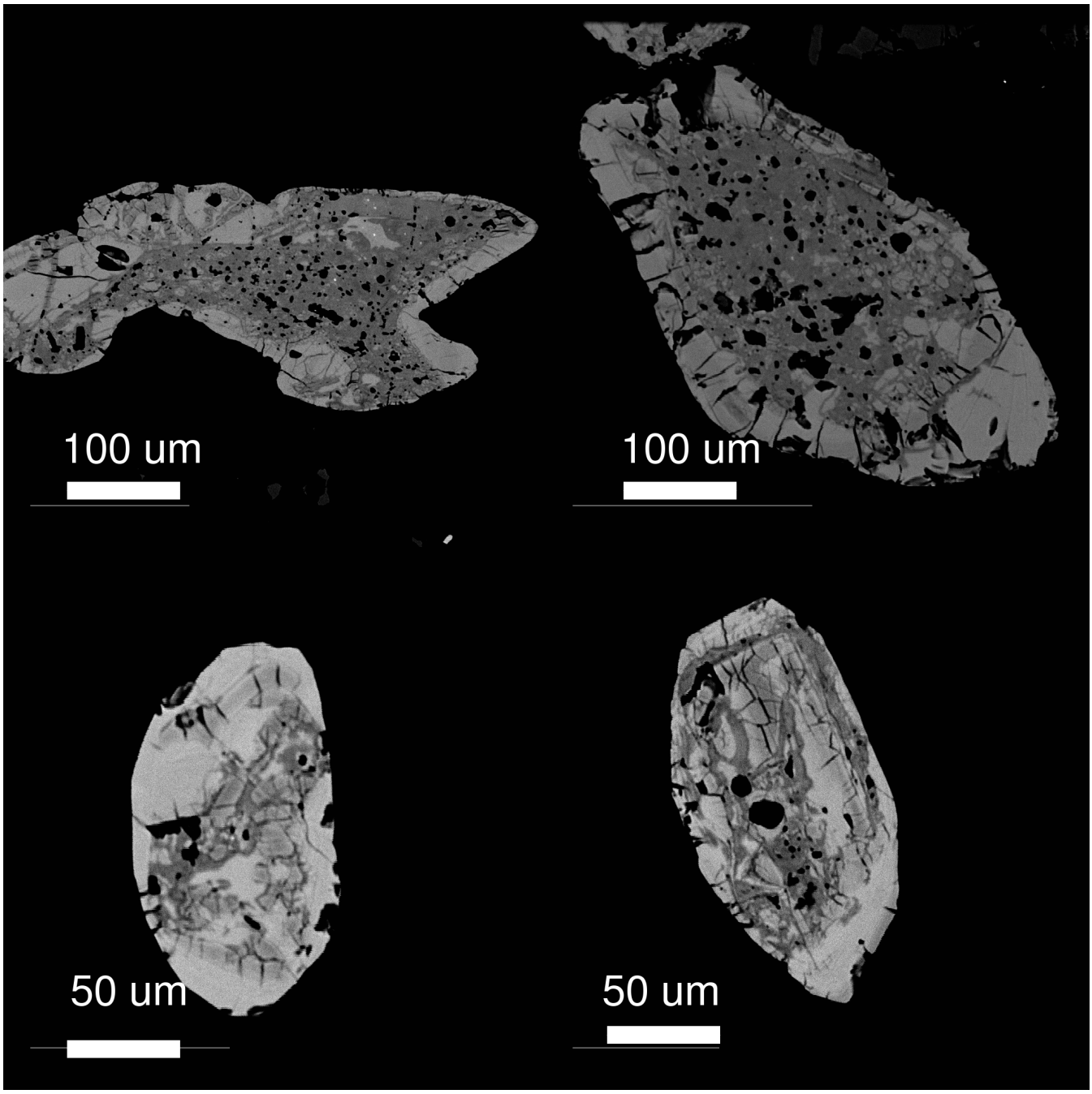

Backscatter electron images of example zircon grains from sample JR12-146 in thin section. Idiwhaa unit sample >4.0 Ga

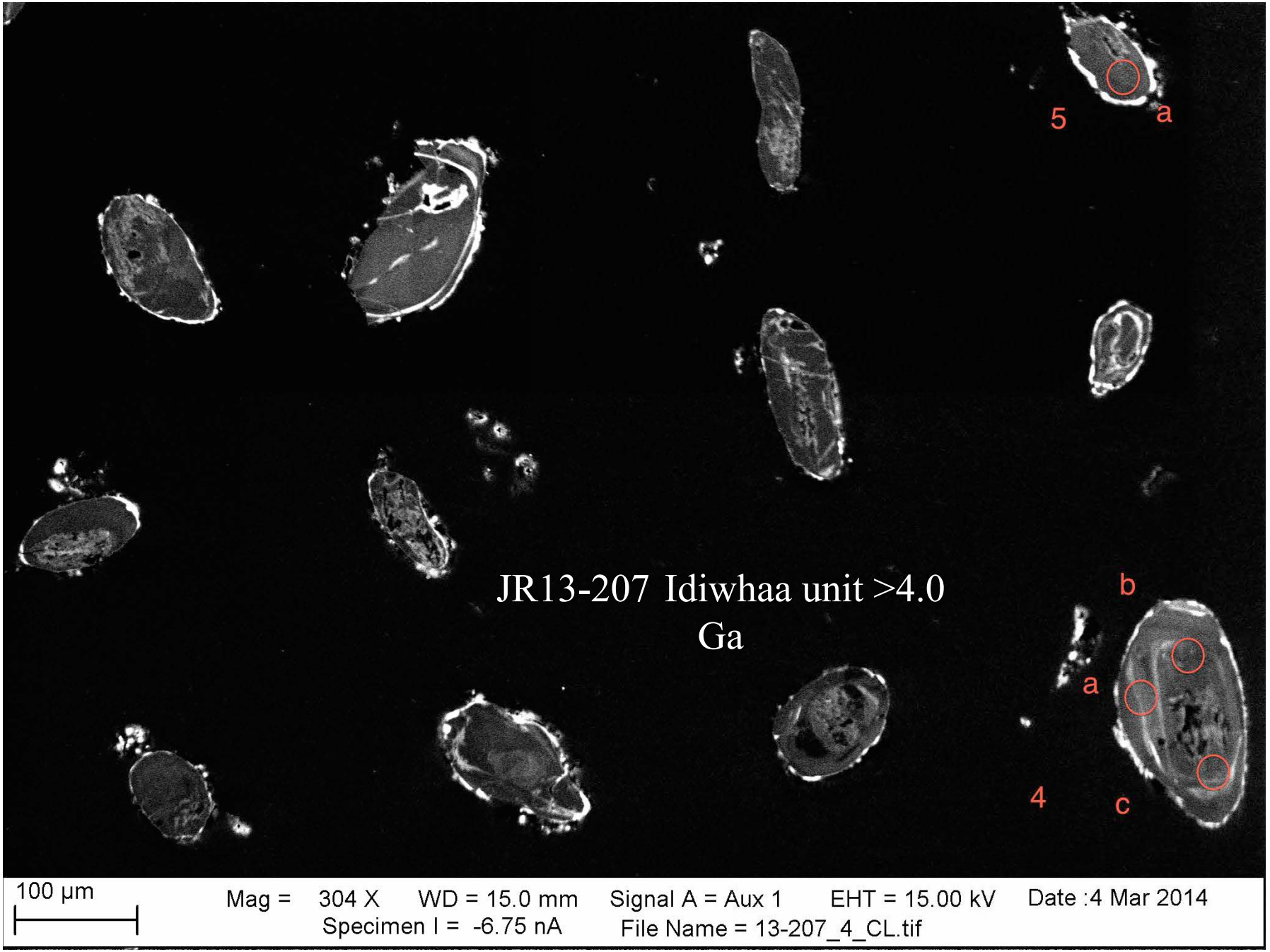
5
a
JR13-207 Idiwhaa unit >4.0
Ga
b
a
4
c
100 µm
Mag = 304 X WD = 15.0 mm Signal A = Aux 1 EHT = 15.00 kV Date :4 Mar 2014
Specimen I = -6.75 nA File Name = 13-207_4_CL.tif

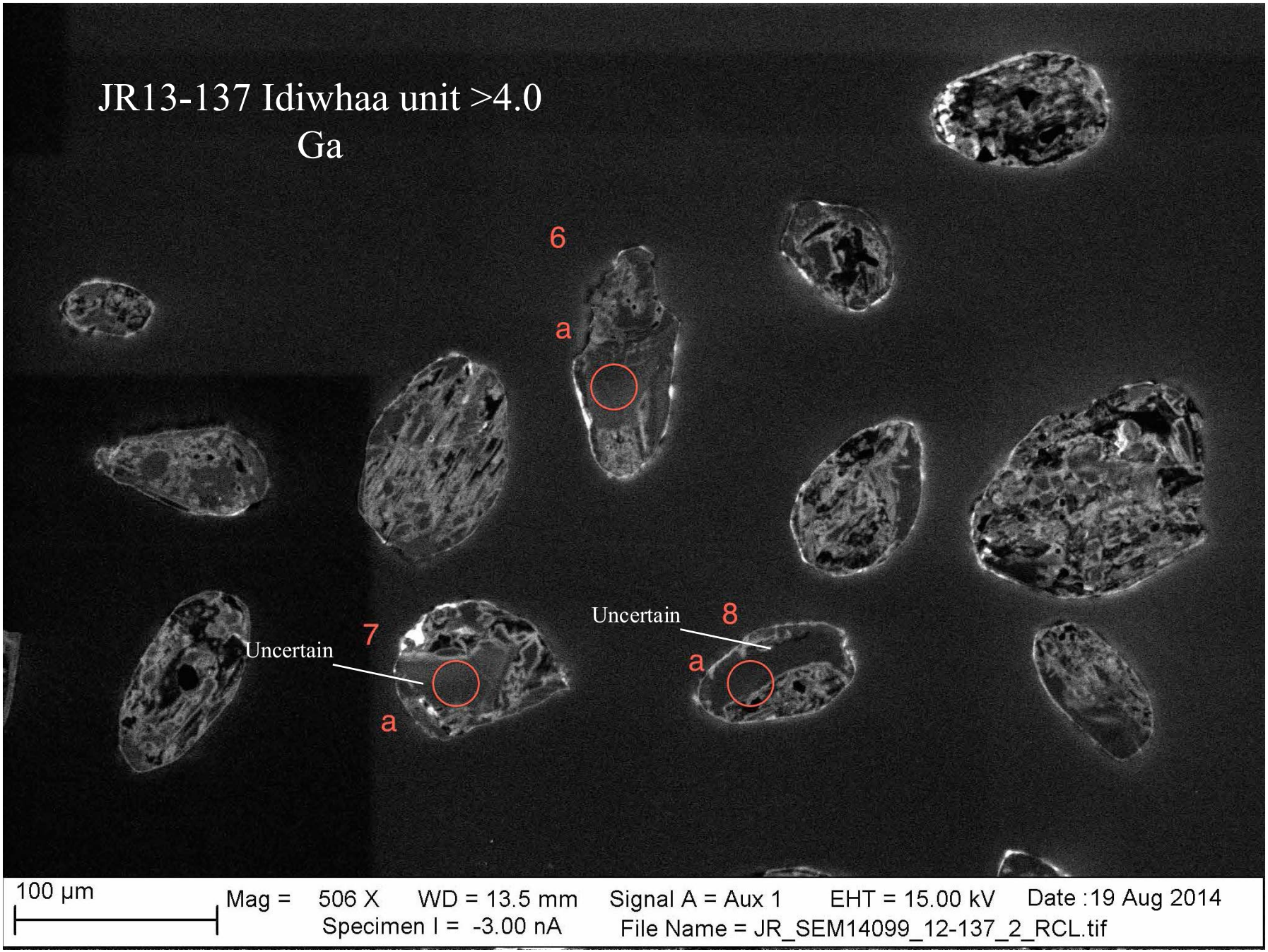
JR13-137 Idiwhaa unit >4.0 Ga
6
a
Uncertain
7
a
Uncertain
8
a
100 µm
Mag = 506 X WD = 13.5 mm Signal A = Aux 1 EHT = 15.00 kV Date :19 Aug 2014
Specimen I = -3.00 nA File Name = JR_SEM14099_12-137_2_RCL.tif

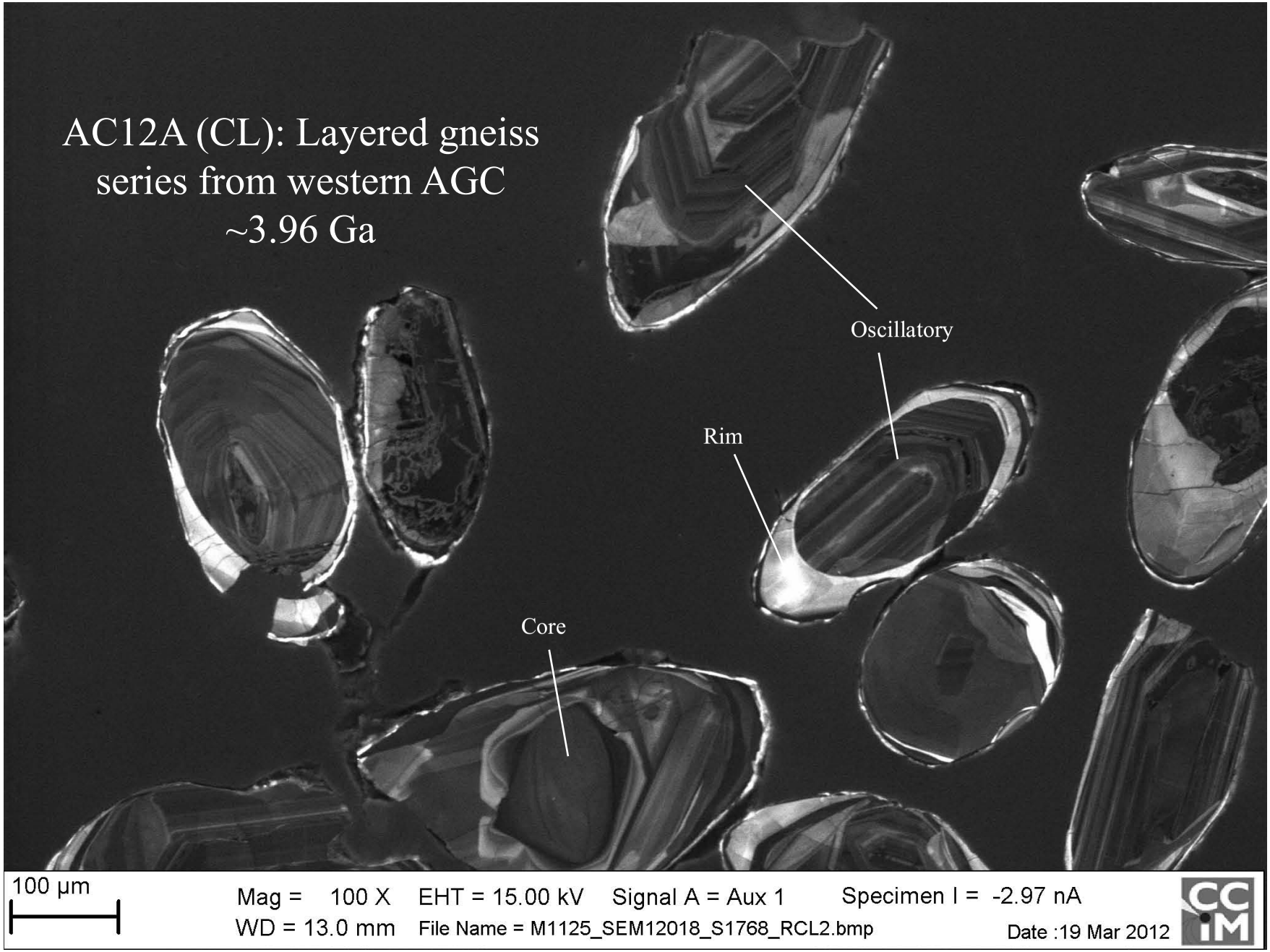
AC12A (CL): Layered gneiss series from western AGC ~3.96 Ga
Oscillatory
Rim
Core
100 µm
Mag = 100 X EHT = 15.00 kV Signal A = Aux 1 Specimen I = -2.97 nA
WD = 13.0 mm File Name = M1125_SEM12018_S1768_RCL2.bmp
Date :19 Mar 2012

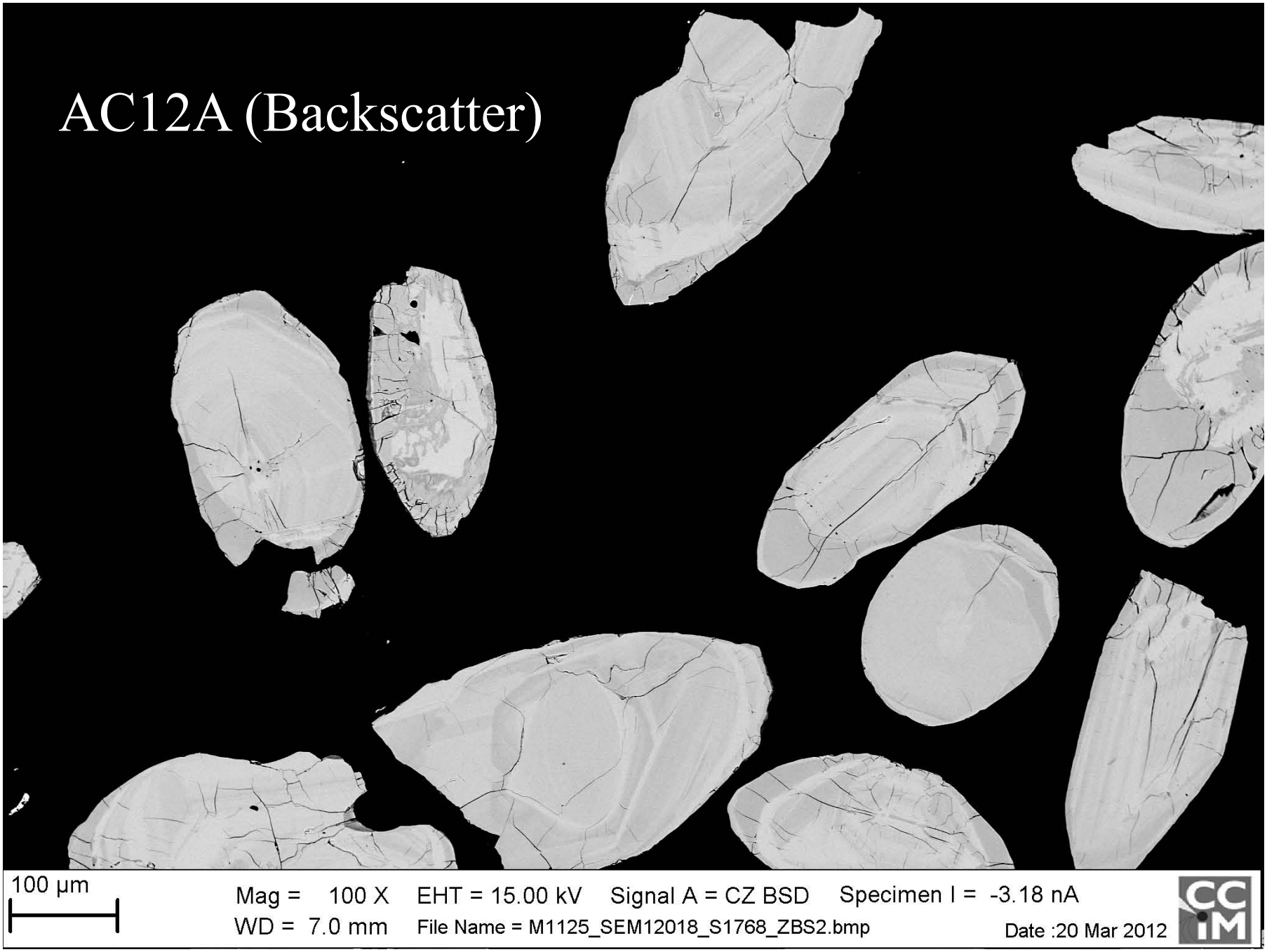
AC12A (Backscatter)
100 µm
Mag = 100 X
EHT = 15.00 kV
Signal A = CZ BSD
Specimen I = -3.18 nA
WD = 7.0 mm
File Name = M1125_SEM12018_S1768_ZBS2.bmp
Date :20 Mar 2012

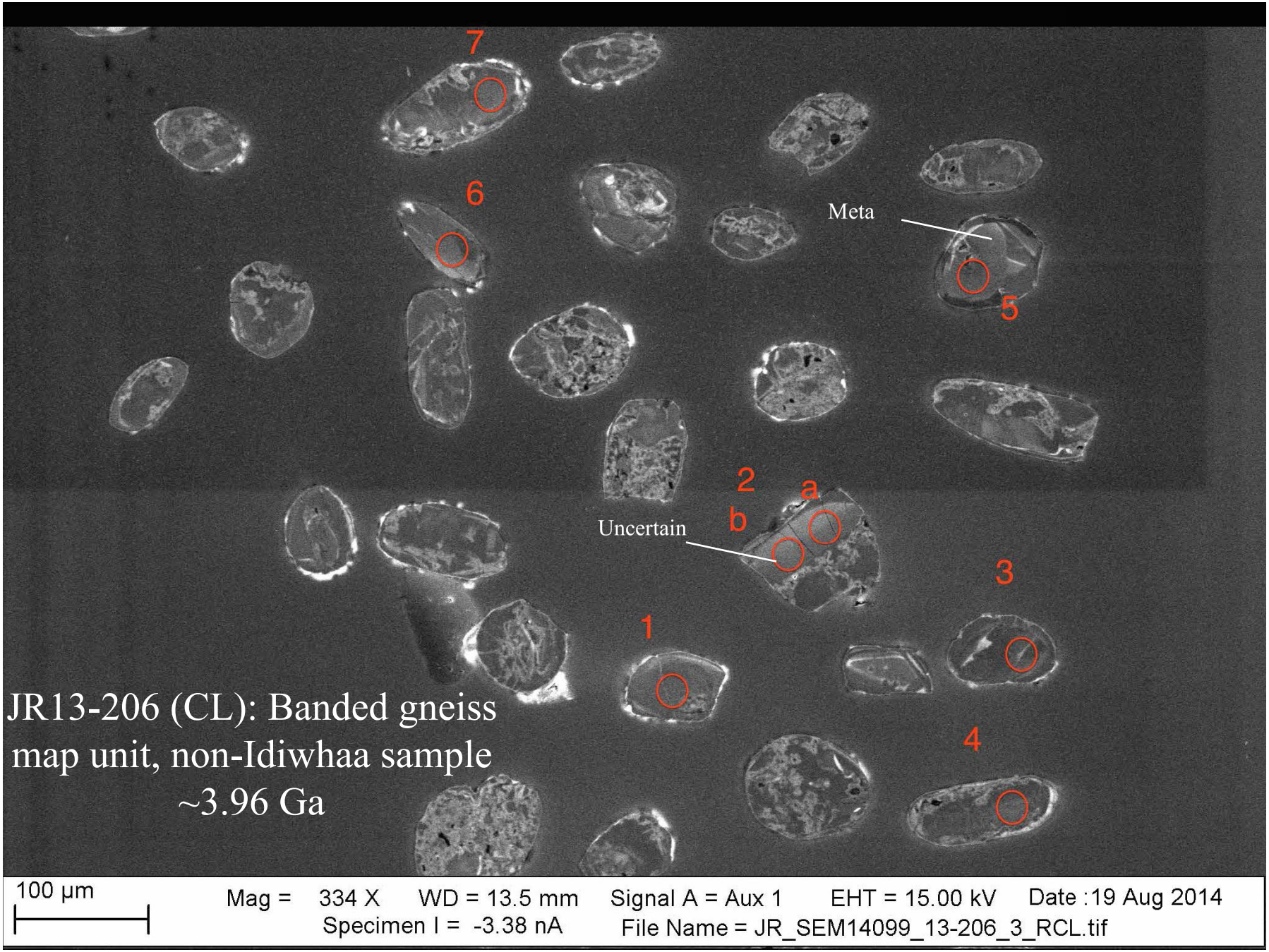
7
6
Meta
5
2
a
b
Uncertain
3
1
4
JR13-206 (CL): Banded gneiss map unit, non-Idiwhaa sample ~3.96 Ga
100 µm
Mag = 334 X WD = 13.5 mm Signal A = Aux 1 EHT = 15.00 kV Date :19 Aug 2014
Specimen I = -3.38 nA File Name = JR_SEM14099_13-206_3_RCL.tif

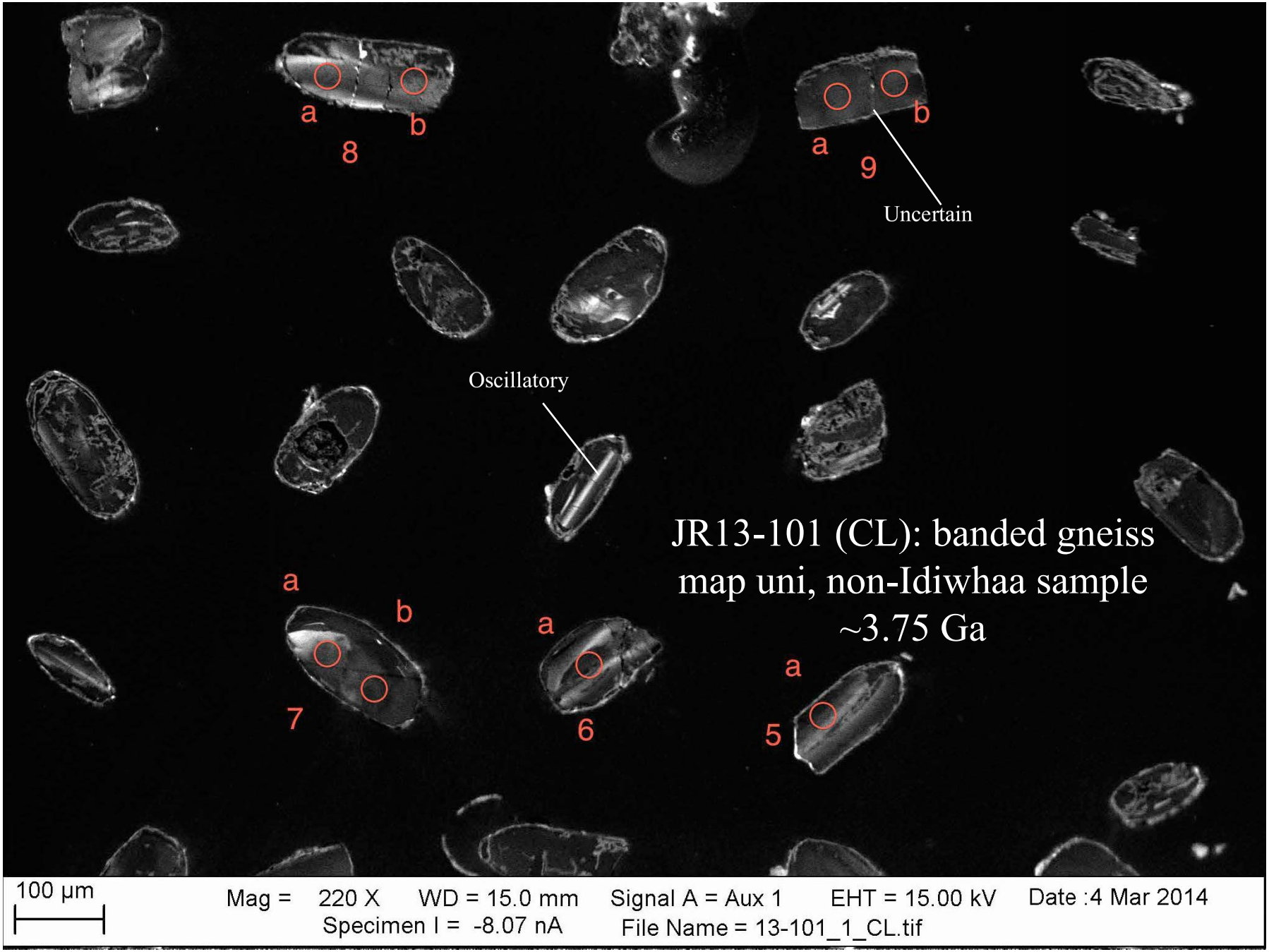
a
b
8
a
b
9
Uncertain
Oscillatory
JR13-101 (CL): banded gneiss
map uni, non-Idiwhaa sample
~3.75 Ga
a
b
7
a
6
a
5
100 µm
Mag = 220 X WD = 15.0 mm Signal A = Aux 1 EHT = 15.00 kV Date :4 Mar 2014
Specimen I = -8.07 nA File Name = 13-101_1_CL.tif

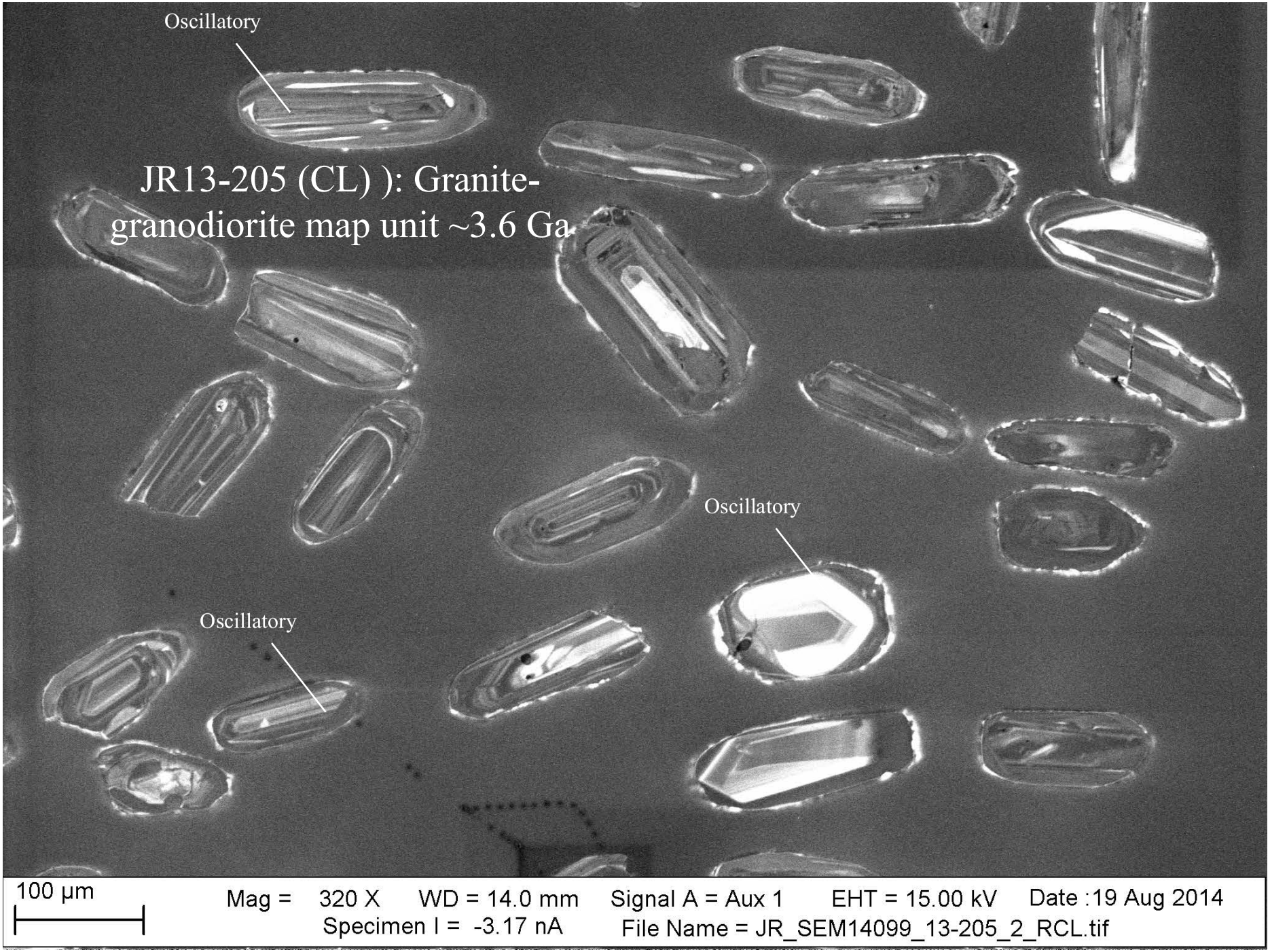
Oscillatory
JR13-205 (CL)): Granite-granodiorite map unit ~3.6 Ga
Oscillatory
Oscillatory
100 µm
Mag = 320 X WD = 14.0 mm Signal A = Aux 1 EHT = 15.00 kV Date :19 Aug 2014
Specimen I = -3.17 nA File Name = JR_SEM14099_13-205_2_RCL.tif

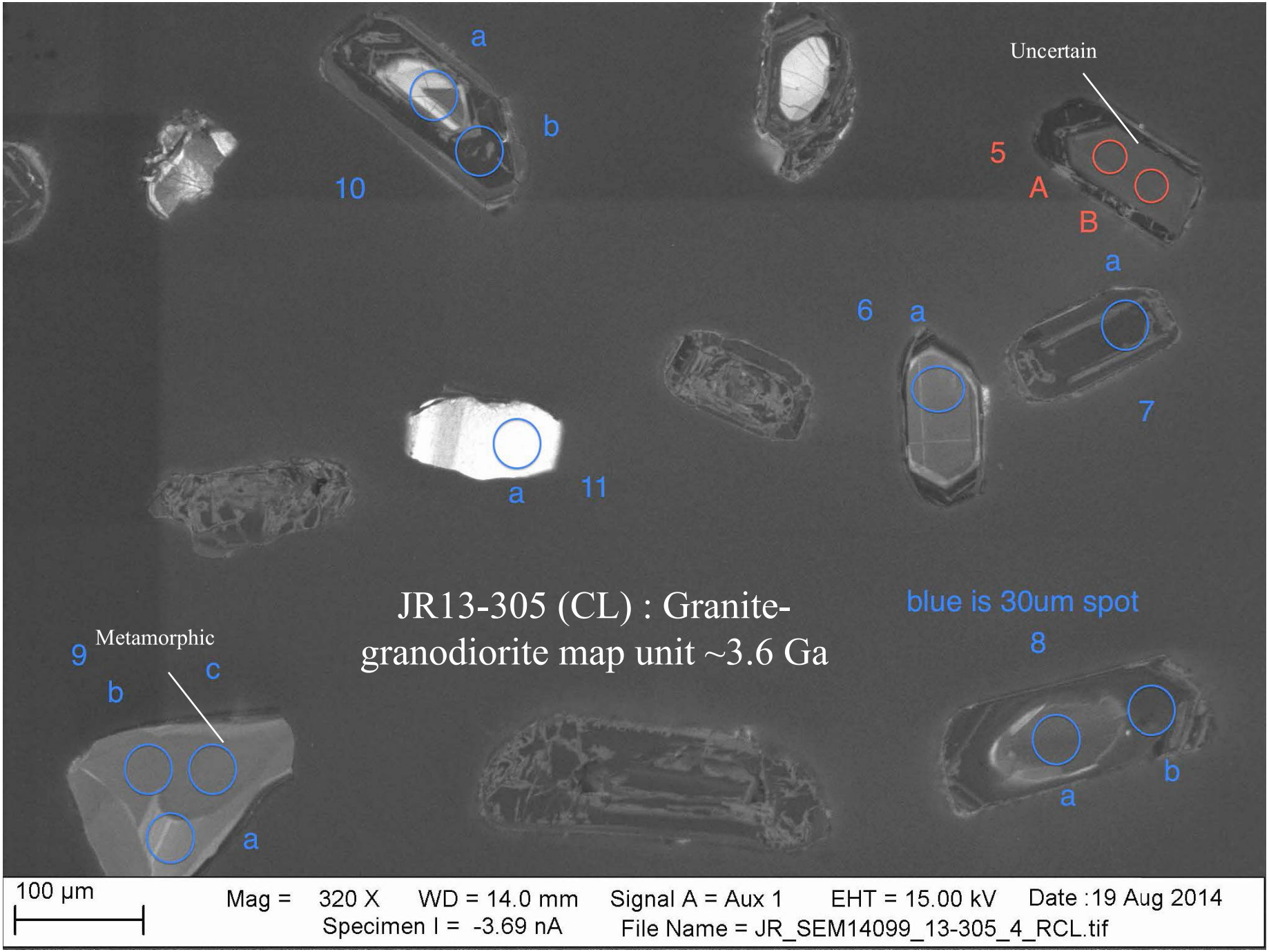
a
b
10
Uncertain
5
A
B
a
6
a
7
a
11
JR13-305 (CL) : Granite-granodiorite map unit ~3.6 Ga
blue is 30um spot
Metamorphic
9
b
c
a
8
a
b
100 µm
Mag = 320 X WD = 14.0 mm Signal A = Aux 1 EHT = 15.00 kV Date :19 Aug 2014
Specimen I = -3.69 nA File Name = JR_SEM14099_13-305_4_RCL.tif

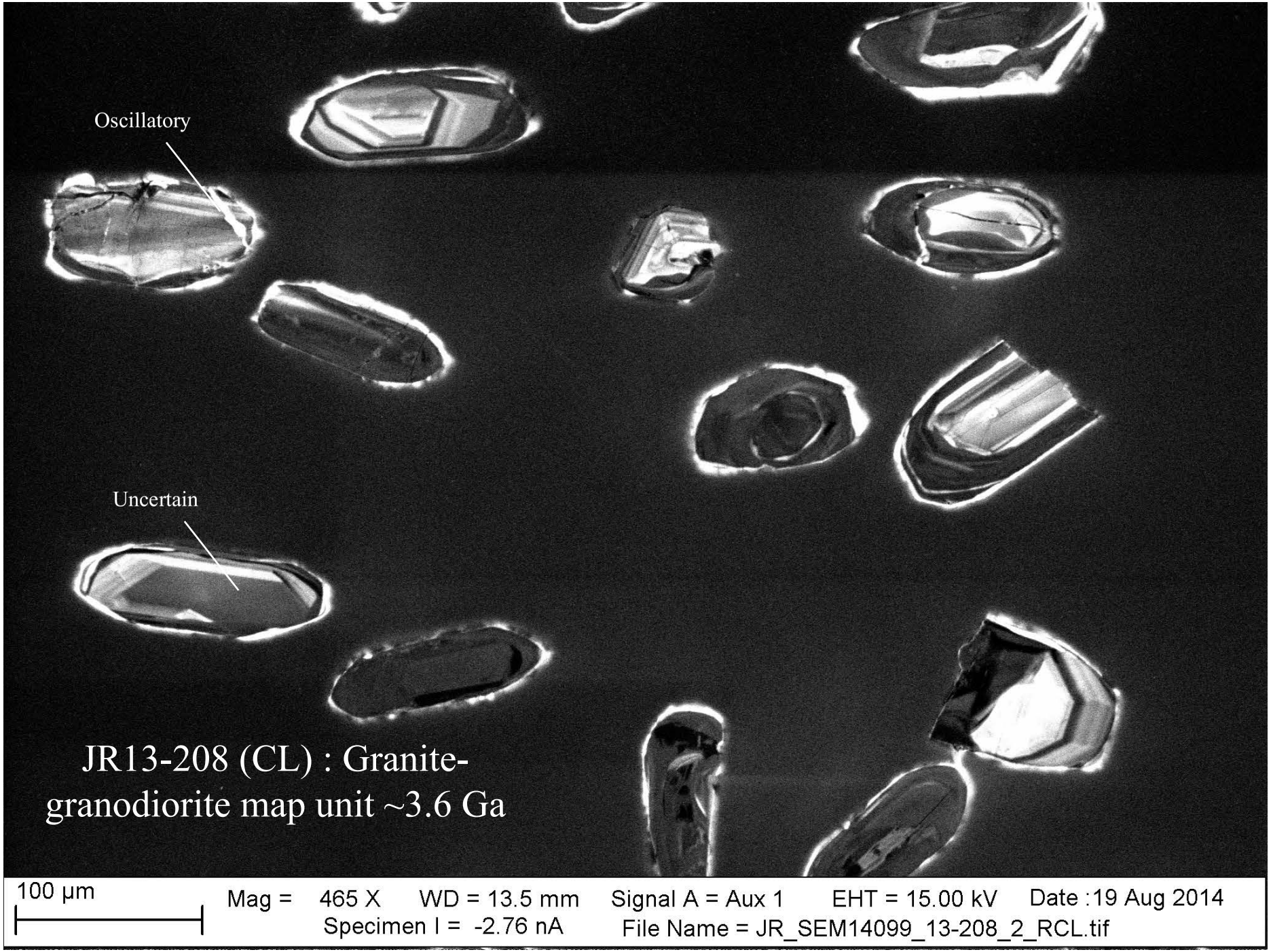
Oscillatory
Uncertain
JR13-208 (CL) : Granite-granodiorite map unit ~3.6 Ga
100 µm
Mag = 465 X WD = 13.5 mm Signal A = Aux 1 EHT = 15.00 kV Date :19 Aug 2014
Specimen I = -2.76 nA File Name = JR_SEM14099_13-208_2_RCL.tif

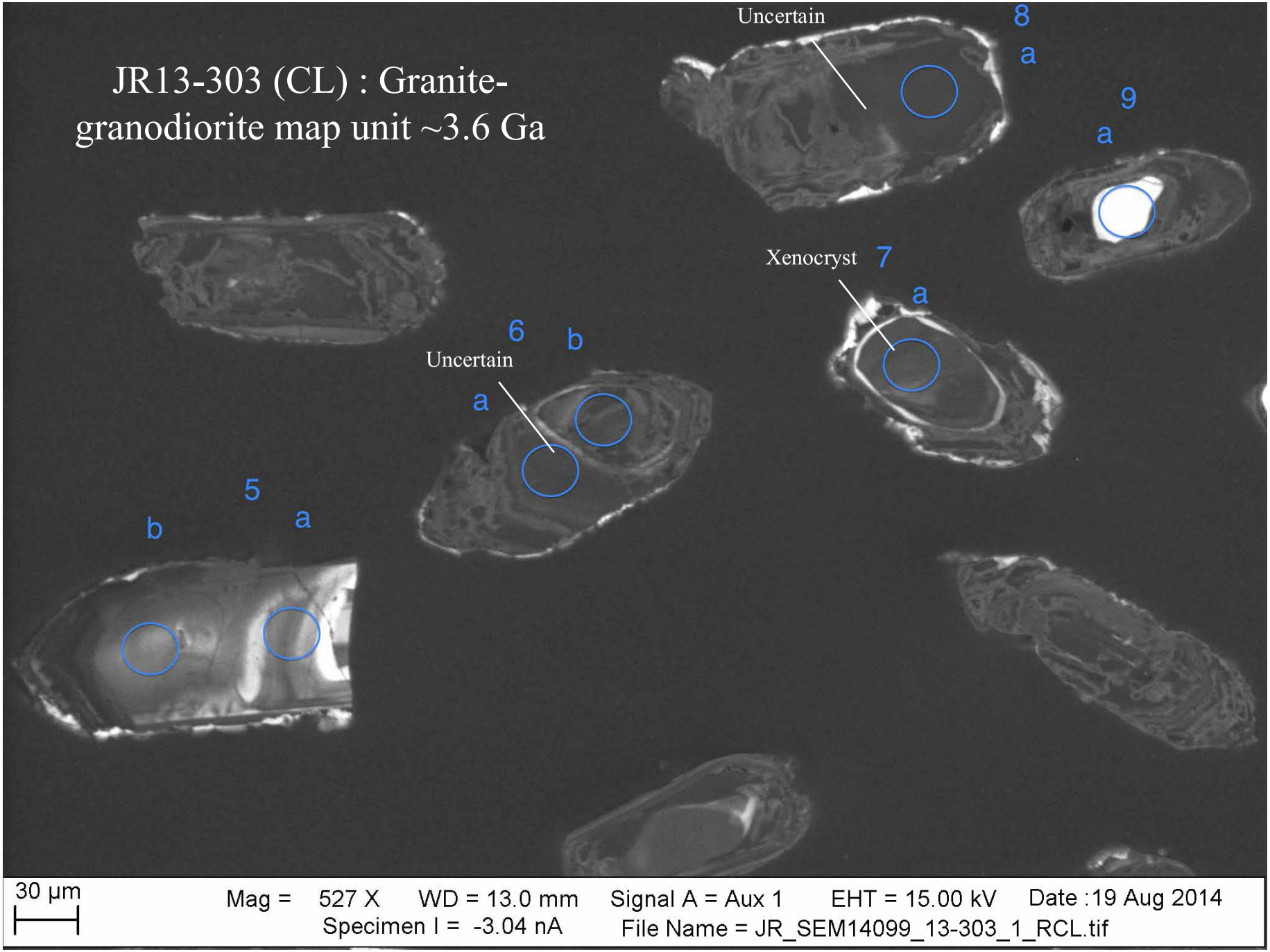
JR13-303 (CL) : Granite-granodiorite map unit ~3.6 Ga
Uncertain
8
a
9
a
Xenocryst
7
a
6
b
Uncertain
a
5
b
a
30 µm
Mag = 527 X WD = 13.0 mm Signal A = Aux 1 EHT = 15.00 kV Date :19 Aug 2014
Specimen I = -3.04 nA
File Name = JR_SEM14099_13-303_1_RCL.tif

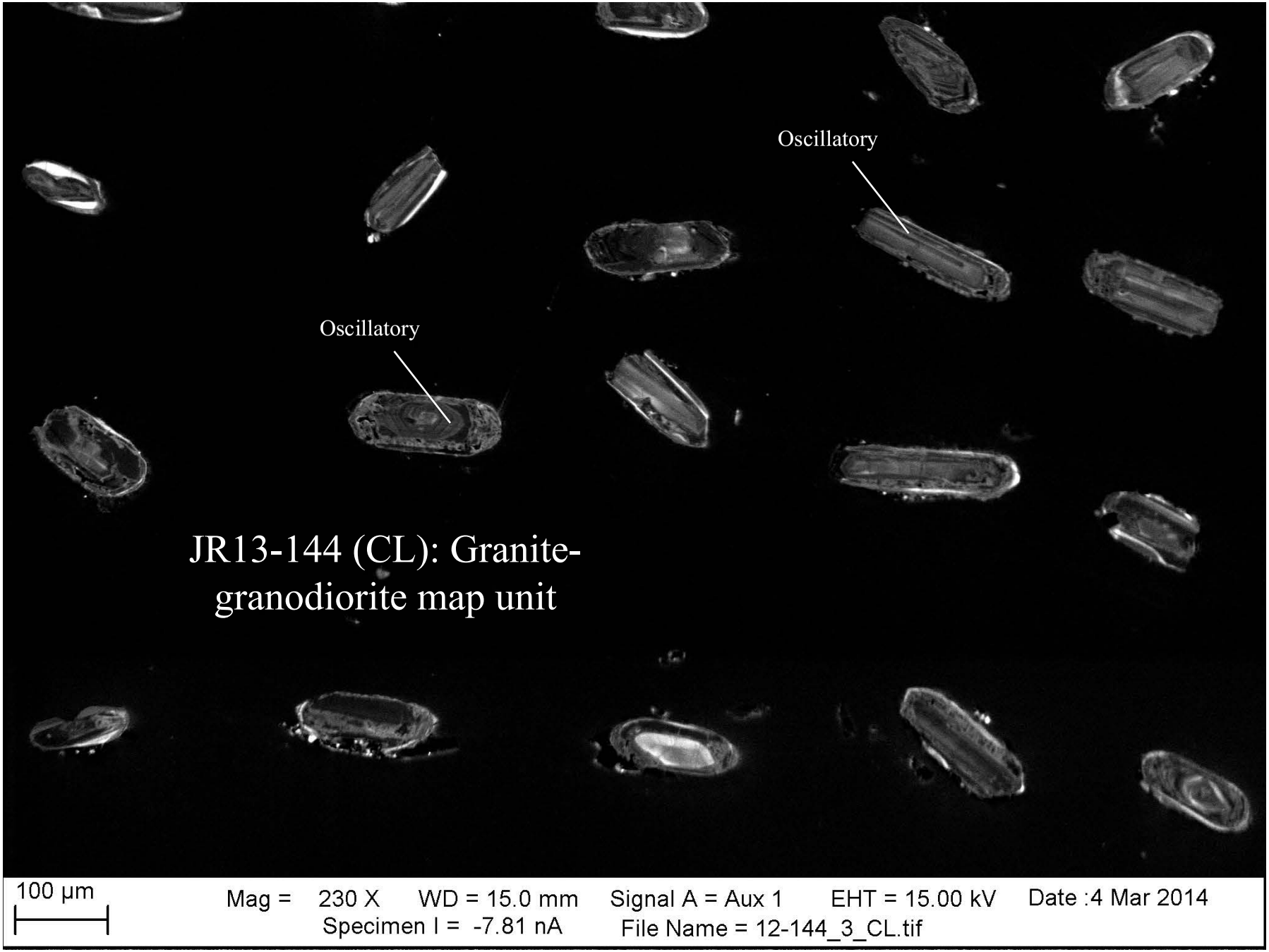
Oscillatory
Oscillatory
JR13-144 (CL): Granite-granodiorite map unit
100 µm
Mag = 230 X WD = 15.0 mm Signal A = Aux 1 EHT = 15.00 kV Date :4 Mar 2014
Specimen I = -7.81 nA File Name = 12-144_3_CL.tif

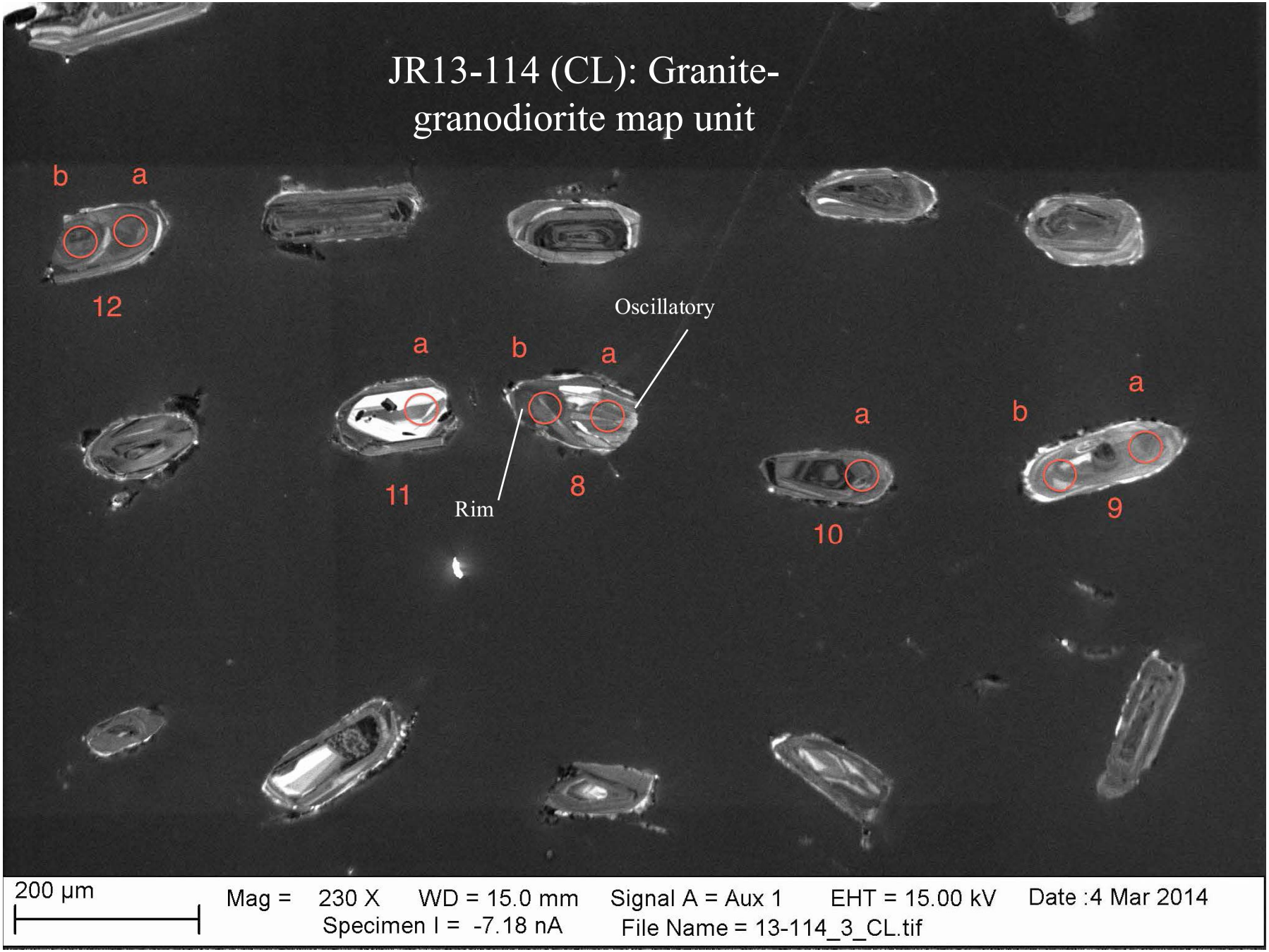
JR13-114 (CL): Granite-granodiorite map unit
b
a
12
a
b
a
Oscillatory
11
Rim
8
a
10
b
a
9
200 µm
Mag = 230 X WD = 15.0 mm Signal A = Aux 1 EHT = 15.00 kV Date :4 Mar 2014
Specimen I = -7.18 nA File Name = 13-114_3_CL.tif

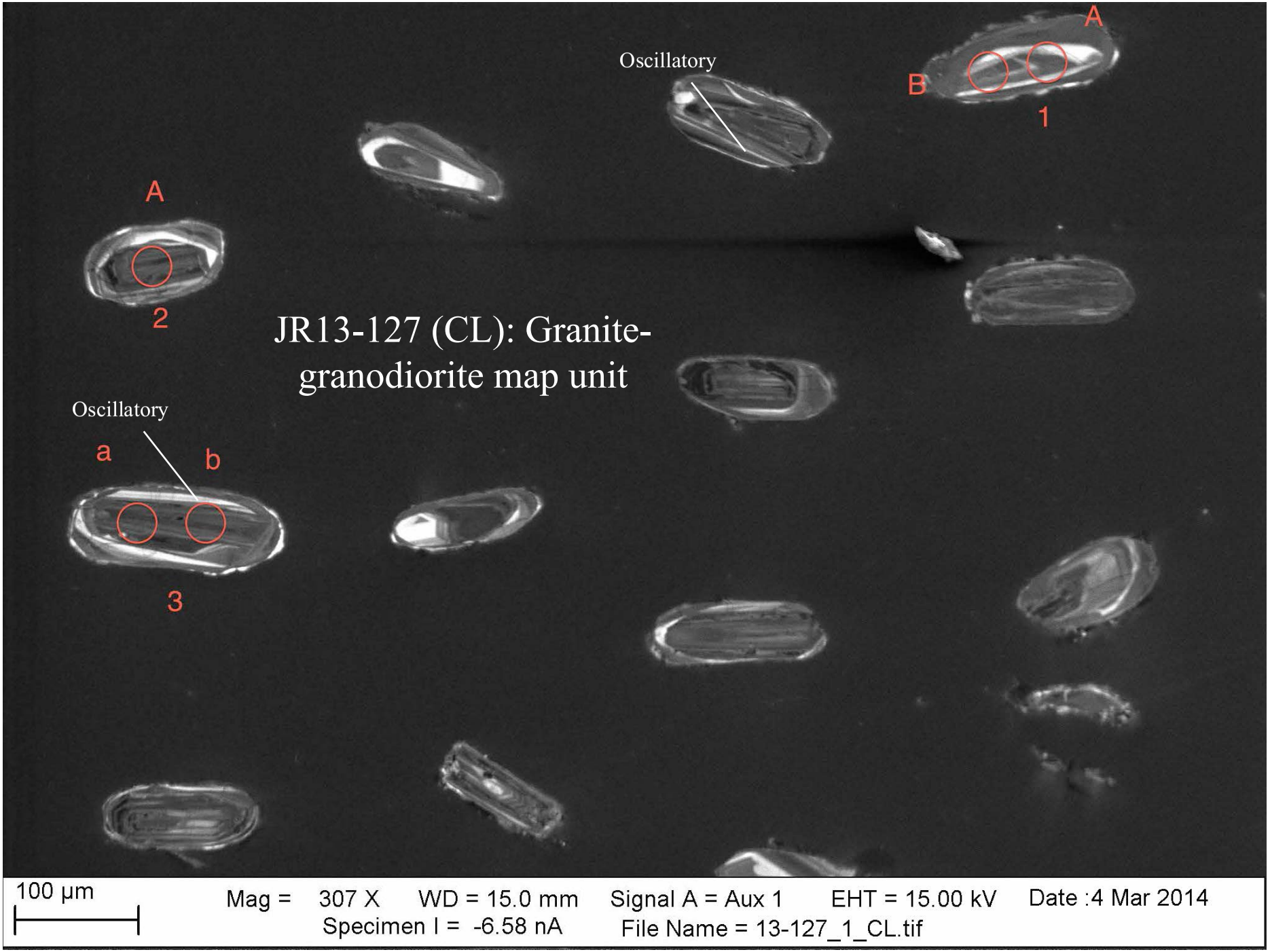
Oscillatory
A
B
1
A
2
JR13-127 (CL): Granite-granodiorite map unit
Oscillatory
a
b
3
100 µm
Mag = 307 X WD = 15.0 mm Signal A = Aux 1 EHT = 15.00 kV Date :4 Mar 2014
Specimen I = -6.58 nA File Name = 13-127_1_CL.tif

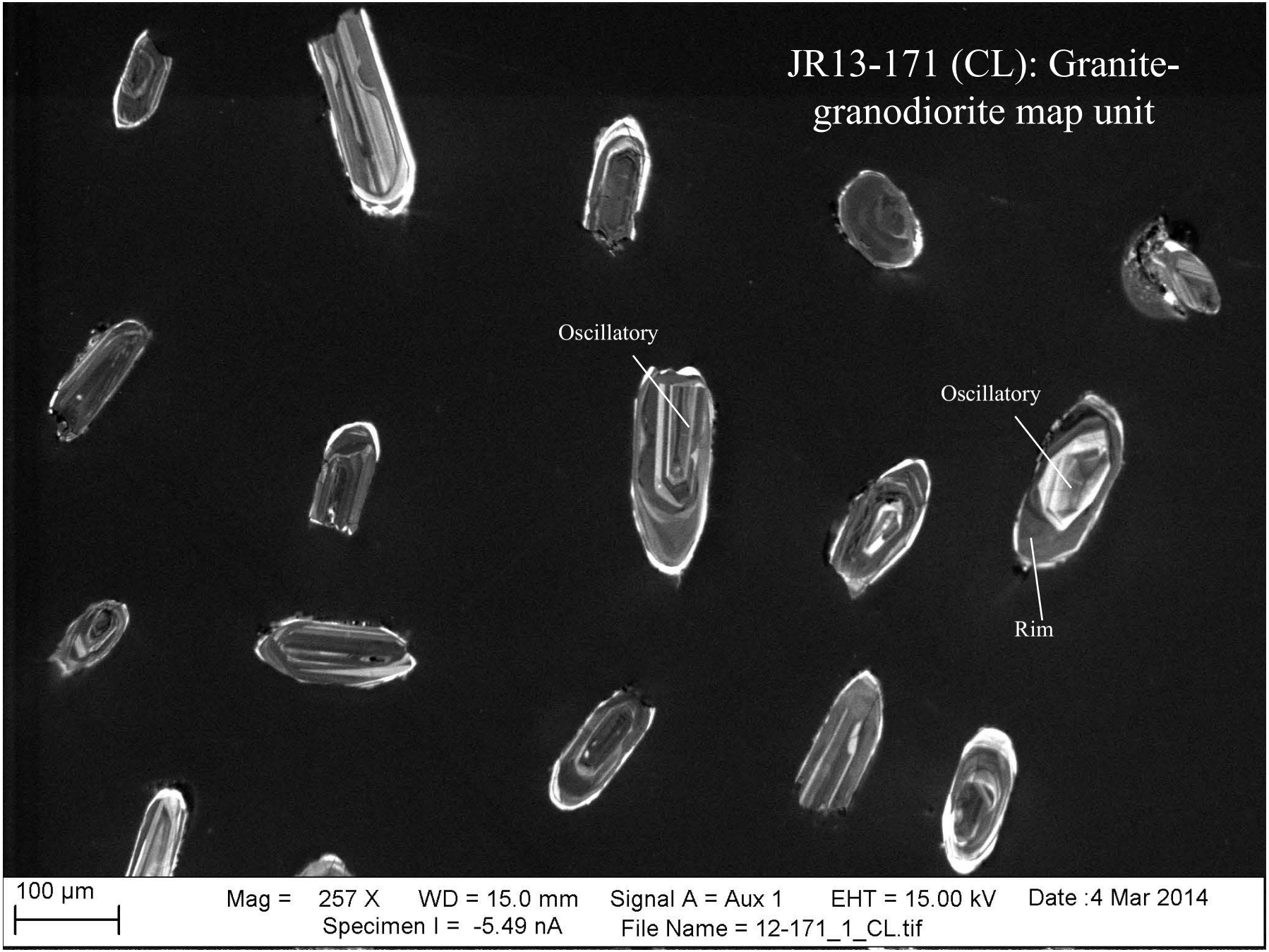
JR13-171 (CL): Granite-granodiorite map unit
Oscillatory
Oscillatory
Rim
100 µm
Mag = 257 X WD = 15.0 mm Signal A = Aux 1 EHT = 15.00 kV Date :4 Mar 2014
Specimen I = -5.49 nA File Name = 12-171_1_CL.tif

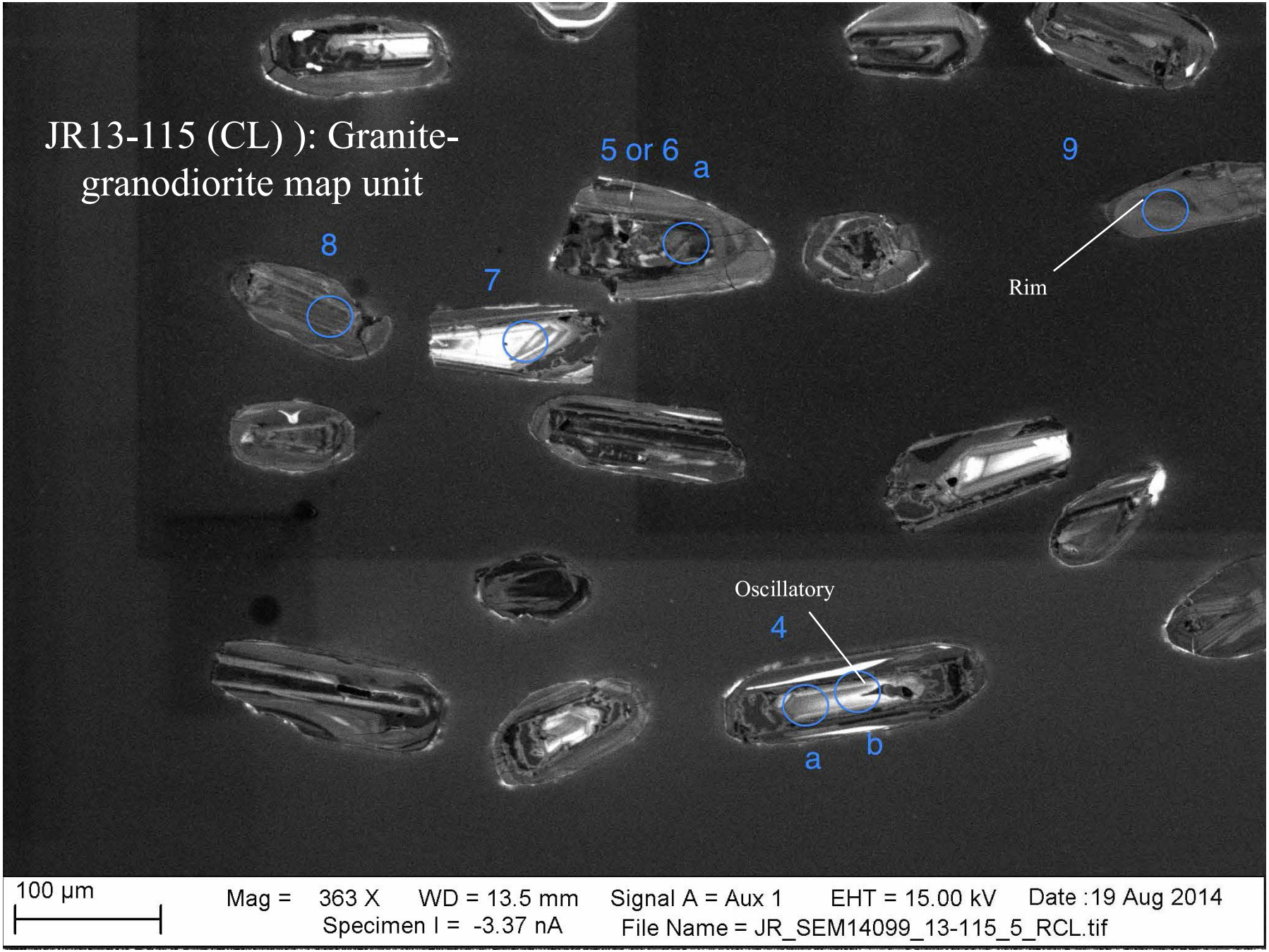
JR13-115 (CL)): Granite-granodiorite map unit
5 or 6
a
9
8
7
Rim
Oscillatory
4
a
b
100 µm
Mag = 363 X WD = 13.5 mm Signal A = Aux 1 EHT = 15.00 kV Date :19 Aug 2014
Specimen I = -3.37 nA File Name = JR_SEM14099_13-115_5_RCL.tif

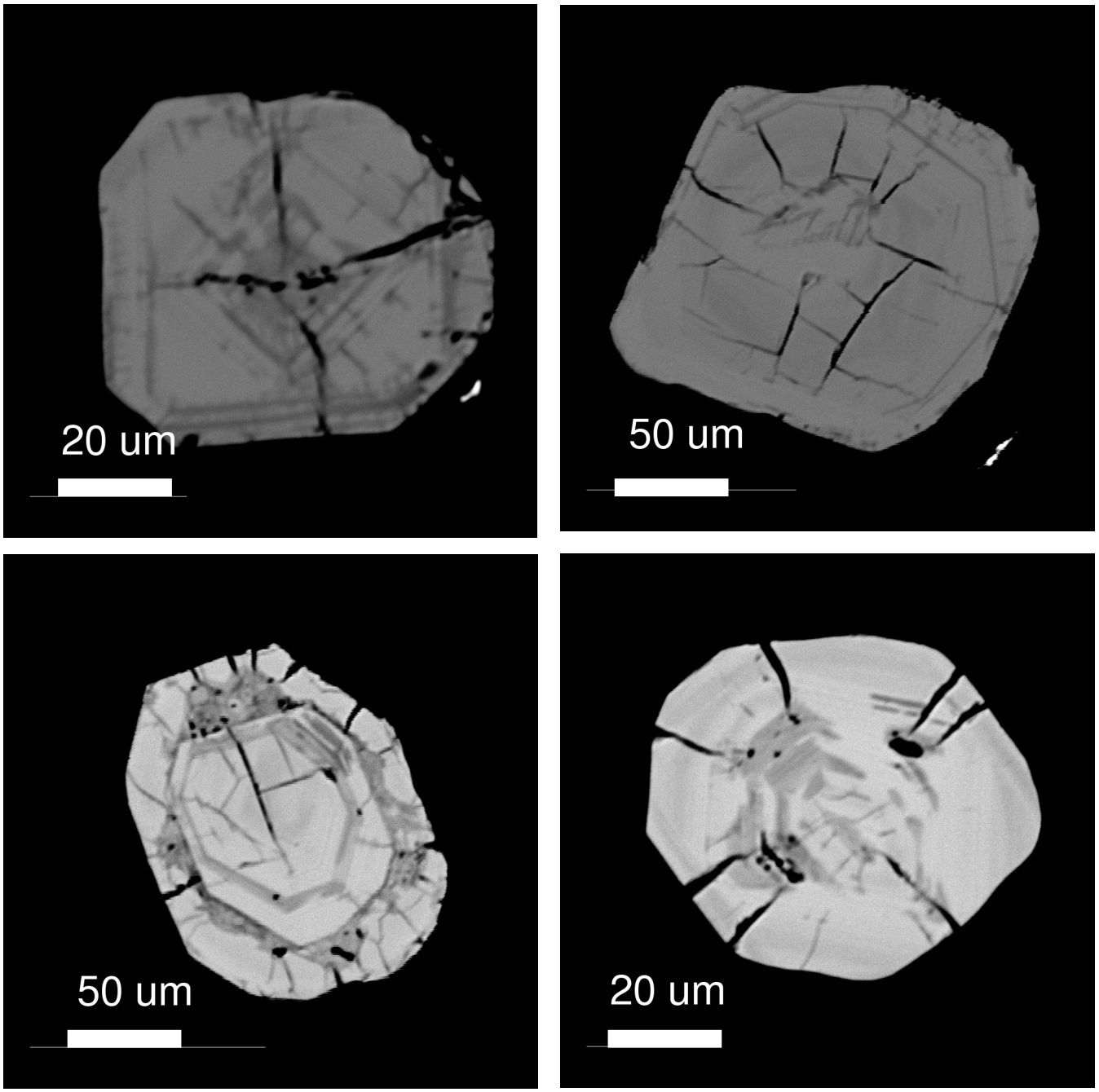

Backscatter electron images of example zircon grains from sample JR13-802 in thin section.

Granite-granodiorite map unit:
~3.37 Ga sample

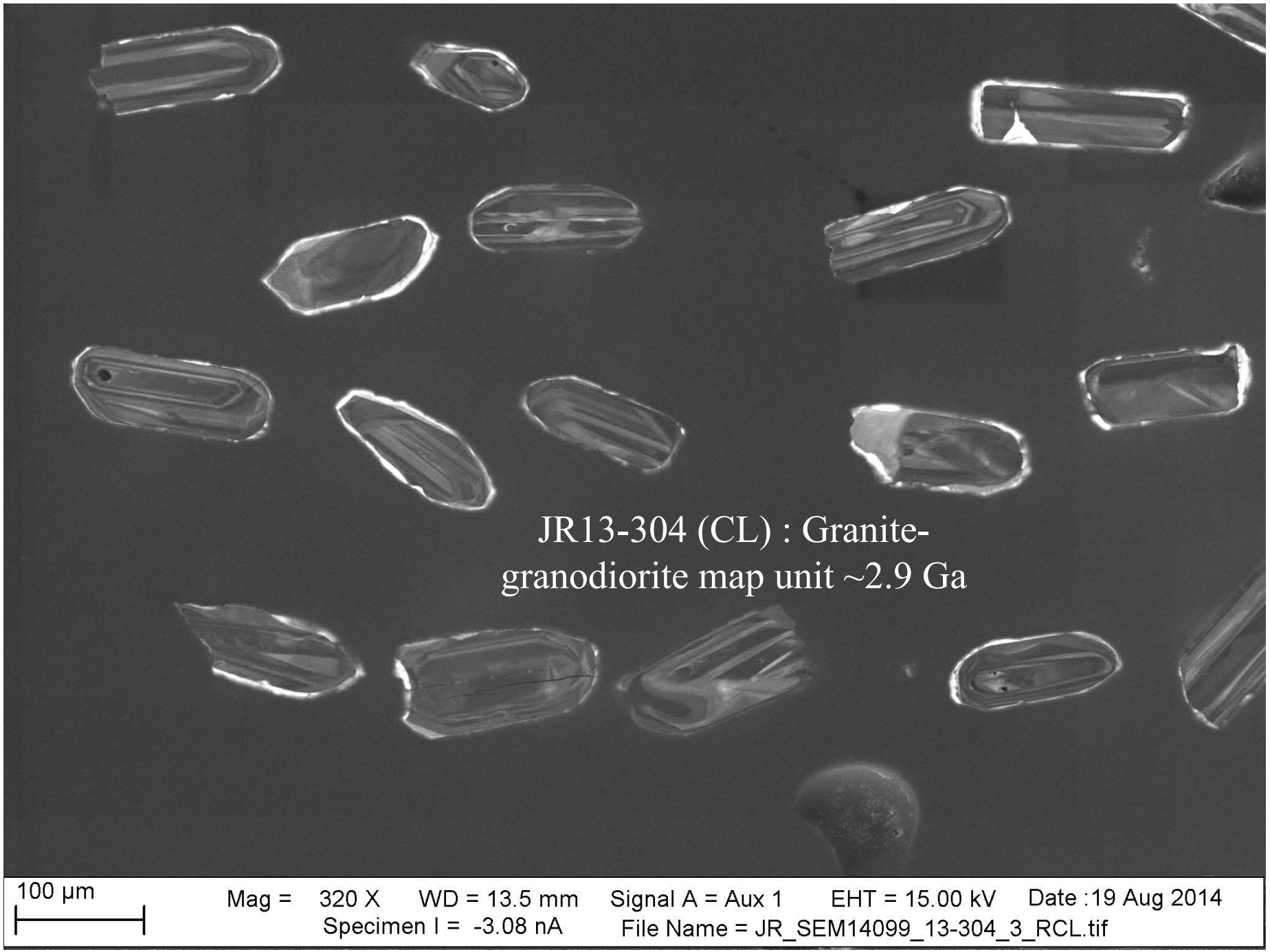
JR13-304 (CL) : Granite-
granodiorite map unit ~2.9 Ga
100 µm
Mag = 320 X WD = 13.5 mm Signal A = Aux 1 EHT = 15.00 kV Date :19 Aug 2014
Specimen I = -3.08 nA
File Name = JR_SEM14099_13-304_3_RCL.tif

Appendix 6: Secondary reference materials analyzed during LA-ICPMS analyses reported here

Date	Method	Analysis name	206Pb (cps)	204Pb (cps)	206Pb/204Pb	207Pb/206Pb	2σ	207Pb/235U	2σ	206Pb/238U	2σ
24-May-12	Mount	OG1-1	75536	56	1357	0.29640	0.00305	28.47090	1.86823	0.69667	0.04515
24-May-12	Mount	OG1-10	155108	65	2400	0.29385	0.00306	27.39820	1.41044	0.67622	0.03409
24-May-12	Mount	OG1-2	67110	40	1677	0.29797	0.00310	27.83781	1.41211	0.67759	0.03364
24-May-12	Mount	OG1-3	58497	19	3108	0.29392	0.00309	27.54545	1.14563	0.67971	0.02735
24-May-12	Mount	OG1-4	151125	28	5466	0.29382	0.00309	25.43302	0.84922	0.62780	0.01990
24-May-12	Mount	OG1-5	97563	27	3608	0.29311	0.00302	27.06693	1.21543	0.66974	0.02927
24-May-12	Mount	OG1-6	105351	36	2900	0.29686	0.00306	26.56789	1.14238	0.64909	0.02709
24-May-12	Mount	OG1-7	101954	40	2576	0.29435	0.00300	25.69340	1.40711	0.63307	0.03407
24-May-12	Mount	OG1-8	153957	67	2290	0.29196	0.00296	26.44811	1.12910	0.65700	0.02724
24-May-12	Mount	OG1-9	166872	21	7777	0.29254	0.00301	27.18924	1.33236	0.67407	0.03229
25-May-12	Mount	OG1-1	84499	29	2913	0.29743	0.00476	27.25462	1.02514	0.66460	0.02263
25-May-12	Mount	OG1-2	88229	44	1990	0.29621	0.00473	27.76768	1.27667	0.67990	0.02931
25-May-12	Mount	OG1-3	89836	49	1835	0.29794	0.00622	29.95609	2.01713	0.72922	0.04668
25-May-12	Mount	OG1-4	91523	88	1040	0.29554	0.00617	29.98715	1.92534	0.73590	0.04468
25-May-12	Mount	OG1-5	81984	30	2714	0.30500	0.00394	32.82457	2.49769	0.78055	0.05853
25-May-12	Mount	OG1-6	55805	96	581	0.30249	0.00396	31.03108	2.23280	0.74402	0.05264
25-May-12	Mount	OG1-7	113004	34	3351	0.30269	0.00391	29.80473	1.86130	0.71413	0.04363
15-Oct-12	Thin Section	OG1-1	307065	10	31593	0.29936	0.00398	29.52524	2.01989	0.71533	0.04800
15-Oct-12	Thin Section	OG1-10	334288	2	153684	0.29676	0.00400	28.40126	1.59189	0.69411	0.03776
15-Oct-12	Thin Section	OG1-11	525645	105	4985	0.29759	0.00408	29.31480	1.62371	0.71443	0.03834
15-Oct-12	Thin Section	OG1-12	253438	133	1906	0.29939	0.00404	29.34816	1.14514	0.71095	0.02603
15-Oct-12	Thin Section	OG1-13	366786	26	14161	0.29952	0.00406	28.39010	1.07021	0.68744	0.02418
15-Oct-12	Thin Section	OG1-14	216937	70	3107	0.29845	0.00403	29.22910	1.16633	0.71029	0.02667
15-Oct-12	Thin Section	OG1-17	294250	1	199650	0.29853	0.00401	28.18898	1.09875	0.68483	0.02506
15-Oct-12	Thin Section	OG1-2	325107	53	6092	0.30260	0.00403	29.93603	2.10990	0.71750	0.04966
15-Oct-12	Thin Section	OG1-3	500667	12	41092	0.29873	0.00398	30.25947	1.85708	0.73465	0.04401
15-Oct-12	Thin Section	OG1-4	491001	48	10322	0.29791	0.00396	29.34752	1.89958	0.71447	0.04526
15-Oct-12	Thin Section	OG1-5	566828	165	3434	0.28761	0.00390	22.67176	1.49279	0.57172	0.03684
15-Oct-12	Thin Section	OG1-6	350086	153	2295	0.29755	0.00398	30.10537	1.86643	0.73382	0.04442

Date	Method	Analysis name	206Pb (cps)	204Pb (cps)	206Pb/204Pb	207Pb/206Pb	2σ	207Pb/235U	2σ	206Pb/238U	2σ
15-Oct-12	Thin Section	OG1-7	470965	3169	149	0.29857	0.00401	29.25396	1.40540	0.71063	0.03278
15-Oct-12	Thin Section	OG1-8	265029	3173	84	0.29872	0.00401	28.90448	1.52156	0.70177	0.03572
15-Oct-12	Thin Section	OG1-9	413947	7	59108	0.29821	0.00400	29.76321	1.45060	0.72387	0.03391
16-Oct-12	Thin Section	OG1-1	224770	22	10034	0.29492	0.00354	29.21867	1.34457	0.71855	0.03192
16-Oct-12	Thin Section	OG1-10	227368	104	2194	0.29852	0.00442	27.66706	1.40119	0.67218	0.03256
16-Oct-12	Thin Section	OG1-11	1107912	188	5903	0.30294	0.00447	29.22534	1.49050	0.69969	0.03416
16-Oct-12	Thin Section	OG1-12	951801	76	12456	0.30141	0.00446	30.61279	1.58953	0.73663	0.03666
16-Oct-12	Thin Section	OG1-13	1009499	89	11382	0.30134	0.00445	29.20715	1.61002	0.70297	0.03734
16-Oct-12	Thin Section	OG1-2	160602	33	4797	0.29614	0.00359	26.79167	1.21622	0.65616	0.02871
16-Oct-12	Thin Section	OG1-3	308495	124	2491	0.29353	0.00351	26.07290	1.14135	0.64422	0.02713
16-Oct-12	Thin Section	OG1-4	254899	47	5423	0.29781	0.00443	29.64835	1.39996	0.72204	0.03236
16-Oct-12	Thin Section	OG1-5	1074553	38	27973	0.30157	0.00446	30.68937	1.76482	0.73808	0.04101
16-Oct-12	Thin Section	OG1-6	1195178	32	36789	0.30178	0.00448	30.07158	1.50157	0.72272	0.03446
16-Oct-12	Thin Section	OG1-7	1226060	170	7213	0.30081	0.00444	30.26646	1.44286	0.72975	0.03308
16-Oct-12	Thin Section	OG1-8	964873	150	6437	0.30048	0.00444	29.47762	1.70324	0.71149	0.03975
16-Oct-12	Thin Section	OG1-9	206193	55	3729	0.29957	0.00446	27.83993	1.30540	0.67400	0.02997
17-Oct-12	Thin Section	OG1-1	432436	81	5356	0.29775	0.00264	27.25379	1.32256	0.66385	0.03167
17-Oct-12	Thin Section	OG1-2	554291	155	3572	0.29818	0.00263	27.93921	1.28162	0.67958	0.03059
17-Oct-12	Thin Section	OG1-3	443547	110	4029	0.29682	0.00261	29.13993	1.36893	0.71202	0.03286
17-Oct-12	Thin Section	OG1-4	375069	134	2790	0.29723	0.00261	29.18114	1.45788	0.71204	0.03502
12-Nov-13	Thin Section	OG1-1	677286	35	19434	0.29718	0.00247	28.92355	1.09566	0.70587	0.02609
12-Nov-13	Thin Section	OG1-10	354037	138	2560	0.29769	0.00301	29.86170	1.46859	0.72752	0.03502
12-Nov-13	Thin Section	OG1-11	415067	38	10885	0.29727	0.00304	29.09082	1.41978	0.70975	0.03387
12-Nov-13	Thin Section	OG1-12	304573	30	10071	0.29671	0.00303	29.48596	1.60650	0.72074	0.03857
12-Nov-13	Thin Section	OG1-13	290772	59	4926	0.29668	0.00303	29.03113	1.37522	0.70970	0.03283
12-Nov-13	Thin Section	OG1-14	279896	45	6156	0.29846	0.00305	29.72120	1.42804	0.72223	0.03391
12-Nov-13	Thin Section	OG1-15	411361	73	5645	0.29858	0.00303	29.58252	1.35165	0.71857	0.03201
12-Nov-13	Thin Section	OG1-18	332074	73	4539	0.29800	0.00302	29.70395	1.29714	0.72293	0.03071
12-Nov-13	Thin Section	OG1-19	417508	86	4846	0.29777	0.00305	30.24249	1.51517	0.73660	0.03612

Date	Method	Analysis name	206Pb (cps)	204Pb (cps)	206Pb/204Pb	207Pb/206Pb	2σ	207Pb/235U	2σ	206Pb/238U	2σ
12-Nov-13	Thin Section	OG1-2	388689	30	12834	0.29751	0.00246	29.34392	1.29247	0.71533	0.03095
12-Nov-13	Thin Section	OG1-3	367999	1	367999	0.29777	0.00250	29.18460	0.97624	0.71084	0.02302
12-Nov-13	Thin Section	OG1-4	291829	1	291829	0.29779	0.00248	29.35974	1.05879	0.71507	0.02509
12-Nov-13	Thin Section	OG1-5	423694	59	7182	0.29536	0.00299	29.85239	1.32888	0.73305	0.03178
12-Nov-13	Thin Section	OG1-6	380136	53	7165	0.29520	0.00299	29.64988	2.06698	0.72845	0.05024
12-Nov-13	Thin Section	OG1-7	453856	79	5773	0.29753	0.00312	29.45424	1.49639	0.71798	0.03569
12-Nov-13	Thin Section	OG1-8	407098	92	4434	0.29583	0.00301	29.53534	1.28924	0.72409	0.03074
12-Nov-13	Thin Section	OG1-9	550139	127	4328	0.29524	0.00302	34.30449	2.47954	0.84272	0.06030
20-May-14	Mount	OG1-1	223137	15	15113	0.29873	0.00316	31.50150	1.40283	0.76482	0.03308
20-May-14	Mount	OG1-10	198057	1	177853	0.29801	0.00315	28.45951	1.32641	0.69261	0.03144
20-May-14	Mount	OG1-10	403189	1	403189	0.29651	0.00310	29.77700	1.26057	0.72836	0.02988
20-May-14	Mount	OG1-11	439074	44	9922	0.29631	0.00311	28.95504	1.16682	0.70871	0.02758
20-May-14	Mount	OG1-12	778073	41	18795	0.29562	0.00311	29.24320	1.26140	0.71746	0.03001
20-May-14	Mount	OG1-13	581978	27	21612	0.29732	0.00316	29.15205	1.16707	0.71112	0.02745
20-May-14	Mount	OG1-14	412005	5	88429	0.29871	0.00316	28.59470	1.20745	0.69429	0.02839
20-May-14	Mount	OG1-15	1151287	6	185442	0.29696	0.00313	29.52302	1.15588	0.72104	0.02719
20-May-14	Mount	OG1-15A	990549	8	117190	0.29663	0.00311	29.01224	1.15465	0.70936	0.02723
20-May-14	Mount	OG1-18	640732	4	153238	0.29774	0.00314	29.00119	1.20212	0.70643	0.02832
20-May-14	Mount	OG1-19	698791	1	726283	0.29756	0.00313	29.41798	1.22733	0.71702	0.02895
20-May-14	Mount	OG1-2	189736	5	35548	0.29810	0.00318	29.98579	1.61379	0.72955	0.03848
20-May-14	Mount	OG1-3	178037	36	4933	0.29835	0.00314	33.13657	1.79128	0.80552	0.04271
20-May-14	Mount	OG1-4	173368	14	12386	0.29773	0.00318	29.39783	2.04291	0.71614	0.04917
20-May-14	Mount	OG1-5	207670	109	1911	0.30158	0.00323	27.84151	1.33348	0.66957	0.03126
20-May-14	Mount	OG1-6	234589	14	17260	0.29847	0.00316	28.78878	1.44436	0.69955	0.03431
20-May-14	Mount	OG1-7	501747	1	501747	0.29988	0.00321	29.11349	1.30840	0.70412	0.03073
20-May-14	Mount	OG1-8	17179145	1	23098741	0.29946	0.00318	28.68489	1.43531	0.69472	0.03397
20-May-14	Mount	OG1-9	440848	1	440848	0.29703	0.00314	28.26169	1.45719	0.69008	0.03482
21-May-14	Mount	OG1-1	492962	338	1456	0.29890	0.00443	29.49300	1.30401	0.71564	0.02981
21-May-14	Mount	OG1-10	557170	92	6072	0.29783	0.00237	29.27947	0.81410	0.71300	0.01899

Date	Method	Analysis name	206Pb (cps)	204Pb (cps)	206Pb/204Pb	207Pb/206Pb	2σ	207Pb/235U	2σ	206Pb/238U	2σ
21-May-14	Mount	OG1-11	913683	122	7514	0.29718	0.00234	29.45758	0.92510	0.71891	0.02185
21-May-14	Mount	OG1-12	666385	112	5952	0.29800	0.00238	29.39988	1.05307	0.71554	0.02499
21-May-14	Mount	OG1-13	185636	65	2870	0.29773	0.00311	29.66271	1.27253	0.72258	0.03007
21-May-14	Mount	OG1-14	203898	71	2874	0.29903	0.00318	29.32658	1.18171	0.71128	0.02765
21-May-14	Mount	OG1-15	291816	78	3755	0.29683	0.00312	29.97538	1.22044	0.73242	0.02881
21-May-14	Mount	OG1-17	234522	67	3504	0.29781	0.00315	28.98898	1.15206	0.70598	0.02704
21-May-14	Mount	OG1-18	233342	54	4349	0.29660	0.00312	29.16997	1.12814	0.71330	0.02655
21-May-14	Mount	OG1-2	525304	340	1546	0.29823	0.00443	29.55606	1.32522	0.71878	0.03041
21-May-14	Mount	OG1-3	673824	351	1922	0.29930	0.00450	28.88696	1.42696	0.70000	0.03293
21-May-14	Mount	OG1-4	258461	278	931	0.29867	0.00443	28.89936	1.44359	0.70176	0.03347
21-May-14	Mount	OG1-5	568797	270	2107	0.29818	0.00445	29.19098	1.53374	0.71001	0.03577
21-May-14	Mount	OG1-6	380996	244	1560	0.29745	0.00441	29.67362	1.30744	0.72353	0.03002
21-May-14	Mount	OG1-7	655927	195	3368	0.29816	0.00444	28.96672	1.25422	0.70460	0.02865
21-May-14	Mount	OG1-8	546619	153	3570	0.29771	0.00442	28.62704	1.28614	0.69740	0.02957
21-May-14	Mount	OG1-9	170317	107	1592	0.29949	0.00444	28.91931	1.32800	0.70032	0.03044
22-May-14	Mount	OG1-1	282137	77	3664	0.29838	0.00506	30.39823	2.04015	0.73889	0.04798
22-May-14	Mount	OG1-2	251765	55	4597	0.29827	0.00506	30.25511	1.85396	0.73568	0.04332
22-May-14	Mount	OG1-3	246275	57	4295	0.29731	0.00501	29.36335	1.72866	0.71630	0.04040
22-May-14	Mount	OG1-4	331602	66	5004	0.29815	0.00507	29.21237	1.77871	0.71062	0.04155
22-May-14	Mount	OG1-6	151077	98	1535	0.29460	0.00509	29.23341	1.75046	0.71970	0.04126
22-May-14	Mount	OG1-7	174772	118	1477	0.29841	0.00504	29.42420	1.81483	0.71513	0.04242
22-May-14	Mount	OG1-8	220193	90	2449	0.29683	0.00502	28.39873	1.65360	0.69389	0.03866
23-May-14	Thin Section	OG1-1	221511	174	1277	0.29547	0.00723	29.64865	1.32798	0.72776	0.02731
23-May-14	Thin Section	OG1-10	319248	40	7943	0.29637	0.00511	26.85504	1.78306	0.65719	0.04214
23-May-14	Thin Section	OG1-11	341099	61	5612	0.29490	0.00511	28.38819	1.81331	0.69817	0.04292
23-May-14	Thin Section	OG1-12	301639	74	4093	0.29534	0.00511	32.55035	2.92884	0.79933	0.07058
23-May-14	Thin Section	OG1-13	266302	33	8007	0.29551	0.00511	29.81675	2.02985	0.73180	0.04818
23-May-14	Thin Section	OG1-14	152512	19	7845	0.29766	0.00513	28.86539	1.91148	0.70333	0.04497
23-May-14	Thin Section	OG1-15	174383	48	3655	0.29355	0.00505	28.32084	1.90316	0.69972	0.04546

Date	Method	Analysis name	206Pb (cps)	204Pb (cps)	206Pb/204Pb	207Pb/206Pb	2σ	207Pb/235U	2σ	206Pb/238U	2σ
23-May-14	Thin Section	OG1-16	224006	18	12599	0.29702	0.00510	27.58646	1.83157	0.67361	0.04320
23-May-14	Thin Section	OG1-17	232835	4	56501	0.29559	0.00509	27.30946	1.77872	0.67008	0.04209
23-May-14	Thin Section	OG1-18	97757	41	2407	0.29806	0.00518	27.14585	1.86097	0.66054	0.04380
23-May-14	Thin Section	OG1-19	101217	62	1627	0.30228	0.00526	26.91563	1.90728	0.64579	0.04436
23-May-14	Thin Section	OG1-2	225350	183	1228	0.29545	0.00723	29.51502	1.40845	0.72452	0.02968
23-May-14	Thin Section	OG1-21	70873	62	1147	0.29860	0.00521	31.78032	2.18035	0.77192	0.05122
23-May-14	Thin Section	OG1-3	240915	172	1403	0.29451	0.00721	29.20325	1.53108	0.71917	0.03334
23-May-14	Thin Section	OG1-4	330507	175	1891	0.29462	0.00720	28.29180	1.33504	0.69646	0.02811
23-May-14	Thin Section	OG1-5	227678	176	1291	0.29313	0.00717	28.13825	1.35005	0.69621	0.02874
23-May-14	Thin Section	OG1-6	180318	205	880	0.29211	0.00714	28.45944	1.41317	0.70660	0.03054
23-May-14	Thin Section	OG1-8	244010	257	951	0.29690	0.00733	25.32537	1.24605	0.61865	0.02633
23-May-14	Thin Section	OG1-9	113596	56	2022	0.29748	0.00517	28.62111	1.99586	0.69780	0.04712
15-Oct-14	MOUNT	OG1-1	369930	50	7341	0.29762	0.00149	30.40001	1.09245	0.74081	0.02636
15-Oct-14	MOUNT	OG1-1	231383	4	63390	0.29856	0.00438	29.84107	1.50406	0.72490	0.03495
15-Oct-14	MOUNT	OG1-10	47744	57	837	0.29598	0.00453	30.38655	2.17301	0.74460	0.05202
15-Oct-14	MOUNT	OG1-10	261050	99	2641	0.29987	0.00439	30.95978	1.51906	0.74880	0.03507
15-Oct-14	MOUNT	OG1-11	360787	86	4214	0.29814	0.00436	29.12917	1.40497	0.70861	0.03257
15-Oct-14	MOUNT	OG1-12	308460	78	3934	0.29797	0.00436	28.63979	1.38290	0.69710	0.03208
15-Oct-14	MOUNT	OG1-13	369662	55	6698	0.29782	0.00436	28.83171	1.60338	0.70212	0.03767
15-Oct-14	MOUNT	OG1-14	342899	50	6854	0.29837	0.00436	28.98489	1.38613	0.70456	0.03209
15-Oct-14	MOUNT	OG1-15	381520	14	26677	0.29701	0.00436	29.40981	1.33001	0.71817	0.03072
15-Oct-14	MOUNT	OG1-16	507571	42	12041	0.27971	0.00511	23.47928	1.22621	0.60879	0.02979
15-Oct-14	MOUNT	OG1-2	313539	24	13063	0.29765	0.00146	29.86747	1.27520	0.72777	0.03087
15-Oct-14	MOUNT	OG1-2	338554	14	24420	0.29825	0.00434	29.53370	1.54142	0.71819	0.03600
15-Oct-14	MOUNT	OG1-3	316694	33	9743	0.29776	0.00139	30.17594	1.16747	0.73502	0.02823
15-Oct-14	MOUNT	OG1-3	356068	1	301534	0.29681	0.00433	30.38762	1.45462	0.74253	0.03385
15-Oct-14	MOUNT	OG1-4	96021	21	4579	0.29956	0.00458	29.87467	1.75335	0.72329	0.04098
15-Oct-14	MOUNT	OG1-4	310947	2	177094	0.29932	0.00440	30.32667	1.48038	0.73483	0.03421
15-Oct-14	MOUNT	OG1-5	250717	42	5940	0.29304	0.00440	26.73562	1.47546	0.66169	0.03514

Date	Method	Analysis name	206Pb (cps)	204Pb (cps)	206Pb/204Pb	207Pb/206Pb	2σ	207Pb/235U	2σ	206Pb/238U	2σ
15-Oct-14	MOUNT	OG1-5	275117	1	275117	0.29675	0.00435	29.19648	1.43706	0.71358	0.03353
15-Oct-14	MOUNT	OG1-6	76010	18	4343	0.29961	0.00473	29.99892	1.58823	0.72619	0.03670
15-Oct-14	MOUNT	OG1-6	416974	1	450249	0.29757	0.00435	29.98357	1.43500	0.73080	0.03330
15-Oct-14	MOUNT	OG1-7	79284	14	5736	0.29676	0.00467	29.24201	1.53488	0.71467	0.03579
15-Oct-14	MOUNT	OG1-7	316861	1	316861	0.29749	0.00434	29.27429	1.60653	0.71370	0.03776
15-Oct-14	MOUNT	OG1-8	79000	15	5382	0.29630	0.00438	29.85604	1.78098	0.73080	0.04224
15-Oct-14	MOUNT	OG1-8	523916	1	884626	0.29593	0.00433	29.67958	1.51444	0.72738	0.03555
15-Oct-14	MOUNT	OG1-9	70858	22	3272	0.29627	0.00449	29.75504	1.59623	0.72841	0.03749
15-Oct-14	MOUNT	OG1-9	319496	17	18921	0.29771	0.00436	29.38235	1.43535	0.71581	0.03336
16-Oct-14	MOUNT	OG1-1	69879	36	1968	0.29837	0.00256	30.79707	1.97868	0.74860	0.04767
16-Oct-14	MOUNT	OG1-1	641230	41	15828	0.29728	0.00265	29.34964	1.39172	0.71605	0.03335
16-Oct-14	MOUNT	OG1-2	116930	47	2495	0.29933	0.00241	30.00742	2.22283	0.72707	0.05354
16-Oct-14	MOUNT	OG1-2	357576	54	6638	0.29751	0.00264	28.89263	1.41997	0.70434	0.03405
16-Oct-14	MOUNT	OG1-3	77454	43	1814	0.29784	0.00236	30.24665	1.94713	0.73654	0.04705
16-Oct-14	MOUNT	OG1-3	286471	79	3622	0.29883	0.00265	30.17094	1.62661	0.73227	0.03894
16-Oct-14	MOUNT	OG1-4	62654	14	4325	0.29532	0.00250	30.34287	1.85498	0.74518	0.04512
16-Oct-14	MOUNT	OG1-4	789856	168	4710	0.29739	0.00263	29.45559	1.40982	0.71835	0.03379
16-Oct-14	MOUNT	OG1-5	728163	164	4430	0.29812	0.00264	29.48153	1.58187	0.71722	0.03796

300

Date	r	207Pb/206Pb age (Ma)	2σ error (Ma)	207Pb/235U age (Ma)	2σ error (Ma)	206Pb/238U age (Ma)	2σ error (Ma)	discordance
24-May-12	0.988	3451	16	3435	62	3408	169	1.6
24-May-12	0.979	3438	16	3398	49	3330	130	4.0
24-May-12	0.979	3460	16	3413	49	3335	128	4.6
24-May-12	0.967	3438	16	3403	40	3343	104	3.5
24-May-12	0.949	3438	16	3325	32	3141	78	10.9
24-May-12	0.973	3434	16	3386	43	3305	112	4.8
24-May-12	0.971	3454	16	3368	41	3225	105	8.4
24-May-12	0.983	3441	16	3335	52	3162	133	10.2
24-May-12	0.971	3428	16	3363	41	3255	105	6.4
24-May-12	0.978	3431	16	3390	47	3322	123	4.1
25-May-12	0.905	3457	25	3393	36	3285	87	6.3
25-May-12	0.938	3451	25	3411	44	3344	112	4.0
25-May-12	0.951	3460	32	3485	64	3531	172	-2.7
25-May-12	0.946	3447	32	3486	61	3555	164	-4.1
25-May-12	0.985	3496	20	3575	72	3719	208	-8.4
25-May-12	0.983	3483	20	3520	68	3585	192	-3.8
25-May-12	0.978	3484	20	3480	60	3474	162	0.4
15-Oct-12	0.981	3467	20	3471	65	3479	178	-0.4
15-Oct-12	0.971	3453	21	3433	54	3398	142	2.1
15-Oct-12	0.969	3458	21	3464	53	3475	143	-0.7
15-Oct-12	0.938	3467	21	3465	38	3462	97	0.2
15-Oct-12	0.933	3468	21	3433	36	3373	92	3.5
15-Oct-12	0.941	3462	21	3461	38	3460	100	0.1
15-Oct-12	0.939	3463	21	3426	38	3363	95	3.7
15-Oct-12	0.982	3484	20	3485	67	3487	184	-0.1
15-Oct-12	0.976	3464	21	3495	59	3551	162	-3.3
15-Oct-12	0.979	3459	20	3465	62	3475	168	-0.6
15-Oct-12	0.979	3405	21	3213	62	2915	149	17.8
15-Oct-12	0.976	3457	21	3490	59	3548	163	-3.4

Date	r	207Pb/206Pb age (Ma)	2σ error (Ma)	207Pb/235U age (Ma)	2σ error (Ma)	206Pb/238U age (Ma)	2σ error (Ma)	discordance
15-Oct-12	0.960	3463	21	3462	46	3461	122	0.1
15-Oct-12	0.967	3464	21	3450	50	3427	134	1.3
15-Oct-12	0.961	3461	21	3479	47	3511	126	-1.9
16-Oct-12	0.965	3444	19	3461	44	3491	119	-1.8
16-Oct-12	0.956	3463	23	3407	48	3314	124	5.5
16-Oct-12	0.957	3485	23	3461	49	3419	128	2.4
16-Oct-12	0.958	3477	23	3507	50	3558	135	-3.0
16-Oct-12	0.963	3477	23	3461	53	3432	140	1.7
16-Oct-12	0.964	3450	19	3376	43	3252	111	7.3
16-Oct-12	0.962	3436	18	3349	42	3206	105	8.5
16-Oct-12	0.949	3459	23	3475	45	3504	120	-1.7
16-Oct-12	0.966	3478	23	3509	55	3563	150	-3.2
16-Oct-12	0.955	3479	23	3489	48	3506	128	-1.0
16-Oct-12	0.951	3474	23	3496	46	3532	122	-2.2
16-Oct-12	0.967	3473	23	3470	55	3464	148	0.3
16-Oct-12	0.948	3468	23	3413	45	3321	114	5.4
17-Oct-12	0.983	3459	14	3393	46	3282	122	6.5
17-Oct-12	0.981	3461	14	3417	44	3343	116	4.4
17-Oct-12	0.982	3454	14	3458	45	3466	123	-0.5
17-Oct-12	0.984	3456	14	3460	48	3466	131	-0.4
12-Nov-13	0.976	3456	13	3451	37	3443	98	0.5
12-Nov-13	0.979	3458	16	3482	47	3524	129	-2.5
12-Nov-13	0.978	3456	16	3457	47	3458	126	-0.1
12-Nov-13	0.982	3453	16	3470	52	3499	143	-1.7
12-Nov-13	0.977	3453	16	3455	45	3457	123	-0.2
12-Nov-13	0.977	3462	16	3478	46	3504	126	-1.6
12-Nov-13	0.975	3463	16	3473	44	3491	119	-1.0
12-Nov-13	0.973	3460	16	3477	42	3507	114	-1.8
12-Nov-13	0.979	3459	16	3495	48	3558	133	-3.7

Date	r	207Pb/206Pb age (Ma)	2σ error (Ma)	207Pb/235U age (Ma)	2σ error (Ma)	206Pb/238U age (Ma)	2σ error (Ma)	discordance
12-Nov-13	0.982	3457	13	3465	42	3479	115	-0.8
12-Nov-13	0.968	3459	13	3460	32	3462	86	-0.1
12-Nov-13	0.973	3459	13	3466	35	3478	94	-0.7
12-Nov-13	0.974	3446	16	3482	43	3545	117	-3.7
12-Nov-13	0.989	3445	16	3475	66	3528	185	-3.1
12-Nov-13	0.978	3457	16	3469	49	3488	133	-1.2
12-Nov-13	0.972	3449	16	3471	42	3511	114	-2.4
12-Nov-13	0.990	3445	16	3619	69	3940	208	-19.3
20-May-14	0.971	3464	16	3535	43	3662	120	-7.5
20-May-14	0.974	3460	16	3435	45	3393	119	2.5
20-May-14	0.969	3452	16	3479	41	3527	110	-2.8
20-May-14	0.966	3451	16	3452	39	3454	103	-0.1
20-May-14	0.970	3447	16	3462	41	3487	112	-1.5
20-May-14	0.964	3456	16	3459	39	3463	103	-0.2
20-May-14	0.968	3464	16	3440	41	3399	107	2.4
20-May-14	0.963	3454	16	3471	38	3500	101	-1.7
20-May-14	0.965	3453	16	3454	38	3456	102	-0.1
20-May-14	0.967	3459	16	3454	40	3445	106	0.5
20-May-14	0.968	3458	16	3468	40	3485	108	-1.0
20-May-14	0.980	3460	16	3486	52	3532	142	-2.7
20-May-14	0.981	3462	16	3585	52	3809	151	-13.3
20-May-14	0.988	3458	16	3467	66	3482	182	-0.9
20-May-14	0.975	3478	16	3414	46	3304	120	6.4
20-May-14	0.977	3462	16	3446	48	3419	129	1.6
20-May-14	0.971	3470	16	3457	43	3436	115	1.2
20-May-14	0.977	3467	16	3443	48	3401	128	2.5
20-May-14	0.979	3455	16	3428	49	3383	131	2.7
21-May-14	0.942	3465	23	3470	43	3480	111	-0.6
21-May-14	0.958	3459	12	3463	27	3470	71	-0.4

Date	r	207Pb/206Pb age (Ma)	2σ error (Ma)	207Pb/235U age (Ma)	2σ error (Ma)	206Pb/238U age (Ma)	2σ error (Ma)	discordance
21-May-14	0.968	3456	12	3469	30	3492	81	-1.4
21-May-14	0.975	3460	12	3467	35	3479	93	-0.7
21-May-14	0.970	3458	16	3476	41	3506	112	-1.8
21-May-14	0.965	3465	16	3465	39	3463	103	0.1
21-May-14	0.966	3454	16	3486	39	3542	106	-3.3
21-May-14	0.964	3459	16	3453	38	3443	101	0.6
21-May-14	0.962	3453	16	3459	37	3471	99	-0.7
21-May-14	0.944	3461	23	3472	43	3491	113	-1.1
21-May-14	0.952	3467	23	3450	47	3421	124	1.7
21-May-14	0.955	3463	23	3450	48	3427	126	1.3
21-May-14	0.959	3461	23	3460	50	3458	133	0.1
21-May-14	0.942	3457	23	3476	42	3509	111	-2.0
21-May-14	0.939	3461	23	3452	42	3438	107	0.8
21-May-14	0.944	3458	23	3441	43	3411	111	1.8
21-May-14	0.946	3468	23	3451	44	3422	114	1.7
22-May-14	0.968	3462	26	3500	64	3566	175	-3.9
22-May-14	0.961	3461	26	3495	59	3555	159	-3.5
22-May-14	0.958	3456	26	3466	56	3482	150	-1.0
22-May-14	0.960	3461	26	3461	58	3461	155	0.0
22-May-14	0.957	3442	27	3461	57	3495	153	-2.0
22-May-14	0.962	3462	26	3468	59	3478	157	-0.6
22-May-14	0.957	3454	26	3433	56	3397	145	2.1
23-May-14	0.838	3447	37	3475	43	3525	101	-3.0
23-May-14	0.966	3451	26	3378	63	3256	162	7.2
23-May-14	0.962	3444	27	3433	61	3414	161	1.1
23-May-14	0.981	3446	27	3567	85	3787	248	-13.1
23-May-14	0.967	3447	27	3481	65	3540	177	-3.5
23-May-14	0.966	3458	26	3449	63	3433	168	0.9
23-May-14	0.967	3437	26	3430	64	3420	170	0.6

Date	r	207Pb/206Pb age (Ma)	2σ error (Ma)	207Pb/235U age (Ma)	2σ error (Ma)	206Pb/238U age (Ma)	2σ error (Ma)	discordance
23-May-14	0.966	3455	26	3405	63	3320	164	5.0
23-May-14	0.964	3447	26	3395	62	3306	160	5.2
23-May-14	0.967	3460	27	3389	65	3269	168	7.0
23-May-14	0.969	3482	27	3380	67	3212	171	9.8
23-May-14	0.859	3447	37	3471	46	3513	110	-2.5
23-May-14	0.967	3463	27	3544	65	3688	184	-8.5
23-May-14	0.884	3442	38	3460	50	3493	124	-1.9
23-May-14	0.855	3442	37	3429	45	3407	106	1.3
23-May-14	0.860	3434	37	3424	46	3406	108	1.1
23-May-14	0.870	3429	37	3435	48	3446	114	-0.6
23-May-14	0.865	3454	38	3321	47	3105	104	12.7
23-May-14	0.968	3457	27	3441	66	3412	176	1.7
15-Oct-14	0.990	3458	8	3500	35	3574	97	-4.4
15-Oct-14	0.957	3463	23	3482	48	3514	129	-1.9
15-Oct-14	0.977	3449	24	3499	68	3588	189	-5.2
15-Oct-14	0.954	3470	22	3518	47	3603	128	-5.0
15-Oct-14	0.953	3461	22	3458	46	3453	122	0.3
15-Oct-14	0.953	3460	22	3441	46	3410	121	1.9
15-Oct-14	0.965	3459	22	3448	53	3429	141	1.1
15-Oct-14	0.952	3462	22	3453	46	3438	120	0.9
15-Oct-14	0.946	3455	23	3467	43	3489	114	-1.3
15-Oct-14	0.937	3361	28	3247	50	3065	118	11.1
15-Oct-14	0.993	3458	8	3482	41	3525	114	-2.5
15-Oct-14	0.960	3461	22	3471	50	3489	134	-1.1
15-Oct-14	0.993	3459	7	3493	37	3552	104	-3.5
15-Oct-14	0.952	3454	22	3499	46	3580	124	-4.8
15-Oct-14	0.965	3468	23	3483	56	3508	152	-1.5
15-Oct-14	0.954	3467	23	3497	47	3551	126	-3.2
15-Oct-14	0.962	3434	23	3374	53	3274	135	5.9

Date	r	207Pb/206Pb age (Ma)	2σ error (Ma)	207Pb/235U age (Ma)	2σ error (Ma)	206Pb/238U age (Ma)	2σ error (Ma)	discordance
15-Oct-14	0.955	3453	23	3460	47	3472	125	-0.7
15-Oct-14	0.955	3468	24	3487	51	3519	136	-1.9
15-Oct-14	0.952	3458	22	3486	46	3536	123	-3.0
15-Oct-14	0.954	3453	24	3462	50	3476	133	-0.8
15-Oct-14	0.964	3457	22	3463	53	3472	140	-0.6
15-Oct-14	0.969	3451	23	3482	57	3536	155	-3.2
15-Oct-14	0.958	3449	23	3476	49	3524	131	-2.8
15-Oct-14	0.959	3451	23	3479	51	3527	138	-2.9
15-Oct-14	0.954	3458	23	3466	47	3480	124	-0.8
16-Oct-14	0.991	3462	13	3513	61	3602	173	-5.3
16-Oct-14	0.982	3456	14	3465	46	3481	124	-0.9
16-Oct-14	0.994	3467	12	3487	70	3522	197	-2.1
16-Oct-14	0.984	3457	14	3450	47	3437	128	0.8
16-Oct-14	0.992	3459	12	3495	61	3558	172	-3.7
16-Oct-14	0.986	3464	14	3492	52	3542	143	-2.9
16-Oct-14	0.990	3446	13	3498	58	3590	165	-5.5
16-Oct-14	0.983	3457	14	3469	46	3490	126	-1.2
16-Oct-14	0.986	3461	14	3470	51	3486	141	-0.9

Appendix 7: Precision estimates for XRF analyses from Washington State University's Geoanalytical Lab

WSU XRF precision, limit of determination (2-sigma)

Mar-06	Replicate r2	Replicate LOD
Unnormalized Major Elements (Weight %):		
SiO2	0.99929	0.58
TiO2	0.99992	0.017
Al2O3	0.99949	0.16
FeO*	0.99948	0.20
MnO	0.99983	0.002
MgO	0.99994	0.076
CaO	0.99976	0.064
Na2O	0.99981	0.045
K2O	0.99992	0.031
P2O5	0.99990	0.005
Estimated LOI	0.966	1.00
SO3	0.989	0.07
Cl	0.992	0.002
Normalized Major Elements (Weight %):		
SiO2	0.99992	0.19
TiO2	0.99996	0.012
Al2O3	0.99987	0.082
FeO*	0.99956	0.18
MnO	0.99988	0.002
MgO	0.99994	0.073
CaO	0.99998	0.043
Na2O	0.99989	0.036
K2O	0.99998	0.015
P2O5	0.99996	0.003
Trace Elements (ppm):		
Ni	0.9992	3.5
Cr	0.9998	3.0
Sc	0.997	1.6
V	0.9996	5.0
Ba	0.9997	11.7
Rb	0.9998	1.7
Sr	0.99992	4.6
Zr	0.99994	3.9
Y	0.9987	1.2
Nb	0.99987	1.2
Ga	0.955	2.7
Cu	0.994	7.4
Zn	0.9991	3.3
Pb	0.9966	2.6
La	0.9941	5.7
Ce	0.996	7.9
Th	0.997	1.6
Nd	0.992	4.3
U	0.983	2.7
Bi	0.758	2.0
Cs	0.365	5.1